The origins of accreted units in the Monian Composite Terrane, North Wales UK

CARDIFF UNIVERSITY
PRIFYSGOL CAERDYDD

Niall Thomas Groome

School of Earth and Environmental Sciences
Cardiff University

Submitted in partial fulfilment of the requirements for the degree of
Doctor of Philosophy (PhD)

2023

ABSTRACT

The subduction complex of the Monian Composite Terrane (MCT) records two distinct episodes of subduction – late Neoproterozoic to early Cambrian, and early Ordovician – separated by a transient transcurrent regime. The first episode is characterised by the high P-T Penmynydd Terrane and the accretionary Gwna Complex, which formed at the continental margin of Gondwana, backed by the Avalonian arc. Transcurrent faulting along the arc front juxtaposed terranes of various origins against one another to assemble the MCT. The lower Ordovician marked a short-lived renewal of subduction before back-arc rifting led to detachment of the Avalonian microcontinent.

This project combines field relations with geochemical petrographic and mineralogical information to discuss the genesis subduction-related MCT units to decipher deformed remnants of past tectonic environments, and to interpret the convergent regime that led to their destruction, and ultimate preservation.

The Gwna Complex preserves a range of deformation states, largely dependent on volume of accreted trench-fill sediments. Block-in-matrix mélange, thick disrupted turbidites and, and olistostromes are common in areas dominated by clastic sediment. Sediment starved areas exhibit predominantly imbricated units of ocean floor material with partially preserved ridge-trench ocean plate stratigraphy (OPS) – semi-coherent fragments of sea floor sedimentary successions and upper parts of igneous substrate from a subducting slab – while block-in-matrix mélange is confined to thin, isolated pelitic beds in highly sheared zones between low shear lenticular units. Basalt substrates exhibit MORB-OIB geochemical signatures with significant variability of enrichment over short distances that may represent off-axis seamount development. Dual OPS sequences are proposed, representing seamount stratigraphy and adjacent ocean floor stratigraphy. Intraplate volcanism, likely in the form of a petit-spot seamount, was also recognised through a combination of field evidence, petrography, and whole rock geochemistry.

Metabasites in the Penmynydd Terrane contain sodic amphiboles including glaucophane and magnesio-riebeckite paired with epidote, indicating peak blueschist facies metamorphism. Relict pillow textures and consistent geochemical compositions with the Gwna Complex indicate formation at the same subduction zone.

The Cemaes Group is recognised as a separate episode of subduction recorded in sedimentary mélange. A continuous volcaniclastic base of continental arc affinity indicates resumption of subduction and arc magmatism, followed by a gradual period of uplift and resultant olistostrome deposition.

ACKNOWLEDGEMENTS

This project was funded by KESS2 via the European Social Fund, in partnership with GeoMôn Anglesey UNESCO Global Geopark. Funding contributions were also made from Natural Resources Wales, Magnox, and the Geologist's Association Curry Fund. This project would not be possible without each of these contributions and the efforts of everybody involved to make the project feasible. The project also benefitted in part from funding through Cardiff University's Hazel Pritchard Award, generously sponsored by SRK Consulting.

I would firstly like to thank my supervisors David Buchs and Åke Fagereng for their guidance, wisdom, and enduring support throughout this project. I would also like to thank Harry Leah for our collaboration both in the field and in the lab, and for general discussions about the project. Jana Horák and the mineralogy & petrology group at National Museum Wales have also been of great help to this project by providing access to resources and preparing thin sections. I am also grateful for the continuous guidance and support from the team at KESS, particularly from Esther Meadows.

I would also like to thank those involved in the project from GeoMôn and NRW – Margaret Wood, Stewart Campbell, Raymond Roberts, Charlotte Hawksworth and Graham Williams – for their assistance with logistics, sharing of knowledge and resources, and general enthusiasm for the project. Additionally, I would like to thank all the volunteers at GeoMôn, who make the geological tours and events possible.

I must say a big thanks to Tony Oldroyd for always being accommodating for a whole range of analytical needs. He has prepared thin sections, overseen sample preparations, assisted chemical lab work, and helped to run XRD analysis over the course of the project – among many other things, I am sure. Also, thanks to Duncan Muir for his assistance and guidance on the SEM – and for organising the Bobble, of course. Geochemical analysis was undertaken by the CAF team at Stellenbosch University, who I recommend highly.

Finally, I would like to thank those who have supported me from outside this project. All of those involved in AFC Cardiff Dragons and the T-Ball Association over the past few years have helped to make my time in Cardiff enjoyable and I miss them dearly. Last, but certainly not least, I would like to thank my family for their tireless support, and Hannah for persistently trying to keep spirits high.

RELATED PUBLICATIONS

The following publications includes contributions from the work presented in this thesis. This list is accurate at the time of writing.

Leah, H., Fagereng, A., Groome, N., Buchs, D., Eijsink, A., & Niemeijer, A., 2022. Heterogeneous subgreenschist deformation in an exhumed sediment-poor mélange. Journal of Geophysical Research: Solid Earth, 127, e2022JB024353. https://doi.org/10.1029/2022JB024353

Roberts, R., Campbell, S., Williams, G., Groome, N., Buchs, D., & Holden, A., 2022. Site 068 – Ynys Llanddwyn late Neoproterozoic-Cambrian Mélange. In: International Union of Geological Sciences. ed. *The First 100 IUGS Geological Heritage Sites*. Spain: International Union of Geological Sciences. pp. 186-187.

TABLE OF CONTENTS

List of Appendices

CHAPTER I
Introduction

1.1 INTRODUCTION

Accretionary complexes form at active convergent tectonic margins from a fragmented mix of material derived from both the footwall and hanging wall. In subduction zones, they can preserve and expose fragments of material derived from subducted oceanic lithosphere, or Ocean Plate Stratigraphy (OPS) (Isozaki et al. 1990; Wakita and Metcalfe 2005). They offer a unique opportunity to characterise the geological history of oceanic crust, from its inception at a spreading centre to its destruction – or recycling – at a subduction zone (Matsuda and Isozaki 1991; Kusky et al. 2013). Accretionary complexes can retain OPS long after cessation of subduction and are valuable geological archives that preserve some of the only remnants of otherwise disappeared oceanic lithosphere. The characterisation of accretionary complexes and associated OPS within them can therefore provide crucial insights into past tectonic events and processes throughout Earth's history (Safonova 2009; Wakita 2012a; Ackerman et al. 2019; Kusky et al. 2020; Yan et al. 2021). Characterising the nature and origin of accretionary complexes is of particular importance in recording pre-Mesozoic tectonic events, where preservation of oceanic crust and other evidence for these events is scarce today (Kusky et al. 2013; Kusky et al. 2020).

While accreted OPS typically consists predominantly of sea floor sedimentary successions and terrigenous arc material, under certain circumstances igneous rocks from upper ophiolitic domains of the oceanic lithosphere, intra-oceanic igneous activity or dissected arcs can be incorporated (Buchs et al. 2009; Kusky et al. 2013; Safonova et al. 2015). Oceanic material, whether in the form of ophiolites, accreted OPS or exhumed highly metamorphosed terranes, can provide rare opportunities to conduct detailed and accessible studies on sea floor material, which is important not only in understanding past tectonic events and oceanic settings, but also in understanding modern oceanic and tectonic environments. Current knowledge of the ocean floor is extremely limited due to the cost, difficulty, and lack of necessity of exploration, and as of writing, less than 20 % of the ocean floor has been mapped to 'modern standards', at resolutions of at least 100 m (data from GEBCO; https://www.gebco.net/).

In North Wales, UK, several units have been identified as possible examples of ancient accretionary complexes formed during a subduction regime that initiated in the Neoproterozoic (Wood 1974; Gibbons 1983a; Carney et al. 2000; Maruyama et al. 2010a; Wood 2012). Subduction of what is interpreted to be the Iapetus Ocean against the margin of continental Gondwana led to the formation of the Avalonian-Cadomian continental arc, providing the initial backdrop for accretion above the subduction interface (Gibbons and Horák 1996; McIlroy and Horák 2006). Igneous rocks within these units may represent some of the few primary remnants of Iapetus oceanic lithosphere, with the former ocean having disappeared entirely by the end of the Silurian (Cocks and Torsvik 2006). The lack of any major destructive overprint from more recent tectonic events makes the units ideal localities to assess potential accretionary processes and preserved OPS from an ancient system.

The potential accretionary units – along with other similarly aged units thought to have derived from a tectonically active setting – form the Monian Composite Terrane (MCT), outcropping primarily on the Isle of Anglesey and across Llŷn Peninsula in North Wales, while also correlating to rocks in southeast Ireland, across the Irish Sea (Tietzsch-Tyler and Phillips 1989; Gibbons et al. 1994). The MCT is a series of juxtaposed terranes of varying metamorphic and tectonic histories, lithologies and origins, ranging from Neoproterozoic to Lower Ordovician in age (Greenly 1919; Gibbons and Horák 1990; Phillips 1991b; Asanuma et al. 2017; Schofield et al. 2020). Given the broad geological range of the MCT, this project will focus on those units of suspected accretionary origin, and units closely related to them.

The MCT sits between several more extensive terranes also linked to this Gondwanan subduction event, including Avalonia to the south and Ganderia to the north. These surrounding terranes – collectively referred to as the peri-Gondwanan terranes – eventually rifted from the margin of Gondwana and migrated towards Laurentia during the lower Palaeozoic, along with the MCT. The terranes extend geographically to North America and continental Europe, and as a result, are well represented in geodynamic interpretations of the tectonic event. The placement of the MCT in this geodynamic setting is rather enigmatic though, and its possible subduction-related rocks may provide unique and critical insight into the peri-Gondwanan tectonic story.

Understanding the geology of the MCT is therefore an important prerequisite in interpreting its role in Gondwanan subduction, and the subsequent rifting and formation of these peri-Gondwanan terranes. The MCT, however, has long been a source of contention among geologists due to its regionally unique and curious geology, its diversity within a concentrated area, and the lack of apparent tectonostratigraphic linkage both between the units that compose it, and with the surrounding regional geology (Shackleton 1975; Barber and Max 1979; Gibbons and Horák 1996; Kawai et al. 2007; Schofield et al. 2020) . Recent conflicting tectonic interpretations of the MCT include a Pacific-style accretion and underplating model (Kawai et al. 2007; Maruyama et al. 2010a; Asanuma et al. 2015), and a Caribbean-style transcurrent system with no evidence for accretionary complexes (Dartnall 2018; Schofield et al. 2020).

1.1.1 Principal aims of the project

This project evaluates the origins and formations of mélange units within the MCT, and looks at their importance in the wider geodynamic evolution of the MCT between the Neoproterozoic and Ordovician periods. The Gwna Complex - being the most widespread, lithologically diverse, and disputed of these units, will occupy the main focus of the project, while mélanges and associated volcaniclastics in the Cemaes Group, as well as the high-grade metamorphic Penmynydd Terrane, are also considered. The Isle of Anglesey is also host to several distinct groups of mafic sheet intrusions. These will also be studied to determine any possible links to MCT-related tectonic activity.

The Gwna Complex provides a rare opportunity to study ocean floor material in detail over a small scale. This study makes use of excellent, accessible exposures at Newborough Nature Reserve as a prime case study of accreted oceanic material, evaluating the formation of the Gwna Complex through reconstruction of OPS, and determining the subsequent processes that led to its accretion. A detailed geochemical study of igneous rocks at the site will analyse any local-scale chemical heterogeneities and their causes. Comparisons to other Gwna Complex localities and potentially related external units are used to provide a regional context to these features.

New geochemical data presented in this study provide the first comprehensive geochemical overview of accreted units and mafic sheet intrusives across Anglesey, building on limited available data (Thorpe, 1993; Ellis, 2009; Saito et al., 2015). Along with mapping, field and mineralogical observations, this data will be used to produce a detailed account of mélange formation in the MCT, and provide a revised interpretation of the tectonic history of the MCT and surrounding peri-Gondwanan terranes.

This thesis is structured into eight chapters, including three primary data chapters, presenting findings from field observations and geological mapping (Chapter II), petrological and mineralogical studies (Chapter III), and whole rock geochemical data (Chapter IV). Chapters V and VI will focus on the interpretations of this data, tackling the origins of the studied units and their wider implications respectively. The purpose of Chapter VII is discussed below in Section 1.1.2.

1.1.2 Geopark collaboration

This project is conducted in collaboration with GeoMôn UNESCO Global Geopark. The aim of the collaboration is to use scientific observations and findings from the project to influence decisions on methods to increase the prominence of the geopark. The collaboration between research and outreach with GeoMôn will be explored in Chapter VII of this thesis.

The collaboration will focus on Newborough Nature Reserve as a primary site of interest. The area is important to this scientific study as it hosts rocks from the Gwna Complex. The site is also of great importance to GeoMôn because it is a major tourist site for the Isle of Anglesey. The complexity and diversity of the geology in the area makes the site ideal for attracting informed visitors and geologists, whilst aesthetically striking outcrops can capture the interest of passive recreational visitors. As part of the collaboration, a geological map of Newborough Nature Reserve will be produced, uncovering the geology of the relatively unexplored Newborough Forest. This map, along with field observations, will be used to locate sites of particular interest to inform decision making, while geological interpretations will be used to produce resources for communicating the geology to the public.

1.2 KEY CONCEPTS

This section aims to provide an overview of the general geological concepts that will provide the basis for this project, discussing relevant plate tectonics, accretionary mechanisms, metamorphism and alteration, and the role of geochemical analysis in the interpretation of these processes.

1.2.1 Anatomy of continental arcs

Active continental-oceanic margins are broadly characterised by subduction of the oceanic plate and the subsequent formation of a volcanic arc. Active margins consist of an arc volcanic front, typically a forearc basin, often an accretionary complex/wedge/prism, and a trench (see Figure 1.1). Arcs form through periods of uplift and magmatic activity near to the continental margin. Forearc basins develop as a catchment for eroded arc and forearc material along the frontal slope. They are contained by a backstop either as a result of forearc faulting or the creation of a topographic high (Clift and Vannucchi 2004). The outer limits of the forearc are marked by a trench, marking the tectonic plate interface in a deep V-shaped basin (van der Werff 1995) that acts as an effective catchment for mass-transport deposits.

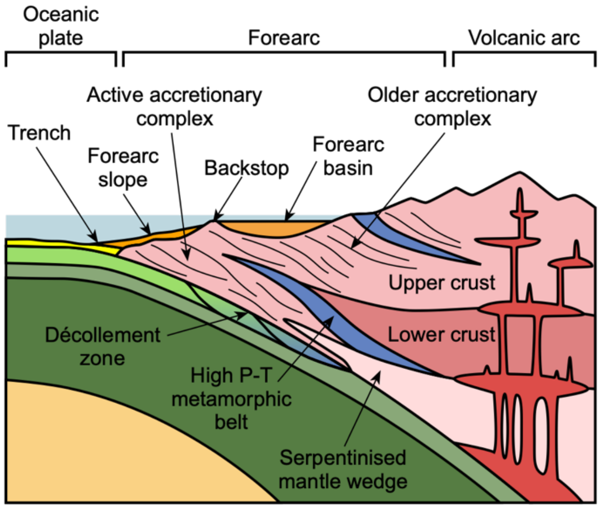

Figure 1.1: Schematic diagram of a volcanic arc showing typical features of a subduction zone and forearc. Modified after (Kusky et al. 2013).

Active subduction zone margins can be considered erosive or accretionary, determined by numerous factors such as relative and absolute plate motions, sediment input rate, and the geometries of the subduction zone and continental margin (Clift and Vannucchi 2004; Ryan et al. 2009; Vannucchi et al. 2013). Erosive margins experience progressive subsidence and landward migration of the trench and arc as upper plate material is eroded by subduction processes (Clift and Vannucchi 2004; Wang et al. 2010). Conversely, accretionary margins are characterised by sustained net accretion and leads to the formation of an accretionary complex at the interface of the continental and subducting oceanic plates.

Compaction and heating of sedimentary material upon a subducting oceanic plate releases great quantities of pore fluids (Bebout 1995), whilst metamorphic reactions at greater depths release more water through dehydration. Lithospheric flexure allows hydrothermal fluids to migrate along pervasive fractures (Schmidt and Poli 2003) towards the upper lithosphere boundary provoking melting of overlying mantle wedge material. These mafic melts rise and mix with felsic material through a complex combination of different processes in the overlying continental crust to produce the intermediate melts characteristic of a continental volcanic arc, although magmatic products can vary greatly through partial melting, fractionation and crustal assimilation (Annen et al. 2006; Winter 2010; Dong et al. 2020).

Accretionary complexes

Accretionary complexes provide unique records of subducted material. They can consist of continentally derived material, ocean floor material and exhumed slivers of high-pT metamorphic units, often being the only remaining records of subducted oceanic material. Accretionary complexes are highly deformed by intense tectonic stresses, often producing mélange by extensive disaggregation and mixing of rock units. The main body of the accretionary complex consists of fault bound coherent units to tectonic mélanges (Kitamura and Kimura 2012) whilst sedimentary mélanges develop along the surface slope and in basins. Potentially coherent duplexes of underplated sea floor material accumulate at the base of the complex along a décollement zone (Cowan 1985). At the front of an accretionary prism, newly accreted material may show differing states of deformation as it is slowly disaggregated and lithified.

Trench sediment input is a major control on accretionary processes. When the trench is thickly sedimented, duplexing and underplating is more common and leads to the preservation of relatively coherent stratigraphy as thick sediment sequences are subducted and the accretionary prism is uplifted. In sediment starved systems, décollement faults do not tend to form to accommodate underplating. This leads to the primary formation of thin belts of chaotic, incoherent mélange (Kusky et al. 1997; Hori and Sakaguchi 2011). Accretion is typically a more sporadic than constant process. Sampling of ocean floor material is rare and is often driven by topographic heterogeneity on the seafloor, where topographic highs are more likely to be accreted (von Huene et al. 2004).

Rapid underplating of trench sediments may be an important mechanism in the exhumation of high-pT metamorphic units from deeper in the subduction zone (Kusky et al. 1997), although the mechanisms that induce exhumation are still poorly understood (Agard et al. 2009; Monié and Agard 2009). Slivers of metamorphic units can be exhumed from deeper along the subduction zone interface and incorporated into accretionary complexes along large-scale thrust faults. The metamorphic units move upwards along the hanging wall of the thrust and are bound by normal faults at the upper surface.

Mélange classifications

Mélange is defined as a mappable rock unit characterised by a lack of internal stratigraphic continuity and by the inclusion of fragments and blocks of various size embedded in a fragmented matrix of finer, often pervasively deformed material (Silver and Beutner 1980; Raymond 1984; Festa et al. 2012). The term covers a wide variety of disordered rocks including chaotic block-in-matrix units, duplexes and fragmented sequences (Kusky et al. 2020). Mélanges can form in a variety of geological settings such as active subduction zone and collisional margins, passive margins, strike-slip regimes, and intracontinental settings. Uniform classification of mélange types has proved challenging historically and currently, mélanges at collisional margins are generally classified into three main types: subduction (or, more generally, tectonic), sedimentary and diapiric (Cowan 1985; Festa et al. 2010). Figure 1.2 demonstrates the different mechanisms that can lead to mélange formation in a subduction zone setting. Diapiric mélanges have not been interpreted in the MCT and are quite distinct from sedimentary and tectonic mélanges. They are vertical crosscutting cylindrical features formed from mud volcanoes that result from mobilisation and upwelling of water, gases and mud (Kopf 2002).

Sedimentary mélange and olistostromes

Olistostromes are considered to be sedimentary mélanges, as they have a similar make-up of chaotic blocks/olistoliths suspended within a matrix, but are formed from entirely sedimentary processes (Hsü 1974; Cowan 1985; Festa et al. 2012). In a forearc setting, they typically form along forearc slope surfaces from downslope mobilisation of partly lithified units (Ogata et al. 2012), or within basins and at the trench as mass-transport deposits. They are transported in a semifluid state and accumulate as massive heterogeneous deposits but may be associated with turbidites. Olistostromes are a product of gravitation instability that can be a result of several methods such as basin subsidence, sediment input rates, pore fluid pressure and changes in climate conditions, but the most prevalent method is through tectonic activity (Nemčok et al. 2005; Festa et al. 2010).

Olistostromes can be distinguished from subduction mélanges due to the rounded and unaligned nature of olistoliths as a result of erosion, while the matrix of an olistostrome is also not pervasively sheared (Hsü 1974). Olistostromes may later become subduction mélanges if subjected to tectonic forces after formation, which is particularly common if deposited into a trench. Tectonised olistostromes are then difficult to distinguish from primary subduction mélanges and they are thought to be common. Most mélanges are polygenetic, originating from sedimentary or diapiric processes before undergoing tectonic overprint (Festa et al. 2019; Wakita 2019).

Subduction mélange

Mélanges that form from subduction zone processes originate either from offscraping and underplating, or from tectonism of mass-transport deposits. This encompasses the bulk of mélange formed within an accretionary prism. Subduction mélange matrices develop a pervasive sheared fabric that anastomoses around roughly parallel oriented clasts. The tectonic fabric is subvertical to steeply dipping towards the arc. Mélanges have a heterogeneous rheology as a result of mixing materials of vastly different competencies. Bulk shear is largely concentrated in the weak mélange matrix, if voluminous enough to accommodate it, with relatively competent clasts subjected to significantly less strain (Fagereng and Sibson 2010). Subduction mélange is a subdivision of tectonic mélange, which has broader connotations and can be applied to numerous geological settings.

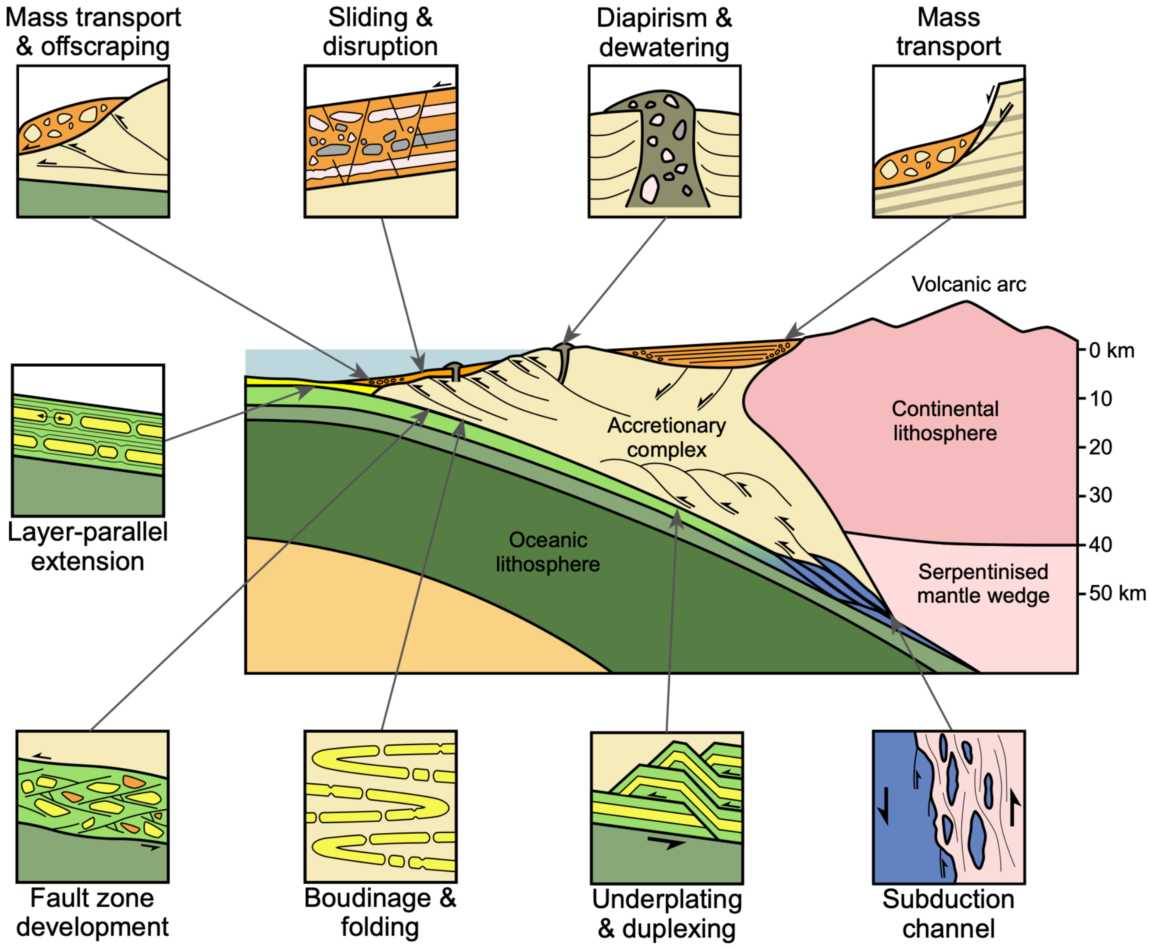

Figure 1.2: Schematic diagram showing various processes of producing different types of mélanges in a subduction zone setting. Modified after Cowan (1985); Kusky et al. (2020). Orange – sedimentary mélanges; green – subduction mélanges; blue – high grade subduction mélanges; grey – diapiric mélanges.

OPS mélange is a distinction of subduction mélange that contains elements of ocean plate stratigraphy – or OPS (Wakita 2015). It is often preserved through underplating, where duplex structures form along décollement fault zones stacking layers against one another (Kusky et al. 2020). Oceanic material is less likely to be mixed and dispersed within less consolidated accreted sediment of the upper accretionary complex this way. The preservation of OPS mélange units through duplexing is described from several accretionary complexes such as the Shimanto Belt, Japan (Onishi et al. 2001; Kimura et al. 2012), and has been interpreted within the Gwna Complex of Anglesey (Maruyama et al. 2010a).

1.2.2 Ocean plate stratigraphy (OPS)

The reconstruction of OPS is the process of decrypting accretionary complex material to uncover the geological evolution of subducted oceanic lithosphere. Accretionary forces subject upper portions of oceanic lithosphere incorporated to intense stresses that lead to extensive deformation and often result in the loss destruction of original stratigraphy order. An understanding of the structural controls and causes of deformation within the accretionary complex is therefore needed to reconstruct the order of deformed and fragmented accretionary units. The concept of OPS is derived from the fundamental structure of accretionary complexes currently observed forming in the Pacific margins around Japan (Isozaki et al. 1990; Kusky et al. 2013). It has developed to represent a template of expected sequence of igneous and sedimentary units that comprise the oceanic lithosphere through the three key phases of its lifecycle (Isozaki et al. 1990; Kusky et al. 2013; Safonova et al. 2016b). Comparisons between OPS from localities across the world and ages spanning from Proterozoic to modern day, show generally consistent similarities in structural controls, major rock components, stratigraphic sequences and basalt geochemistry (Kusky et al. 2013). Comparisons between modern and ancient accretionary complexes can therefore provide crucial insight into both past and present geodynamic processes (Safonova 2009; Maruyama et al. 2010a; Wakita 2012b; Safonova et al. 2016a; Robertson 2019).

A 'standard' ridge-trench OPS model, as illustrated in Figure 1.3, includes fragments from the uppermost stages of Penrose ophiolites, intracontinental seafloor sedimentary successions and continental material deposited in and around a subduction trench. The base of an OPS sequence (Stage I) may begin with upper ophiolitic volcanic rocks, although these are rarely preserved in accretionary complexes. Pelagic seafloor sediments such as cherts and shales make up the base of overlying sedimentary sequences, being deposited between stage I and II. Towards the trench of a subduction zone, terrigenous material is introduced causing the deposition of hemipelagic sedimentary units. Greywacke-shale turbidite sequences and olistostromes accumulate around the trench as the oceanic lithosphere enters stage III and begins to undergo subduction and accretion (Kusky et al. 2013; Safonova et al. 2015).

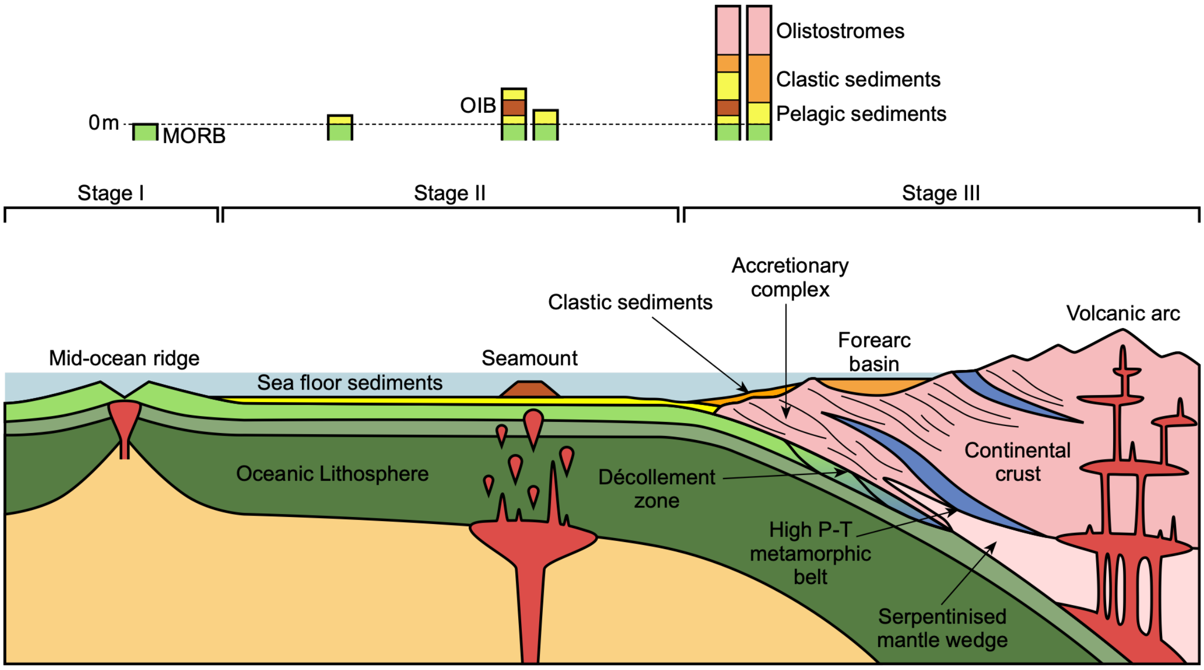

Figure 1.3: Schematic diagram showing the ridge-trench transition of oceanic lithosphere and the development of standard ridge-trench OPS across three key stages of development. Stage I – axial ridge volcanic activity; Stage II – intraplate pelagic sedimentation and possible seamount production; Stage III – clastic trench fill sedimentation and accretion/reworking. Modified after Kusky et al. (2013).

Intraplate volcanism and seamount OPS

Irregularities in seafloor topography can have major implications for accretionary processes. Features such as seamounts and island arcs can clog subduction zones slowing subduction rates and acting as a catalyst for accretion due to their relative height and buoyancy (von Huene et al. 2004; Pickering and Hiscott 2016). Accumulation of continental sediments upon these features would also be typically less prominent than on its surroundings. The subduction of seamounts does promote increased deposition of continental material around them, however, since their prominence beneath the forearc can lead to slope instability at the surface (von Huene et al. 2004). In accretionary complexes, seamounts therefore have biased representation, as they are considerably more susceptible to accretion than flat ocean floor.

Seamounts are widespread across modern-day ocean floors, ranging from large volcanic ocean islands to small, relatively insignificant topographic irregularities, with approximately 90% of seamounts being less than 500 m high (Wessel et al. 2010; Buchs et al. 2015). Modern ocean islands and seamounts close to sea level are much more accessible and geographically significant, and therefore hold a biased representation in geological understanding of intraplate volcanism. Smaller seamounts such as petit-spots

(Hirano et al. 2001; Hirano et al. 2006) show that there is significant variation in intracontinental processes and an effective method of studying these is in accretionary complexes (Mertz et al. 2001; Buchs et al. 2013). Figure 1.4 shows some of the general diversity in the distribution, size and setting of seamounts.

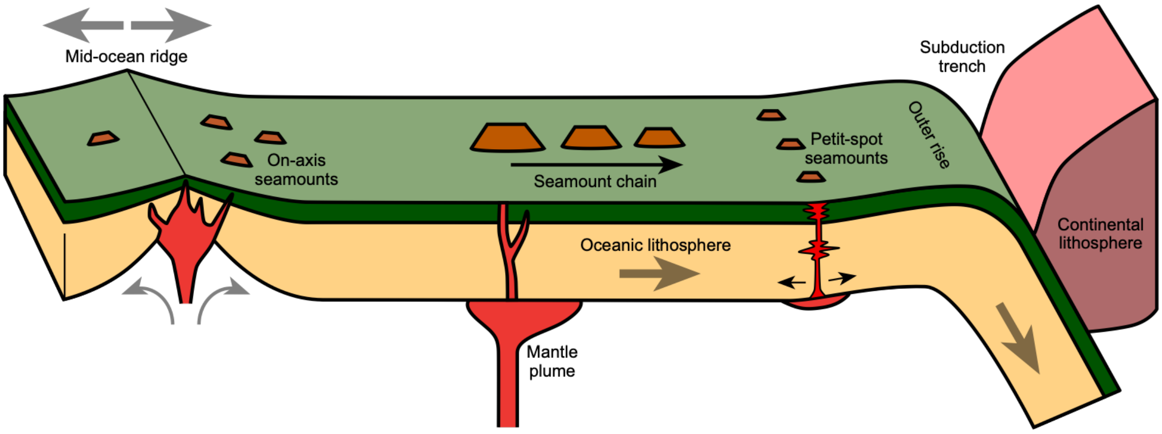

Figure 1.4: Schematic demonstration of some established methods of seamount formations including off-axis seamounts near spreading centres, variably distributed mantle plume-derived seamounts and petit-spot seamounts derived from flexure around the outer rise of subducting oceanic lithosphere.

Seamounts typically consist of basaltic lavas similar in morphology to mid-ocean ridges, although more evolved magmatic suites may also be produced. This creates difficulties in distinguishing basalts of different origins in accretionary complexes, where tectonic origins are not obvious. A key discriminating factor is that seamounts create localised environments that lead to the preservation of distinct OPS sequences, as outlined in Figure 1.5. Seamounts typically develop a cap of carbonate sediments (peak above CCD) or other shallow marine sediments. Upon seamount slopes, carbonate breccias, volcaniclastics and other clastic material is deposited through erosion and instability of the seamount summit, transitioning into distal mudstones around the base (Safonova 2008; Kusky et al. 2013; Safonova et al. 2015).

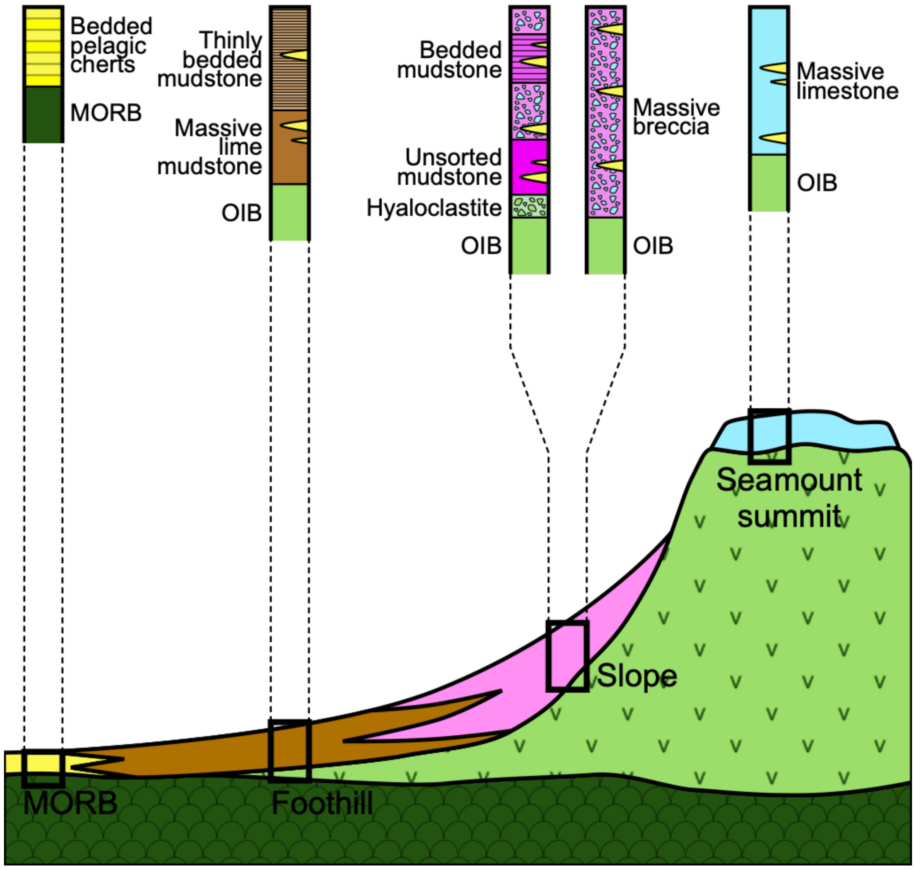

Figure 1.5: Schematic cross-section of a seamount showing the development and variation of seamount OPS at different stages of the seamount, including distal seafloor OPS and OPS developed around the seamount foothill, along the slope and at the summit. Modified after Sano and Kanmera (1991); Safonova (2009).

1.2.3 Geochemical diversity of basalts

Basalt is the most diverse, widespread volcanic rock found on Earth and can be produced in various tectonic environments including spreading centres, intraplate volcanoes, and volcanic arcs. Whilst OPS and other indicating factors can produce an idea of tectonic setting, supplementation of geochemical data can be extremely useful in discriminating magmatic origins. Integrating other supporting evidence, rocks can then be attributed to their most likely tectonic settings, based on processes occurring in modern-day analogues (Wood 1980; Pearce 2008; Humphreys and Niu 2009; Gale et al. 2013; Pearce 2014). It should be noted that highly depleted ophiolitic rocks such as boninites can be common in many subduction systems, however there is no evidence of their presence in the units studied in this project, and therefore will not be focused on in great detail.

Mid-ocean ridges

At mid-ocean ridges, melts are produced through decompression melting of a mantle source at shallow depths (<80 km), driven by mantle convection beneath thin, buoyant lithosphere. Resulting volcanic products are generally constrained to tholeiitic basalts, limited by the fractionation of olivine + clinopyroxene + plagioclase at low pressures (15 – 20 kbar). They contain relatively low contents of Al_2O_3 (<0.2 %), TiO_2 (<2 %) and alkalis, and have a high Mg# that evolves along an Fe-enrichment trend. Mid-ocean ridge basalts (MORB's) are also characterised by low concentrations of incompatible elements (Rollinson 1993; Winter 2010).

MORB's can be subcategorised into N-MORB ('normal'), E-MORB/P-MORB ('enriched', or 'plume-influenced'), and D-MORB ('depleted'), with N-MORB representing a most statistically likely MORB composition between E-MORB and D-MORB respective statistical end-members (Gale et al. 2013). The upwelling mantle source of basalt is thought to largely originate from an upper mantle depleted in incompatible elements. A component of this upwelling mantle may also originate from the deeper, more fertile mantle, capable of producing E-MORB melts with an enriched concentration of incompatible elements.

Spreading rates of mid-ocean ridges may lead to some compositional variability within MORB products. At ridges with slower spreading rates, a cooler thermal structure and thicker lithosphere means relatively lower degrees of partial melting and episodic volcanic activity, since the bulk of the system remains comfortably below the liquidus temperature. Convection and magma mixing are therefore limited, leading to variable geochemical compositions, albeit remaining within the MORB array (Sinton and Detrick 1992). At fast-spreading ridges, continuous convection leads to the production of heterogeneous magmas from an almost steady-state magma chamber. They tend to produce slightly more enriched N-MORBs with lower Mg# (Sinton and Detrick 1992). Fast-spreading ridges are typically associated with the production of off-axis seamounts, where melts erupt directly onto the seafloor on the flanks of axial ridges. Forming from deeper melt pockets, they can bypass the main mixing centre directly beneath the mid-ocean ridge and avoid further fractionation, leading to compositional heterogeneity relative to on-axis magmas (Perfit and Chadwick 1998; Davis and Clague 2000). Off-axis seamounts are typically tholeiitic and can reach E-MORB compositions (Perfit and Chadwick 1998).

Intraplate volcanism

Mantle plumes are largely considered to be the main drivers behind intraplate volcanism and production of ocean island basalt (OIB) melts in the formation of ocean islands and seamounts, along with larger scale flood basalts and plateaus. Plumes are thought to originate from the deep mantle, most likely from the D” layer at the core-mantle boundary (Courtillot et al. 2003; Foulger and Jurdy 2007). The source material is heterogeneous and relatively enriched in incompatible elements through the recycling of oceanic lithosphere and sediments. OIB and MORB incompatible element compositions can be expressed along a MORB-OIB array as respectively enriched and depleted sources can interact, with E-MORB representing an intermediate (Pearce 2008). Generalised geochemical distinctions are demonstrated in Figure 1.6. The suite is most extensively evident in Iceland, where the mid-Atlantic ridge intersects the Iceland plume, resulting in basalt trace element compositions ranging between N-MORB and OIB (Fitton et al. 1997).

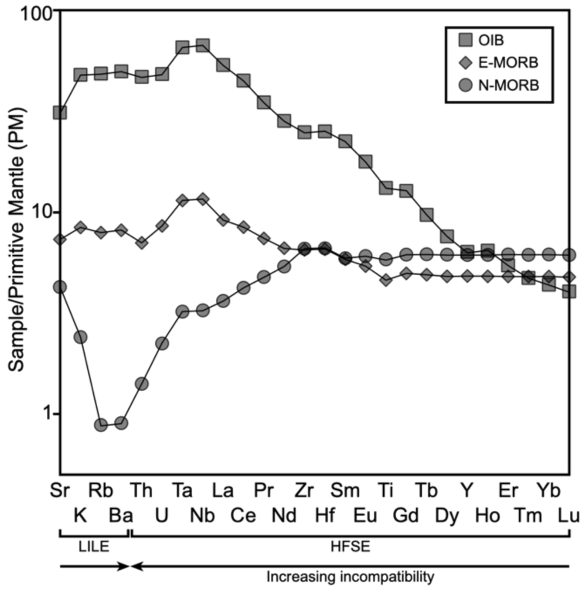

Figure 1.6: Multivariate plot of average OIB, E-MORB and N-MORB compositions showing compositional changes against relative compatibility of elements. Data from (Sun and McDonough 1989).

Partial melting of the plume head mostly occurs at the base of the oceanic lithosphere, which acts as a density filter. Oceanic lithosphere thickness therefore acts as a primary control on OIB compositions (Humphreys and Niu 2009; Niu et al. 2012; Niu 2021). Beneath older, thicker lithosphere, decompression melting of plumes occurs at greater depths and higher pressure, within the garnet stability zone as opposed to the shallower spinel stability zone. The presence of garnet greatly affects REE (rare-earth element) distributions for example, as garnet preferentially retains HREE’s (heavy REE) at much greater rates than LREE’s (light REE) (Niu 2021).

Plume-derived magmatism most commonly produces tholeiitic to alkali basalts but may also produce a suite of more differentiated rocks reaching rhyolite compositions, or phonolites in silica-undersaturated systems (Winter 2010; Suetsugu et al. 2013). Compared to MORB compositions, OIB’s are typically enriched in alkalis (Na + K) and large-ion lithophile elements (LILE's) with the exception of Sr, and with relatively low K/Rb and K/Ba ratios (Pearce 1976; Schilling et al. 1983; Sun and McDonough 1989). OIB's are also progressively more enriched in more incompatible elements (Schilling et al. 1983; Sun and McDonough 1989; Rollinson 1993; Gale et al. 2013). This results in steeper normalised REE patterns with preferential enrichment in LREE's.

Although mantle plumes produce the most prominent seamounts, seamounts have great variety and can form through several different processes, as shown in Figure 1.4. On-axis seamounts are derived from decompression melting at mid-ocean ridges and typically have N-MORB to E-MORB compositions (Davis and Clague 2000). Petit-spots are small intraplate seamounts that are derived from lithospheric flexure, enabling the migration of small melt pools accumulated at the base of the lithosphere to penetrate to the surface (Hirano et al. 2006; Yamamoto et al. 2014; Sato et al. 2018). These seamounts also have an OIB-like composition but are distinguishable from plume-derived OIB's by their sodic compositions (low K_2O/Na_2O ratios) and a relative depletion of Zr and Hf compared to other HFSE's (Hirano et al. 2006).

Volcanic arcs

Subduction-related basalts form from a deeply complex set of volcanic arc magmatic processes. Erupted basalts do not fully represent their primary melt compositions and will typically experience some degree of fractionation, partial melting, assimilation or magma mixing during ascension through the arc (Tatsumi and Eggins 1995; Winter 2010). Basalts rarely reach the surface in continental arcs as they are denser than the continental crust and are likely to remain stalled towards the base of the crust.

The difference in crustal thickness between ocean island and continental arcs creates a compositional array comparable to the MORB-OIB relationship. Continental arc basalts (CAB's) are progressively more enriched in incompatible elements than island arc basalts (IAB's) and have relatively steep REE patterns, although both typically originate from garnet-bearing sources (Pearce 2008; Niu 2021).

Principally, IABs and MORBs originate from similar depths and mantle sources, and this is reflected by their similar major element and HFSE compositions. The voluminous presence of fluids introduced to the mantle source from the downgoing slab leads to greatly enriched LILE's contents in volcanic arc basalts (VAB's). A key difference geochemically between the MORB-OIB array and the VAB array is the significant enrichment of Th, sourced from melting of subducted sediments (Pearce and Peate 1995; Pearce 2008).

Both continental and oceanic arc settings may produce back-arc basins with basaltic components (BABBs) (Sinton and Fryer 1987; Taylor and Martinez 2003). These basalts derive from an N-MORB-like source through the same process of lithospheric thinning and may sit compositionally within the MORB-OIB array. The mantle source is often influenced by subduction and arc processes, with greater influence closer to the arc, causing BABB compositions to stray between the MORB-OIB and VAB arrays (Pearce 2008; Saccani 2015). They are more geochemically erratic than MORB's and are enriched in LILEs and LREEs, whilst the thinner nature of ophiolite formation produces relatively high Al and low Fe compositions (Sinton and Fryer 1987; Saccani 2015).

1.2.4 Sea floor alteration

Greenly (1919) described the extrusive volcanics of his Gwna Group under the term 'spillites'. Spillite is a term applied to magmatic rocks that have undergone alteration, replacing much of its original mineralogy and leaving no visible phenocrysts. The volcanic rocks studied from the Gwna Complex on Llŷn Peninsula have been similarly altered (Saito et al. 2015). Spillitic alteration is a good indicator of volcanic activity in oceanic conditions and is commonplace in pillow lavas. Throughout the lifespan of an ocean floor, passive seawater circulation in the upper lithosphere results in slow, low temperature alteration, potentially aided by the presence of hotter hydrothermal fluids sourced from shallow magma chambers (Kelley et al. 2002).

Seawater fluid circulation within oceanic crust, can have significant, widespread effects on its geochemistry, mineralogy and physical properties of oceanic rocks (Edmond et al. 1979; Humphris et al. 1980; Thomson et al. 2014). Sea floor alteration of oceanic crust is a dynamic process, varying according to factors such as lithospheric depth, primary mineralogy and texture, fluid composition, structure of secondary phases, permeability, distance from spreading axes and sea floor sedimentation rate (Stroncik and Schmincke 2001; Becker and Davis 2004; Franzson et al. 2008; Zhang and Smith-Duque 2014). The main alteration processes of submarine volcanic rocks include deuteric alteration, seafloor weathering, hydrothermal circulations of fluid solutions and regional metamorphism (Hékinian 1982).

In the volcanics of the upper lithosphere (< 600 m), large volumes of hydrothermal fluids circulate at 0 – 150 °C, characterised by high fluid flux (Alt, 2004). At greater depths, alteration is characterised by hotter fluids and much lower permeability, leading to the formation of pervasive greenschist facies mineral assemblages (Becker & Davies, 2004; Staudigel, 2003). Most low-temperature alteration occurs within approximately 8 – 10 Ma as secondary mineral precipitation and sedimentary cover begins to restrict fluid pathways (Grevemeyer et al. 1999; Alt and Teagle 2003; Nedimović et al. 2008).

Three major alteration trends are common in mature upper lithosphere volcanics: albitisation, chloritisation and epidotisation (Hernández-Uribe et al. 2021). Albitisation involves the replacement of primary magmatic plagioclase by albite through ion exchange reactions, replacing Ca with Na from salt-rich seawater (Rosenbauer et al. 1988). Chloritisation and epidotisation are characterised mostly by the replacement of mafic minerals that make up the remaining bulk mineralogy of a basalt (clinopyroxene and olivine). Chloritisation involves the replacement of mafic minerals by smectite group clay minerals and chlorite, leading to overall enrichment in Mg and Fe primarily, whilst Ca and Si are removed (Mottl 1983; Alt 2004; Kiss et al. 2008). Epidotisation involves the replacement of both clinopyroxene and plagioclase with an assemblage of epidote + chlorite + quartz, driven by oxidised fluids and leading to an enrichment of Ca (Bach et al. 2013).

The earliest form of alteration in submarine basalt is the deuteric, non-pervasive infilling of pore spaces and fractures with celadonite ± nontronite ± Fe-oxyhydroxides to create a dark rim often seen around pillow basalts. This process can also involve the replacement of olivine phenocrysts (Humphris et al. 1980; Alt 2004). Deuteric alteration is followed quickly by palagonisation of volcanic glass. Due to its non-crystalline form, volcanic glass is highly reactive and is rapidly replaced in situ by palagonite, along with clay and zeolite minerals (Staudigel and Hart 1983; Alt 2004; Franzson et al. 2008).

These rapid early phases are followed by more comprehensive alteration as primary mineral components of mafic rocks are broken down over a longer timescale. Plagioclase is primarily affected by albitisation, whilst mafic minerals are replaced in high abundance by smectite-group clay minerals like saponite and nontronite at low temperatures (Alt and Teagle 2003). The formation of Fe-oxyhydroxides also takes place and pyrite can often form in reducing conditions. Palagonite is also broken down into smectites through thermodynamic changes of circulating fluids, leading to re-enrichment of Si, Al and Mg, enrichment in K and removal of Ti (Stroncik and Schmincke 2001; Stroncik and Schmincke 2002).

Smectite group minerals can be further replaced by illite and chlorite during burial beneath accumulating sea floor sediments and progressive increase in fluid temperature (Tardy and Duplay 1994; van de Kamp 2008). Illite formation is constrained to occur in temperatures of 90 – 115 °C, whilst chlorite forms from the breakdown of saponite at 60 – 70 °C (Tardy and Duplay 1994). At higher temperatures (> 200 °C), illite converts to muscovite and results in the steady release of Si, Fe and Mg from the system, whilst consuming Al and K (Totten and Blatt 1993; van de Kamp 2008).

Both albitisation and chloritisation result in significant losses of Ca, leading to the circulation of fluids rich in Ca and depleted of alkalis. Additional Ca may also be introduced from interactions with seafloor carbonate sediments. Epidotisation and the formation of carbonates, as well as carbonate precipitation as veins or amygdales, are important processes in returning Ca to the system from these fluids (Staudigel et al. 1981; Kiss et al. 2008; Bach et al. 2013).

The outcome of these alteration processes is that mafic igneous rocks that were emplaced on the sea floor are likely to have been subjected to a complex combination of these processes, leading to the mobility – to some extent – of most major elements and LILE's. This is important to recognise when analysing rock of this type.

1.2.5 Subduction-related metamorphism

Metamorphic facies are a set of domains representing pressure and temperature (P-T) conditions under which, rocks will generally experience solid-state changes. Each domain is associated with a particular metamorphic mineral assemblage for standard protolith rock types of a constant whole rock composition (Eskola 1921; Eskola 1939; Turner 1981). P-T paths reflect the metamorphic history of a rock through a record of metamorphic facies. There are three broad prograde P-T path gradients that a rock may be subjected to, each reflecting different tectonic or magmatic influences on their changing conditions (Miyashiro 1961; Spear 1995). Low P-T paths are driven by temperature and are associated with contact metamorphism. Intermediate P-T paths are most variable and typically relate to burial, governed largely by standard geothermal gradients. High P-T paths record a high pressure increase relative to temperature. Figure 1.7a outlines the conditions of these paths, which generally correlate to distinct domains of a subduction zone setting (see Figure 1.7b).

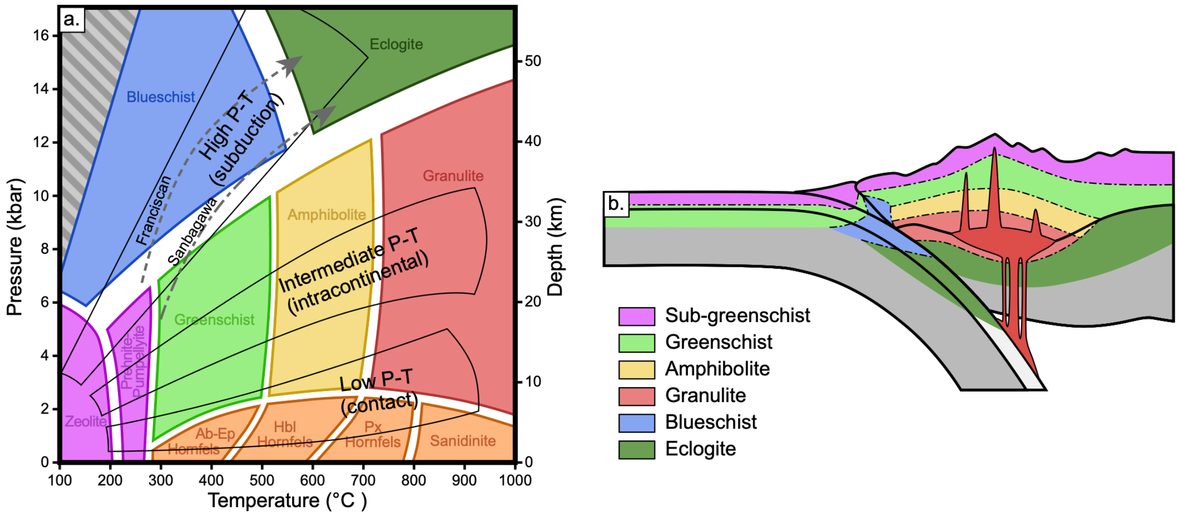

Figure 1.7: Diagram showing (a) P-T conditions of metamorphic facies outlining the P-T paths of two well-known blueschist belts and (b) schematic domains of metamorphic facies in an active subduction zone setting. Modified after (a) Miyashiro (1994); Spear (1995); Winter (2010) with P-T paths from Maruyama et al. (2010a) and (b) Ernst (1973).

High P-T rocks

High P-T paths are synonymous with subduction zones, where latent heating effects result in cold subducting oceanic lithosphere being subjected to increasing pressure at depth but with a characteristically low geothermal gradient. Subduction-related metamorphic paths develop along a typical prograde path through zeolite, prehnite-pumpellyite (both also jointly referred to as sub-greenschist), blueschist and ultimately eclogite facies. Along paths with a relatively lower P-T gradient, the rock may experience greenschist facies conditions prior to blueschist facies (Turner 1981; Liou et al. 1996). Since no occurrences of eclogites have been reported on Anglesey, this section will primarily focus on blueschists.

Blueschist facies is distinguished by its blue colour owed to the presence of glaucophane, a blue sodic amphibole, that forms from mafic protoliths. A mineral assemblage of glaucophane + lawsonite/epidote/zoisite is diagnostic of blueschist facies metabasite (Evans 1990; Spear 1995; Fettes et al. 2007). An assemblage including jadeite + quartz is indicative of high-pressure blueschist facies and a blueschist without jadeite, whilst also containing epidote over lawsonite is considered to be a 'low-pressure' blueschist (Evans 1990; Tsujimori and Ernst 2014; Xu et al. 2018; Pourteau et al. 2019). The Sanbagawa blueschist belt in circum-Pacific Japan is an example of a 'low-pressure' blueschist (Banno and Sakai 1989; Otsuki and Banno 1990). An example of a 'high-pressure' jadeite + lawsonite-bearing blueschist belt is in the Franciscan Complex, California (Moore 1984; Maruyama and Liou 1988). Pelitic blueschists are defined by a mineral assemblage of phengite + chlorite/talc + garnet, and can also contain chloritoid (Yardley 1989).

Exhumation of high P-T rocks

Blueschists and other high-pressure subduction zone rocks are thought to be exhumed rapidly (within approximately 15 My) by flow and/or faulting in accretionary wedges or upper parts of subducted crust, or may be influenced by buoyancy if associated with low-density metapelitic continental crust (Agard et al. 2009; Kusky et al. 2013). Subducted material may be exhumed up to depths of around 70 km, at which point the negative buoyancy of the downgoing oceanic lithosphere is rarely overcome (Agard et al. 2009). In order to preserve blueschist facies rocks, which transition to eclogite facies at 40 – 50 km (Tsujimori and Ernst 2014), the subduction-exhumation process must happen rapidly.

To be subducted to depths where high grade metamorphism occurs, material must stay attached to the substrate in the subduction channel. Mechanisms behind subsequent detachment are largely related to changes in mechanical properties, such as melting, metamorphic hydration, strain weakening and foliation development, which can act to create weak zones that can facilitate detachment, as well as influencing buoyancy (Warren 2013). Subsequent mechanisms for exhumation are complex and can vary even across the lifespan of a single subduction zone, but are driven largely by buoyancy, tectonic forces, and spatial fluctuations, as demonstrated in Figure 1.8. Exhumation may occur contemporaneously with subduction, or be driven by processes such as slab break-off, which can lead to eduction (Agard et al. 2009; Warren 2013).

Exhumed shallow-dipping metamorphic belts in subduction systems are typically emplaced within overlying accretionary complexes. The juxtaposition of high P-T metamorphic belts against low P-T accretionary terranes creates 'paired metamorphic belts' (Miyashiro 1994; Brown 1998; Brown 2002). An example of a paired metamorphic belt is the pairing of the Sanbagawa high P-T metamorphic belt and the Ryoke low P-T metamorphic belt, consisting of accreted arc-derived sedimentary sequences (Miyashiro 1961; Miyashiro 1994). High P-T metamorphic belts are typically bound by a thrusted base and normal faulted roof as a product of wedge exhumation and may also undergo significant strike-slip movement (Maruyama et al. 1996; Kawai et al. 2006).

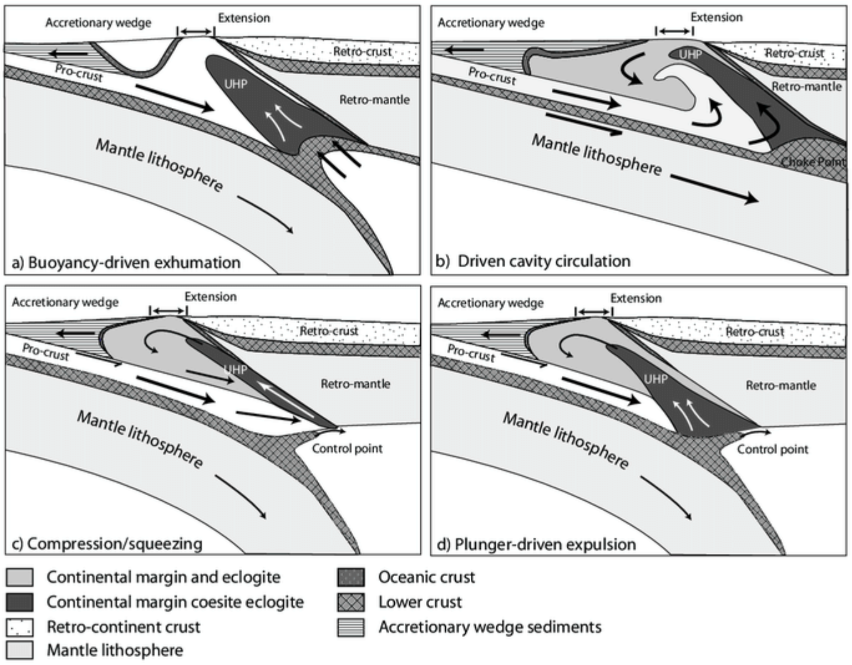

Figure 1.8: Schematic diagrams of UHP exhumation mechanisms in subductions zones including (a) buoyancy-driven exhumation; (b) driven cavity flow initiated by traction of the subducting plate; (c) compression of material between denser or more competent material; and (d) plunger-driven expulsion, expelling weaker material from the subduction channel. From Warren (2013).

Precambrian blueschists

Most known occurrences of exhumed blueschists are Mesozoic-Cenozoic in age. The Neoproterozoic blueschists of Anglesey (Greenly 1919; Gibbons and Mann 1983; Dallmeyer and Gibbons 1987) are one of only a handful of known Proterozoic blueschist occurrences, and are some of the oldest in the world (Liou et al. 1990; Maruyama et al. 1996; Brown 2007). The establishment of modern plate tectonics is a long-debated topic, but general current consensus is that modern systems were established by the Archean-Proterozoic transition (Cawood et al. 2018; Condie 2018; Johnson et al. 2019; Palin et al. 2020). Despite this, blueschists are underrepresented in the Proterozoic geological record and debates have arisen around whether blueschist formation would have been possible throughout the Proterozoic (Ernst 1973; Maruyama et al. 1996; Brown 2007). The Aksu blueschist belts in Xinjiang Province, China, with metamorphic age constraints of 754 – 602 Ma (Maruyama and Liou 1988; Zhu et al. 2011) for example, confirm that blueschists were viable by the mid-Neoproterozoic (Maruyama et al. 1996).

It has been speculated that the low geotherm needed to facilitate blueschist facies conditions may not have been possible, particularly in the early stages of the

Neoproterozoic, due to the production of relatively thin lithosphere and a higher geothermal gradient. These effects have diminished over time through secular cooling and subsequent tectonic and magmatic changes (Liou et al. 1990; Maruyama et al. 1996; Pollack 2007). Another theory for the underrepresentation of blueschists, is that oceanic basalts would have been relatively rich in MgO, therefore forming greenschist mineral assemblages at what are today considered to be blueschist facies conditions (Palin and White 2016).

Alternatively, it has been suggested that secular cooling has had little influence on blueschist production throughout the history of modern plate tectonics and that lack of Pre-Mesozoic blueschist preservation is more likely the product of preservation bias (Valley et al. 2005; Watson et al. 2006). The exhumation of blueschists is a dynamic process that requires rapid and continuous uplift and erosion, making the appearance of blueschists at the surface a transient event, unless this process ceased at an appropriate time (Richardson 1970).

1.3 THE MONIAN COMPOSITE TERRANE (MCT)

The MCT, also referred to as the Mona Complex in various literature (Greenly 1919; Gibbons and Ball 1991; McIlroy and Horák 2006), will be defined in this study as a collection of units older than the Floian overstep that outcrop across Anglesey and Llŷn Peninsula, bound to the northwest of the Menai Strait Fault Zone (MSFZ). It is important to note that the term 'MCT' is used in this case to highlight a group of rock units of defined age and spatial limits that will be considered the overall focus of this study. Potential links to other terranes outside these spatial parameters should not be dismissed. Figure 1.9 shows a simplified geological map of the MCT across Anglesey and Llŷn Peninsula. This section aims to provide a summarised overview of the MCT by integrating past literature with the recently proposed tectonostratigraphy of Anglesey by Schofield et al. (2020), which will be used as a basis for the geological background in this thesis.

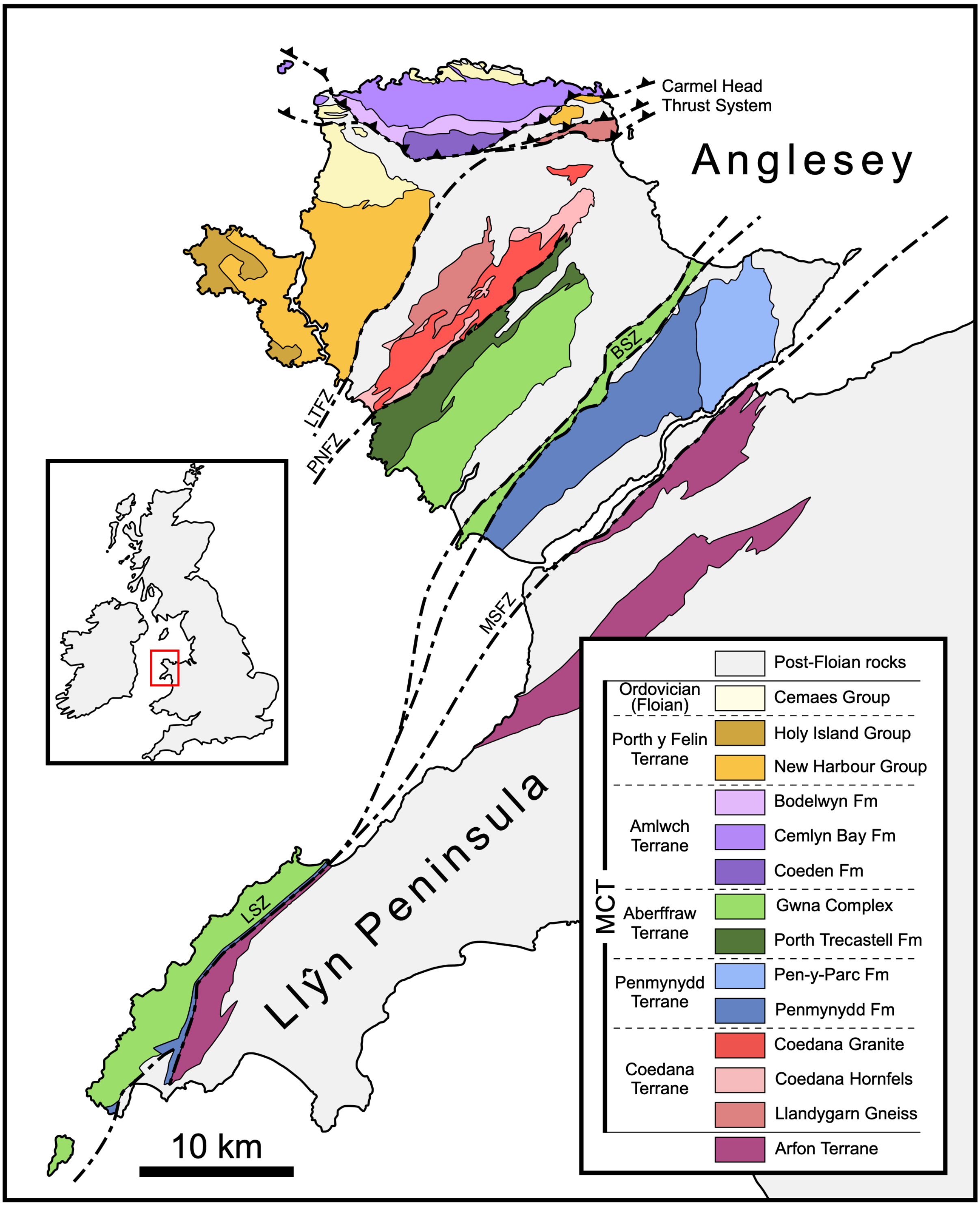

Figure 1.9: Geological map of the Monian Composite Terrane outlining the key units of each terrane across Anglesey and Llŷn Peninsula. The Arfon Terrane represents arc material from the Avalonian Composite Terrane. LTFZ – Llyn Traffwyl Fault Zone; PNFZ – Porth Nobla Fault Zone; BSZ – Berw Shear Zone; MSFZ – Menai Strait Fault Zone; LSZ – Llŷn Shear Zone. Modified after *(Gibbons and Horák 1996; Schofield et al. 2020)*.

The Floian overstep that will define the upper age limit of the MCT, unconformably overlies all units of the MCT across Anglesey, along with the high angle transcurrent faults that separate terranes. Ages constraints between terranes are outlined in Figure 1.10. Although relatively minor episodes of reactivation have occurred since, the cessation of major transcurrent activity along these shear zones is marked by the Floian overstep (Bates 1974; Beckly 1987; Phillips 1991a). The exact age of the unconformity on Anglesey is slightly uncertain. It was typically assumed to occur at the base of the Floian (477.7 Ma) based on fossil records, however the classification of the underlying Cemaes Group rocks as also Floian age means that it must have occurred later (474 – 470 Ma) in the Floian epoch (Bates 1972; Schofield et al. 2020). The Floian overstep also correlates to unconformities across North Wales such as the Arenig and Nant Ffrancon unconformities (Kokelaar 1988; Carney et al. 2000). Beyond this point in the lower Ordovician, the geology of Anglesey and mainland Wales become somewhat parallel as the extensional regime of the Welsh basin is opened (Kokelaar 1988; Pothier et al. 2015).

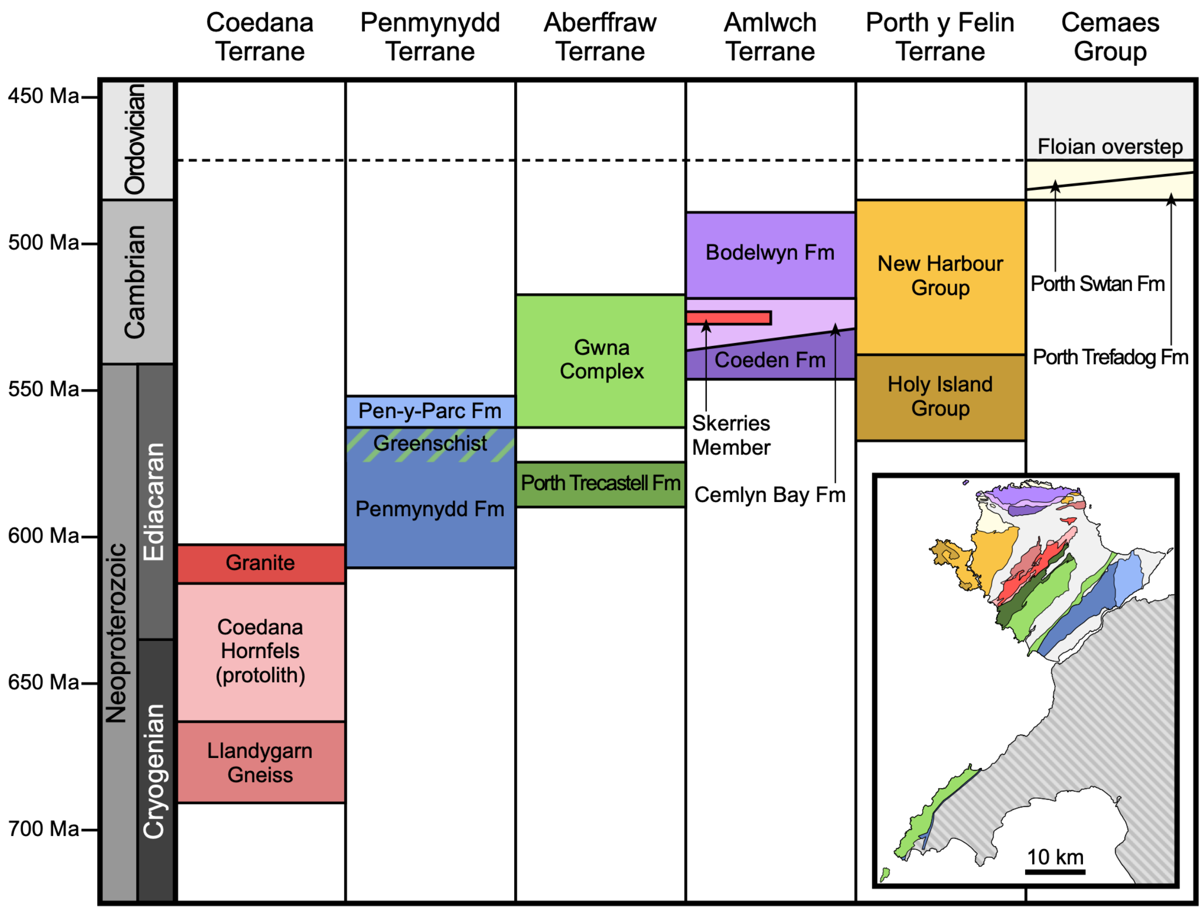

Figure 1.10: Age ranges determined for the terranes of the MCT based on various interpretations of absolute and relative constraints. After Carney et al. (2000); Asanuma et al. (2017); Dartnall (2018); Schofield et al. (2020).

1.3.1 Tectonostratigraphic interpretations of the MCT

The first substantial survey of Anglesey's geology was conducted by Henslow (1822), who recognised four major units including the Mona Complex (referred to in this study as the MCT). Blake (1888) later described the occurrence of 'glaucophane schists' within the MCT, now well-known as the Penmynydd blueschist belt. This was followed by the distinguished work of Edward Greenly, who thoroughly documented the lithostratigraphy and geology of Anglesey through a series of publications, including a 1-inch geological map of the island and accompanying memoir (Greenly 1919; Greenly 1920). This map and general lithostratigraphy have since remained the primary reference framework for the geology of Anglesey. Greenly defined the three terranes of the Mona Complex: the Coedana, Aethwy/Penmynydd and Monian Supergroup. The tectonostratigraphy of the MCT has been reinterpreted numerous times since, but typically remain close to Greenly's framework, with most issues revolving around the order of the Monian Supergroup (Shackleton 1954; Shackleton 1969; Shackleton 1975; Barber and Max 1979; Gibbons and Ball 1991).

Greenly's work also introduced the concept of 'mélange', used to describe rocks from the Gwna Group, part of the Monian Supergroup, in place of Henslow's previously termed 'crush breccia'. Greenly's descriptions of autobreccia mélanges across Anglesey were used as justification for tectonic – rather than sedimentary – origins of similar occurrences in the Carpathians and Franciscan (Hsü 1968; Sengör 2003). Whether the Gwna mélanges described by Greenly are derived from tectonic or sedimentary processes is still debated. A major problem with the tectonic interpretation was that the Gwna mélanges appeared to be stratigraphically above other, less deformed units of the Monian Supergroup. This led to non-tectonic processes such as submarine landslides being proposed for their origin (Shackleton 1954; Shackleton 1969; Wood 1974). Development of plate tectonic theory brought new insights into how tectonic processes could produce mélanges with propagating slip planes on the scale of subduction zones (Sengör 2003). Coupled with the significance of the Penmynydd blueschists, it became clear that the formation of the MCT was, to some extent, linked to an ancient subduction complex (Wood 1974; Thorpe et al. 1984). Despite this, the origin of the Gwna Complex is still disputed as of writing, with recent studies interpreting either tectonic (Kawai et al. 2007; Maruyama et al. 2010a; Wood 2012; Asanuma et al. 2015) or sedimentary (Dartnall 2018; Schofield et al. 2020) origins.

Recognition of large-scale transcurrent movement along the major high-angle boundaries between terranes allowed the MCT to be viewed as a series of juxtaposed terranes, alleviating some constraints opposing Greenly's tectonostratigraphy (Kohnstamm and Mann 1981; Nutt and Smith 1981; Gibbons 1983a; Gibbons 1987) . This also opened the possibility of linking the MCT and the surrounding regional geology (Gibbons and Horák 1996; Horák et al. 1996; McIlroy and Horák 2006; Kawai et al. 2007; Waldron et al. 2011; Schofield et al. 2020) .

Improvements in geochemical and geochronological analytical capabilities in more recent times have provided further insights into the tectonic relationships and formation of MCT units, establishing a clearer tectonostratigraphic understanding (British Geological Survey 1980; Gibbons et al. 1994; McIlroy and Horák 2006; Kawai et al. 2007). Whole rock geochemical studies have been conducted on various units to attempt to determine their origins or provenance (Thorpe 1972; Phillips 1991b; Thorpe 1993; Saito et al. 2015). Age constraints were determined for various units using several chronostratigraphic methods (Beckinsale and Thorpe 1979; Dallmeyer and Gibbons 1987; Tucker and Pharaoh 1991; Collins and Buchan 2004; Strachan et al. 2007; Asanuma et al. 2015; Asanuma et al. 2017; Dartnall 2018). Units of the MCT are now considered to range from Neoproterozoic to lower Ordovician, as opposed to being entirely Precambrian – or Precambrian to lower Cambrian – as previously interpreted. However, without comprehensive, well constrained age relationships of all units, stratigraphic ambiguities still exist between some units.

The tectonostratigraphy of the MCT, developed by Greenly (1919), defined three terranes: the Coedana Terrane, the Penmynydd/Aethwy Terrane, and the Monian Supergroup. Although variations of this stratigraphy have been proposed since, most interpretations adhere to this three-terrane framework. However, a recent comprehensive tectonostratigraphic synthesis of Anglesey by Schofield et al. (2020) distributes pre-Floian rocks across five terranes: the Coedana Terrane, Penmynydd Terrane, Aberffraw Terrane, Porth y Felin Terrane and Amlwch Terrane. The publication covers a vast amount of geology and introduces new terminology without much focus on integrating its new stratigraphy with the previous framework. This section will aim to synthesise the geology of the MCT using the newly proposed tectonostratigraphy of Scofield et al. (2020), covering the changes between new and old interpretations, shown in Figure 1.11.

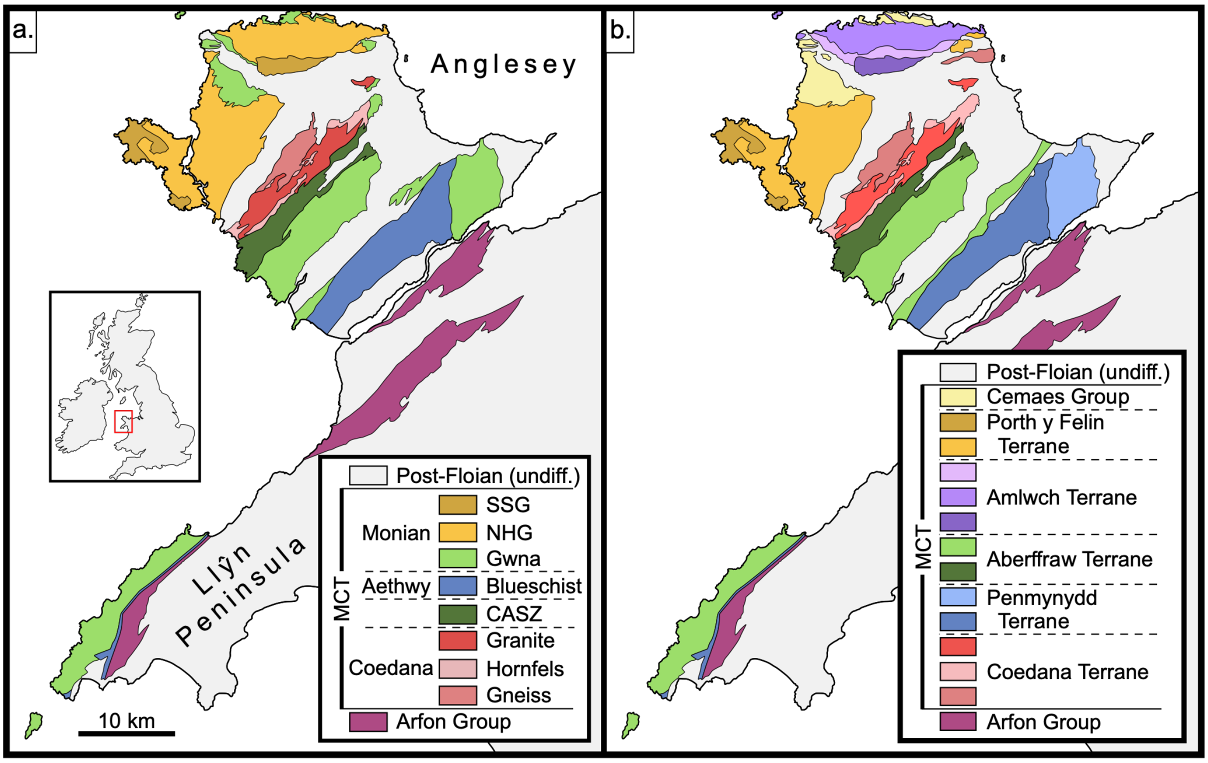

Figure 1.11: Geological map comparison of tectonostratigraphic interpretations between (a) original framework *(British Geological Survey 1980; Gibbons et al. 1994; McIlroy and Horák 2006; Kawai et al. 2007)* and (b) revised framework that will be used in this project (Schofield et al. 2020). SSG – South Stack Group; NHG – New Harbour Group; Gwna – Gwna Group; CASZ – Central Anglesey Shear Zone.

1.3.2 Aberffraw Terrane

The Aberffraw Terrane outcrops through central Anglesey and across northern Llŷn Peninsula, extending onto Bardsey Island. It is juxtaposed against the Coedana Terrane to the northwest by the PNFZ, and against the Penmynydd Terrane to the southeast by the BFZ on Anglesey and the LFZ on Llŷn Peninsula. The terrane is divided into the Porth Trecastell Formation and the Bodorgan Formation.

Porth Trecastell Formation

Also known as the Central Anglesey Shear Zone (Mann 1986; Gibbons and Horák 1996) , the Porth Trecastell Formation comprises polydeformed schistose metapelitic-psammitic sequences with quartzite, carbonate, and rare occurrences of mafic rocks that have undergone greenschist to amphibolite facies metamorphism (Asanuma et al. 2017; Schofield et al. 2020). The Porth Trecastell Formation has long been interpreted as a major transcurrent shear zone including highly deformed remnants of Gwna Complex sedimentary material (Gibbons and Mann 1983; Mann 1986; Gibbons and Horák 1990) .

More recent interpretations have considered the unit as a regional metamorphic belt, similar to the blueschists of the Penmynydd Terrane (Asanuma et al. 2017).

A maximum age of deposition for the sedimentary protoliths of the Porth Trecastell Formation is interpreted at 585±30 Ma based on U-Pb dating of detrital zircons (Asanuma et al. 2017; Dartnall 2018). K-Ar analysis of phengites from metasedimentary rocks yield a peak amphibolite facies metamorphic age of 575±11 Ma and 578±11 Ma for the Porth Trecastell Formation (Asanuma et al. 2017). Estimated peak metamorphic temperature based on K-Ar phengite closure temperatures ranges 400 – 600°C (Asanuma et al. 2017).

Gwna Complex

The Gwna Complex (or Bodorgan Formation) is a chaotic assemblage of largely disassembled lithologies including basalts, carbonates, quartzites, and pelagic-hemipelagic rocks that have been interpreted as clasts of a regional-scale mélange emplaced within several types of mélange matrices (Greenly 1919; Gibbons and McCarroll 1993; Kawai et al. 2007; Asanuma et al. 2015). It incorporates much of Greenly's Gwna Group mélanges across eastern Anglesey and Llŷn Peninsula. Alternative interpretations describe the unit as a crudely-bedded mega-conglomerate formation of sedimentary, rather the tectonic nature (Dartnall 2018; Schofield et al. 2020).

Detrital zircons samples from sandstones throughout the Bodorgan Formation have yielded various ages from different localities based on dates acquired from U-Pb analyses (Asanuma et al. 2015; Asanuma et al. 2017). A maximum depositional age of 571±20 Ma is interpreted from the Bodorgan area in central Anglesey (Asanuma et al. 2017), whilst maximum depositional ages yielded from Llŷn Peninsula range from 608±4 Ma to 539±19 Ma (Asanuma et al. 2015). Sandstones from Newborough yield a maximum deposition age of 550±24 Ma (Asanuma et al. 2017). Reassessments of U-Pb analyses suggests that formation of the Bodorgan Formation likely took place at 552 – 537 Ma on Anglesey, and <530 Ma on Llŷn Peninsula (Dartnall 2018).

Basalts from the Bodorgan Formation exhibit a geochemical composition within the MORB-OIB suite (Thorpe 1993; Saito et al. 2015). Whilst a small number analyses of basalts from Anglesey show MORB compositions, basalts from Llŷn Peninsula exhibit both MORB and OIB geochemical signatures (Saito et al. 2015). OIB-like pillow basalts on Llŷn Peninsula have been noted to be typically overlain by more oxidised sediments, whereas MORB pillow basalts are more commonly overlain by anoxic sediments (Sato et al. 2015; Asanuma et al. 2017). This difference is supported by ages of sedimentation in the Gwna Group, where detrital zircons from oxidised sediments yield an age of 539±19 Ma, and from anoxic sediments yield a distinctly older age of 601±6 Ma (Asanuma et al. 2015). Geochemical data available for the Gwna Complex is primarily sourced from Llŷn Peninsula (Saito et al. 2015), while localities across Anglesey are underrepresented. Given the geochemical heterogeneity observed in Llŷn Peninsula, a more comprehensive study of Anglesey localities is necessary.

Newborough Nature Reserve

The area of Newborough, in SE Anglesey, hosts a narrow wedge of Gwna Complex rocks bound between strands of the BFZ, and was recently termed the Llanddwyn Volcanic Member (Schofield et al. 2020). The area is of particular interest in understanding the geology of the Gwna Complex, where many characteristic features can be found in a concentrated, well-exposed and accessible area (Greenly 1919; Carney et al. 2000; Maruyama et al. 2010a).

Llanddwyn Island, Newborough, has been described as possessing more coherent structural controls than the chaotic assemblages elsewhere in the Gwna Complex. Three 'textbook' duplex structures, each dividing into a series of horse structures, have been inferred across the island, shown in Figure 1.12 (Kawai et al. 2008; Maruyama et al. 2010a). Each duplex is interpreted as representing a different stage of OPS, repeated within each individual horse structure. The OPS from these three duplexes combines to complete a classic example of Pacific-type OPS, with pillow basalts overlain by various sedimentary units deposited in different environments of the sea floor along its progression from mid-ocean ridge to subducting trench (Isozaki et al. 1990; Maruyama et al. 2010a; Kusky et al. 2013). The Gwna Complex in Newborough extends beyond Llanddwyn Island, though, and the extent of these proposed duplexes beyond Llanddwyn Island has not been fully explored.

Glacial dropstones have been reported within a single hemipelagic mudstone bed on Llanddwyn Island, evincing a Neoproterozoic glaciation event during a period of ongoing tectonic activity around Avalonia (Kawai et al. 2008). The deposition of dropstone-bearing beds is estimated to coincide with the Gaskiers glaciation event at ~580 Ma (Trindade and Macouin 2007; Pu et al. 2016), overlapping with the formation dropstone beds and diamictites in Scotland and Ireland (Condon and Prave 2000).

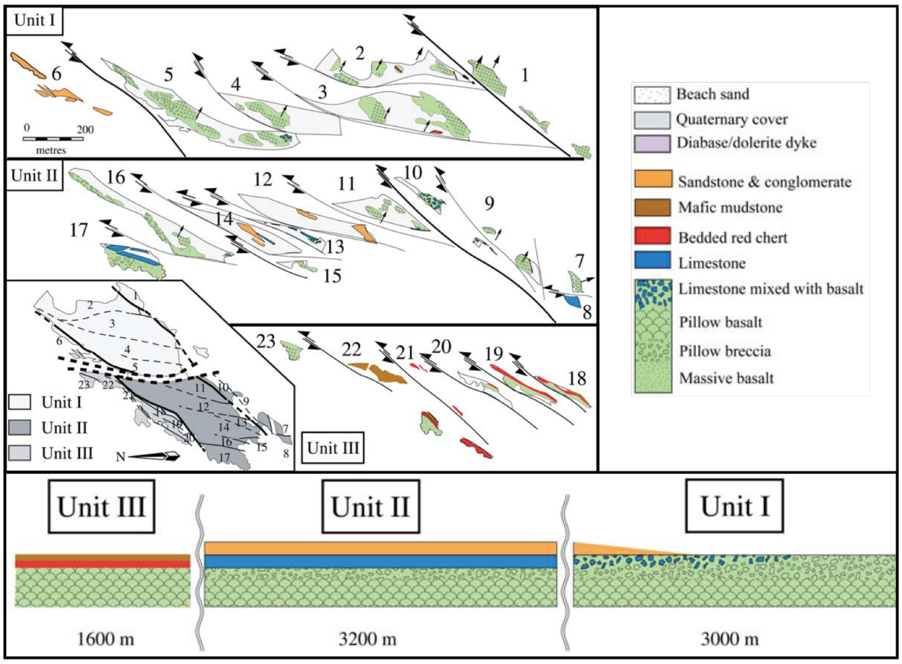

Figure 1.12: Proposed duplex system across Llanddwyn Island, Newborough, with different OPS stages recognised between the duplexes. From Maruyama et al. (2010b).

Formation of the Aberffraw Terrane

The Gwna Complex has been interpreted as representing a Pacific-type accretionary complex, likened to modern examples off the coast of Japan, with interpreted OPS from Newborough and Llŷn Peninsula bearing strong similarities (Kawai et al. 2008; Maruyama et al. 2010a; Asanuma et al. 2015). Alternative theories interpret the Gwna Complex as a sedimentary-derived mega-conglomerate deposit in a proximal basin (Dartnall 2018; Schofield et al. 2020), meaning that further investigation is required.

Metasediments in the Porth Trecastell Formation appear to be analogous to sedimentary lithologies in the Gwna Complex, suggesting that the formations may be related by a shared protolith source (Mann 1986; Asanuma et al. 2017). The older Porth Trecastell Formation has undergone a period of metamorphism before the unconformable deposition of the Bodorgan Formation. Detrital zircons from both The Porth Trecastell Formation and Bodorgan Formation show similar provenance, with a dominant Ediacaran age peak likely corresponding to a peri-Gondwanan source, although the provenance of the Porth Trecastell Formation is more ambiguous (Dartnall 2018).

The Porth Trecastell Formation reaches a metamorphic grade similar to those intermediately occurring along the prograde P-T path of the Penmynydd Formation blueschists (discussed in Section 1.3.3). Along with similarities in dominant protoliths, this has led to suggestions that both metamorphic units have a similar origin as subducted oceanic material that reached different depths of a subduction zone (Asanuma et al. 2017), with the higher grade blueschists descending to greater depths. Similarities in peak metamorphic age suggest a common cause for the exhumation of both units, speculated to be the subduction of a spreading centre (Kawai et al. 2006; Kawai et al. 2007; Asanuma et al. 2017). However, unlike the Penmynydd Terrane, the Porth Trecastell Formation does not share a high-angle sheared contact with the Gwna Complex (Schofield et al. 2020).

1.3.3 Penmynydd Terrane

The Penmynydd Terrane – also known as the Aethwy Terrane – exposed along the SE of Anglesey, is a narrow (<10 km) NE-SW striking terrane bound by the MSFZ to the east and the BFS to the west (Gibbons 1987). It has also been traced across to Llŷn Peninsula, occurring as a very narrow unit along the LSZ (Gibbons 1981; Gibbons 1983b; Gibbons and McCarroll 1993). It consists of the Penmynydd Formation, including the well-renowned blueschists of Anglesey, and the Pen-y-Parc Formation, formerly included within the Gwna Group (Greenly 1919; British Geological Survey 1980; Schofield et al. 2020). The Pen-y-Parc Formation is thought to be thrust upon (Schofield et al. 2020) the stratigraphically lower Penmynydd Formation along a N-S striking contact, although evidence for this is not clearly described.

Penmynydd Formation

The Penmynydd Formation consists of a series of lenticular metabasite units orientated NE-SW within a metapelitic-psammitic phengite-mica schist matrix (British Geological Survey 1980; Gibbons 1983a; Kawai et al. 2006). These lenticular metabasite units range up to several kilometres in size and show evidence of variable peak metamorphic grades between them (Kawai et al. 2006).

Metabasites in the Penmynydd Formation contain a range of amphibole species from actinolite to glaucophane, with amphibole species acting as a proxy for maximum metamorphic grade (Gibbons and Gyopari 1986; Kawai et al. 2006). Chemical zonation in amphiboles, consisting of actinolite cores grading to barroisite, with glaucophane/crossite rims have been described from the unit, preserving a prograde metamorphic progression (Gibbons and Mann 1983; Horák and Gibbons 1986) . It should be noted that crossite is a discontinued term for an amphibole of intermediate composition between glaucophane and magnesio-riebeckite (Leake et al. 1997; Hawthorne et al. 2012). Use of the term has persisted in metamorphic studies because crossite acts as a useful pressure-dependant intermediary between high-pressure glaucophane and low-pressure riebeckite (Matsumoto et al. 2003).

Using amphibole species as a proxy for peak metamorphism, the Penmynydd Terrane has been divided into roughly N-S trending isograd zones with a crossite-barroisite-bearing high-grade central zone surrounded by lower grade zones (Kawai et al. 2006; Kawai et al. 2007). Along with schistosity orientations, this has been interpreted as a shallow dipping antiform (Kawai et al. 2007; Treagus 2007) with a higher metamorphic grade in its core and lower along the outer flanks.

Ar-Ar dating of amphiboles and phengites from Anglesey suggests an initial greenschist facies metamorphic event with a peak age of 580-590 Ma, followed by a separate blueschist facies subduction-related event with a peak age of 550-560 Ma (Dallmeyer and Gibbons 1987). Newer K-Ar dates acquired from phengites, interpret a similar, slightly earlier peak metamorphic age of 566±11 Ma whilst blueschists outcropping along Llŷn Peninsula yield slightly younger peak metamorphic ages of 530±10 Ma, 545±10 Ma and 549±10 Ma (Asanuma et al. 2017). A later phase of retrograde greenschist metamorphism has not been dated (Gibbons and Gyopari 1986; Dallmeyer and Gibbons 1987). Whole-rock geochemical analysis of a single blueschist facies metabasite sample was undertaken by Thorpe (1972), yielding N-MORB-like immobile trace element signatures with a tholeiitic protolith. This single analysis, however, does not provide a comprehensive geochemical overview of the formation, where metabasites occur in multiple lenses of variable metamorphic grades.

In the surrounding mica schists, localised lawsonite-bearing schists have been reported from several localities concentrated within thin (<1 m wide), localised bands that seemingly coincide with mylonitic shearing in the crossite isograd (Gibbons and Mann 1983; Kawai et al. 2006). Lawsonite indicates relatively higher pressures and/or lower temperatures than in lawsonite-absent blueschists (Xu et al. 2018; Pourteau et al. 2019). These conditions may be localised due to excessive shearing along the isograd (Kawai et al. 2006), or lawsonite may be more widespread in the Penmynydd Formation, rarely found due to poor exposure and the rarity of preserving lawsonite at low P-T conditions (Comodi and Zanazzi 1996). Localised high concentrations of lawsonite tend to occur from the closed-system homogenisation of carbonates and metapelites (Lefeuvre et al. 2020). The presence of lawsonite in blueschists of such age is extremely rare and it has only been reported from a handful of pre-Mesozoic localities on Earth (Gibbons and Mann 1983; Liou et al. 1990; Tsujimori and Ernst 2014).

Pen-y-Parc Formation

Like the rocks of the Penmynydd Formation, the Pen-y-Parc Formation consists of lenticular slivers of metabasites interleaved within schistose metapelites and metapsammites. The Pen-y-Parc Formation has however been subject to lower grade metamorphism, reaching greenschist facies (Greenly 1919; Schofield et al. 2020). Detrital zircons from metasediments in the Pen-y-Parc Formation yield a maximum depositional age of 566±16 Ma (Asanuma et al. 2017). No definitive ages published for subsequent greenschist facies metamorphism have yet been published.

Mineral isograds constructed by Kawai et al. (2006) suggest that an eastern section of the Pen-y-Parc Formation only reaches sub-greenschist facies. The material was therefore considered part of the Gwna Group, with the rest of the Pen-y-Parc Formation not being distinguished from the Penmynydd Formation. Some previous studies of the area have also constructed similarly adjusted boundaries, not distinguishing a separate unit equivalent to the Pen-y-Parc Formation, shown in Figure 1.13 (Dallmeyer and Gibbons 1987; Gibbons and Ball 1991).

Formation of the Penmynydd Terrane

Blueschist facies metamorphism of the Penmynydd Formation is a clear indicator of formation at high pressure and low temperature conditions, synonymous with a tectonic subduction zone setting (Thorpe et al. 1984). Metabasalts can tentatively be described as having a MORB geochemical signature (Thorpe 1972), suggesting that the unit represents oceanic material that has underwent subduction to estimated peak metamorphic conditions of 8 – 9 kbar and 400 - 500°C at depths of >25 km, before being exhumed along an anticlockwise P-T-t path (Gibbons and Gyopari 1986; Kawai et al. 2006). Exhumation may have been onset by subduction of a spreading ridge (Kawai et al. 2006; Kawai et al. 2007) and coincided with an episode of retrograde greenschist facies metamorphism (Dallmeyer and Gibbons 1987). The anticlinal structure of the Penmynydd Terrane is typical of exhumed high-pressure metamorphic belts in accretionary complexes (Kawai et al. 2006; Agard et al. 2009; Kusky et al. 2013).

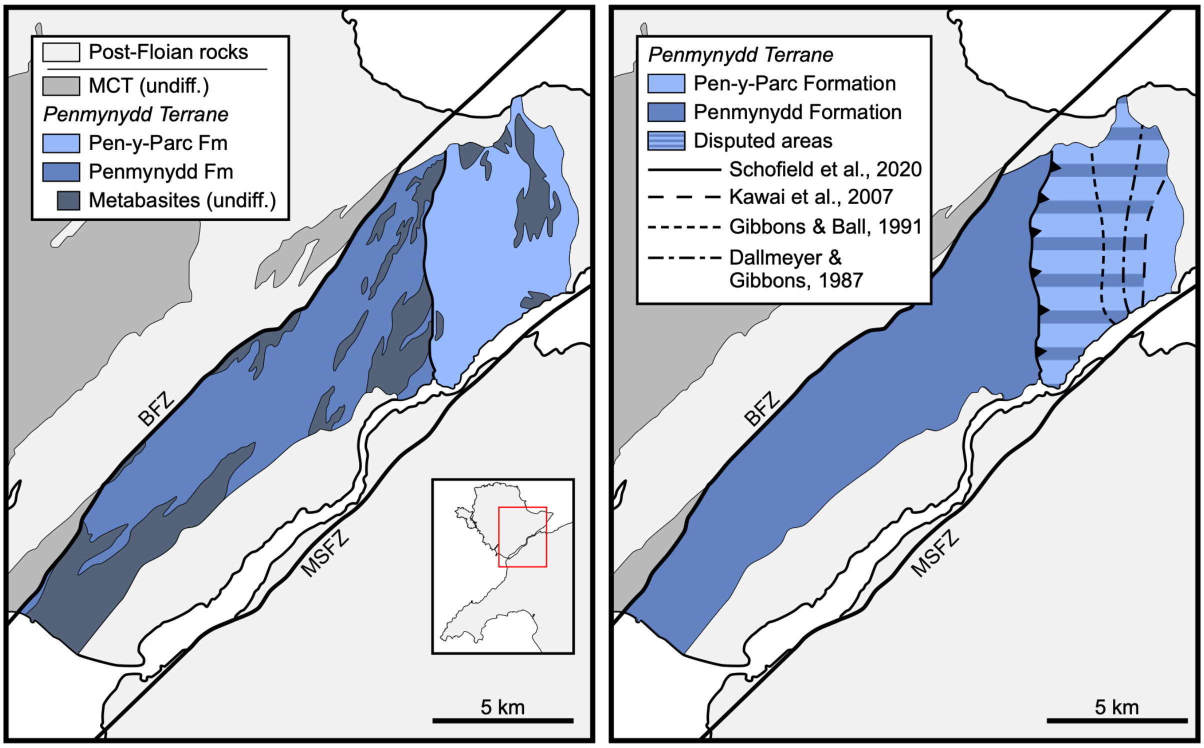

Figure 1.13: Maps of the Penmynydd Terrane showing (a) metabasite lens distribution after British Geological Survey (1980) and (b) different interpretations of the extent of the Penmynydd Formation after Dallmeyer and Gibbons (1987; Gibbons and Ball (1991); Kawai et al. (2007); Schofield et al. (2020).

The Penmynydd Terrane is thought have been incorporated into the Aberffraw Terrane upon its exhumation to relatively shallow depths along high-angle fault zones (Kawai et al. 2006; Kawai et al. 2007; Asanuma et al. 2017). This model does not consider that the Penmynydd Terrane metamorphic belt is bound by transcurrent shear zones, which obscures the tectonic relationship between the two units (Gibbons and Ball 1991).

The maximum age of sediment deposition for the Pen-y-Parc Formation overlaps very closely to the age of peak blueschist facies metamorphism in the Penmynydd Formation, both at around 566 Ma (Asanuma et al. 2017). This indicates that whilst sedimentation of the Pen-y-Parc Formation took place, the Penmynydd Formation was subducted at depths of >25 km (Gibbons and Gyopari 1986), suggesting that there is no direct link between the units and that they were juxtaposed against one another during accretion or later. Both units experienced later greenschist metamorphism, although these are unlikely to be related since the Penmynydd Formation likely experienced this during exhumation (Gibbons and Gyopari 1986).

The maximum deposition age of the Pen-y-Parc Formation is similar to those yielded from the formerly associated Gwna Complex (Asanuma et al. 2017). Eastern regions of the Pen-y-Parc Formation, also have a similar low grade metamorphic history to the Gwna Complex (Kawai et al. 2006). The Pen-y-Parc Formation is included in the Penmynydd Terrane, based on closely related structural deformation histories (Schofield et al. 2020), although it is not clear where the evidence for this derives and if it accounts for the Pen-y-Parc Formation in its entirety. The affinity of the Pen-y-Parc Formation therefore requires some clarification.

1.3.4 Coedana Terrane

The Coedana Terrane outcrops in across central Anglesey and is bound to the southeast by the PNFZ and overstepped by Ordovician (Floian) sedimentary successions to the north and west. It is dominated by the plutonic Coedana Granite, which is hosted within basement gneisses and metasedimentary rocks.

The Llandygarn Gneiss contains the oldest rocks in the Coedana Terrane, consisting of compositionally variable amphibolite to migmatitic paragneisses of semi-pelitic protoliths that reach sillimanite-kyanite metamorphic grade (Gibbons and Horák 1990; Carney et al. 2000; Strachan 2012). The minimum age of the gneisses is 666±7 Ma based on U-Pb analysis of zircon rims, interpreted as the peak amphibolite facies metamorphic age (Strachan et al. 2007). The presence of sillimanite, along with plagioclase-hornblende thermometry estimate that the gneisses were subject to peak metamorphic conditions of 4 – 5 kbar and 650 – 750°C (Horák 1993; McIlroy and Horák 2006) . The gneisses are unconformably overlain by less deformed metasedimentary rocks, which have undergone contact metamorphism to low-grade hornfels, through emplacement of the Coedana granite (Schofield et al. 2020).

The Coedana Granite yields a U-Pb zircon age of 613±4 Ma (Tucker and Pharaoh 1991). The discordia has an upper intercept of 1443 Ma, which is fairly consistent with ε_{Nd} model ages of 1300-1430 Ma, indicating the incorporation of older crustal material during magmatism (Davies et al. 1985; Horák 1993). The granite is a geochemically variable, highly evolved peraluminous monzogranite with a calc-alkaline signature and I-type affinity (Horák 1993). Both the mineralogy and whole rock geochemical signatures of the granite signify an arc-related origin that is consistent with generation in the Avalonian arc (Horák 1993; McIlroy and Horák 2006). Although less deformed than the surrounding basement gneisses, the granite has been pervasively affected by ductile deformation (Greenly 1919; Horák 1993).

Formation of the Coedana Terrane

Consistencies in geochemical signatures and age constraints suggest that the Coedana granite is related to a period of Avalonian arc magmatism. Two main theories exist to account for the segregation of the Coedana Terrane from Avalonia and its placement in the MCT. Kawai et al. (2007) proposed a tectonic model that included the Coedana Terrane as an outlying klippe that has been isolated from Avalonia exhumation processes undercutting arc material, eventually becoming detached through erosion (see Figure 1.14a). Interestingly, geophysical gravity surveys suggest that the Coedana granite is a relatively shallow feature (Kohnstamm and Mann 1981; Pharaoh et al. 2020).

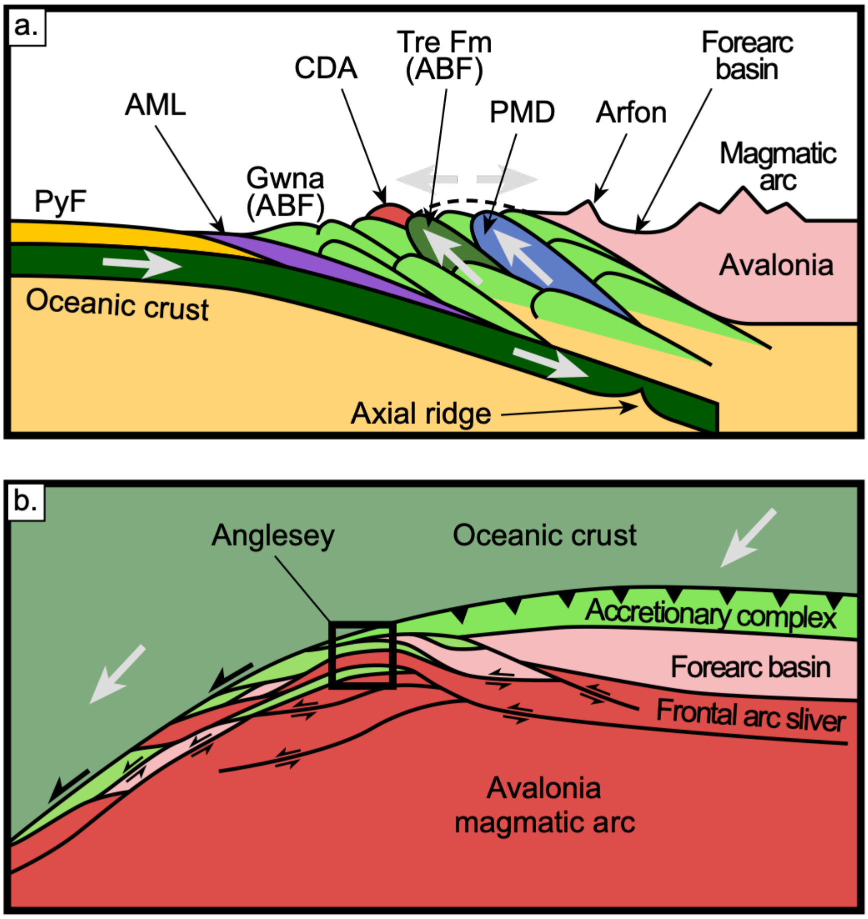

Figure 1.14: Schematic diagrams of tectonic interpretations for the placement of the Coedana Terrane showing (a) isolation as a klippe due to exhumation of metamorphic belts after (Kawai et al. 2007; Asanuma et al. 2015) and (b) emplacement along major transcurrent fault networks driven by oblique subduction after *(Gibbons and Horák 1996)*. PyF – Porth y Felin Terrane; AML – Amlwch terrane; ABF – Aberffraw Terrane; CDA – Coedana Terrane; PMD – Penmynydd Terrane.

The more established model shown in Figure 1.14b suggests that the Coedana Terrane was emplaced as a tectonic sliver against accreted material through transcurrent fault movement occurring along the Avalonian arc margin (Gibbons and Horák 1996;

Strachan et al. 2007). Geochemical distinctions between the Coedana Granite and Sarn granitoids of the Arfon Terrane in NW Wales, suggest that the Coedana granite has been transported from elsewhere along the Avalonian arc front (Horák 1993).

1.3.5 Porth y Felin Terrane

The Porth y Felin Terrane outcrops across western Anglesey and Holy Island. It consists of the Holy Island Group (formerly South Stack Group) and the New Harbour Group, both of which comprised two of the three units of the old Monian Supergroup (Gibbons and Ball 1991; Phillips 1991b; Schofield et al. 2020). The Porth y Felin Terrane is thought to represent sedimentation within a NE-SW trending basin with no evidence of formation within an accretionary prism (Wood 1974; Phillips 1991b).

The Holy Island Group comprises of the lower South Stack Formation, the Holyhead Formation and the upper Rhoscolyn Formation, all of which are lightly (sub-greenschist facies) metamorphosed (Phillips 1991b; Collins and Buchan 2004) with a cryptic deformation history (Treagus et al. 2013; Lloyd 2018). The lower South Stack Formation is dominated by pelitic sequences with interbedded sandstones. The sequences of the overlying Holyhead and Rhoscolyn Formations are more sandstone-dominated, with the Holyhead Formation including the 150 – 200 m thick Holyhead quartzite (Phillips 1991b; McIlroy and Horák 2006). Numerous sedimentary structures identify the Holy Island Group as a classic turbidite sequence, likely deposited in a deep-water, 'poorly efficient' turbidite fan, with sediment provenance interpreted as having derived predominantly from a continental source (Phillips 1991b; Treagus et al. 2013).

The New Harbour Group mainly consists of sequences of highly foliated, polydeformed metapelitic chlorite-mica schists with subordinate interbedded sandstones (Phillips 1991b). Within the New Harbour Group, there are also sporadic occurrences of highly deformed, metamorphosed basic-intermediate lavas and tuffs with volcanic arc geochemical signatures (Thorpe 1993). Masses of gabbros and serpentinites outcrop within New Harbour Group schists around Holy Island (Wood 1974; Maltman 1977). Although these have been speculated to be related to the preservation of ophiolitic material (Thorpe 1978), evidence from serpentinite textures and the lack of ultramafic clasts in accretionary units suggests that their presence is not related to subduction and they are likely part of an unrelated intrusive suite (Maltman 1975; Maltman 1979).

Upper units of the basal South Stack Formation yield maximum depositional ages of 501±10 Ma (Collins and Buchan 2004), 569±18 Ma and 522±16 Ma (Asanuma et al.

2017) for the Holy Island Group. Reassessed U-Pb dates suggest a depositional age of <530 Ma for the Holy Island Group (Dartnall 2018). Preserved skoliths (vertical trace burrows) of Early Cambrian age within the South Stack and Rhoscoyln Formations support deposition occurring largely in the Cambrian (Greenly 1919; Barber and Max 1979; McIlroy and Horák 2006; Treagus et al. 2013). The minimum age of deposition for the New Harbour Group is constrained by greenschist facies metamorphism at 474±9 Ma, whilst the maximum deposition ages have been reported at 520±33 Ma, 530±7 Ma and 533±9 Ma (Collins and Buchan 2004; Asanuma et al. 2017; Dartnall 2018). Depositional age constraints therefore favour contemporaneous deposition of these groups. The provenance of sediments in the New Harbour Group is also interpreted to be different to those in the Holy Island Group (Phillips 1991b; Dartnall 2018).

The stratigraphic relationship between the two groups has been contentious due to the more deformed New Harbour Group seemingly overlying the Holy Island Group. It has been suggested that the Holy Island Group has been tectonically emplaced below the New Harbour Group through the process of underplating proximal to a subduction zone trench, with comparisons made to modern analogues around Japan (Kawai et al. 2007; Asanuma et al. 2017). This process has been used to explain the greater intensity of deformation observed in the stratigraphically higher New Harbour Group (Kawai et al. 2007). However, the New Harbour Group has been observed conformably overlying the Holy Island Group across a boundary of continuous sedimentation with no evidence of shearing (Treagus et al. 2013). The differences in style and intensity of deformation have therefore been attributed to lithological and subsequent rheological differences between the two units.

1.3.6 Amlwch Terrane

The Amlwch Terrane is a largely sedimentary succession that outcrops in northern Anglesey, north of the Carmel Head Thrust System. It consists of units that were formerly shared with the Porth y Felin Terrane, but have been reinterpreted as separate terranes (Schofield et al. 2020). The Carmel Head Thrust System represents a later period of Acadian deformation related to the docking on Laurentia in the Devonian (Matley 1899; Bamousa 2008). The Amlwch Terrane consists the lower Coeden Formation, the Bodelwyn Formation and the upper Cemlyn Bay Formation, all separated by thrusted boundaries (Schofield et al. 2020). The Coeden and Bodelwyn Formations consist of pelitic-psammitic sedimentary sequences (Schofield et al. 2020). Both units are poorly exposed, and their origins are therefore relatively ambiguous, particularly the Coeden Formation. The Cemlyn Bay Formation is more lithologically diverse, including turbiditic sandstone-mudstone sequences and metasedimentary volcaniclastic sequences (Greenly 1919; Phillips 1991b; Bamousa 2008; Schofield et al. 2020). Maximum depositional ages of the Cemlyn Bay Formation have been interpreted at 548±9 Ma and 515±13 Ma (Asanuma et al. 2017).

1.3.7 Ordovician rocks

The Floian overstep effectively marks the end of the formation of the MCT and gives rise to uniform sedimentation across Anglesey (Bates 1974; Beckly 1987; Phillips 1991a). Ordovician stratigraphy is therefore best sorted into pre- and post-overstep units. The Cemaes Group is thought to be Floian in age and is overstepped by both the Porth Wen Group and the Llyn Alaw Group, both Floian to Darriwillian in age (Schofield et al. 2020). Upper Ordovician rocks also overlie these mid-Ordovician strata and correlate well with those in the Welsh basin (Bates 1972).

The Porth Wen Formation consists of thick quartzites overlain by cross-bedded sandstones with Floian brachiopods, limited to northern Anglesey where they unconformably overlie the Cemaes Group as an alluvial fan deposit (Bates 1972; Schofield et al. 2020). The Llyn Alaw Formation is more widespread across Anglesey, consists of mudstone-dominated mass transport deposits with interbedded coarse sediment sequences. It is interpreted as a basin formation in an extensional setting, adjacent to other related basins – including the Welsh basin – across mainland Wales (Bates 1972; Beckly 1987; Kokelaar 1988; Pothier et al. 2015).

Cemaes Group

The Cemaes Group comprises of the Porth Trefadog Formation and the overlying Porth Swtan Formation (Barber and Max 1979; Schofield et al. 2020), separated by a gradational boundary (Bamousa 2008; Dartnall 2018). The lower Porth Trefadog Formation comprises thick-bedded turbiditic sequences of ash flow tuffs and tuffaceous sandstones, also known as the Church Bay tuffs and Skerries grits respectively (Greenly 1919; Shackleton 1969; Phillips 1991a; Bamousa 2008). The andesitic Skerries grits are thought to represent the unroofing of a volcanic arc and the provenance of the Church Bay tuffs is thought to be very similar (Phillips 1991b).

The Porth Swtan Formation represents a polymictic mass transport deposit with clasts of unmetamorphosed sediments, predominantly carbonates, sandstones and greywackes, dispersed throughout a foliated, unbedded semi-pelitic matrix (Greenly 1919; Wood and Nicholls 1973; Carney et al. 2000). Partly-dolomitised limestones are stromatolitic (Wood and Nicholls 1973; Muir et al. 1979) and would likely have been deposited in shallow waters, possibly upon the summits of seamounts (Wood 2012). Figure 1.15 shows the Porth Swtan Formation around the Cemaes area in northern Anglesey.

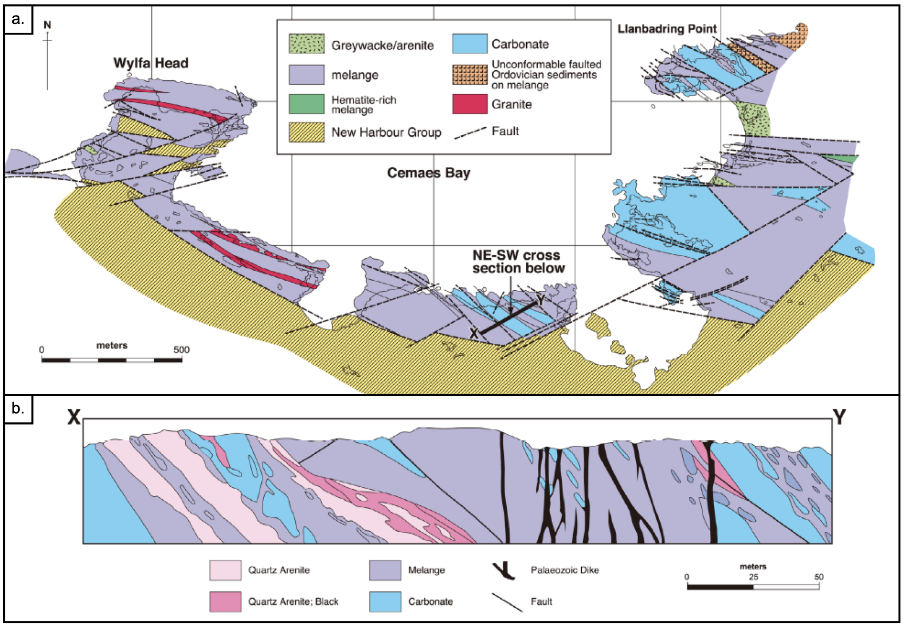

Figure 1.15: Geological map (a) and cross section (b) of the Cemaes area in northern Anglesey showing the components of the Porth Swtan Formation. From Wood (2012).

The rocks of the Porth Swtan Formation were included within the Gwna Group, and were prominent in Greenly's description of the Gwna mélanges (Greenly 1919). Greenly (1919) distinguished them as being more of a pseudo-conglomerate than elsewhere – referring to rocks of the Gwna Complex – and having less of a parallel structure. The soft division of the Gwna Group that existed between 'Cemaes-type' and 'Llanddwyn-type' mélanges largely matches the current parameters of Porth Swtan and Bodorgan formations (Greenly 1919; Wood and Nicholls 1973; Schofield et al. 2020). Similar to the Bodorgan Formation, the nature of the mélange is still debated between accretionary processes (Wood 2012) and mass wasting at the margin of an extensional basin (Dartnall 2018; Schofield et al. 2020).

Strontium isotope analysis shows that limestone clasts from the Porth Swtan Formation in Llanbadrig, northern Anglesey, formed in the early Neoproterozoic at 860 – 800 Ma (Horák and Evans 2011), however the date of mélange formation has not been directly analysed. The timing of formation of the Cemaes Group is tightly constrained under the interpretation that it post-dates deformation and metamorphism of the Porth y Felin and Amlwch Terranes at 474±9 Ma (Collins and Buchan 2004; Schofield et al. 2020).

1.3.8 Dolerite dykes

Two major sets of NW-SE trending mafic dykes are known to occur across Anglesey (Greenly 1919; Piper 1976; Bevins et al. 1996). The youngest set was observed to intrude the Upper Palaeozoic rocks of Anglesey, making it of likely Cenozoic age (Greenly 1900). A single dyke along the northern coast of Anglesey from this set was determined to have an age of 55±2 Ma (Allott & Lomax 1988; Hailwood et al. 1992). This set of Paleogene intrusions have been geochemically linked to the Antrim basalts in Ireland (Ellis 2009), establishing a connection to the British Paleogene Igneous Province (BPIP), the result of magmatism onset by rifting of the North Atlantic (Barrat and Nesbitt 1996; Kent and Fitton 2000; Hansen et al. 2009).

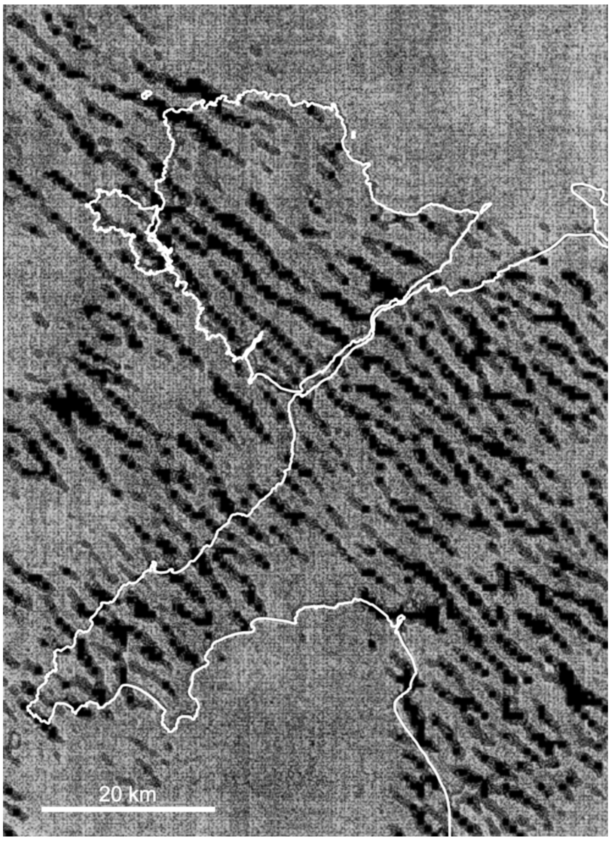

Figure 1.16: Distribution of mafic dykes across NW Wales as outlined by aeromagnetic data after (Bevins et al. 1996).

The older set of mafic intrusions have been studied in less detail and their age has not been constrained beyond field relationships, estimating a lower-mid Palaeozoic age (Greenly 1919; Piper 1976). While not part of the MCT, these lower Palaeozoic intrusions may be related to igneous activity in an adjacent volcanic arc (Howells et al. 1991; Gibbons and Young 1999). Several subtle methods of field identification have been outlined, based largely around the more mafic compositions of the Paleogene dykes, making them more susceptible to weathering (Harker 1887; Greenly 1900).

1.3.9 Extent of the MCT beyond NW Wales

Correlations have been made between the MCT and the Rosslare Terrane in SE Ireland, spatially linking the terranes along the NE-SW striking MSFZ across an unexposed 120 km distance beneath the Irish Sea (Tietzsch-Tyler and Phillips 1989; Gibbons et al. 1994; Waldron et al. 2014a). The stratigraphy of metasedimentary formations in the Cahore Group correlates to the South Stack Group and is also thought to be Cambrian-Ordovician in age (Tietzsch-Tyler and Phillips 1989; Phillips 1991b). High-grade mylonitic paragneisses and amphibolites are also seen to be juxtaposed against the low-grade Cahore Group metasediments by high-angle NE-SW sinistral shear zones (Murphy 1990), similar to the organisation of the MCT. The paragneisses and amphibolites of the Rosslare Terrane correlate in age to those of the Coedana Terrane on Anglesey, whilst the intruding St Helens gabbroic pluton is of similar age to the Coedana granite intrusion and other Avalonian magmatic events (Max and Roddick 1989). The Rosslare Terrane is also unconformably overlain by less deformed post-Floian Ordovician rock (Tietzsch-Tyler and Phillips 1989; Murphy 1990).

Tracing the MCT across northern England has proved more challenging. The high-angle NE-SW faults that intersect the MCT become obscured offshore from North Wales and are thought to correlate to the Ribblesdale fault system in northern England (Pharaoh et al. 2020). Monian stratigraphy has not been successfully correlated in northern England although the comparisons in deformation history and likely age suggest a link with the Ingleton Group (Soper and Dunning 2005). The Ingleton Group comprise basement rocks of Silurian and Carboniferous stratigraphy in the Pennines. Further inland to the East of the South Craven fault, the distribution of the MCT and Avalonian terranes become more uncertain (Pharaoh et al. 2020).

1.4 EVOLUTION OF THE PERI-GONDWANAN TERRANES

Towards the end of the Neoproterozoic, the Avalonian-Cadomian belt at the northwestern margin of Gondwana experienced a rapid transition from subduction-driven formation of an Andean-style continental arc to a transcurrent-dominant regime (Nance and Thompson 1996; McIlroy and Horák 2006; Nance et al. 2008; Ackerman et al. 2019). This was followed by diachronous rifting of several peri-Gondwanan landmasses that began to propagate in the late Cambrian, driven by the back-arc emergence of the Rheic

Ocean and closure of the Iapetus Ocean between the peri-Gondwanan terranes and Laurentia (Keppie et al. 2003; Linnemann et al. 2008; Pollock et al. 2009; Nance et al. 2010; Sánchez-García et al. 2019). The Caledonide-Appalachian orogeny marks the culmination of this event lasting from the Ordovician to mid-Devonian, recording the collision of the peri-Gondwanan terranes (and Baltica) against the margin of Laurentia (van Staal et al. 1996; Murphy et al. 2004; Woodcock et al. 2007; Zagorevski et al. 2012; Waldron et al. 2014a; Waldron et al. 2019a). Three of these peri-Gondwanan terranes occur across the British Isles – located to the south of the Iapetus suture across England, Wales, and southern Ireland – and the MCT sits geographically between them with uncertain affinity, as shown in Figure 1.17.

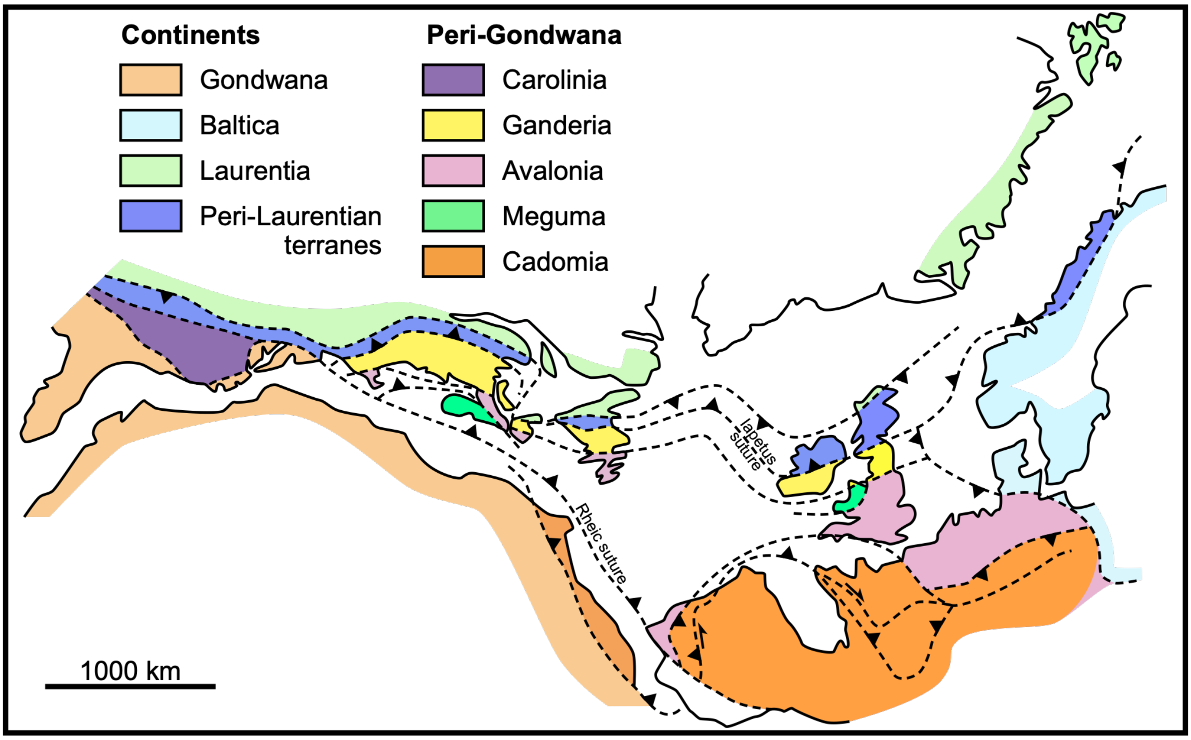

Figure 1.17: Distribution of peri-Gondwanan terranes across modern-day landmasses superimposed onto a pre-Mesozoic palinspastic reconstruction. Modified after van Staal et al. (2012); Waldron et al. (2014a); Pothier et al. (2015).

Constraining mechanisms and kinematics behind this tectonic event have proven challenging. Peri-Gondwanan terranes across Europe and North America are largely obscured by the Variscan (Europe) and Alleghanian-Ouachita-Marathon (North and Central Americas) orogenies that were caused by the Permo-Carboniferous collision of Laurasia and Gondwana, and subsequent formation of Pangea. In addition, several peri-

Gondwanan terranes such as Avalonia are now divided between North America and Europe by the opening of the Atlantic Ocean, making comprehensive studies challenging.

1.4.1 Terrane links to the MCT

The Avalonian-Cadomian belt extended along the margins of the Amazonian and West African cratons of Gondwana, consisting of numerous described peri-Gondwanan terranes that can be split between the Avalonian and Cadomian domains (Murphy et al. 2004). Four main Avalonian terranes have been identified as rifting from Gondwana around the Cambrian-Ordovician boundary – (West and East) Avalonia, Meguma, Ganderia and Carolinia (Murphy et al. 2004; Pollock et al. 2009; Wen et al. 2020). Of these terranes, Avalonia, Meguma and Ganderia are thought to be represented on the British Isles (see Figure 1.18), with all three claimed to have affinity with the MCT in various studies. Evidence of transcurrent relocation of terranes, along with potential links of arc magmatic rocks with those in North Wales created a potential link between the MCT and Avalonia (Gibbons 1983a; Horák 1993; Gibbons and Horák 1996; Kawai et al. 2007). Larger scale studies of peri-Gondwanan terranes, however, favour the MCT as being related to Meguma (Schofield et al. 2016; Schofield et al. 2020) or Ganderia (Pollock et al. 2009; Waldron et al. 2011; Waldron et al. 2014b) rather than Avalonia.

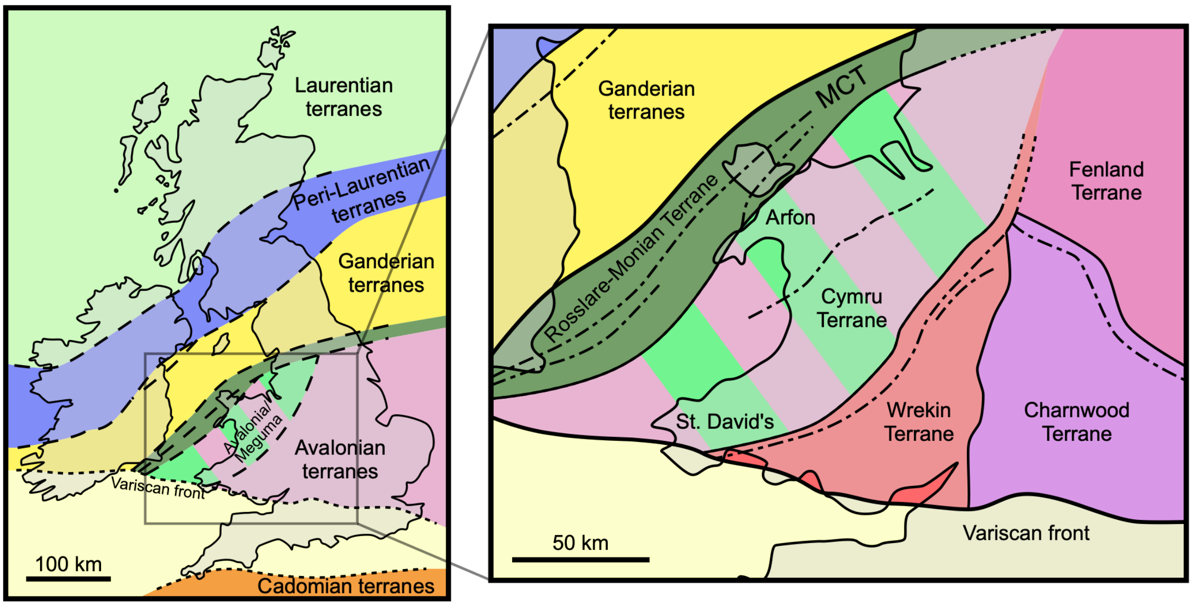

Figure 1.18: Distribution of peri-Gondwanan terranes across the British Isles in relation to the MCT and (inset) distribution of the Avalonian Composite Terrane. After Carney et al. (2000); McIlroy and Horák (2006); Waldron et al. (2019b).

The peri-Gondwanan terranes are closely related and are thought to have rifted together along the same rift system based on their sediment provenance, timing of their departure and subsequent collision with Laurentia, palaeomagnetic data and fossil records (Murphy et al. 2004; van Staal et al. 2012; Pothier et al. 2015; Waldron et al. 2019b). Ganderia is thought to have originated adjacent to the Amazonian craton of Gondwana, whilst East Avalonia and Meguma, and parts of West Avalonia likely derived from a more easterly source closer to the West African craton (van Staal et al. 2012; Shellnutt et al. 2019; Waldron et al. 2019b). Other provenance studies and palaeomagnetic data suggest that Avalonia may have closer affinity to Amazonia (Pollock et al. 2009; Wen et al. 2020).

Avalonia

The division of East and West Avalonia is not purely derived from modern-day locations (Europe and North America respectively) but also through geodynamic and geochemical differences that may be representative of a composite terrane (Waldron et al. 2014a). They are considered to be closely related in formation, but may have become dispersed during rifting (Waldron et al. 2011; Schofield et al. 2016). Avalonian magmatism across the British Isles (East Avalonia) closely resembles activity recorded in West Avalonia and Meguma (Schofield et al. 2016). However, isotopic differences in Neoproterozoic magmatic rocks suggest that East Avalonia may have been at least partly separated from West Avalonia, with possible links to Ganderia (van Staal et al. 2020).

East Avalonia records two separate phases of arc development, with initial Neoproterozoic continental arc development (Horák et al. 1996), and secondary Ordovician arc development during rifting (Howells et al. 1991). On the British Isles, East Avalonia is divided between four terranes (Carney et al. 2000; McIlroy and Horák 2006; Schofield et al. 2016). The Cymru Terrane is split between Arfon and St. David's domains in northern and southern Wales respectively. The Wrekin Terrane has the longest recorded magmatic history during Neoproterozoic arc activity. Along with the Charnwood Terrane, exposures are limited to a small series of localities in the West Midlands. The Fenland Terrane is a theoretical terrane known only from a small number of borehole-derived outcrops. Ordovician arc-related magmatism was confined within the Cymru Terrane, separated by a marginal basin (Kokelaar 1988; Howells et al. 1991).

Avalonia was the first of the peri-Gondwanan terranes to be linked to with MCT, establishing similarities between Coedana Terrane and the Arfon rocks of the Cymru

Terrane and linking them by transcurrent faulting (Gibbons and Horák 1996; Horák et al. 1996). Links between the age and isotopic signatures of the Coedana granites, and Sarn Complex granites and Arfon ignimbrites, as well as basement rocks, provided a strong link to the Cymru Terrane (Tucker and Pharaoh 1991; Horák 1993; Horák et al. 1996) as shown in Figure 1.14. The MCT is proposed under this linkage to represent forearc fragments of the Avalonian arc (Gibbons and Horák 1996; Kawai et al. 2007). Further provenance studies show close similarities between Llandygarn gneisses and basement rocks of the Malverns Complex of Avalonia (Strachan et al. 2007). Several outcrops interpreted as tectonically emplaced Arfon Group outliers have been reported on Anglesey in the form of the Baron Hill beds and the Bwlch Gywn tuff, however their affinity remains uncertain (Greenly 1919; Reedman et al. 1984).

Meguma

The Meguma Terrane mostly outcrops in a single area in Nova Scotia, North America, positioned to the south of Avalonian rocks. Meguma is closely linked with Avalonia and it is unclear whether Meguma represents a separate peri-Gondwanan landmass or the terranes migrated contiguously, although it is clear that they formed independently (Nance et al. 2010; Shellnutt et al. 2019). The Meguma Terrane may have formed between the separated landmasses of East and West Avalonia (Waldron et al. 2011; Pothier et al. 2015).

The terrane consists of thick Cambrian sequences of siliciclastic turbidites. Correlations between the Meguma Terrane and the turbidites that comprise the Porth y Felin Terrane of the MCT, as well as the Rosslare Complex, have led to a linkage between the terranes (Waldron et al. 2019b). Zircon provenance studies have further complicated the extent of the Meguma Terrane in the British Isles by suggesting that the Cymru Terrane may originate from Meguma rather than Avalonia (Waldron et al. 2014a; Pothier et al. 2015). Provenance results suggest that the Cymru Terrane may have been isolated from the main Avalonian arc and has an affinity more closely related to Meguma (Schofield et al. 2016). The thick Cambrian turbidite deposits of the Harlech Dome, which are situated upon arc material in North Wales, provide further correlation to Meguma sequences in Nova Scotia (Waldron et al. 2011; Schofield et al. 2020).

Ganderia

Ganderia is situated to the north of the MCT and separates the Avalonian Terranes from peri-Laurentia across Europe and North America (Hibbard et al. 2007; van Staal et al. 2012), having reached the Laurentian margin earlier in the Late Ordovician-Early Silurian (Zagorevski et al. 2008; van Staal and Barr 2012). It extends across the northern Appalachians of North America and have been correlated with the Leinster-Lakesman Terrane of southern Ireland, and by extension across northern England (van Staal et al. 1996; van Staal et al. 2012; Waldron et al. 2014a). The Leinster-Lakesman Terrane records a predominantly Ordovician deep-water deposits overlain by late Ordovician arc-related magmatic rocks of the Lake District (McConnell et al. 1999; Barnes et al. 2006). Overlying Late Ordovician-Early Silurian sediments record the collision with Laurentia (Stone and Evans 1995).

Ganderia represents a composite terrane that formed separately from Avalonia and records a similar Neoproterozoic basement and arc magmatic history (van Staal et al. 2012; Barr et al. 2014; Waldron et al. 2014a). The Ganderian clastic wedge was deposited along the margin of the Amazonian domain of Gondwana – as opposed to the stronger West African provenance of Avalonia and Meguma – and originated from a relatively distal position relative to the subduction regime of Avalonia-Cadomia (Nance et al. 2008; van Staal et al. 2012; Shellnutt et al. 2019). Ganderia and Avalonia may have been brought together through soft arc-arc collision along the Gondwanan margin during the late Neoproterozoic, leading towards the end of arc magmatism (van Staal et al. 2020).

Despite preserving no late Neoproterozoic magmatic activity or basement rocks, detrital zircon provenances from Cambrian and Ordovician rocks of the Leinster-Lakesman Terrane show close similarities to Ganderian rocks across North America (Waldron et al. 2014a). The Leinster-Lakesman Terrane is thrust upon the MCT in Rosslare, SE Ireland, and Ordovician-Silurian sediment provenances share close affinity (Tietzsch-Tyler and Phillips 1989; Waldron et al. 2014a). As a result, the MCT is often included within Ganderia, with the MSFZ marking the southern boundary against Meguma/Avalonia (van Staal et al. 2012; Waldron et al. 2014b; Pothier et al. 2015; Waldron et al. 2019a). Despite this, the MCT is clearly distinguished from the Leinster-Lakesman Terrane below the Arenig unconformity by its Neoproterozoic basement and polydeformed Monian terranes.

1.4.2 Convergence along Gondwanan margin

Evidence of an initial, largely Proterozoic convergent regime is most extensively recorded through the preservation of continental arc material in the form of the Avalonian-Cadomian belt, supported by evidence from arc-related environments like accretionary complexes. Long-lasting, stable subduction and Avalonian and Ganderian arc formation began to take place around 640 Ma after a complex series of short-lived collisions beginning in the Tonian (van Staal et al. 2020).

Arc formation

Avalonian arc volcanism occurred over three distinct magmatic episodes, beginning with early-stage magmatism in the Wrekin Terrane, with intermediate-felsic plutonic rocks in the Malvern Complex dated at 677±2 Ma (Thorpe et al. 1984; Tucker and Pharaoh 1991; Carney et al. 2000). The main stage of mostly calc-alkaline felsic magmatism with some intermediate magmas, was more widespread and occurred 620 – 600 Ma, including the generation of the Coedana granite of the MCT (Tucker and Pharaoh 1991; Horák et al. 1996; Compston et al. 2002). Late-stage magmatism occurred 570 – 550 Ma and was largely limited to the Malvern Borderlands of the Wrekin Terrane, with some activity in the Arfon Terrane (Tucker and Pharaoh 1991; Compston et al. 2002). This late activity overlaps with ages of Penmynydd blueschist metamorphism and possible trench-fill sediments in the Gwna Complex. Magmatic rocks from this phase are more compositionally variable, ranging from tholeiitic basaltic to rhyolitic, with geochemical signatures that suggest that rifting had initiated (Thorpe et al. 1984; Carney et al. 2000). The main and late-stage phases of arc magmatism correlate well with calc-alkaline magmatic suites from West Avalonia in North America (Gibbons and Horák 1996).

Ganderian arc-related magmatic activity also occurred in three distinct stages, separated by intervening periods of platform sedimentation. Arc magmatism occurred between 675 – 647 Ma, 625 – 600 Ma and 580 – 530 Ma, with the third stage being most voluminous (Barr et al. 2003; Lin et al. 2007; Barr et al. 2014). Magmatic activity largely overlapped with regional metamorphism. Intermediate phases overlap broadly with those in Avalonia and may represent short-lived periods of soft terrane collisions (van Staal et al. 2020).

Accretionary margin development

The MCT is an important potential record of this subduction regime. It hosts the only known occurrences of blueschists from the Avalonian-Cadomian belt – key indicators of subduction. The Blovice accretionary complex (BAC) in Czechia is the only other known example of a recognised accretionary complex attributed to the Avalonian-Cadomian belt where elements of OPS can be determined. It is characterised by a Franciscan-type mélange that accreted during the late Neoproterozoic-Cambrian, backed by a volcanic arc, and has been compared to the setting of the MCT, recording subduction beneath the Avalonian-Cadomian margin (Hajná et al. 2013; Ackerman et al. 2019). Both complexes are thought to represent similar processes occurring around the same time that are situated hundreds of kilometres apart.

Transition to transcurrent regime

Synmagmatic transcurrent shearing occurred within the Avalonian arc, suggesting oblique subduction dynamics before the end of arc magmatism (Gibbons and Horák 1990; O'Brien et al. 1994). Volcanic arc activity in Avalonia ceased from 550 Ma as subduction was replaced by a transcurrent dominant regime for the majority of the Cambrian until departure of the peri-Gondwanan terranes. This led to the dismemberment, relocation and interchange of arc-proximal material prior to rifting throughout the peri-Gondwanan terranes (van Staal et al. 2020). This is primarily observed in the MCT and likely led to the composite juxtaposition of terranes from different environments, as illustrated in Figure 1.14b (Gibbons and Horák 1996).

1.4.3 Rifting of peri-Gondwanan landmasses

Rifting of Ganderia from the Gondwanan margin occurred in the mid- to late-Cambrian (509 – 485 Ma), closely followed by Avalonia in the early Ordovician (485 – 470 Ma). Rifting saw the resumption of arc-related magmatism at scattered volcanic centres, predominantly across Snowdonia and SW Wales (Kokelaar 1988; Howells et al. 1991; Thorpe et al. 1993b). Renewed magmatic activity occurred in three distinct episodes between the Tremadocian and Katian epochs (ca. 488 – 454 Ma) (Kokelaar 1988; Howells et al. 1991; Schofield et al. 2008). Avalonian magmatism ceased before collision with Laurentia and may have been a result of a soft collision with Baltica, or perhaps due to slab breakoff.

The onset of rifting led to the formation of sedimentary basins across the British Isles that initiated in the Cambrian and continued throughout the Ordovician and Silurian and coincided with high sea levels (Pothier et al. 2015). The most prominent of these are the Welsh Basin, which extends across central and southern Wales, and the Midland Platform across central England (Strachan 2012). Smaller parallel basins such as the Arfon Basin in North Wales, and the Anglesey Basin opened separately under the same extensional regime. An influx of Monian material in the Welsh Basin suggests that the MCT had been juxtaposed with Meguma/Avalonia by the Tremadocian epoch (Pothier et al. 2015).

Rifting occurred diachronously, propagating from west to east along the Avalonian-Cadomian belt (Sánchez-García et al. 2019; van Staal et al. 2020). Numerous palinspastic reconstructions have been proposed to model this tectonic event, with two models holding prominence in the form of a ‘Caribbean-style’ model and a ‘Baja-style’ model, named after modern-day analogues. Both models acknowledge the tectonic activity along the margins of both Gondwana and Laurentia, include prominent strike-slip components, and result in the closure of the Iapetus Ocean with the subsequent opening of the Rheic Ocean.

'Baja-style' model

The 'Baja-style' generally assumes a linear translation of the peri-Gondwanan terranes between Gondwana and Laurentia (Keppie et al. 2003; Cocks and Torsvik 2006; Pollock et al. 2009; Shellnutt et al. 2019). The possible causes that led to cessation of subduction and transition to transcurrent and extensional regimes include slab rollback or slab breakoff leading to the formation of a back-arc basin (Pollock et al. 2009). The most plausible cause given current evidence is the oblique subduction of a mid-ocean ridge (Sánchez-García et al. 2019). Oblique subduction is the most likely mechanism for transcurrent faulting across the Avalonian arc and would also induce the staggered rifting that is evident across peri-Gondwanan terranes (Horák et al. 1996; Keppie et al. 2003; Sánchez-García et al. 2019).

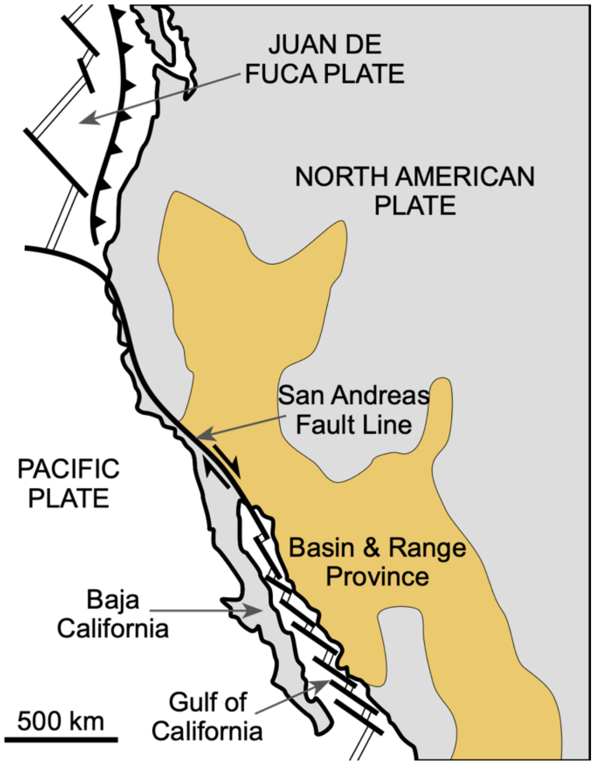

Figure 1.19: Modern day tectonic setting of the Californian coast of North America, showing the basis of the 'Baja-style' rifting system, with oblique subduction of an axial ridge leading to the propagation of basins and rifting along the continental margin along with transcurrent terrane movement. After Dickinson (2006).

The proposed model has been compared to the modern-day tectonic setting of the western coast of North America, shown in Figure 1.19 (Keppie et al. 2003; Strachan 2012; Sánchez-García et al. 2019). The oblique subduction of the East Pacific Rise (spreading ridge between Pacific and Cocos/Juan de Fuca oceanic plates) beneath the North American continental margin has resulted in the rifting of Baja California as a peninsula migrating from the mainland. It is parted from the mainland by the propagation of the Gulf of California, with extensional regimes extending northwards (Condie 1997; Dickinson 2006). Baja California is connected to the mainland via the San Andreas transcurrent fault network. The Gulf of California rifting centre is connected to the oceanward Juan de Fuca Ridge spreading centre along the prominent San Andreas transcurrent fault system.

'Caribbean-style' model

Rather than a rapid change between collision and rifting, the 'Caribbean-style' model proposes that prominent transcurrent faulting is responsible for the departure of the peri-Gondwanan landmasses from the continental margin, part of a singular curved fault system that connects to tectonic activity on the Laurentian margin (Waldron et al. 2019b; Schofield et al. 2020). This would involve an arching tectonic plate interface similar to that of the Caribbean plate, transitioning from largely transcurrent regimes along the northern and southern interfaces to an arching convergent margin to the east (Kerr and Tarney 2005; García-Casco et al. 2011).

Rotation of Peri-Gondwanan landmasses

The Caribbean-style model assumes complete rotation of the peri-Gondwanan landmasses during translation towards Laurentia along a singular curved fault system. The Baja-style system, however, leaves more leeway in terms of terrane rotation and can accommodate a curved or linear path for peri-Gondwanan landmasses (Keppie et al. 2003; Pollock et al. 2009). On a linear path, terranes would not be rotated during translation. However, rotation could be possible by assuming greater diachronous spreading rates of the Rheic Ocean, where fast spreading rates would cause the rotation of early rifted landmasses that could dock obliquely against Laurentia.

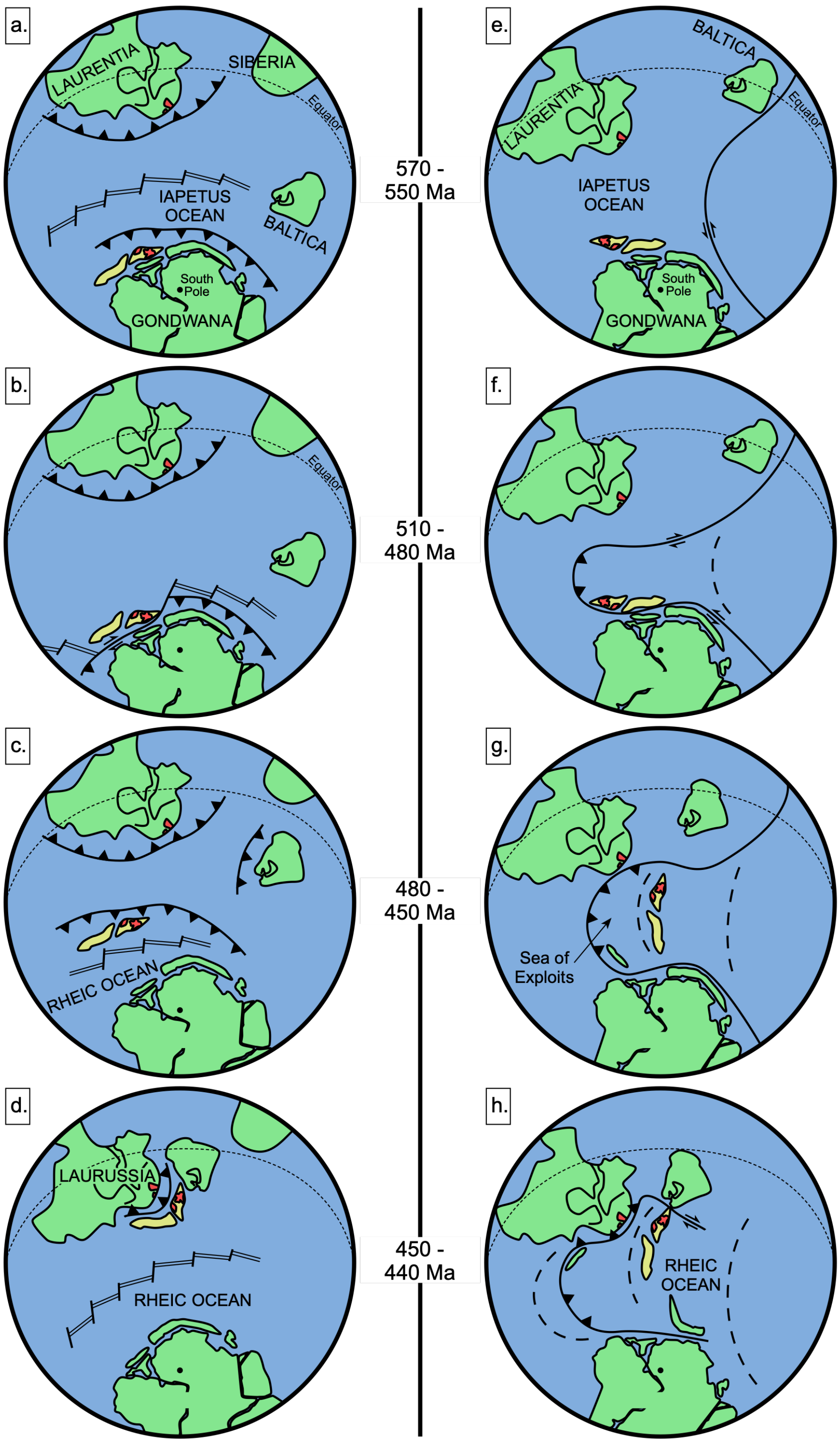

Figure 1.20: Schematic overview of the two favoured palinspastic models of peri-Gondwanan rift evolution including (a-d) Baja-style model modified after *(Keppie et al. 2003; Linnemann et al. 2008; Pollock et al. 2009; Ackerman et al. 2019; Sánchez-García et al. 2019)* and (e-h) Caribbean-style model modified from (Waldron et al. 2014b; Pothier et al. 2015; Schofield et al. 2020). Yellow terranes highlight Avalonia; red areas represent modern extent of British Isles.

The polarity of subduction kinematics is a good indicator of whether rotation of terranes has occurred. Peri-Gondwanan terranes seemingly show a mix of polarities, with evidence in West Avalonia to suggest rotation of the terrane derived from a northerly subduction polarity (Keppie et al. 2003). This rotation is not observed, however, in East Avalonia or Carolinia. Geomagnetic data interpretations seemingly indicate rotation of Avalonia during its passage from Gondwana to Laurentia, although original positions were not determined (Wen et al. 2020).

1.4.4 Collision with Laurentia

The migration of the Peri-Gondwanan landmasses saw the closure of the Iapetus Ocean and subsequent opening of the Rheic Ocean (Nance et al. 2010; Waldron et al. 2014b). Upon the closure of the Iapetus Ocean, the terranes docked against the northern continent of Laurentia, along with the continent of Baltica to the east. The resulting Caledonide-Appalachian orogeny occurred throughout the Ordovician to mid-Devonian as a pulsed event as landmasses individually arrived at the Laurentian margin. Zircon provenance studies suggest a staggered collision, with Laurentian material recorded in Ganderia in the late Ordovician (Waldron et al. 2014a). East Avalonia is thought to have collided later in the Silurian (Cocks and Torsvik 2002; Waldron et al. 2014a).

On Anglesey, the collision with Laurentia led to the SSE thrusting of Carmel Head, along with prevalent Acadian deformation and SSE shortening of Devonian and Silurian stratigraphy (Bamousa 2008; Schofield et al. 2008; Strachan 2012). Acadian deformation is largely absent from mainland Britain since Avalonia generally avoided significant Acadian deformation (Woodcock et al. 2007; Schofield et al. 2008).

CHAPTER II

Field Geology of the MCT

2.1 OVERVIEW OF STUDY AREAS

This chapter will describe field evidence from various units across the MCT, including the Gwna Complex, Penmynydd Terrane, Cemaes Group, and from various mafic sheet intrusions from across the Isle of Anglesey. These units will provide the basis for the rest of this study and samples from the locations described in this chapter will be analysed further in Chapters 3 and 4. This section will give an overview of the material studied and provide geological context to the units. Mapping in the Gwna Complex will be used to determine stratigraphic and structural features in order to evaluate interpretations of a tectonic or sedimentary origin, as proposed in previous studies.

The Gwna Complex has been divided between four distinct, tectonically, and geographically separated study areas (I-IV). These divisions will be described separately to provide a more comprehensive overview and to identify potential differences between the areas. While the mafic intrusives explored in this chapter are not part of the MCT, the estimated Lower Palaeozoic age of a particular set of dykes suggests that they may originate from arc magmatism related to the MCT. Figure 2.1 shows an overview of the study areas across Anglesey and Llŷn Peninsula covered in this chapter. A record of samples collected from all study areas is available in Appendix A.

2.2 METHODOLOGY

Fieldwork and sampling were undertaken in each of the study areas described in this chapter. Samples were collected from outcrops of interest for the purposes of whole-rock analyses or for hand-scale or microscale textural observations. Protected GCR, RIGS SSSI or AONB sites such as Newborough Nature Reserve required permission to undertake sampling, which was conducted discreetly to limit disruption and maintain the appearances of outcrops. Access to outcrops situated on private land was sought with landowners' permissions.

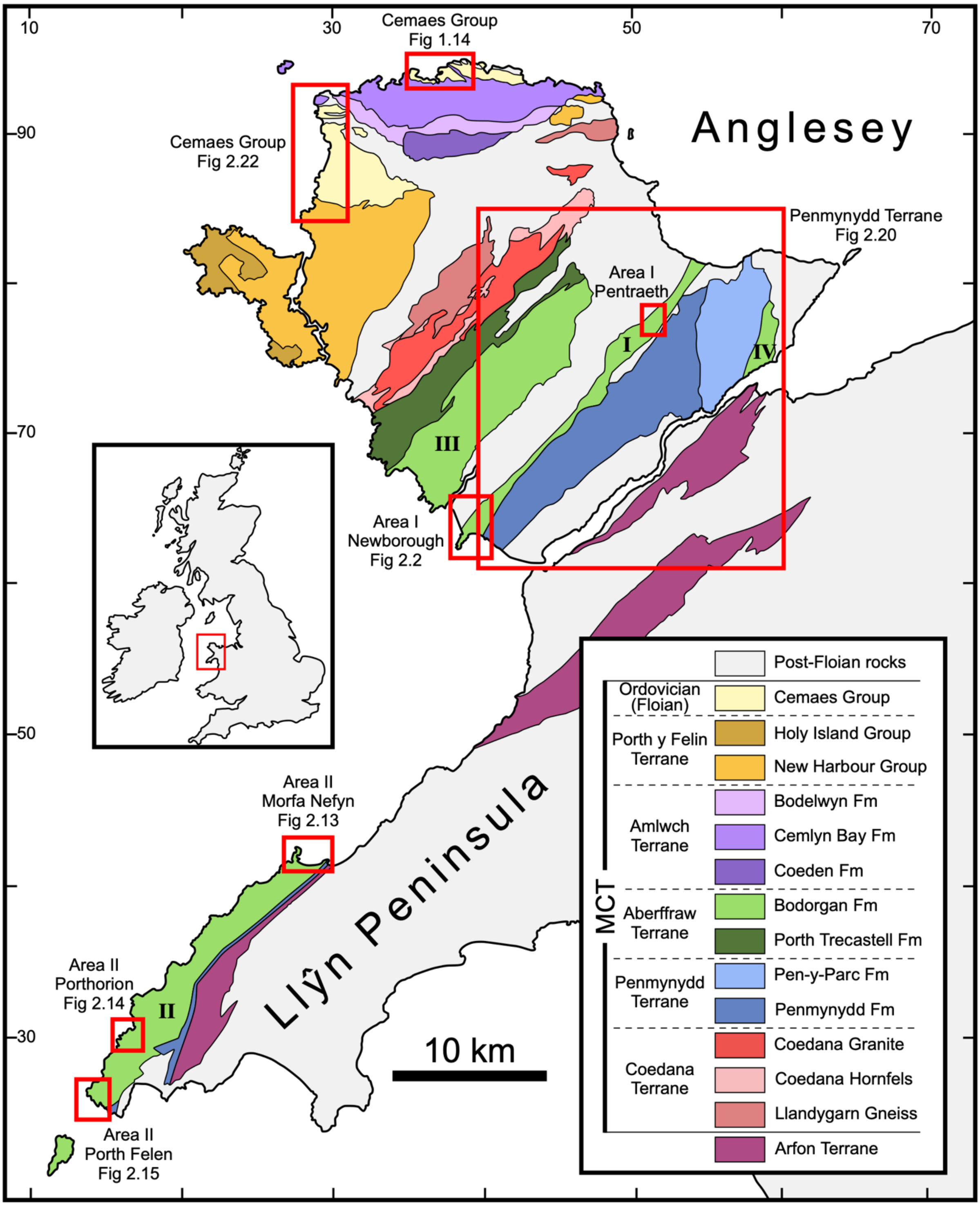

Figure 2.1: Simplified geological map of the MCT highlighting key localities and study areas discussed in this chapter.

Fieldwork on Anglesey presents consistent challenges with limited outcrop exposures of variable quality. Anglesey is a flat, low-lying island draped in glacial till, meaning that exposures are limited to low coastal outcrops of variable access, and inland roche moutonnée. This is particularly apparent in the Penmynydd Terrane for example, where exposures are limited and rarely extensive.

Gwna Complex Area I represented an area of particular interest and outcrops throughout Newborough Nature Reserve were mapped in detail. Positioning in Newborough Forest – where prominent reference landmarks are very limited – was determined using a combination of GPS and LiDAR composite digital terrane model (DTM) data at 50 cm resolution (Edina LIDAR Digimap Service 2016).

2.3 GWNA COMPLEX – AREA I (NEWBOROUGH)

Area I of the Gwna Complex is confined within strands of the NE-SW striking BFZ (Pharaoh et al. 2020; Schofield et al. 2020), bound by Gwna Complex Area III and unconformably overlying Carboniferous strata to the west, and the Penmynydd Terrane to the east. Area I material is well exposed over a relatively continuous area entirely within the bounds of Newborough Nature Reserve in southern Anglesey, extending across both Newborough Forest (SH 39 64) and Llanddwyn Island (SH 38 62) to the south. The area contains some of the most complete Gwna Complex exposures on Anglesey, highlighting its lithological diversity and structural heterogeneity. Area I outcrops to the north of Newborough are rare, and links to outcrops in Pentraeth (SH 52 78) are discussed in Section 2.3.5.

The mapped area shown in Figure 2.2 (2 km x 3 km) consists of interleaved lenticular units of variable thickness (0.5 – 120 m) of 12 distinguishable lithologies that repeat with varying degrees of stratigraphic order and have been subjected to low-grade (sub-greenschist) metamorphic conditions. The units are uniformly orientated along a general strike of 020-040˚ and have been tilted subvertically. Preserved volcanic textures including concave pillow lava bases and hyaloclastite horizons, along with graded bedding in sedimentary units, indicate that units consistently dip steeply (> 70˚) SE. A pervasive foliation strikes parallel to the orientation of the units and dips subvertically NW, creating an offset of 10-20˚ between foliation dip and stratigraphic dip.

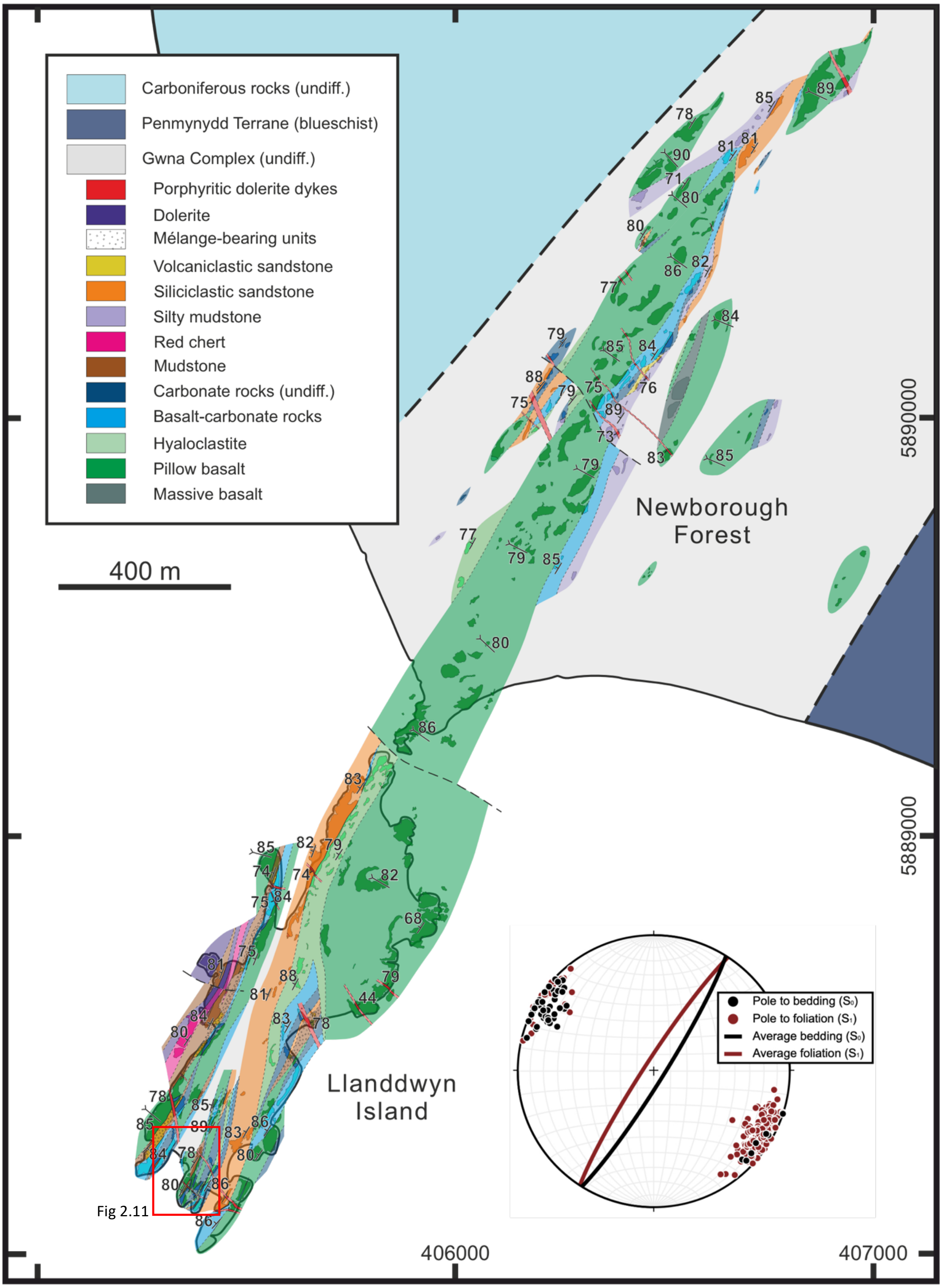

Figure 2.2: Geological map of Newborough (Gwna Complex Area I) with stereonet plots of bedding and foliation orientations.

The wedge-shaped boundaries of the Gwna Complex Area I were no observed but inferred through various methods. To the west, the BSZ was traced along topographic markers paired with evidence from existing geological and geophysical maps. To the east, outcrops of Penmynydd Terrane metabasites from north of Newborough Forest were delineated and extrapolated along prevailing foliation through the mapped area. While Penmynydd Terrane outcrops are common in the surrounding area, thicker sand dune coverage of the eastern parts of Newborough Forest covers any occurrences in the mapping area.

Regional deformation in Area I is heterogeneous, concentrated within high-strain shear zones that surround relatively undeformed, low shear lenticular slices 20 – 250 m thick and up to 2 km long. Figure 2.3 shows a tectonic map of Newborough, identifying 16 low shear units (1-16) intercalated with highly sheared zones of dismembered sequences of highly deformed rocks that form a large-scale mélange. Area I is dominated by thick mafic magmatic sequences – mostly pillow basalts – that comprise the bulk of coherent sequences and individual coherent units. Coherent sequences are topped by a suite of thinner sedimentary-dominated units including carbonate rocks, cherts, mudstones, and sandstones. Incoherent high-strain shear zones comprise the same rock types, often as thinner slices – although weaker lithologies are more abundant – and retain no stratigraphic integrity.

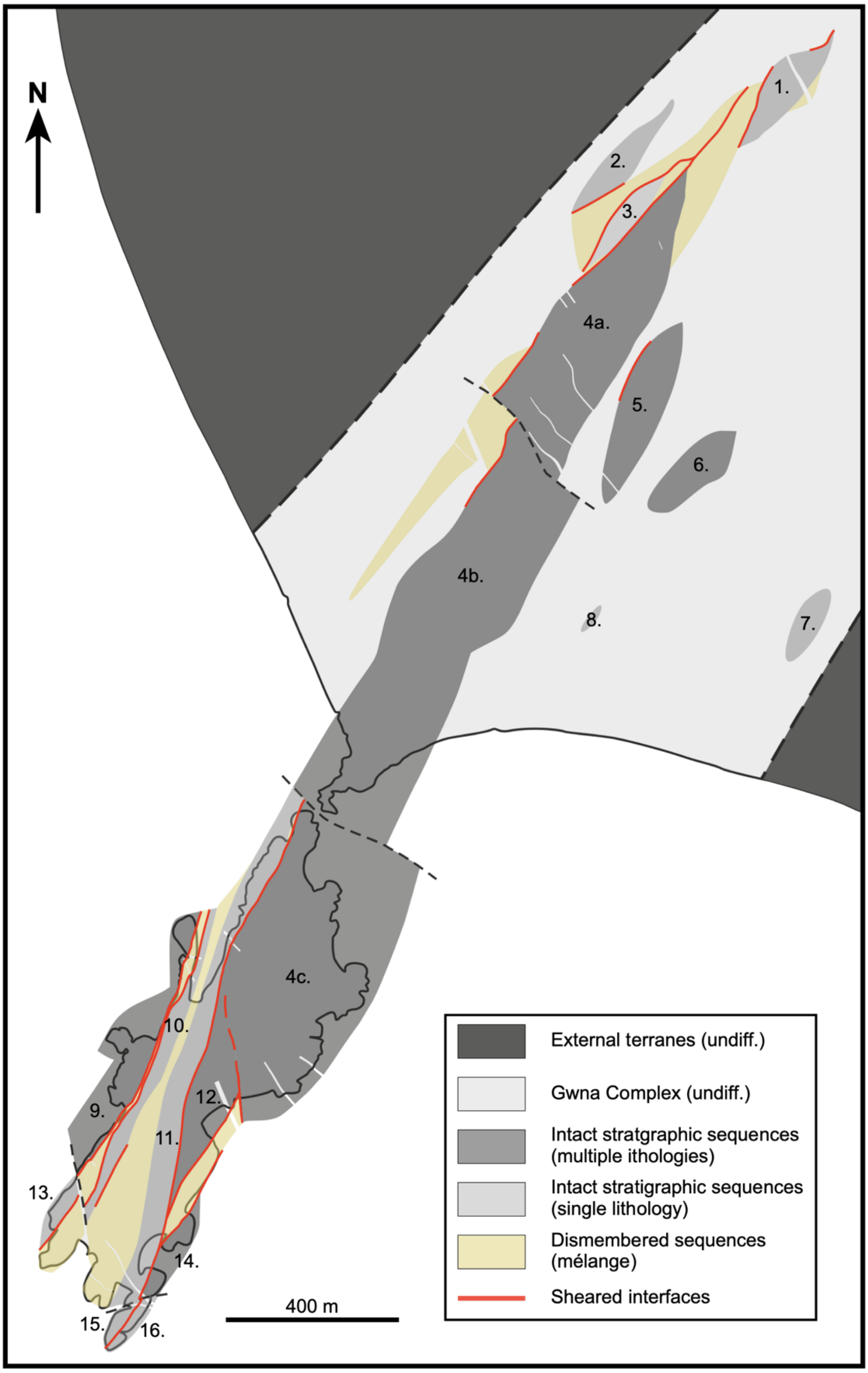

Figure 2.3: Tectonic map of Newborough (Gwna Complex Area I) distinguishing areas of low shear that preserve pre-deformation stratigraphic features or sequences (1-16) and areas of high shear mélange where highly deformed slices are tectonically juxtaposed with not stratigraphic order preserved. Unit 4 has been divided into three sections (4a-c) along later strike-slip faults that crosscut Area I.

2.3.1 Lithologies

Of the twelve distinct Gwna Complex lithologies identified in Area I, four are magmatic in nature, five consist predominantly of pelagic sedimentary components, two consist of predominantly clastic components and one is of tectonic origin. Porphyritic dolerite dykes also crosscut the rocks of this area, and their emplacement postdates the formation of the Gwna Complex. All mapped porphyritic dolerite dykes are classified as Group 1 intrusives (see Section 2.9).

Magmatic suite

The Gwna Complex igneous suite is composed of closely related basaltic rocks including pillow basalts and subordinate hyaloclastites and massive basalts. Pillow lavas are the dominant magmatic rocks type (see Figure 2.4a), with massive lavas and hyaloclastites often found as components within pillow lava sequences, but both also occur as singular mappable lithological units.

Pillows are typically 30 – 70 cm in diameter and consistent in average size between units, with occasional lobate basalts that can reach 2 m in length. Parallel sets of feeder channels establish a consistent orientation for the sequences. Each pillow typically has a chilled rim 1 – 10 mm wide. While most pillow sequences in Newborough are non-vesicular, those in Units 9 and 13 are exceptions, with radial elongate vesicle patterns (see Figure 2.4b). Interpillow spaces are filled by a chlorite-clay-rich matrix with well-developed concentric foliation around pillow outlines, likely the product of extensively altered volcanic glass. Red jasper masses are commonplace in these interpillow spaces and in occasional drainage cavities in pillow cores. Carbonate material also infills these spaces particularly towards the upper stratigraphical regions, and both are interpreted to be hydrothermal in origin. Larger linear masses of red jasper develop along occasional fractures within pillow basalt sequences (eg. SH 3914 6304). These jasper formations have been interpreted as red chert layers of sedimentary origin (Maruyama et al. 2010a), however they are limited to fracture zones where high fluid mobility likely led to increased hydrothermal activity. Pillows may exhibit a frothing texture at their core associated with epidote formation, which may have resulted from volatiles concentrated in late-stage magmas of crystallising pillows.

Hyaloclastites occur as individual units, and as intermittent continuous or discontinuous horizons within pillow basalt units that are typically 1 – 5 m wide. They contain irregular, rounded to subangular basaltic clasts varying from fragments < 0.1 mm in diameter to fully preserved pillow basalts up to 30 cm in length. The fragments are supported by a highly foliated, calcite-rich chloritic matrix that is interpreted to be comprehensively altered volcanic glass (see Figure 2.4e). Clasts are often substantially fractured and infilled by matrix material, and often show zoned alteration effects. Examples of lateral gradation between pillow lavas and hyaloclastites (see Figure 2.4c) indicate that they formed concurrently, likely controlled by geographical variations during formation. Clast density ranges from approximately 25 – 75 % with relatively minor internal variations. Lateral variations in clast size and density within hyaloclastites (see Figure 2.4f) are also likely a product of flow variability during formation. Some hyaloclastites contain rare examples of juvenile clasts of featureless, irregular lobate basalt that appears to have intruded freshly erupted hyaloclastites, creating a self-peperitised texture (eg. SH 3907 6297).

Massive basalt occurrences are rare and mostly localised to small horizons within pillow basalt units, occurring as single discontinuous sheet flows typically < 2 m in thickness (eg. SH 3906 6294). A single larger example of a massive basalt (AN17020) occurs in Unit 5, where most of the observed lower magmatic sequence consists of a massive basalt flow stratigraphically between series of pillow basalts. The massive basalt is notably darker in colour, a dark purple colour, in contrast to the green pillows above and below, and is cut by thin jasper veins that form along fracture networks. Along what appears to be the upper surface of the flow, autobrecciation textures have developed, consisting of rounded basalt clasts 5 – 50 mm in diameter densely packed within a basaltic matrix (see Figure 2.4d).

A fourth magmatic lithology – dolerite, found as a set of sills exclusively in Unit 9 – is interpreted to represent a separate magmatic event from the dominant basalt sequences. The dolerite shows common features of a sheet intrusive, including chilled margins and variable grain size based on sill thickness. It is dark grey and amphibole-bearing, with no evidence of olivine, indicating an intermediate composition. Unlike the later porphyritic dolerite dykes, the dolerite is aphyric and non-vesicular. The sills have also been structurally incorporated into the Gwna Complex, rather than crosscutting sequences. Like other magmatic rocks in Area I, the dolerites have undergone extensive low-grade alteration.

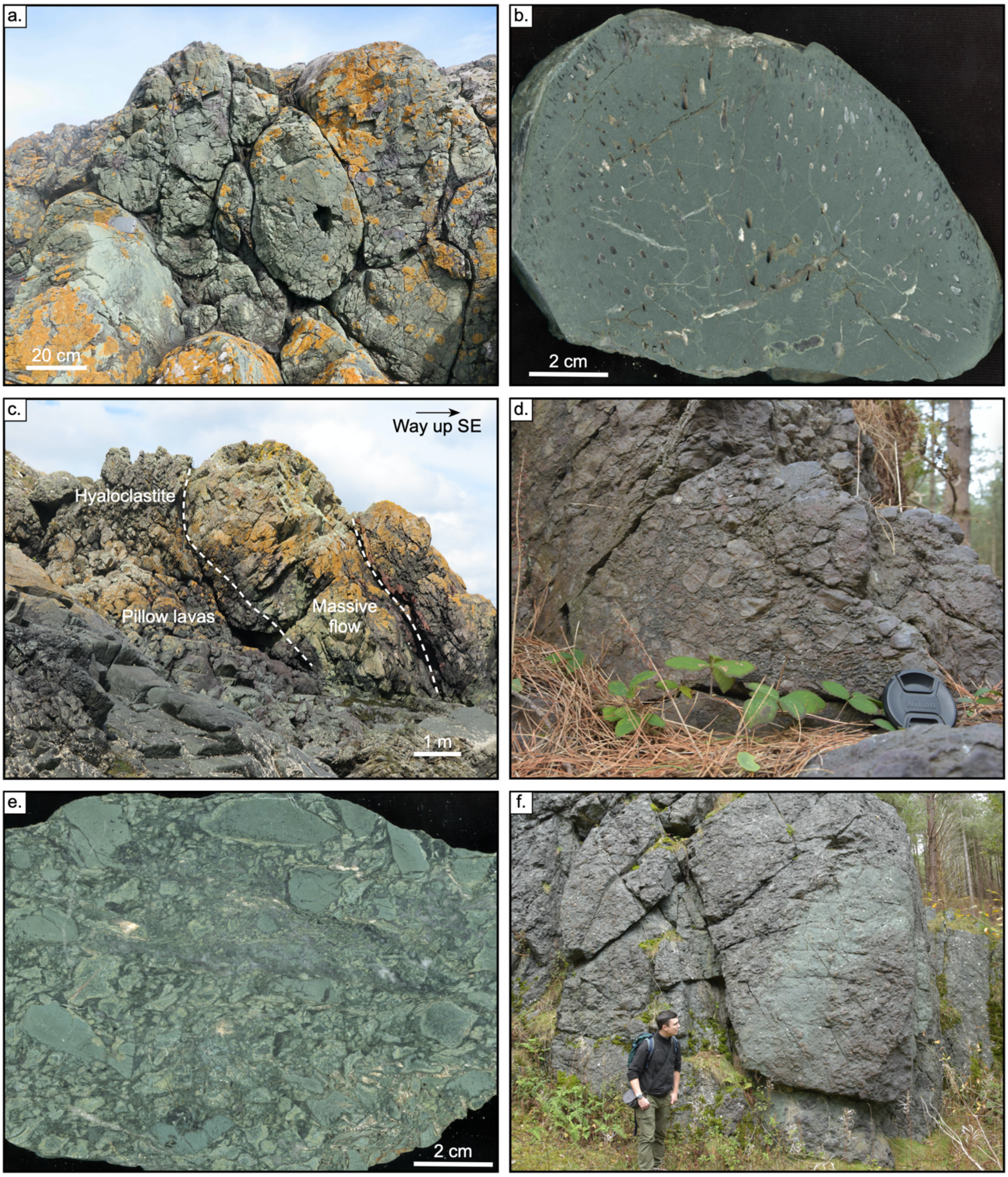

Figure 2.4: Various representative magmatic rocks from Gwna Complex Area I including (a) grey-green pillow basalts from Unit 4b (SH 3909 6347) showing a way-up direction to the right (SE) with an example of a drainage cavity within a pillow; (b) polished slab of a vesicular/amygdalar pillow basalt from Unit 9 (AN18014; SH 3877 6320) showing a radial pattern with carbonate and zeolite amygdales and a thin light green pillow rim; (c) assemblage from Unit 4c (SH 3906 6294) of pillow lavas grading laterally into hyaloclastites, overlain by a massive basalt lave flow 2 – 3 m thick; (d) possible autobrecciation texture in massive basalt of Unit 5 (SH 3978 7431); (e) polished slab of hyaloclastite from Unit 4c (SH 3906 6344) showing basaltic clasts of variable size and shape within a calcite-rich dark green matrix; and (f) hyaloclastite outcrop in Unit 4b (AN17024; SH 3924 6391) showing lateral variability in clast size and density highlighted by the change in density of reddened basalt clasts within the green matrix.

Basalt-carbonate rocks

Complex interactions between pillow basalts and carbonate rocks occur in numerous localities but rarely in stratigraphic succession, observed only in Units 4 and 12. The primary emplacement of basalt into otherwise structureless carbonate material has led to pillow formation and extensive fracturing, leading to intrusion of pillows by surrounding carbonate material. In Newborough Forest, Unit 4 (a and b) provides a prime example of how these interactions act as a transitional phase between the lower igneous suite and overlying sedimentary sequences (see Figure 2.5). Progressively larger quantities of carbonate material – predominantly dolomitic – begin to infill interpillow spaces in the upper 10 – 20 m of the pillow basalts. The transition into the basalt-carbonate lithological unit is marked by the pillows becoming individually supported within a carbonate matrix (see Figure 2.5d). Proceeding upward through the unit over approximately 20 m, pillow basalts are progressively more less abundant until becoming absent (see Figure 2.5b), completing the transition to the carbonate rocks lithology.

Carbonate veins crosscut the pillows as a secondary process, infiltrating cracks in the pillows and producing a brecciated appearance that becomes generally more enhanced in upper parts of the sequence, where carbonates become more voluminous relative to basalt. In carbonate-dominated domains where basalt is rare, pillows typically have an exploded appearance, appearing as a scattered assemblage of basalt fragments larger than average non-brecciated pillow lavas. Basalt also undergoes replacement by carbonate material, particularly affecting pillow cores. Cores often appear to be almost entirely replaced by carbonate material, with remnant strands of basalt preserved (see Figure 2.5c). Chilled pillow rims are typically not replaced however, creating hollow pillow textures. Within surrounding carbonate rocks, strands of basaltic material and high amounts of jasper are also disseminated.

Unit 4 also demonstrates how upper regions of pillow basalt sequences (roughly 30 m thickness) contain progressively reddened haematite-bearing basalt (see Figure 2.5e), likely due to proximity to overlying carbonate rocks. This continues through the basalt-carbonate rocks, which always contain reddened, haematite-rich basalts. Dolomite formation through carbonation of limestones likely oxidised nearby basaltic rocks leading to this process. Deformed basalts in high-strain shear zones often display similar characteristics, maybe as a result of increased fluid flow along sheared pathways.

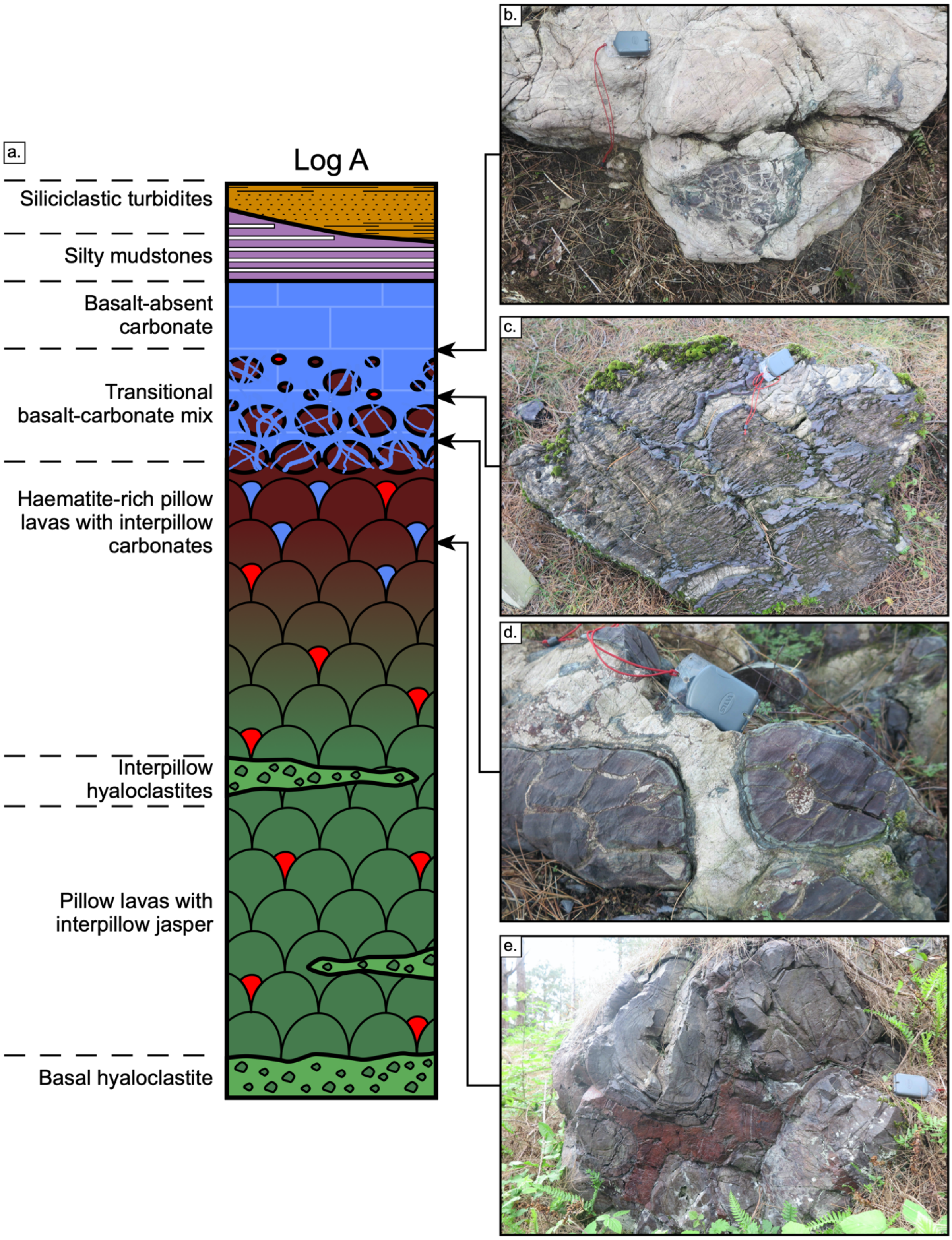

Figure 2.5: logged section through Unit 4a (see Figure 2.9) showing a stratigraphically coherent transition between pillow basalts and overlying carbonate rocks showing (b) uppermost parts of the basalt-carbonate interaction where sporadic, highly altered pillows have been extensively replaced and partly disseminated into surrounding carbonate rocks; (c) preserved pillow rims where cores have been largely replaced by carbonate material; (d) intact pillows within carbonate matrix with some dispersed basaltic material, with fractures and drainage cavities infilled by carbonate and jasper; and (e) upper parts of pillow basalt unit where pillows have become reddened by haematite, also showing interpillow jasper.

Pelagic sedimentary rocks

Interactions with the magmatic suite suggest that the carbonate rocks are pelagic in nature. Carbonate rocks are described as undifferentiated due to their complex nature. They are predominantly composed of dolomite that was a product of pre-deformation dolomitisation, but multiple stages of reworking mean that calcite is also present, mostly in veins. The rocks are white-yellow and occasionally present slightly pink, potentially due to a rhodochrosite component. Extensive recrystallisation and reprecipitation has thoroughly overprinted most primary sedimentary features, however some evidence of relict bedding/layering is preserved occasionally (eg. SH 3948 6446). There is no evidence of stromatolitic features as observed in limestones blocks of the Porth Swtan Formation in northern Anglesey (see Section 2.8).

The distinctly coloured layered red cherts are exclusively found in Unit 9 and consist of repeated thin beds (2 – 20 cm) of cherty material with minor mud and silt components (see Figure 2.6a) that exhibit graded bedding fining towards SE. The cherts are interbedded with hemipelagic mudstones with a deep green/purple appearance that alternates throughout exposures (see Figure 2.6c). Mudstones appear to be massive, however excessive shearing may have obscured bedding features. The deep colouration suggests a high mafic content and the mudstones likely represent tuffs from a mafic/intermediate source.

Silty mudstones are thinly interbedded cherts, mudstones and siltstones (see Figure 2.6b) that represent a transition between pelagic sedimentation and periodic influx of fine clastic material. The alternating sequence includes clearly defined laterally continuous beds 0.5 – 20 cm thick where concentrations of cherty and silty layers vary throughout the sedimentary sequence. Coarser beds are occasionally graded. Tight folds expose soft sediment deformation as tougher chert beds – and even silt beds – become locally truncated or fragmented and incorporated into mud layers. Perpendicular fractures in cherty layers are common particularly close to folds, and are infilled by quartz, suggesting fluid release related to deformation.

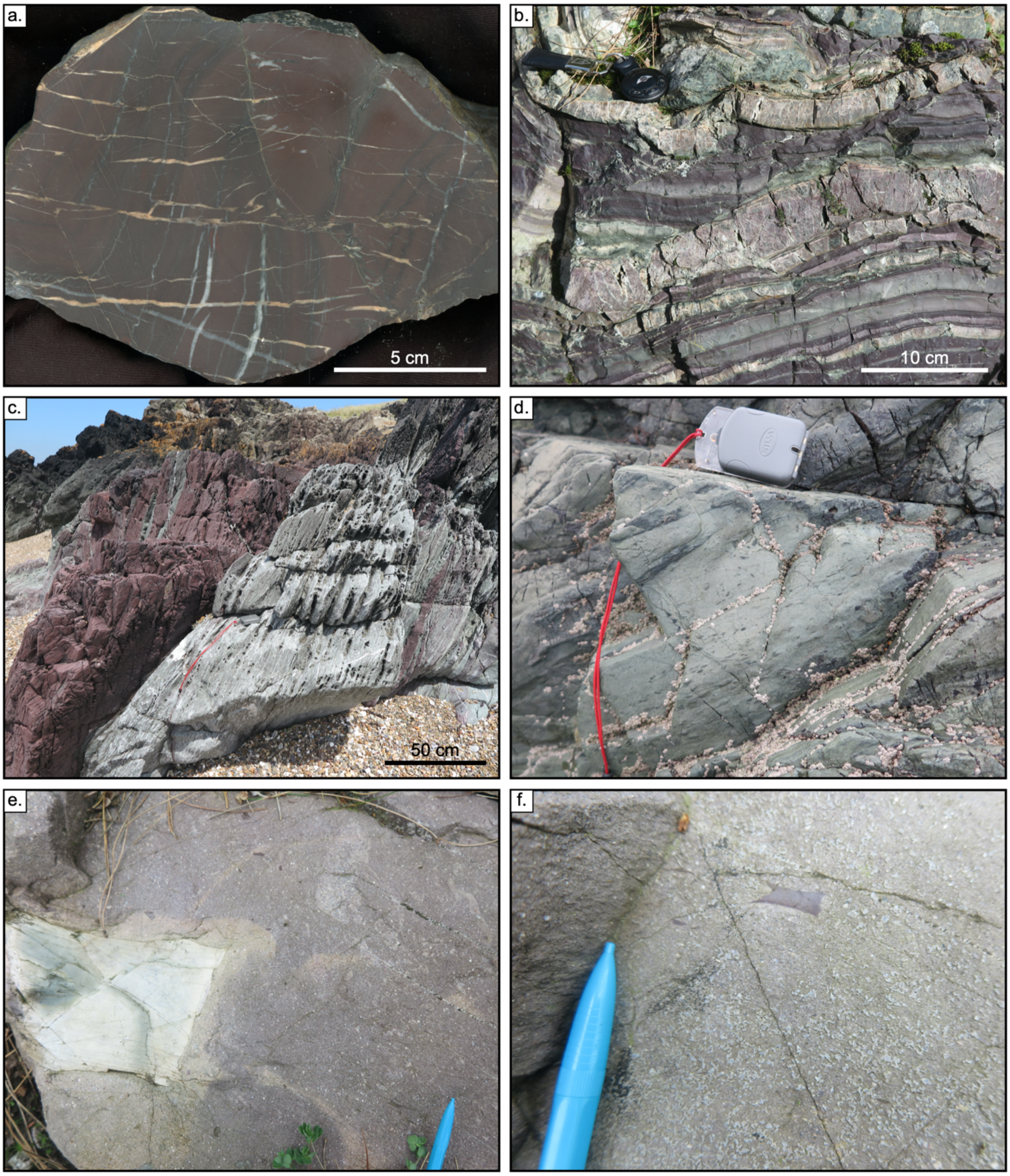

Figure 2.6: Various representative sedimentary rock types from Gwna Complex Area I including (a) polished slab of red chert from Unit 9 (AN18002; SH 3865 6294) showing folding, displacement along carbonate veins, and feint grading from the inclusion of clastic material; (b) disturbed layering of silty mudstones (SH 3995 6495) showing deep purple mudstone layers, light purple/green silty layers with graded bedding and light chert layers with perpendicular quartz veins; (c) contrasting red/purple and green/grey colours in mudstone succession in Unit 9 (AN19011 – red, AN19012 – green; SH 3862 6281); (d) green chloritic sandstone from Unit 11 (SH 3895 6335) with dark patches that may represent evidence of bioturbation; (e) brown siliciclastic sandstone containing large chert rip-out clast and (f) small purple mudstone rip-out clast from Unit 4c (SH 3966 6432).

Clastic sedimentary rocks

The predominant clastic lithology in Area I is a grey-green interbedded sandstone-mudstone unit interpreted as a volcaniclastic sandstone. Chloritic spots in the arkosic sandstones appear to represent altered mafic lithic clasts or feldspars. Sandstone beds are commonly fine to medium grained with sporadic coarse beds up to 50 cm thick. Coarser sandstone beds host small elliptical features of dark muddy material (see Figure 2.6d) which may represent rip-out clasts of lower mudstone beds or bioturbation.

In Unit 4c, a minor turbiditic sequence of brown mudstones and medium to very coarse arenitic sandstones is exposed. This sequence is interpreted as a separate sandstone lithology based on a dominant siliciclastic component rather than volcaniclastic. Sandstone components host juvenile rip-out clasts of underlying cherts and purple mudstones (see Figures 2.6e and f).

Tectonic units

Localised 'mélange units' develop from mechanically weak lithologies in high strain zones and around at lens interfaces, particularly where they are juxtaposed against stronger units. In Area I, these tectonic units develop in mudstones and clast-poor hyaloclastites. Units are no thicker than 20 m and consist typically of a highly sheared matrix that hosts fragments of lithologies primarily sourced from neighbouring units.

Mudstones are the most widespread host rocks for mélange beds. Sandstone clasts are most common, whilst basalt and jasper are also frequently abundant (see Figure 2.8a and b). Rarer examples of chert, silty mudstone (see Figure 2.8c), dolomite, and mudstone clasts have also been observed. Clasts are rounded to subangular, ranging generally from millimetre to decimetre scale, although larger clasts up to 2 m in length are found in the mélange beds of Unit 12 (see Figure 2.8c and d). Clasts are also uniformly orientated with long axis parallel to foliation and commonly develop tails through shearing. Foliation typically deflects around clasts (see Figure 2.8e).

The clasts of mélange beds in Unit 9 (SH 3853 6264) have previously been interpreted as dropstones (Kawai et al. 2008). The study describes preferential distortion of laminae around the base of clasts; however, laminations were generally observed to deflect above and below clasts. Along with the aligned orientation and deformation of clasts, this suggests that distortion is a result of tectonic shearing rather than soft sediment impact deformation. Clast lithologies also originate entirely from units found in Gwna Complex Area I, with concentrations of clasts correlating with surrounding units.

To justify this, dropstones would have to originate from glacially eroded material from higher, subaerial components of the Gwna Complex and deposited in active sedimentary environments. This is highly unlikely since other study areas of the Gwna Complex – discussed below – exhibit voluminous amounts of other clastic lithologies that have not been described in Area I.

The mélange beds at Unit 9 occur at the upper interface of the unit. At the described locality of the dropstones, the mélange is bordered by more competent sandstone horizons and an overlying pillow basalt exhibiting localised shortening of pillows. The vast majority of clasts in the mélange are sandstone, basalt and jasper, suggesting that clasts from both margins have been incorporated into the mudstone through intensive shearing, as shown in Figure 2.7. Although clasts show consistent shear flattening parallel to foliation, evidence of asymmetric shear deformation is relatively rare and unpronounced.

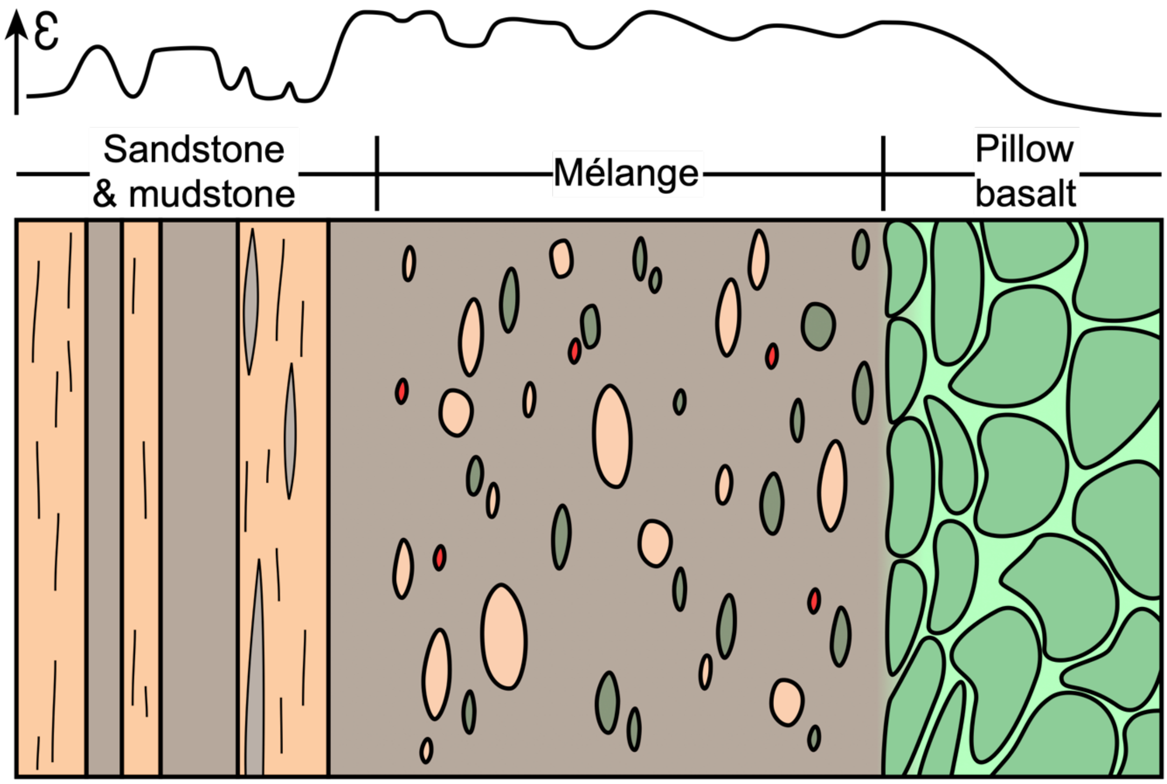

Figure 2.7: Schematic cross section across lens interface (ca. 10 m wide) at the top of Unit 9 showing the formation of mélange along a highly sheared mudstone horizon showing the incorporation of orientated clasts from the relatively competent bordering lithologies of sandstone and pillow basalt (with jasper). The upper sandstone-mudstone sequence becomes locally boudinaged while pillow lavas undergo shortening around the interface.

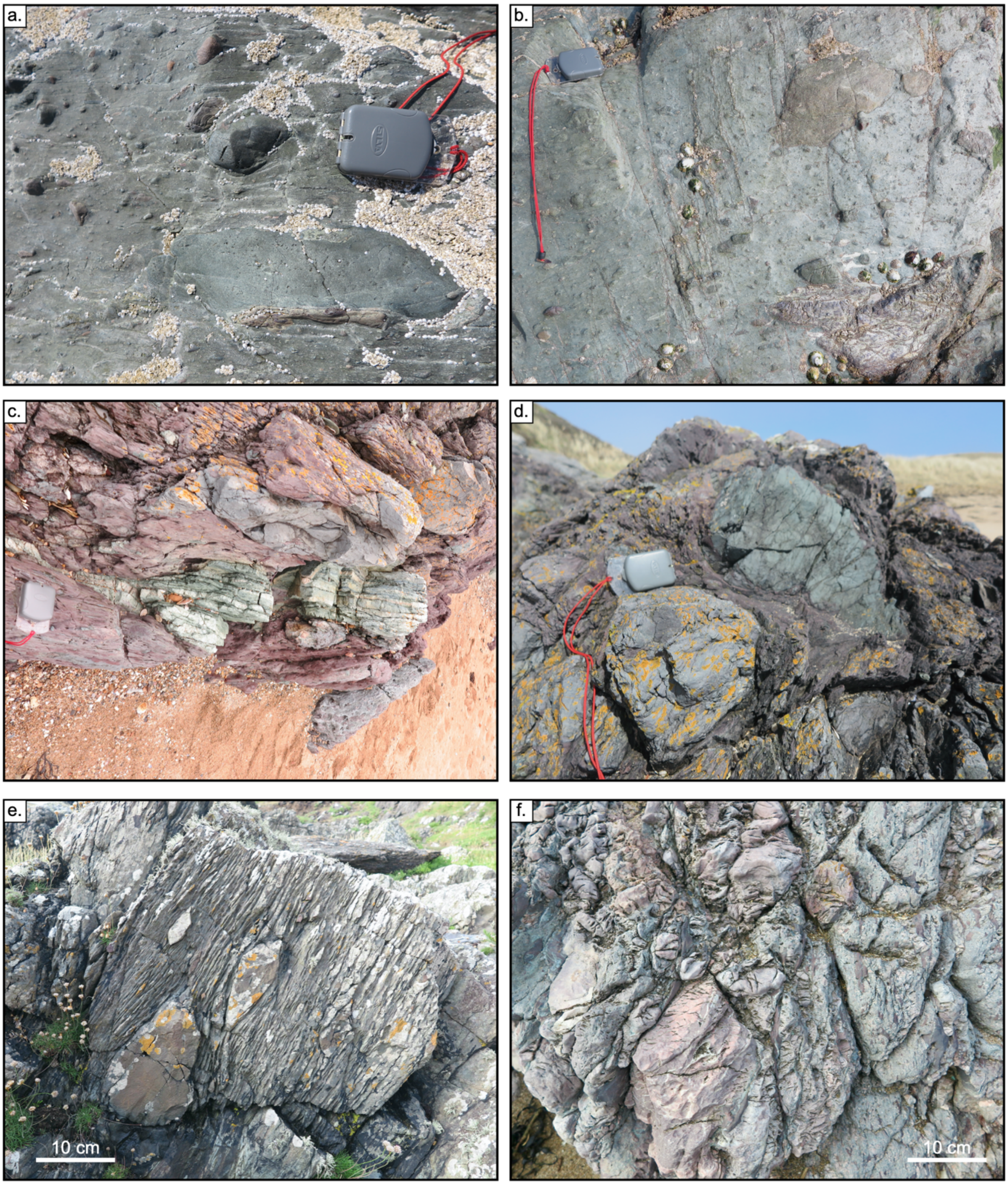

Figure 2.8: Examples of localised mélange formation in Gwna Complex Area I showing (a-b) assortment of clast types within a light green mudstone matrix (SH 3848 6252); (c-d) large clasts within a red mudstone matrix above Unit 12 (SH 3886 6279) showing the inclusion of a large, elongate siliceous mudstone clast along with sandstone and basalt clasts; (e) sandstone clasts in a mudstone matrix above Unit 9 (SH 3862 6283) showing foliation deflected evenly around clasts and elongation of clasts parallel to foliation; and (f) white/pink dolomite clasts within a light green hyaloclastite matrix with deformed purple basalt clasts of magmatic origin (SH 3858 6242).

In the South of Llanddwyn Island, a hyaloclastite with low clast density acts as a matrix for small-scale mélange formation, incorporating blocks of dolomite from the adjacent unit within a high shear assemblage (see Figure 2.8f). Dolomite clast abundance dissipates away from the contact between the units, suggesting mixing along a single interface. This is a distinct difference from the mudstone mélange beds, where clast mixing appears to be sourced from both margins, homogenising clast distributions.

2.3.2 Low shear semi-coherent units

Elongate lenticular slices of largely undeformed material that preserve original magmatic and depositional details, are interwoven between areas of highly sheared, dismembered sequences that do not retain stratigraphic context. Of the 16 preserved stratigraphic sequences outlined in Figure 2.9a, six preserve multiple lithologies that retain stratigraphic order. The remaining nine sequences consist of single lithologies – seven of which are pillow basalts, one of which is basalt-carbonate (Unit 15) and another that comprises chloritic sandstone (Unit 11). The size and extent of most lenses is uncertain due to exposure limitations, however Unit 4 shows that they can extend over several kilometres in length, with stratigraphic thicknesses of several hundred metres.

The six semi-coherent imbricate slices present largely repeating sequences – or parts of sequences – that each have their own stratigraphic or textural variations as outlined by stratigraphic logs (A-H) in Figure 2.9b. Three separate logs have been constructed for Unit 4 (logs A-C) to compare lateral changes in stratigraphy across the largest exposed lens in the area. Unit 4 is offset by two notable strike-slip faults that naturally segment the lens into three components (Unit 4a-4c). The logs have been constructed using a baseline where sedimentary components are first introduced. The basal magmatic sequences are interpreted to represent upper lithosphere material, the upper surface of which marks the sea floor. This baseline is useful to denote the relative thicknesses of both volcanic and sedimentary domains between units.

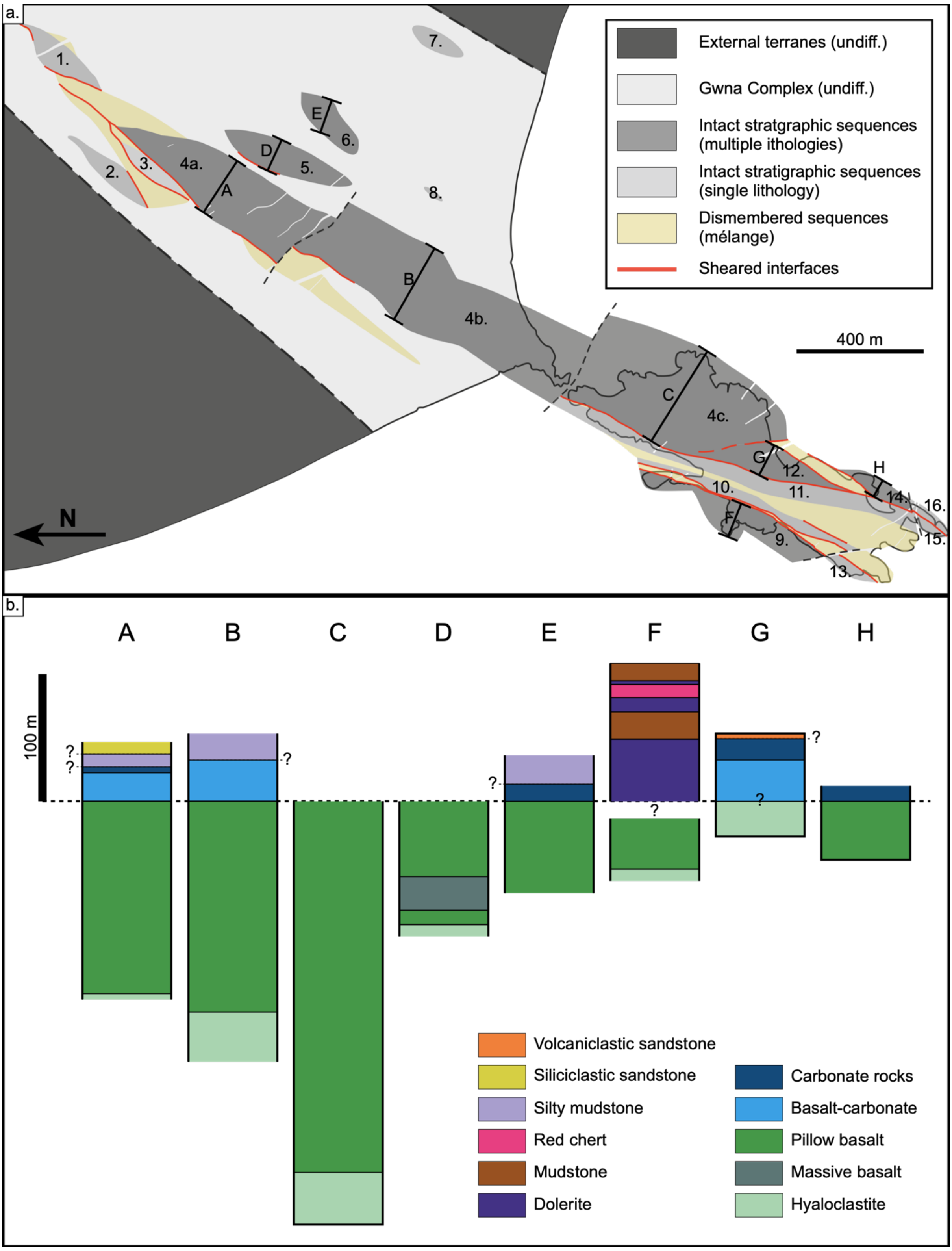

Figure 2.9: Tectonic map of Newborough (Gwna Complex Area I) with logged transects (A-H) of stratigraphic successions from low shear units with multiple lithologies, where stratigraphic uncertainties caused through lack of exposure are highlighted using the symbol '?'.

Each log – with the exceptions of Logs F and G – consists of a substantially thicker basal magmatic component than overlying sedimentary component. Magmatic domain thickness ranges from roughly 30 – 350 m thick. Six of the eight logs are marked by basal hyaloclastites – the least coherent rock type in the igneous substrate. Out of the 14 units that include basal magmatic components, only five (Units 1, 3, 10, 14 and 16) have observed lower interfaces not marked by a hyaloclastite. Pillow basalts are the main lower magmatic component in all logs except for Log G. In five examples of recorded magmatic-sedimentary transitions, carbonates directly overlie basalts in all cases, either through a basalt-carbonate transitional unit or through an apparently sharp transition to carbonate rocks. Direct upper contacts between carbonate rocks and overlying sedimentary rocks were not observed in any units. In Unit 4a, a potential contact with overlying silty mudstone is obscured and may not show a conformable contact. Silty mudstones are observed overlying carbonates in three of four examples, however. Sandstones (both volcaniclastic and siliciclastic) are observed at the top of both sequences in which they occur in (Logs A and G). Additionally, Unit 11 shows a volcaniclastic sandstone – with no observed links to lower stratigraphy, due to lack of exposure – in contact with the base of overlying Units 4c and 12, indicating that it sits at the top of an underlying succession. The logs show that stratigraphic successions are only partly preserved, but key stratigraphic relationships may be used to recover a composite stratigraphy.

Identified low shear units are generally buffered by high shear mélanges around unit interfaces, however there are potential examples of direct unit contacts. The contact between Units 4c and 12 is ambiguous due to lack of exposure but outcrops seem to suggest a boundary marked by the basal hyaloclastite of Unit 4. The relationship of the hyaloclastite to Unit 12 is unclear as it appears to split along the bases of both units. In outcrops along the northern coast of Llanddwyn Island (SH 3906 6344), textural differences marked by slip planes may represent the stacking of hyaloclastite components. Whether the basal hyaloclastite of Unit 12 is indeed a representation of volcanic stratigraphic succession or is part of the interfacing mélange is uncertain. Additionally, the contact between Unit 11 and various overlying sequences (Units 4c, 12 and 14) is marked by a localised high shear contact, while sedimentary features are preserved throughout the unit otherwise. Units 14, 15 and 16 are also marked by localised zones of intense deformation over 1 – 5 m along interfaces.

Log A (Unit 4a)

Log A represents the most lithological diversity of the stratigraphic sequences on Newborough, preserving six distinct lithologies (seven represented in total in Unit 4a). Log A best demonstrates the gradational transition between pillow basalts and carbonate rocks, via the transitionary lithology of basalt-carbonate, as explained in Section 2.3.1. Contacts between the carbonates and overlying silty mudstone, and between the silty mudstone and overlying sandstone are unexposed. Some internal slip must be present along the upper margins of Unit 4a, as the stratigraphic order of silty mudstones and siliciclastic sandstones is locally inverted. While both seemingly occur above of each other at different localities, rip-out clasts of juvenile chert and purple mudstone clasts found within coarse siliciclastic sandstone beds indicate that the siliciclastic sandstones overlie the silty mudstones stratigraphically.

Towards the north of Unit 4a, volcaniclastic sandstones are found overlying silty mudstones, while siliciclastic sandstones become notably absent – not shown by Log A. The rip-out clasts provide direct evidence of siliciclastic sandstones directly overlying the silty mudstones, while no such evidence was found from the volcaniclastic sandstones. The units are both turbiditic and occupy similar positions towards the top of the stratigraphic succession.

Log B (Unit 4b)

Log B shows great similarities to Log A, containing a slightly thicker pillow basalt component (approximately 10 – 20 m difference). It also exposes a more substantial basal hyaloclastite component, measuring up to 20 m thick. The carbonate component is very similar in thickness to Log A. Although only basalt-carbonate rocks were recorded, it is possible that carbonate rocks are present towards the top of the unit but not exposed. Carbonate rocks are also overlain by silty mudstones, which occur in greater thickness that in Log A. The contact between the lithologies is not observed however, so stratigraphic continuity is questionable.

Log C (Unit 4c)

Unlike Logs A and B, Log C does not include an upper sedimentary, as it presumably continues offshore to the east of Llanddwyn Island. The pillow basalt component of Log C is notably thicker than Logs A and B, and is the thickest recorded unit in Area I by over 100 m (ca. 300 m total thickness). This continues a trend of progressive thinning of the pillow basalts towards the north throughout Unit 4, presumably since Unit 4 seemingly pinches out to the north, while its southern extent is unknown and likely continues offshore. Structural interpretations of Llanddwyn Island by Maruyama et al. (2010) determined that Unit 4c represented a duplex consisting of X sheared horses. No evidence was uncovered to support any systematic shearing has occurred across the unit, and it is considered to be a single, continuous succession.

Basal hyaloclastites make up the only other recorded lithology in Log C, and shows a comparable thickness to Log B, being slightly thicker but also providing a lower contact that is not exposed in Log B. As mentioned, there is potential evidence of stacked hyaloclastites at the base of Unit 4c.

Log D (Unit 5)

Log D also contains only igneous lithologies without any observed overlying sedimentary rocks. A small exposure of hyaloclastite marks the observed lowest lithology. Within the pillow basalt sequence, is a substantial massive basalt component roughly 30 m thick, which is laterally continuous. It is expected that the massive basalt is a result of changing variables within volcanic processes that formed the pillow basalts, and that the unit does not hold major significance in terms of the stratigraphic record, given that pillow lavas occur both stratigraphically above and below.

Log E (Unit 6)

Like Logs A and B, Log E contains silty mudstone overlying carbonate rocks, but with no direct contact exposed. The transition between lower pillow basalts and overlying carbonate rocks is also poorly exposed although progressive reddening on upper pillows were observed. The presence of a basalt-carbonate component is unclear, although given the relatively low thickness of the carbonate component, this may represent a shorter transitional phase not buffered by mingling basalt as in Log H.

Log F (Unit 9)

Unit 9 is the most unique lithological sequence preserved in Area I. It contains two lithologies not found elsewhere – in Area I or any other areas of the Gwna Complex. It also contains thick packages of mudstones that are only seen elsewhere in dismembered high shear mélange. A lower basaltic component is ambiguous, but a series of vesicular pillow basalts with a lower hyaloclastite are observed in contact with mudstones, sharing the tectonostratigraphic position of the lowest dolerite sill. These vesicular basalts at the northern headland of Unit 9 (AN18014; see Figure 2.4b) may correlate to vesicular pillow basalts in the southern Unit 13 (AN18031; SH 2385 3626). The unit accommodates lateral slip along the mudstones to accommodate the contact with both basalt and dolerite but is difficult to determine given the intensely foliated nature of the mudstones and bedding-parallel shearing. Any evidence of transition between basalt and carbonate rocks – as seen in other logs – is missing, also likely because of shearing.

Dolerite sills of variable thickness (0.2 m – 50 m) are seen to intrude red cherts and are therefore considered to post-date the pillow basalts, along with some of the lower sedimentary stratigraphy observed in other logs. Thicker bodies exhibit well developed chilled margins and several relatively thin intrusions < 1 m thick (AN19026; see Figure 2.10a) are relatively fine grained. The sills are not continuous beyond the bounds of Unit 9 and are considered to have intruded before regional shearing. Their potential chemical relationships to surrounding igneous rocks and the larger igneous system in Newborough is explored further in Section 4.4.3.

The upper surface of Unit 9 is marked by a distinctive hyaloclastite (AN19029; see Figure 2.10c and d) roughly 3 m thick with a high volatile content. The hyaloclastite is dissected heavily by chaotic networks of carbonate veins and basalt clasts are highly distorted. Jasper is common and has been overprinted by densely packed carbonate rhombs with pink cores grading into white edges. Directly above a sheared contact, another hyaloclastite (AN19030; see Figure 2.10b) exhibits more common textures and much lower fluid concentrations, marking the transition interface of Unit 9. This is a unique example of a hyaloclastite occurring in the upper domain of a sequence, and it may represent a minor extrusive component related to the intrusive dolerite sills, whose presence within the sedimentary domain already indicates near-surface magmatic activity.

Aside from the potential secondary phase of magmatism recorded in Unit 9, the sedimentary succession does not correlate directly to logged successions from other units. Cherts are found elsewhere as layers within silty mudstones, but not as continuous chert deposits. The mudstones of Unit 9 are seen elsewhere in mélanges but not in preserved stratigraphic successions. Due to the intense bedding-parallel shearing of the unit, its relationship to the red cherts is unclear, although they units may be thickly interbedded. Both lithologies have similar pelagic depositional environments. The deep colours of the mudstones are similar to the mudstone components in the silty mudstones.

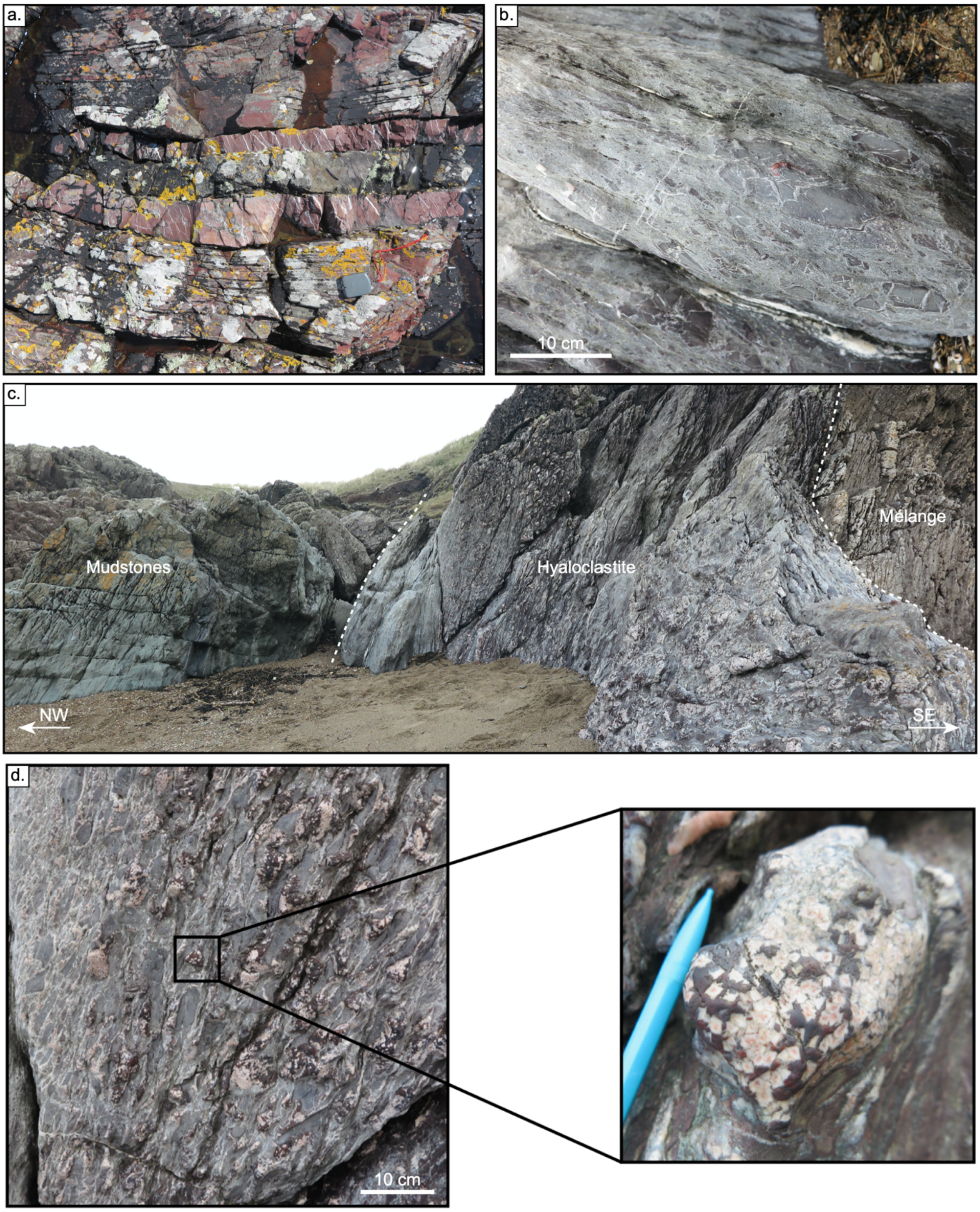

Figure 2.10: Distinguishing features as evidence of a secondary magmatic event preserved in Unit 9 including (a) small dolerite sill intruding layered red cherts (AN19026; SH 3867 6293); (b) hyaloclastite from the overlying high-strain shear zone (AN19030) showing textures commonly observed from lower magmatic sequences; (c) hyaloclastite overlying mudstones in the upper stratigraphy of Unit 9 (AN19029; SH 3864 6282); (d) the unique texture of the upper hyaloclastite with dense networks of carbonate veins, high carbonate concentrations within the matrix, and carbonate rhombs imposed on the surfaces of abundant jasper blocks.

Log G (Unit 12)

While not exposed, it is possible that a small amount of pillow basalt separates hyaloclastite from overlying basalt-carbonate – assuming that the hyaloclastite is part of the stratigraphic succession. This is likely due to the nature of the lower basalt-carbonate units, which comprises complete, densely packed pillows rather than smaller basalt fragments with a hyaloclastic texture. The contact between carbonate rocks and overlying volcaniclastic sandstone is once again ambiguous.

Log H (Unit 14)

The smallest unit of stratigraphic sequences containing multiple lithologies, Log H shows pillow basalts overlain directly by carbonate rocks, with only a small amount of the sequence exposed. It accommodates a much shorter and sharper transition between basalt and carbonate than seen in Logs A, B and G. Unlike other units, Unit 14 is not marked by a hyaloclastite component at the base, and instead is in contact with several relatively sheared lithologies. Towards the base, pillows are locally shortened over ca. 5 m thickness, leading to the localised development of parallel foliation.

2.3.3 Heterogeneous deformation

Within low shear units, coherence is disrupted by internal slip, particularly in the upper sedimentary domain. The widely variable mechanical properties of the juxtaposed lithologies, results in sheared horizons within weak horizons such as hyaloclastites and mudstones – both of which have high phyllosilicate contents. The exploitation of structural weaknesses along continuous hyaloclastite horizons is a likely mechanism for sampling the relatively thick magmatic suite that is preserved in the Gwna Complex. Intermittent weak mudstone layers are likely the reason for commonly disrupted upper sedimentary domains. Interestingly, basalt-carbonate units are also relatively weak, with highly altered reddened basalt components providing a structural weakness that may coalesce into slip planes. Silty mudstones, however, are relatively strong as pervasive folding prevents slip along mudstone layers. The behaviour of these different lithologies within shear zones on Llanddwyn Island is discussed in much greater detail by (Leah et al. 2022).

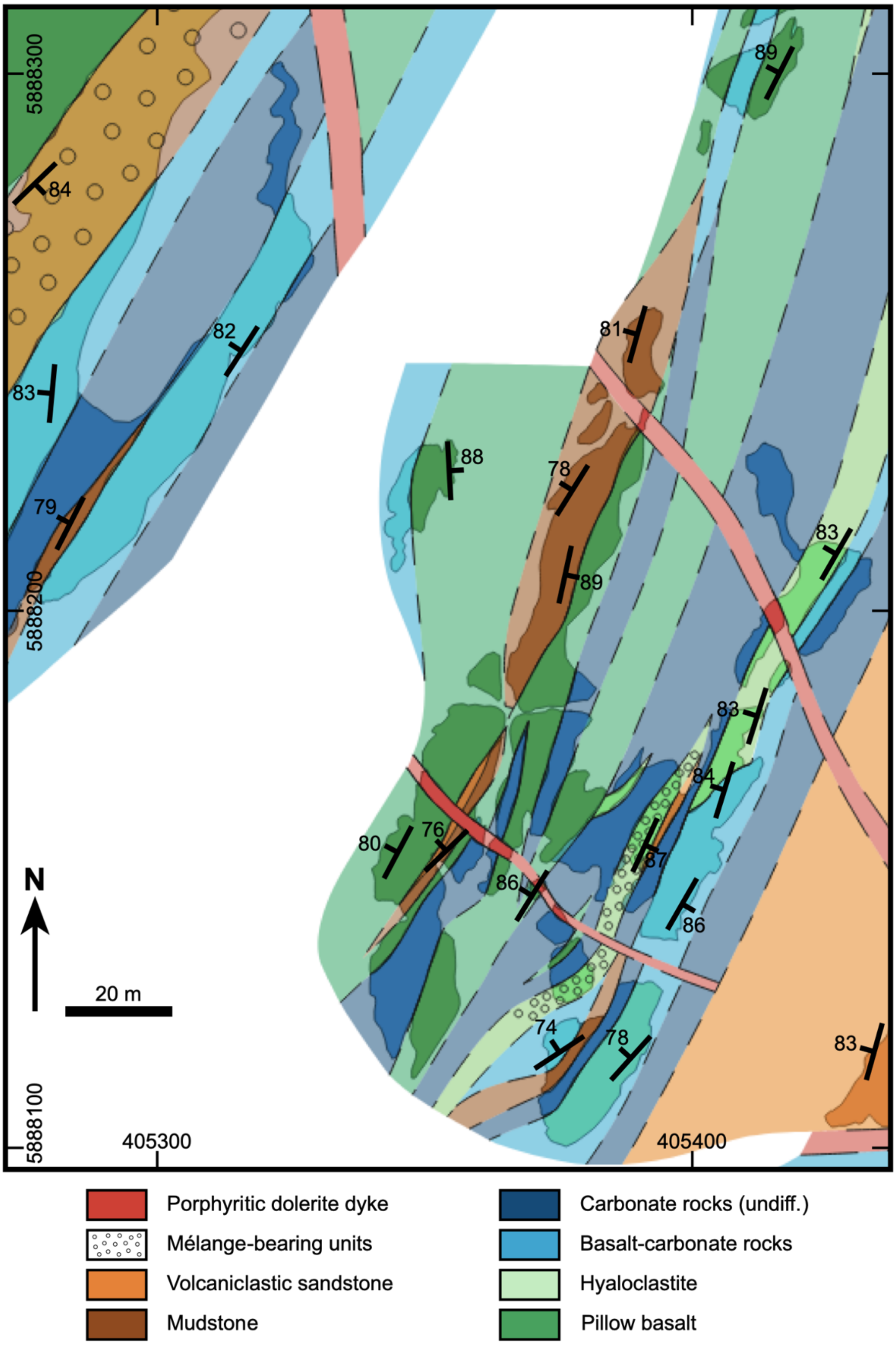

Figure 2.11: Geological map of southern Llanddwyn Island (Gwna Complex Area I) showing a well-exposed high shear mélange zone comprising thinly imbricated units of various lithologies juxtaposed with no stratigraphic order where units can be seen regularly pinching out and the formation of localised mélange-bearing units.

Low-strain shear unit interfaces are highly sheared thrust zones of variable thickness (5 – 20 m) that mark the transition from low shear to high-strain shear zones (see Figure 2.7). Upper unit interfaces were rarely observed but typically occur along pelitic horizons within sandstones (eg. Units 11 and 12), while lower interfaces are marked by hyaloclastites most commonly, or by pillow basalts. Mudstones and hyaloclastites are both rich in phyllosilicates and highly foliated from shearing, and may become mélange-bearing (eg. Unit 9 and 12). Pillow basalts at unit interfaces (eg. Unit 14) typically undergo shortening, which results in elongation parallel to shearing and may lead to development of a localised foliation.

High-strain shear zones between coherent lenticular units comprise the same suite of lithologies, but components are generally thinner and lack any evidence of stratigraphic succession, instead being juxtaposed through shearing. While block-in-matrix mélange is a common occurrence in other areas of the Gwna Complex, the mélange in Area I consists of disorganised fragments imbricated directly against one another, rather than being suspended in an encompassing matrix – with the exception of localised mélange-bearing beds discussed in Section 2.3.1. Large-scale tectonic deformation is therefore accommodated predominantly by these juxtaposed fragments.

High-strain shear assemblages are best exposed in southern Llanddwyn Island, shown in Figure 2.11. Intense deformation is seen even in mechanically stronger units such as pillow basalts and carbonates. Pillow basalts are plastically deformed, elongating, and distorting pillow textures, and can also be subject to size reduction and foliation development in increasing interpillow spaces (see Figures 2.12e and f). A prime example of carbonate deformation shows a dolomitic unit (ca. 5 m thick) that has been entirely brecciated and recemented by a dolomite matrix (see Figure 2.12d). Rotated sets of multiple vein generations show that the brecciation is not a sedimentary texture, while small dolomitic veins crosscut neighbouring units. The eastern interface also develops a localised mélange within the bordering hyaloclastite.

Deformation within the high-strain shear zones is also seen to be heterogeneous. In the northern section of the mapped area, silty mudstones to the north of Unit 3 are relatively well preserved (SH 3995 6495), albeit with no stratigraphic context. Tracing the lithology southwards in the mélange buffering Units 2 and 3 however (SH 3983 6490), the silty mudstones are highly disintegrated, with fragmented chert clasts scattered throughout the foliated mudstone component that now acts as a uniform matrix. This may be due to a localised increase in strain due to the closer proximity of two low shear units.

2.3.4 Kinematic indicators

Various way-up indicators suggest that Area I rocks have been uniformly tilted steeply towards SE, including pillow orientation, intermittent hyaloclastite horizons and grading of basalt-carbonate units. Despite the abundance of high-strain shear zones and various clast-bearing assemblages, kinematic shear indicators such as clast asymmetry are rare. Shear flattening of clasts is extremely common in mélange beds, hyaloclastites and basalt-carbonate units, for example. Rare shear indicators from veined clasts are observed in hyaloclastites, such as in southern Llanddwyn Island (SH 3866 6243; see Figure 2.12d), where a quartz vein intersecting an elongated pillow indicated downstepping of units towards NW (downwards movement of NW block relative to SE block across subvertical shear zone). Rare and often poorly defined examples of asymmetric strain in mélange bed clasts support these kinematics. Minor bedding-parallel isoclinal folds in the red cherts of Unit 9 (see Figure 2.12a) also indicate downstepping of NW blocks. Microscale interactions between slip planes and veins within highly sheared material from southern Llanddwyn Island consistently support these kinematics (Leah et al. 2022; in press). Additionally, the consistent 10-20˚ difference in dip angle between bedding and cleavage is also consistent with an overall shear sense of downstepping NW.

Folded silty mudstones verge predominantly SE (see Figure 2.12c), with a minor oblique folding component along subvertical fold axes. Faults propagate from the folds fracturing chert and silt layers, while mudstone components infill fractures and incorporate fractured fragments. This soft sediment deformation of partially lithified sediments must predate regional-scale shear deformation, in which the folded units act competently. Folded chert sequences are common in subduction zone settings. They remain soft sediments until hardening through diagenesis at conditions within a subduction zone, meaning that initial slumping towards the trench and early subduction-driven folding are common (Kameda et al. 2017).

Consistent kinematic indicators across Newborough show that units throughout Newborough are orientated subvertically towards the SW, imbricated along high-shear zones. Repeated lithological sequences suggest that blocks have been emplaced in imbricated and repetitive units progressively from the NW.

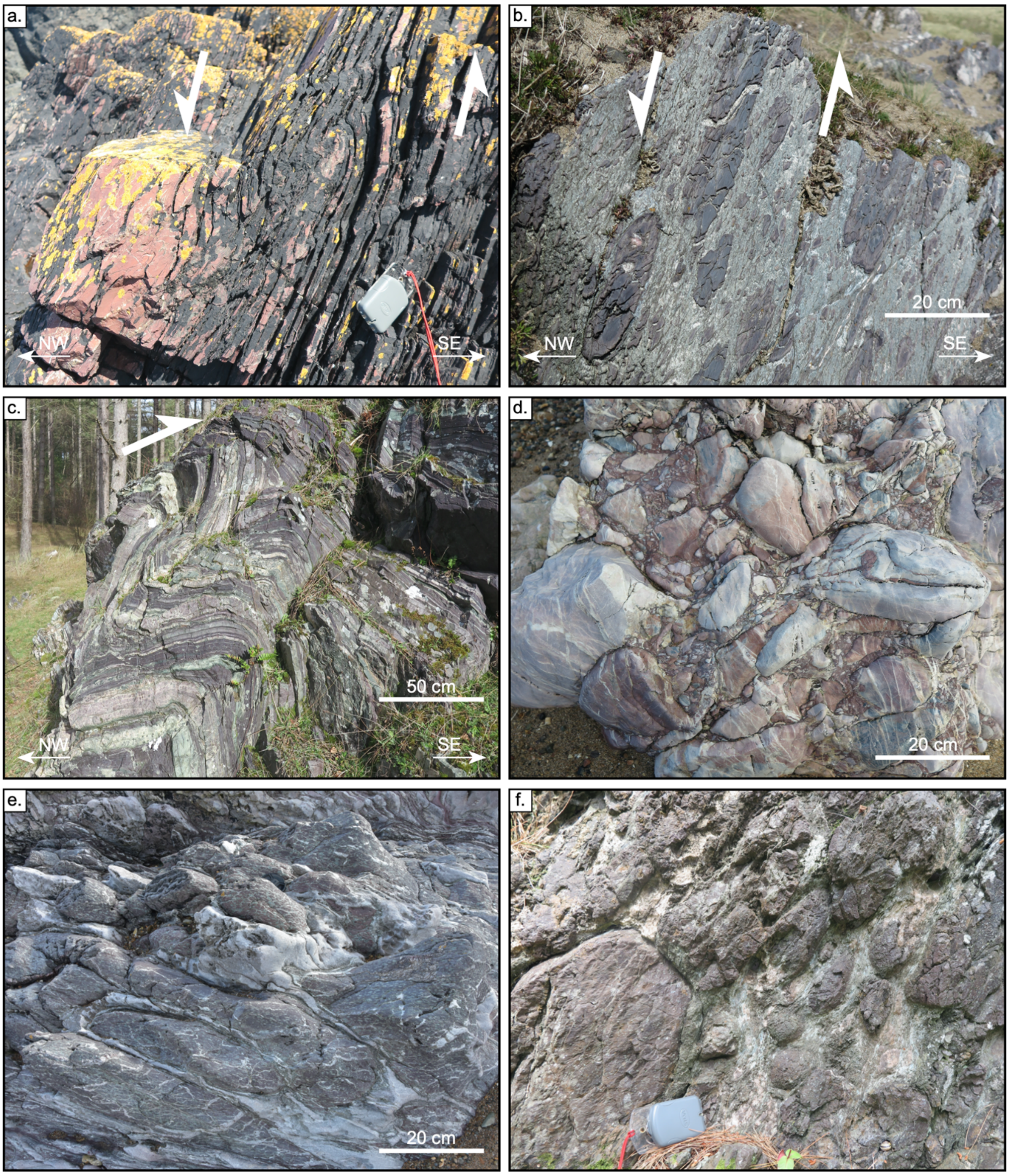

Figure 2.12: Various deformation features and kinematic indicators from Gwna Complex Area I showing (a) small isoclinal folds in layered red cherts showing downstepping of NW block (SH 3862 6286); (b) elongated basalt pillows within a hyaloclastite matrix with a sheared pre-deformation vein that indicates downstepping towards NW (SH 3861 6247); (c) silty mudstone sequence in Unit 4c (SH 3960 6422) showing pre-shearing folds that verge SE; (d) dolomite breccia from a high-strain shear zone (SH 3857 6241) showing brittle disaggregation of a carbonate unit and further cementation by dolomite, while vein orientations show clast rotation; (e) deformed pillow lavas elongated parallel to foliation within carbonate-rich matrix from high-strain shear zone (SH 3852 6246); and (f) shortening and reduction of pillow lavas and formation of a localised foliation fabric (SH 3957 6403).

2.3.5 Area I linkage to Pentraeth

Figure 2.1 highlights two outcrop zones in Gwna Complex Area I – Newborough, and a small concentration of isolated outcrops around the village of Pentraeth (SH 52 78). These have been interpreted by Schofield et al. (2020) as a continuation of a single, continuous unit (Area I) along the NE-SW striking BSZ, as shown in the map of Figure 2.1. Outcrops in Pentraeth are limited to a small series of crags concentrated in NNE-SSW orientations, largely obscured by farmland and vegetation. They are dominated by pillow basalts with subvertical SE-dipping orientations (eg. AN19036; SH 5242 7777), consistent with those in Newborough. The pillows are 50 – 70 cm in diameter and largely undeformed, with a chloritic interpillow matrix with occasional examples of jasper. Minor outcrops of dolomitised yellow-white dolomitic carbonate rocks were also observed. These carbonates are representative of those observed in Newborough and showed no similarities to the fossiliferous, bedded, calcite-dominant Carboniferous limestones found nearby.

Like in Newborough Forest, the thicker, less deformed basalt sequences form topographic highs and are preferentially exposed, while very little other material is exposed. While there is no evidence of continuous exposure of Area I along the BSZ between Newborough and Pentraeth, there are clear consistencies between the areas to justify linking them as an inferred single unit. At the very least, these outcrops in Pentraeth do appear to represent Gwna Complex material.

2.4 GWNA COMPLEX – AREA II (LLŶN PENINSULA)

Area II extends approximately 20 km along the northern coast of Llŷn Peninsula – between Morfa Nefyn and Aberdaron – and continues onto Bardsey Island, situated 3 km offshore to the west of the mainland. It is bound to the south by the NE-SW trending LSZ that runs roughly parallel to the coastline through the centre of the peninsula. The area consists largely of various assemblages of schists and large-scale mélanges with sporadic occurrences of igneous rocks with overlying sedimentary sequences that resemble the framework that dominates Area I.

2.4.1 Preserved oceanic sequences

Magmatic rock occurrences are relatively uncommon in Area II and tend to be appear in concentrated areas across Llŷn Peninsula. Four key localities are described below. Basaltic rocks in Area I are associated with overlying sedimentary sequences, and these have also been recognised in Area II at Porth Felen. Substantial preserved sequences are otherwise seemingly absent, but evidence of dismantled sequences is found within some of these concentrations of basalts, such as Morfa Nefyn and Porthorion, which also host sedimentary lithologies of oceanic origin.

Morfa Nefyn

The headland at Porth Dinllaen (SH 27 41) – and along the bay towards Penrhyn Nefyn – consists predominantly of pillow basalt (see Figure 2.13). Penrhyn Nefyn (SH 29 41) marks the contact between the Gwna Complex and the Arfon Terrane across the LSZ. The Gwna Complex side of the shear zone is marked by intensely deformed, highly foliated basaltic schist with localised mylonitic zones. Foliation and mylonitic zones are orientated NE-SW, parallel to the shear zone, and dip NW at 30-50˚. Despite the intensity of deformation, basaltic schists remain at sub-greenschist facies mineralogy with no presence of amphiboles. Westward away from the shear zone, deformation intensity is progressively alleviated, and Porth Dinllaen peninsula consists of undeformed pillow basalt sequences with sporadic hyaloclastites (see Figure 2.17a).

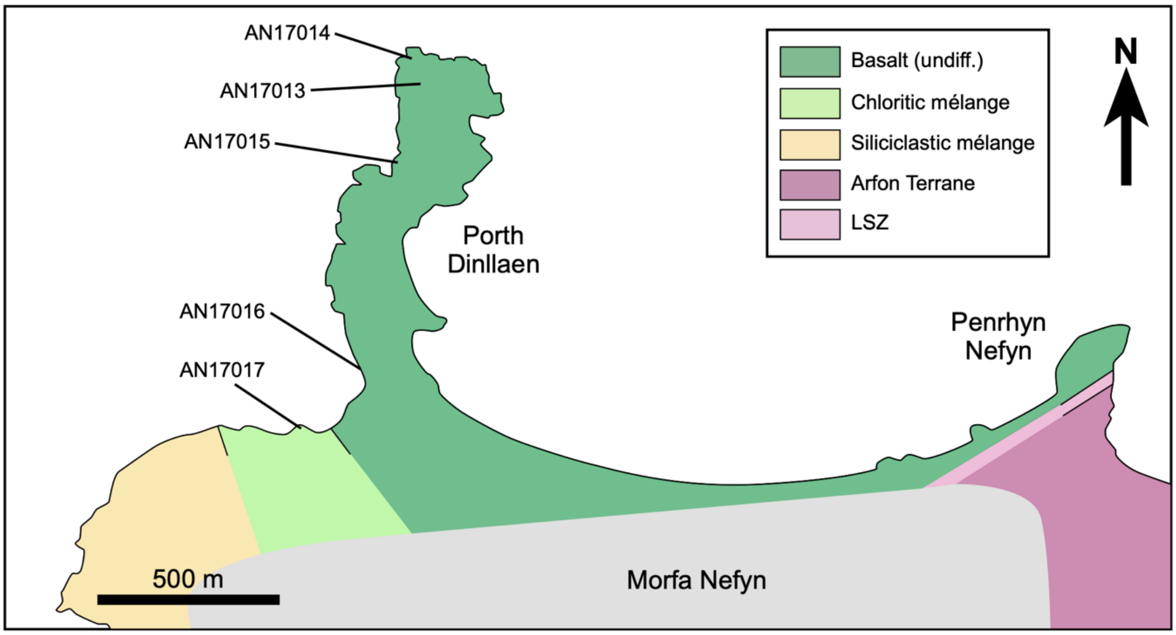

Figure 2.13: Simplified geological map of Morfa Nefyn after Gibbons and McCarroll (1993); Kawai et al.(2007) showing sample localities from the area.

The pillow basalt sequences consistently dip subvertically SE and are occasionally overturned, much like exposures in Area I. Pillow sequences are up to 200 m thick and are dissected by fault planes. The pillow basalts are green, vesicular and aphyric, with no examples of haematite-rich sequences, and contain high amounts of jasper. They tend to be smaller (30 – 40 cm) on average than those in Area I. While jasper is typically found between in interpillow spaces and drain cavities in basalts of the Gwna Complex, jasper at Morfa Nefyn also frequently infills fractures as veins and vesicles as amygdales (eg. AN17013; SH 2763 4179).

Faulted blocks of chloritic schists are juxtaposed regularly against the pillow basalts. At the western base of the peninsula (SH 273 411), a NW-SE trending faulted contact marks the extent of the pillow lavas, and coastal outcrops to the west are dominated by chloritic schists. The schists are light green and are populated by calcite veins that increase in density towards fault zones. Elongate sandstone clasts (< 10 cm length) are scattered throughout along a moderate foliation that while locally variable, dips steely along a NE-SW strike. Clasts of dolomitic carbonate and purple mudstone sit sporadically within the schist, along with small lenses of potentially highly deformed basalt – or a basaltic breccia such as a hyaloclastite (eg. SH 2721 4108).

Porth Iago

To the south of Porth Iago (SH 16 31), multiple basaltic clasts outcrop within chloritic schist and purple mudstone matrices and are particularly prominent at Trwyn Glas (SH 165 311), where relatively undeformed pillow structures show a SE dip direction. Smaller outcrops are generally heavily faulted and deformed. Minor carbonate clasts and silty mudstones are also included as clasts within the purple mudstone matrix.

Porth Oer – Porthorion

Outlying headlands of pillow basalt occur at Dinas Bach (SH 157 293), Dinas Fawr (SH 155 290), and Porthorion (SH 155 286), along with inland outcrops at Capel Carmel (SH 161 291) as shown in Figure 2.14. The pillow lavas show a generally shallow dip (30-50°) SE, as opposed to the subvertically tilted outcrops at Morfa Nefyn. Pillows tend to be moderately deformed, with magmatic textures commonly obscured. The sequences here do not seem to show any preservation of stratigraphy, and the basaltic headlands have faulted contacts with the bay side outcrops. The bay side outcrops exhibit a mélange consisting of a highly foliated purple/green mudstone matrix that host various clasts of silty mudstone, basalt, carbonate, and basalt-carbonate rocks up to 50 m in length.

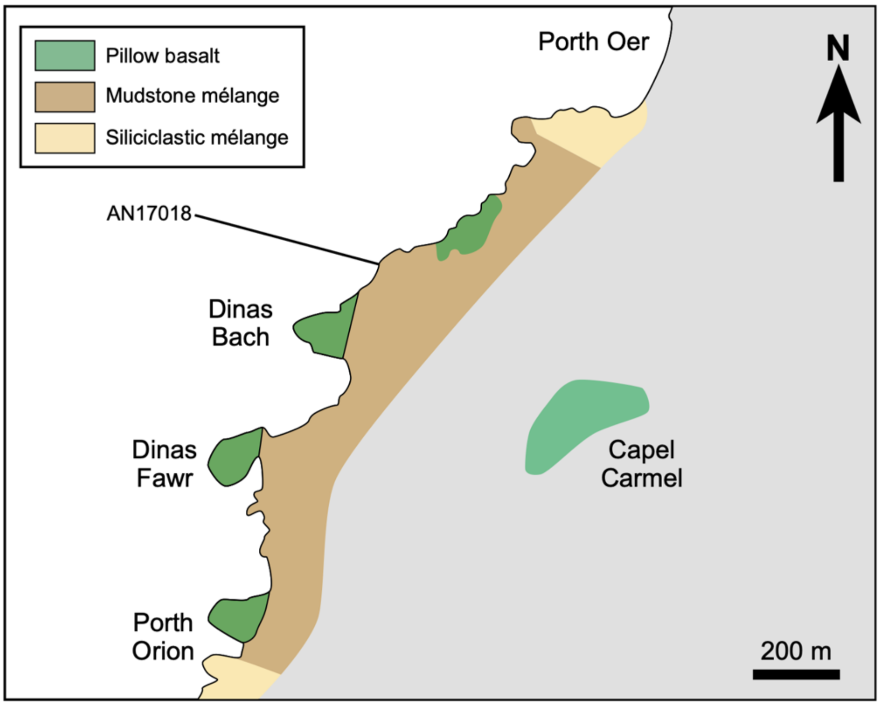

Figure 2.14: Simplified geological map of area from Porth Oer to Porthorion after Gibbons and McCarroll (1993); Saito et al. (2015) showing sample localities from the site. Pillow basalt units highlighted are relatively undeformed, while basalt and basalt-carbonate clasts are common within the mudstone mélange but are more substantially deformed.

Unlike the headlands, basalt clasts in the mélange are reddened by the presence of haematite and are highly disrupted by carbonate material that intersects pillows as chaotic networks of dolomitic veins with varying density between clasts (eg. SH 156 291). To the south of Dinas Fawr, a carbonate-rich basalt clast is juxtaposed – with a small amount of intermittent mudstone matrix – against a large basalt-carbonate clast that extends southwards for approximately 50 m across the seafront (SH 156 289). The basalt-carbonates are carbonate-dominated, comprising approximately 80 % of the rock volume, evenly distributed throughout the clast (see Figure 2.17e and f). The clast has undergone significant deformation, regularly fracturing the carbonates and infilling spaces with more malleable, highly altered basalt. In more extreme conditions, strands of basalts coalesce along fracture planes, producing small-scale block-in-matrix textures. There is evidence of true peperitic interactions between the components, with angular, irregular-shaped basalt clasts dispersed within unfractured carbonate host material. These features were not observed from similar occurrences in Area I.

Porth Felen

The area between Trwyn Maen Melyn (SH 13 25) and Trwyn Bychestyn (SH 14 24) exhibits pillow basalts preserved from two distinct settings (see Figure 2.15). The area around Trwyn Maen Melyn is characterised by a regional-scale, deformed mélange consisting of siliciclastic pelite schist matrix hosting rounded (mega)clasts of Gwyddel beds, quartzites, carbonates and basalts. Along the coastal headland of Trwyn Maen Melyn, an approximately 100 m long exposure of deformed, reddened pillow basalts (AN19022; see Figure 2.17d) sits at the edge of the mélange bound by schists to the north and sitting along a fault to the south. Small (< 2 m) lenses of calcite-dominant carbonate rocks and mudstones have been emplaced within the pillow basalt unit along fault planes. The pillows dip SE, elongated along a NE-SW axis and are heavily fractured but consistently large (ca. 50 – 80 cm).

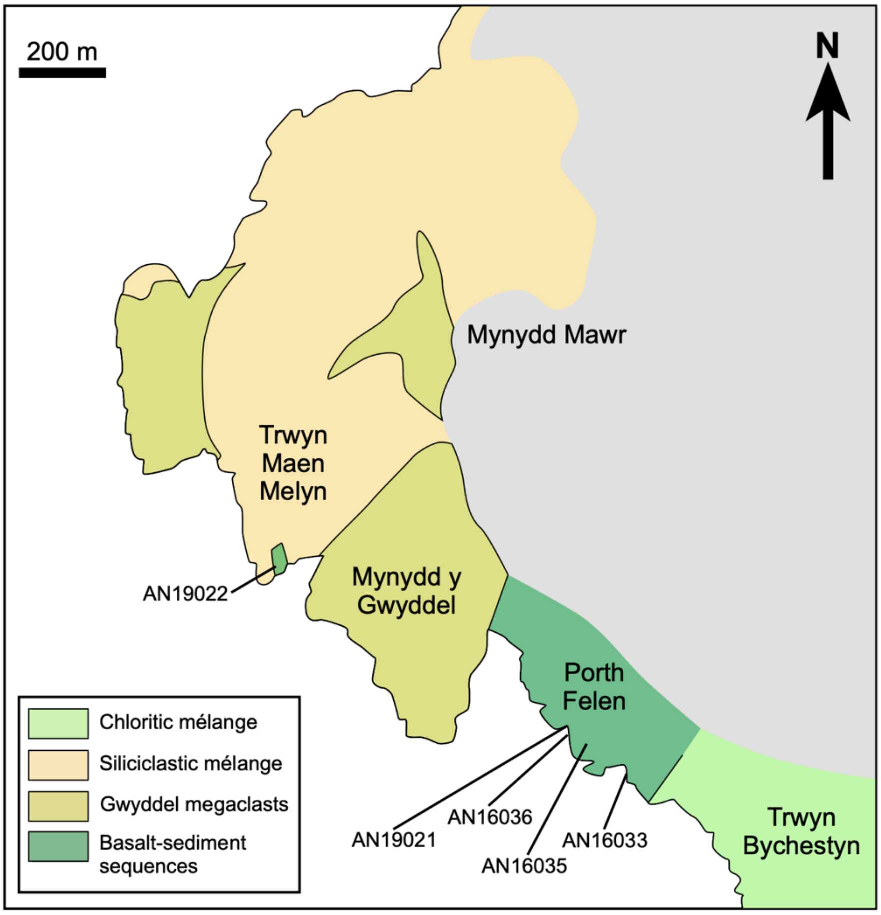

Figure 2.15: Simplified geological map of Porth Felen area after Gibbons and McCarroll (1993; Saito et al. (2015) showing sample localities from the site. Basalt-sediment sequences consist of pillow basalts overlain by sea floor sediments and are overlain by disrupted siliciclastic turbidites.

To the east at Porth Felen, basalt becomes a prominent lithology in a series of four identified semi-repeated sequences (1-4; see Figure 2.16). The orientations of sequences vary across the locality, which is influenced by high-angle faulting and large-scale N-S folding. Most of the area exhibits a shallow (< 20˚) but varying dip generally towards NE. The sequences consist of pillow basalts generally overlain by carbonate rocks and topped by turbiditic sandstones and mudstones. Two types of mudstones also occur variably between carbonates and sandstones in Sequences 2 and 4. Upper and lower extents of sequences are not exposed. Further east at Trwyn Bychestyn the basaltic sequence gives way to massive clast-bearing chloritic schist across another high-angle fault.

The pillow basalts at Porth Felen have good shape, are largely undeformed and have been reddened by haematite to a lesser extent than those at Trwyn Maen Melyn. They are also smaller in comparison (ca. 40 – 50 cm). Carbonate rocks overlie the pillow basalts with little evidence of interaction or mixing between the lithologies, and the rocks are often fractured along contacts. The carbonates are predominantly dolomitic with a deep yellow-brown appearance. They range from massive to laminated, although do not appear to be stromatolitic like the layered carbonates of the Cemaes Group. Carbonate units range from 1 – 5 m thick with some lateral variability. Silty mudstones are occasionally seen in small quantities below siliciclastic turbidite sequences. The mudstones are discontinuous and outcrop as lenses < 2 m thick. Turbidite sequences are also highly sheared, creating more of a crude mélange rather than an interbedded sequence, however they do not locally host clasts of multiple lithologies as observed in Trywn Maen Melyn. They are brown-grey in colour with little chlorite content. The sandstones are medium-gritty arenites, suggesting a predominantly continental sediment source.

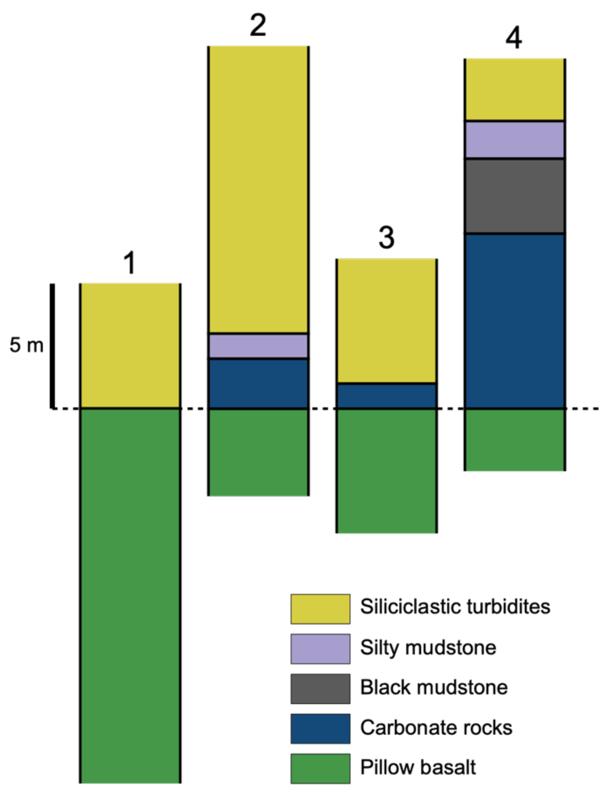

Figure 2.16: Schematic logs of semi-repeating sequences at Porth Felen that show fundamental similarities to those described in Gwna Complex Area I.

Sequence 1 consists only of pillow basalts and overlying turbiditic sedimentary rocks, and is the only sequence not to contain carbonate rocks. It sits within the headland of Porth Felen, and the observed pillow basalt component is at least 20 m thick. Geochemical analyses from Porth Felen by Saito et al. (2015) show compositional differences between the pillow basalts from Sequence 1 from those in Sequence 4, although the pillow basalts are texturally very similar.

In Sequence 4, layered dolostone is overlain by a black shaly mudstone lens (AN19021; see Figure 2.17b) that pinches out in either direction after approximately 40 m. The upper parts (ca. 0.5 m) of the underlying dolostone – along with horizons within the black mudstone – are populated by small euhedral pyrite crystals up to 5 mm in diameter. The underlying dolostone shows evidence of oblique folding (see Figure 2.17c), while the base of the black mudstone shows multiple slip surface orientations. The mudstone lens is described in detail by Sato et al. (2015) and represents a unique occurrence in the Gwna Complex. It is partially overlain by small quantities of silty mudstone that also outcrops as a lens that pinches out above the black mudstone.

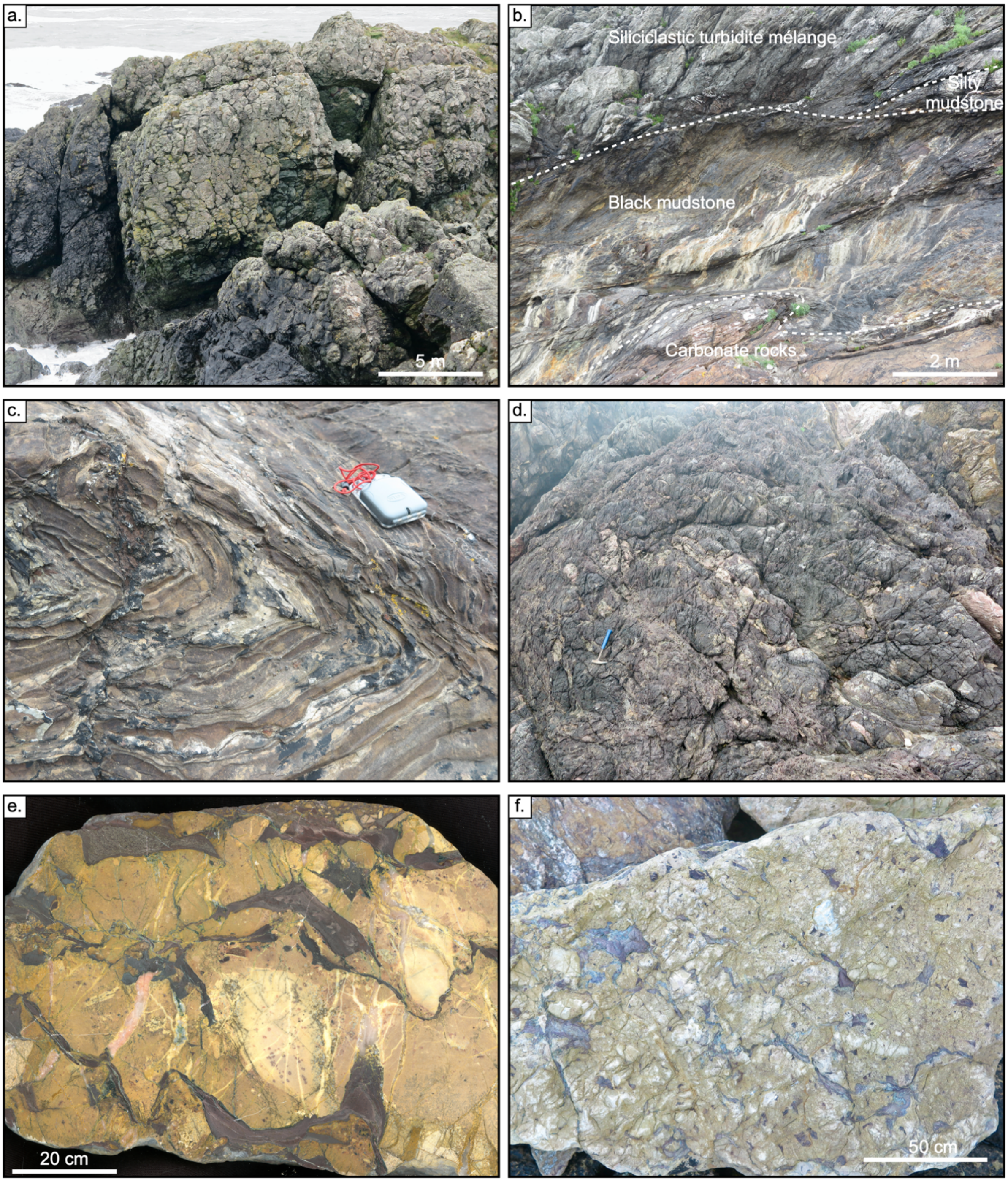

Figure 2.17: Various volcanic rock and sea floor sediments preserved from Gwna Complex Area II including (a) undeformed pillow basalt sequences from Morfa Nefyn (SH 2765 4210) showing steep SE dipping orientation much like pillows of Gwna Complex Area I; (b) Sequence 4 at Porth Felen (SH 1457 2472) showing black mudstone (AN19021) overlying carbonate rocks, topped by a discontinuous silty mudstone lens and siliciclastic mélange; (c) layered dolomitic carbonate rocks of Sequence 4 at Porth Felen showing isoclinal folding and the presence of euhedral pyrite crystals; (d) deformed carbonate-rich pillow basalts within the siliciclastic mélange of Porth Maen Melyn (AN19022; SH 1385 2518); (e-f) basalt-carbonate rocks within large clast in mudstone mélange at Porthorion (SH 156 289) showing basalt strands disseminated throughout fractured, deformed carbonate-dominated unit with evidence of peperitic juvenile basalt clasts.

2.4.2 Regional-scale mélange

Structurally and lithologically, Area II has notable differences to Area I. Vast quantities of clastic sediments dominate large parts of Area II that are much less – or not at all – represented in Area I. The influx of high volumes of chloritic schists and siliciclastic turbidites has led to regional-scale mélange formation across much of Area II, leaving the preservation of stratigraphically coherent material confined to few small areas. Additional lithologies such as quartzites and the Gwyddel beds populate these mélanges. Quartzites are white, coarse quartz arenites with massive form that often occur as large masses in excess of 20 m, and are common clast types throughout Area II (see Figures 2.18a and b). The Gwyddel beds are more geographically constrained, outcropping as megaclasts (up to 1 km) in siliciclastic turbidite mélanges between Anelog (SH 15 28) and Mynydd y Gwyddel (SH 14 24; see Figure 2.18c). They consist of isoclinally folded, layered coarse quartzitic material with thin silt/mud intervals and are interpreted as tuffaceous sandstones (Matley 1928; Gibbons and McCarroll 1993).

Siliciclastic turbidites are the dominant mélange host rock across the southern parts of Area II, composed of disrupted sequences of pelites and fine-gritty arenites. In Area I, a singular occurrence of siliciclastic sandstone with interbedded mudstone was observed. This is a possible analogue for the siliciclastic turbidites of Area II. Clasts within the siliciclastic mélange between Anelog and Mynydd y Gwyddel are generally rounded and vary greatly in size with no primary orientation. They are likely the product of olistostromal mélange formation with a pervasive tectonic overprint, as opposed to the tectonically juxtaposed slices of the mélange dominating Area I. Stratigraphic repetitions buffered by siliciclastic mélange at Porth Felen suggest that some material is tectonically imbricated, however.

Chloritic schists consist predominantly of thick, foliated mudstones with disrupted horizons of fine lithic greywackes (see Figures 2.18e and f). They have a consistent green colour that indicates a high chlorite content and are frequently intersected by white calcite and quartz veins. They may correlate to the chloritic sandstones of Area I, which are generally composed of coarser material but become locally schistose.

Purple/green mudstones – that are sporadic in Area I but are the typical host units for localised mélange – are common in Area II but tend to be more localised that the more widespread chloritic and siliciclastic mélange fabrics. As in Area I, the mudstones are mélange bearing in Area II, but can incorporate much larger clast sizes given their greater quantities (see Figures 2.18c and d).

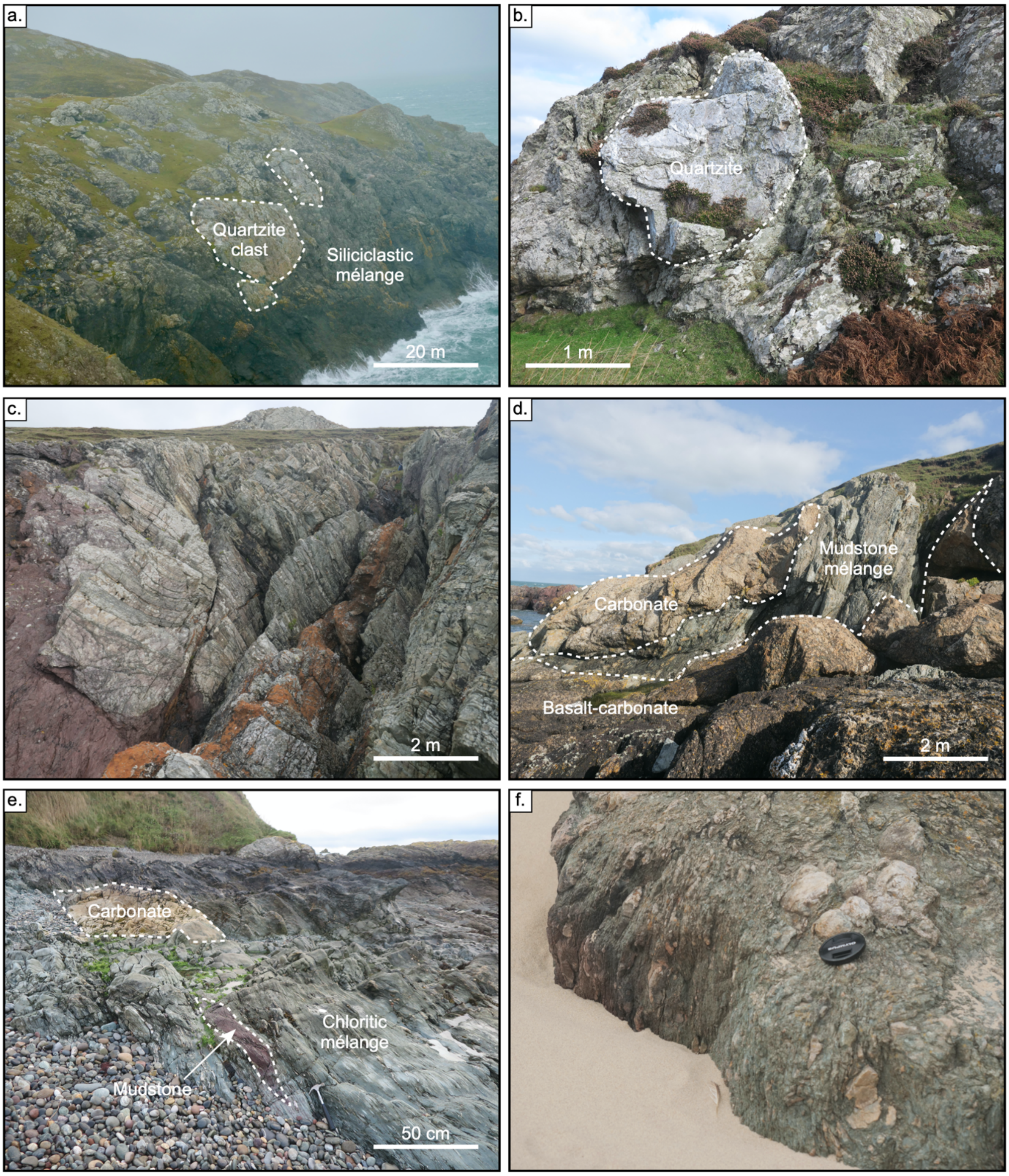

Figure 2.18: Various mélange features that characterise Gwna Complex Area II including (a) rounded quartzite megaclasts within siliciclastic matrix at Trwyn Maen Melyn (SH 1376 2537); (b) quartzite clast within siliciclastic mélange at Anelog (SH 1469 2718); (c) Gwyddel beds megaclast (white, bedded) within massive purple mudstone matrix, cut by siderite-rich brecciated fault zone; (d) carbonate and basalt-carbonate clasts within a mudstone mélange matrix at Porthorion (SH 156 289) showing evidence of duplexing with downstepping towards NW; (e) carbonate and mudstone clasts within a chloritic mélange at Morfa Nefyn (SH 2728 4104); and (f) quartzite clasts within a schistose chloritic mélange.

2.5 GWNA COMPLEX – AREA III (BODORGAN)

Area III outcrops across southern Anglesey between Aberffraw and Bodorgan, extending NE across central Anglesey. It is tectonically separated from Area I by the BSZ and is unconformably overlain by Carboniferous stratigraphy (eg. SH 3886 6669). The angular NE-SW contact with the polydeformed metasediments (orientated subvertically roughly N-S) of the Porth Trecastell Formation is exposed at the eastern headland of Porth Cwyfan (SH 3375 6754) and is obscured by later oblique faulting.

The area is dominated by subvertical turbiditic sandstones and mudstones intermittently hosting elongate lenses aligned parallel to the prevailing NE-SW foliation orientation, consistent with orientations throughout Area I. The fine to gritty arenites and mudstones are brown-grey in colour, suggesting low chlorite content. Quartzite is the most common clast component, with lenses up to 20 m thick (SH 3593 6677). Lenses are common throughout the area, including the headlands south of Traeth Mawr, where repeated mud-rich turbidite sequences are otherwise interrupted for 100 – 200 m. Around Porth Cadwaladr (SH 361 664) the turbiditic sequence gives way to a chloritic schist matrix that extends roughly 300 m. The schist is highly deformed with wildly undulating foliation that flows around relatively dense populations of quartzite and dolomitic carbonate clasts ranging from < 5 cm to 10 m in thickness.

Intermittent occurrences of dolomitic carbonate clasts, purple/green mudstones and chloritic schists – occasionally including chert layers – are recognisable from other Gwna Complex areas and often occur near one another. The mudstones occur sporadically as highly sheared zones within the turbiditic schists that act as a matrix for clasts of multiple lithologies. If the mudstones are clasts within the turbidites themselves, then this would suggest that the stratigraphy of Area III has been reworked.

Igneous rocks are relatively uncommon in Area III. Along the coast between Aberffraw and Bodorgan, igneous material is confined to several elongate lenses (< 5 m wide) of deformed basalt-carbonate rocks concentrated along the eastern headland of Traeth Mawr (SH 3582 6748). The lenses are mixed with dolomitic carbonate lenses within a foliated mudstone matrix that alternates intermittently between purple and green. Basalt components have been greatly deformed, distorting pillow shapes, which are densely intersected by carbonate veins. Interestingly, these three lithologies are common in Area I, where turbiditic sedimentary rocks are much less voluminous.

Further inland, between the settlements of Soar (SH 38 71) and Capel Mawr (SH 41 72), the largest volumes of igneous rocks from Area III occur as a series of concentrated basaltic lenses (eg. AN19042; SH 3880 7235). The NE-SW orientated lenses outcrop as prominent roche moutonnée headlands, showing basaltic sequences more than 50 m thick. The lenses are moderately deformed, consisting of poorly preserved pillows with massive lava intervals. Outer parts of lenses are relatively highly deformed, with no pillow textures preserved, high concentrations of fractures and local reddening. Lenses are bordered by intensely foliated turbiditic schists or purple/green mudstones.

2.6 GWNA COMPLEX – AREA IV (MENAI STRAIT)

Area IV was categorised within the bounds of the Pen-y-Parc Formation (Penmynydd Terrane) in the revised tectonostratigraphy of Anglesey by Schofield et al. (2020). However, observations from outcrops along the Menai Strait between Gallow's Point (SH 595 750) and Glyngarth (SH 580 740) show much greater affinity to the Gwna Complex than inland outcrops of the Pen-y-Parc Formation, around Llansadrwn (SH 56 76) and Llanddona (SH 57 79), for example. The evidence used to define the proposed Pen-y-Parc Formation (Schofield et al. 2020) is not described in detail but appears to have originated predominantly from these westerly localities, while traditional geological boundaries (British Geological Survey 1980) have been maintained. Here, the boundary (see Figure 2.1) has been delineated based on the mineral isograds determined Kawai et al. (2007), which are congruent with field observations of outcrop lithologies in the area. No contact between Gwna Complex Area IV and the Penmynydd Terrane was observed due to the sparse nature of outcrops inland.

Exposure of Gwna Complex Area IV is largely confined to coastal outcrops is disrupted by numerous crosscutting doleritic dykes and faults, likely due to its proximity to the MSFZ. It exhibits highly disrupted sub-greenschist material consisting mostly of pelitic to gritty chloritic schists with occurrences of deformed basalts, dolomitic carbonate rocks, cherty mudstones, and possibly tuffaceous mudstones. Lithological contacts are typically faulted, obscuring many stratigraphic relationships. The area is gently folded along NW-SE trending axial planes.

Basalt occurrences are distinguished from the metabasites of the Penmynydd Terrane by their lack of amphiboles. All occurrences of basalt are green due to high chlorite abundance, and relict plagioclase phenocryst spots (1 – 5 mm) are visible locally. Basalts in Area IV occur in three main units – along with some minor occurrences – which are 20 – 50 m wide. Two of these outcrops (AN19023; SH 5884 7463 and AN19024; 5933 7487) consist of uniform massive basalt with internal laminations – of black phyllosilicate-rich material 1 – 5 mm thick – bound by highly deformed chloritic schists and mudstones. The remaining outcropping unit exposes distorted, elongated pillow lavas (AN17009; see Figure 2.19a). The pillows are surrounded by more massive basalt with no evidence of a primary volcanic transition between the two lithologies. The pillows are relatively small (20 – 40 cm diameter), bordered by thick, dark green interpillow rims up to 5 cm thick. Interpillow jasper is also present. Above these pillows, discontinuous basalt breccias consist small basaltic clasts (< 10 cm) populating a similar dark green, foliated matrix that may be representative of a deformed hyaloclastite component, or a continuation of pillow lavas deformed to a greater extent. As the extent of deformation increases and pillows are elongated, interpillow material coalesces into linear planes (see Figure 2.19b). It is therefore likely that the laminations observed in other basaltic units are relicts from destroyed pillow textures.

The chloritic schists are similar to those in the Pen-y-Parc Formation although generally containing less recrystallised quartz. Quartz layers and deformed clasts are present in concentrated areas throughout the chloritic schists of Area IV however (see Figure 2.19e). The schists are clast-bearing (see Figure 2.19d) and act as the dominant matrix for Area IV in the absence of large quantities of siliciclastic material as observed in Area II. The schists grade from pelitic to medium grade arkose, like the chloritic sandstones of Area I. Coarser components of the chloritic schist preserve original sedimentary textures and are not commonly observed to be clast-bearing but are laminated (see Figure 2.19f). Unlike Area I, thin interbedding of the units is not seen here, and occurrences are more massive and varying in grain size between outcrops.

Carbonate rocks are yellow-grey and dolomitic, occurring as elongate blocks up to 20 m in length. They are massive and show no internal structural features. Minor occurrences of lightly folded, finely interbedded quartzites and mudstones have a white-green appearance and appear as blocks within the schistose mélange. They are similar in appearance to the Gwyddel beds described from Area II. Quartzite clasts are common but tend to be more limited in size (< 2 m) than in Area II and III. Purple/green mudstones are also present and are highly sheared, distorting the form of units. These rocks correlate to those described in Areas I, II and III, and are observed to be clast-bearing (see Figure 2.19c).

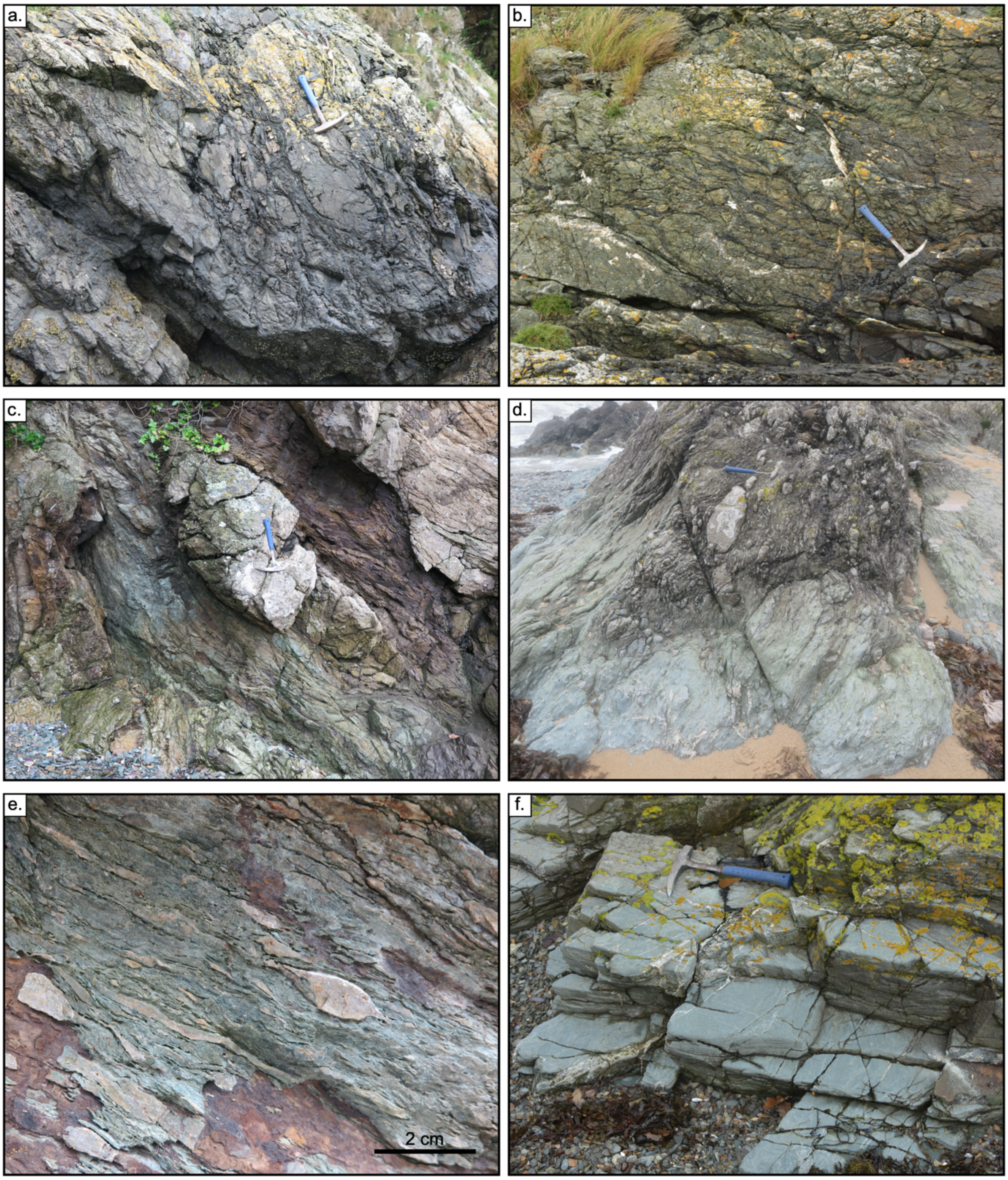

Figure 2.19: Various features from Gwna Complex Area IV including (a) highly deformed pillow basalts showing pillow shortening and reduction (SH 5865 7448); (b) intensely deformed pillow basalts and propagation of a foliation, partly erasing pillow textures; (c) elongated quartzite clast orientated parallel to foliation within a surrounding mudstone matrix ; (d) small quartzitic clasts within a highly foliated chloritic mélange with schistose texture; (e) chloritic schist with elongate, augen-like quartz orientated along foliation; and (f) more competent psammitic component to chloritic schist that does not locally contain clasts but is still highly foliated.

2.7 PENMYNYDD TERRANE

The Penmynydd Terrane is characterised by interleaving polydeformed bodies of amphibole-bearing, mica-bearing and chloritic schists ranging from greenschist to blueschist facies mineral assemblages. Smaller, sporadic occurrences of quartzitic schists, felsic schists and carbonate rocks were also observed. Schists commonly become locally mylonitic, particularly near lithological interfaces. Samples of metabasic (amphibole-bearing) schists were collected from 13 localities across the Penmynydd Terrane. Figure 2.20 outlines the localities of these samples overlain on a geological map (British Geological Survey 1980) that highlights metabasic lens distribution.

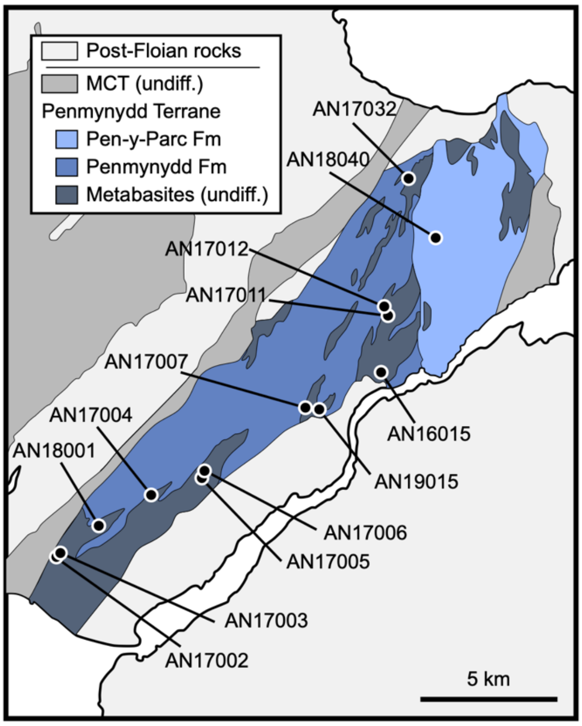

Figure 2.20: Simplified geological map of the Penmynydd Terrane showing the distribution of metabasite lenses throughout both the Penmynydd and Pen-y-Parc Formations and showing sample localities, after British Geological Survey (1980); Kawai et al. (2007); Schofield et al. (2020).

2.7.1 Metabasites of the Penmynydd Formation

Metabasic rocks in the Penmynydd Terrane are identified by their mineral assemblages, consisting of amphibole (sodic-calcic) + epidote + quartz ± haematite. They have a darker, more uniform appearance than the metasedimentary rocks and are less friable. In appearance, they are typically massive and polydeformed, with variable prominence in syn-metamorphic foliation that commonly shows the development of tight, isoclinal folds and crenulation textures. Quartz is present in lower abundances, forming thin veins and augen-like structures, although larger masses can accumulate locally. Amphiboles are the dominant mineral phase and vary from green (calcic; likely actinolite or hornblende) to blue (sodic; likely glaucophane), reflecting different species that act as a rough proxy for peak metamorphism. The schists often possess a layered appearance, with amphibole-rich layers, quartz-rich layers, and epidote-chlorite-dominant layers (see Figure 2.21a and e). In Pentraeth Forest (AN17032; SH 544 787), the metabasite schist appears to consist of alternating blue and green bands 2 – 10 cm thick governed largely by amphibole species. Haematite content varies between localities and is usually a minor phase, but relatively high contents create reddish overtones in some places, for example at Llansadrwn (AN18040; SH 562 768). While rare lawsonite occurrences along the boundary of the Penmynydd and Pen-y-Parc Formations have been documented in metabasites (Gibbons and Mann 1983), no occurrences were identified in this study.

Intense foliation that becomes locally mylonitic affects metabasic schists throughout the Penmynydd Terrane. Some exposures, however, appear to preserve rare evidence of deformed pillow lava structures within the schists. At Llanfair (SH 534 715) isolated, unfoliated elliptical structures are orientated along the intensely foliated surrounding schist (aspect ratio 1:4 – 1:8). Boudinage, perpendicular joints and oblique quartz-bearing fractures are common features related to tensile deformation and stretching. Larger examples (> 50 cm) tend to have lower aspect ratios (see Figure 2.21b) while smaller structures are highly elongated with more prominent tensile deformation features (see Figure 2.21c). Similar structures are better preserved at Castellior (SH 544 740), where they have been stretched less intensely (aspect ratio approx. 1:1.5 – 1:2). The structures are asymmetrical and are in different states of rotation, ranging from rounded to dome-like shapes with flat bases that resemble the forms of pillow lavas (see Figure 2.21d). They are roughly 50 – 70 cm in length, which is similar to typical pillow lava occurrences in the Gwna Complex.

2.7.2 Metasedimentary rocks of the Penmynydd Terrane

Metabasite lenses are interleaved with amphibole-absent metasedimentary rocks predominantly in the form of mica schists and chloritic schists. Mica schists dominate the Penmynydd Formation – although not exclusively – while chloritic schists are more common in the Pen-y-Parc Formation. The mica schists are blue-grey in appearance with typically high quartz contents that occurs as bands of variable distribution and thickness with interlayered white-grey mica (muscovite – phengite) with a blue sheen. Chlorite is present in small amounts within micaceous layers. Minor rusting is also evident, particularly along the micaceous layers. The chloritic schists are similarly quartz-dominated with horizons of rich in chlorite, producing a grey-green appearance.

Garnets rarely populate mica schists but were not identified in metabasites or chloritic schists. In Plas Cadnant (SH 554 732), euhedral garnets (1 – 4 mm diameter) occur locally in light blue mica schists close to the contact with chloritic schists to the north. In Star (AN16001; SH 510 719), smaller euhedral garnets (< 1 mm diameter) occur in mica schists close to a large metabasite lens around Llanfair.

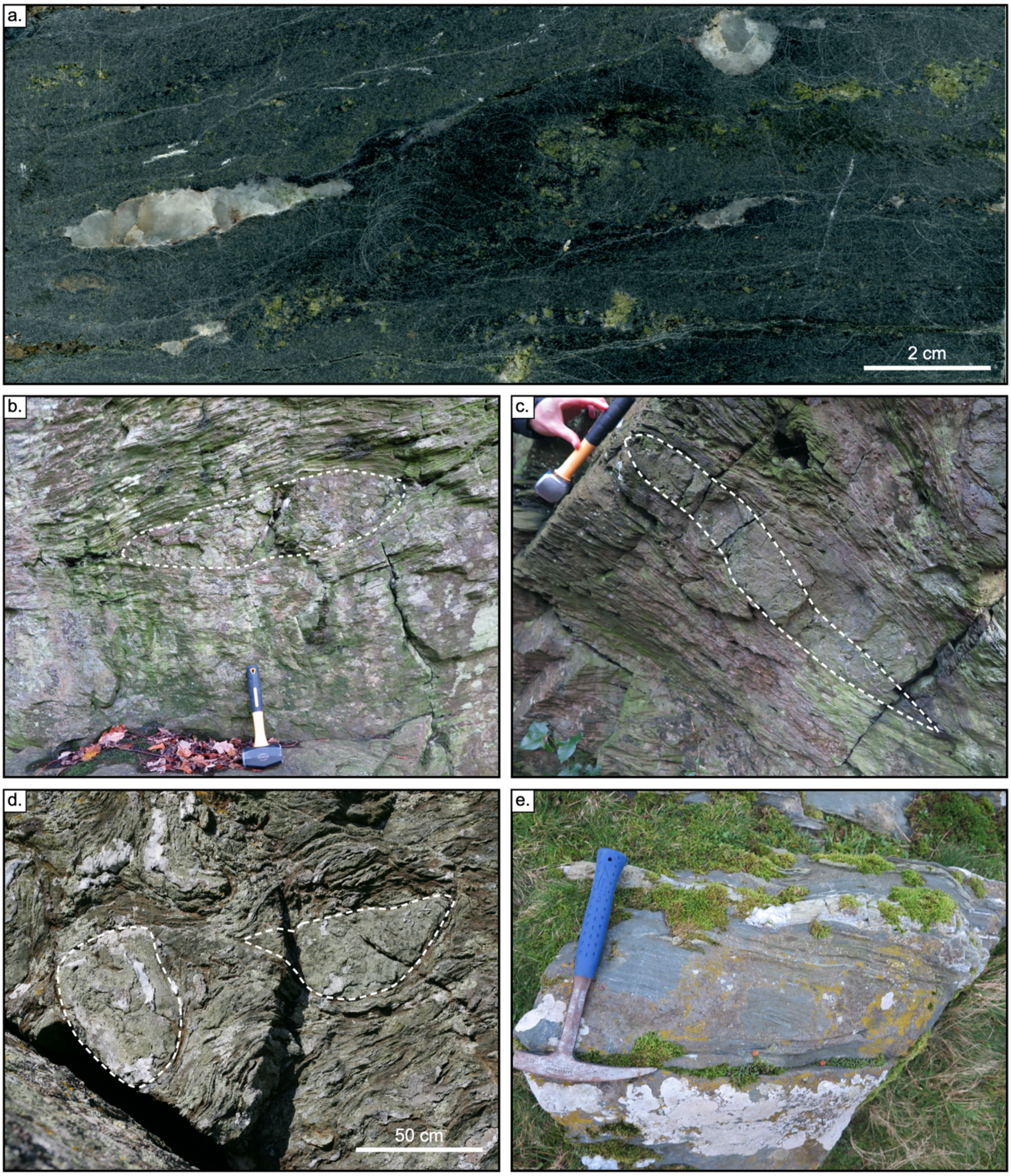

Figure 2.21: Various textures of metabasites from the Penmynydd Terrane including (a) polished block showing the deep blue colour of the fine grained, amphibole-rich rock with elongate masses of quartz and concentrations of light green epidote (AN16015; SH 5342 7156); (b) relict pillow lava texture elongated along plane of foliation with oblique tensile fractures from Llanfair (SH 5343 7157); (c) reduced relict pillows with smaller size and greater aspect ratio from Llanfair; (d) relict pillows from Castellior (SH 544 740) that have been rotated within a foliated metabasite that deflects around the structures, photo courtesy of Stewart Campbell; (e) relatively clear outcrop (AN17003; 4154 6495) showing blue colour and foliation with mineralogical banding and foliation-parallel quartz layers.

Light grey carbonate blocks 5 – 50 m in diameter occur sporadically and are more commonly found in the Pen-y-Parc Formation (eg. Plas Cadnant; SH 558 731) and are orientated along the dominant direction of foliation of surrounding schists. The carbonates are significantly less deformed surrounding rocks. Quartzitic blocks also occur infrequently throughout the Pen-y-Parc Formation with similar form to the carbonate blocks, although extent of deformation is more variable.

Towards the BSZ along the western margin of the Penmynydd Terrane (eg. Pentre Berw; SH 485 727), lenses of grey-pink felsic schists containing alkali feldspars are interleaved with mica schists and metabasite lenses. The schists are quartz-rich with occasional augen-like alkali feldspar occurrences within quartz layers or lenticles, intervened by layers of mica. Relative quartz and mica compositions vary greatly between localities. These occurrences have not been observed towards the eastern parts of the terrane, however. They are seemingly related to occurrences of gneisses around the area, which have been interpreted as basement material from the Arfon Terrane, termed the Holland Arms Gneisses (Beckinsale and Thorpe 1979; Kawai et al. 2007).

2.7.3 Structure of the Penmynydd Formation

Foliation orientation varies greatly over short distances, but prevailing orientations are relatively stable, ranging broadly from N-S in the north of the terrane to NE-SW towards the south. This largely follows the mapped orientations of metabasite lenses (British Geological Survey 1980). Localised mylonitic zones seemingly develop towards lithological interfaces, such as between metabasite schists and mica schists, suggesting more intense deformation towards the outskirts of lenses. This may be the reason for potential pillow lava relics being observed only in localities towards the centres of larger metabasite lenses. This would be consistent with the findings of Gibbons and Gyopari (1986), who identified preserved greenschist cores of metabasite lenses in road cuttings – also within the Llanfair metabasite lens – suggesting that metamorphism and deformation effects were greater around the boundaries of lenses, while their cores were relatively preserved.

Syn-metamorphic deformation between mica schists and metabasites was observed near Star (SH 5302 7234), creating an anastomosing lithological contact that exhibits isoclinal folding and NNE-SSW trending mineral lineation. This suggests that the unit had been exposed to further deformation after emplacement of the metabasite lenses within the mica schist matrix. The overall structure of the unit shows orientated, elongate lenses of metabasic rocks within a thick, voluminous metasedimentary matrix with a dominant pelitic protolith and local examples of multiple lithologies, which is similar in many ways to the structure of the Gwna Complex.

Pen-y-Parc Formation

The area of the Pen-y-Parc Formation roughly to the east of Glyngarth has been assigned to the Gwna Complex (Area IV) based on field observations outlined in Section 2.6. The relationship between the Penmynydd Formation and the Pen-y-Parc Formation is rather unclear. The mapped boundary is not well exposed, although lithological differences are observed between Plas Cadnant and Castellior (SH 55 73), marking the boundary between mica schists and metabasites to the west and chloritic greenschists to the east. The Pen-y-Parc Formation is also dominated by chloritic schist and contains carbonate and quartzite blocks.

Despite this, amphibole-bearing metabasite lenses occur in both units, with AN18040 sampled from the Pen-y-Parc Formation, among other examples particularly in the northern areas around Llanddona (SH 57 80). There are no clear differences in protolith or metamorphic grade that can be determined between the units. Additionally, mica schists occur in the Llanddona area, along with chloritic schists. While there are enough differences between the units to support the current division, there appears to be a closer relationship between them than presented by Schofield et al. (2020).

2.8 CEMAES GROUP

The Cemaes Group consists of the Porth Trefadog Formation and seemingly overlying Porth Swtan Formation. The Porth Trefadog Formation outcrops over a 4 km span between Porth Defaid (SH 28 85) and Porth Swtan (SH 29 89), along the western coast of Anglesey see Figure 2.22. The Porth Swtan Formation also outcrops at Porth Swtan but is seen more extensively along the northern coast of Anglesey, in the area around Cemaes (SH 37 94).

2.8.1 Base of the Cemaes Group

The lower boundary of the Porth Trefadog Formation is marked by an ENE-WSW thrust fault through Porth Defaid (SH 2890 8569), in contact with the underlying green/blue polydeformed chloritic schists of the New Harbour Group to the south. On the northern side, a doleritic dyke (AN20001) crosscuts the Porth Trefadog Group subparallel to the fault within several metres of the contact. The intrusion has previously led to misinterpretation of the boundary as an unconformable sequence marked by a subaerial lava flow (Dartnall 2018). However, textural observations of the unit are consistent with Group 3 dolerite intrusives from elsewhere across Anglesey (see Section 2.9). Localised fault fabrics and steepening foliation within the lower New Harbour Group rocks indicate that the contact is faulted rather than unconformable. This tectonostratigraphic relationship appears to have been used to constrain the relative age of the Cemaes Group (Schofield et al. 2020).

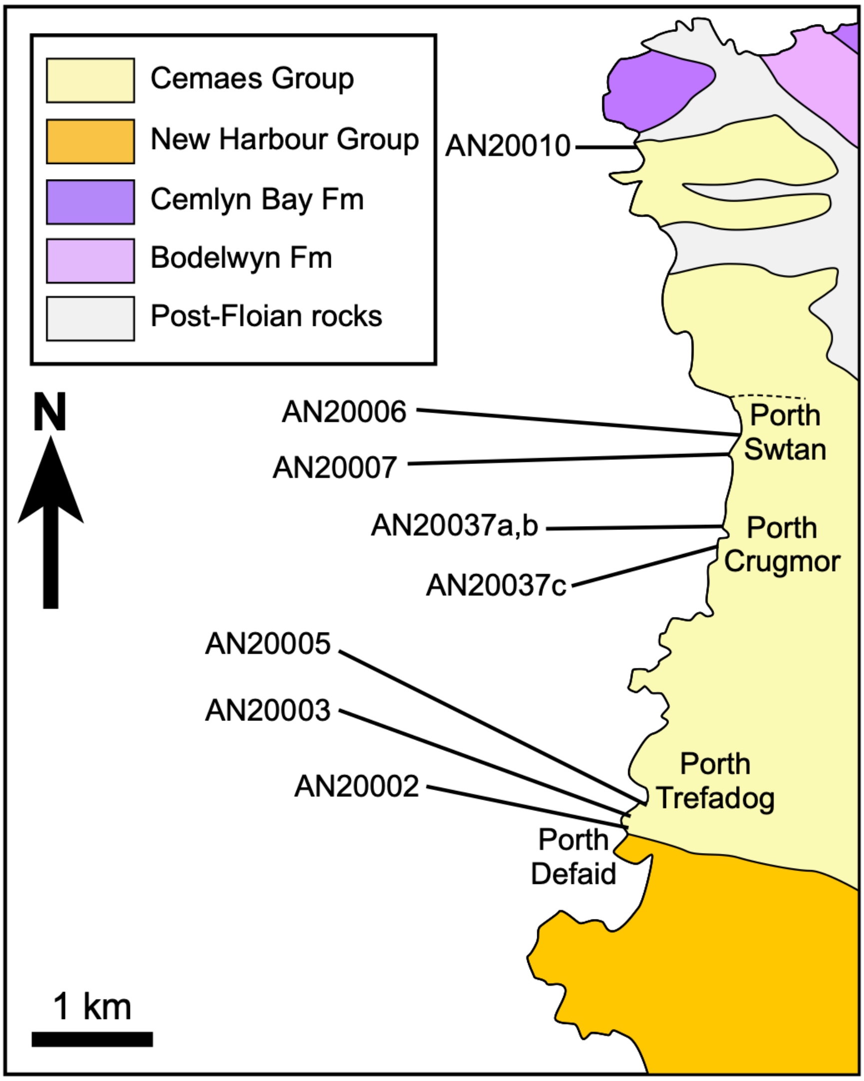

Figure 2.22: Simplified geological map of Western Anglesey after Schofield et al. (2020) showing the extent of the Cemaes Group and showing sample localities from the area. The dashed line at Porth Swtan marks the boundary between Porth Trefadog Formation (south) and Port Swtan Formation (north).

2.8.2 Porth Trefadog Formation

The Porth Trefadog Formation is characterised by a thick sequence of tuffs and tuffaceous sandstones, estimated to be 200 – 300 m thick. Between Porth Trefadog and the southern headlands of Porth Swtan, the sequence is very uniform with no major lithological changes recorded. The rocks are gently folded – in comparison to the New Harbour Group schists – and dip generally northwards along open E-W trending folds. The sequence represents repetitive volcanic turbidites consisting of mud (AN20037a) to fine greywacke layers 5 – 50 cm thick with sporadic medium to coarse horizons (AN20037b). The volcaniclastics are grey-green but often exhibit a distinct yellow-brown weathered appearance.

The base of the formation – between Porth Defaid and Porth Trefadog – is more texturally heterogeneous than the rest of the unit. Towards the base, a foliated red mudstone horizon (AN19002) roughly 2 m thick outcrops between fine volcaniclastic beds and other green mudstone horizons. Dolomites and quartz clasts occur locally. At the northern headland of Porth Defaid, coarser beds common, interbedded with laminated mudstones and finer sandstones. Several coarse beds up to 2 m thick contain rounded quartz clasts up to 1 cm in diameter and may represent ignimbrite horizons (AN20005; see Figure 2.23a). Northwards across Porth Trefadog, the sequence becomes more consistent and finer grained.

Porth Trefadog Fm – Porth Swtan Fm relationship

At Porth Swtan, the uniform volcaniclastic turbidites of the Porth Trefadog Formation gradationally transition into debris flow deposits, incorporating quartzitic ribbons parallel to bedding. This transition occurs over approximately 300 m, interrupted by numerous high-angle E-W striking normal faults. At the south of Porth Swtan, successions become moderately disturbed, with coarser beds fragmented and boudinaged (see Figure 2.22b). Coarse quartz arenite clasts increase in size, thickness, and abundance northwards across Porth Swtan (see Figures 2.22c to d). At the northern end of Porth Swtan (SH 3011 8948), a large high-angle fault marks the progression into the Porth Swtan Formation, consisting of thick, elongate quartz arenite clasts orientated within a mudstone matrix. Carbonate clasts are also incorporated to a lesser extent, exposed further up the stratigraphy (SH 2958 8995).

The contact between these two units appears to be a continuous progression of the transitional change in the upper parts of the Porth Trefadog Formation. However, the faulted contact obscures this transition, leaving the true nature of their relationship uncertain. Similarly orientated faults intersect the Porth Trefadog Formation across Porth Swtan, exposing blocks at different transitional stages based on the relative abundance of quartzitic clasts in a fault block. Therefore, it is likely that the units are a continuous progression that has been further interrupted by this faulting regime.

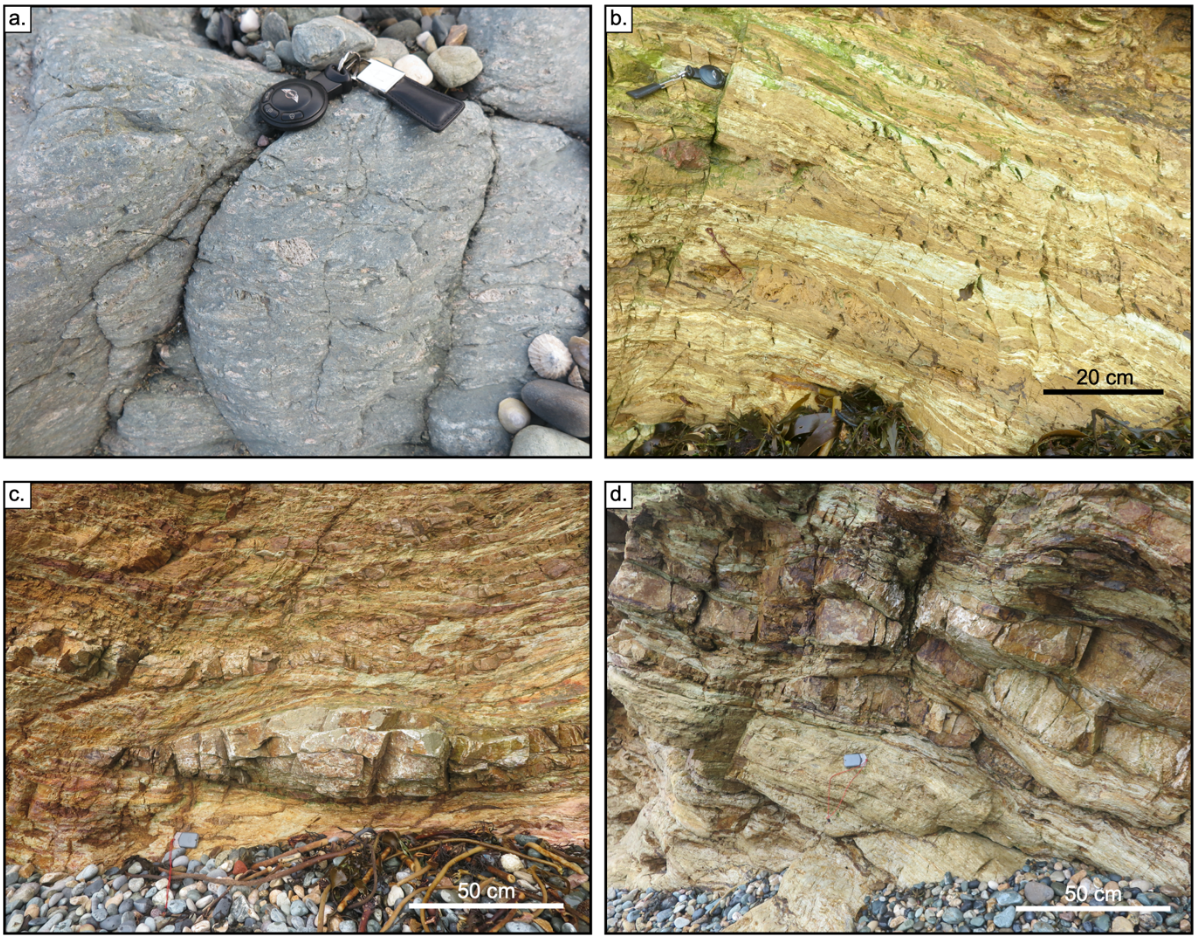

Figure 2.23: Various stages of the Porth Trefadog Formation showing (a) coarse volcaniclastic sandstone with large ellipsoid quartz grains towards base of the formation at Porth Defaid (AN20005; SH 2891 8581); (b) bedded volcaniclastics with distinct weathered yellow/brown appearance, showing minor disturbances in bedding towards Porth Swtan (SH 2992 8914); (c) volcaniclastic sequence intact but more disrupted with sporadic ribbon-like quartzite lenses stacked horizontally (SH 3004 8924); and (d) densely stacked quartzite lenses arranged parallel to one another and the foliation of the volcaniclastic matrix at the upper stages of transition from Porth Trefadog Formation volcaniclastic turbidite sequence to Porth Swtan Formation block-in-matrix mélange unit (SH 3010 8929).

Skerries volcaniclastics

The Skerries volcanic member (Schofield et al. 2020) outcrops in an isolated fault-bound sequence to the north of Porth Swtan (AN20010; SH 2963 9029). It outcrops most extensively across the Skerries islands off the northwestern coast of Anglesey (SH 26 94), but the islands were not visited in this study. The Skerries volcanic member is a dark, coarse arkosic volcaniclastic unit. Its relationship to the volcaniclastics of the Porth Trefadog Formation is unclear.

2.8.3 Porth Swtan Formation

The Porth Swtan Formation outcrops more extensively along the northern coast of Anglesey, between Wylfa Head (SH 35 94) and Llanbadrig (SH 38 95). As in Porth Swtan, the area consists of brown/grey carbonate and white quartz arenite clasts that range from a scale of millimetres to hundreds of metres, suspended within a pervasively foliated matrix that ranges from mudstone to gritty greywacke shown in Figure 2.24. The arrangement of elongate, broadly aligned clasts within the largely massive, unbedded pelitic matrix creates a block-in-matrix mélange texture. Strain is accommodated preferentially within the matrix, while clasts show little evidence of plastic deformation, only autoclastic fracturing. Where clasts densely populate the matrix, duplex structures form, marked by pervasive slip layers (see Figure 2.24c).

Carbonate megaclasts, such as at Trwyn-y-Parc (SH 347 940), can occur in excess of 250 m long. These larger clasts expose partial dolomitisation of primary limestone, which pervades clasts from the clast boundaries inwards and along fracture planes. The majority of smaller (< 10 m) carbonate clasts have been fully dolomitised. Primary limestone such as that observed in Gadlys Quarry (see Figure 2.24f), preserves stromatolitic banding with rare stromatolite domes and vesicularites (Wood and Nicholls 1973) within thickly bedded, light grey sequences.

The distribution of clasts throughout the Porth Swtan Formation appears to be somewhat zonal, with areas alternating between carbonate-dominant and arenite-dominant clast assemblages. Wylfa Head, for example, consists predominantly of densely packed, discontinuous arenite ribbons, while Trwyn-y-Parc is populated by mostly carbonate clasts, including several megaclast occurrences. Horizons of roughly aligned clasts of the same lithologies show evidence of sporadic ghost stratification (Woodcock and Morris 1999) in an otherwise chaotic assemblage. At Llanbadrig, this can be seen through the juxtaposition of dolomitic carbonate, limestone, and sandstone horizons.

The mélange matrix is consistent throughout the formation, although incorporates grain-sized clasts of the local prevailing clast lithology. It is generally dark brown and clay rich (see Figure 2.24b). There is no evidence of multiple matrix lithologies as seen in the Gwna Complex, or a significant chloritic component that was seemingly present in the underlying Porth Trefadog volcaniclastics. This suggests that along with an influx of clastic material, the transition into the Porth Swtan Formation involved a change in dominant sediment input from volcaniclastic to siliciclastic.

The rocks of the Porth Swtan Formation – and Cemaes Group as a whole – are notably less deformed than similar mélanges observed in the Gwna Complex. Clasts in the Porth Swtan Formation generally show relatively low levels of deformation, with an absence of intensely sheared clast-matrix interfaces and a pervasive cleavage. Another notable difference with the Gwna Complex is the lack of magmatic or pelagic material lithologies. Small, worked jasper pits (SH 3731 9458) may hint at the presence of some unexposed igneous material, since jasper in the Gwna Complex is associated with hydrothermal activity around basal magmatic rocks.

Figure 2.24: Various textures from the Porth Swtan Formation in the Cemaes area showing (a) large orientated quartzite clast within highly foliated pelitic fabric; (b) dark mudstone matrix with deflected foliation around a limestone clast, with sporadic smaller fragments incorporated into the matrix that have undergone foliation-parallel shear deformation; (c) densely packed sandstone clasts (top) separated from limestone clast (bottom) by mudstone-dominated, highly sheared mélange fabric with duplexed clasts; (d) clasts concentrated along subparallel horizons that appear to be boudinaged; (e) sideritic carbonate clast within dark mudstone matrix surrounded by other clasts of predominantly sandstone; and (f) stromatolitic limestone from Gadlys Quarry (SH 3741 9408) where the core of a carbonate megaclast has remained free from dolomitisation.

2.9 MAGMATIC INTRUSIVES

Mafic sheet intrusions are common occurrences across Anglesey. Samples of 14 dykes were collected from different localities across the island with various hosting country rocks. All observed intrusions included here are younger than units of the MCT. They are therefore considered to have no genetic relationship to the doleritic sills of the Gwna Complex in Area I, or any other magmatic rocks of the Gwna Complex. Figure 2.25 shows localities of sampled mafic intrusives across Anglesey, displaying recorded orientation data that supports the NW-SE dominant trends described by Bevins et al. (1996). The intrusives were categorised into three groups (Groups 1 – 3) based on textural distinctions.

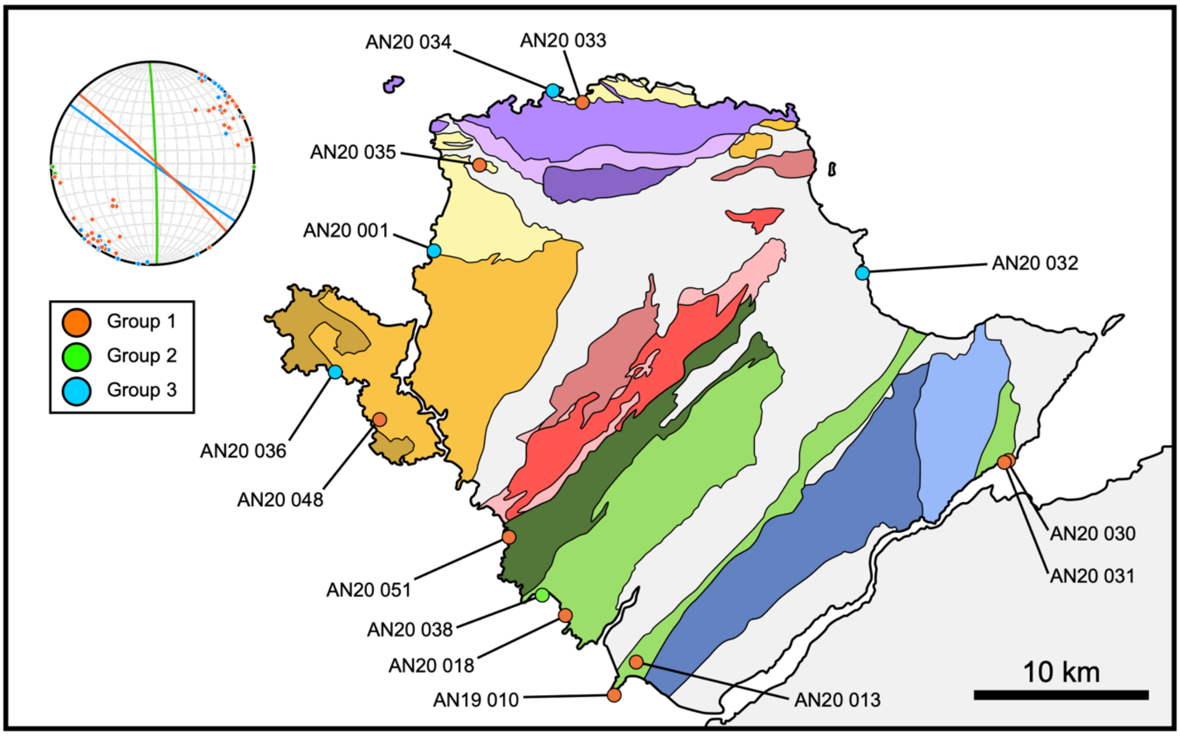

Figure 2.25: Dyke sample localities plotted on a geological map of Anglesey with orientation data measured from both samples and unsampled dykes across Anglesey. Poles represent individual data while planes represent group averages.

Group 1 intrusives show the most variable textures and roughly correlate to the supposed Lower Palaeozoic dyke set, although absolute dates have not been determined (Harker 1887; Greenly 1919). Group 2 describes a single occurrence of an unusual biotite-bearing dyke with a distinct orientation. Group 3 describes a set of Paleogene intrusives related to the BPIP where the emplacement of AN20034 has an established age of emplacement (Allott & Lomax 1988; Hailwood et al. 1992). Similarly, AN20036 was sampled from Porth Dafarch, which was also sampled and analysed in the geochemical study of Paleogene dykes on Holy Island by Ellis (2009).

2.9.1 Group 1 intrusives

Intrusives were observed crosscutting the Aberffraw Terrane, Porth y Felin Terrane, Amlwch Terrane and Cemaes Group, including the Porth Swtan Formation, which represents the supposed youngest rocks in the Cemaes Group (AN20033; SH 3748 9468). In the cliffs of Ogof Fawr, along the northern coast of Anglesey, a Palaeozoic dyke intrudes Lower Ordovician post-Floian sedimentary sequences of the Llyn Alaw Formation (SH 4870 9215). This represents the youngest stratigraphic relationship found between Group 1 intrusives and country rock; however, this does not disregard the possibility that the dykes may be significantly younger or comprise multiple sets of intrusives with different emplacement ages.

Texturally, Group 1 dykes are doleritic, generally with a moderate-dark grey appearance. They have a low olivine content (ca. 0 – 5 %) in comparison to Group 3 dolerites, representing a relatively more intermediate composition. This seemingly has a distinguishing effect on the weathering profiles of Group 1 and 3 intrusives. The darker, more mafic Group 3 intrusives are generally more susceptible to weathering and tend to be less prominent than the Group 1 intrusives.

Group 1 intrusives typically contain altered phenocrysts of plagioclase consisting of sugary white material, likely an assemblage of white micas and zeolites. Plagioclase pseudomorph phenocrysts were observed in most dykes, varying in size between dykes, from 0.5 – 5 cm average length. Some examples of dykes with exceptionally large phenocrysts include Llanddwyn Island (AN19010; SH 3888 6318) and Porth Trecastell (AN20051; SH 3307 7070). In these examples, phenocrysts are concentrated towards the centres of dykes decreasing in both size and abundance towards outer regions. The aforementioned Llanddwyn Island dyke shows evidence of multiple phases of injection, with an outer dyke of relatively small phenocrysts and a core of larger, highly concentrated phenocrysts. Most intrusives are vesicular to some extent and vesicles are often stretched laterally. Small patches (2 – 5 cm) of concentrated pyrite are uncommon.

Relationships between intrusives and surrounding country rock tend to vary, even over small distances. For example, along Menai Strait (Gwna Complex Area IV), several dykes are observed over ca. 50 m stretch of outcrop (SH 59 74), and while most dykes (eg. AN20031) are planar with straight, sharp contacts to the country rock schists, the largest dyke (AN20030) demonstrates an irregular, wavy contact on both sides that deviates from planar form. This also occurs on Llanddwyn Island, where a dyke traversing the southern beaches shows a similarly irregular boundary (AN19010), although this happens on a small scale allowing the dyke to maintain its planar shape.

While cooling joints are common but not prominent, Group 1 intrusives are also commonly crosscut by tectonic joints that sporadically accommodate displacement, although typically on a scale of <1 m. Examples of tectonically deformed dykes occur at Llanddwyn Island through reactivation along shear zones (SH 3888 6318), and Ogof Fawr through prolonged activity along the Carmel Head Thrust System (SH 4870 9215).

2.9.2 Group 2 intrusives

In the headland of Parlwr, south from the village of Aberffraw, a single N-S trending dyke displays unusual textures relative to any other intrusives seen on Anglesey (AN20038; SH 3515 6785). It intrudes, and therefore postdates, rocks from the Aberffraw Terrane – but its age cannot accurately be constrained beyond this. The dyke has been subjected to minor sinistral offsets along NW-SE striking planes. Similar tectonic offsets occur in Group 1 intrusives but have not been identified from Group 3 intrusives. Several dolerite dykes of Group 1 affinity strike NW-SE across the surrounding area but no intersections between the intrusive groups were observed.

The Parlwr dyke interestingly contains grains of biotite up to 2 mm, although typically smaller, occasionally occurring as euhedral hexagonal crystals. The dyke is light grey although weathered orange/brown in many places. The colour largely attributes to a groundmass rich in extensively altered plagioclase, seen here as interstitial as opposed to the euhedral laths of dolerite dykes in Groups 1 and 3.

2.9.3 Group 3 intrusives

Numerous Group 3 intrusives crosscut Carboniferous limestone sequences throughout Anglesey, for example across the northern coast at Traeth Bychan (AN20032; SH 5170 8458), and along the eastern coast at Plas Newydd (SH 5212 6921). They show a consistent NW-SE orientation (see Figure 2.25) and have variable widths that can be much wider than Group 1 or 2 intrusives. The Porth Dafarch dyke (AN20036; SH 2326 7998), for example, measures consistently in excess of 20 m thickness.

Intrusives are dark grey to black, but often have a rusted brown appearance due to extensive surface weathering. They often contain phenocrysts of white plagioclase laths up to 5 mm in length without primary orientation. Unlike Groups 1 and 2, plagioclase appears to be relatively unaltered. Olivine phenocrysts are also common and may be altered. Many of the dykes are vesicular. Grain size is typically varied because of chilled margins, ranging from fine or very fine outer margins to medium or coarse centres. Dykes exhibit prominent cooling joints, mainly perpendicular to strike but also parallel to strike in larger dykes, for example at Porth Dafarch (AN20036), and spheroidal weathering commonly develops along these joint systems. The Plas Newydd dyke (SH 5212 6921) shows evidence of metasomatic interaction and low-grade contact metamorphism with Carboniferous limestone country rock.

CHAPTER III
Mineralogy & Mineral Chemistry

3.1 INTRODUCTION

This chapter will outline the mineral assemblages and compositions of the various rock types encountered in this study, combining petrographic observations, semi-quantitative whole rock XRD data and quantitative mineral compositional data. Samples collected in this study are outlined in Chapter 2. A total of 56 thin sections were prepared for petrographic observations. A total of 25 samples were analysed using scanning electron microscopy (SEM) and a total of 22 samples were analysed using x-ray diffraction (XRD). Samples collected by Eijsink (2017) were also incorporated into this study and can be identified by the prefix 'AN16'. These samples include previously prepared thin sections and hand specimens that were prepared for whole rock analysis during this project.

3.2 ANALYTICAL TECHNIQUES

Samples were prepared for analysis at the School of Earth & Environmental Sciences, Cardiff University. Samples were cut using a diamond-encrusted circular saw to remove dirt and weathered surfaces, and reduced into blocks of approximately 10 cm in diameter ready for crushing. Thin section blocks were cut from the same material as their corresponding whole rock samples. Cut samples were then cleaned and dried before crushing.

A Fritsch Pulverisette 1 jaw crusher, equipped with Mn-steel jaws, was used to grind the samples into an aggregate of <10 mm in diameter. From the aggregate, a 100g representative sample was extracted for milling. A Retsch PM 400 planetary ball mill with agate grinding jars was used to further reduce grain size to <125 µm. The jaw crusher, mill and associated equipment were cleaned thoroughly between uses to minimise the risk of sample contamination. Rock powders were prepared for use both in XRD analysis and whole rock geochemical analysis (see Chapter 4.2).

Polished, uncovered 30 µm thin sections were produced at the Department of Natural Sciences, National Museum Wales or the School of Earth & Environmental Sciences, Cardiff University. Thin section samples selected for scanning electron microscope analysis were coated in a carbon film 10 – 15 µm thick to prevent charge build-up from the electron beam.

3.2.1 X-Ray Diffraction

Whole rock XRD preparation and analysis was conducted at the School of Earth & Environmental Sciences, Cardiff University using sample rock powders. Full scans were run using a Philips PW1710 Automated Powder Diffractometer using Cu Kα radiation at 35 kV and 40mA, between 2 – 70° 2θ at a scan speed of 0.02° 2θ/s. From the scans, phases were identified from diffractogram peaks using Philips PC-Identify 1.0b software, matching closest phase profiles to a diffractogram with support from thin sections or EDS analysis where needed. Broad dominant amphibole phases could be determined by XRD (ie. Na- or Ca-amphibole species), although multiple amphibole phases in a single sample (as discussed in Section 3.3) could not be accurately discriminated. Semi-quantitative analysis of phase proportions was performed by measuring corresponding peak areas and applying weight normalisations to determine relative abundances (Johns et al. 1954; Weaver 1961; Biscaye 1965).

3.2.2 Scanning Electron Microscope

Quantitative energy-dispersive X-ray spectrometry (EDS) was conducted at the School of Earth & Environmental Sciences, Cardiff University to analyse in-situ mineral chemistry, using a ZEISS Sigma HDVP field emission scanning electron microscope (SEM) equipped with two Oxford Instruments X-Max^N EDS detectors. Operating conditions were set at 15 kV and aperture size of 60 µm with a current of 4 nA and a working distance of 8.9 nm. Analytical drift checks were undertaken every 30 minutes using a Co reference standard.

Quantitative EDS analysis of different minerals was undertaken using one of several programs calibrated to appropriate standards. Pyroxene, amphibole and epidote analyses were calibrated to an ASTIMEX Kakanui hornblende standard, chlorite analyses were calibrated to an ASTIMEX chlorite standard and feldspar analyses were calibrated to an ASTIMEX plagioclase standard. Calibration was undertaken using suites of

ASTIMEX and Smithsonian standard materials. Secondary standard checks were performed regularly during data collection. Analyses were generally conducted with three closely clustered spots to highlight anomalous data, such as spots that intercept fractures or inclusions. Feldspars were scanned over an area of 10 μm^2 to avoid small-scale heterogeneity. Backscatter electron (BSE) imaging was carried out with EDS analysis.

3.2.3 Data calculations & software

Quantitative EDS data were grouped with similar data from the same analytical sites, which were deemed to be slight variations of the same compositions. An uncertainty of 2 standard deviations (2σ) has been applied and presented with data consisting of analyses from more than one point. Anomalous data were removed if deemed unreliable, for example anomalous analyses taken proximal to grain boundaries or inclusions.

Analyses were grouped by analytical sites, and similar data was grouped together to create data sets. Feldspars were homogenous across samples and were therefore grouped into single data points for whole samples. Amphiboles in the Gwna Complex were analysed using their individual spectra as data points, with anomalous spectra removed. Since EDS analysis cannot distinguish Fe^{3+} from Fe^{2+}, the data for FeO represents FeO_{total} and therefore ΣFe atoms per formula unit. Ratios of $Fe^{3+}/\Sigma Fe$ for clinopyroxene were then calculated based on stoichiometry and charge balance (Droop 1987).

Amphibole mineral formulae and site occupancies were calculated using methods presented by Locock (2014), with ratios of $Fe^{3+}/\Sigma Fe$ were estimated based on charge balance and assumptions on site occupancy. Amphibole species and subgroups were determined according to amphibole nomenclature recommended by the International Mineralogical Association (Hawthorne et al. 2012).

3.3 GWNA COMPLEX

Across the four areas of the Gwna Complex, a total of 34 thin sections were prepared, while 14 samples were analysed using SEM and 15 analysed using XRD. Magmatic and sedimentary samples will be discussed separately, with basalt-carbonate rocks included in sedimentary discussions.

3.3.1 Mineralogy of igneous rocks in the Gwna Complex

Four igneous lithologies – pillow basalts, hyaloclastites, massive basalts, and dolerites – were identified from across the Gwna Complex (see Chapter 2) and all will be discussed in this section. All samples exhibit evidence of pervasive alteration which has largely obscured magmatic mineralogy and textures. This alteration is largely accounted for by assemblages of albite, chlorite, quartz, carbonates and illite. Actinolite, which is a primary indicating mineral for greenschist facies, is absent in all magmatic samples except those from Unit 9 of Area I, which will be discussed separately. The Gwna Complex magmatic rocks have therefore undergone alteration in largely sub-greenschist conditions.

Pillow basalts

The magmatic texture of pillow basalts is generally semi-ophitic, with sprawling interstitial clinopyroxene masses up to 5 mm in diameter encasing randomly orientated plagioclase laths typically 0.5 – 1 mm long (see Figures 3.1a and b). Few samples such as AN19022 and AN19036 contain larger feldspars exceeding 2 mm length. Vesicles in samples such as AN18013 and AN18014 are infilled by assemblages of chlorite, zeolites, and calcite. Clinopyroxene is rarely preserved and was only identified in five samples (AN16029, AN18012 and AN18023 from Area I, and AN17013 and AN17015b from Area II) through various analytical methods. In samples analysed by XRD, clinopyroxene (augite/diopside) is a major constituent in the sample mineralogy, accounting for 18 – 26 % total volume. Clinopyroxene bearing samples all originate from undeformed pillow basalt sequences and do not contain haematite.

Plagioclase has been extensively albitised in all samples, and albite is typically the most abundant mineral phase (40 – 66 % ab). Chlorite (clinochlore), quartz and clay minerals (illite) are the main alteration products from mafic minerals and groundmass, with additional Fe-Ti oxides, epidote, prehnite, calcite and muscovite. It should be noted that due to crystallographic and compositional similarities, distinctions between illite and muscovite were in many cases difficult to resolve. Chlorite is ubiquitous in analysed pillow basalt samples (3 – 10 % ab) and often comprises the bulk of interstitial spaces between feldspar laths, presumably occupying the spaces of clinopyroxene and potentially other replaced mafic minerals, typically alongside illite and associated phyllosilicate minerals. Quartz and carbonate minerals are typically present in varying quantities, often buffered by the presence of veins in samples that have undergone deformation.

Reddened pillow basalts such as AN16028 and AN17022 contain haematite (up to 11 % ab) and are associated with elevated abundances of quartz, carbonates and illite (see Figure 3.1c). Conversely, chlorite seems to be less widespread. No primary magmatic minerals were found in these samples. While reddened pillows tend to be more deformed and therefore populated by more veins, quartz and carbonate minerals are seen commonly within alteration assemblages.

AN17015a and b represent samples taken from interpillow schist and pillow basalt respectively. The interpillow schist is dominated by quartz (48 % ab), calcite (31 % ab) and chlorite (15 % ab), with only a small quantity of albite (6 % ab). While no distinct masses of jasper or carbonate were present in the sample, silica and carbonate activity has had a major pervasive effect on interpillow spaces.

Hyaloclastites

Like the interpillow schist AN17015a, hyaloclastites contain very little albite, and are predominantly composed of quartz and carbonate minerals, with subordinate abundances of chlorite and illite. These minerals comprise hyaloclastite matrices, which are generally fine grained and arranged into complex bands of alternating dominant minerals that defines a foliation. AN18022, a carbonate-rich hyaloclastite, develops coarser granular areas dominated by carbonates, with slip planes developed along patches of intergranular chlorite.

AN17024 contains small amounts (3 % ab) of haematite that has resulted in reddened clasts. Preservation state of clasts ranges between samples, but no samples retain any primary magmatic minerals. Clasts in AN17024 and AN18022 for example, retain magmatic textures, with randomly orientated albite laths and extensively altered interstitial spaces filled by chlorite and clay minerals (see Figure 3.1f). However, smaller clasts in these hyaloclastites have been incorporated into the matrix fabric, have undergone elongation and have been extensively replaced by carbonates, quartz, chlorite, clay minerals, and Fe-Ti oxides. Extensive clast alteration often appears zonal, and AN18022 shows zonal alteration in clasts of all sizes (see Figure 3.1e).

Massive basalts

A singular sample of massive basalt (AN17020) was analysed, showing consistent mineral assemblages with reddened pillow basalts, containing relatively high amounts of quartz (19 % ab), illite (11 % ab) and haematite (7 % ab) that fill interstitial spaces. Albitised feldspars in the sample are relatively elongate, thin laths 2 – 4 mm long (see figure 3.1d).

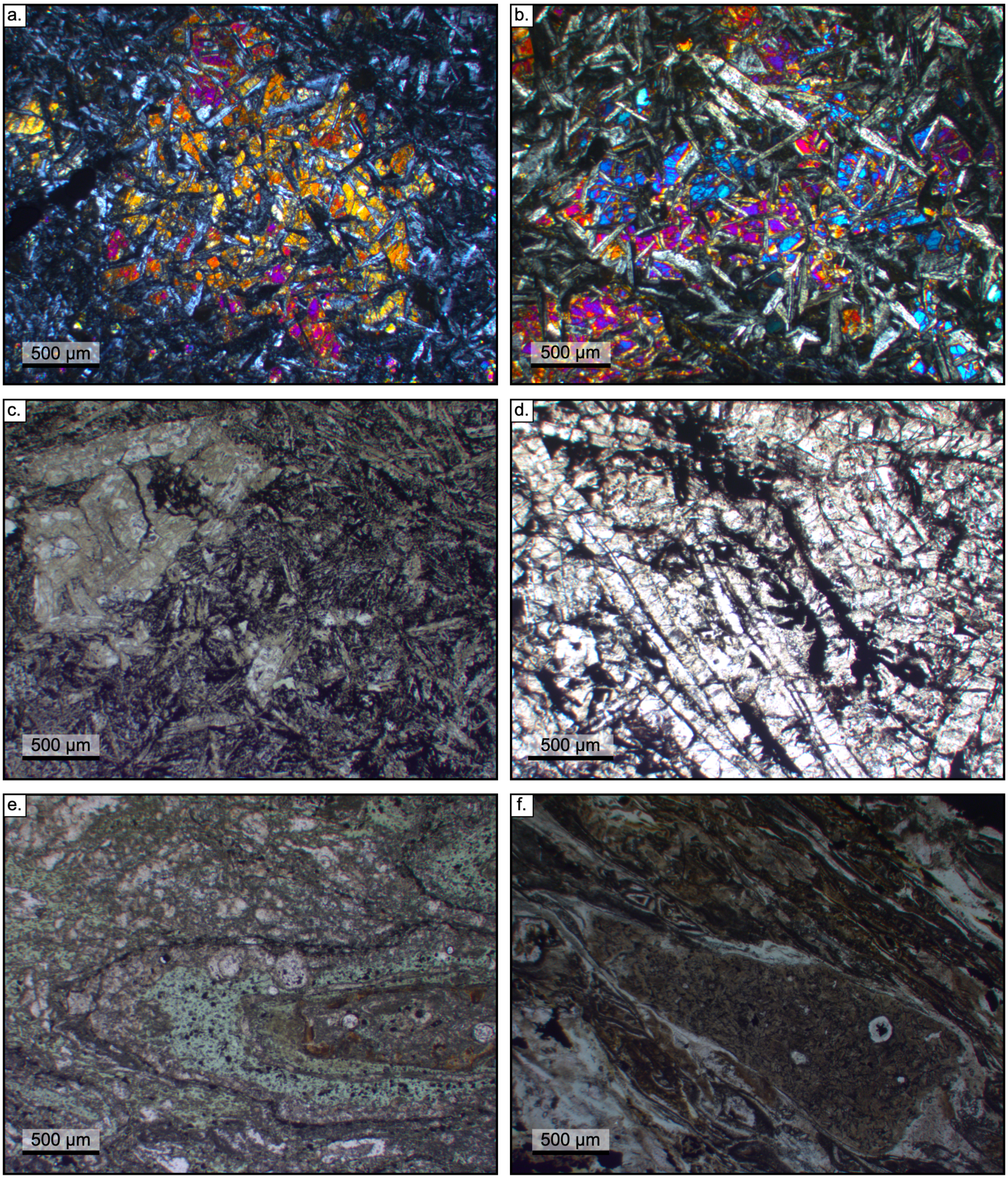

Figure 3.1: Microscopic images from basaltic rocks in the Gwna Complex showing a selection of textural features including (a) semi-ophitic textures in a pillow basalt (AN18012) outlined by a rare occurrence of magmatic-derived clinopyroxene with altered rims, occupying interstitial spaces between altered plagioclase laths; (b) well-preserved clinopyroxene (AN18023) showing partially euhedral shape around albitised plagioclase laths; haematite-bearing pillow basalt (AN19022) consisting largely of an altered opaque groundmass of haematite + clay minerals + quartz, with an albitised feldspar phenocryst to the left; massive basalt (AN17020) showing a haematite-bearing interstitial assemblage around light, elongated feldspars; (e) chlorite-rich hyaloclastite (AN18019) showing zoned alteration of an elongated basalt clast with a carbonate-dominated rim, chloritic mantle rich in Fe-Ti oxides and a clay-rich core; (f) elongated basalt clast (AN17024) within a highly sheared hyaloclastite matrix consisting of alternating, flowing bands dominated by carbonates, chlorite and clay minerals with intermittent remnants of smaller basalt clasts.

Area I – Unit 9

Five analysed samples from Unit 9 of Gwna Complex Area I include pillow basalt (AN18014), dolerite (AN18015, AN19026 and AN19028) and hyaloclastite (AN19029). The uniqueness of these rocks within Area I was discussed in Section 2.3.2. Mineralogically, the rocks are also significant, in that they are the only actinolite-bearing rocks found within the Gwna Complex. Actinolite was found within the pillow basalt and dolerite samples (8 – 14 % ab) but was not found in the hyaloclastite. Estimates from XRD suggest that AN18014 and AN18015 have very similar compositions, with high albite contents (64 – 57 % ab), along with quartz (8 – 11 % ab), chlorite (5 – 10 % ab) and actinolite. Epidote was estimated at 7 % abundance in AN18015 but was not detected in AN18014 despite being confirmed in thin section.

In both rock types, actinolite is acicular and intergrown with chlorite and minor amounts of titanite. Within dolerites, the assemblages form in distinctly elongate patches 1 – 2mm long in various orientations and may be pseudomorphs of subhedral prismatic minerals. Similar textures have been reported in dolerite sills forming from the alteration of clinopyroxene or titanomagnetite (Fowler and Zierenberg 2016). Relatively high concentrations of titanite suggest that titanomagnetite was involved. These textures are also present in AN18014, although assemblages are smaller (0.2 – 0.5 mm long) and less defined spatially. Assemblages of chlorite and epidote fill interstitial spaces throughout these rocks, with epidote often concentrated along interfaces with albite.

AN19029 shows a highly altered and deformed hyaloclastite consisting of carbonates (70 % ab), quartz (14 % ab) and chlorite (13 % ab). Clasts have been elongated and replaced extensively by calcite and subordinate quartz and chlorite, while the highly sheared matrix consists of chlorite with clay minerals and Fe-Ti oxides. Alignment of clasts has allowed slip planes to develop along planar channels of matrix, marked by linear concentrations of clay minerals.

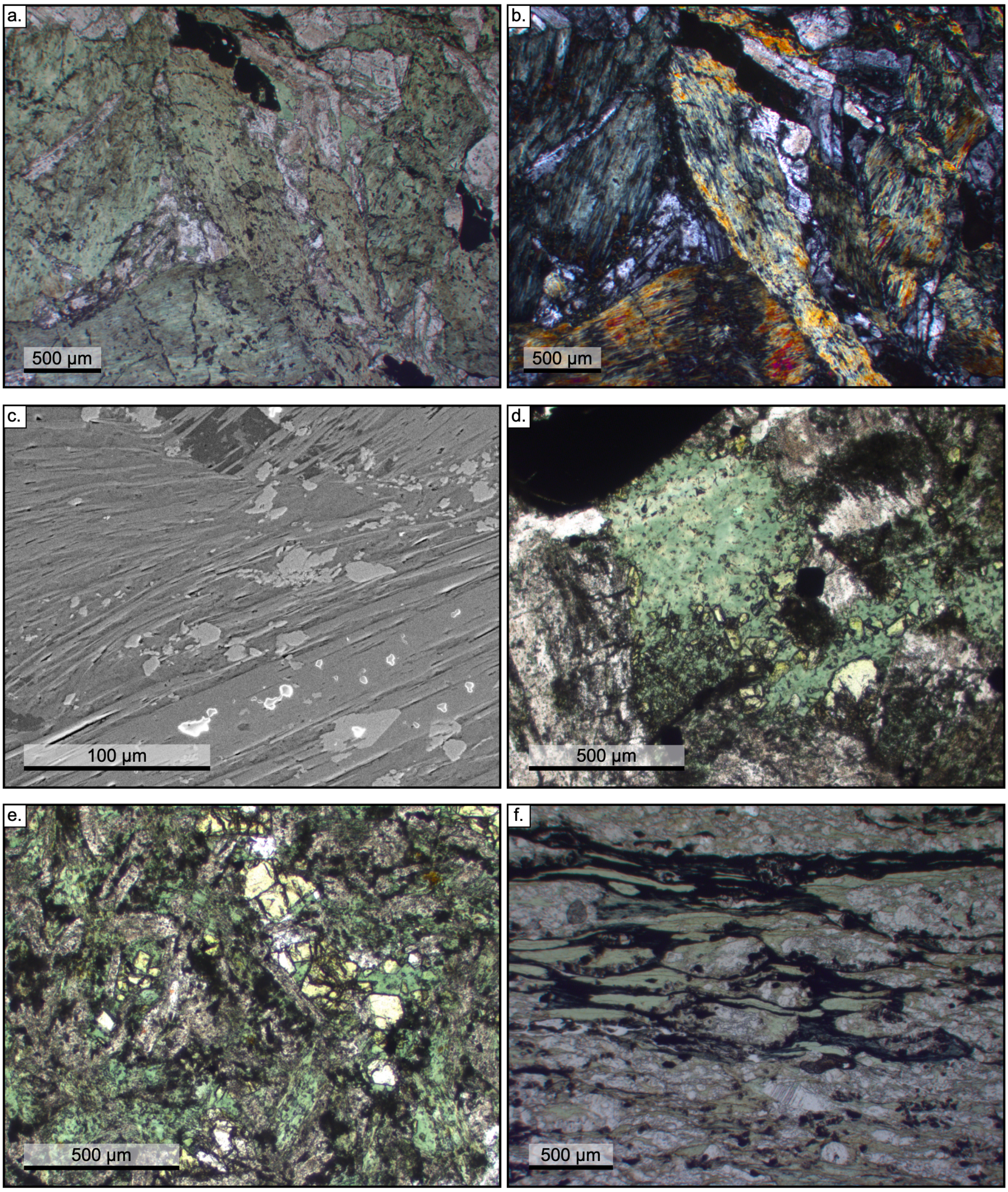

Figure 3.2: Various petrographic textures from magmatic rocks in Gwna Complex Unit 9 including (a-b) multiple randomly orientated assemblages of actinolite + chlorite + titanite that have seemingly replaced a primary mafic mineral from AN19028; (c) BSE image of AN19028 showing the closely intergrown nature of the alteration assemblage and the relatively prominent occurrences of titanite; (d) interstitial chlorite between albitised plagioclase laths with dense occurrences of epidote that are clustered around the chlorite-albite interface in AN18015; (e) the finer grained pillow basalt texture of AN18014 showing the same alteration features as observed in the diorites; (f) the Unit 9 hyaloclastite (AN19029) showing a chlorite-rich matrix surrounding elongated basalt clasts that have been extensively altered to carbonates with subordinate quartz and chlorite.

3.3.2 Mineral chemistry of igneous rocks in the Gwna Complex

Clinopyroxene

Clinopyroxene was quantitatively analysed from three pillow basalt samples – AN17013, AN18012 and AN18023. All samples are rich in Mg and produce an Mg# range between 60.5 and 82.1, with most analyses showing an Mg# above 75. Bivariate plots in Figure 3.3 show decreasing Ti (0.058 – 0.020 apfu), Mn (0.012 – 0.004 apfu), Fe (0.42 – 0.18 apfu) and Na (0.043 – 0.019 apfu) with increasing Mg#. Conversely, Al and Ca show broadly positive correlations to Mg#. AN17013 contains increased Al and Ti, directly offsetting relatively low Si contents (1.74 – 1.76 apfu) compared to other samples (1.83 – 1.91 apfu). The balance of these compositional changes within the T-site is shown in Figure 3.4a, which also highlights a relative imbalance between Ti and Al in AN18023-8a and 8b in favour of additional Ti (Ti/Al = 0.41 – 0.42; Ti/Al range in other samples = 0.16 – 0.24). Similarly, AN18012-4a is shown to have elevated Si (1.91 apfu) and relatively low Al (0.10 apfu) and Ti (0.02 apfu). It also shows minor depletions in Ca and Na, with higher Mg contents balancing the M2 site.

The three samples have overlapping compositional ranges, with Mg# ranges of 70.2 – 78.5 in AN17013, 74.7 – 82.1 in AN18012 and 60.5 – 79.0 in AN18023. AN18023-8a and 8b are the only analyses with Mg# values below 70. They follow the compositional trends set by AN18012 and AN18023. AN18023-8a and 8b were analysed from a single clinopyroxene grain, and their differences represent internal chemical heterogeneities. However, the greater compositional differences from other analyses in AN18023 show that chemical variation is greater between individual grains than through internal heterogeneity.

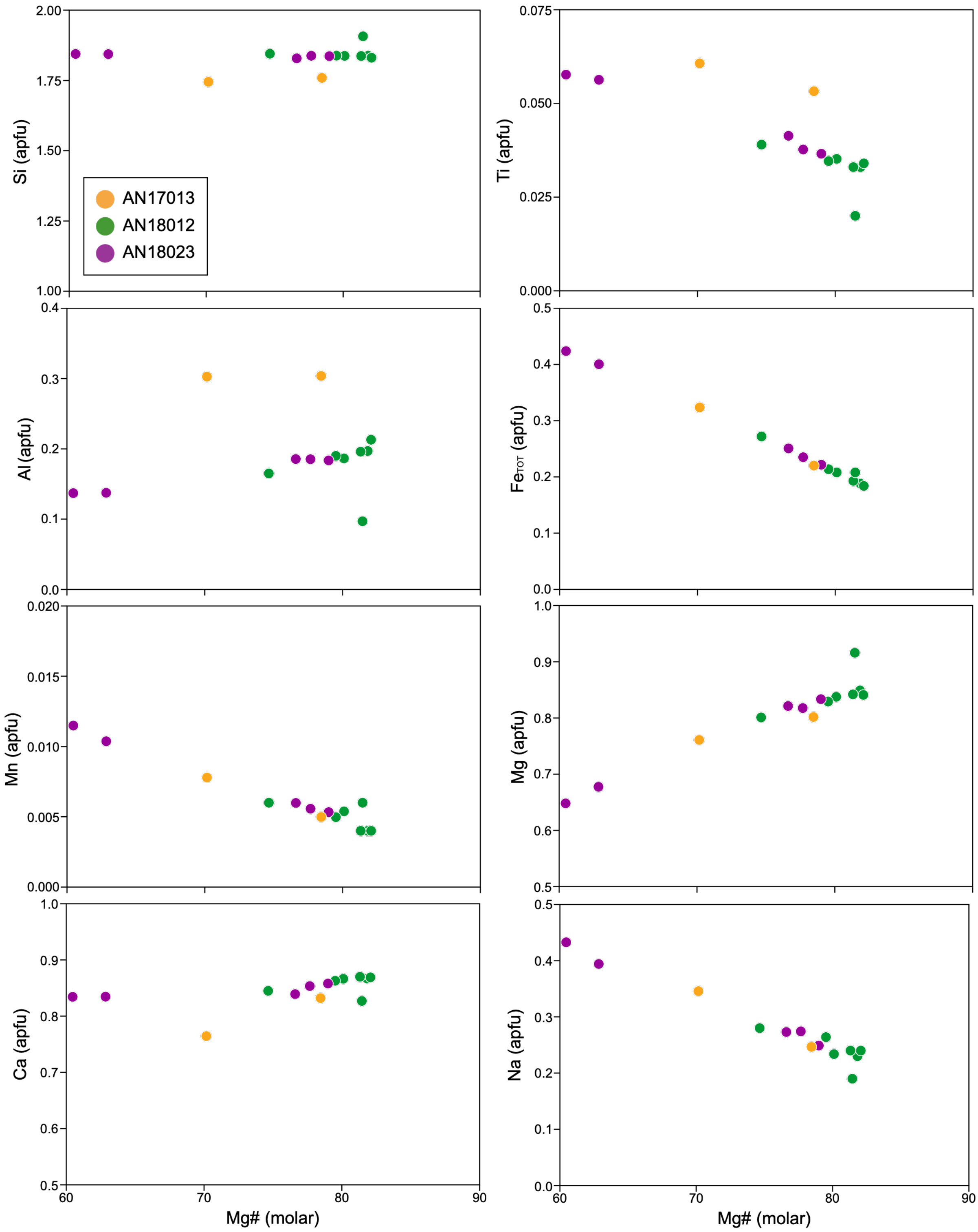

Figure 3.3: Bivariate plots of molar Mg# against major elements for clinopyroxenes in magmatic rocks of the Gwna Complex.

Figures 3.4b and c show tectonic discrimination plots using clinopyroxene compositions, with samples plotting largely within the MORB fields. Both samples from Area I – AN18012 and AN18023 – plot very closely within the MORB fields while AN17013 – from Area II – plots above the MORB field in Figure 3.4b and within the E-MORB field in Figure 3.4c, suggesting that they derive from a more enriched basalt. All analysed clinopyroxenes are diopsides (see Figure 3.4d), with compositional end-member ranges of X_{Wo} 41.3 – 45.9, X_{En} 34.0 – 47.0 and X_{Fs} 9.7 – 22.2.

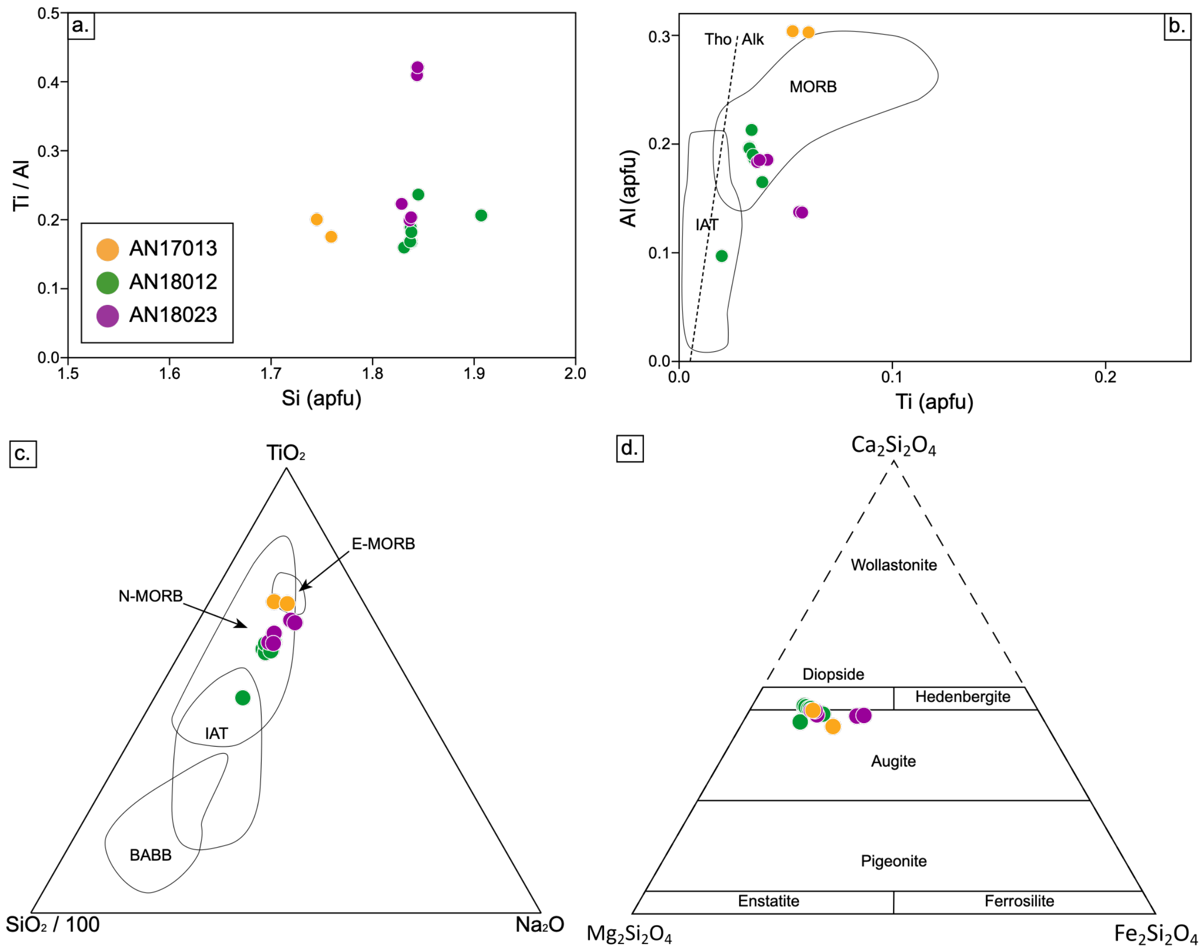

Figure 3.4: Various chemical plots of clinopyroxenes from the Gwna Complex showing (a) the relationships between constituents occupying the T site; (b) tectonic discrimination plot using Al and Ti as pressure indicators, after Leterrier et al. (1982); (c) ternary tectonic discrimination plot, after Nisbet and Pearce (1977); pyroxene classification plot, after Morimoto et al. (1988).

Amphibole

Amphiboles were quantitatively analysed from three samples from Area I Unit 9 of the Gwna Complex – AN18014 (pillow basalt), AN18015 and AN18028 (both dolerites). Amphibole compositions are predominantly within the tremolite-ferro-actinolite series with some analyses straying towards magnesio-ferri-hornblende compositions, (see Figure 3.5a). Analyses represented by triangles create a secondary cluster characterised by low A site cation sums (0.021 – 0.087; main range 0.037 – 0.158), the inclusion of Fe^{2+} (0.018 – 0.163 apfu) within the B site to offset low Ca (1.718 – 1.907 apfu; main range 1.918 – 2.000 apfu), and high Fe^{3+} contents (0.224 – 0.523 apfu) in place of Fe^{2+} in the C site. Hollow triangles represent analyses within this trend that reach magnesio-ferri-hornblende compositions. All samples within the main cluster contain between 2.5 and 4.5 Mg cations in the C site, placing them within the actinolite field of the tremolite-ferro-actinolite series (see Figure 3.5b).

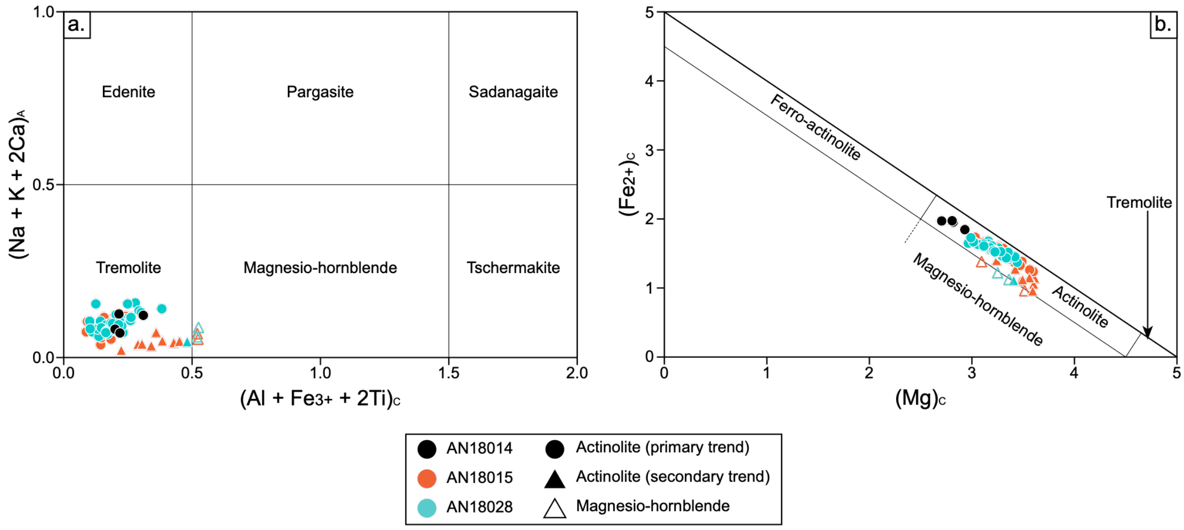

Figure 3.5: Amphibole species classification diagrams for amphiboles from magmatic rocks in the Gwna Complex showing (a) classification based on constituents of A and C sites; and (b) classification of species within the tremolite-ferro-actinolite series based on C site constituents.

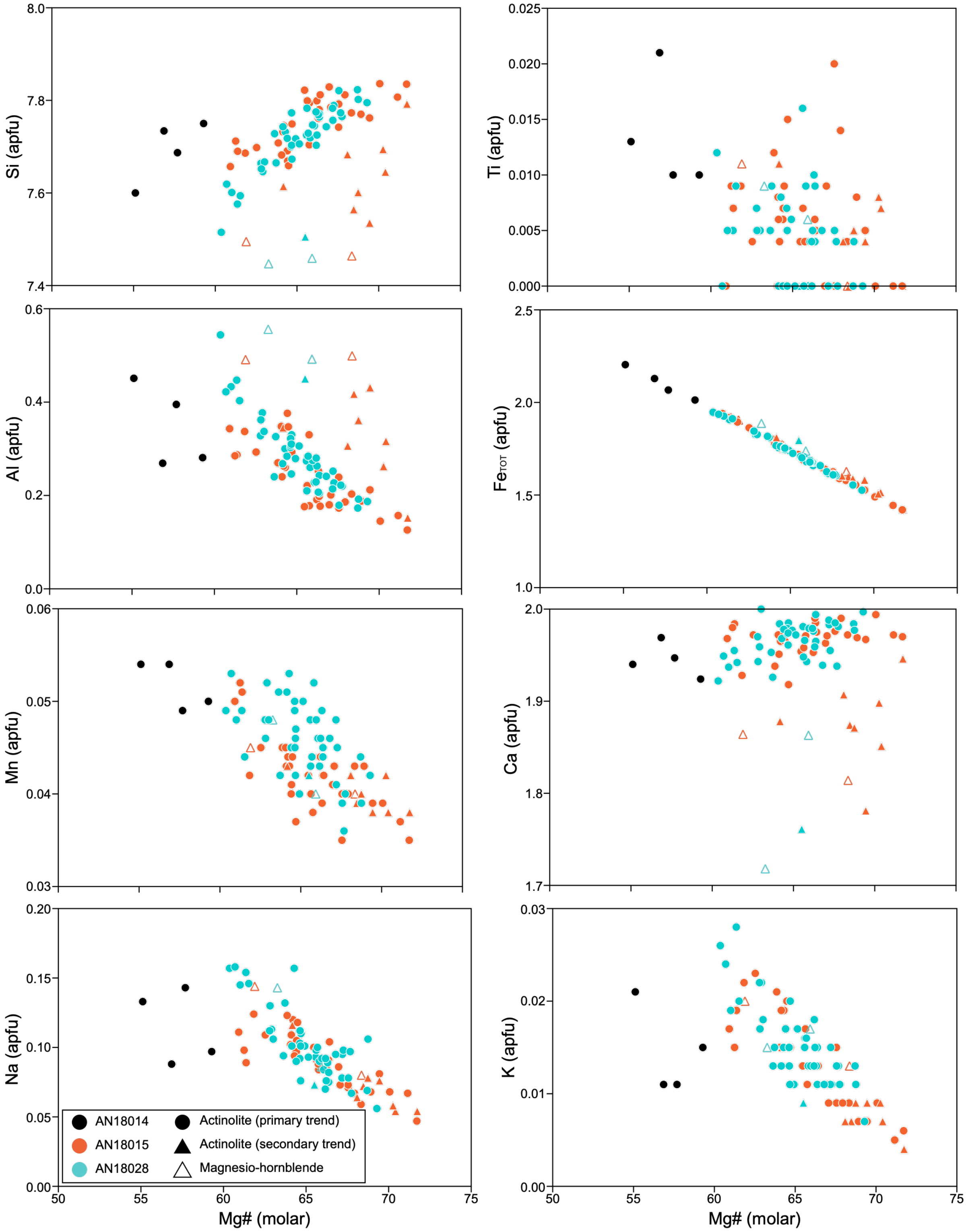

Figure 3.6: Bivariate plots of amphiboles from the Gwna Complex plotting molar Mg# against major elements.

Analyses from AN18014 have a distinctly lower Mg# range (55.1 – 59.3) than those from AN18015 (60.9 – 71.7) and AN18028 (60.4 – 69.3), as shown by the multivariate plots of Figure 3.6. They have low Mg contents (12.2 – 13.4 % MgO) and subsequently high Fe contents (16.3 – 17.7 % FeO) relative to the main trend (13.8 – 16.8 % MgO; 11.8 – 16.1 % FeO). AN18014 is otherwise compositionally similar to the main trend. For all analyses, increasing Mg# coincides with decreasing Al (3.3 – 0.7 % Al_2O_3), total Fe (17.7 – 11.8 % FeO), Mn (0.43 – 0.29 % MnO), Na (0.56 – 0.17 % Na_2O) and K (0.15 – 0.02 % K_2O). Conversely, Si increases (51.1 – 54.9 % SiO_2) with Mg#, along with Mg (12.2 – 16.8 % MgO). From the secondary trend, low Si and subsequently high Al in the T site is reflected in the bivariate plots of Figure 3.6, along with low Ca.

Feldspar

Albitisation of magmatic plagioclase has been comprehensive throughout all analysed samples in the Gwna Complex. Average compositions from seven basaltic or doleritic samples produce compositional ranges of X_{AN} 0.2 – 2.5, X_{AB} 97.1 – 99.5, X_{OR} 0.3 – 1.5. The two samples with the lowest albite components – AN18012 (X_{AB} = 97.1) and AN18023 (X_{AB} = 97.1) – both contain magmatic clinopyroxene, suggesting that albitisation in these samples was incomplete due to less intense alteration.

3.3.3 Petrography of sedimentary rocks in the Gwna Complex

Basalt-carbonate rocks

Basalt clasts in basalt-carbonate rocks are heavily altered in a similar manner to those in hyaloclastites. They have a very dark appearance, suggesting high haematite and clay mineral contents. Multiple generations of carbonate veins extensively infiltrate basalt and isolate smaller fragments. Alignment of clay minerals creates networks of slip planes throughout the altered basalt clasts, accommodating plastic deformation of basalt and stretching of clasts (see Figure 3.7a). Small elongate fragments of relatively tough altered basalt remain between these slip planes. AN20021 shows the replacement of the interior of a basalt pillow by carbonate material (see Figure 3.7b). The fine-grained carbonates form along anastomosing bands that flow around elongate altered basalt remnants, seemingly along the clay-rich slip planes. It is possible that these slip planes opened fluid pathways allowing an influx of carbonate material into clast interiors, and carbonates have precipitated in place of these weak horizons, while relatively robust altered basalt has remained in place.

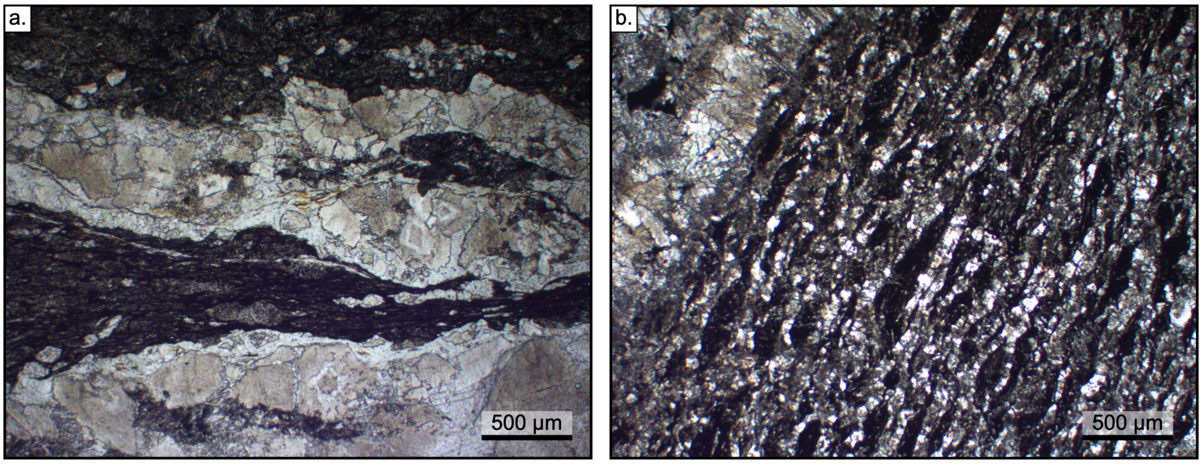

Figure 3.7: Textures of basalt-carbonate rocks showing (a) plastic deformation of basalt along clay-rich slip planes flowing around residual basalt fragments, pinched between carbonate veins; and (b) partly replaced pillow basalt interior with strands of remnant basalt surrounded by carbonate material.

Chloritic sandstone

AN17025 and AN19025 both represent chloritic sandstones from Area I. AN17025 is finer grained and seems to have been more altered. Grains are up to 0.1 mm in diameter and are rounded to subrounded. Common rounded grains of chloritic material represent altered clasts of lithic fragments and/or feldspars. The matrix consists of clay-rich material that included some chlorite. Elongate ovoid features – shown at outcrop scale in Figure 2.6d – sit parallel to foliation and are coarser grained, with a less abundant, more chloritic matrix. AN19025 contains subangular to subrounded clasts up to 0.5 mm in diameter, consisting of significant amounts of both feldspar and various lithic fragments, classifying the sample as a lithic arkose. The sandstone is more densely packed with a matrix consisting of chlorite with subordinate clay minerals.

Chloritic schist

Chloritic schists consist predominantly of quartz and albite (> 75 % ab), with quartz being more abundant. Muscovite, chlorite, and clay minerals comprise most of the remaining volume, concentrated and aligned to create schistose foliation. Calcite also occurs in all analysed samples, present in veins or as an alteration product. All samples have been greatly deformed, leading to quartz recrystallisation, locally heterogeneous grain sizes and the development of occasional porphyroclasts within a reduced matrix.

3.4 PENMYNYDD TERRANE

Thin sections were prepared for eight metabasite samples, along with two samples of metasedimentary rocks. Seven metabasite samples were analysed using SEM and six were analysed using XRD, while two metasedimentary samples were analysed using SEM.

3.4.1 Mineralogy of the Penmynydd Terrane

Metabasites

Mineral assemblage of the metabasites consists primarily of sodic to calcic amphiboles, albite, and epidote, with chlorite, quartz and illite. Titanite, rutile and pyrite occur as accessory minerals. Samples all show distinct foliation propagated by alignment of amphiboles (see Figure 3.8a). Amphiboles tend to dominate samples, accounting for 33 – 85 % total rock volume. Albite is mostly found within elongate pockets or bands between amphibole-dominated layers and has a variable abundance (see Figure 3.8c). In most samples, albite accounts for 29 – 37 % total rock volume, however it is particularly abundant in AN19015 (48 % ab) and was not detected by XRD in AN16015 – which consequently has an amphibole content of 85 %. Quartz was identified by XRD in three samples (up to 9 % ab) and is typically found alongside albite.

Only a dominant amphibole species could be determined using XRD due to the crystallographic similarities between closely related species. Dominant amphibole species range from calcic actinolite (AN17006, AN17011 and AN17032) to sodic glaucophane (AN16015 and AN19015) and riebeckite (AN17003). Petrographically, samples show zoned amphiboles with green (calcic) cores that grade towards blue (sodic) rims to various extents. Samples show different components based on their colour range. AN16015 and AN19015 for example contain predominantly blue amphiboles with only small cores of green phases. AN17006 and AN17032, for example, are dominated by green amphiboles with faintly blue rims seen sporadically. While amphibole zonation is generally observed to be gradual, AN16015 demonstrates a sharp transition between calcic core and sodic rim (see Figure 3.8d). Sodic amphiboles are indicative of blueschist facies metamorphism, while actinolite is a characteristic greenschist facies mineral. This relationship therefore represents stages of prograde metamorphic replacement of actinolite by sodic amphiboles. Sporadic examples of larger amphiboles from AN17011, however, suggest possible retrograde zoning, with light green rims around blue-green cores (see Figure 3.8b).

All samples contain epidote (4 – 11 % ab) with the exception of AN17011, which instead contains clinozoisite (8 % ab). Epidote commonly occurs in concentrations as granular or elongate crystals orientated parallel to foliation, typically within amphibole dominated bands. In several samples, large epidote grains (> 0.5 mm) distort amphibole fabrics and develop asymmetric pressure shadows that are commonly filled by chlorite and quartz (see Figure 3.8e). Chlorite (clinochlore) was measured in all samples analysed by XRD (3 – 11 % ab) and occurs as a product of alteration, mostly within amphibole dominated bands. Illite was also identified in four of six samples analysed by XRD (6 – 14 % ab) and is another alteration product that formed through retrogression.

Mica schists

The mica schists of the Penmynydd Formation consist of predominantly quartz with foliated layers of phengitic mica. Albite is found within quartz assemblages, while small grains of titanite and Fe-Ti oxides are scattered throughout phengite layers. In AN16001, euhedral garnets up to 0.5 mm in diameter sparsely populate phengite layers of a mica schist (see Figure 3.8f). Foliation deflects around the garnets, which show evidence of rotation. Chlorite occurs as an alteration product throughout phengite layers but is found in highest concentrations around garnets. Chlorite fills pressure shadows around garnets and infills fractures within garnets.

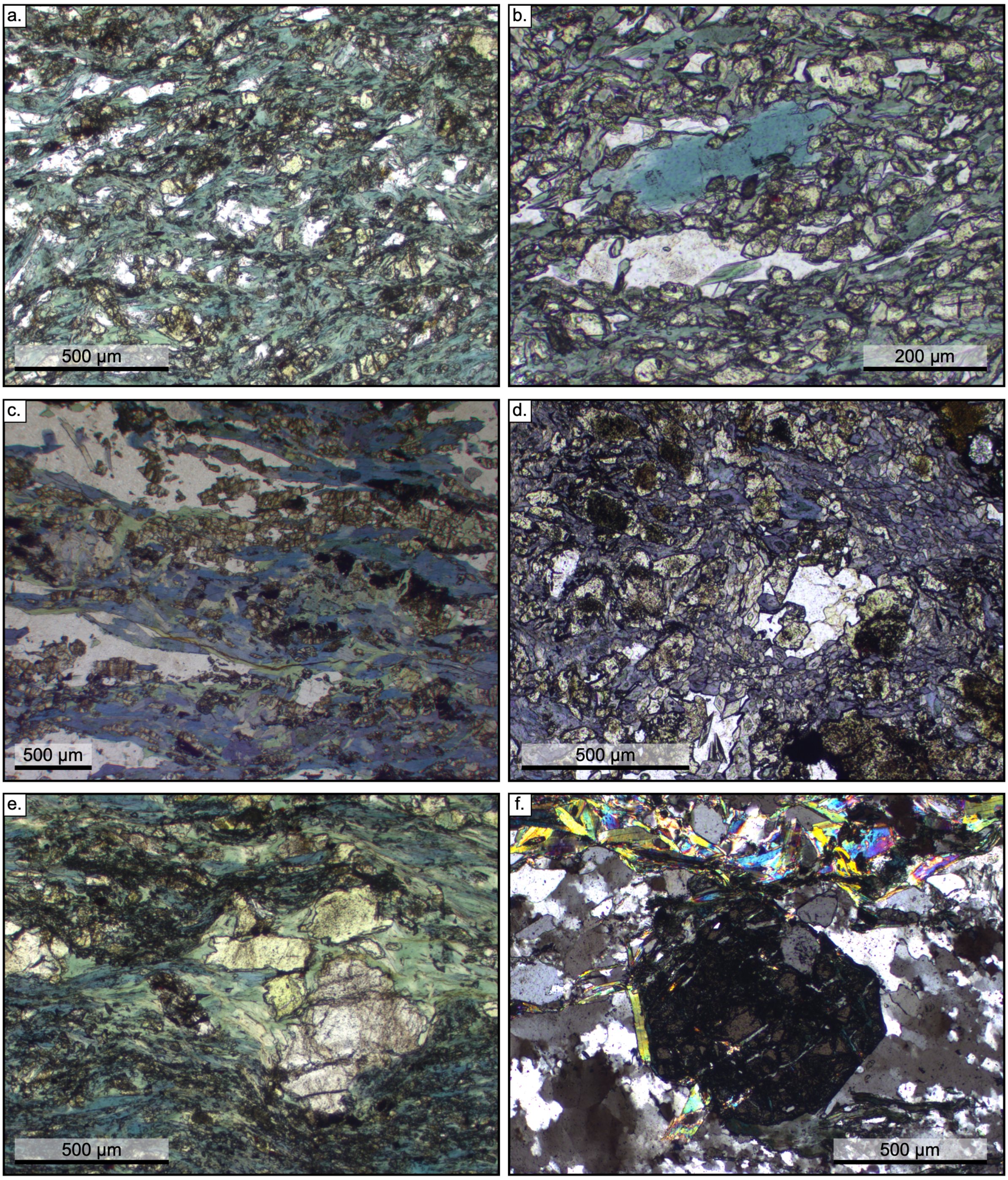

Figure 3.8: Various petrographic features from rocks in the Penmynydd Terrane including (a) foliated fabric of predominantly green amphiboles with a lightly developed crenulation in AN17006 with epidote and albite; (b) zoned amphibole with blue-green core and light green rim in AN17011; (c) banded zones of blue amphiboles, chlorite and titanite with intermittent albite in AN19015; (d) glaucophane-dominated texture in AN16015 showing sharp amphibole zonation with green cores and blue rims; (e) epidote porphyroblast in AN17003 with a metamorphic fabric deflected asymmetrically around, with chlorite concentrated within pressure shadows; and (f) euhedral, partially altered garnet within a mica schist (AN16001).

3.4.2 Mineral chemistry of the Penmynydd Terrane

Amphibole

Amphiboles were quantitatively analysed from eight metabasite samples from the Penmynydd Terrane. Compositional subgroups range between calcic, sodic-calcic, and sodic. Most samples have compositional ranges from calcic to sodic-calcic amphiboles (AN17006, AN17011, AN17032 and AN17007). AN16015 and AN19015 have amphibole compositional ranges from sodic-calcic to sodic. AN17003 is the only sample that shows a compositional range from calcic to sodic amphiboles. AN17004 contains only calcic amphiboles.

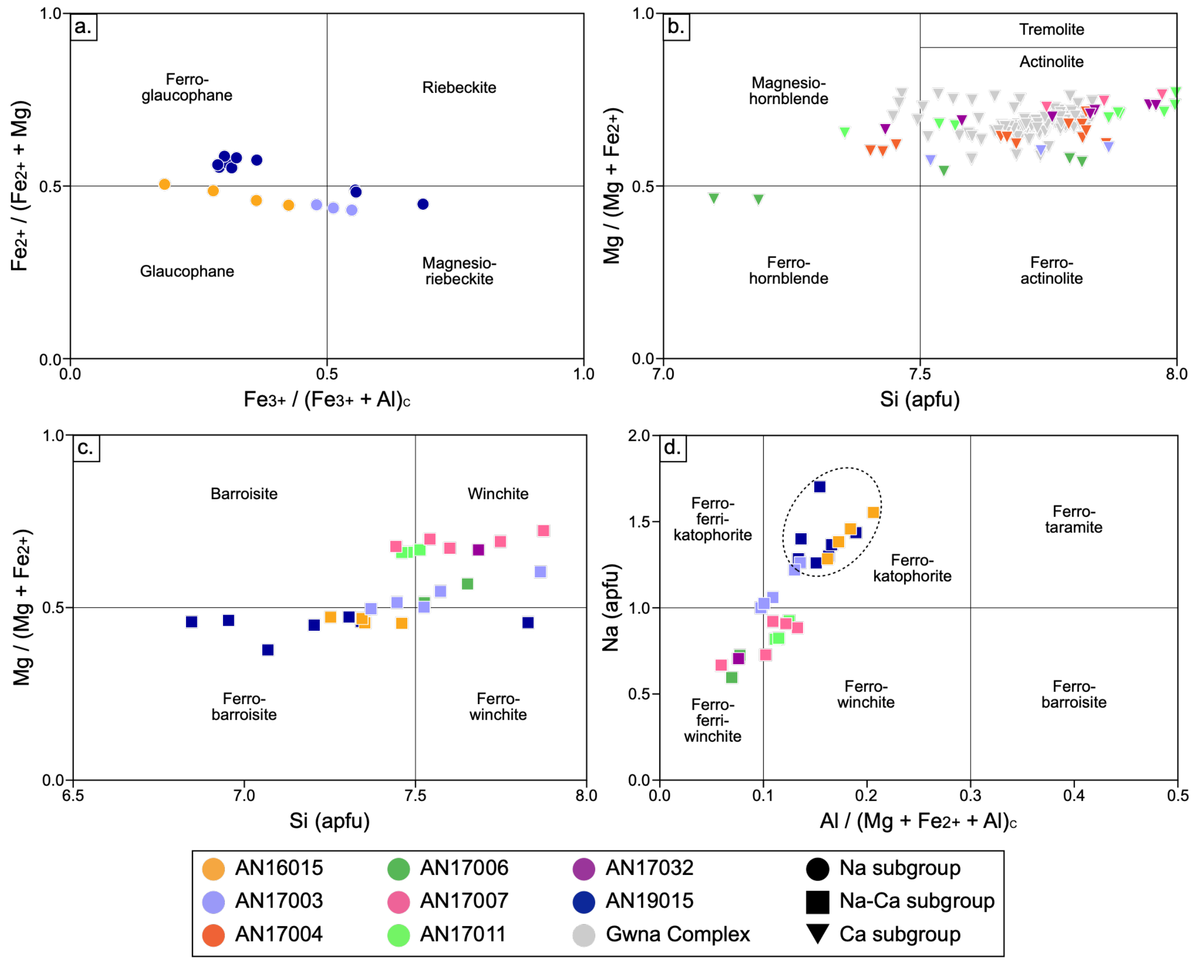

Figure 3.9: Amphibole species classification diagrams for amphiboles from Penmynydd Terrane metabasites showing (a) sodic amphibole classification; (b) calcic amphibole classification; (c) sodic-calcic amphibole classification based on mafic and silica contents; and (d) sodic-calcic classification based on C site constituents to show that analyses plotting in the ferro-barroisite field of Figure 3.9c actually represent ferro-katophorite (circled data).

Sodic amphiboles are indicative of blueschist facies metamorphic conditions, whilst calcic amphiboles such as actinolite, are characteristic greenschist facies mineral indicators. The relationship between Ca and Na contents in these amphiboles is therefore a reliable proxy for relative metamorphic grade, where increasing Na indicates a prograde reaction, and an increase in Ca – as seen towards the rims of some samples discussed below – would indicate retrograde reactions.

Sodic amphibole species range from ferro-glaucophane – glaucophane – magnesio-riebeckite, controlled largely by Fe^{2+}/Fe^{3+} ratios in the C site (see Figure 3.9a). Sodic-calcic amphiboles range from ferro-katophorite – ferro-winchite – ferro-ferri-winchite - ferri-winchite – winchite (see Figure 3.9c and d). The Na-Ca amphiboles are split between two groups. Ferro-katophorites and similar compositions with low Mg and relatively high Na (> 1 apfu) originate from samples with sodic amphibole rims. Winchites, however, originate generally from the rims of calcic amphiboles. Calcic amphiboles range from actinolite – magnesio-hornblende – magnesio-ferri-hornblende – ferro-hornblende (see Figure 3.9b). Samples occupy similar compositional ranges to one another and are comparable amphiboles from the Gwna Complex. Two ferro-hornblende analyses – both from AN17006 – are compositional outliers.

The bivariate plots of Figure 3.10 show a linear decrease in Si from calcic (48.3 – 57.8 %) to sodic-calcic (45.8 – 55.1%) phases across variable ranges within samples. Sodic phases show a sharp increase in Si contents (53.0 – 56.9 %) relative to this linear trend. Negative linear relationships with Si can be seen with Al (0.53 – 10.90 %), Ti (0 – 0.34 %), Na (0.68 – 5.90 %) and K (0.01 – 0.28 %) between calcic and sodic-calcic phases. Sodic phases show decreases in Ti (0 – 0.1 %) and K (0 – 0.05 %) in proportion to their increase in Si. They also show a decrease in Al (4.55 – 8.44 %) to a lesser extent. In contrast, Na increases along with Si from calcic-sodic to sodic (5.8 – 6.8 %). Broadly linear correlations with Si can be seen in Mg (6.96 – 17.60 %) and Ca (2.15 – 12.15 %) for calcic to sodic-calcic phases. Sodic phases show no relative changes in Mg (6.90 – 8.72 %) from sodic-calcic phases, and a decrease in Ca (0.97 – 2.58 %). Negative relationships between Si and Fe in calcic to sodic-calcic phases are split between parallel trends of different samples. AN16015, AN17003, AN17006 and AN19015 have relatively high Fe (16.38 – 23.06 %), while AN17004, AN17007, AN17011 and AN17032 have relatively low ranges (10.04 – 17.34 %). Sodic phases show similar Fe contents to their sodic-calcic counterparts, with AN16015 showing a minor decrease in Fe in sodic phases.

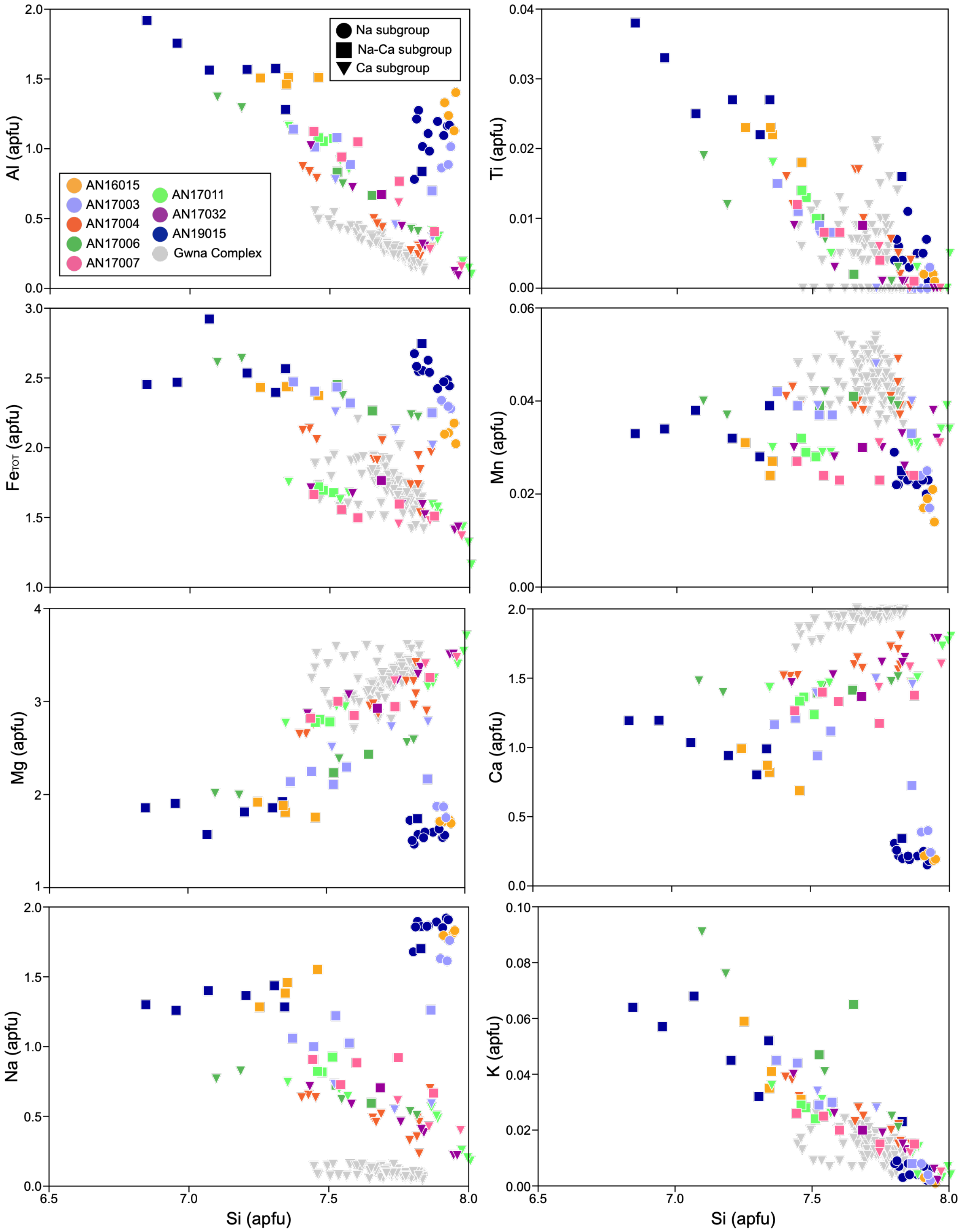

Figure 3.10: Bivariate plots of compositions of amphiboles from Penmynydd Terrane metabasites, plotting Si cations against other major element cations. Gwna Complex amphiboles (see Section 3.3.2) are also included for reference.

Gwna Complex calcic amphiboles (predominantly actinolite) have distinct compositional differences from the calcic amphiboles of the Penmynydd Terrane. They have relatively high Ca, Mg and Mn contents, along with relatively low Na and Al contents, along with consistently low Na/Al ratios (see Figure 3.11).

Compositional variability in the Penmynydd Terrane amphiboles is predominantly controlled by zonation, grading from relatively calcic cores to relatively sodic rims (see Figure 3.11). Compositions in AN17004 and AN17006 show greater variations between grains rather than through internal heterogeneity. Mg# decreases uniformly from calcic to sodic phases (43.0 – 76.1 calcic; 35.0 – 68.3 sodic-calcic; 36.5 – 45.5 sodic). AN16015, however, has higher Mg# values in sodic phases than its corresponding calcic phases. Cation proportions Na/Al generally decrease from calcic to calcic-sodic phases and subsequently increase again in sodic phases. AN17003 shows increasing Na/Al ratios from calcic through to sodic phases, suggesting that lower Mg# values (< 56) may influence Na/Al ratios.

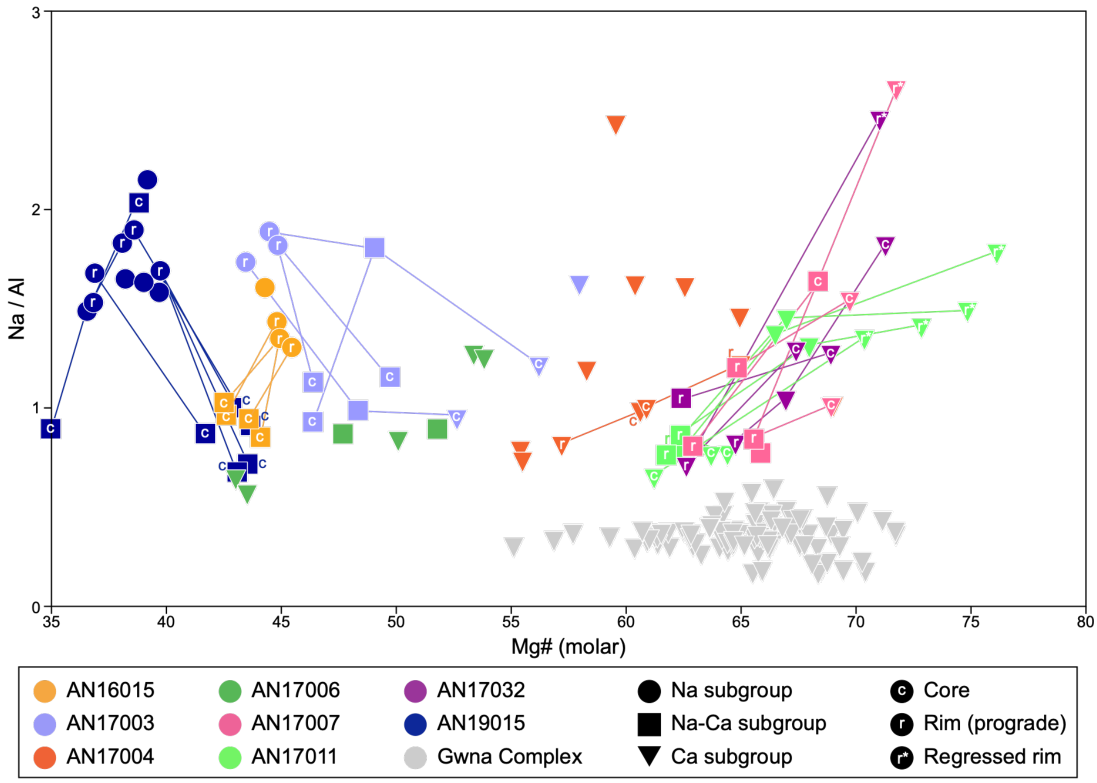

Figure 3.11: Bivariate plot of amphibole compositions from Penmynydd Terrane metabasites showing chemical zonation trends between cores and rims of samples.

Three samples – AN17007, AN17011 and AN17032 – have calcic outer rims showing evidence of minor retrograde reactions. These retrograde rims occur within calcic-dominated samples but were not observed in samples containing sodic amphiboles. Retrograde amphiboles are all actinolite with high Mg# values (> 70). The rims tend to be very thin (< 10 μm) and overprint the initial prograde zonation.

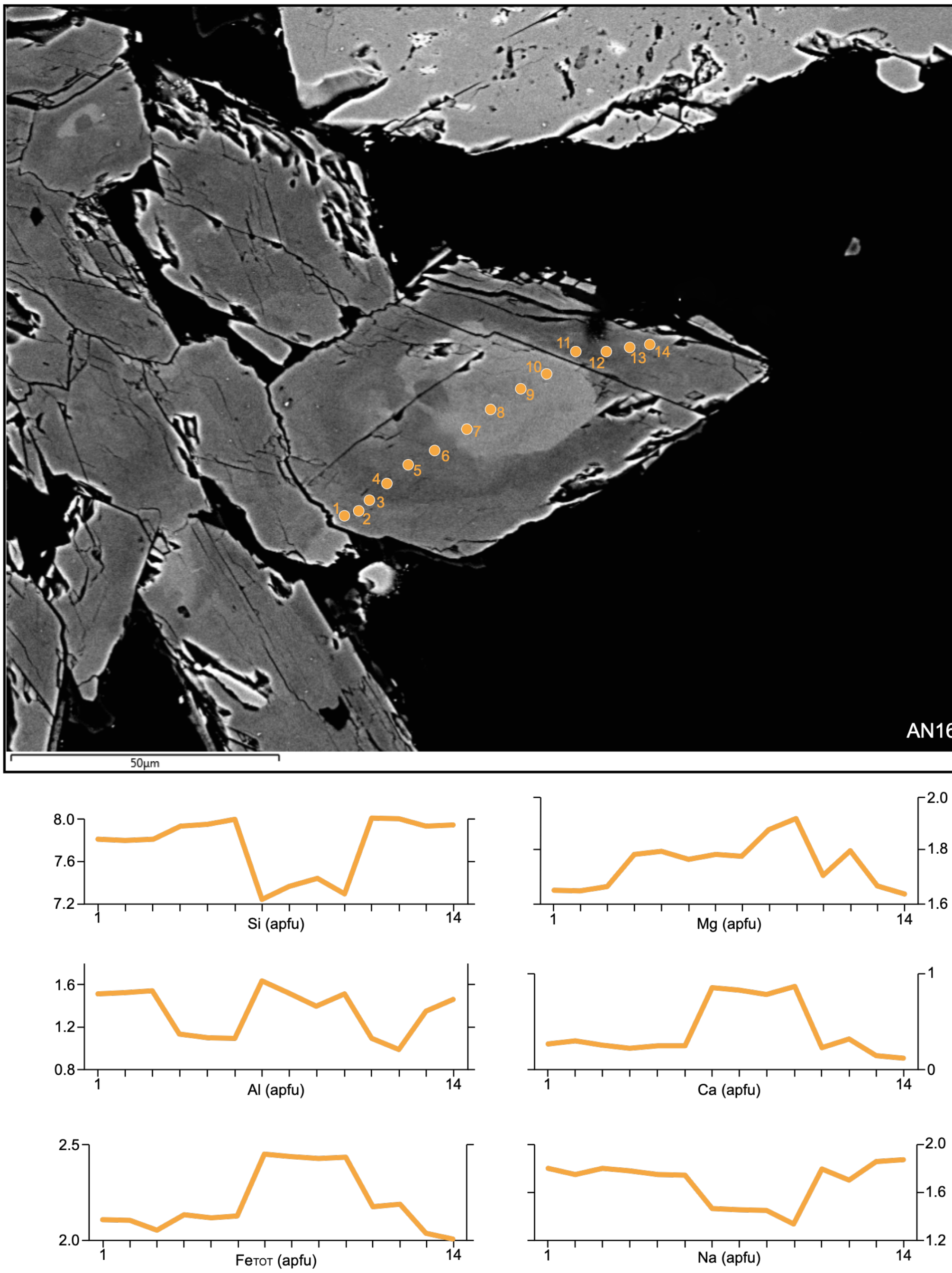

Figure 3.12: Compositional variation of selected major elements measured across a zoned amphibole from AN16015 with an Na-Ca amphibole core and Na amphibole rim.

Zonation between Na-Ca and Na amphibole components generally occurs sharply, as shown. Compositions of sodic rims are relatively consistent, although some grains may show relatively minor sharp, zoned compositional changes, as shown in Figure 3.12. Core-rim compositions for AN16015 and AN19015 are therefore relatively binary. Zonation between Ca and Na-Ca amphiboles, however, is more gradational and occasionally irregular. Samples containing calcic amphiboles therefore create a broader suite of compositions. AN17003 shows gradational calcic to sodic-calcic cores surrounded by chemically uniform sodic rims.

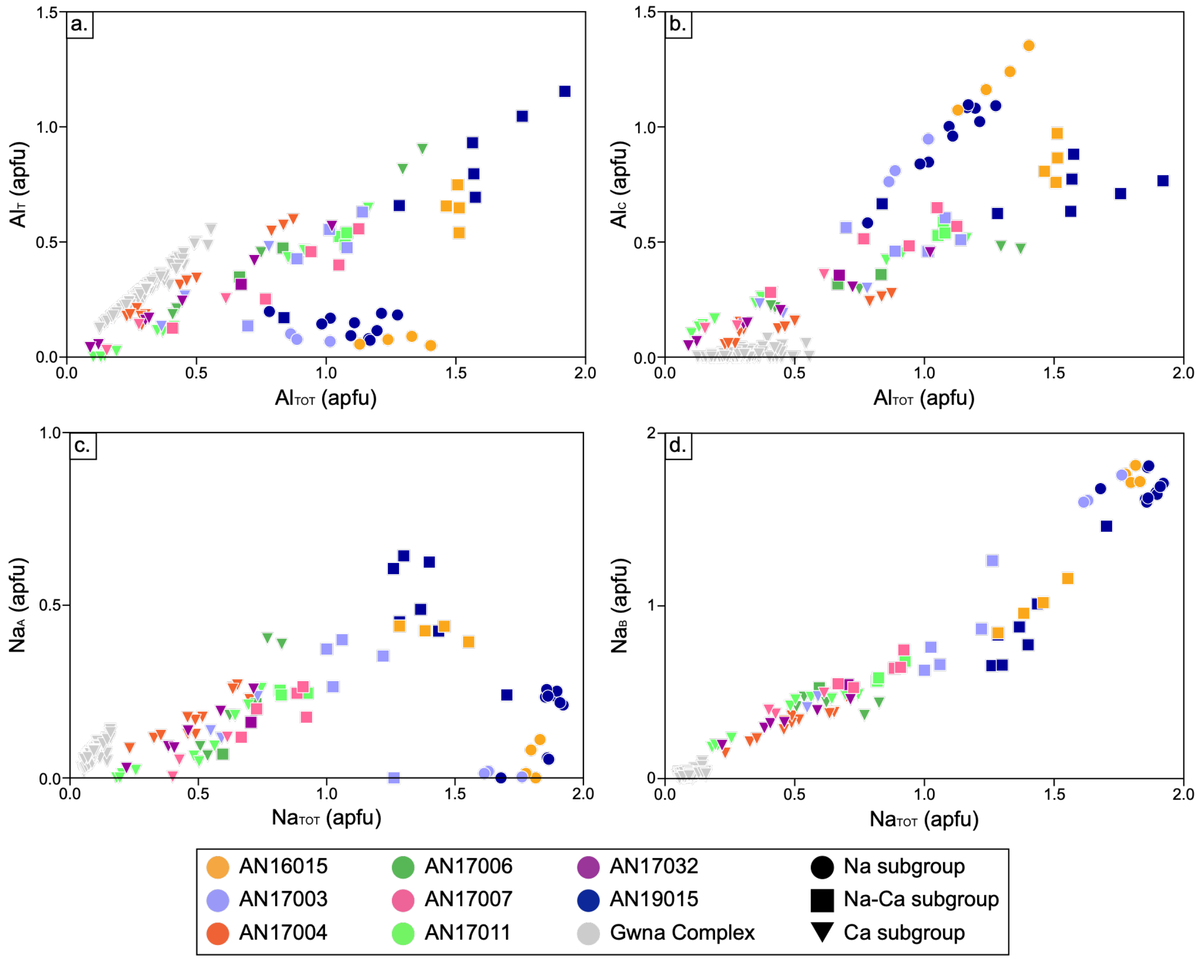

Figure 3.13: Site allocation plots for amphiboles of Penmynydd Terrane metabasites showing (a-b) Al site allocations for the T and C sites plotted against total Al; and (c-d) Na site allocations for the A and B sites plotted against total Na.

Along with compositional changes, crystallographic arrangements also vary between the different amphibole components. Crystallographic distributions of Al and Na are linear between calcic and sodic-calcic phases, but both cations undergo significant site reassignments in sodic phases (see Figure 3.13). Sodic amphiboles contain less or roughly equal total Al (0.78 – 1.40 apfu) than their sodic-calcic counterparts (0.70 – 1.92 apfu), however Al presence in the C site increases (0.67 – 1.53 apfu). This is facilitated by removal of Al from the T site (0.05 – 0.20 apfu sodic; 0.43 – 1.15 apfu sodic-calcic) and coincides with increasing Si in sodic phases. Similarly, Na is redistributed from the A site (0.24 – 0.64 apfu sodic-calcic; 0 – 0.11 apfu sodic) into the B site (0.63 – 1.46 apfu sodic-calcic; 1.60 – 1.81 apfu sodic) in sodic phases, replacing removed Ca.

Feldspar

Albite is the overwhelmingly dominant feldspar phase in the Penmynydd Terrane metabasites. Average compositions from seven metabasite samples produce compositional ranges of X_{AN} 0.1 – 0.5, X_{AB} 99.1 – 99.8, X_{OR} 0.1 – 0.6. Small, singular grains of K-feldspar occur rarely but was not analysed quantitatively.

Garnet

Garnets from AN16001 – a metasedimentary mica schist – were analysed semi-quantitatively. Estimated compositional ranges were X_{ALM} 18 – 28, X_{PRP} 0, X_{GRS} 34 – 36, X_{SPS} 19 – 33, X_{UVA} 0, X_{AND} 15 – 17. Pyrope and uvarovite components were not measured as MgO and Cr_2O_3 were not detected. The garnets are Fe-rich, and their compositional variability is determined by their relative contents of FeO and MnO.

3.5 CEMAES GROUP

Five thin sections were prepared from the Porth Trefadog Formation. Observations of the Porth Swtan Formation mélange were made using thin sections prepared by Eijsink (2017) from rocks around Cemaes.

Porth Trefadog Formation

The Porth Trefadog Formation sandstones consist of poorly sorted subangular fragments with significant proportions of altered feldspar and lithic clasts within a clay-rich matrix (see Figure 3.14a), classifying the rocks as lithic arkose. Chlorite is subordinate within the matrix and is more common in finer grained layers along with fine white micas. Towards the base of the unit, large quartz clasts more than 2 mm are incorporated into finer grained beds such as AN20003. The beds are foliated with evidence of shearing, with phyllosilicate-rich layers deflected around quartz clasts, which have been elongated and show tensile fractures (see figure 3.14b).

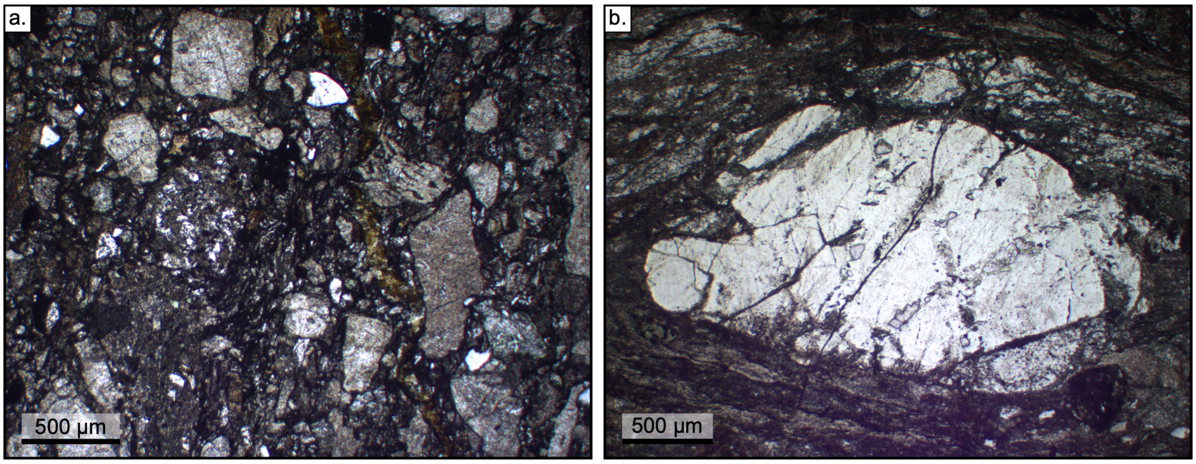

Figure 3.14: Petrographic textures of Porth Trefadog Formation sandstones showing (a) a textural overview from a coarse bed from the centre of the formation (AN20037c); and (b) large quartz clasts within lower sandstones at Porth Trefadog (AN20003) with a deflected foliated fabric and lightly fractured asymmetric clast.

Porth Swtan Formation

The Porth Swtan Formation consists predominantly of arenitic and carbonate clasts that consist mostly of dolomite. AN16009, AN16011 and AN16012 show consistent, well rounded, well sorted medium to coarse quartz arenites with rare feldspar grains. Quartz grains are bound by pressure solution, with small amounts of clay matrix. The mélange matrix of the Porth Swtan Formation is a consistent mudstone with series of parallel slip planes anastomosing around subrounded to subangular fragments of quartz and larger rounded clasts of arenites that may be fractured.

3.5 MAFIC INTRUSIVES

A total of six representative thin sections were prepared from mafic intrusives across Anglesey for petrographic observation. The samples have been organised in terms of their assigned groups (1-3), determined from field observations in Section 2.9. Mineralogical and petrographic observations from these samples are discussed below.

Group 1

Group 1 dykes have undergone extensive alteration that has largely replaced the original magmatic mineral assemblages. All samples contain over 50 % plagioclase, occurring as thick euhedral/subhedral laths that have been variably overprinted by sericitic alteration. Plagioclase in AN19010 has been completely replaced by coarser assemblages of muscovite with chlorite and clay minerals. AN19010 contains plagioclase phenocrysts that may exceed 1 cm in length, along with randomly orientated laths 0.5 – 2 mm long that make up the bulk of the rock (see Figure 3.15a).

Mafic mineral assemblages have been completely replaced in all samples. Altered assemblages primarily consist of chlorite, along with clay minerals, quartz, calcite, and micas. Assemblages are brown to green depending on the relative abundances of clay minerals to chlorite respectively. These assemblages typically occur interstitially between plagioclase laths, with the exception of AN20035, where large chloritic masses seemingly represent subhedral pseudomorphs of mafic phenocrysts (see Figure 3.15b). Smaller surrounding brown alteration patches of clay minerals, quartz, chlorite, micas, and calcite likely represent a second mafic mineral phase.

Opaque minerals are common occurrences throughout Group 1 rocks, occurring as small (< 0.2 mm diameter) euhedral/subhedral grains that can account for over 10 % total rock volume (eg. AN19010). AN20035 has a relatively low abundance of opaque minerals (ca. 2 % total volume) where subhedral/anhedral masses are mostly concentrated in altered mafic assemblages.

Group 2

Like Group 1 dolerite dykes, the Group 2 dyke (AN20 038) has undergone extensive alteration. The rock is medium grained, consisting of a dense assemblage of euhedral crystals within an altered matrix of predominantly feldspar and opaque minerals. The groundmass has been altered to mostly clay minerals, carbonates, pockets of chlorite, and relatively minor occurrences of quartz.

Two sets of larger euhedral minerals comprise approximately 50 % of the rock volume. The larger of these are long prismatic crystals 1 – 2 mm in length that have undergone complete alteration to dark brown opaque minerals, likely assemblages of clay minerals. The prisms have distinct hexagonal bases and were most likely amphiboles (see Figure 3.15c). Smaller but more abundant biotite is commonly observed as grains 0.5 – 2 mm length with carbonate and chlorite infiltrating along cleavage planes and grain boundaries (see Figure 3.15d). Altered black grains with similar size and form are likely biotite pseudomorphs, and some biotite grains have been partially altered in this manner. These pseudomorphs are more common that fresh biotite.

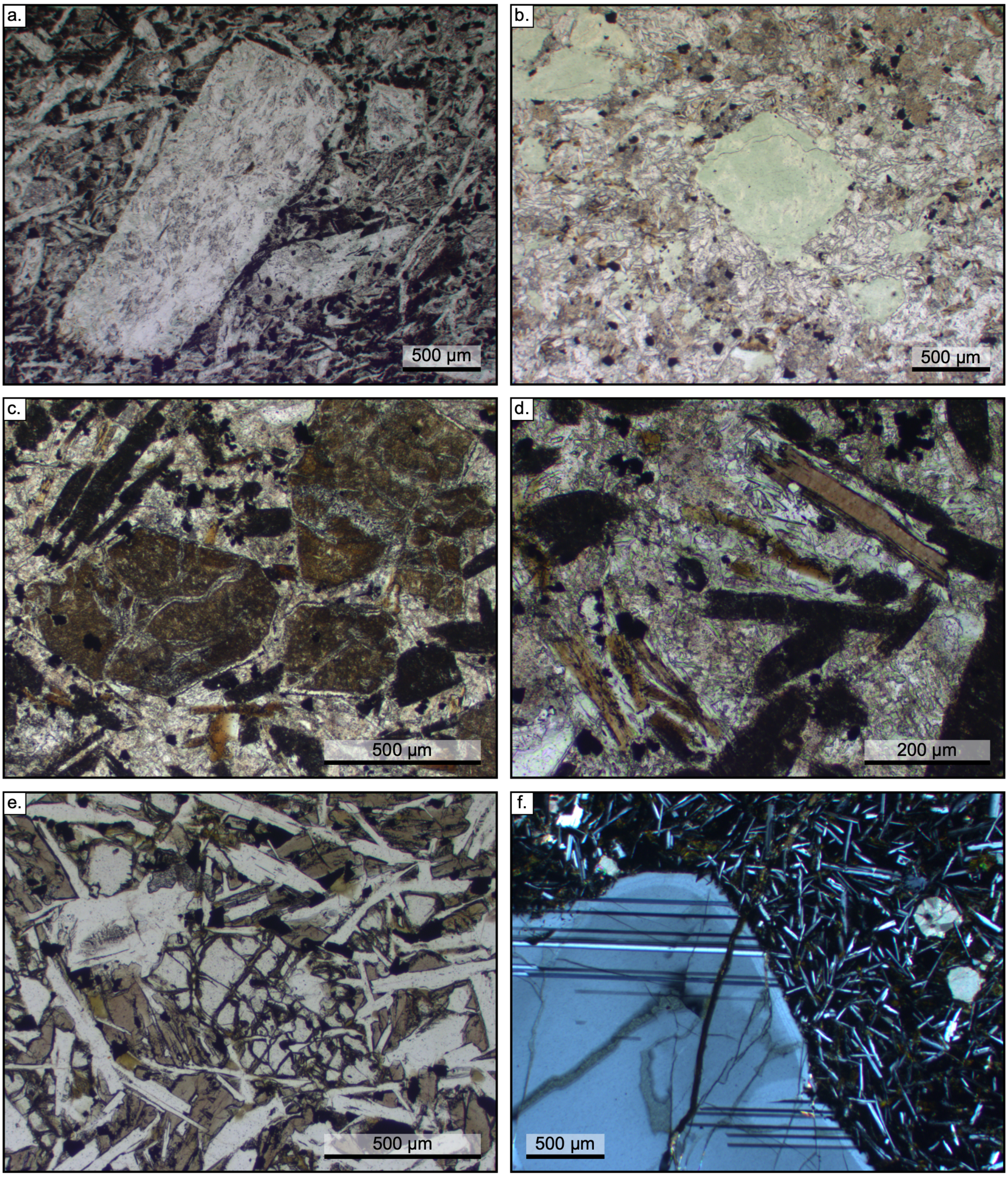

Figure 3.15: Petrographic features of mafic intrusives of (a-b) Group 1, (c-d) Group 2 and (e-f) Group 3, showing (a) altered plagioclase phenocryst (AN19010); (b) chloritic masses likely the product of alteration of a mafic phenocryst (AN20035); (c) euhedral amphibole phenocrysts with biotite and a groundmass of predominantly feldspar (AN20038); (d) partially altered biotite with chlorite and calcite alteration products (AN20038); (e) euhedral olivine, feldspar laths and interstitial clinopyroxene (AN20001); and (f) large, partially resorbed plagioclase phenocryst (AN20032).

Irregular, rounded masses up to 2 mm in diameter have quartz-rich cores, which become more carbonate-dominated towards rims, with high contents of opaque mineral aligned along irregular fracture planes. Biotite and opaque minerals have preferentially formed around the rims of these features, which may represent highly altered xenocrysts.

The largest features reach up to 5 mm in length and have euhedral tabular form. They have also been subjected to complete recrystallisation, comprising of quartz and carbonates. Opaques are abundant and concentrated along planes that seemingly represent fractures and cleavage planes. Rims of carbonate, opaque minerals and biotite surround the crystals, with grains of biotite concentrated around the boundary.

The dominant occurrence of both amphibole and biotite, along with high contents of matrix-bound feldspars suggest a high K content, although this may not be evident from whole rock geochemistry after alteration. The mineral assemblage and texture is consistent with lamprophyres (Le Maitre 2002), which commonly occur as dykes.

Group 3

Group 3 dykes are comprised primarily of plagioclase, olivine and clinopyroxene, with minor opaque minerals and accessory titanite (see Figure 3.15e). Vesicles (< 1 mm in diameter) are common throughout the dykes and are often infilled, or partially infilled, by carbonates. Plagioclase occurs as randomly orientated euhedral-subhedral laths typically 0.5 – 2 mm in length that account for roughly 50 % of total rock volume or greater across all samples. Larger (2 – 5 mm) rounded plagioclase phenocrysts occur in some samples such as AN20032 (see Figure 3.15f). These distinct phenocrysts have irregular shapes with concentric zonation and partly resorbed edges. Unlike feldspars of Groups 1 and 2, the plagioclase in Group 3 is relatively unaffected by alteration.

Clinopyroxene is the most common mafic mineral and commonly fills interstitial spaces between plagioclase along with opaque minerals. Olivine is present in all samples, occupying up to 10 % rock volume. It sits either within interstitial spaces or forms relatively large (0.5 – 1 mm) subhedral crystals. Both mafic minerals are commonly altered to various extents, with clay minerals and zeolites being the most common alteration products.

CHAPTER IV
Whole Rock Geochemistry

4.1 OVERVIEW OF GEOCHEMICAL STUDIES

In this chapter, whole rock geochemical results are presented for five distinct groups of samples. These groups include the igneous rocks of the Gwna Complex (Chapter 4.4), the sedimentary rocks of the Gwna Complex (Chapter 4.5), the metabasites of the Penmynydd Terrane (Chapter 4.6), volcaniclastic/tuffaceous material from the Porth Trefadog Formation (Chapter 4.7), Cemaes Group, and an assortment of mafic sheet intrusions from across Anglesey (Chapter 4.8). A total of 91 samples were analysed across the five rock type groups. Full results tables are available in Appendix A.

Several geochemical studies of MCT rocks have been conducted in the past, most notably that of Saito et al. (2015), which analysed igneous rocks of the Gwna Complex, predominantly sampled from Llŷn Peninsula (Area II). The data produced (24 samples) by Saito et al. (2015) will be incorporated to supplement the Gwna Complex igneous rocks dataset collected during this study to increase the size and scope of the dataset. Earlier studies of relevance conducted on Penmynydd Terrane metabasites (Thorpe 1972) and Gwna Complex basalts (Thorpe 1993). Data from these studies will not be included due to limitations with the data including small sample sizes, smaller suites of analysed elements and questions over data reliability, as would be expected from these older studies.

4.2 ANALYTICAL TECHNIQUES

Samples were prepared for analysis at the School of Earth & Environmental Sciences, Cardiff University. Samples were cut using a diamond-encrusted circular saw to remove dirt and weathered surfaces, and reduced into blocks of approximately 10 cm in diameter for crushing. Thin sections blocks were also cut from the same material as their corresponding whole rock samples. Cut samples were then cleaned and dried before crushing.

A Mn-steel jaw crusher was used to grind the samples into an aggregate of <10 mm in diameter. From the aggregate, a 100g representative sample was extracted for milling. An agate ball mill was used to further reduce grain size to <125 µm. The jaw crusher, mill and associated equipment were cleaned thoroughly between uses to minimise the risk of sample contamination. Rock powders were prepared for use both in geochemical analysis and XRD analysis (see Chapter 3.2).

Whole rock geochemical characterisation was done using the methods of X-ray fluorescence (XRF) coupled with laser ablation induced coupled plasma mass spectrometry (LA-ICP-MS). Both methods were carried out in the central analytical facilities of Stellenbosch University, South Africa. XRF analysis was used to characterise major elements whilst LA-ICP-MS was used to characterise trace elements.

Major element analysis was conducted by XRF using a Rh tube with 3 kWatt energy. Loss of ignition (LOI) was calculated gravimetrically based on sample weight reduction when heated to 1000°C for a duration of several hours, as expressed in the following equation:

$$LOI\ (wt\ \%) = \frac{(initial\ mass - mass\ upon\ ignition)}{initial\ mass} \times\ 100$$

For LA-ICP-MS trace element analysis, powdered rock samples were fused with lithium tetraborate at a sample/flux ratio of 1:10. Some samples with particularly low trace element concentrations were also analysed with a sample/flux ratio of 1:5 to increase count rates where appropriate. Analysis was conducted using an Agilent 7700 ICP-MS fitted with a photomultiplier detector, and a Resonetics M50SE 193 nm excimer laser. Due to the generally low contents of trace elements in basalts and metabasalts, a relatively large ablation spot size (200 – 240 µm) was used in order to increase count rates of trace elements of low concentration so that they did not fall below the detection limits during corrections. Ablation time of analyses was 35 seconds with 15 seconds background time.

Samples were analysed 2-3 times each and the calculated mean value for each trace element is used in results tables. An uncertainty calculated from the standard deviation of the analyses has been applied and presented within a full raw geochemical data set, which is available in Appendix A. Due to high LOI values in many Gwna Complex igneous rocks, both major and trace elements were normalised to anhydrous state, in order to remove its influence on relative trace element concentrations.

4.3 ELEMENT MOBILITY THROUGH ALTERATION

Whole rock geochemical analysis – and subsequent petrogenetic interpretations – of rocks should be undertaken with an understanding of any changes to initial compositions caused by secondary processes, such as metamorphism, metasomatism, weathering or diagenesis. Remobilisation of elements through these processes can lead to major discrepancies between analysed whole rock compositions and initial compositions upon formation. This is particularly relevant when studying rocks in the MCT, given its age, general tectonic history, and the subaqueous palaeoenvironments of many of the studied rock types. Both the igneous and volcaniclastic rocks of the Gwna Complex display key indicators of element mobility through extensive alteration, where original mineralogy has been comprehensively replaced in many areas. Subaqueous basalts are commonly associated with seafloor alteration due to the high quantities of fluids to facilitate alteration, high exploitable surface area, and presence of unstable materials and minerals such as volcanic glass and olivine respectively. The protoliths of the Penmynydd Terrane blueschists have also evidently undergone significant metamorphism and were likely subject to similar subaqueous alteration as Gwna complex volcanic rocks prior to metamorphism.

The potential to remobilise an element through secondary processes is dependent on a complex series of factors and conditions. Within the conditions that the studied materials have been subjected to, the mobility of an element is expected to relate closely to its ionic potential (charge/radius). Elements of intermediate ionic potential (2 – 8) produce strong cation-oxygen bonds and therefore stable solids. These intermediate elements are mostly HFSE's such as Zr, Ti, Nb and REE's, which are generally considered immobile under most conditions (Rollinson 1993). Elements of high ionic potential, such as Cr and Mo, and low ionic potential, such as LILE's, both produce less stable solids more prone to element mobility due to cation-cation repulsion and weak cation-oxygen bonds respectively. Melting temperatures of oxides of hard cations are generally concordant with ionic potential, and the immobility of elements of intermediate ionic potential begins to decline above upper amphibolite metamorphic conditions, which are not reached in the studied material (Pearce 1996). Other factors such as salinity and pH can also play large factors in element mobility under extreme conditions that are not necessary to consider in this study (Markl and Baumgartner 2002).

Alteration indexes were determined for both the volcanic material of the Gwna Complex and the metabasites of the Penmynydd Terrane. For the Gwna Complex, the dolerite sills of Llanddwyn Island and potentially associated volcanic rocks from Unit 9 were omitted as they are likely not cogenetic. Samples from all four areas across the Gwna Complex have tentatively been included and do not greatly impact results relative to those of a singular area, suggesting a cogenetic relationship between all four areas. For the Penmynydd Terrane, the inclusion of samples across multiple metabasite lenses throughout the terrane must also be considered, along with the relatively small number of analysed samples.

To determine the alteration index of an element in a given system, the element is correlated against the most stable, immobile element, which is typically assumed to be Zr (Cann 1970; Pearce 1996). An element's alteration index is then determined by the strength of its correlation (R^2 value) to Zr, which acts as a proxy standard. This method cannot account for variability in the formation of the studied material, so data sets of assumed cogenetic samples were used. While Zr is often assumed to be most immobile, an initial test can be used to establish the most immobile element from a select group of typically highly immobile elements (Guice 2019).

Eight elements (Zr, Y, Yb, Ho, Th, Nb, Hf and Ti) were correlated against one another, all HFSE's, and all analysed elements. The mean R^2 results from each group showed that Zr is the most compatible element in the Gwna Group basalts and showed moderate-strong correlation with each of the other seven elements (mean R^2 value of 0.73). Therefore, Zr is to be used in constructing R^2 values for each element. For the Penmynydd Terrane metabasites, Zr, Hf and Ti produce very similar R^2 values, and while Hf has a higher mean R^2 value (Zr – 0.71, Hf – 0.73, Ti – 0.72) compared the selected immobile elements, Zr and Ti show an equal mean correlation (Zr – 0.50, Hf – 0.49, Ti – 0.50) with all elements. Therefore, Zr will also be used for calculating R^2 values of elements in the Penmynydd Terrane for cohesion with the Gwna Complex calculations, although any of Zr, Hf or Ti would be equally suitable.

The alteration index of an element is based on its determined R^2 value, categorised as high ($R^2 \leq 0.667$), moderate ($R^2 \leq 0.334, \geq 0.667$) or low ($R^2 \geq 0.334$). Those with high correlations are deemed to be relatively immobile, while those with low correlations are assumed to have been mobilised to a significant degree.

Table 4.1 shows R^2 results for Gwna Complex basalts, showing that all major elements apart from Ti have been heavily mobilised. This means that traditional methods of classification based on major element analysis for igneous rocks, such as TAS (Le Maitre 2002) and R1-R2 (De la Roche et al. 1980) discrimination diagrams, are not reliable in this system. This is shown by the scattered range of data in Figure 4.1a, which plots Gwna Complex pillow basalts on a TAS diagram, with data plotting across numerous unlikely fields including foidite, basanite and andesite. While most samples plot within the basalt or basaltic andesite field as expected, there is a clear scatter caused by significant variations in both alkali and silica content. In comparison, Figure 4.1b shows the same data is plotted in a similar classification diagram (Pearce 1996; Hastie et al. 2007) that relies on HFSE's with moderate to high R^2 values, displaying a much tighter grouping confined to the basalt and alkali basalt fields.

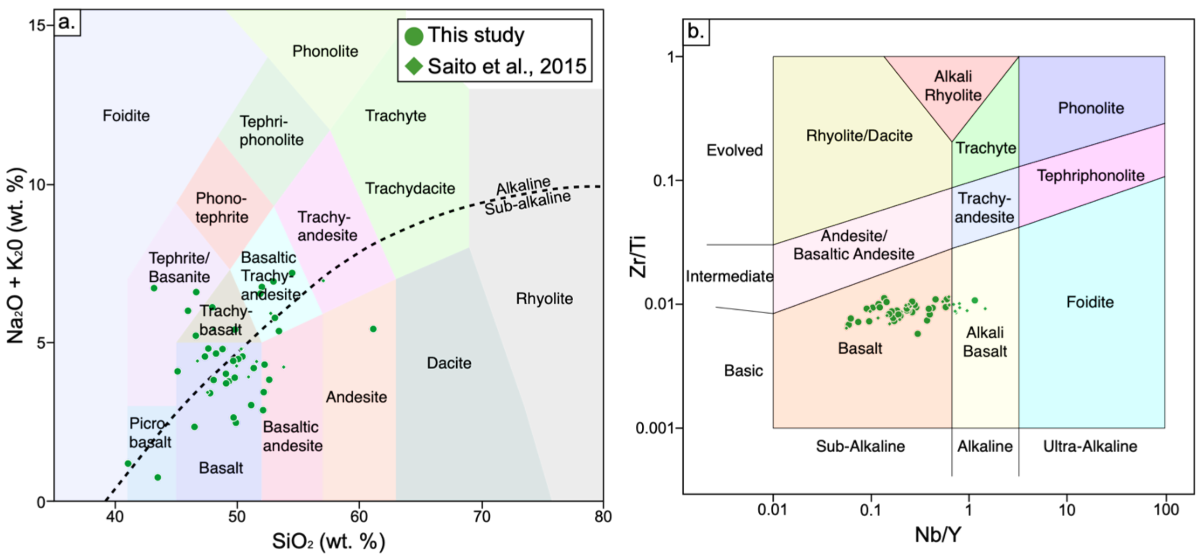

Figure 4.1: Gwna Complex igneous samples plotted in (a) TAS volcanic classification diagram (Le Maitre 2002) with alkaline – sub-alkaline trend curve after (Irvine and Baragar 1971) and (b) volcanic classification scheme based on immobile HFSE ratios (Pearce 1996).

Table 4.1: calculated alteration indexes (R^2 values) for elements from samples of Gwna Complex basalts.

Element	R^2	Correlation	Element	R^2	Correlation
SiO_2 (wt. %)	0.069	Low	Mo	0.026	Low
TiO_2	0.927	High	Cs	0.227	Low
Al_2O_3	0.109	Low	Ba	0.120	Low
Cr_2O_3	0.187	Low	La	0.745	High
Fe_2O_3	0.170	Low	Ce	0.742	High
MnO	0.098	Low	Pr	0.715	High
MgO	0.178	Low	Nd	0.753	High
CaO	0.065	Low	Sm	0.771	High
Na_2O	0.061	Low	Eu	0.635	Moderate
K_2O	0.051	Low	Gd	0.737	High
P_2O_5	0.447	Moderate	Tb	0.703	High
Sc (ppm)	0.005	Low	Dy	0.657	Moderate
V	0.415	Moderate	Ho	0.624	Moderate
Cr	0.157	Low	Er	0.589	Moderate
Co	0.002	Low	Tm	0.515	Moderate
Ni	0.154	Low	Yb	0.493	Moderate
Cu	0.160	Low	Lu	0.396	Moderate
Zn	0.153	Low	Hf	0.911	High
Rb	0.200	Low	Ta	0.669	High
Sr	0.017	Low	Pb	0.093	Low
Y	0.574	Moderate	Th	0.667	High
Nb	0.682	High	U	0.360	Moderate

Moderate to high R^2 values were calculated for most HFSE with the exception of U, which appears to have been mobilised. While LREE's and MREE's have high correlations, HREE's become progressively less correlated, with Lu having an R^2 value of below 0.5. This progressive decline is likely a magmatic product, where variability of HREE's is greater than LREE's, rather than an alteration product.

Table 4.2 shows calculated alteration indexes for Penmynydd Terrane metabasites. Like the Gwna Complex basalts, major elements generally show evidence of mobilising, although to a lesser extent. For example, Ca and P are highly correlated, while Mg and K also show moderate correlations to Zr. Similarly, high ionic potential elements like Cr, Co, Ni and Zn are moderately correlated. Penmynydd Terrane blueschists show similarly high correlations for HFSE's as in the Gwna Complex basalts. Ti, Hf, LREE's and MREE's all have high correlations, while Nb, Y, Th and HREE's have moderate correlations. Unlike the Gwna Complex basalts, U also has a high correlation in the Penmynydd Terrane metabasites.

Table 4.2: calculated alteration indexes (R^2 values) for elements from samples of Penmynydd Terrane metabasites.

Element	R^2	Correlation	Element	R^2	Correlation
SiO_2 (wt. %)	0.009	Low	Mo	0.042	Low
TiO_2	0.956	High	Cs	0.365	Moderate
Al_2O_3	0.020	Low	Ba	0.362	Moderate
Cr_2O_3	0.404	Moderate	La	0.689	High
Fe_2O_3	0.235	Low	Ce	0.756	High
MnO	0.005	Low	Pr	0.834	High
MgO	0.593	Moderate	Nd	0.903	High
CaO	0.725	High	Sm	0.989	High
Na_2O	0.286	Low	Eu	0.985	High
K_2O	0.472	Moderate	Gd	0.882	High
P_2O_5	0.854	High	Tb	0.780	High
Sc (ppm)	0.130	Low	Dy	0.652	High
V	0.043	Low	Ho	0.516	Moderate
Cr	0.553	Moderate	Er	0.509	Moderate
Co	0.337	Moderate	Tm	0.411	Moderate
Ni	0.521	Moderate	Yb	0.427	Moderate
Cu	0.253	Low	Lu	0.411	Moderate
Zn	0.433	Moderate	Hf	0.961	High
Rb	0.555	Moderate	Ta	0.707	High
Sr	0.169	Low	Pb	0.319	Low
Y	0.563	Moderate	Th	0.633	Moderate
Nb	0.632	Moderate	U	0.688	High

While the calculations of Tables 4.1 and 4.2 show R^2 values for each element, the table cannot be used to detect clusters of data, which may result from variations in source material rather than through the product of alteration. Figure 4.2 shows bivariate diagrams of representative elements plotted against Zr. Potential clusters within the Gwna Complex basalts can be seen in bivariate plots with P, Rb and U. This suggests either variation within the source material affecting these elements, or focused alteration affecting some samples over others, potentially through heterogeneous deformation or fluid activity. While variation is seen within the Penmynydd Terrane metabasites, there are no clear clusters observed, although this may be due to the relatively small sample size.

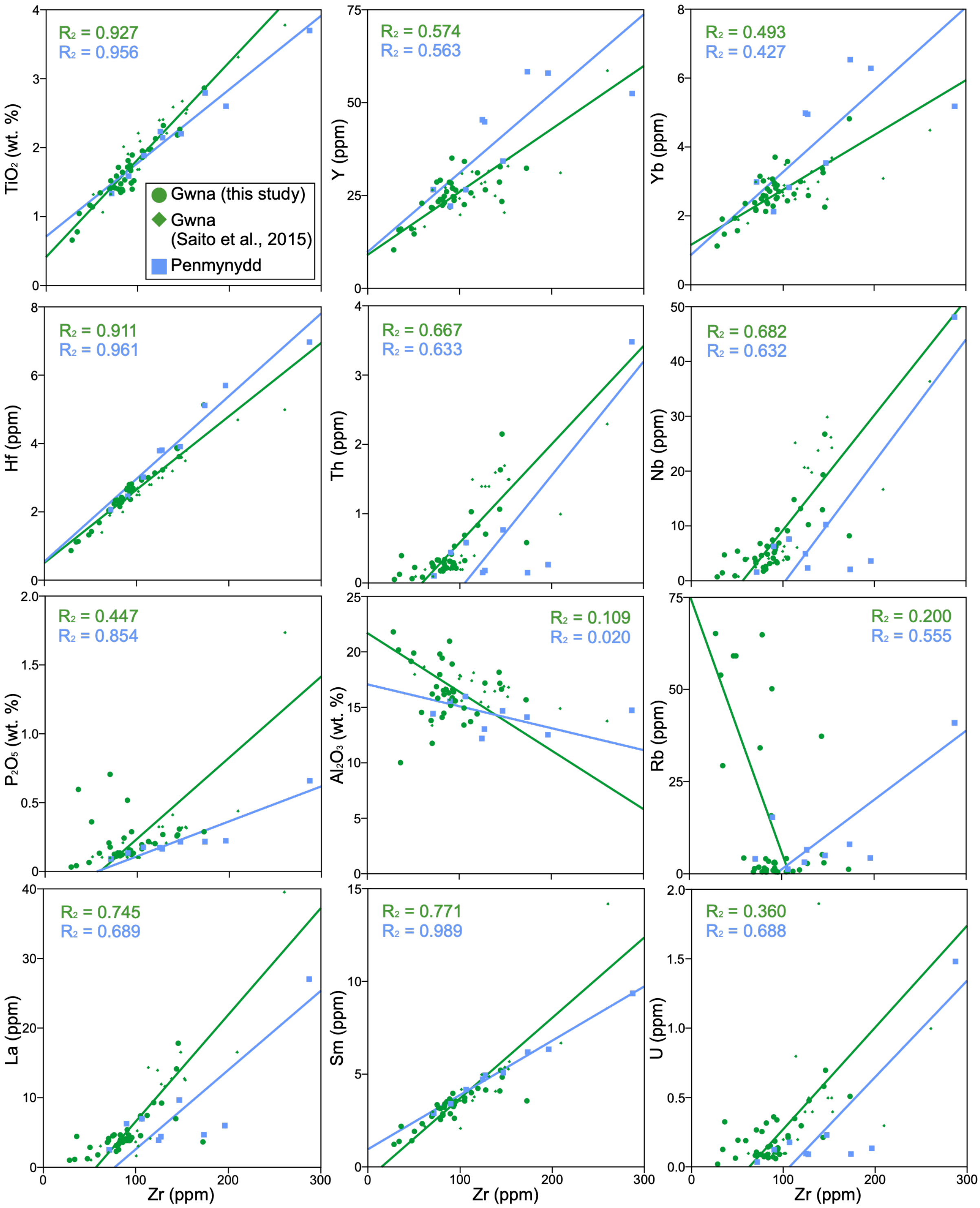

Figure 4.2: bivariate plots for selected elements against Zr to show R^2correlations for Gwna Complex igneous rocks and Penmynydd Terrane metabasites.

4.4 GEOCHEMISTRY OF GWNA COMPLEX IGNEOUS ROCKS

A total of 45 samples were analysed from Gwna Complex igneous rocks across all four study areas, while supplementary from 23 samples analysed by (Saito et al. 2015) have also been added. Two basalt-carbonate samples were also analysed and are discussed in Section 4.4.3, but have not been included in more general analyses due to the influence of carbonate material. As discussed in Chapter 4.3, all major elements except for Ti appear to have been significantly mobilised within the Gwna Complex, so tectonic classifications will rely heavily on less mobilised HFSE's. Three sample groups were distinguished based on geochemical variations, divided into an N-MORB-like tholeiitic compositional group (Group 1), an E-MORB-like intermediate group (Group 2) and an enriched OIB-like alkaline group (Group 3). These distinctions are discussed in Section 4.4.2.

4.4.1 Major elements

Although generally affected by mobilisation, coarse major element trends have been retained, as shown by the TAS diagram in Figure 4.1a. This disruption of major element compositions is highlighted again by the Harker diagrams of Figure 4.3. Contents of SiO_2 generally falls between 40 – 55 %, with several outliers above this value and an anomalously low sample of 34 % belonging to a heavily fluid-influenced hyaloclastite (AN19029). Contents of Al_2O_3 ranges from 12.5 – 23 % with several exceptions below this range. There is a negative linear correlation between SiO_2 and CaO, likely the product of alteration processes, which certainly influences the high and variable CaO contents. This negative correlation is also seen with MgO, supporting observations of dolomite being the primary carbonate alteration product in basalts. Lower MgO is however more associated with more enriched samples of Groups 2 and 3, suggesting that alteration effects are more imposed upon magmatic variability than seen for CaO. More enriched samples of Groups 2 and 3 also have generally higher TiO_2 and P_2O_5 contents than Group 1 samples, although there is not much distinction between Groups 2 and 3. The majority of samples contain <1 % K_2O, however several exceptions exceed this, with LLY37B reaching over 4 %. These exceptions are not specific to any groups and are likely a result of alteration processes primarily affecting certain samples.

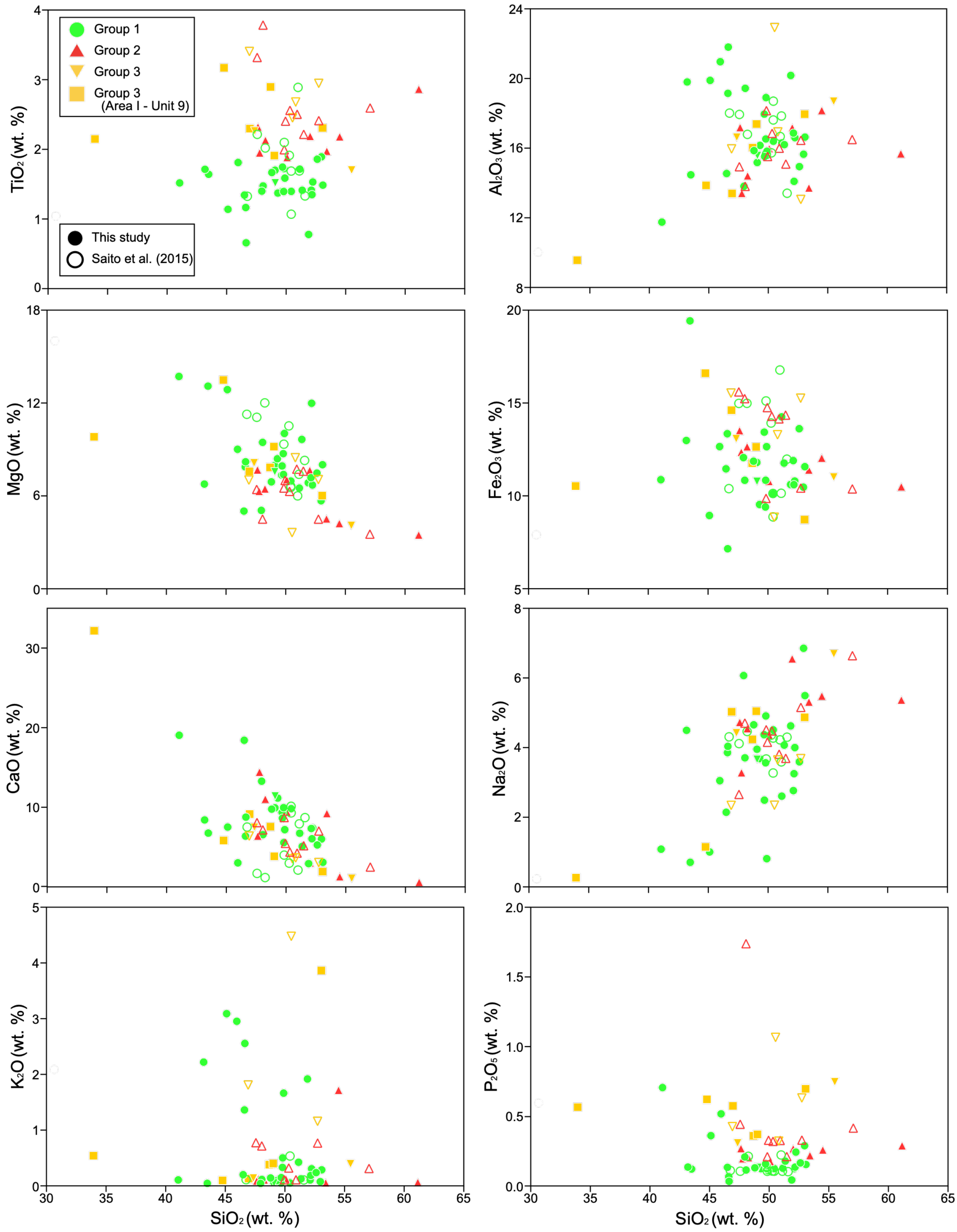

Figure 4.3: Harker diagrams showing major element compositions of Gwna Complex igneous rocks.

Samples show variable but low MgO contents – typically <12.5 % – resulting in a large range in Mg#, ranging from 37 – 74.

$$Mg\#\ (molar) = 100 \times \left(\frac{Mg}{Mg + Fe}\right)$$

Figure 4.4 shows a negative correlation between Mg# and TiO_2, where more enriched samples tend to have higher TiO_2 contents and lower Mg# values. Group 3 samples tend to have moderate Mg# values (42 – 65), while also being enriched in TiO_2 to similar degrees as Group 2 samples.

4.4.2 Trace elements

As shown in Figure 4.1b, the Gwna Complex igneous rocks produce a singular, largely continuous evolutionary trend ranging between basalt and alkali basalt compositions. Figures 4.5 and 4.6 show a range of tectonic discrimination diagrams, which consistently plot samples within the MORB-OIB array, ranging from primarily tholeiitic compositions to alkali compositions (Figures 4.5a-b). The samples produce a surprisingly variable suite of compositions, ranging from approximately mean N-MORB to mean OIB end members (Figures 4.5c-d). Within this progression, three compositional groups have been identified based on a series of trace element ratios, corresponding closely to a tholeiitic N-MORB composition (Group 1), an intermediate E-MORB composition (Group 2), and an alkaline OIB composition (Group 3). Group 1 is most populated with 40 samples, while 17 samples sit within Group 2. Group 3 is made up of 12 samples, six of which are identified as potentially related to intraplate igneous activity in Area I (from Units 9 and 10; see Section 2.3). These six samples have therefore been distinguished from the remaining samples in Group 3.

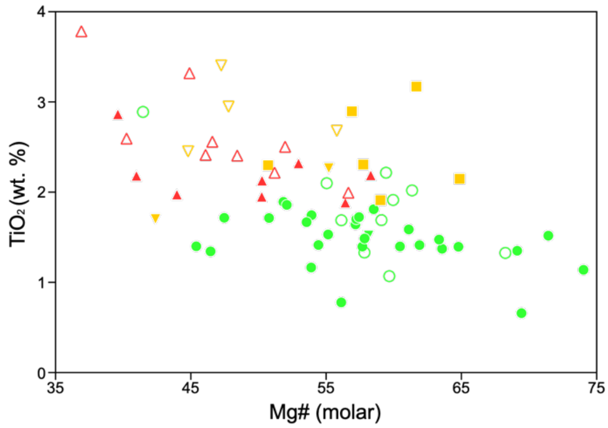

Figure 4.4: bivariate plot showing variations in Mg# plotted against immobile TiO_2 within Gwna Complex igneous rocks. Legend in Figure 4.3.

The tectonic discrimination diagrams of Figures 4.5 and 4.6 show samples categorised by these groups juxtaposed against the study areas that samples were collected from. From this, a large compositional spread can be seen across each study area. Areas I, II and IV have samples plotted within each of the three compositional groups, while Area III, which is represented by just two samples, plots within Groups 1 and 2. Areas I and II, which are more thoroughly represented, show the greatest compositional range, and the ranges are very similar to one another, as demonstrated best in Figure 4.5c and 4.6c.

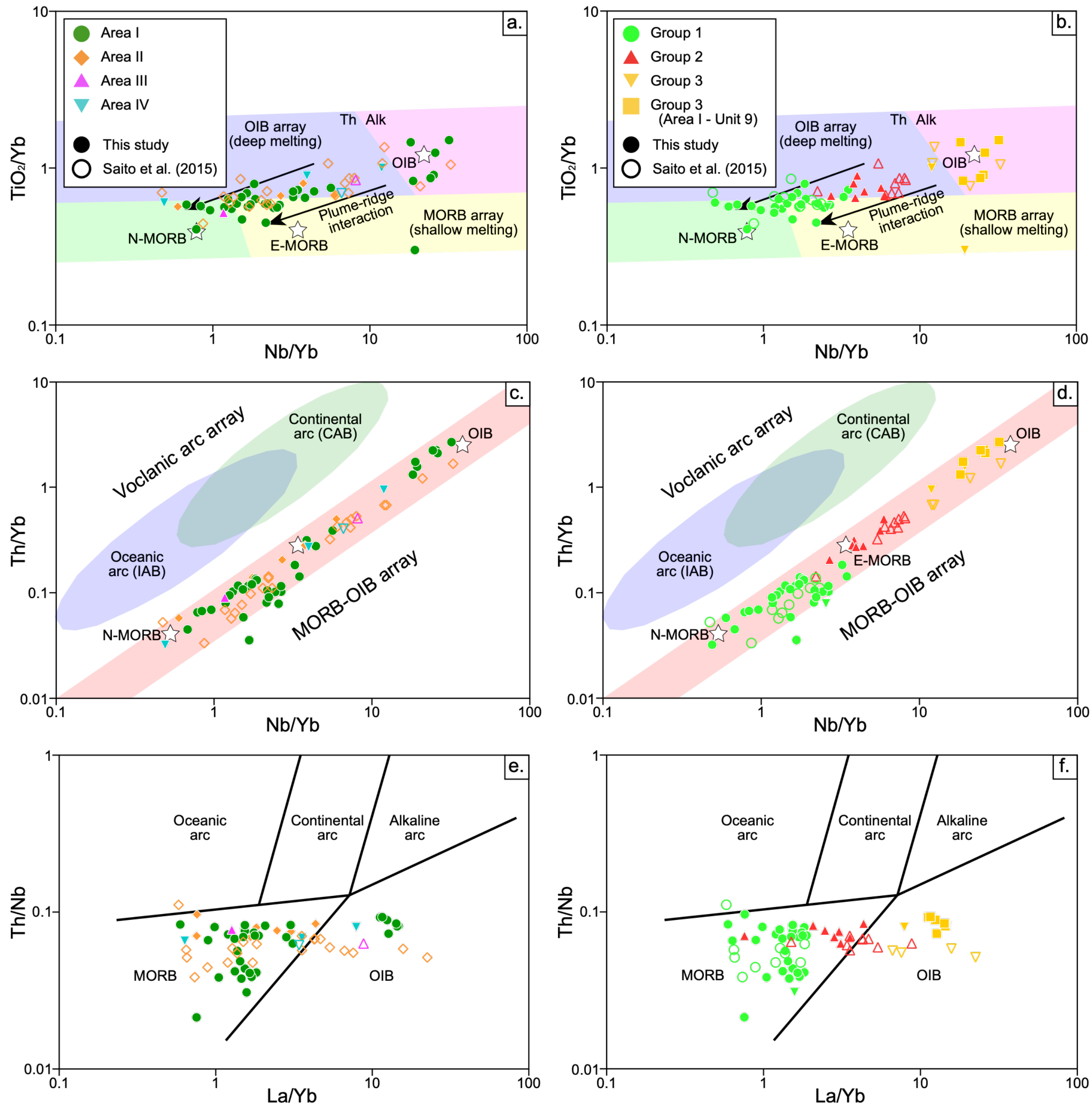

Figure 4.5: immobile element discrimination diagrams for Gwna Complex igneous rocks distinguished by sample area (a, c, and e) and geochemical group (b, d, and f). (a-b) tectonic discrimination of igneous rocks utilising Ti as a key variable (Pearce 2008); (c-d) tectonic setting discrimination for igneous rocks using Th (Pearce 2014); (e-f) tectonic setting classification using Th/Nb and REE ratios (Hollocher et al. 2012).

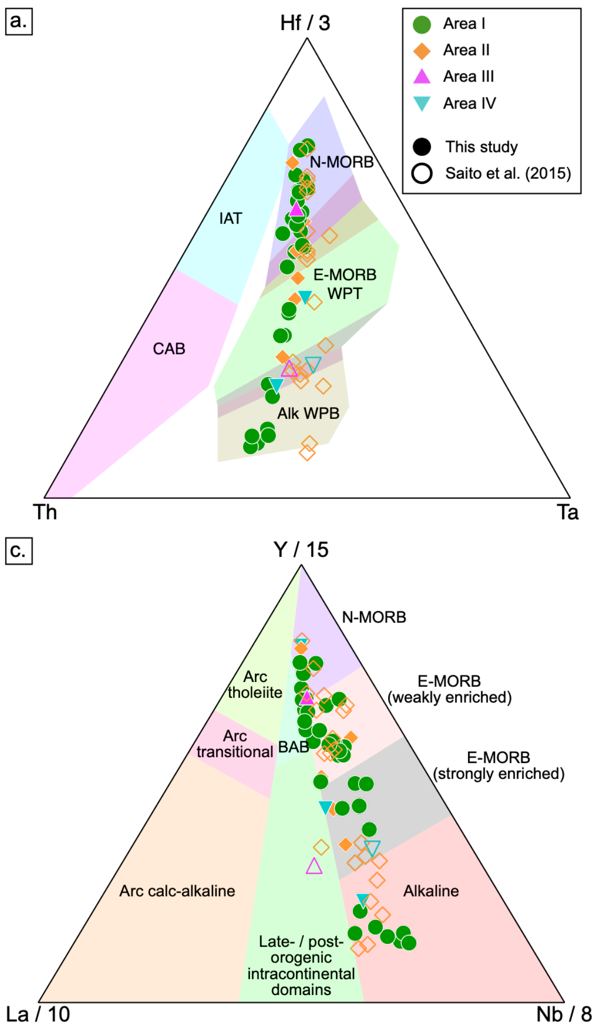

Figure 4.6: ternary discrimination diagrams for Gwna Complex volcanic rocks distinguished by sample area (a and c) and by geochemical group (b and d). (a-b) Basalt tectonic discrimination diagram (Rollinson 1993); (c-d) tectonic classification diagram for mafic igneous rocks (Cabanis and Lecolle 1989).

As shown from Figures 4.5b and 4.5d, some samples have anomalous compositions, with one from each group primarily identified. Figure 4.7 highlights the compositional ranges of groups; however, three anomalous samples have been excluded and plotted individually. In Group 1, AN19036 is continuously depleted in all HFSE's except for LREE's, which are close to the lower limit of other Group 1 samples (see Figure 4.8a). Figures 4.5d and 4.5h demonstrate how AN19036 falls anomalously below Group 1 trends, particularly affected by low Th content (Th = 0.06 ppm), leading to the sample plotting below the MORB-OIB array in Figure 4.5d. In Group 2, ANG24 is relatively enriched in LREE's (La/Sm_{PM} = 1.80) and produces an unusual convex LREE trend (see Figure 4.7b). It is seemingly enriched in REE's relative to other HFSE's, which have similar concentrations to other samples in Group 2. This is seen in Figure 4.6d, where high La concentrations (La = 40.6 ppm) pull the sample from the MORB suite into the intracontinental domains field. In Group 3, AN18006 is anomalously enriched, particularly in Zr (Zr/Zr* = 1.75), Hf and HREE's. It has a strongly negative Ti anomaly (Ti/Ti* = 0.41), and this is reflected in Figure 4.5b, where the sample plots far below others in Group 3, otherwise confined to the alkaline OIB field.

The multivariate plots in Figure 4.7 show a progressive enrichment from Group 1 (least) to Group 3 (most). Group 1 samples produce a flat, broadly convex normalised REE trend (La/Lu_{PM} = 0.39 – 1.39), while Groups 2 and 3 produce broadly linear REE patterns with increasing negative gradient between Group 2 (La/Lu_{PM} = 0.50 - 4.47) and Group 3 (La/Lu_{PM} = 4.47 – 16.94; see Figure 4.8b). Several samples in Group 2 – notably and AN16036 and LLY387 – exhibit negative Eu anomalies (Eu/Eu* = 0.61 – 0.65) although most do not (Eu/Eu* = 0.89 – 1.13). Despite the large variation in LREE concentrations between and within the groups, HREE concentrations are similar between all groups.

Samples from Group 3 – with the exception of AN18006 – plot fairly consistently on discrimination diagrams, although Group 3 samples associated with Units 9 and 10 of Llanddwyn Island are generally more enriched in Th (see Figure 4.6b). The multivariate plots of Figure 4.8 show that there are several minor differences between the subgroups, including relative Th enrichment (Th = 2.76 – 6.23 ppm to 1.70 – 4.90 ppm), seen in Figure 4.8a. Unit 9 and 10 samples also show a steeper mean REE trend and are more depleted in HREE's (Yb = 1.81 – 2.76 ppm) than other samples in Group 3 (Yb = 2.42 – 3.42 ppm) despite sharing very similar LREE concentrations.

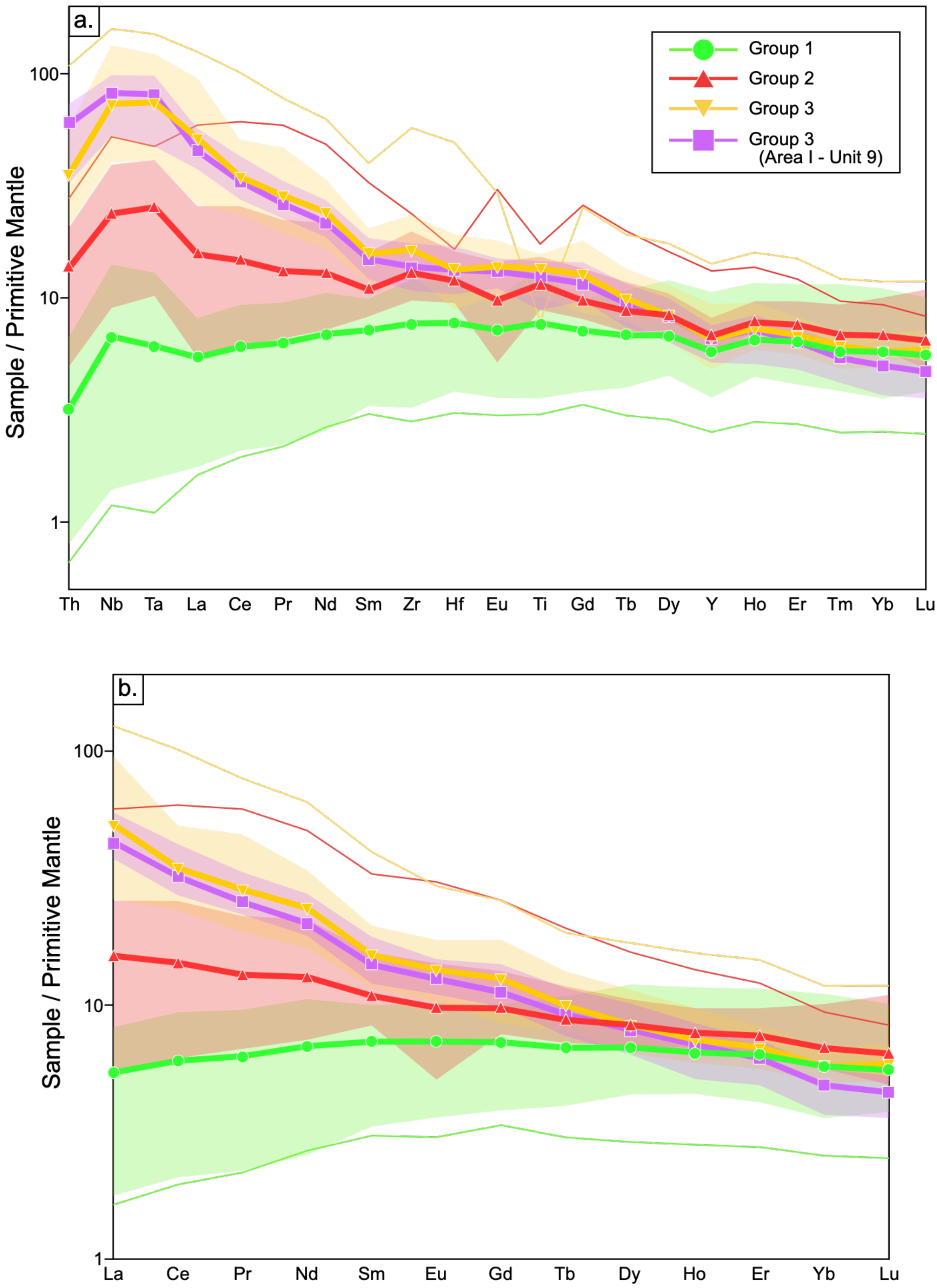

Figure 4.7: multielement plots featuring (a) immobile HFSE elements and (b) REE elements normalised to primitive mantle (Sun and McDonough 1989). Fields show compositional ranges for each geochemical group while thick lines with corresponding shapes represent mean values excluding anomalous samples shown by thin lines.

4.4.3 Igneous rocks of Area I

The igneous material of Area I is divided between many units with ranging states of preservation and deformation, as outlined in Chapter 2. A total of 36 samples of igneous rocks were analysed. Of these, 30 originated from ten of the units defined in Figure 2.3. A further two samples were analysed from a unit isolated in the north of Newborough Forest (Unit 17) along strike of the main outcropping area of Figure 2.2. Three samples were analysed from igneous material within highly sheared mélange zones across Newborough. Another sample was analysed from Pentraeth in northern Anglesey. The most sampled unit was Unit 4 (12 samples) because of its size and relatively complete exposure. This allowed for observations of geochemical changes laterally and with depth, along with monitoring the compositions of basal and internal hyaloclastites. Of the samples analysed, 22 were pillow basalts, seven were hyaloclastites, three were basalt-carbonate rocks, three were dolerites and a single sample was massive basalt.

Variability between units

Despite the variable composition of igneous rocks across Area I, compositions within individual units are relatively consistent – shown in Figure 4.8 – with the variability deriving largely from between units rather than internally. All units (apart from Unit 9, discussed below) are tholeiitic with compositional ranges between N-MORB and E-MORB. Despite the seemingly continuous evolutionary trend of the Gwna Complex across all areas, Area I shows a clear compositional gap between tholeiitic E-MORB that comprises most units, and alkaline OIB in Units 9 and 10, shown clearly in the ternary plots of Figure 4.9.

The largest internal geochemical differences within units are seen with Units 9 and 17. In Unit 17, the large variation between AN18006 and AN18025 is difficult to explain, and AN18006 has been discussed as a geochemical anomaly in Section 4.4.2. Based on the geochemical compositions of other units, it is expected that AN18025 is a more accurate representation of the unit, with a tholeiitic, weakly enriched MORB-like composition.

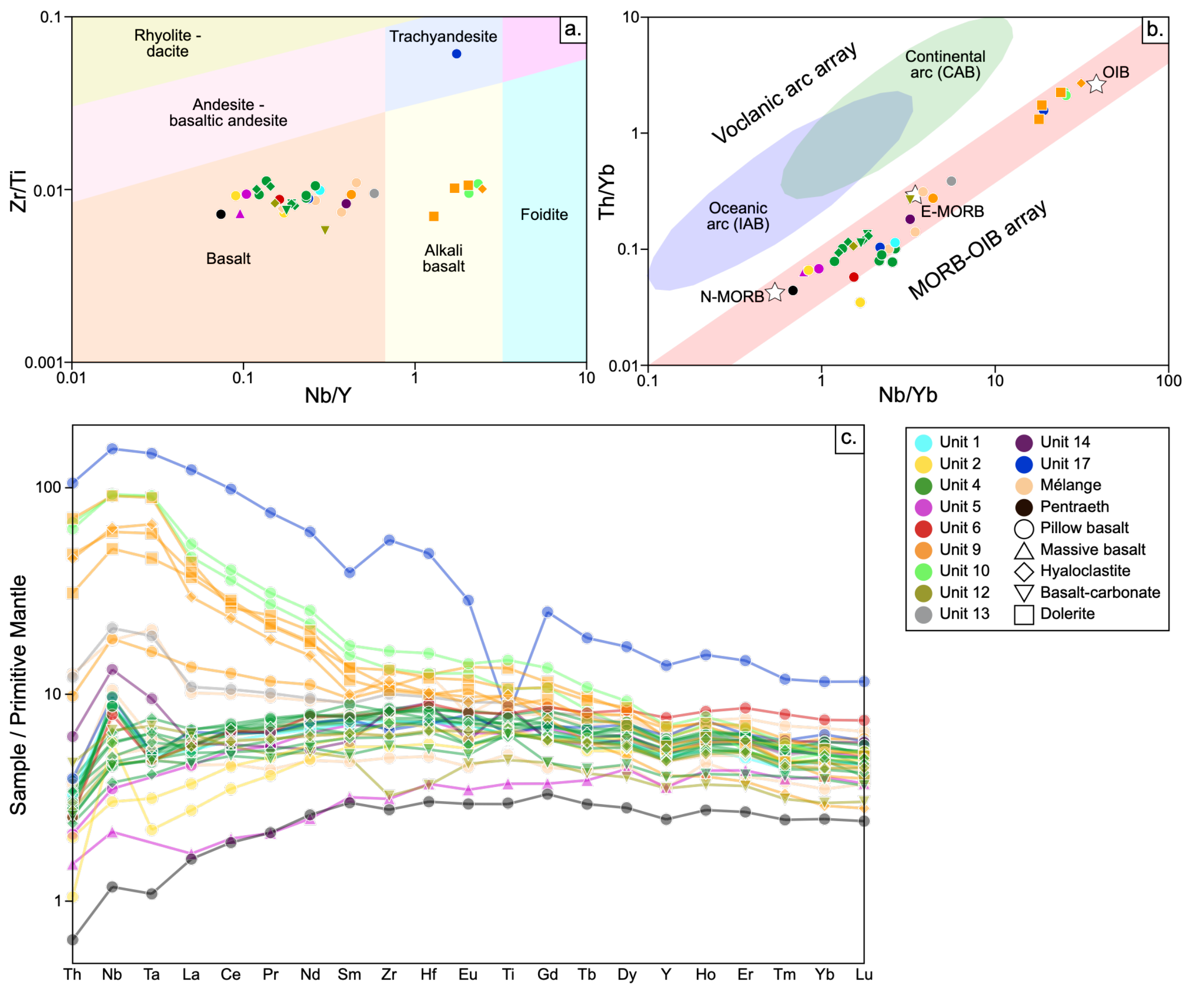

Figure 4.8: plots of Gwna Complex Area I igneous rocks distinguished by tectonostratigraphic units and rock type showing (a) volcanic rock classification scheme (Pearce 1996), (b) tectonic discrimination plot (Pearce 2014), and (c) multielement plot of immobile HFSE elements normalised to primitive mantle (Sun and McDonough 1989).

Geochemical differences in Unit 9 are expected under the consideration that the dolerite sills and overlying hyaloclastites are representative of a secondary magmatic event. These samples are display very similar OIB-like compositional signatures, despite major element differences expected between the different lithologies. The exception to this is AN18014, a vesicular pillow basalt, which is assumed to act as the primary igneous base to Unit 9, although its stratigraphic placement is not certain. AN18014 is still relatively enriched compared to most basaltic rocks in Area I, with an E-MORB-like composition (Figure 4.8b), however it is compositionally much more similar to the other primary igneous occurrences in Area I than the apparent secondary OIB-like igneous rocks of Unit 9. AN18014 is geochemically most similar to AN18031 of Unit 13, another vesicular pillow basalt unit occurring along strike to the south. It is therefore possible that these rocks mark a continuation of a single unit offset along obliquely orientated faults. These two samples – along with AN16028 from a high-strain shear zone – are the only Group 2 samples in Area I, showing that they are more geochemically enriched than other primary igneous rocks in Area I, all of which sit within Group 1.

The OIB-like samples of Unit 9 are similarly matched by the pillow basalts of Unit 10, which runs stratigraphically above Unit 9, separated by a narrow zone of highly sheared lithologies. Interestingly, AN19030 sits within this intermediate mélange zone and has a distinctly tholeiitic, weakly enriched composition (La/Lu_{PM} = 1.40). Unit 10 contains slightly higher HFSE's on average and produces very similar REE patterns relative to other OIB-like samples from Area II, for example.

AN19036, sampled from Pentraeth, is the least enriched sample analysed from Area I and is consistently depleted in all HFSE's. It is particularly depleted in LREE's, producing a positive REE gradient (La/Lu_{PM} = 0.66) that levels and becomes slightly negative across MREE's and HREE's (Gd/Lu_{PM} = 1.35), which remain consistently less abundant than in other samples. Despite this it retains very similar HFSE signature to other tholeiitic samples from Area I, particularly Units 2 and 5, which also show comparatively little enrichment.

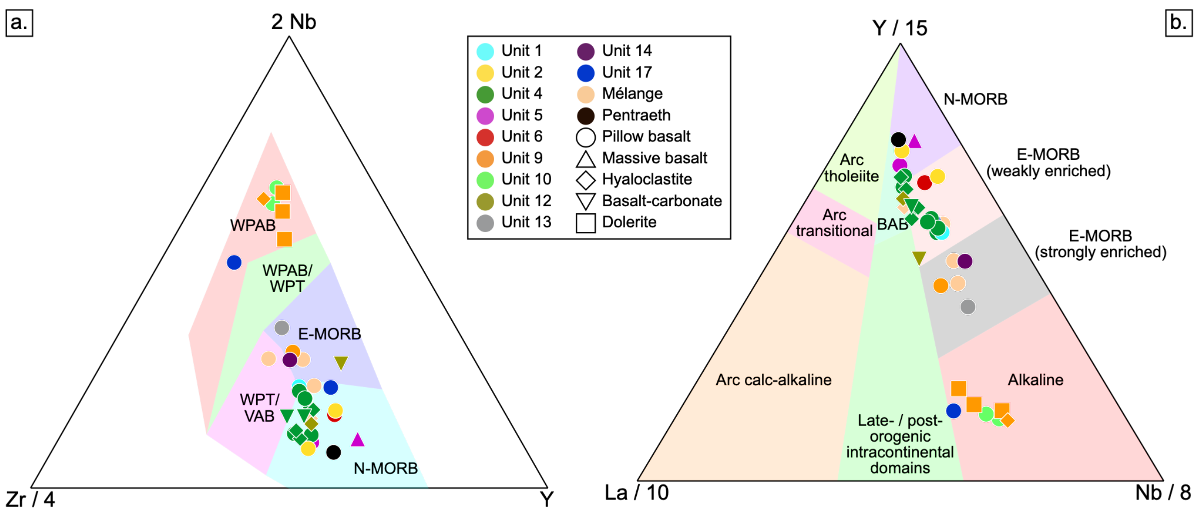

Figure 4.9: ternary tectonic discrimination plots for Gwna Complex Area I igneous rocks showing (a) basalt tectonic discrimination diagram (Rollinson 1993) and (c) tectonic classification diagram for mafic igneous rocks (Cabanis and Lecolle 1989).

Variability between lithologies

The compositional variability of basalt carbonates is controlled by the relative proportions of basalt and carbonate within a sample. Increased carbonate content leads to an increase in Ca, Mg, Mn, K, P and LOI, while Si, Al and Na are reduced. Despite the influence of two mixing rock types, trace element concentrations are largely unaffected and HFSE ratios remain predominantly influenced by the basalt component. All three basalt-carbonate samples produce geochemical signatures consistent with those produced by pillow basalts throughout Area I. Samples AN17021 and AN20021 – despite different basalt-carbonate ratios – display very similar geochemical signatures that are very consistent with other pillow basalts from Unit 4. Hyaloclastites generally follow similar major element trends, with carbonate content also highly variable through the influence of veins and alteration of matrix material. Hyaloclastites from both internal and basal hyaloclastites were analysed from Unit 4 and all hyaloclastites produced very similar trace element compositions to Unit 4 pillow basalts.

4.4.4 Igneous rocks of Area II

Samples of igneous rocks from Area II originate from three key localities across Llŷn Peninsula in Nefyn, Porth Orion and Porth Felen. Given the compositional diversity exhibited in samples from Area II, it is important to uncover any geochemical variations based on location and to potentially determine their relationship to stratigraphic or textural variations. Figure 4.10 shows Area II igneous rocks distinguished by these key localities.

On average, samples from Nefyn and Porth Orion have similar geochemical compositions, while those from Porth Felen are generally more enriched. Samples from Nefyn have the smallest compositional range and are tholeiitic to transitional with an E-MORB-like signature. Of seven samples, three plot in Group 1 and four in Group 2. In comparison to Area I, the samples in Area II show a more continuous progressive enrichment path along the MORB-OIB array (Figure 4.10b).

Samples from Porth Orion are split between two compositional trends. Of 11 samples, eight plot within Group 1 and a single sample (LLY16) plots within Group 2, marginally outside of Group 1. This grouping plots between N-MORB and E-MORB, and generally less enriched than samples from Nefyn. Two other samples, LLY37b and LLY81, plot in Group 3. These two samples originate from the east of the main headlands that other samples were collected from. LLY37b originates from a small basalt lens within schist, while LLY81 also comes from a basalt block surrounded by schist, although it is not clear whether the block is faulted or also incorporated in the schist.

Porth Felen is represented by ten samples, with two plotting in Group 1, six in Group 2 and two in Group 3. Six of the samples originate from a large basalt outcrop within the bay of Porth Felen, and all plot within a similar E-MORB-OIB compositional range. Repeated sequences of basalt overlain by sediments continue to the southeast, represented by AN16035, AN16036 and A325. Both AN16036 and A325 have very similar tholeiitic N-MORB-E-MORB compositions, although AN16036 has a notably higher Zr-Hf anomaly (Zr/Zr* = 2.00 to 1.42). AN16035 is more enriched however, as shown by REE patterns (La/Lu_{PM} = 3.20 to 0.50 – 0.51) and is much more similar in composition to the group to the west. Several samples show moderate Eu anomalies, although this is not specific to a locality. AN19022 is the least enriched sample from Porth Felen, with a tholeiitic N-MORB composition and no enrichment in Th, Nb or Ta, showing a weakly negative Nb anomaly (Nb/Nb* = 0.94). The sample originates from a large basalt block within mélange, situated on the headland to the west of the bay at Porth Felen and appears to be tectonically distinct from other samples from the area.

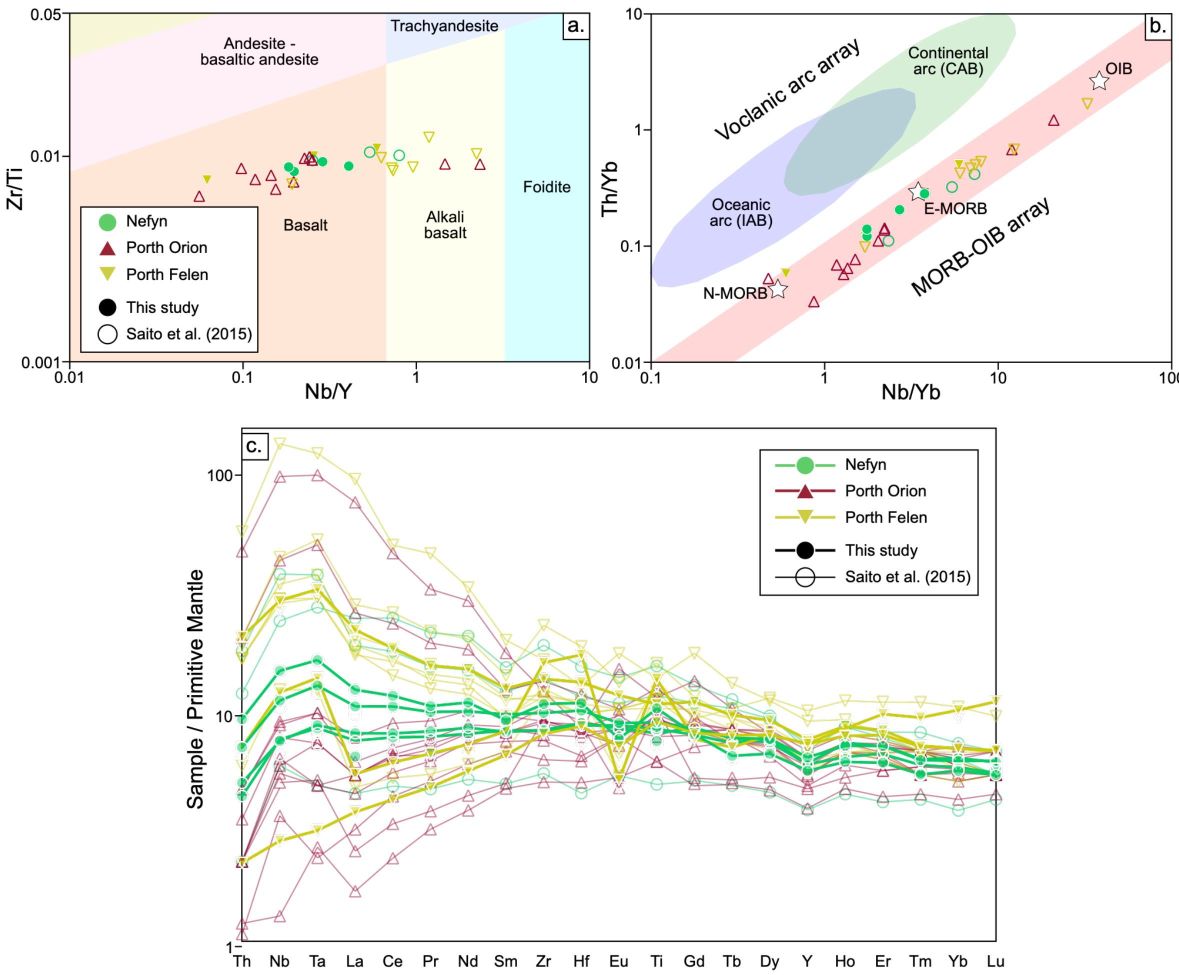

Figure 4.10: plots of Gwna Complex Area II igneous rocks distinguished by key localities showing (a) volcanic rock classification scheme (Pearce 1996), (b) tectonic discrimination plot (Pearce 2014), and (c) multielement plot of immobile HFSE elements normalised to primitive mantle (Sun and McDonough 1989).

4.5 GEOCHEMISTRY OF GWNA COMPLEX SEDIMENTS

A total of 14 samples from various sedimentary rocks across Areas I, II and IV were analysed from the Gwna Complex. Five samples are chloritic schists from Areas II and IV. Also included is a sandstone sample, a red chert sample, a silty mudstone samples and two mudstone samples from Area I, and a black mudstone sample from Area II. Three other samples (jasper AN18002 and carbonates AN20014 and AN20020) will be discussed separately in Sections 4.5.4 and 4.5.5 respectively.

4.5.1 Major elements

Figure 4.11 shows the major element compositions of analysed samples through Harker diagrams. The samples analysed range between 65.1 – 82.9 % SiO_2, with red chert unsurprisingly having highest silica content. Mudstones from Area I have the lowest abundance (65.1 – 65.4 %), while the black mudstone of Area II has relatively high 75.1 %. Schists range between 65.9 – 74.4 %, while the sandstone and silty mudstone of Area I have 70.4 % and 67.3 % respective SiO_2 abundances. Contents of Al_2O_3 are closely correlated to SiO_2, with a range of 7.5 – 18.0 % that decreases with increasing SiO_2. One notable exception is the black mudstone, which has a relatively high Al_2O_3 abundance (16.1 %). The black mudstone also has the lowest abundances of MgO, Fe_2O_3, CaO, Na_2O and P_2O_5, while having the highest K_2O abundance. It is worth noting that the black mudstone also has the lowest MnO content of analysed sediments (0.02 %).

Samples generally have low MgO contents, ranging between 0.7 – 2.8 %, while having higher Fe_2O_3 (2.0 – 6.7 %). Schists generally have MgO and Fe_2O_3 abundances concordant with SiO_2 however AN16033 is relatively low in both. The schists and sandstone have highest CaO contents (0.9 – 1.6 %), while mudstones contain slightly less (0.7 %) and the silty mudstone and red chert are relatively depleted with concentrations < 0.25 %. Abundances of Na_2O range between 0.3 – 5.1 %, while K_2O ranges between 1.1 – 4.8 %. Samples with high Na_2O generally have subsequently low K_2O, as seen with AN17008 and AN17025. AN17018 and AN19012 show the revers of this trend.

Of the two Area I mudstones, AN19011 represents reddened mudstone and AN19012 represents green mudstone. They are compositionally quite similar with two key differences. AN19011 contains greater Fe_2O_3 (6.7 % to 6.2 %) and subsequently less MgO (2.0 % to 2.5 %). The largest difference is that AN19011 has a relatively high Na_2O (5.0 % to 1.9 %) content, with low K_2O (3.1 % to 4.7 %) and Al_2O_3 (16.2 – 18.0 %).

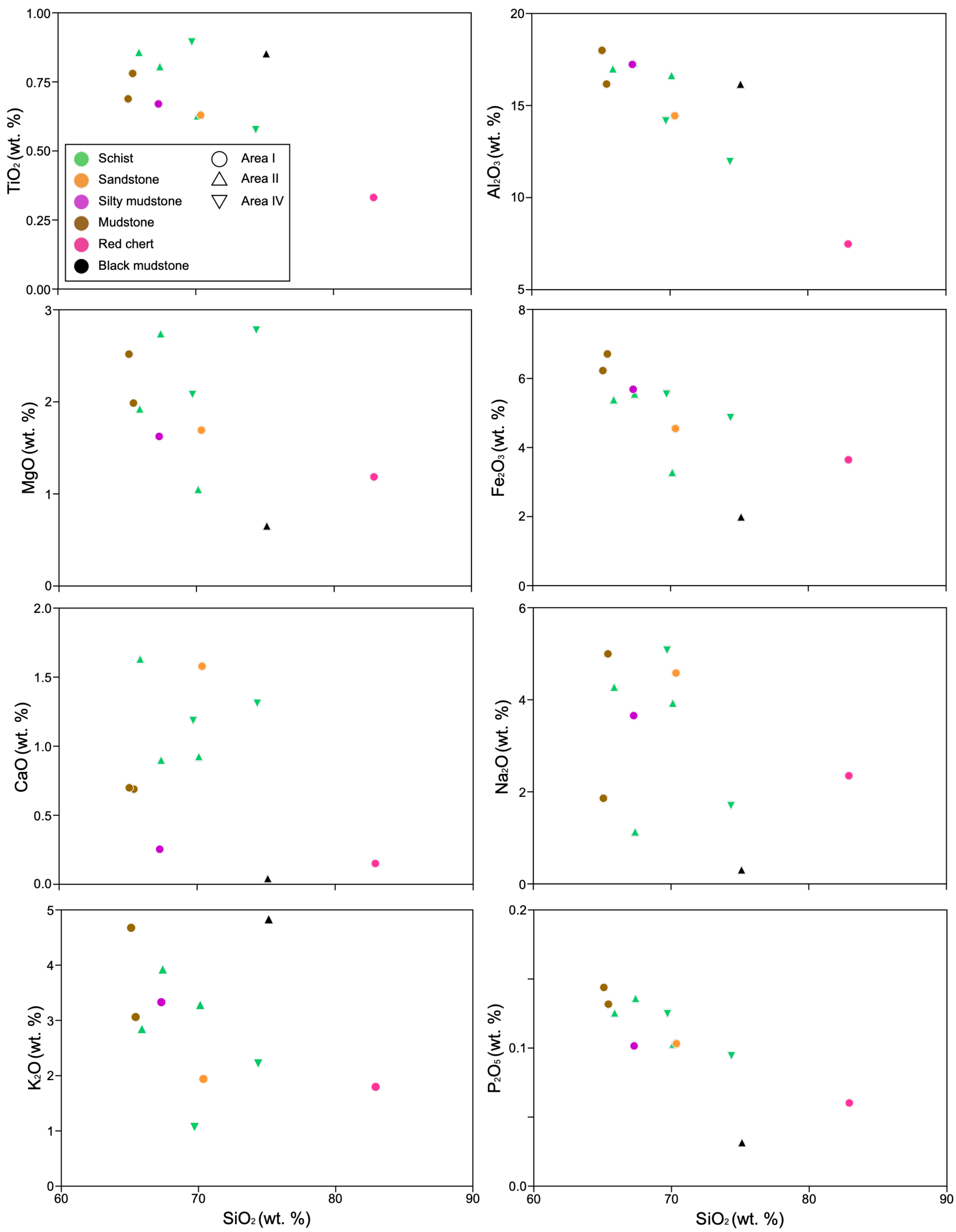

Figure 4.11: Harker diagrams showing major element compositions of various sedimentary rocks from the Gwna Complex, distinguished by rock type and sample area.

Figure 4.12 utilises major element compositions to classify clastic rocks. Because the plot is targeted at clastic rocks, the red chert, and black mudstone should not be considered as strongly, and the plot is more useful to classify the schists and sandstone. Samples plot largely within the greywacke field, with three samples (AN17010, AN17018 and AN19012) plotting in the litharenite field.

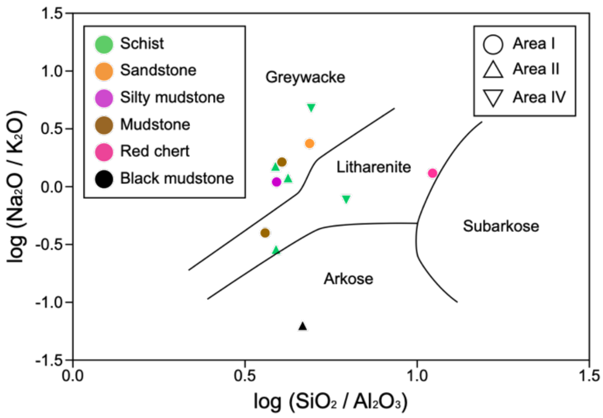

Figure 4.12: major element geochemical classification scheme for clastic rocks (Pettijohn et al. 1972) to classify sedimentary rocks from across the Gwna Complex.

4.5.2 Trace elements

Multivariate plots in Figure 4.13 show that the schists and sandstone display very similar HFSE trace element patterns, with negative Nb-Ta anomalies (Nb/Nb* = 0.23 – 0.30) and Ti anomalies (Ti/Ti* = 0.58 – 0.75), positive Zr-Hf anomalies (Zr/Zr* = 1.62 – 2.20) and gently negative sloping REE patterns (La/Lu_{PM} = 4.12 – 8.02) with weakly negative Eu anomalies (Eu/Eu* = 0.67 – 0.86). Mudstones display very similar patterns, with a slightly more defined negative Eu anomaly (Eu/Eu* = 0.65). Despite great similarities, AN19012 is more enriched in LREE's, while AN19011 has a less pronounced Nb-Ta anomaly. The silty mudstone shows a unique REE pattern, displaying a positive Ce anomaly (Ce/Ce* = 2.08), moderate negative Eu anomaly and weakly positive HREE trend (Gd/Lu_{PM} = 1.48). Other HFSE abundances closely follow those in from the schists and sandstone. Red chert shows a comparatively weak Zr-Hf anomaly (Zr/Zr* = 1.384), more pronounced negative Ti anomaly (Ti/Ti* = 0.46) and more steeply negative HREE pattern (Gd/Lu_{PM} = 1.47). The black mudstone is comparatively enriched in LREE's, which subsequently produce a steely negative pattern (La/Sm_{PM} = 7.19), along with a strong negative Eu anomaly (Eu/Eu* = 0.51).

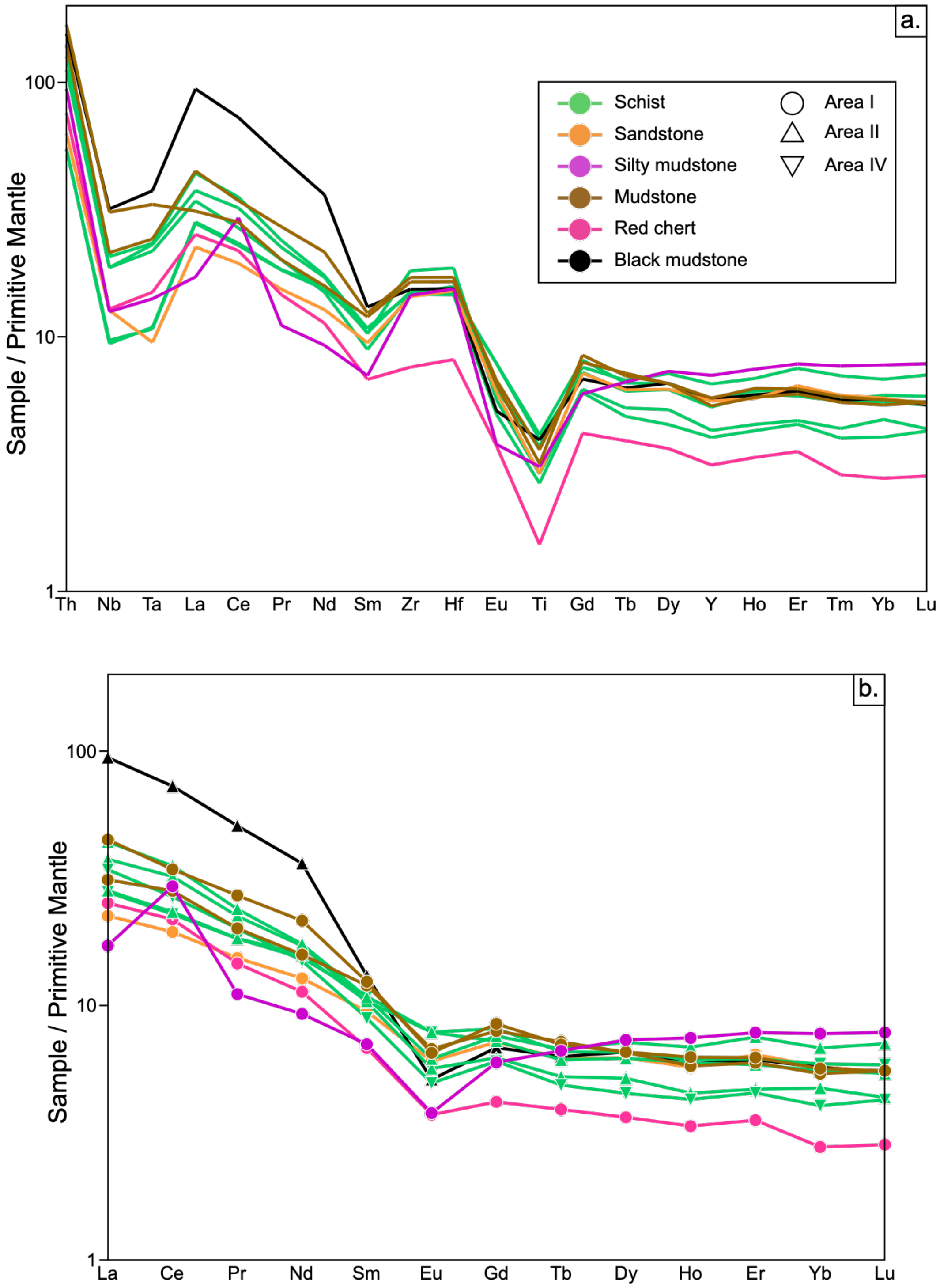

Figure 4.13: multielement plots featuring (a) immobile HFSE elements and (b) REE elements normalised to primitive mantle (Sun and McDonough 1989) showing sedimentary samples from the Gwna Complex distinguished by rock type and sample area.

4.5.3 Provenance

Figure 4.14a uses major elements to discriminate tectonic setting. Samples are spread between the arc field and continental margin field, while the black mudstone falls within the passive margin field. Figures 4.14b uses major element discriminant functions to analyse sediment provenance, with samples largely plotting between the felsic and intermediate igneous fields, with a group of four samples plotting around the quartzitic sedimentary field. Figures 4.14c and d have both been used as methods to analyse sediment source derivations. Samples plot within the intermediate field in Figure 4.14c, clustered around andesite, while several samples plot towards the felsic field. Samples in Figure 4.14d plot within the felsic field although schist samples with relatively high TiO_2 plot very close to the felsic-intermediate boundary.

The ternary plots of Figures 4.14e and f examine trace element ratios to determine the provenance of clastic sedimentary rocks. Samples are split between two groups in Figure 4.14e, plotting within the continental island arc and oceanic island arc fields respectively. The clusters split schist samples from both Areas II and IV. The oceanic island arc cluster plots close to the continental island arc boundary. In Figure 4.14f, all samples plot in a single cluster around the continental island arc field. The samples have La/Sc and Th/Sc ratios ranging between 0.7 – 4.6 and 0.26 – 0.95 respectively, which is indicative of an intermediate to felsic sediment source (Cullers and Podkodyrov 2000). Ratios of La/Co and Th/Co range between 1.0 – 3.3 and 0.4 – 1.4 respectively, which is also indicative of an intermediate to felsic source (Cullers and Podkodyrov 2000). It should be noted that AN19021 was not included in the La/Co and Th/Co ranges due to its low Co contents (0.825 ppm), which led to anomalously high ratios.

4.5.4 Interpillow jasper

The occurrences of layered red cherts in Area I (Unit 9) has often been conflated with basalt-associated red jasper across the Gwna Complex, leading to conclusions that interpillow jasper is a sedimentary product. Maruyama et al. (2010), for example mapped large jasper occurrences along fracture zones in Unit 4c, as the same lithology as the red cherts of Unit 9 in their geological map of Llanddwyn Island. AN17014 represents jasper samples from between pillow basalts in Area II. It is composed of 95.5 % SiO_2 and 4.2% Fe_2O_3 with very low trace element abundances and shows no geochemical similarities to AN18002.

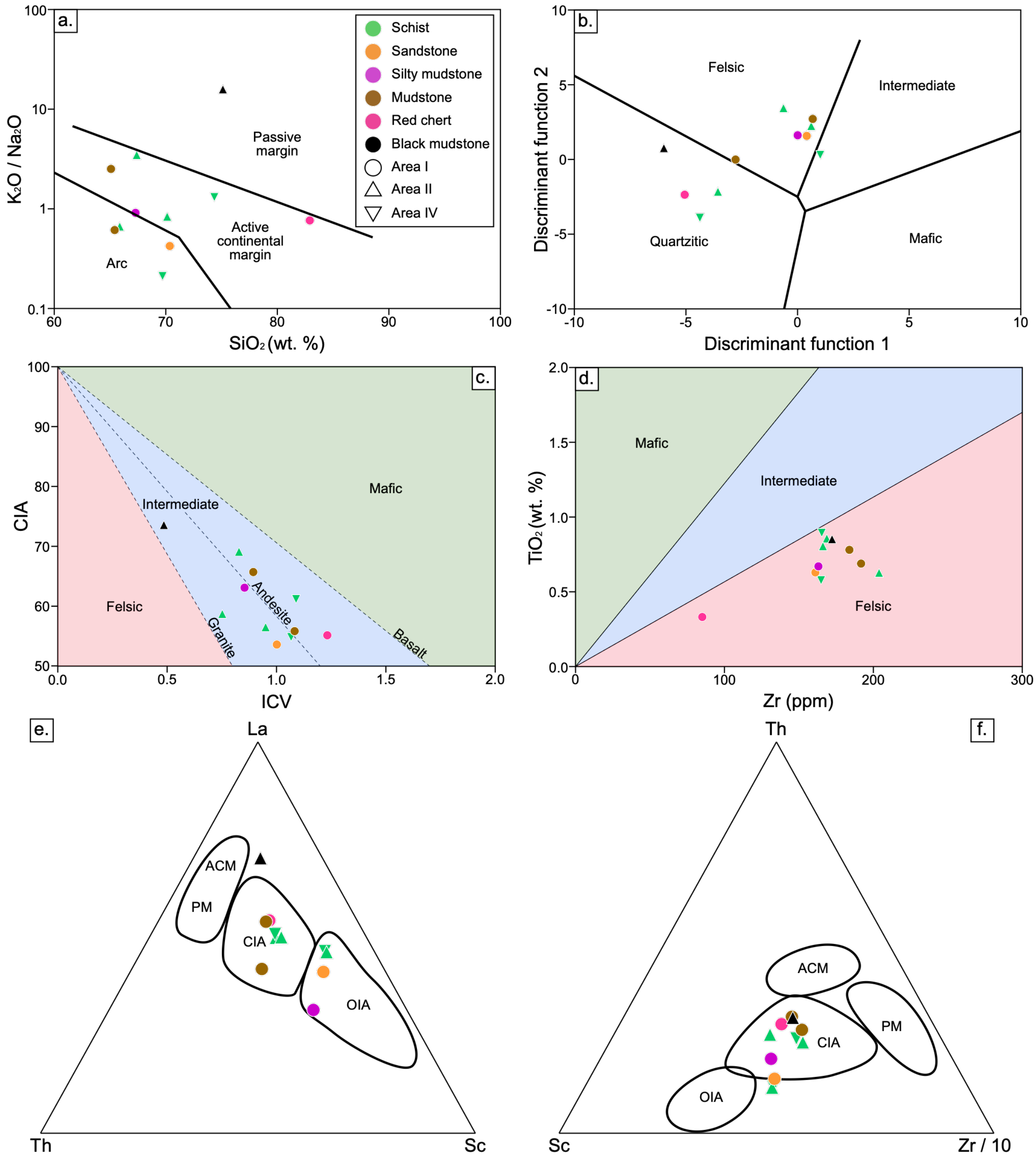

Figure 4.14: geochemical plots to geochemically discriminate sediment provenance for Gwna Complex sedimentary rock samples showing (a) tectonic setting determination for sandstones and mudstones (Roser and Korsch 1986), (b) major element based discriminant function diagram (Roser and Korsch 1988), (c) chemical index of alteration plotted against index of chemical variation as a proxy for sediment sources (Potter et al. 2010), (d) bivariate Ti/Zr plot used as a proxy for sediment provenance (Hayashi et al. 1997), (e-f) ternary tectonic discrimination plots for sandstones (Bhatia and Crook 1986). For 4.13b: Discriminant Function 1 = $(-1.773*TiO_s) + (0.607*Al_2O_3) + (0.760*Fe_2O_3) + (1.500*MgO) + (0.616*CaO) + (0.509*Na_2O) + (-1.220*K_2O) - 9.090$; Discriminant Function 2 = $(0.445*TiO_s) + (0.070*Al_2O_3) + (-0.250*Fe_2O_3) + (-1.142*MgO) + (0.438*CaO) + (1.475*Na_2O) + (-1.426*K_2O) - 6.861$.

4.5.5 Carbonate rocks

Two samples of carbonate rocks were analysed from Area I (AN20014 and AN20020). While AN20014 was sampled from a purely carbonate unit, AN20020 was sampled from the carbonate component of a basalt-carbonate unit. Both samples have minor SiO_2 components (2.7 % in AN20014, 5.5 % in AN20020), with AN200020 most likely influenced in part by interactions with basalt. The samples are composed of 17.7 – 19.4 % MgO, 31.1 – 31.8 % CaO and 43.7 – 43.9 % CO_2, making dolomite the overwhelmingly dominant carbonate phase. AN20014 contains 3.5 % Fe_2O_3 opposed to 0.7 % in AN20020, along with slightly higher Al_2O_3 (0.6 % in AN20014, 0.2 % in AN20020).

4.6 GEOCHEMISTRY OF PENMYNYDD BLUESCHISTS

A total of nine samples were analysed from metabasites within the Penmynydd Terrane. Data from the Penmynydd Terrane has been overlain with data from Gwna Complex igneous rocks (discussed in Section 4.4) to compare the magmatic origin of the rock types. As with the Gwna Complex igneous rocks, the Penmynydd Terrane has experienced significant geochemical alteration (see Section 4.3), so classifications will rely largely on HFSE's and other immobile elements. Mineral assemblages in these rocks range from greenschist to 'low-pressure' blueschist facies (see Section 3.4), conforming with P-T calculations by Kawai et al. (2006). These peak conditions (8-9 kbar at 25 km depth; 400 – 500 ˚C) are not likely to have significantly affected the mobility of HFSE's.

4.6.1 Major elements

Despite evidence of alteration, the metabasites show consistent major element compositions, as seen in the Harker diagrams of Figure 4.15. Contents of SiO_2 range between 48.5 – 51 %, with the exception of AN17003 (44.2 %) while Al_2O_3 ranges between 12 – 16 %. They are relatively Fe-rich with 11 – 18 % Fe_2O_3 and 4 – 8 % MgO, rendering Mg# between 36 – 58. Figure 4.16 shows the broadly negative trend between Mg# and TiO_2 content. Samples AN18040 and AN19015 show different compositional trends to the remaining samples. They have the lowest MgO and Cao content, along with highest TiO_2, Na_2O and P_2O_5 contents. Interestingly, they do not have the highest Fe_2O_3 contents suggesting another controlling mechanism beyond magmatic evolution. There are also notable differences between the two samples, such as the lack of K_2O enrichment in AN19015, its notably lower Al_2O_3 content and more moderate CaO and P_2O_5 contents.

The remaining samples have relatively consistent compositions, with 1.3 – 2.8 % TiO_2, 9 – 12 % CaO, 0.1 – 0.8 % K_2O and 0.10 – 0.25 % P_2O_5.

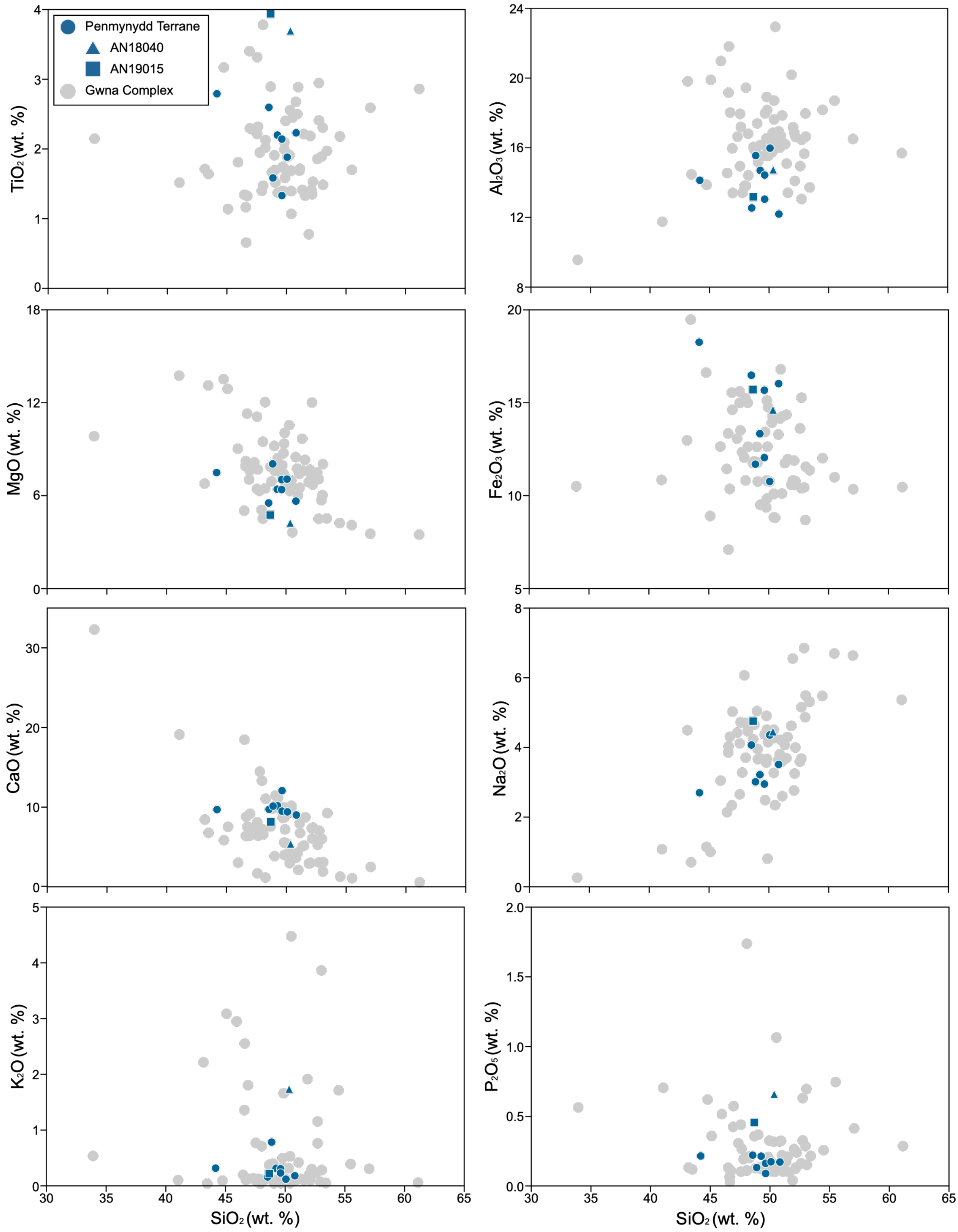

Figure 4.15: Harker diagrams showing major element compositions for Penmynydd Terrane metabasite samples plotted against Gwna Complex igneous rocks.

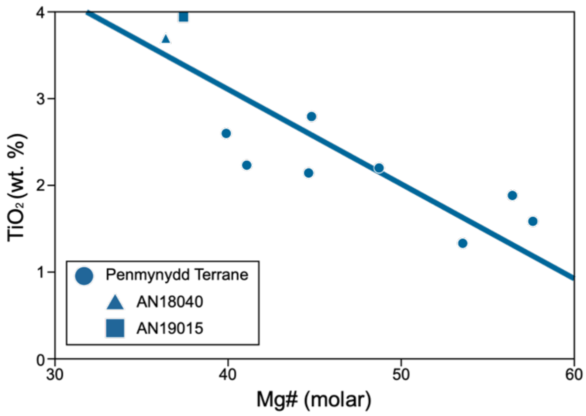

Figure 4.16: bivariate plot showing relationship between Mg# and TiO_2 in metabasite samples of the Penmynydd Terrane.

The Penmynydd Terrane metabasites have very similar mean major element compositions to the igneous rocks of the Gwna Complex. Both data sets produce a mean SiO_2 content of around 49 %, with mean Al_2O_3, Fe_2O_3, CaO and MgO falling within a 2.5 % difference. Mean contents of Na_2O and K_2O are within a 0.5% difference and P_2O_5 content is around 0.3 % for both groups. Penmynydd Terrane metabasites have generally higher Fe_2O_3 contents and subsequently less MgO. Differences between CaO and Na_2O are less distinct, and the Penmynydd Terrane metabasites generally have slightly more CaO and slightly lower Na_2O and K_2O. The Penmynydd Terrane metabasites are also generally lower in Al_2O_3. Mean TiO_2 is slightly higher, although contents between samples are quite variable. While all samples fall within the range of the Gwna Complex compositions for other major elements, AN18040 has a higher TiO_2 content than the highest Gwna Complex sample (ANG24) at 3.9 %, while AN19015 has a similarly high content at 3.7 %.

4.6.2 Trace elements

In Figure 4.17c, samples from the Penmynydd Terrane cluster within the basalt classification field, with the exception of AN18040, which plots as alkali basalt. Similarly, samples plot between the tholeiitic and transitional field in Figure 4.17a, while AN18040 and AN19015 plot within the calc-alkaline field. Figures 4.17b, d, e and f show samples plotting within the MORB-OIB array, much like igneous rocks of the Gwna Complex. A key exception to this is AN19015, which shows consistent continental arc geochemical signatures. Within the MORB-OIB array, AN18040 consistently plots towards alkaline OIB fields with geochemical signatures between E-MORB and OIB composition. The remaining samples are split between two well-defined groups of N-MORB (AN16015, AN17003, AN17006, AN17011 and AN18001) and moderately enriched E-MORB (AN17004 and AN17032) compositions. The N-MORB group tend to have relatively depleted compositions compared with the least enriched Gwna Complex samples.

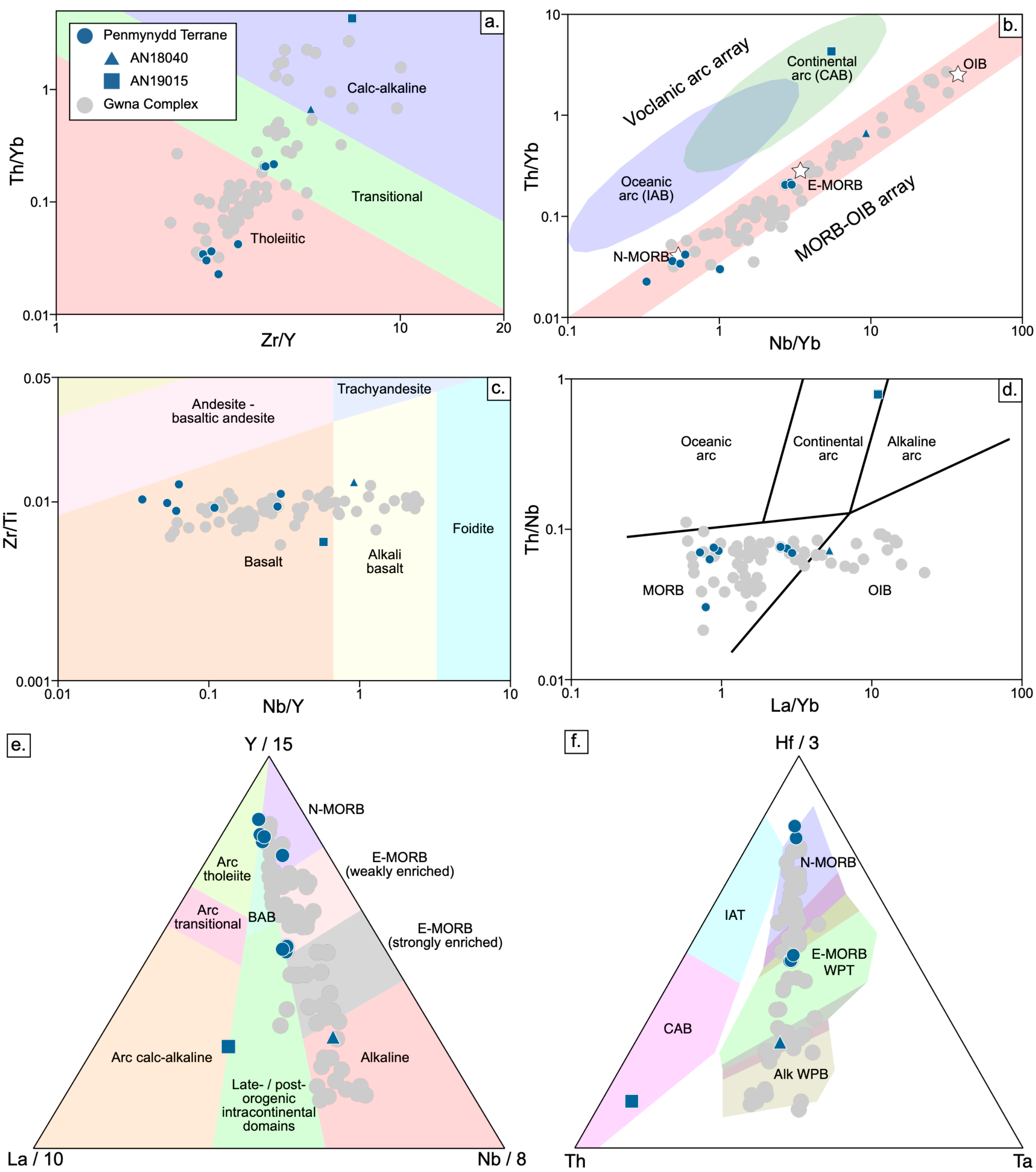

Figure 4.17: geochemical discrimination plots for Penmynydd Terrane metabasite samples plotted against Gwna Complex igneous rocks showing (a) magmatic affinity diagram *(Ross and Bédard 2009)*; (b) tectonic setting discrimination for igneous rocks using Th (Pearce 2014), (c) volcanic rock classification scheme (Pearce 1996), (d) tectonic setting classification using Th/Nb and REE ratios (Hollocher et al. 2012), (e) basalt tectonic discrimination diagram (Rollinson 1993) and (f) tectonic classification diagram for mafic igneous rocks (Cabanis and Lecolle 1989).

The volcanic rock classification scheme of Pearce (1996) in Figure 4.17c is not only useful in classifying rock types, but also in identifying differences in source material between samples. The Zr/Ti ratio acts as a differentiation index, since Ti has a greater affinity to oxides and pyroxenes and is therefore preferentially removed in greater relative quantities than Zr in more differentiated melts (Floyd and Winchester 1978; Rollinson 1993). The Penmynydd Terrane metabasites and the Gwna Complex igneous rocks show very similar Zr/Ti ratios, which suggests a similar magmatic source for protoliths in both groups. AN19015 has a relatively low Zr/Ti ratio (Zr/Ti = 0.006) compared to other Penmynydd Terrane samples (Zr/Ti = 0.009 – 0.013) and may represent an outlier from this trend.

The multivariate plots of Figure 4.18 highlight the geochemical differences of AN19015, which shows significant negative Nb and Ta anomalies (Nb/Nb* = 0.23), while showing enrichment in Zr (Zr/Zr* = 1.65), Hf and Ti (Ti/Ti* = 3.95). It shows a steeply negative REE trend (La/Lu_{PM} = 7.93) which declines steeply through LREE's (La/Sm_{PM} = 3.69) and flattens off towards HREE's (Gd/Lu_{PM} = 1.51). There is also a moderately negative Eu anomaly (Eu/Eu* = 0.61) that is much more defined than in any other Penmynydd Terrane samples (Eu/Eu* = 0.84 – 1.03). As a result, AN19015 is relatively depleted in HREE's. AN18040 shows similar multivariate trends to strongly enriched E-MORB/OIB igneous rocks from the Gwna Complex, with a more uniform negative REE trend (La/Lu_{PM} = 3.73), HREE contents similar to less enriched samples, and moderate enrichment in Nb (Nb/Nb* = 1.682), Ta and Zr (Zr/Zr* = 1.35).

The remaining samples match trends of the Gwna Complex igneous rocks well. E-MORB samples are enriched in Th, Nb and Ta, as well as LREE's to a lesser extent, relative to the N-MORB group. They show a weakly negative REE trend (La/Lu_{PM} = 2.00 – 2.08) and are relatively depleted in HREE's. In contrast, N-MORB samples show a weakly positive REE trend (La/Lu = 0.52 – 0.65) with weak Eu anomalies (Eu/Eu* = 0.84 – 0.89). AN17011, part of the N-MORB group, is systematically depleted in REE's yet shows the same REE pattern, with HREE's similar in concentration to the E-MORB samples. N-MORB samples also appear to be notably low in Ta relative to Nb.

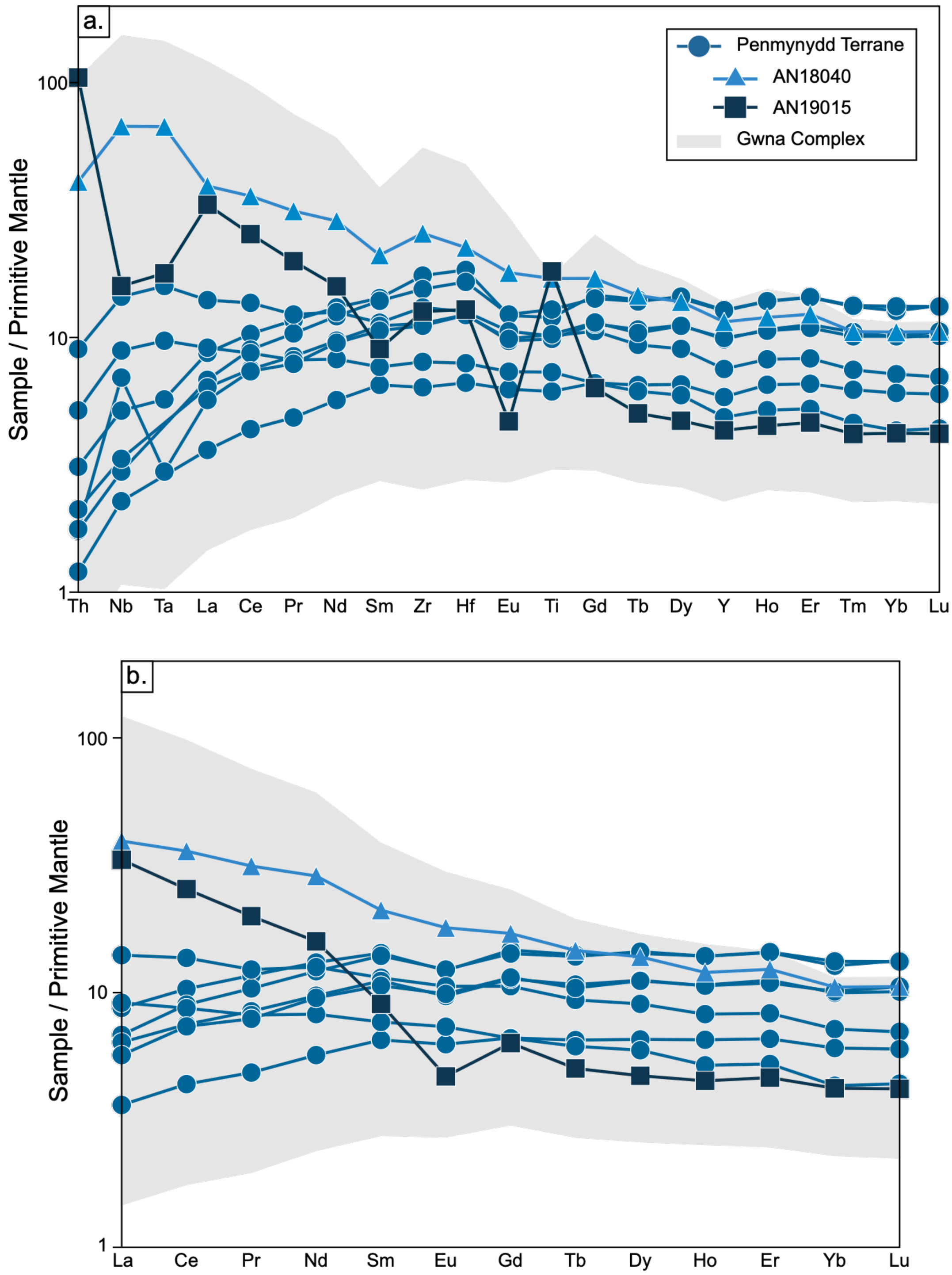

Figure 4.18: multielement plots featuring (a) immobile HFSE elements and (b) REE elements normalised to primitive mantle (Sun and McDonough 1989) showing Penmynydd Terrane metabasite samples plotted against the compositional range of Gwna Complex igneous rocks.

4.7 GEOCHEMISTRY OF THE PORTH TREFADOG FORMATION

The Porth Trefadog Formation is interpreted as a volcaniclastic sequence that sits stratigraphically below the Porth Swtan Formation mélange (see Section 2.8). Unlike many other units in the MCT, no absolute ages have been determined for the Cemaes Group. The provenance of these volcaniclastics may therefore give insight into the origin and context of the Cemaes Group. Nine samples were analysed from across the Porth Trefadog Formation along the western coast of Anglesey, including AN20010 from the Skerries Member. Porth Trefadog Formation samples have been split into three subgroups based on their locality, which acts as a proxy for stratigraphic height. Samples from around Porth Trefadog (AN20002, AN20003 and AN20005) are stratigraphically low, samples from around Porth Swtan (AN20006 and AN20007) were collected towards the top of the formation, while those from around Porth Crugmor (AN20037a, b and c) sit stratigraphically between.

4.7.1 Major elements

The content of SiO_2, the biggest control on major element compositions, ranging between 58.1 – 74.2 %, as expressed in the Harker diagrams in Figure 4.19. This wide range produces broadly negative correlations with other major elements as they are diluted by increasing silica content. Both Al_2O_3 (11.0 – 18.3 %) and TiO_2 (0.50 – 0.77 %), have strong negative correlations to SiO_2. Samples have generally low MgO contents (1.1 – 3.0 %) relative to Fe_2O_3, which is more variable, ranging between 4.3 – 8.4 %. Stratigraphically low samples from around Porth Trefadog show slightly higher MgO and Fe_2O_3 contents relative to SiO_2 than other samples, while the Skerries volcaniclastic has relatively high MgO. Both CaO and K_2O defy the negative correlation to SiO_2. Samples from Porth Swtan are relatively depleted in CaO (0.3 – 0.4 % compared with 1.6 – 4.8 %), while AN20037c, the most SiO_2-rich sample from Porth Crugmor, is relatively CaO poor compared with other samples from the location. It is also relatively enriched in Na_2O. While K_2O abundances are generally between 2.5 – 3.4 %, AN20007 contains an anomalously high 4.5 %. This is balanced by its relatively low Na_2O contents relative to AN20008, which is otherwise very similar compositionally. AN20002, the most silica-rich sample has low Na_2O content (0.24 %), while other samples range between 1.9 – 4.2 %.

Using a TAS classification scheme in Figure 4.20a, samples plot between (trachy)andesite, dacite and rhyolite fields, although the low alkali content of AN20002 (2.9 %) is suspect. Other samples maintain consistent alkali contents, ranging between

5.3 – 6.8 %, showing a slight negative correlation to increased SiO_2, as seen in the Harker diagrams of Figure 4.19. All samples plot within the calc-alkali field of Figure 4.20b, with the exception of AN20002 on account of its depleted alkali content. It plots within the tholeiitic field.

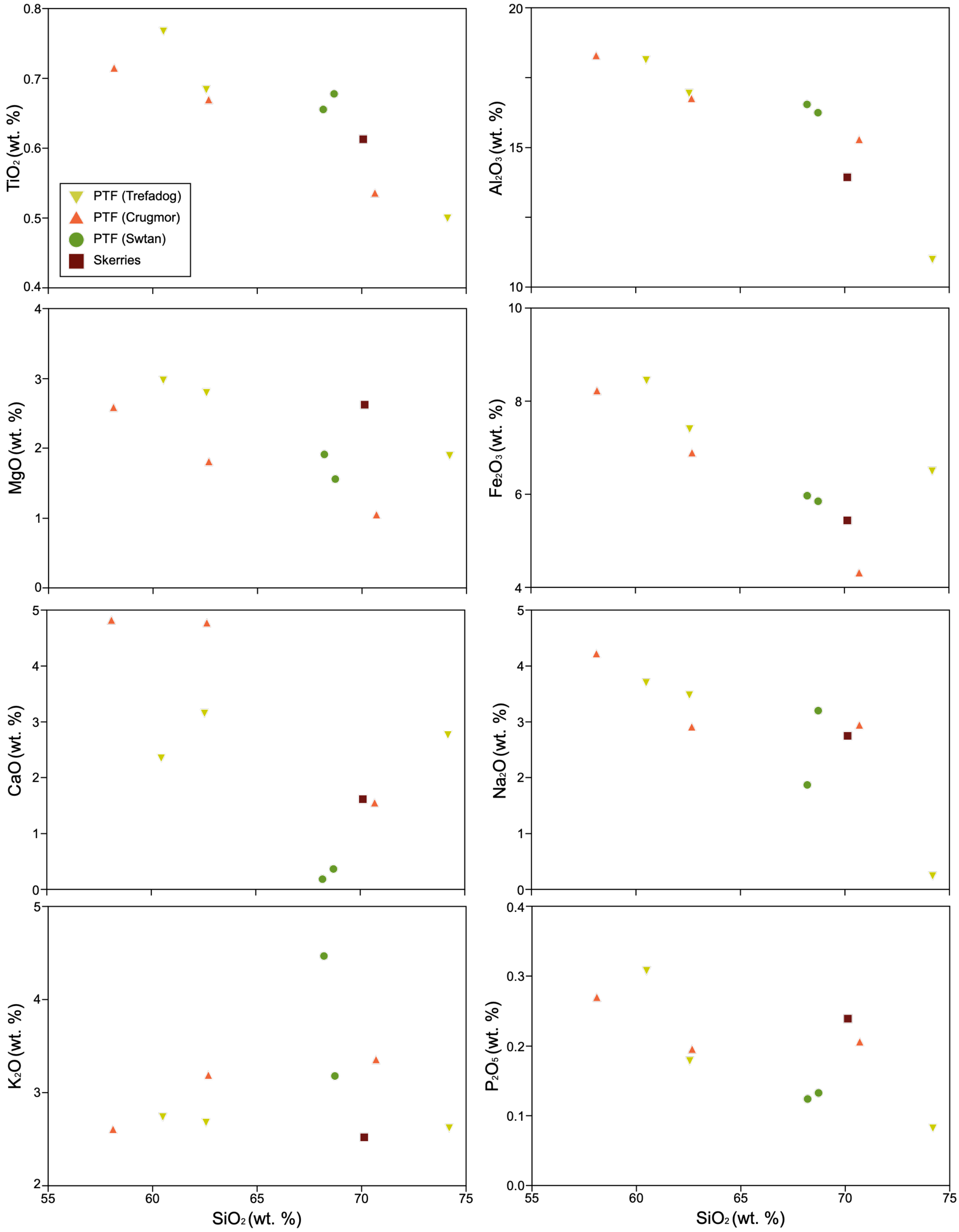

Figure 4.19: Harker diagrams showing the major element compositions of volcaniclastics from the Porth Trefadog Formation (PTF), distinguished by locality as a proxy for stratigraphic position.

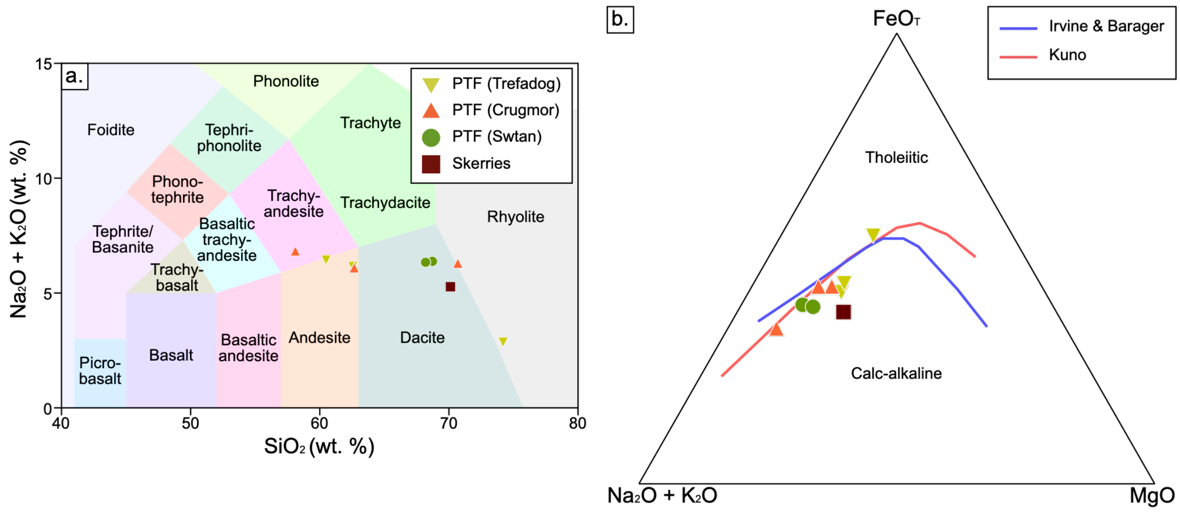

Figure 4.20: (a) TAS volcanic classification diagram (Le Maitre 2002) and (b) AFM diagram (Rollinson 1993) to characterise Porth Trefadog Formation volcaniclastic samples. 4.20b differentiation curves: blue after (Irvine and Baragar 1971), red after (Kuno 1968).

4.7.2 Trace elements

Unlike igneous rocks discussed in this chapter, LILE's show relatively stable concentrations in the Porth Trefadog Formation volcaniclastics, as shown by the multivariate plot of Figure 4.21a. This suggests that alteration has not greatly affected compositions, although Cs, Ba and Sr show signs of mobilisation. Samples show large negative Nb-Ta anomalies (Nb/Nb* = 0.12 – 0.23), with lowest anomalies correlating to Porth Swtan samples. AN20010 (Skerries volcaniclastic) closely follow the trends of the lowest stratigraphic samples from Porth Trefadog. Porth Swtan samples show positive Zr-Hf anomalies (Zr/Zr* = 1.42 – 1.65) that are not seen in other samples (Zr/Zr* = 0.85 – 1.07). All samples show a similarly large negative Ti anomaly (Ti/Ti* = 0.34 – 0.71). Figure 4.21b shows that all samples show similar normalised REE patterns, with negative convex LREE trends (La/Sm_{PM} = 2.76 – 4.12) and gently negative to flat HREE trends (Gd/Lu_{PM} = 1.20 – 1.87). Although all samples have similar LREE contents, they become sorted stratigraphically towards the HREE's, with those from Porth Swtan having highest concentrations and those from Porth Trefadog having lowest. All samples show weakly negative Eu anomalies (Eu/Eu* = 0.67 – 0.88). The Skerries volcaniclastic has a very similar REE trend to the Porth Trefadog samples.

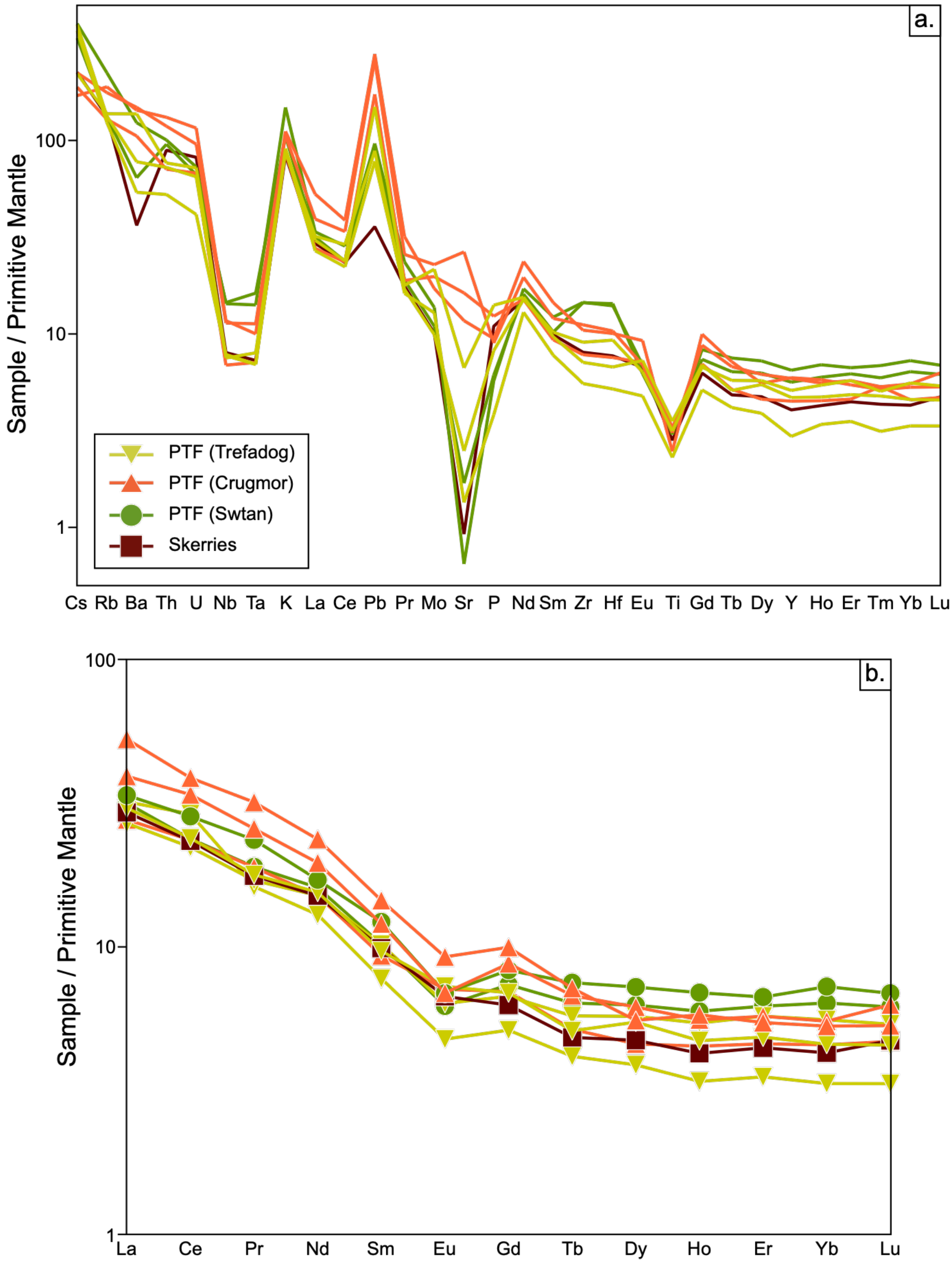

Figure 4.21: multielement plots featuring (a) suite of LILE and HFSE elements and (b) REE elements normalised to primitive mantle (Sun and McDonough 1989) showing compositions of Porth Trefadog Formation samples.

Based on the trace element classification in Figure 4.22a, samples plot around the sub-alkaline andesite/basaltic andesite field, which correlates with the andesite/dacite TAS classification in Figure 4.20a. Figure 4.22b shows that all samples plot closely within the continental arc field. While this classification is primarily developed for igneous rocks, Figures 4.22c and d are tectonic classifications developed primarily for sandstones. Both plots show samples plotting around island arc fields, split between continental and oceanic island arc fields.

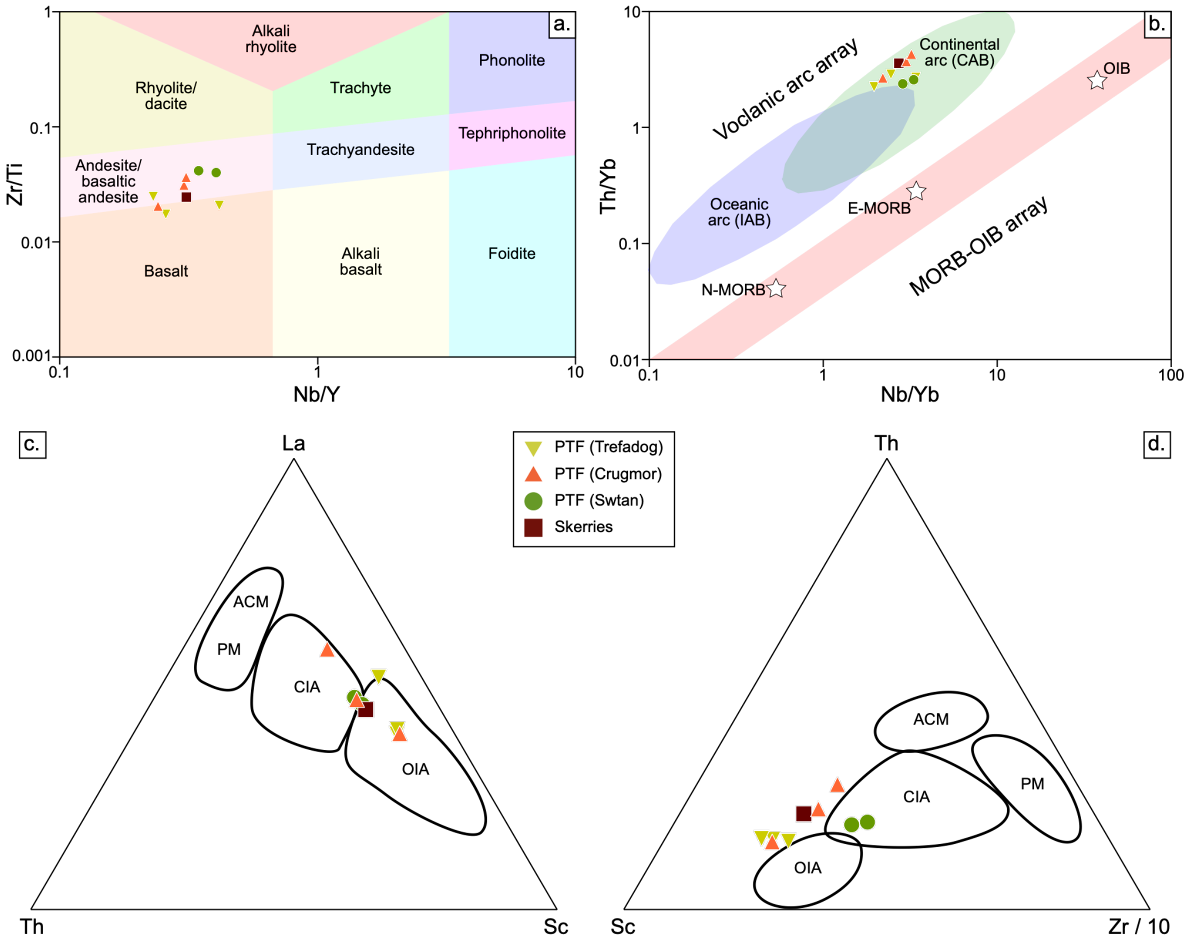

Figure 4.22: trace element discrimination plots for Porth Trefadog Formation rocks showing (a) volcanic rock classification scheme (Pearce 1996), (b) tectonic setting discrimination for igneous rocks (Pearce 2014) and (c-d) ternary tectonic discrimination plots for clastic rocks (Bhatia and Crook 1986).

4.8 GEOCHEMISTRY OF ANGLESEY'S MAFIC INTRUSIONS

A total of 17 mafic intrusive igneous rocks were analysed from across Anglesey including nine Group 1 intrusives (dolerites of assumed Palaeozoic age), one Group 2 intrusive (biotite-bearing lamprophyric dyke) and four Group 3 intrusives (dolerites of Paleogene age). Three doleritic sills from Gwna Complex Area I, have also been included for comparison and are discussed further in Section 4.4. Group 1 intrusives have been subdivided into four groups (a-d) based on geochemical distinctions. These groups, while determined geochemically, are consistent to sampling areas across Anglesey. Group 1a consists of two samples from Northern Anglesey (AN20033 and AN20035). Group 1b consist of two samples from Area I of the Gwna Complex (AN19010 and AN20013) and another from Area III (AN20018), all occurring along around the southern coast of Central Anglesey. Group 1c consists of two samples from Area IV of the Gwna Complex (AN20030 and AN20031), in Northeast Anglesey. Group 1d consists of a single sample from Porth Trecastell, also in Southern Anglesey but distinct from others in Group 1b.

4.8.1 Major elements

As shown in Chapter 3, Group 1 rocks have undergone significant alteration, which likely affects major element concentrations to a greater extent than samples from Groups 2 and 3. Figure 4.23 shows major element compositions plotted through Harker diagrams. Group 1 samples show greatest variation in SiO_2 (46.4 – 53.9 %) and Al_2O_3 (13.6 – 18.1 %) abundances. While these variations generally transcend subdivisions, Group 1c samples have comparatively low Al_2O_3 contents. MgO abundances range between 3.9 – 8.4 % while Fe_2O_3 ranges between 11.4 – 17.3 % with a broadly inverse correlation. CaO ranges from 5.9 – 9.1 %, and Na_2O generally ranges from 2.4 – 4.5 % although two samples (AN19010 and AN20051) fall below 1 % Na_2O. Both samples also show unusually high K_2O abundances of around 3.6 % – along with similarly enriched AN20030 – whereas other samples sit below 1.5 % abundance.

Along with low Al_2O_3 contents, Group 1c also shows relatively low MgO abundances, along with relatively high SiO_2, TiO_2, Fe_2O_3 and P_2O_5. Group 1 samples generally show P_2O_5 abundances below 0.5 %, whereas Group 1c samples exceed 1 %. Group 1c samples are compositionally consistent in all major elements except K_2O, which is notably high in AN20030, and Fe_2O_3, which is relatively high in AN20031. Group 1a contains relatively low TiO_2, and moderately low Fe_2O_3, conversely with moderately MgO contents. Group 1d similarly shows relatively low TiO_2 and Fe_2O_3 along with moderately high MgO and CaO. Group 1b acts as an intermediate composition, although shows greater compositional range than other subgroups. AN19010 is notably depleted in Na_2O and high in K_2O, but also has relatively high TiO_2 and Fe_2O_3 abundances, with comparatively low Al_2O_3.

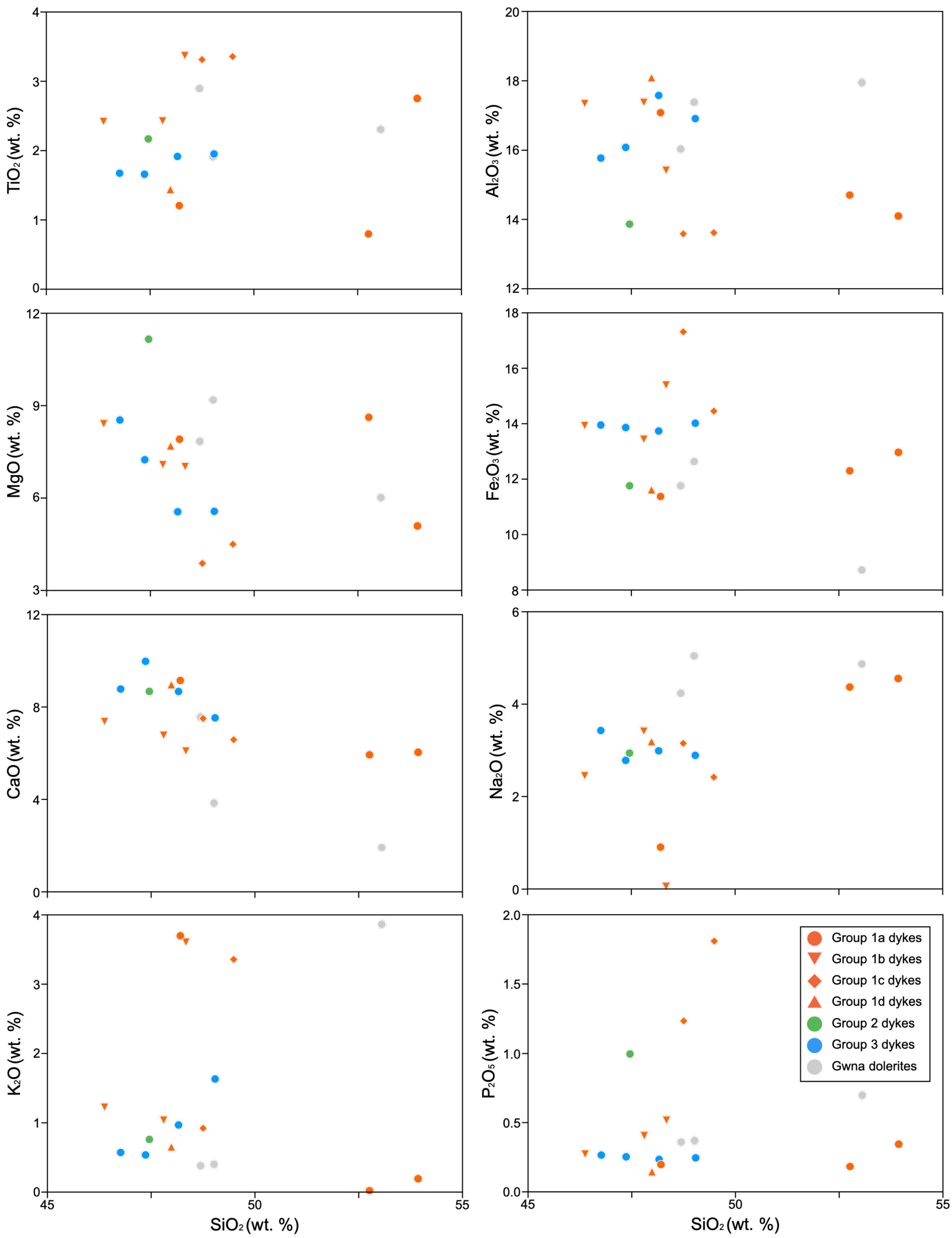

Figure 4.23: Harker diagrams showing the major element compositions of mafic intrusive rocks from Anglesey, split into textural groups with Group 1 subdivided (1a-d) based on geochemical variations.

The single Group 2 sample, AN20038, is distinguished by its relatively high MgO content (11.2 %), and subsequently high Mg# of 65.3. Despite this, other major element abundances are close to mean abundances for Groups 1 and 3. Its relatively average abundance of Fe_2O_3 (11.8 %) means that the sample has a higher total mafic content than other samples. Moderate exceptions include relatively low Al_2O_3 (13.9 %) and relatively high P_2O_5 (1 %), both of which are similar to compositions of samples in Group 1c.

Group 3 samples show similar major element compositions with very stable TiO_2 (1.7 – 1.9 %), Fe_2O_3 (13.7 – 14.0 %), Na_2O (2.8 – 3.4 %) and P_2O_5 (0.25 – 0.27 %) contents. SiO_2 abundance ranges from 46.7 – 49.0 %, Al_2O_3 between 15.8 – 17.6 %, and CaO between 7.5 – 10.0 %. The most significant variation is seen with MgO, which ranges between 5.6 – 8.5 %, producing an Mg# between 44.0 – 54.8.

4.8.2 Trace elements

Figure 4.24a shows that intrusives from Groups 1 and 3 are weakly to moderately calc-alkaline, with the exception of Group 1d, which is tholeiitic. Group 2 by contrast, is strongly calc-alkaline. Groups 1a and 2 have similarly high Th/Yb ratios (Group 1 = 0.66 – 0.84), while Groups 1b and 1c have lower Th/Yb ratios (0.20 – 0.59) but relatively high Zr/Y ratios (6.29 – 8.15). Figure 4.24c classifies Groups 1a and 2 as basalts, Group 1b between basalt and alkali basalt, and Group 1c as basaltic andesite based on its high Zr/Ti ratios (0.030 – 0.037). Group 2 is classified as alkali basalt.

Group 1d is clearly the least evolved intrusive group, and plots consistently within tholeiitic fields, leaning towards island arc affinity over MORB affinity (see Figures 4.24b, d, e and f). Groups 1b and 1c plot within the MORB-OIB array, with Group 1c showing E-MORB signatures and Group 1b showing greater enrichment towards OIB compositions (see Figures 4.24b and f). Figure 4.24e shows that high La in these groups pulls them from the MORB-OIB array towards the late/post-orogenic intracontinental domain along with Groups 1a and 2. Group 1a shows consistent volcanic arc affinity on enriched Th contents, but unlike Group 1d, is most likely associated with continental arc rather than oceanic (see Figures 4.24d and f). Group 2 is also most likely associated with continental arc magmatism, although from a much more alkaline domain than Group 1a.

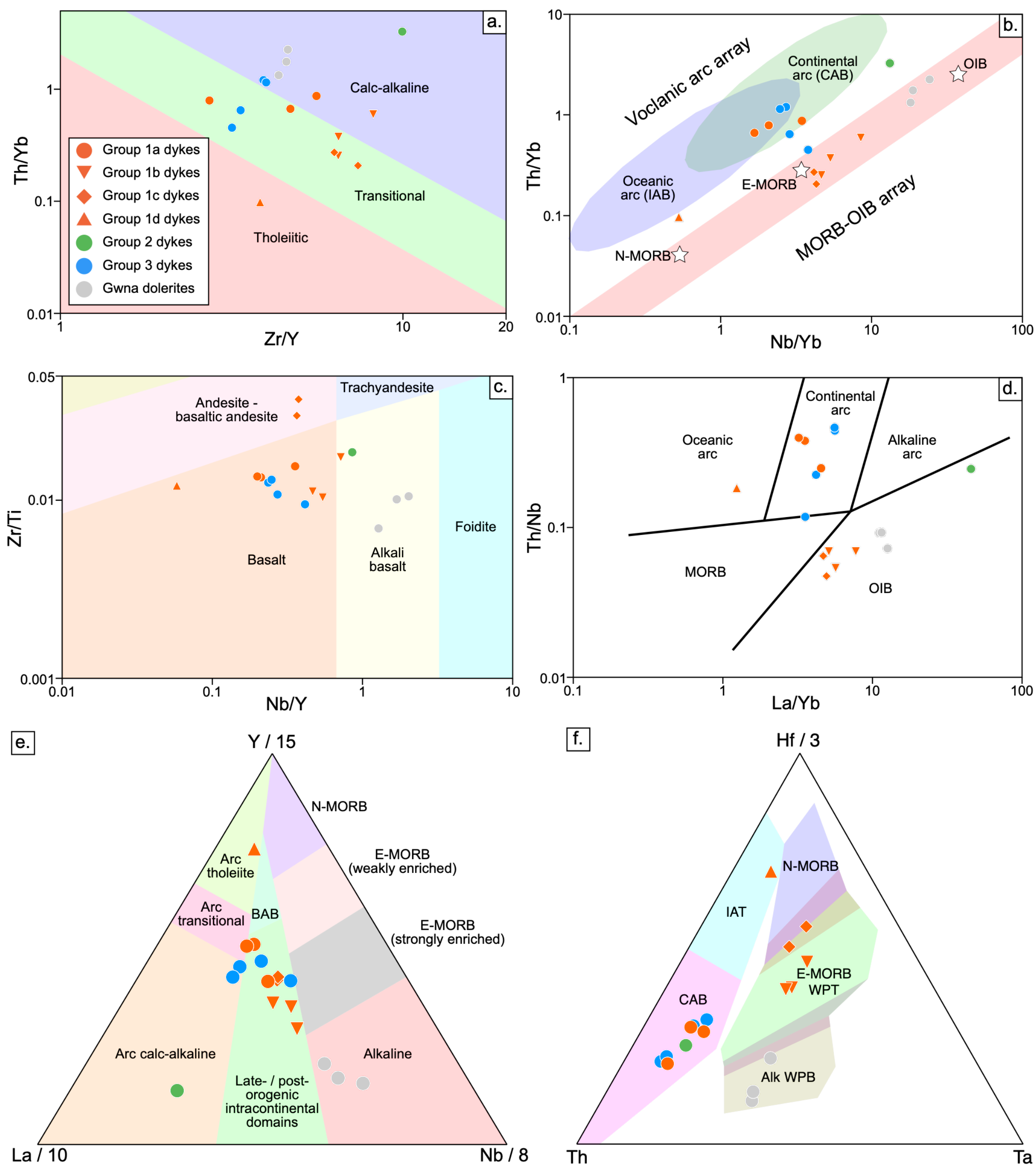

Figure 4.24: immobile trace element discrimination plots for mafic intrusive rocks from Anglesey showing (a) magmatic affinity diagram *(Ross and Bédard 2009)*; (b) tectonic setting discrimination for igneous rocks using Th (Pearce 2014), (c) volcanic rock classification scheme (Pearce 1996), (d) tectonic setting classification using Th/Nb and REE ratios (Hollocher et al. 2012), (e) tectonic classification diagram for mafic igneous rocks (Cabanis and Lecolle 1989) and (f) basalt tectonic discrimination diagram (Rollinson 1993).

Group 3, associated with the BPIP and opening of the Atlantic (Ellis 2009), shows a surprising set of geochemical signatures that range from E-MORB to CAB, occupying transitional spaces between the MORB-OIB and VAB arrays (see Figures 4.24b, d and e).

The dolerite sills of the Gwna Complex are clearly not related to any of the intrusives focused on in this section.

The multivariate plots of Figure 4.25 clearly show the effects of different Th/Nb and Th/Ta ratios between the groups, with Groups 1a, 1d, 2 and 3 – all of arc affinity – showing negative Nb-Ta anomalies (Nb/Nb* = 0.32 – 0.58), while Groups 1b and 1c – of MORB-OIB array affinity – show positive Nb-Ta anomalies (Nb/Nb* = 1.15 -1.30), along with Zr (Zr/Zr* = 1.39 – 1.84) and, to a lesser extent Hf. Groups 1c and 2 show moderate negative Ti anomalies (Ti/Ti* = 0.67 – 0.74), while other groups show positive affinities (Ti/Ti* = 1.04 – 1.91). Group 1d is particularly depleted in Th, Nb, Ta and LREE's. Group 1c is consistently enriched in HFSE's (except for Ti) relative to Group 1b, which shows similar multivariate trends. Group 2 is strongly enriched in LREE's and Th, but relatively depleted in Nb, Ta (Nb/Nb* = 0.35), Zr and Hf (Zr/Zr* = 0.95). It shows a steeply negative REE gradient (La/Lu_{PM} = 34.93), with the lowest HREE abundances of all analysed intrusives. With the exception of Group 1d, which has a positive LREE gradient (La/Sm_{PM} = 0.67) and overall, gently convex REE pattern (La/Lu_{PM} = 0.88), the remaining samples show similar moderately negative linear to slightly concave REE patterns (La/Lu_{PM} = 2.25 – 5.54).

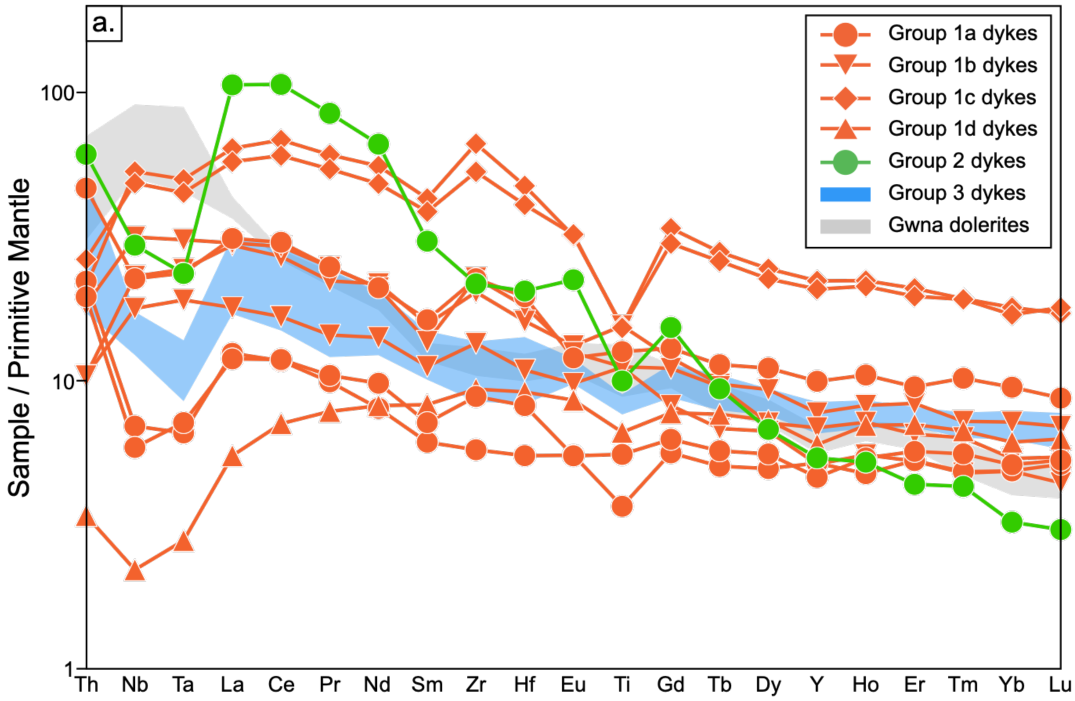

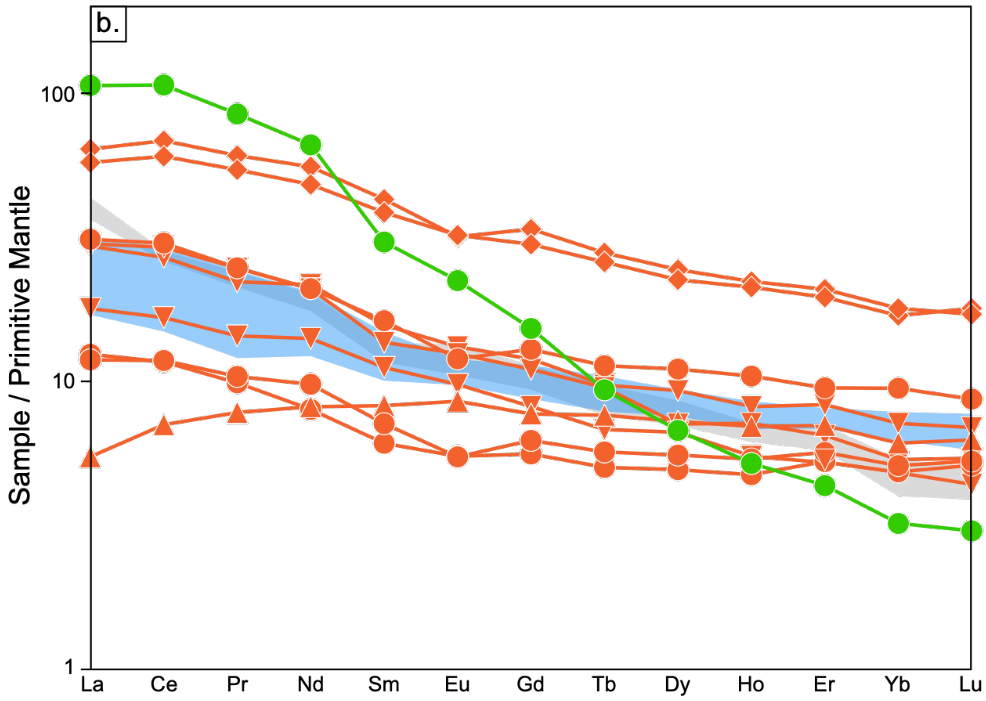

Figure 4.25: multielement plots featuring (a) immobile HFSE elements and (b) REE elements normalised to primitive mantle (Sun and McDonough 1989) showing the geochemical variability of mafic igneous intrusives from Anglesey.

CHAPTER V

Reconstruction of accreted material in the MCT

5.1 ACCRETIONARY EVIDENCE IN THE GWNA COMPLEX

Over the four studied areas, the Gwna Complex has proven to be structurally and lithologically diverse. Despite this, key similarities exist across all units that suggest that the units are closely related. Each area is affected by a pervasive NE-SW trending deformation fabric, although locally disturbed in Areas II and IV. The areas share a suite of core lithologies, including variable volumes of turbiditic sediments, quartzites, pelagic to hemi-pelagic sediments, and pillow-dominated basaltic sequences (see Table 5.1). Terrigenous and hemi-pelagic sedimentary rocks are derived from similar felsic-intermediate continental arc sources, varying between dominant volcaniclastic and siliciclastic components. Geochemical signatures of basaltic rocks all plot within the MORB-OIB array, further supported by consistent clinopyroxene compositions across Areas I and II (also with MORB-OIB compositions), suggesting a uniform magmatic source. Consistent mineral assemblages of basaltic rocks show that all areas were subjected to similarly low P-T metamorphic conditions (sub-greenschist facies). The anomalous occurrence of apparent greenschist facies mineral assemblages in mafic rocks of Area I Unit 9 is discussed in Section 5.1.4.

The relative prominence of these core components seemingly corresponds to the local structural framework of an area, ranging from repeated stratigraphic successions of basalts and pelagic to hemi-pelagic rocks in Area I, to more chaotic block-in-matrix regimes dominated by siliciclastic material in Area II. This section aims to provide a singular model of formation for the Gwna Complex, incorporating the variability across all four study areas.

5.1.1 Evidence for a tectonic origin

In Gwna Complex Area I, rocks are consistently tilted subvertically, with shear kinematic indicators from numerous sources suggesting downstepping of NW units against those to the SE. Semi-repetitive sequences in low shear units uniformly exhibit evidence of younging directions towards the SE. The interfaces of these low shear zones are marked by intense shear deformation and the development of mélange, showing that strain has been concentrated within the interface of these units. This suggests that repeated units – corrupted by pervasive shearing – have been imbricated against one another, stacked sequentially towards the SE. Kinematic indicators show that younger sequences originating from the NW have repeatedly underplated older units to the SE.

Table 5.1: Lithological diversity of the Gwna Complex showing the relative abundance of lithologies present within the four studied areas. Rare lithologies have single occurrences within an area, while uncommon lithologies outcrop in multiple areas but in relatively low volumes compared to common lithologies.

Lithology	Area I	Area II	Area III	Area IV
Clastic sedimentary rocks				
Gwyddel beds	None	Common	None	None
Quartzite	None	Common	Common	Uncommon
Siliciclastic turbidites	Rare	Common	Common	Uncommon
Volcaniclastic turbidites	Uncommon	Common	Uncommon	Common
Pelagic/hemipelagic sedimentary rocks				
Mudstone	Uncommon	Common	Uncommon	Common
Black mudstone	None	Rare	None	None
Silty mudstone	Common	Uncommon	Rare	Rare
Red chert	Rare	None	None	None
Carbonate rocks	Common	Common	Uncommon	Common
Basalt-carbonate rocks	Common	Uncommon	Rare	None
Magmatic rocks				
Dolerite	Rare	None	None	None
Pillow basalt	Common	Common	Uncommon	Uncommon
Massive basalt	Uncommon	Rare	None	Common
Hyaloclastite	Common	Uncommon	None	Rare

Area I lithologies are dominated by MORB-OIB basalt sequences that are overlain by pelagic to hemi-pelagic sedimentary sequences and small quantities of clastic turbidites derived from a continental arc setting. Such sequences are characteristic of ridge-trench OPS (Isozaki et al. 1990; Wakita and Metcalfe 2005; Kusky et al. 2013). Imbricated repetitions of OPS units buffered by shear zones are features found within subduction mélanges, resulting from the accretion of subducting material through sequential underplating (Onishi et al. 2001; Kimura et al. 2012; Wakabayashi 2017; Regalla et al. 2018).

Although Area I is uniformly characterised by this structural setting, other areas of the Gwna Complex are more variable, ranging between similar irregular imbrication of tectonic slices and block-in-matrix mélange. Table 5.1 shows that Area I is relatively starved of continent-derived clastic sediments. Areas II, III and IV, meanwhile, are characterised by volumetrically dominant clastic turbidites and less frequent occurrences of magmatic rocks.

Localised mélange-bearing beds in Area I show that its structural deformation style can support development of well mixed block-in-matrix fabrics, although they are limited by low, isolated volumes of phyllosilicate-rich material needed to act as a mélange host. The greater influx of turbiditic material into other Gwna Complex areas facilitates block-in-matrix mélange development on a much greater scale, resulting in lithological units often being hosted by a mélange fabric as opposed to directly imbricated against one another. Other more tectonically disrupted areas of the Gwna Complex are therefore seen to be analogous to the accretionary mechanisms interpreted for Area I, with deformation style controlled by the distribution and relative abundance of those core lithological components.

Repeated OPS sequences of multiple lithologies are also preserved in Area II, however they are separated by oblique faulting, rather than being imbricated along shear zones. Subvertically tilted low shear units of basalts also occur in Areas II and III, with a consistent way-up direction towards the SE, surrounded by highly sheared sequences. These sequences represent single-lithology units of OPS. Similar low-shear units of predominantly pillow basalt are the most common forms of OPS preservation in Area I.

The Gwna Complex is therefore considered to be a product of OPS accretion at a continental margin, where deformation styles are influenced by relative lithological volumes. Schematic endmembers of deformation styles in a subduction zone setting are shown by Figure 5.1. Area I shows the least disruption, preserving imbricates of OPS that can be reassembled (see Figure 5.1a) and, given the lithological continuity across the Gwna Complex, applied across all areas, where stratigraphic order has largely been disrupted by block-in-matrix mélange formation (see Figure 5.1b).

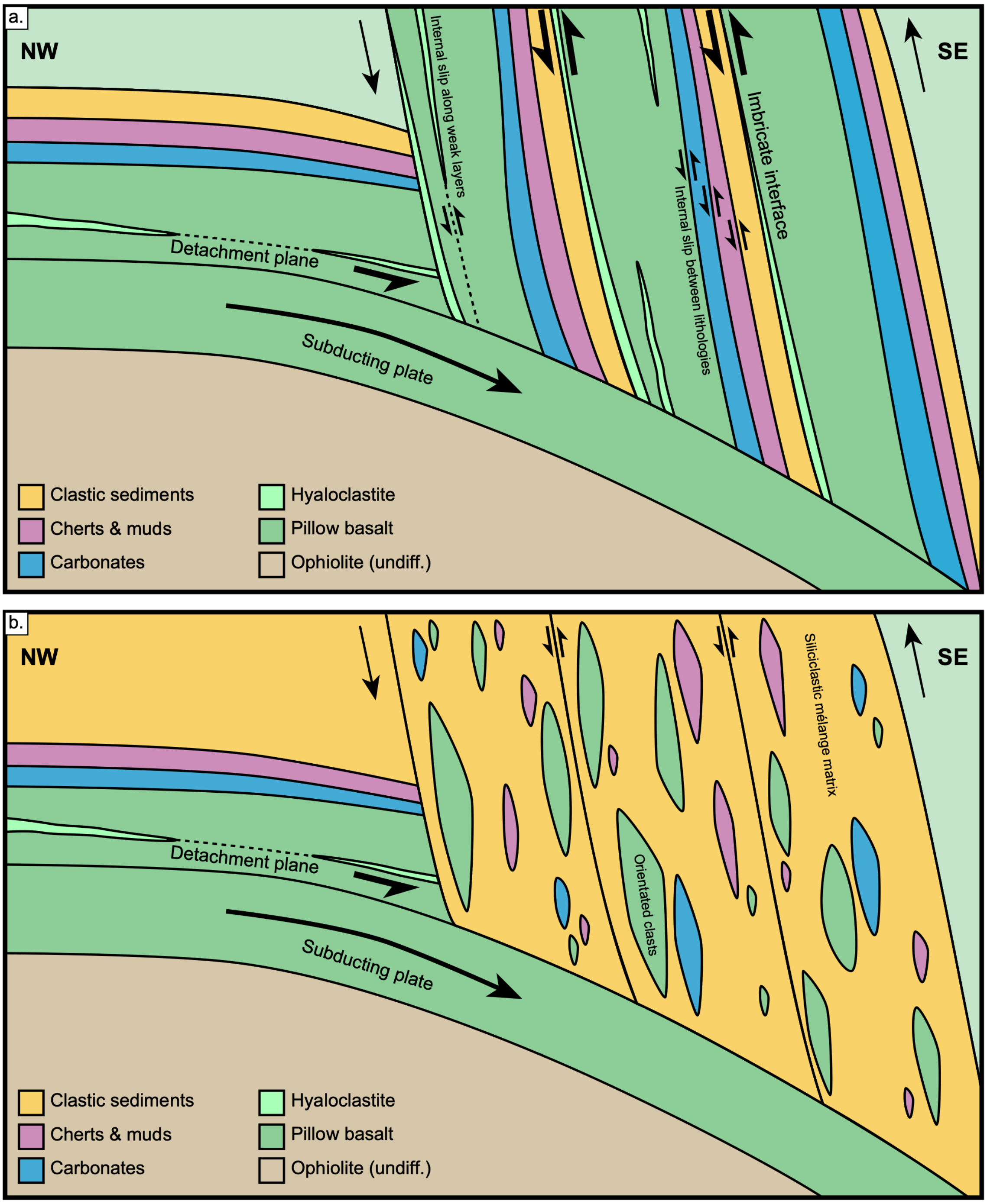

Figure 5.1: Schematic deformation endmembers for the formation of the Gwna Complex in an accretionary setting where delamination is dependent on the depth of weak hyaloclastite horizons in an ophiolitic basalt sequence, showing (a) imbricates of basalt-dominated OPS sequences buffered by highly concentrated shear interfaces with internal slip along weak layers in a system starved of siliciclastic sediments; and (b) block-in-matrix mélange formation in a siliciclastic dominated system where lower OPS units have become disaggregated and mixed in an enveloping foliated matrix.

5.1.2 Origins of the basal magmatic rocks

While the magmatic rocks of the Gwna Complex plot consistently within the MORB-OIB array, they should not be assumed to originate from a mid-ocean ridge without further scrutiny, since tectonic settings such as arc-related basins can produce similar basalts with overlapping geochemical signatures (Piercey 2011; Yang et al. 2021). Opposing interpretations have classified the Gwna Complex as an accretionary (Kawai et al. 2007; Maruyama et al. 2010a; Saito et al. 2015) or arc-proximal basin setting (Dartnall 2018; Schofield et al. 2020). Accreted basalts from a mid-ocean ridge and basalts uplifted from the closure of a basin would both originate from shallow mantle melting, producing similar geochemical compositions. However, their tectonic settings and methods of preservation are significantly different.

Ocean floor or arc-proximal basin

Figure 5.2 plots the Gwna Complex magmatic rocks against two data sets of mafic volcanics from within the Avalonian-Cadomian belt, comparing the rocks to hypothetical equivalents of accreted Iapetus ocean floor basalts (Ackerman et al. 2019) and basin-derived basalts from the back-arc rifting of Avalonia from the Gondwanan margin (Sánchez-García et al. 2003; Sánchez-García et al. 2008; Sánchez-García et al. 2010; Sarrionandia et al. 2012). Gwna Complex rocks are displayed in the geochemical groups established in Section 4.4. The groups roughly translate to data groups in for the rifted basalts (N-MORB-type, subalkaline and alkaline/peralkaline groups), which are also constructed from compositional variations (Sánchez-García et al. 2010; Sánchez-García et al. 2019). Ocean floor basalts have been similarly distinguished by tholeiitic and alkaline compositions (Ackerman et al. 2019).

Data from ocean floor basalts originates from accreted OPS in the Blovice accretionary complex in the Bohemian Massif. The accretionary complex is similarly Neoproterozoic-Cambrian in age, consisting of oceanic material accreted along the margins of the Avalonian-Cadomian belt while still attached to Gondwana (Nance et al. 2010; Hajná et al. 2014; Hajná et al. 2018; Ackerman et al. 2019). The accretionary complex may be analogous to the Gwna Complex, forming somewhat contemporaneously at another point along the expansive Andean-type arc subduction system of the Avalonian-Cadomian belt (Linnemann et al. 2008; Nance et al. 2008; Nance et al. 2010). Accreted material is largely dismembered within a block-in-matrix mélange, and is interpreted to have recorded ridge-trench OPS with a significant component seamount OPS originating from an intraplate mantle plume (Ackerman et al. 2019).

Data from rift systems is sourced from the Ossa Morena Zone in Iberian Autochthon (Sánchez-García et al. 2003; Sánchez-García et al. 2008; Sánchez-García et al. 2010; Sarrionandia et al. 2012). The mafic rocks in focus were produced through back-arc rifting and subsequent bimodal magmatism within the Avalonian-Cadomian as convergence was replaced by a passive transcurrent regime (Murphy et al. 2004; Quesada 2006; Linnemann et al. 2008; Sánchez-García et al. 2019). This geodynamic transition was diachronic and active in Iberia by 540 – 520 Ma (Pereira et al. 2006). Rift-related magmatic activity occurred over three stages, with basalts predominantly occurring within the main (middle) and late stages, along with subordinate rhyolites and intermediate lavas (Sánchez-García et al. 2010; Sánchez-García et al. 2019).

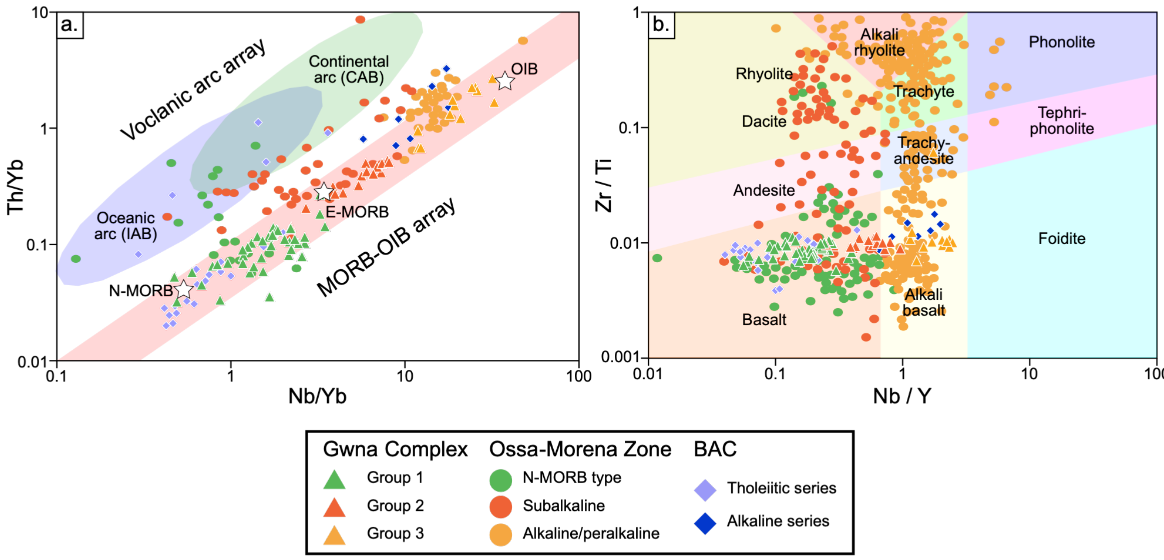

Figure 5.2: Geochemical discrimination diagrams of Gwna Complex mafic rocks plotted against data from the Ossa-Morena Zone back-arc rift system *(Sánchez-García et al. 2019)* and accreted OPS sequences from the Blovice accretionary complex (Ackerman et al. 2019) showing (a) tectonic discrimination between MORB-OIB and VAB arrays (Pearce 2014); and (b) volcanic discrimination diagram (Pearce 1996).

The tectonic discrimination diagram in Figure 5.2a shows that mafic rocks from both the main and late rifting stages in the Ossa-Morena Zone share a similar Nb/Yb ratio range to the Gwna Complex, ranging from slightly enriched N-MORB to OIB. However, a significant number of analyses migrate from the MORB-OIB array towards the VAB array. This occurs in N-MORB, E-MORB and OIB samples alike, and suggests that a crustal component had interacted with the source. From Nd isotope analysis, crustal dwell times are interpreted as being very low, limiting the ability for extensive crustal interaction (Sánchez-García et al. 2019). However, this interaction still appears to have notably affected compositions. Accreted OPS basalts in the Blovice accretionary complex are largely distributed within the MORB-OIB array, except for five samples that plot within the VAB array. These three samples are not the result of crustal assimilation and are thought to represent a changing mantle source, possibly a result of early BABB generation before maturation to the dominant MORB-OIB regime (Ackerman et al. 2019). Samples firmly within the MORB-OIB array are divided between two sample clusters – tholeiitic N-MORB and alkaline OIB. This leaves a significant compositional gap around E-MORB. OIB-like samples are entirely attributed to plume-derived seamounts, whereas the Gwna Complex seemingly shows a continuous compositional range from N-MORB to OIB. The majority of OIB-like analyses from the Blovice accretionary complex also stray above the MORB-OIB array, indicating some source interaction or heterogeneity. Tholeiitic compositions are mostly clustered around N-MORB, and many are moderately depleted towards D-MORB. Figure 5.2b shows the bimodal distribution of magmatic products in the Ossa-Morena Zone, from basalt to alkali rhyolite classifications. Basalts from the Blovice accretionary complex occupy a similar compositional range to the Gwna Complex, however analyses from the alkaline series have higher Zr/Ti ratios than in the tholeiitic series, as well as corresponding Gwna Complex analyses.

Mafic rocks from the Gwna Complex do not show evidence of crustal input that is present throughout rift-related rocks, as shown by consistent Th/Nb ratios. Additionally, there is no evidence in the Gwna Complex of bimodal magmatism that characterises the Ossa-Morena Zone rift magmatic sequences. The Gwna Complex may therefore be seen as an ocean floor sequence like the later basalts of the Blovice accretionary complex. However, the compositional range of basalts is much greater than those of mid-ocean ridge origin in the Blovice accretionary complex, and similar to the Ossa-Morena Zone basalts that have not been contaminated. Despite not showing affinity towards a back-arc setting, the compositional variability of the Gwna Complex suggests that it may also not originate from simple mid-ocean ridge volcanism.

Geochemical variability of Gwna Complex basalts

Basalts across the Gwna Complex show a relatively continuous evolutionary geochemical trend that fits within the MORB-OIB array, spanning approximately from mean N-MORB to mean OIB compositions (Sun and McDonough 1989). This variability is also observed over small areas such as across the basalts of Area I, and the OPS sequences at Porth Felen in Area II, for example. While there is evidence of two episodes of magmatic activity in the Gwna Complex, the dominant magmatic trend appears to be singular and continuous. Heterogeneity of melts at mid-ocean ridges is typically lost as magmas coalesce in shallow magma chambers that promote efficient mixing and homogenisation (Sinton and Detrick 1992; Gregg et al. 2012; Keller et al. 2017).

Off-axis seamounts form through upwelling melts from isolated chambers that have not effectively mixed with other melts in shallow magma chambers during their converging ascent (Niu and Batiza 1997; Niu et al. 2002). They therefore record the compositional diversity of melts produced in a mid-ocean ridge setting. Off-axis seamounts generally exhibit more variable compositions than mid-ocean ridge basalts, with heterogeneity recorded on a relatively local scale within individual seamounts (Haase et al. 2009; Anderson et al. 2021). Off-axis seamount data sets were sourced from Niu and Batiza (1997) and Anderson et al. (2021), both of which analyse seamounts around the East Pacific Rise.

Heterogeneity at mid-ocean ridges is promoted by thorough efficient mixing and aggregating of melts, which relates directly to spreading rates (Niu 2021). Fast spreading ridges such as the East Pacific Rise (EPR) are buffered by continuous mantle melting, leading to efficient mixing in a constantly supplied magma chamber. Slow spreading ridges, such as the Mid-Atlantic Ridge (MAR) may lose magma chamber convection during inactive periods, leading to less efficient mixing and greater magmatic heterogeneity (Perfit and Chadwick 1998; Perfit 2001). Figures 5.3 and 5.4 plot Gwna Complex magmatic rocks against data sets from off-axis seamounts, along with fast and slow spreading centres – from the EPR and MAR respectively.

Data sets for the EPR were sourced from Thompson et al. (1989); Bach et al. (1994); Batiza et al. (1995); Teagle et al. (2006); Teagle et al. (2007); Goss et al. (2010); Jenner and O'Neill (2012); Gale et al. (2013); Mougel et al. (2014); Chen et al. (2019); Mallick et al. (2019); and Sano and Yamashita (2019). The data were downloaded from the PetDB Database (www.earthchem.org/petdb) using the following parameters: feature name = East Pacific Rise; and rock type = mafic volcanic. Additional data is included from Perfit (unpublished) and Hinds (unpublished) that was submitted directly to PetDB. Analyses from off-axis samples were filtered out. Data sets for the MAR were sourced from Debaille et al. (2006); Jenner and O'Neill (2012); and Yang et al. (2018). The data were downloaded from the PetDB Database (www.earthchem.org/petdb) using the following parameters:

feature name = Mid-Atlantic Ridge; and rock type = mafic volcanic. Additional data is included from Lawson (unpublished) that was submitted directly to PetDB. MAR analyses influenced by the Iceland plume were selectively filtered out as its influence obscures mid-ocean ridge compositional variability.

Compositional ranges of the data sets are best observed in Figure 5.3a, which shows all data plotting along a singular linear trend of the MORB-OIB array. The EPR shows the most homogeneity, with the vast majority of analyses plotting around N-MORB with slight enrichment towards E-MORB. A small cluster of depleted analyses plot towards D-MORB. Analyses from the MAR show a broader compositional range, from D-MORB to E-MORB, with some analyses showing enrichment beyond mean E-MORB. Off-axis seamounts show the greatest variability, however, approaching OIB compositions very similar to Group 3 samples of the Gwna Complex. The compositional range of off-axis seamounts includes significantly more depleted basalts than Group 1 samples from the Gwna Complex, reaching D-MORB compositions. Samples depleted relative to N-MORB comprise approximately 11 % of the data set.

Figure 5.3b further emphasised these trends along the MORB-OIB array. It also highlights relatively enriched TiO_2 contents in the Gwna Complex and off-axis seamounts relative to the mid-ocean ridges. Differences in TiO_2 contents within both the MAR and EPR begin to define multiple trends, reflecting large-scale heterogeneity along the ridges. Figure 5.3c shows similar patterns between Gwna Complex and off-axis seamount analyses, which have slightly elevated Zr/Y ratios relative to La/Yb, particularly in more evolved analyses. Some Gwna Complex Group 3 samples show anomalously low Nb/Y, although this is largely attributed to samples from Area I Unit 9, possibly originating from a separate magmatic system. The Gwna Complex rocks have relatively low Zr/Ti, with comparable ranges to the off-axis seamounts (Figure 5.3d). The ternary tectonic discrimination plots of Figures 5.3e and f show preferential enrichment of Zr in off-axis seamounts and slight Ti enrichment in the Gwna Complex, relative to the mid-ocean ridges, which plot predominantly in the MORB fields, spanning to within-plate basalt fields.

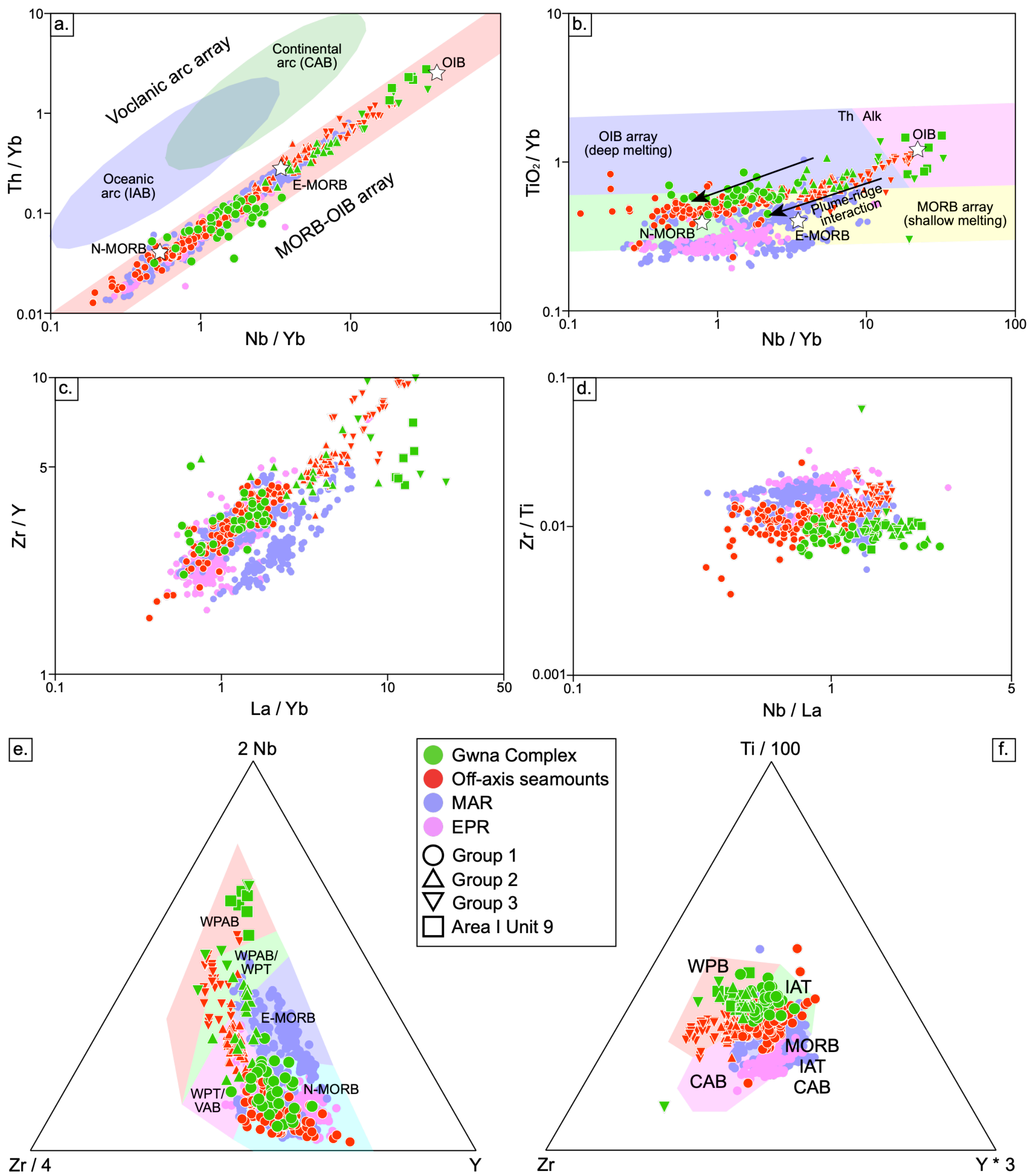

Figure 5.3: Geochemical discrimination diagrams plotting Gwna Complex mafic rocks against data from off-axis seamount basalts from the Pacific Rise, along with mid-ocean ridge basalts from the slow-spreading Mid-Atlantic Ridge (MAR) and the fast-spreading East Pacific Rise (EPR), showing (a) tectonic discrimination diagram distinguishing MORB-OIB and VAB arrays (Pearce 2014); tectonic discrimination diagram using Ti (Pearce 2008); (c) immobile element plot showing melt evolution against REE abundances; (d) immobile element diagram of Zr/Ti melt evolution against Nb/La as a proxy for source heterogeneity; (e) ternary tectonic discrimination diagram distinguishing MORB and OIB compositions (Rollinson 1993); and (f) ternary tectonic discrimination diagram (Pearce and Cann 1973). Data sources outlined in main text.

The multivariate plots of Figure 5.4 plot MAR and EPR analyses as shadows showing 1σ to mean values. Off-axis seamounts have been divided into three groups using the same criteria used to geochemically distinguish the Gwna Complex magmatic rocks (Ross and Bédard 2009), with mean compositions for each group plotted against the Gwna Complex equivalents. Mid-ocean ridges exhibit predominantly flat mean REE patterns characteristic of N-MORB, with the MAR being slightly more enriched on average (La/Lu_N = 1.30) than the EPR (La/Lu_N = 0.82). Off-axis seamounts show a distinct positive Zr anomaly which is not mimicked in Hf. This pattern is evident in analyses from all three groups, becoming more exaggerated in more evolved samples. The Gwna Complex rocks also show a minor Zr enrichment, and a Zr-Hf anomaly of similarly low amplitude is seen in EPR analyses.

Off-axis seamounts otherwise show very consistent patterns to Gwna Complex samples when applied to the same geochemical groupings. This suggests that D-MORB analyses are not significant components in the off-axis seamounts, with most Group 1 slightly enriched from N-MORB, like in the Gwna Complex. From 228 included data, 134 place in Group 1, 59 in Group 2 and 35 in Group 3. Therefore, 59.8 % of analyses fit into Group 1 (55.9 % in Gwna Complex), 25.9 % in Group 2 (35.2 % in Gwna Complex) and 15.4 % in Group 3 (8.8 % in Gwna Complex excluding Area I Unit 9). Compositional distributions between the units are therefore similar.

The geochemical variability observed in the Gwna Complex is not feasible to produce directly from the axis of a mid-ocean ridge. In order for evolved Group 3 compositions to form at a mid-ocean ridge, either plume interference would be needed (Fitton et al. 1997; Kelley et al. 2013), or the source magma chamber(s) must not be homogenous. Without evidence of an accreted ocean island or geochemical evidence of plume interference, the latter is more likely. Off-axis seamounts along the EPR generate a compositional range very close the observed range in the Gwna Complex, with the full heterogeneous suite observed as locally as within individual seamounts (Anderson et al. 2021). Small-scale heterogeneity is a significant factor in the Gwna Complex, with compositional variability common between lenses in Area I, while heterogeneity has been recorded from within basaltic blocks in Area II at Porth Felen and Porthorion. Like the Gwna Complex, basalts are predominantly N-MORB but can reach OIB compositions. A small number of D-MORB analyses were recorded in off-axis seamounts but were not recorded in the Gwna Complex.

Another factor attributing to the geochemical heterogeneity of the Gwna Complex is the interpreted presence of intraplate magmatism in relation to Newborough Unit 9 and the alkaline nature of the sampled material, illustrated in Figure 5.3. Field evidence and alkaline compositions suggest that this sequence may potentially represent petit-spot magmatism, as outlined in Section 1.2.2. This concept will be evaluated further in Section 5.1.4.

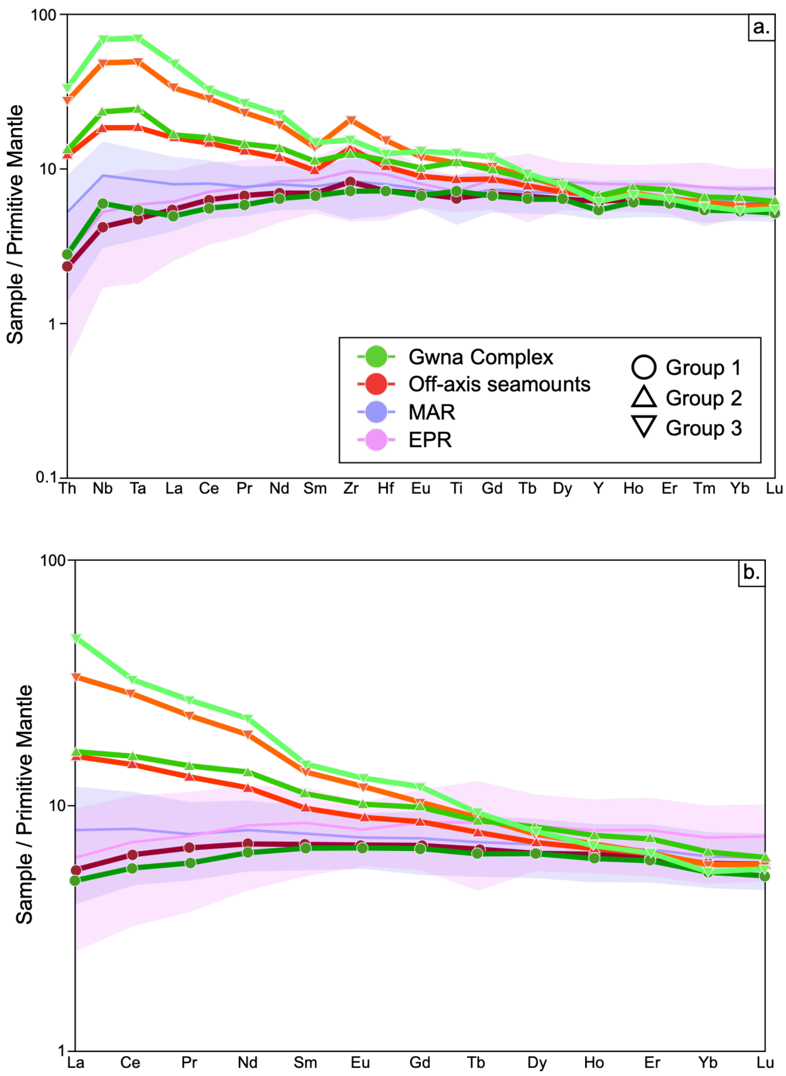

Figure 5.4: Multivariate plots of Gwna Complex mafic rocks against data from off-axis seamount basalts from the Pacific Rise, along with mid-ocean ridge basalts from the slow-spreading Mid-Atlantic Ridge (MAR) and the fast-spreading East Pacific Rise (EPR), showing mean compositions of Gwna Complex and off-axis seamount analyses for three defined geochemical groups, and compositional shadows of 1σ to mean for mid-ocean ridges. Normalised to primitive mantle composition after Sun and McDonough (1989).

5.1.3 OPS in Area I

Six low-shear units in Area I preserve multiple lithologies in apparent stratigraphic continuity, reflecting partial records of OPS. None of these units provide a full, uninterrupted OPS record, however, observed lithological relationships can be used to construct a composite OPS for Area I.

Magmatic base

Subduction mélanges are typically dominated by terrigenous siliciclastic material, with accretion of ophiolitic material being rare (Ujiie 2002; Remitti et al. 2011; Wakita 2012b; Kusky et al. 2020). Accreted magmatic material commonly originates from prominent intraplate features such as seamounts and plateaus, which are preferentially accreted over flat-lying basalts derived from a mid-ocean ridge (Safonova 2009; Kerr 2014; Safonova and Santosh 2014; Wakita 2019). In Area I of the Gwna Complex, basaltic rocks are dominant lithologies with sequences more than 300 m thick. This suggests that delamination of mid-ocean ridge derived basalts would have occurred from significant depths along a planar sequence. Alternatively, thick occurrences of basalts may originate from seamounts, where delamination would not need to occur within the substrate of the ocean floor.

The base of the OPS in Area I consists of basaltic rocks of variable thickness, and lower interfaces are typically marked by highly sheared hyaloclastite layers. This suggests that OPS units have been delaminated preferentially along these hyaloclastite horizons, which are seen intermittently throughout pillow lava dominated sequences. High phyllosilicate contents and pervasive slip planes characterise hyaloclastite matrices, making them highly susceptible to shearing. The depths of laterally continuous hyaloclastites within a subducting magmatic sequence therefore influences the depth of delamination, and subsequently the thickness of magmatic material that is accreted.

Basalt-carbonate transition

Carbonate rocks overlie the basaltic sequences, typically across a transitional basalt-carbonate phase that represents contemporaneous volcanic activity and sediment deposition. In standard models of ridge-trench OPS, basal mid-ocean ridge volcanics are typically overlain by pelagic mudstones and cherts (Isozaki et al. 1990; Wakita and Metcalfe 2005; Kusky et al. 2013; Wakita 2019). Interactions between pillow basalts and carbonates are not common features of mid-ocean ridge settings due to lack of sediment deposition, and are more associated with seamount summits (Rojay et al. 2001; Jordan et al. 2008; Troll and Carracedo 2016). Precipitation of carbonate mud indicates that volcanic activity is occurring above the CCD.

In a mid-ocean ridge setting, this would require a low CCD at the time of volcanism. Although predicting CCD levels in past oceans is difficult, vast influxes of alkaline material following the cessation of major glaciation events would have facilitated generally low CCD levels throughout large periods of the Ediacaran (Liu et al. 2014). Large sediment influx over a short timeframe would also be necessary to explain how enough carbonate material was deposited in a syn-magmatic pelagic environment to fully support intruded pillow lavas. Alongside rapid sediment influx, sufficient carbonate coverage would require irregular volcanic activity along a slow-spreading mid-ocean ridge. While this would provide geochemical heterogeneity, it would not produce the more enriched basalts of the Gwna Complex without additional influence (see Section 5.1.2).

Alternatively, using a seamount model would allow for a higher CCD and is a more common environment for basalt-carbonate mixing to occur. Cap carbonates would potentially lead to the formation of carbonate breccias along seamount slopes (Sano and Kanmera 1991; Safonova 2009; Safonova et al. 2016b) or the inclusion of carbonate fragments within surrounding pelagic sea floor sediments (Wakita 2019) due to atoll collapse. There is no evidence of carbonate clasts being included in chert or mudstone sequences in Area I – except for mélange clasts. A singular example of carbonate breccia on Llanddwyn Island is also interpreted to be tectonic in origin. The breccia is tectonically mixed with a bordering hyaloclastite matrix, and randomly orientated carbonate veins present only in clasts suggest that the unit had undergone deformation before brecciation, which would be unlikely in young carbonate cap material.

Dolomitisation appears to have occurred before deformation, given the further evidence of deformation, and crosscutting of veins. Given the likely age of the carbonates, there is a possibility that they may have formed through primary dolomite deposition in the aftermath of significant ice ages that took place throughout the Cryogenian and lower Ediacaran (ca. 730 – 580 Ma). These events – particularly the Marinoan glaciation – have been linked with globally distributed dolostone cap carbonate formation (Shields 2005; Li et al. 2013; Liu et al. 2014).

Cherts and mudstones

The relationship between carbonate rocks and other pelagic to hemi-pelagic rocks in Area I is unclear. Carbonate rocks are overlain by silty mudstones in three of four possible units, although direct contacts were not observed in either. Silty mudstones comprise layers of mudstones, cherts, and siltstones. Siltstone components represent intermittent distal clastic sediment input. Both mudstones and cherts occur as singular units with limited clastic input, occurring as thickly interbedded packages in Unit 9. This suggests that mudstones and cherts should underlie the silty mudstones – assuming that there is no other proximal clastic sediment source to supply to siltstone components. However, this is not reflected in the observed stratigraphic logs from Area I.

Mudstones and cherts occur as singular units solely within Unit 9, which has a rather unusual stratigraphy (discussed in Section 5.1.4). The tuffaceous mudstones are seen in thick packages that are seen elsewhere in Area I within mélange zones, but are not preserved within other low shear sequences. This may be due to the mechanical weaknesses that such thick, planar packets create. They would likely concentrate large amounts of shear and may well be removed from preserved sequences as a result, along with interbedded chert layers. Their assumed stratigraphic preservation in Unit 9 may be related to the presence of doleritic sills, which may have galvanised the sediments locally through low-grade contact metamorphism and increased hydrothermal activity. Silty mudstones are relatively thinly interbedded, and the transition from thick packets to thin beds – along with the inclusion of mechanically stronger siltstone layers – may also have worked to dissipate strain between layers.

Alternatively, Unit 9 may represent a separate, divergent OPS. Pillow basalts are overlain directly by mudstones, although the contact is heavily sheared, and it is therefore unclear whether a carbonate component may have been present within the stratigraphic sequence of Unit 9. There is no evidence of reddening towards the upper parts of the pillow basalts. If carbonates were not present, mudstone and chert sequences would overlie pillow basalts directly. This may be representative of bimodal deposition around a seamount, where carbonate material is deposited at the seamount summit – above the CCD – while siliceous material is deposited below, on the surrounding sea floor (see Figures 5.5a and b). Silty mudstones are likely and extension of the mudstones and cherts, and they commonly overlie carbonate rocks, suggesting that OPS would converge by this stage, as the seamount summit falls below the CCD (see Figure 5.5c). This may explain the common occurrences of tuffaceous mudstones throughout the Gwna Complex while not identified within OPS sequences outside of Unit 9. Further evidence may include basal pillow lavas of Unit 9 being highly vesicular and relatively small, possibly distinguishing mid-ocean ridge pillow basalts from seamount pillow basalts. However, Unit 9 pillow basalts have relatively enriched E-MORB geochemical signatures and show no clear distinctions to other basalts of the Gwna Complex.

In modern ocean settings, it is common that mid-ocean ridges would form at depths above the CCD (Parsons and Sclater 1977; Boudreau et al. 2010). While this is more difficult to attribute to Late Neoproterozoic settings, it is highly possibly that the ridge may have formed above the CCD. However, this still leaves the issue of promoting sufficient sedimentation of carbonate material onto an active ridge to host series of pillow basalts. It is more likely that this would have occurred on the ridge away from the axis, whether through off-axis seamounts or other means.

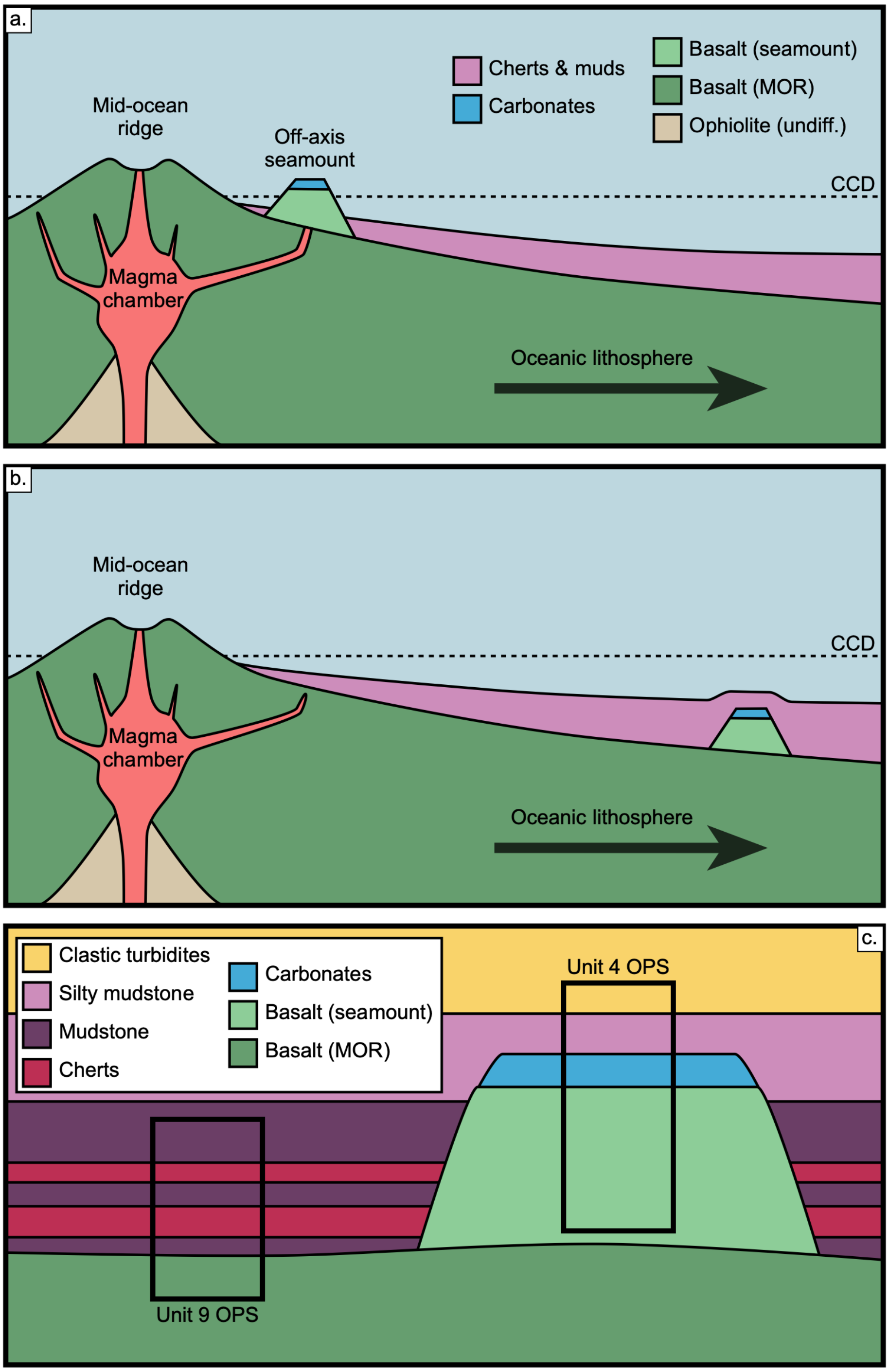

Figure 5.5: Schematic cross section of an axial ridge illustrating lower OPS development in the Gwna Complex, showing (a) emplacement of an off-axis seamount with an assumed summit above the CCD, facilitating carbonate cap formation while siliceous muds are deposited around the seamount base, below the CCD; (b) progressive spreading from the axial ridge causes the seamount to descend below the CCD through lithospheric cooling, leading to pelagic-hemipelagic sedimentation above both seamount and seafloor sequences, leading to convergence of OPS; and (c) schematic representation of adjacent seafloor environments relative to observed, logged OPS in Area I.

Mudstones and cherts are therefore assumed to be deposited above or alongside carbonates, representing a secondary, more voluminous phase of pelagic sedimentation that occurs below the CCD. A bimodal deposition is most likely, as this does not require the total absence of lithologies from within multiple apparently coherent low-shear units. Figure 5.5c shows a schematic model for the formation of these two adjacent environments and their produced OPS, projected through logs of Units 4 (seamount OPS) and Unit 9 (MOR OPS). Silty mudstones are interpreted to represent an intermediate transitionary stage between the pelagic to hemi-pelagic mudstones-chert sequences and overlying clastic sedimentary units. They represent the distal approach of the sea floor towards a continental landmass, where eroded clastic material is periodically deposited in graded beds at the far reaches of turbiditic flows.

Clastic sedimentary units

Where preserved in low shear units (Units 4 and 12), clastic lithologies typically mark the upper interface of the unit. Rip-out clasts of silty mudstone components in siliciclastic sandstones confirm its position at the top of the OPS of Area I. Geochemical signatures confirm that the sediments originate from a continental arc, suggesting that they represent deposits around the trench of a subduction zone. Similar geochemical signatures in mudstones and silty mudstones suggest a progression from distal to proximal deposition from the same dominant arc source throughout the ocean lifecycle.

Composite OPS of Area I

Two main OPS interpretations have been laid out for Area I of the Gwna Complex. The first suggests a singular, uniform OPS that includes a stratigraphic placement for all lithologies observed in Area I (see Figure 5.6). The second interpretation proposes two adjacent OPS sequences that converge upwards from around the transition to hemi-pelagic sedimentation (see Figure 5.7). It should be noted that the occurrence of intraplate volcanism related to dolerite sills in Unit 9 is not included in these models and is discussed separately in Section 5.1.4.

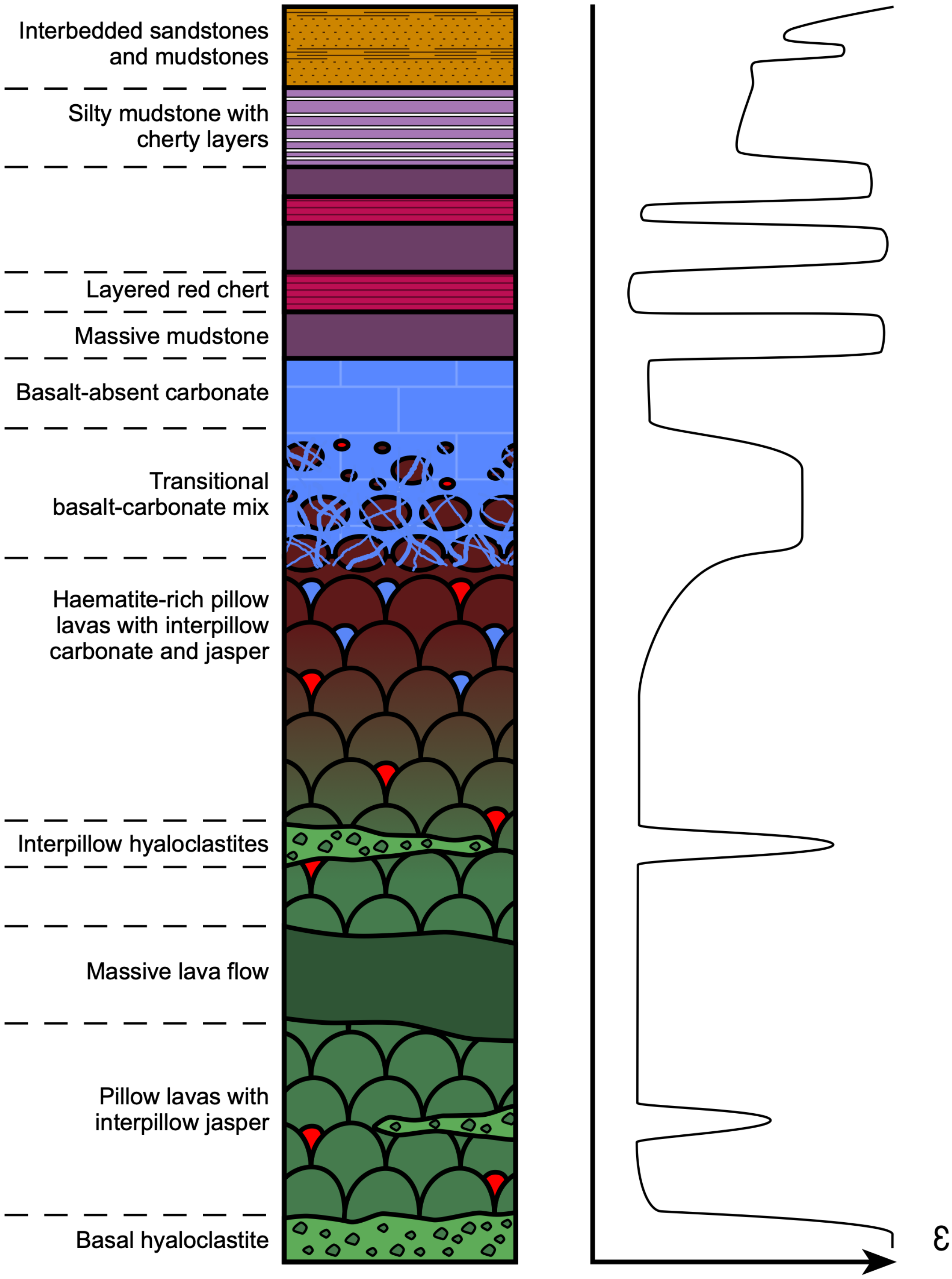

Figure 5.6: Composite singular OPS model for Area I of the Gwna Complex, comprising a basaltic substrate overlain gradationally by carbonate rocks and other pelagic to hemi-pelagic sea floor sedimentary rocks, as clastic continental material is progressively introduced towards during the approach to a subduction trench. Strain intensity is illustrated quantitatively, identifying weak horizons in the OPS where structural disintegration of stratigraphic units is most likely to have occurred.

The singular OPS model incorporates mudstones and cherts from Unit 9 but is presented with the issue of explaining their absence in other coherent units, with shearing along mudstones being the most feasible explanation. This is illustrated in Figure 5.6 by the relative strain intensity gauged for each locality. This shows the variability of mechanic strength between lithologies and highlights potential weak horizons that lead to disordering of stratigraphic successions. Likewise, the lack of carbonates in Unit 9 may be explained by insufficient outcrop. This OPS can be applied to both mid-ocean ridge and off-axis seamount interpretations for the origin of the basal magmatic rocks by assuming that either environment makes the transition from above to below the CCD through progression away from the spreading centre.

The dual OPS model accounts for the lithological differences between Unit 9 and other low-shear units. It proposes adjacent sequences of mid-ocean ridge OPS and off-axis seamount OPS to distinguish contemporaneous carbonate and siliceous pelagic sedimentation. Mid-ocean ridge OPS is based around observations from Unit 9. However, this still poses a problem in that its upper interface is marked by mudstones (and a hyaloclastite). The lack of upper hemi-pelagic to clastic sedimentary rocks means that the proposed OPS convergence cannot be confirmed. Seamount OPS is much more commonly preserved in Area I than mid-ocean ridge OPS and this may be a result of accretionary bias. Section 5.1.4 discussed the possibility of a small seamount preserved in association to Unit 9, which may have helped to facilitate its accretion.

The most likely scenario is the dual OPS model since it maintains the observed stratigraphic order logged within low-shear units. The model is comparable to accretionary complexes in SW Japan, where mid-ocean ridge OPS and seamount OPS are both accreted (Maruyama 1997; Wakita 2012b; Safonova et al. 2015; Safonova et al. 2016b; Wakita 2019). Seamount cap carbonates and ocean floor chert deposits developed coevally and were both overlain by silicic tuffs of similar late Permian ages (Safonova et al. 2015; Safonova et al. 2016b). However, basalt-limestone mélanges of the seamount OPS were accreted alongside sandstone-chert OPS sequences from the mid-ocean ridge. Mid-ocean ridge OPS became dominated by late trench-fill clastic sediments while seamount OPS did not record any siliciclastic cover (Wakita 2012b; Wakita 2019). In Gwna Complex Area I, basalts and mudstones are preserved in the mid-ocean ridge OPS without a relatively high-volume siliciclastic input, while clastic turbidites are present in seamount OPS, albeit in low volume. The Gwna Complex shows less stratigraphic disparity, perhaps indicating seamounts of less prominence, as would be reasonable for off-axis formations (Allan et al. 1987; Jaroslow et al. 2000; Choi et al. 2021).

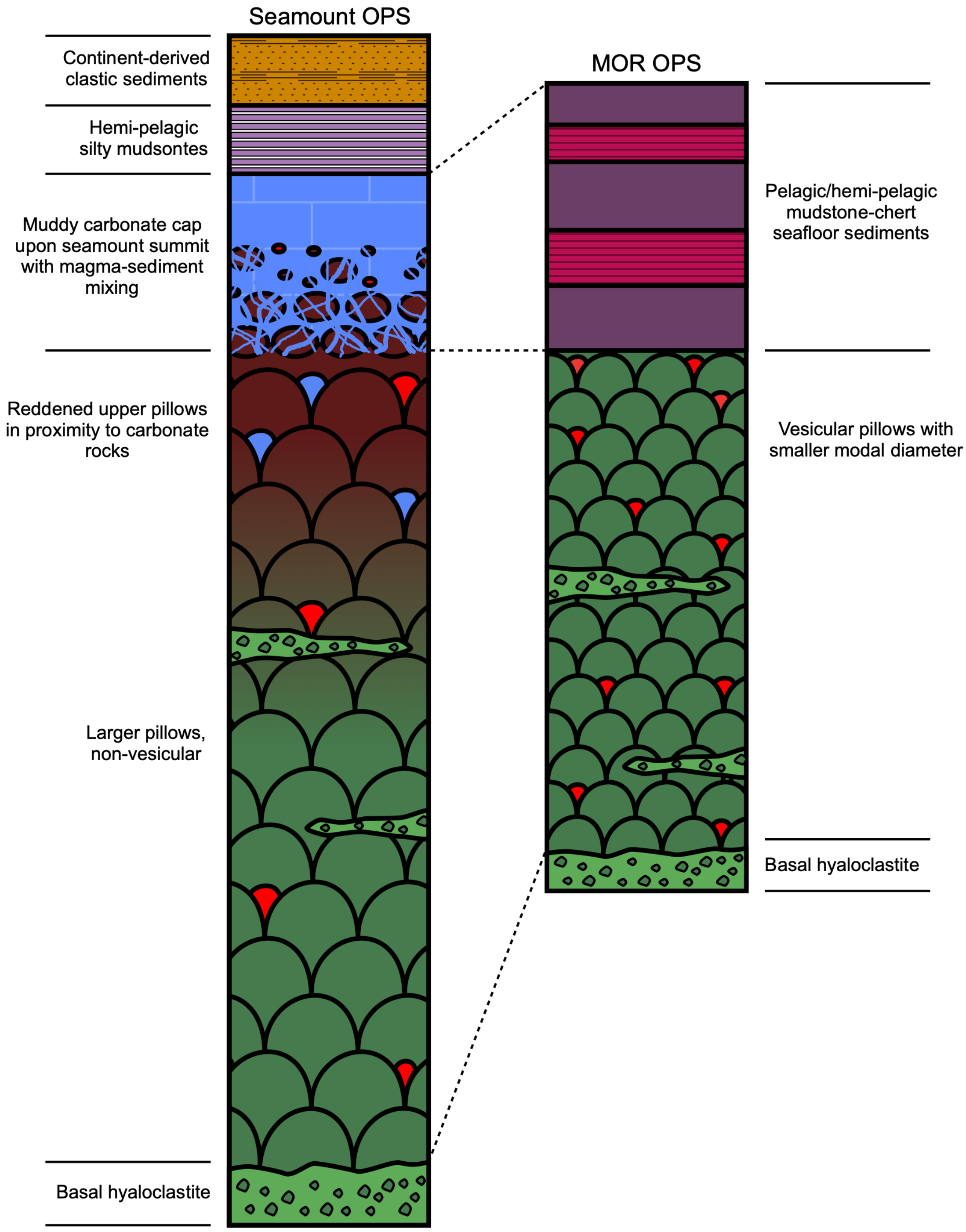

Figure 5.7: Dual OPS composite logs showing juxtaposition of seamount OPS and mid-ocean ridge (MOR) OPS, where basaltic bases represent formation on or off the axis of a spreading centre, with seamounts overlain by carbonate mud and mid-ocean ridge basalts overlain by siliceous material. OPS likely converge by hemi-pelagic dominant sedimentation.

5.1.4 Intraplate Magmatism in Area I Unit 9

The geology of Unit 9 in Area I, along the western flanks of Llanddwyn Island, is unique within the Gwna Complex. As discussed, the widespread presence of colourful, tuffaceous mudstones and cherty material throughout all areas of the Gwna Complex suggests that the unit is not genetically distinct but may represent a divergent OPS representing ocean floor material surrounding the more abundant seamount OPS. The dolerites and associated volcanics, however, appear to represent a single, isolated example of pre-subduction intraplate magmatic activity.

Dolerite sills were not observed elsewhere in the Gwna Complex, and they are geochemically distinct to the primary basalts of the Gwna Complex, with OIB geochemical signatures. Associated Unit 9 pillow basalts are highly vesicular in comparison to surrounding sequences, and both rock types are actinolite-bearing – the only examples found in the Gwna Complex. The relative timing of emplacement is well constrained since dolerite sills are seen to intrude – and must therefore postdate deposition of – pelagic to hemi-pelagic sedimentary rocks. The sills are incorporated into the accreted OPS of Unit 9, meaning that they predate subduction and subsequent accretionary deformation.

Metamorphic grade

The presence of actinolite, along with other greenschist facies minerals such as chlorite, epidote, and albite, raises the issue of whether Unit 9 has undergone a separate tectonic history and been subjected to higher P-T conditions than the surrounding Gwna Complex rocks. Despite similar mineral assemblages to lower grade actinolite-dominated samples from the Penmynydd Terrane (eg. AN17007, AN17011 and AN17032), the volcanics of Unit 9 are texturally different and their actinolites are chemically different. Greenschist facies metabasites of the Penmynydd Terrane are schistose and polydeformed, whereas the magmatic rocks of Unit 9 are not, and even retain well preserved magmatic features such as vesicles, pillow shapes and relict magmatic petrographic textures.

Chemically, actinolites from Unit 9 are relatively low in Na and Al while containing high proportions of Ca. The site allocations of Na and Al are also distinct from Penmynydd Terrane amphiboles, with Al hosted almost entirely within the T site and Na hosted predominantly in the A site. The distributions of Al and Na within the crystallographic structure of amphiboles are governed by the physical conditions – most influentially pressure and temperature – under which crystallisation takes place.

Allocation of Al and Na into the C site and B site respectively are associated with increasing pressure, while incorporation into the T site and A site respectively are more dependent on temperature conditions (Raase 1974; Brown 1977; Holland and Richardson 1979; Ruiz Cruz 2010). The chemistry of Unit 9 actinolites is therefore indicative of relatively low-pressure formation. A secondary compositional trend was observed in the Unit 9 amphiboles, reaching magnesio-hornblende compositions. Figure 5.8 shows how these divergent compositions are chemically more representative of igneous-derived amphiboles. These amphiboles may represent relict compositions of largely replaced magmatic amphiboles. It is more likely – due to the intergrowths of chlorite and high content of epidote – that the alteration assemblage has replaced clinopyroxenes at low pressure prehnite-pumpellyite facies conditions, and similar assemblages have been described from thermally metamorphosed metabasites (Terabayashi 1988; Shibuya et al. 2010).

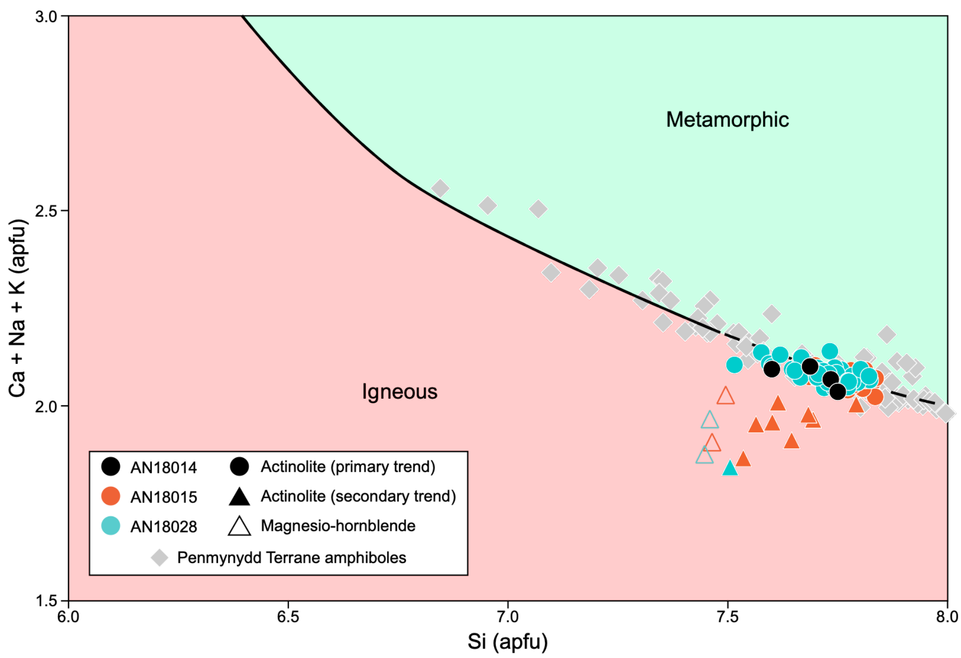

Figure 5.8: Compositional plot of amphiboles in Unit 9 mafic rocks of the Gwna Complex plotted with Penmynydd Terrane amphiboles to show potential igneous affinity of some Unit 9 amphiboles. After (Leake 1971).

The rocks of Unit 9 were therefore likely subjected to the same tectonic history as the Gwna Complex as a whole, however formation of actinolite suggests a localised increase in temperature. This may have been buffered by the intraplate magmatic activity itself. Dolerite intrusions occurred at shallow depths within presumably unlithified cherts and mudstones, and extruded onto the sea floor. This would have promoted localised hydrothermal activity under higher temperatures. Increased hydrothermal activity and higher temperatures may also be responsible for the red colouration of the cherts through oxygenation of circulating fluids (Montgomery and Kerr 2009), while other cherts of the Gwna Complex are predominantly white.

Stratigraphic structure of Unit 9

The lower stratigraphic regions of Unit 9 continue offshore, obscuring its stratigraphic order. There are also unexposed discontinuities that affect the unit, leading to the lateral juxtaposition of dolerite sills and pillow basalts. The pillow basalts underlie a continuous mudstone with mélange-bearing components, and therefore likely represents the magmatic base of Unit 9. These relatively small, vesicular pillow basalts may link to those in Unit 13, which have a similar appearance and are also overlain by mélange-bearing mudstone. Unit 13 sits directly to the south of Unit 9, separated by a NW-SE fault. The basalts are geochemically very similar, with E-MORB compositions (see Figure 5.9).

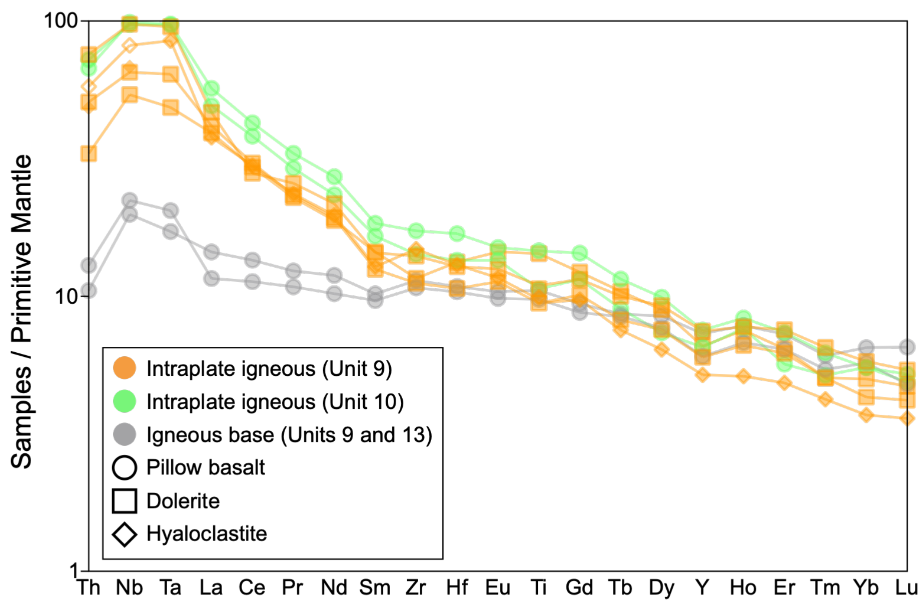

Figure 5.9: Multivariate plot of immobile elements for igneous rocks from Gwna Complex Area I – Unit 9 and potentially associated rocks from surrounding OPS units, showing the relationship between OIB-like intrusives in Unit 9 with potential extrusive equivalents in Unit 10, and a likely link between basal vesicular pillow basalts from Units 9 and 13.

Figure 5.9 shows the close geochemical similarities between the pillow basalts of Unit 10 with the intraplate magmatic rocks of Unit 9. The hyaloclastite at the upper surface of Unit 9 (AN19029) represents a minor extrusive component of the intraplate magmatism, shown by its consistent geochemical signatures with the dolerites. The pillow basalts of Unit 10 also appear to be geochemically related as another potential extrusive component. However, Unit 10 is separated from Unit 9 by a thin (5 – 20 m) buffer of mélange. If the units are related, then the pillow basalts of Unit 10 must have been removed partially from the upper surface of Unit 9, facilitated along weak horizons created by hyaloclastites and mudstones.

Aside from the 3 – 5 m thick hyaloclastite and 20 – 30 m thick pillow basalts of Unit 10, no other potential extrusive components were found. Seamounts and other prominent sea floor features have greater likelihood of being accreted (von Huene et al. 2004). It is therefore likely that the extrusive components of Unit 9 are minor, or more OIB basalts would likely dominate Area I. If Unit 9 represents a divergent ocean floor OPS, then the formation of a volcanic edifice may have facilitated accretion.

Sills are uncommonly associated with plume-derived 'hot-spot' seamounts but have been described in association with petit-spot magmatism (Mertz et al. 2001; Hirano et al. 2006; Buchs et al. 2013). Accreted sequences from the Franciscan (Mertz et al. 2001) and the Santa Rosa accretionary complexes (Buchs et al. 2013) both exhibit sets of alkaline dolerite sills intruding radiolarian red cherts, with those from Santa Rosa overlain by an extrusive basaltic component. Petit-spots are relatively minor form of intraplate magmatism that form low volume (< 1000 m height) extrusive components of highly vesicular/amygdalar hyaloclastites and pillow basalts (Hirano et al. 2001; Hirano et al. 2006; Machida et al. 2015), as shown in Figure 5.10.

Petit-spots are tectonically derived, forming in response to plate flexure, rather than through upwelling of mantle material in plumes or at mid-ocean ridges. Small pools of melt at the base of the lithosphere migrate upwards along tensile stress fields developed by this flexure (Machida et al. 2015; Sato et al. 2018). Oceanic plate flexure is typically caused by buckling around the outer rise in response to subduction (Hirano et al. 2006; Hirano 2011; Hirano et al. 2013), and petit-spots have also resulted from extensional basin regimes (Valentine and Hirano 2010) and glacial rebound (Uenzelmann-Neben et al. 2012). Intraplate magmatic systems are typically defined by the processes of their formation, and while these can be determined in current oceans, determining the genesis of accreted, dismembered seamounts is much more challenging.

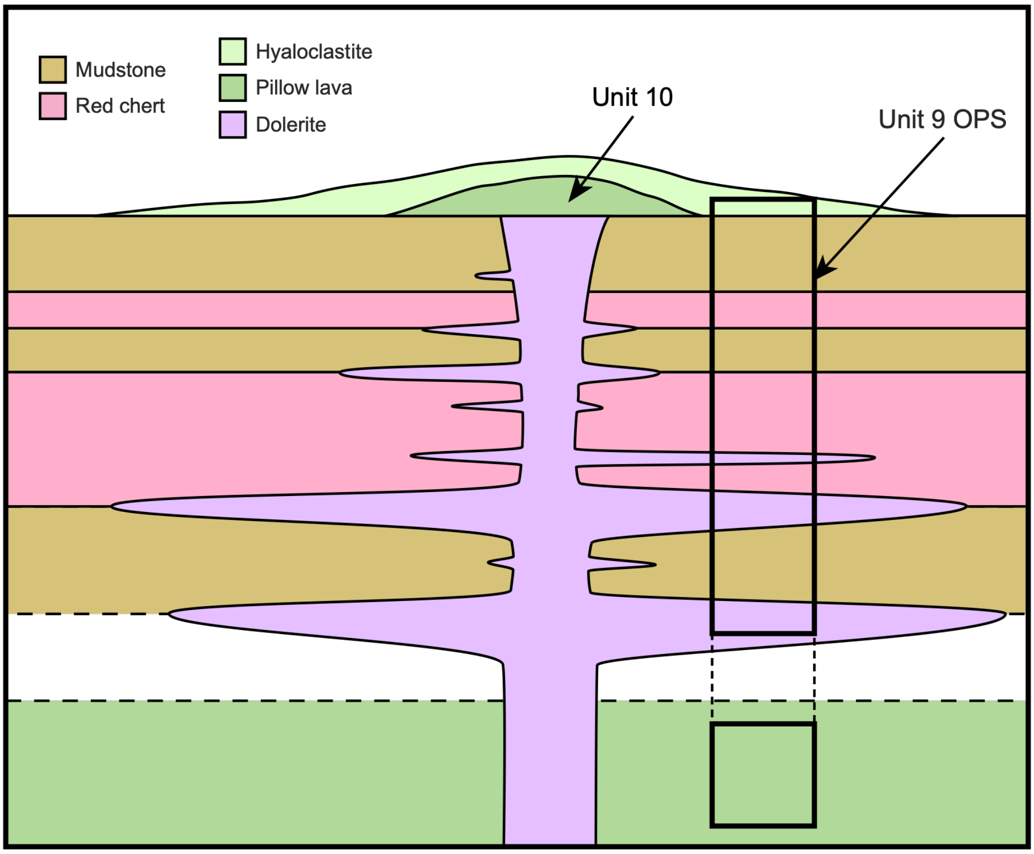

Figure 5.10: Schematic diagram illustrating a potential petit-spot framework of Unit 9 by imposing logged OPS (Log F) upon a cross section of a standard petit-spot seamount, after Hirano et al. (2006).

Source of intraplate magmatism

Petit-spot seamounts, much like plume-derived seamounts, exhibit typical OIB-like geochemical signatures since both originate from melts at the base of oceanic lithosphere. A combination of field observations and whole rock geochemistry has been used to discriminate petit-spot magmatism from plume-derived magmatism in an accretionary setting (Mertz et al. 2001; Buchs et al. 2013). Basalts or basaltic rocks from both settings have a predominantly OIB-like geochemical signature and petit-spots can only be distinguished from subtle geochemical differences. Although some of these geochemical differences have been highlighted in previous literature, no clear compositional limits have been defined and no petit-spot compositional range has been established.

Petit-spot seamounts are alkaline (high K_2O + Na_2O content), with a relatively high potassic component (high K_2O/Na_2O ratio). Plume-derived seamounts are typically tholeiitic to alkaline with a much more sodic alkali content (low K_2O/Na_2O ratio). Figure 5.11 shows that petit-spot seamounts tend to have total alkali contents of above 5 % and

K_2O/Na_2O ratios of 0.8 – 1.6. However, numerous analyses plot with ratios of 0.2 – 0.3, amongst tholeiitic plume-derived basalts showing that petit-spot seamounts may have wide compositional ranges. While alkali ratios are good geochemical indicators of petit-spot volcanism, factors such as seafloor alteration make them unreliable in many settings, including the Gwna Complex.

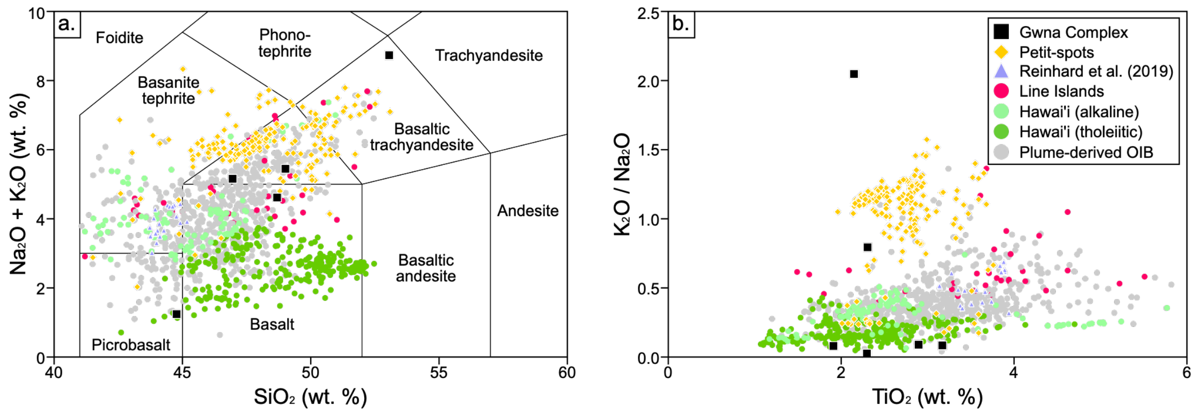

Figure 5.11: Major element geochemical diagrams of intraplate magmatic rocks from Gwna Complex Area I plotted against data from various petit-spot and plume-derived seamounts (data sources included in main text) showing (a) total alkali rock type classification for extrusive rocks (Le Maitre 2002); and (b) plot of potassic contents against Ti.

The geochemical plots in Figures 5.11, 5.12, 5.13 and 5.15 compare the compositions of Gwna Complex intraplate magmatic samples against geochemical data from selected plume-derived seamounts and petit-spot seamounts. Data for plume-derived seamounts are compiled from studies from selected seamounts around the world, including Ascension Island (Jicha et al. 2013), the Azores archipelago (Millet et al. 2009; Beier et al. 2012; Larrea et al. 2013; Hildenbrand et al. 2014; Métrich et al. 2014; Zanon and Pimentel 2015; Zanon and Viveiros 2019; Waters et al. 2020), the Cook-Austral Islands (Dupuy et al. 1989; Hauri and Hart 1997; Kogiso et al. 1997; Lassiter et al. 2003; Takamasa et al. 2009; Hanyu et al. 2013), the Line Islands (Schlanger et al. 1976; Davis et al. 2002), Peter I Island (Prestvik et al. 1990; Hart et al. 1995; Kipf et al. 2014), the Pitcairn Islands (Woodhead and McCulloch 1989; Dostal et al. 1996; Delavault et al. 2015; Garapić et al. 2015; Wang et al. 2018; Bonnand et al. 2020) and Samoa (Workman et al. 2004; Jackson et al. 2007; Hart and Jackson 2014; Reinhard et al. 2019). Average OIB composition has also been included after Sun and McDonough (1989).

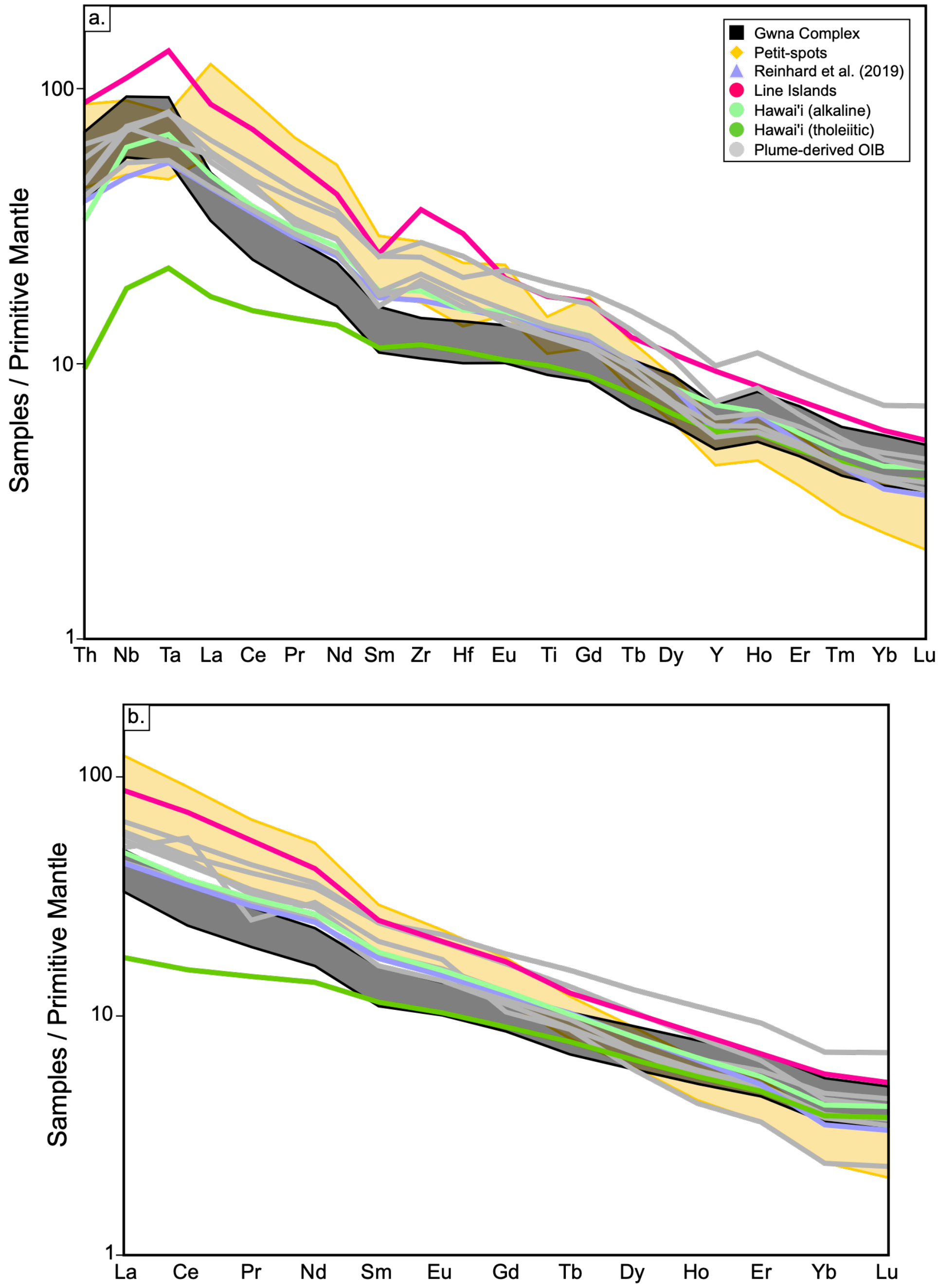

Figure 5.12: Multivariate element diagrams plotting intraplate magmatic rocks from Gwna Complex Area I against mafic rocks from petit-spot seamounts and from selected plume-derived seamounts, plotting mean compositional lines or shadows representing 1σ to mean. Data sources available in main text. Normalised to primitive mantle composition (Sun and McDonough 1989).

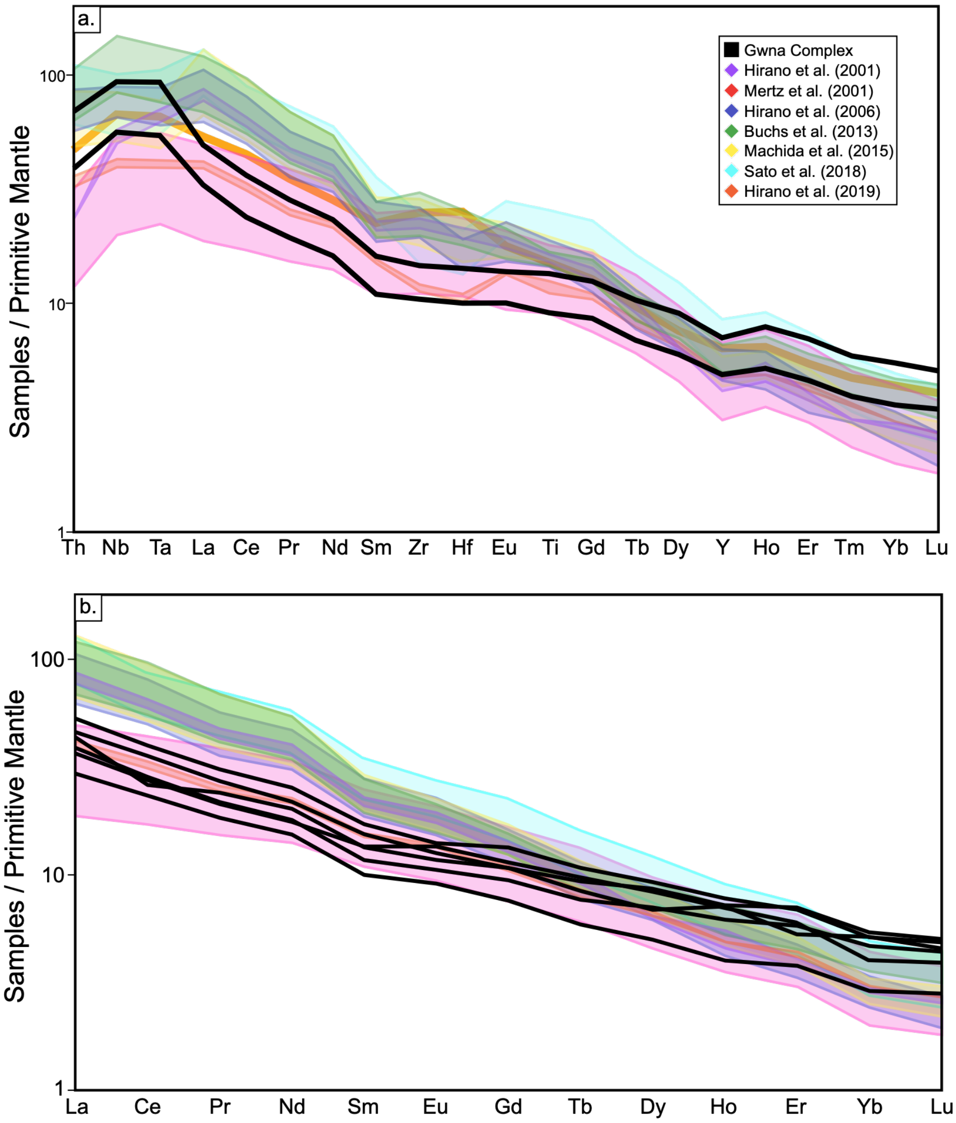

Figure 5.13: Multivariate element diagrams plotting intraplate magmatic rocks from Gwna Complex Area I against individual studies of petit-spot seamounts, plotting mean compositional lines or shadows representing 1σ to mean. Normalised to primitive mantle composition (Sun and McDonough 1989).

Data for plume-derived Hawaiian basalts are compiled from (Coombs et al. 2004; Morgan et al. 2007; Dixon et al. 2008; Sisson et al. 2009; Hanano et al. 2010; Hanyu et al. 2010; Rhodes et al. 2012; Cousens and Clague 2015). The Hawaiian data has been discriminated into tholeiitic and alkaline samples based on their alkali and silica contents (Irvine and Baragar 1971). The large size of the Hawaiian plume is a result of a high degree of partial melting, meaning that the melts are generally less differentiated than smaller plume-derived basalts, directly in contrast with small, highly differentiated petit-spot melts. Less differentiated tholeiitic basalts from the Hawaiian hotspot therefore offer an opposing endmember proxy to petit-spot melts, so have been highlighted from other plume-derived seamount geochemical data. Compared to other plume-derived seamounts, basalts from the Line Islands have relatively high-K compositions, creating an interesting comparison to highly alkaline, potassic petit-spot seamounts.

Rejuvenated magmatism in Samoa has been proposed to be a result of petit-spot volcanism as a result of tectonic uplift outboard of the Tonga Trench subduction zone, based on their geochemical similarities to petit-spot seamounts in the NW Pacific (Reinhard et al. 2019). These rejuvenated magmas are superimposed upon initial plume-derived volcanism. Data for the rejuvenated basalts have been highlighted as potential petit-spot volcanism.

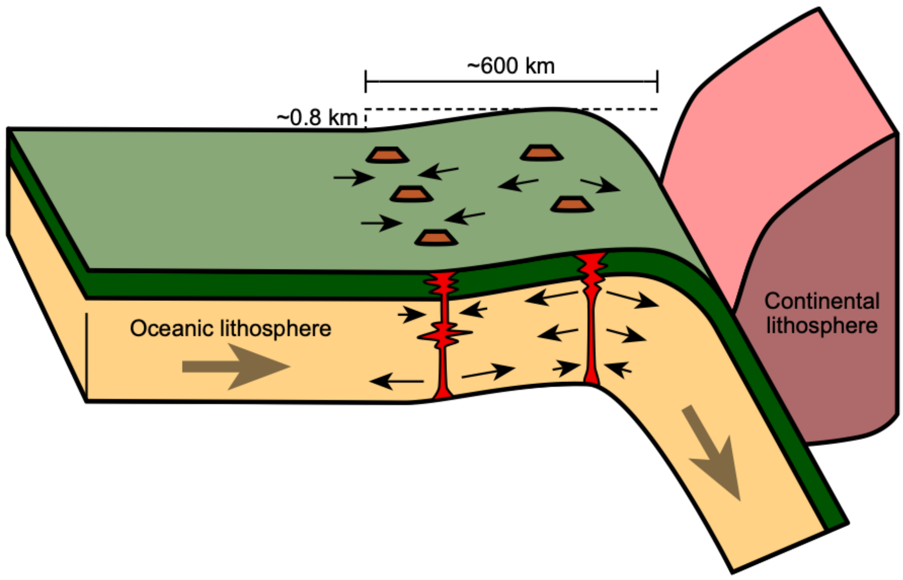

Figure 5.14: Schematic diagram of a subducting ocean floor illustrating most likely scenarios for petit-spot emplacement in response to plate flexure through subduction, demonstrating how oceanward petit-spot melts stall in the mid-lithosphere as tensile stress fields are inverted, while those at the base of the outer rise are emplaced with minimal disruption. Modified after Sato et al. (2018).

Petit-spot data has been compiled from previous geochemical studies from NW Pacific (Hirano et al. 2001; Hirano et al. 2006; Machida et al. 2015; Sato et al. 2018; Hirano et al. 2019), as well as in accreted sequences from the Franciscan complex, California (Mertz et al. 2001) and the Santa Rosa complex, Costa Rica (Buchs et al. 2013). The study by Machida et al. (2015) differentiates petit-spots in the NW Pacific based on their eruption position relative to the outer rise, corresponding to variable lithospheric stress differentials (see Figure 5.14). Stress fields at the outer rise remain tensile through the ascent of magma to the surface, producing alkaline petit-spot magmas reflective of their source. Oceanward of the outer rise, however, tensile stresses at the base of the lithosphere are inverted in the upper lithosphere, stalling the ascending melts in the mid-lithosphere, promoting interactions with surrounding peridotites and resulting in a less evolved petit-spot magma (Machida et al. 2015; Sato et al. 2018).

Plume-derived seamounts show ranges in compositions with an average composition (Sun and McDonough 1989) providing a mean representation. Petit-spot seamounts generally show relatively steep REE patterns (mean La/Lu_{PM} = 33.14), particularly evident by relatively depleted HREEs (mean Gd/Lu_{PM} = 5.34; see Figures 5.13, 5.15a and c). Petit-spot data from Mertz et al. (2001) and Hirano et al. (2019) show slightly depleted LREEs relative to other petit-spots but still show similar HREE patterns (see Figure 5.12). Seamounts of the Line Islands and Samoa contain similar LREE abundances within the range of petit-spot seamounts but do not show such steep depletion of HREE's (mean Gd/Lu_{PM} = 2.37 Line Islands; 3.12 Samoa).

Another distinction of petit-spots is a relative depletion of Zr and Hf ($Sm/Zr_{PM} <$ 1.0 generally compared to plume-derived seamounts with $Sm/Zr_{PM} >$ 1.0). This is shown in Figures 5.12 and 5.15e, where the majority of plume-derived seamounts fall below a ratio of 1.0, with the exception of mostly alkaline seamounts. Figure 5.15f shows that petit-spot seamounts generally plot above 1.0, although analyses from Mertz et al. (2001), Hirano et al. (2001) and Buchs et al. (2013) largely fall just below 1.0. Analyses from Machida et al. (2015) range above and below 1.0, with those falling below having undergone more extensive metasomatism. Analyses from Mertz et al. (2001) and Hirano et al. (2001) also have relatively depleted Th (see Figures 5.15d and f) more similar to tholeiitic seamounts.

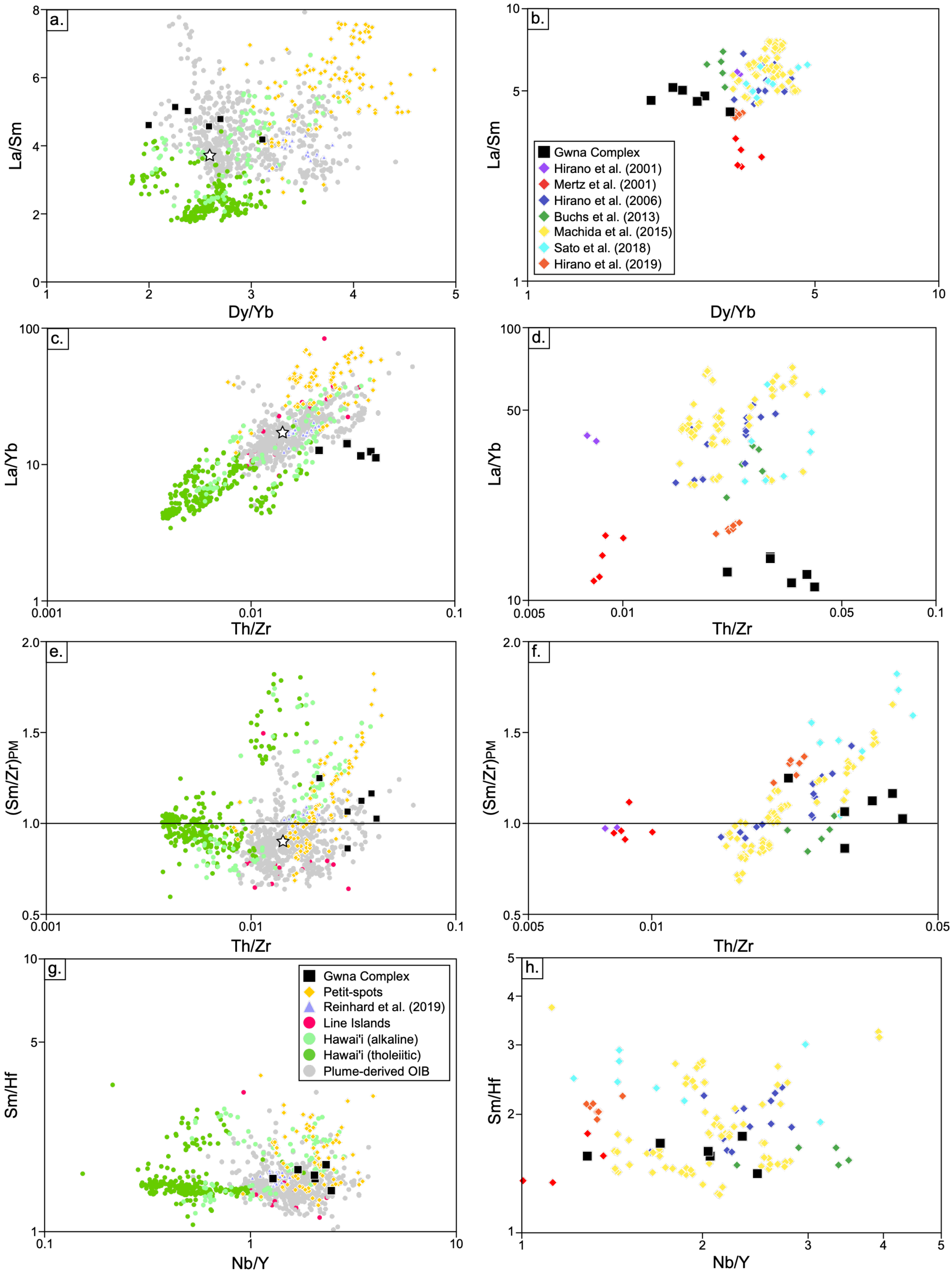

Figure 5.15: Geochemical diagrams of intraplate magmatic rocks from Gwna Complex Area I plotted against data from various petit-spot and plume-derived seamounts (data sources included in main text) showing (a-b) representations of LREE and HREE slope patterns; (c-d) trace element ratio plot of REE patterns against Th/Zr; (e-f) trace element ratio diagram showing the relative enrichment or depletion of Zr against Sm; and (g-h) trace element ratio diagram plotting Sm/Hf against alkalinity (Nb/Y).

Gwna Complex analyses display distinctly concave multivariate patterns. They contain very similar Th, Nb and Ta contents to petit-spot seamounts but with notably shallower REE patterns (mean La/Lu_{PM} = 9.68), starting with relatively low HREEs (mean La/Sm_{PM} = 1.05) but becoming relatively enriched in HREEs (mean Gd/Lu_{PM} = 2.48). The overall REE pattern is more similar to relatively evolved plume-derived basalts like the alkaline Hawaiian basalts (mean La/Lu_{PM} = 11.3), and are also similar to potential petit-spot rejuvenated lavas from Samoa (Reinhard et al. 2019). These analyses, however, are not as highly enriched in Nb and Ta as the Gwna Complex rocks and other petit-spot seamounts. Figures 5.15d and f show that the Gwna Complex samples have very similar Th/Zr ratios to the bulk of petit-spot analyses, along with an average $(Sm/Zr)_{PM} < 1.0$. Figure 5.15h shows that the Gwna Complex samples have slightly elevated Sm/Hf ratios, along with high Nb/Y ratios, both of which are similar to petit-spot seamounts and alkaline plume-derived seamounts.

Highly alkaline plume-derived seamounts produce basalt compositions that overlap with those of petit-spots. Distinguishing petit-spot seamounts based on geochemistry alone is therefore not viable. Additionally, petit-spots show a wide compositional range that cannot be solely explained by mid-lithosphere interactions with peridotites. Petit-spot analyses from Mertz et al. (2001) and Hirano et al. (2019) show geochemical signatures more similar to those in alkaline plume-derived seamounts, while potential rejuvenated petit-spots in Samoa (Reinhard et al. 2019) also fall into the same category. Given the small number of studies on petit-spot seamounts since their recent discovery, it is highly likely that their compositional range has yet to be truly observed, and some controls on their genesis have yet to be realised.

Geochemically, the Gwna Complex rocks are quite distinct, but show close affinities with petit-spot seamounts and highly alkaline plume-derived seamounts. The Gwna Complex samples have similar HFSE contents to petit-spot seamounts, importantly including depleted Zr and Hf in comparison to other HFSE's. However, the REE patterns of the Gwna Complex samples do not conform with petit-spot seamounts – and they are rather distinct from plume-derived seamount patterns also.

Despite geochemical uncertainties, field evidence and magmatic textures are very comparable to previous petit-spot descriptions (Mertz et al. 2001; Hirano et al. 2006; Buchs et al. 2013; Machida et al. 2015). It is therefore likely that Gwna Complex Unit 9 is representative of an accreted petit-spot seamount. Compared to analyses from Machida et al. (2015), the compositions are intermediate, suggesting formation was likely oceanward from the outer rise, facilitating a moderate dwell time in the mid-lithosphere. Differences in REE patterns may reflect a relatively thin oceanic lithosphere preserved in the Gwna Complex.

5.1.5 Correlating Area I across the Gwna Complex

Area I is rather unique to the Gwna Complex, in that its comparatively low volumes of terrigenous clastic material have resulted in ophiolitic basalts and sea floor sedimentary sequences dominating its stratigraphy. Block-in-matrix mélange is the prevailing fabric across other areas of the Gwna Complex, facilitated by voluminous matrices of chloritic schists, pelite-dominated siliciclastic turbidites, and mudstones. Basalt substrates across all four study areas show textural similarities and overlapping geochemical variability within the MORB-OIB array, suggesting consistent formation processes.

OPS comparisons

Repeated occurrences of OPS comprising multiple lithologies were recorded from Porth Felen (Area II), and broadly match the framework of OPS in Area I. The Porth Felen sequences are not imbricated along shear zones, but are separated by brittle faults. There are fundamental linkages between the areas, although Porth Felen comprises notably thinner sea floor sedimentary units. The upper surface of OPS in Porth Felen extends beyond the headland, composed of disrupted turbidites that are thicker than clastic sequences in Area I.

Basalt-carbonate transitions were not seen in Porth Felen. Basalts were directly overlain by layered carbonate rocks, but contacts were typically marked by slip planes populated by precipitated jasper and carbonate masses. Substantial blocks of basalt-carbonate rocks were observed, however, in mélange blocks at Porthorion. Similarly, interleaved basalt-carbonate blocks in Area III mélange show a progressive increase in carbonate components to the SE, consistent with the grading direction in Area I. Their absence in Porth Felen does therefore not imply that basalt-carbonate interactions are features confined to Area I OPS. Basalts in Porth Felen have relatively enriched (E-MORB to OIB) compositions.

The black mudstone of Porth Felen matches the interpreted stratigraphic position of mudstones in Area I – between lower carbonate rocks and overlying silty mudstones. However, the mudstones do not directly correlate to one another. The mudstones of Area I are tuffaceous with a continental arc geochemical signature, including a red/purple haematitic component. The black mudstone, however, is representative of anoxic sedimentation (Sato et al. 2015), and exhibits geochemical affinities of a passive margin without continental arc input. The mudstones show no evidence of manganese nodule formation or Mn enrichment, which are regular features of pelagic sea floor sediments in oxidised ocean conditions (Fike et al. 2006). Black mudstones may therefore represent older seafloor material in the Gwna Complex, deposited prior to the global Ediacaran oxidation event, although the event is not well constrained in deep oceans and may have involved fluctuating conditions (Fike et al. 2006; Sato et al. 2015). Sedimentation of black mudstones appears to be very limited, and its only occurrence in Porth Felen is heavily sheared into a single discontinuous lens. It is likely that the low-volume, mechanically weak unit is disseminated elsewhere in the Gwna Complex by shearing. The tuffaceous mudstones are more common and occur in all four study areas. They are representative of more voluminous pelagic to hemi-pelagic sedimentation that – along with cherts – dominate abyssal sedimentation and are more representative of Gwna Complex OPS. Assuming stratigraphic continuity between the carbonates and black mudstones at Porth Felen, this would support the singular OPS of Area I (see Figure 5.6), where mudstones overlying carbonates could only be inferred.

Clastic sedimentary rocks in Area I are divided between volcaniclastic and siliciclastic sandstones, which correlate to chloritic schists and siliciclastic turbidites respectively. Clear end members are observable in Area I, however, the more voluminous nature of clastic sediments in other areas has led to intermixing of clastic components. This may be partially a result of sedimentary grading through sediment source evolution, but is probably facilitated predominantly by tectonic mixing. This would be achieved through greater sediment volumes, with block-in-matrix textures allowing for sediment-sediment interactions in the matrix. In Area I, relatively thin occurrences are more confined between elongate imbricates.

Composite OPS for the Gwna Complex

Aside from localised features such as petit-spot magmatism in Area I and anoxic black mudstones in Area II, lithological frameworks across study areas are consistent.

Areas III and IV are more similar structurally to Area II, comprising turbidite-dominated mélanges with concentrated occurrences of basalts and pelagic to hemi-pelagic sedimentary sequences. Increased sediment variability and volume outside of Area I represent the only systematic changes in OPS, all related to continental erosion and trench-fill sedimentation. Quartzite clasts are common to uncommon in Areas II, III and IV but are absent in Area I. Clastic lithologies in Areas III and IV are otherwise continuous from Area I, but occurring in substantially greater volume. Olistostromes in Area II represent further lithological changes, with the input of Gwyddel bed clasts. Basalt clasts within the olistostromes (eg. AN19022) have compatible Group 1 (N-MORB) compositions and may represent reworking of previously accreted material. Figure 5.16 illustrates a composite Gwna Complex OPS recorded to reflect conditions of formation at various stages of an ocean lifecycle.

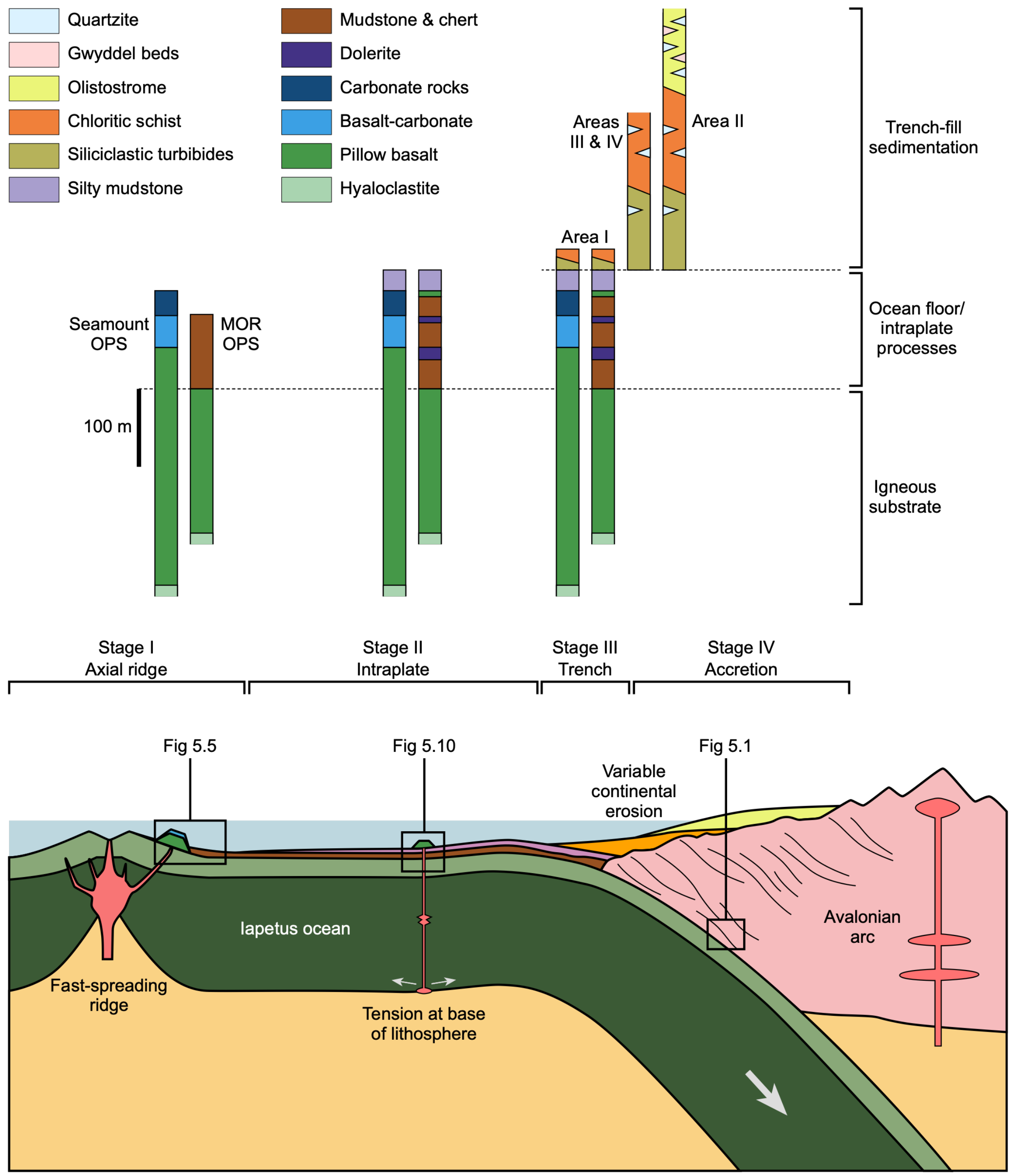

Figure 5.16: Schematic composite diagram of tectonic and depositional settings encountered during the formation of ridge-trench OPS in the Gwna Complex, showing (I) axial ridge magmatism with divergent mid-ocean ridge (MOR) OPS and off-axis seamount OPS with varying pelagic sedimentation; (II) intraplate hemi-pelagic sedimentation as dual OPS converges, along with localised petit-spot volcanism in MOR sequences in response to subducting plate flexure; (III) variable trench-fill sedimentation from continental sources, showing large differences in sediment input between Area I and Area II; and (IV) the descent of OPS into the subduction zone where it is accreted into the active Gwna Complex.

5.2 ORIGIN OF PENMYNYDD TERRANE

The Penmynydd Terrane consists of highly deformed greenschist to blueschist facies sequences that are indicative of a subduction regime. Zoned amphiboles, with relatively low P-T calcic to sodic-calcic compositions, indicate a previous greenschist facies metamorphic event. The terrane is structurally similar to the Gwna Complex in many ways, with elongate clasts of relatively strong metabasites hosted within weaker mica schist and chloritic schist matrices.

5.2.1 Blueschist protolith

The metabasites of the Penmynydd Terrane generally plot as tholeiitic basalts within the MORB-OIB array, ranging from N-MORB to E-MORB (see Figure 4.17). Relict pillow textures throughout multiple metabasite localities confirm that the Penmynydd Terrane represents subducted oceanic material. Peak metamorphism ages (560 – 530 Ma) largely coincide with siliciclastic sedimentation in the Gwna Complex (549 – 530 Ma), suggesting roughly similar basalt protolith ages (Dallmeyer and Gibbons 1987; Asanuma et al. 2017). Geochemical similarities enforce this link, and both units most likely formed from the same oceanic material, preserved through different subduction zone processes.

High P-T metabasites are more likely to originate from ocean floor material, which has a lower probability of accretion than relatively prominent seamounts. Metabasites would therefore be expected to be less enriched than Gwna Complex basalts, assuming a predominantly off-axis seamount origin. The majority of analysed metabasites have N-MORB compositions, plotting amongst the least enriched Gwna Complex basalts. Two samples from opposite ends of the terrane (AN17004 and AN17032) exhibit very similar compositions approaching E-MORB. AN18040 has been highlighted as an anomaly due to its unusual geochemistry (slightly alkaline E-MORB) and high haematite contents. There are no clear spatial or metamorphic links between these compositional variants.

Although most samples imply a less enriched ocean floor environment of emplacement, AN18040 provides an exception. It occurs in the Pen-y-Parc Formation, rather than the Penmynydd Formation, which coincides with the more common occurrence of carbonate blocks. This provides some similarities to the Gwna Complex OPS. Another exception if AN19015, which exhibits an alkaline continental arc signature. The sample shares mineralogical and major element compositional properties with other metabasites but is clearly of different origin. It most likely represents tuffs from a mafic lava.

5.2.2 OPS in the Penmynydd Terrane

Although original stratigraphic successions are not retained in the Penmynydd Terrane, links to the Gwna Complex can be used to infer a schematic OPS based on preserved relationships between similar rocks (or protoliths). As mentioned, the Pen-y-Parc Formation seems to preserve more common occurrences of carbonate and quartzite clasts, both of which are common in the Gwna Complex. The Penmynydd Formation consists of predominantly metabasites and mica schists, with little evidence of other lithologies. Mica schists originate from pelite-dominated sedimentary protoliths. They can be correlated to the voluminous pelite-dominated turbidites in Areas II, III and IV of the Gwna Complex as continent-derived sediments (see Figure 5.17). The general absence of carbonates in the Penmynydd Formation may correlate to MOR OPS proposed from the Gwna Complex. Localised occurrences of carbonate clasts and enriched metabasites (AN18040) in the Pen-y-Parc Formation may represent subordinate occurrences of seamount material.

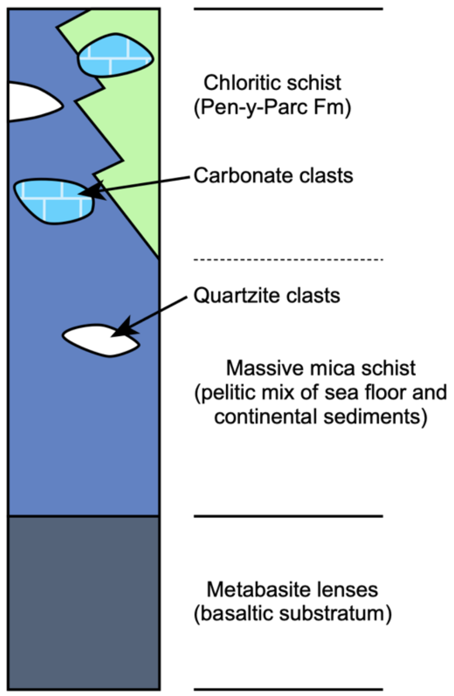

Figure 5.17: Schematic OPS reconstruction of the Penmynydd Terrane and the relations of protoliths with OPS lithologies in the Gwna Complex.

5.2.3 Metamorphic conditions

Metabasites in the Penmynydd Terrane are all characterised by metamorphic amphiboles, ranging from calcic to sodic compositions. Calcic compositions are representative of relatively low-grade greenschist facies conditions and often confined to amphibole cores, while higher grade calcic-sodic and sodic rims generally represent a prograde core-rim zonation towards blueschist facies. Calcic amphibole cores in even the lowest P-T samples represent an initial greenschist facies metamorphic event that has affected the Penmynydd Formation. This initial metamorphism occurred 20 – 30 Ma before peak metamorphism and has been attributed to seafloor metamorphism (Gibbons and Gyopari 1986; Dallmeyer and Gibbons 1987). This could therefore be attributed to sea floor basalts that were exhumed from deep within the substrate, although this would not explain the presence of AN19015.

Peak metamorphism varies between samples, with the highest-grade amphiboles in AN17004 remaining calcic, for example. The distribution of peak metamorphism between samples is not well constrained. Most samples comply with metamorphic isograds outlain by Kawai et al. (2007), however AN17007, AN17011 and AN17032 all plot within zone the highest grade (Zone III) but contain sodic-calcic amphibole prograde rims. Curiously, AN17007 and AN19015 were sampled within several hundred metres from each other, yet AN17007 contains mostly calcic amphiboles with some sodic-calcic rims, and AN19015 contains sodic-calcic to sodic amphiboles only. The Mg# of these samples also varies greatly, from > 60 in AN17011, to < 45 in AN19015.

Like peak metamorphic grade, the minimal preserved metamorphic state is also variable between samples. Those with higher peaks (Na-amphibole rims) typically have sodic-calcic amphibole cores, whilst those with relatively low grade generally preserve calcic cores (see Figure 3.11). Amphiboles accommodate Al into the T-site and Na into the B-site at the same rates across calcic to calcic-sodic compositions, suggesting prograde metamorphism along a single P-T path (see Figure 3.13). In sodic amphiboles, calcic-sodic cores mean that intermediate phases along this path have been more effective at replacing initial calcic amphiboles, which can be explained in two possible ways. Firstly, metabasite lenses have been exhumed from variable depths and tectonically mixed during exhumation, thus recording different metamorphic conditions. Secondly, metamorphic reactions occurred more efficiently around the outer parts of metabasite lenses, buffered by fluid interactions, while alteration in the centres took longer and remained incomplete.

Metamorphic zonation is most likely, given the consistent nature of the mica schists. Evidence for this zonation has also been observed previously (Gibbons and Gyopari 1986). These disequilibrated cores of lenses, however, have been preferentially subjected to retrograde metamorphism, which is not seen affecting sodic amphiboles.

5.3 CEMAES GROUP

The block-in-matrix mélange of the Porth Swtan Formation directly overlies the volcaniclastic turbidite succession of the Porth Trefadog Formation. This immediately suggests that the Porth Swtan Formation mélange is sedimentary in origin, since there is very little evidence to suggest that the lightly deformed, continuous Porth Trefadog Formation succession has been accreted. Pervasive foliation and highly sheared blocks that are present throughout the Gwna Complex are not as well defined in the Porth Swtan Formation. Thick, mostly fine-grained arkosic sequences in the Porth Trefadog Formation are locally interrupted but have not been dismembered like similar clastic sequences in the Gwna Complex, which typically show evidence of extensive shearing and a well-developed foliation.

The Porth Trefadog Formation volcaniclastics have very consistent geochemical compositions throughout, exhibiting a continental arc signature. Skerries volcaniclastics show highly compatible geochemical compositions. While the upper boundary of the Porth Trefadog Formation is observable, the sheared lower boundary at Porth Defaid opens the possibility that the Skerries volcaniclastics may be related to the Porth Trefadog Formation, comprising part of the lower, more psammitic stratigraphy.

Carbonate rocks

Carbonate rocks in the Porth Swtan Formation that have not been overprinted by dolomitisation are stromatolitic with low mud content. They are indicative of shallow marine environments of deposition, in contrast to the deep-water carbonates of the Gwna Complex. Figure 5.18 compares the geochemical compositions of carbonate rocks from the Porth Swtan Formation and the Gwna Complex. The carbonates of the Porth Swtan Formation produce a distinct positive correlation between Mn/Sr ratios and MgO content (see Figure 5.18a) across a range of carbonate compositions from limestone to dolostone. Dolomitic carbonates from the Gwna Complex do not follow this trend and have low Mn contents (140 – 150 ppm) more like Porth Swtan Formation limestones than dolomitised carbonates. Additionally, Gwna Complex carbonates have notably higher Rb contents than corresponding Porth Swtan Formation dolostones (see Figure 5.18b). This suggests that dolomitisation occurred as separate processes between the two units, under different conditions.

Formation of the Cemaes Group

The Cemaes Group includes a separate mélange unit from those in the Gwna Complex and the Penmynydd Terrane. The mélange has not been subjected to less intense deformation forces and potential ghost stratigraphy is indicative of a gravity slide. The transition between thick depositions of volcaniclastic turbidites to assemblages of siliciclastic sediments and shallow marine limestones suggests a gradual but significant increase in continental erosion in an arc proximal setting. The unit has been previously interpreted as accretion of a seamount (Wood 2012), however accreted seamount material would be expected to include some volcanics, especially if they are large enough features to host shallow sea atolls.

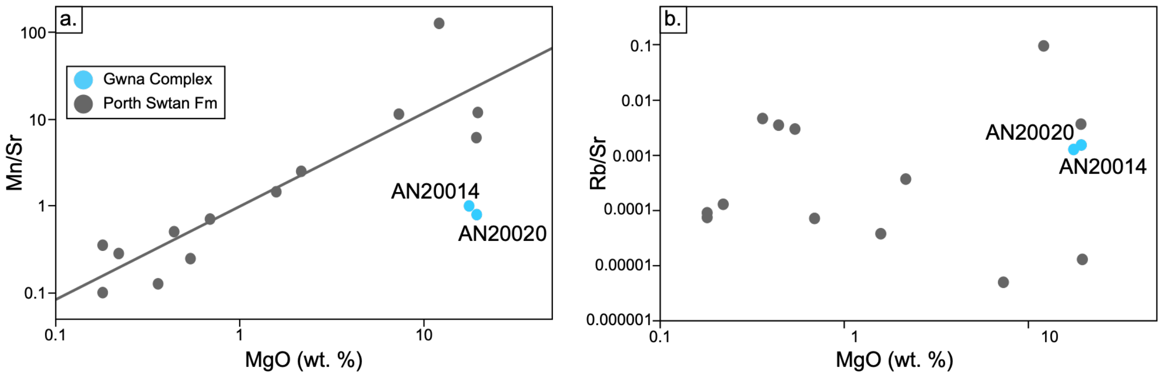

Figure 5.18: Compositional diagrams of Gwna Complex carbonate rocks plotted against carbonate rocks from the Porth Swtan Formation in Cemaes *(Horák and Evans 2011)*.

5.4 BIASES IN ACCRETED OPS

Seamounts are most commonly associated with upwelling mantle plumes, however, they may also form through several known alternative processes. This chapter outlines likely occurrences of two distinct types of seamounts in an accretionary complex, neither of which relate to mantle plumes. Off-axis seamounts form close to fast-spreading centres from isolated pockets of decompressed mantle melts (Davis and Clague 2000; Niu et al. 2002). Petit-spots form from upwelling of small melt pools at the base of the lithosphere through plate flexure (Hirano et al. 2006). Since both features are relatively minor – with edifices typically below several hundred metres – they are often overlooked in modern sea floor environments and are likely also underrepresented in the rock record.

Calculated estimates suggest approximately 125000 seamounts over 1 km in height populate the modern ocean floor, with 8 – 80 million at heights above 100 m (Wessel et al. 2010). Seamounts therefore populate a significant portion of the ocean floor and processes involved in their formation – particularly smaller edifices – are poorly understood. Accretion at continental margins is often sporadic. Subduction zones are highly dynamic systems, and accretion is driven by numerous factors, with one key factor being topographic height of the upper surface of the subducting crust (Watts 2001; Clift and Vannucchi 2004; Hajná et al. 2014). Accretion is therefore biased towards thick trench-fill sedimentary deposits and seamounts.

Off-axis seamounts are estimated to be the most common form of seamount populating current ocean floors (Hillier 2007; Buchs et al. 2015). Despite not being as tall or voluminous as many plume-derived seamounts (Jaroslow et al. 2000; Choi et al. 2021), they have a greater probability of being accreted that surrounding ocean floor, especially in systems with relatively low continental sediment input. Despite this, off-axis seamounts are seldom interpreted within accretionary complexes. Basalt sequences of the Gwna Complex has previously been reported as mid-ocean ridge origin (Thorpe 1993; Saito et al. 2015), but unusual features such as basalt-carbonate transitions and compositional variability have not been effectively scrutinised. It is possible that these features have been misinterpreted in other accretionary complexes due to the absence of traditional seamount OPS – designed around larger edifices (Sano and Kanmera 1991; Safonova 2009) – and overlooked geochemical variability. Off-axis seamounts have predominantly tholeiitic N-MORB to E-MORB compositions (Niu and Batiza 1997; Anderson et al. 2021), but the more enriched components that define them from MOR derived basalts may be overlooked, or attributed to secondary intraplate magmatism.

Petit-spot seamounts represent an emerging field of study that has largely been centred around analysis of the current sea floor (Hirano et al. 2001; Hirano et al. 2006). Some studies have recognised accreted petit-spot products in the form of both intrusive and extrusive components, providing crucial insight into the anatomy of these features (Mertz et al. 2001; Buchs et al. 2013). Despite this, knowledge of petit-spots is still evolving, and methods of recognising petit-spot magmatism in accreted sequences have not yet been fully realised. Geochemical characterisation has proven to be a useful method, but the compositions of some petit-spots – including those in the Gwna Complex – may overlap with plume-derived seamounts, and require further field evidence for clarification. Additionally, sea floor alteration may obscure alkali and potassic ratios in older rocks, which are prime geochemical indicators of petit-spots.

The ocean floor is more variable than is often perceived, and this variability may not be reflected adequately in the rock record in the form of OPS. Relatively minor oceanic features may be misrepresented in accretionary complexes, where indicative geospatial and topographical information has been lost. This chapter outlines combined petrographic, geochemical, and field observations used to interpret the presence of seamounts of two distinct geneses, that can be applied to identification in other accretionary complexes.

CHAPTER VI
Tectonic evolution of the MCT

6.1 TECTONIC SETTINGS OF STUDIED UNITS

The nature of formation for units studied in this project gives insight into the development of the MCT, and its placement within a larger regional geological context. The following chapter will analyse these units with respect to their tectonic evolution. These findings and their implications on the formation of the MCT will then be placed into a larger context, regarding formation of the Avalonian-Cadomian arc system and subsequent rifting of peri-Gondwanan microcontinents.

6.1.1 Gwna Complex

The Gwna Complex represents accretionary material from a subduction mélange that preserves OPS from a subducted ocean floor at the margin of a continental arc. Variable volumes of trench-fill clastic input across the four study areas of the Gwna Complex may be driven by sea floor topography or by external geodynamic factors. Area I represents a sediment starved system, with very little clastic sediment accreted, whereas Areas II and III are dominated by thick turbidites and olistostromal deposits. As discussed in Section 5.1, accreted basaltic material may derive predominantly from seamounts, generated off-axis from a spreading centre. Thicker accumulations of trench-fill sediment can be expected on low-lying ocean floor material than upon prominent features like seamounts, where sediment cover would be lower, depending on the height of the feature (Kusky et al. 2013; Wakita 2019). However, in Area I, Unit 9 rocks are potentially reflective of sea floor OPS but are not topped by relatively thick clastic sediment accumulations. While they may be associated with petit-spot seamount formation, the extrusive components of petit-spots are typically no more than 200 – 300 m tall (Hirano et al. 2006; Hirano 2011; Hirano et al. 2019). Conversely, seamount OPS sequences with enriched basaltic bases at Porth Felen are topped by thick siliciclastic turbidite deposits. Therefore, clastic sediment input is likely controlled by external geodynamic changes.

Comparative U-Pb maximum depositional ages of zircons from clastic sediments from Areas I and II suggest that sequences in Area II are older (Area I <537 Ma; Area II <549 Ma) (Asanuma et al. 2017; Dartnall 2018), possibly representing an evolution in the geodynamic setting of the subduction zone. Continental arc erosion has therefore seemingly decreased in the time between deposition Area II and Area I trench-fill sediments. Late-stage arc magmatism in the Avalonian arc occurred 570 – 550 Ma, and 580 – 530 in the Ganderian arc (Tucker and Pharaoh 1991; Compston et al. 2002; Barr et al. 2014). Avalonian magmatism overlaps with the deposition of Gwna Complex Area II clastic sediments but has ceased – or at least subsided – by the deposition of Area I clastic sediments (see Figure 6.1).

Magmatic activity in an arc setting promotes thermal uplift along with construction of volcanic edifices. This promotes high erosional rates and therefore high sediment supply to the trench. Conversely, the lack of magmatic activity during deposition of Area I sediments may reflect changes in the subduction environment such as the onset of transition from convergent to passive setting. Late-stage Avalonian magmatism is associated not only with the Gwna Complex, but the subduction of the Penmynydd Terrane (peak metamorphic ages 566 – 530 Ma) (Dallmeyer and Gibbons 1987; Asanuma et al. 2017). No accreted MCT rocks are thought to predate these units, suggesting that late-stage Avalonian magmatism may represent the onset – or resumption – of subduction after a passive phase (see Figure 6.1a). This may have also allowed passive sediment accumulation on earlier accreted sea floor (Area II), which were not given time to accumulate during ongoing subduction upon later accreted sea floor (Area I).

Clastic sediment in Area I is predominantly volcaniclastic in nature, whereas Area II comprises prominent volcaniclastic and siliciclastic components. Rifting and subsidence throughout East Avalonia and Ganderia during the Cambrian led to the formation of the Welsh Basin, Lakes-Manx Basin and Leinster Basin (Prigmore et al. 1997; Barnes et al. 2006; Brenchley et al. 2006; Waldron et al. 2011; Rushton et al. 2011; Strachan 2012). Basin formation along the peri-Gondwanan arcs would have significantly limited continental sediment supply to the continental margin, leaving the isolated arcs as singular, limited sediment source rich in volcanic material. This progression would therefore affect not only clastic sediment volume, but also sediment composition in the trench, reflected in the differences between Areas I and II.

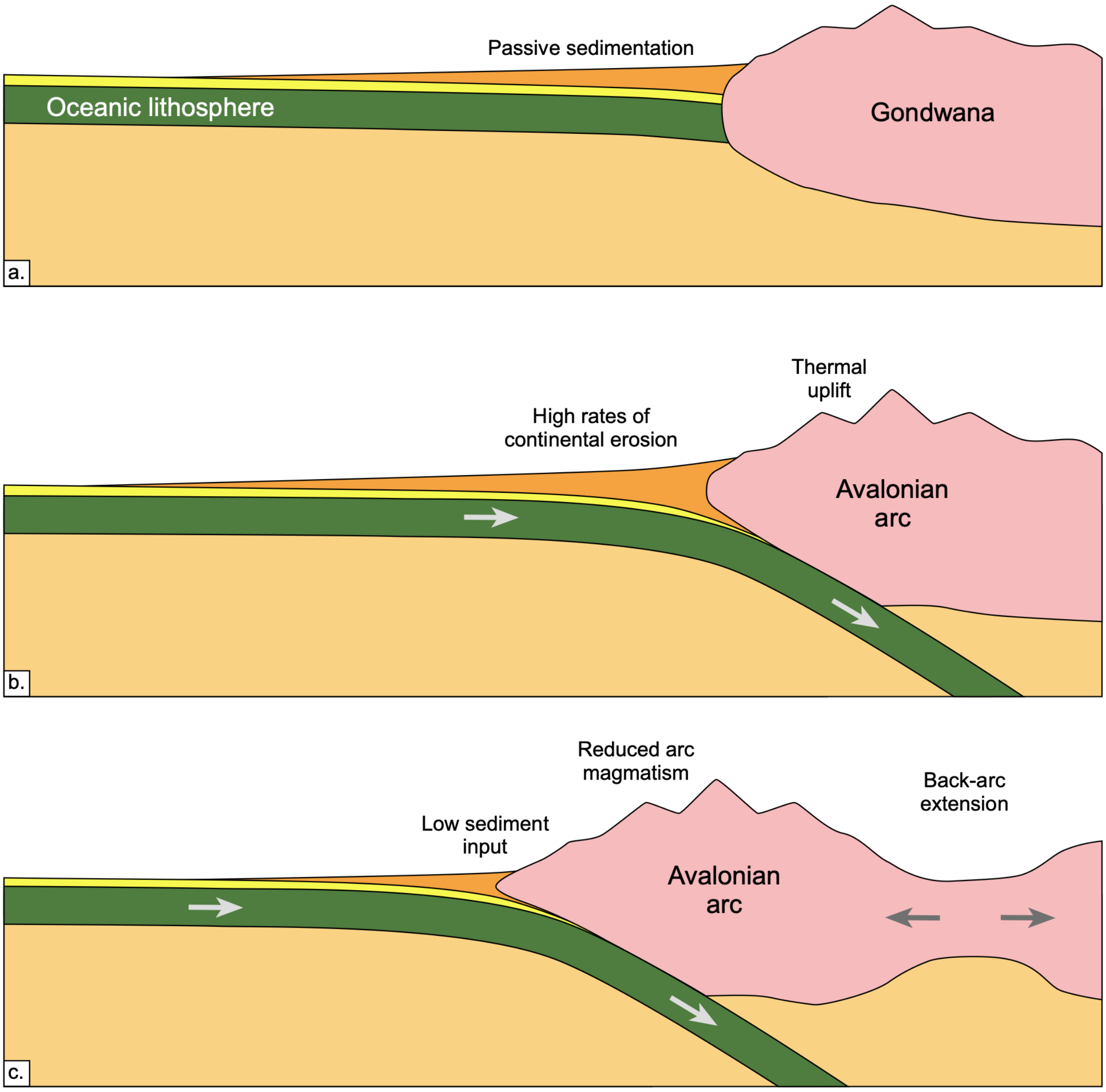

Figure 6.1: Schematic evolution of the Gwna Complex as a result of potential changes in tectonic environment, illustrating (a) an initial passive margin setting, promoting accumulation of eroded continental material on the sea floor, (b) subduction initiation leads to arc magmatism and continental uplift, leading to greater erosion rates and volcaniclastic sediment availability, resulting in high trench-fill sedimentation rates; and (c) back-arc basin formation isolates the Avalonian margin from Gondwanan sediment sources, while decreasing arc magmatic activity reduces volcaniclastic input, leading to a sediment starved subduction zone.

6.1.2 Penmynydd Terrane

The Penmynydd Terrane is thought to have been directly exhumed into the overlying low P-T accreted material of the Gwna Complex, forming a metamorphic pair (Kawai et al. 2006; Kawai et al. 2007; Maruyama et al. 2010a). However, inclusions of lenses of felsic material and the Holland Arms Gneiss along its western margin show that the unit has undergone some localised mixing with terranes not limited to the Gwna Complex. These foreign clasts appear to be of continental arc origin, and the Holland Arms Gneiss protolith has been attributed to the basement gneisses of the Coedana or Arfon Terrane of Avalonia (Greenly 1919; Beckinsale and Thorpe 1979; Horák 1993; Kawai et al. 2006; McIlroy and Horák 2006). While the Holland Arms Gneiss has been described as an unconformable outlier (Kawai et al. 2006), sheared felsic material seemingly occurs as elongate lenses that have been incorporated into the mica schist fabric of the Penmynydd Terrane parallel to the prevailing NE-SW trending regional shear, indicating tectonic mixing.

The eastern margin of the Penmynydd Terrane is also poorly defined, with the addition of chloritic schists along with mica schists as a prominent matrix component in the Pen-y-Parc Formation. It is unclear whether the sediments are mixed with the chloritic schists of the bordering Gwna Complex Area IV, or if the rocks are a coinciding result of low to moderate P-T metamorphism of a similar pelitic protolith. Metabasite lenses have not been mixed between the terranes, suggesting that terranes are not mixed. Likely correlations of OPS between the Gwna Complex and Penmynydd Terrane (see Section 5.2) suggest that a shared pelitic protolith is likely.

Exhumation of the blueschists typically occurs within 10 – 20 My after peak metamorphism (Agard et al. 2009), which would place Penmynydd Terrane exhumation at roughly 550 – 530 Ma. This would be consistent with ongoing convergence and formation of the Gwna Complex. While the Penmynydd Terrane was likely exhumed into the Gwna Complex as a metamorphic pair, the later transcurrent regime has led to interactions with slivers of continental arc – akin to the Coedana Terrane – along its western margin. This transcurrent disorder is further demonstrated by the occurrence of blueschist material in direct contact with the Arfon Terrane to the SE within the LSZ (Gibbons 1981; Gibbons 1983b). Transcurrent faulting along the western margin with Gwna Complex Area IV is less clear and both units may have been faulted as a single tectonic slice.

6.1.3 Cemaes Group

The Porth Swtan Formation represents a separate mélange from the Gwna Complex, indicating a second accretionary – or mélange forming – event. The Cemaes Group has not been subjected to NE-SW deformation and shearing that characterises most terranes of the MCT, and therefore likely post-dates the transcurrent tectonic regime that was in effect throughout the Cambrian (Gibbons 1983a; Gibbons and Horák 1990; Strachan 2012). Schofield et al. (2020) assumes an Arenig age for the Cemaes Group based on an unconformable relationship with the Porth y Felin Terrane. Evidence to suggest that this contact – seen at Porth Defaid – is faulted relieves the constraints on relative maximum age, however the lack of deformation would still place its formation around the lower Ordovician.

Renewed arc-related volcanism in the Welsh Basin initiated around 488 Ma, in the Tremadocian epoch (Kokelaar 1988; Howells et al. 1991; Brenchley et al. 2006). This volcanism may therefore be seen as a potential source of the Porth Trefadog Formation volcaniclastics. Magmatic activity was bimodal throughout the Tremadoc-Caradoc series, producing rhyolites and basalts, with subordinate intermediate components (Howells et al. 1991; Thorpe et al. 1993b).

Figure 6.2 plots the Porth Trefadog Formation volcaniclastics against rhyolites, basalts, and intermediate rocks from the Tremadoc-Caradoc series in Snowdonia, the closest of two main Ordovician volcanic centres in the Avalonian domain. Also plotted for comparison is AN19015, a Penmynydd Terrane blueschist with an arc-related mafic protolith. Rhyolites have been divided into two groups based on their SiO_2 contents (Rhyolite I – 70 – 80 wt %; Rhyolite II – 60 – 70 wt %). Volcaniclastics from the Porth Trefadog Formation show similar HFSE compositional trends to the Rhyolite II group but with systematically lower concentrations. Rhyolite II analyses exhibit similarly pronounced negative Ti anomalies (Ti/Ti* = 0.24 – 0.31), while Rhyolite I analyses have a larger anomaly (Ti/Ti* = 0.04 – 0.11). This is evident in Figure 6.3a, which also displays similar Mg# ranges between Rhyolite II (32.3 – 56.3), icelandites (32.3 – 47.8), and the Porth Trefadog Formation (32.4 – 48.8). Figure 6.3b shows that despite high SiO_2 contents, Rhyolite II was produced from intermediate melts of similar compositions to the icelandites, within a sub-alkaline system. Porth Trefadog Formation volcaniclastics fit closely within the range of Rhyolite II and the icelandites.

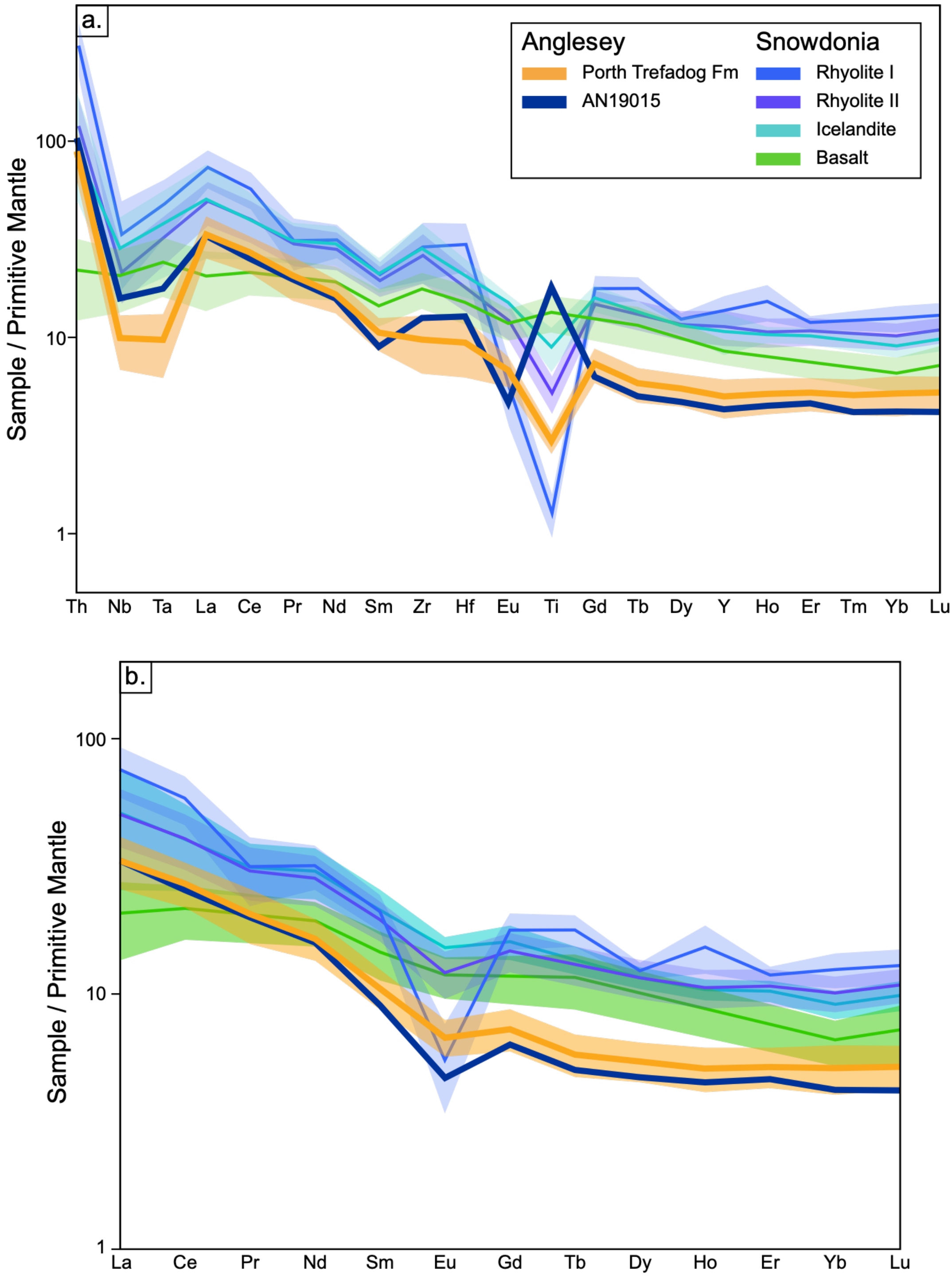

Figure 6.2: Multivariate diagrams of immobile elements plotting Porth Trefadog Formation volcaniclastics and an arc signature Penymyndd Terrane blueschist against magmatic rocks from Snowdonia, normalised to primitive mantle composition (Sun and McDonough 1989). Snowdonia data from Howells et al. (1991); Thorpe et al. (1993b).

Despite slightly low HREE abundances, Porth Trefadog Formation volcaniclastics show close affinity to Rhyolite II compositions. Rhyolite II is populated by analyses of both intrusive and extrusive rocks belonging to the early-stage Llewellyn Volcanic Group. The Llewellyn Volcanic Group is Sandbian in age (Howells et al. 1991), which would be too young to produce the Porth Swtan Formation, given that Arenig rocks overlie the Cemaes Group. However, sustained arc magmatism in North Wales suggests that earlier eruptions of felsic-intermediate material from the same Tremadoc-Caradoc system are the likely source of the volcaniclastics.

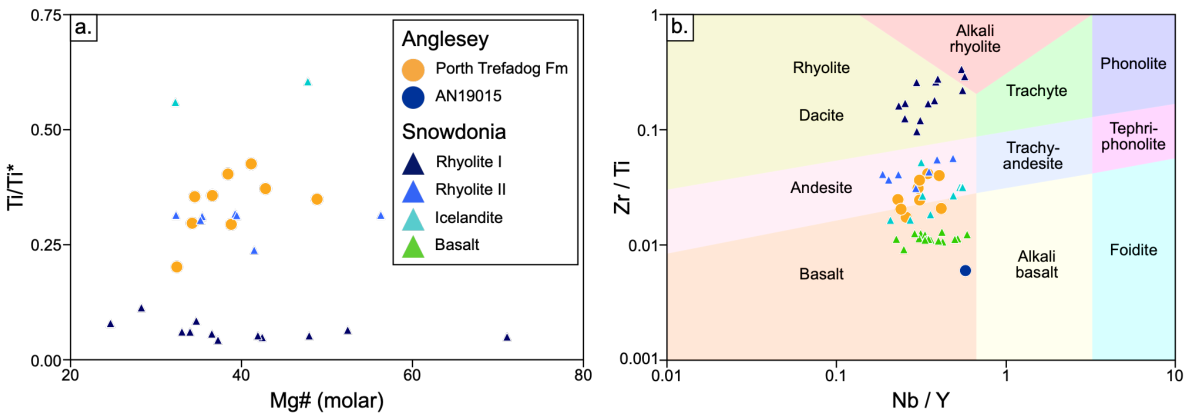

Figure 6.3: Geochemical plots of Porth Trefadog Formation volcaniclastics and an arc signature Penymyndd Terrane blueschist against magmatic rocks from Snowdonia showing (a) Ti/Ti* plotted against molar Mg#; and (b) volcanic classification scheme based on HFSE ratios (Pearce 1996). Snowdonia data from Howells et al. (1991); Thorpe et al. (1993b).

The gradational transition from largely fine grained volcaniclastic turbidites in the Porth Trefadog Formation to the mélange of the Porth Swtan Formation suggests a large increase in sedimentation rates. This is likely related to progressive uplift caused by renewed magmatic activity and/or back-arc rifting. Relatively undeformed sequences sat conformably below a mélange indicate a lack of any significant tectonic disruption during formation.

Various dating methods have placed the initial deposition of carbonates from Porth Swtan Formation clasts within the Tonian (Horák and Evans 2011; Dartnall 2018). Given the likely lower Ordovician age of the Porth Swtan Formation, this suggests that the carbonates were recycled from sedimentary successions around the continental margin, rather than being accreted seamount atolls. Multiple complex arc-arc collisions along the Gondwanan margin throughout the Tonian-Cryogenian (van Staal et al. 2020) imply that the harbouring of seamounts in a geodynamically mobile, intra-oceanic setting for such a long period is highly unlikely. This favours a sedimentary mélange formation for the Porth Swtan Formation. The inclusion of Tonian carbonates as clasts (and megaclasts) suggests a distinct change in sediment supply from other Gwna Complex terranes. While there are several possibilities, a plausible explanation is that transcurrent faulting along the arc front has introduced passive sedimentary sequences to the active continental margin – or through cratonic basin formation in the arc front onset by transcurrent faulting. Alternatively, they could be sourced from unroofing of an established sedimentary sequence.

6.1.4 Mafic intrusives of Anglesey

Group 3 doleritic intrusives are much younger than the MCT and do not have a bearing on its evolution. Mafic intrusives from Groups 1 and 2, however, may be linked to various magmatic processes throughout the subduction-rifting-collision geodynamic system in which the MCT has formed.

Group 1

Doleritic intrusives belonging to Group 1 have been split into four subgroups based on their geochemical compositions. These four subgroups exhibit geochemical signatures which indicate different tectonic environments of formation. Group 1a shows likely continental arc affinity, Groups 1b and 1c exhibit E-MORB characteristics with distinct REE patterns, and Group 1d shows an oceanic arc signature with relatively low Th and Nb, possibly indicating MORB with a crustal component.

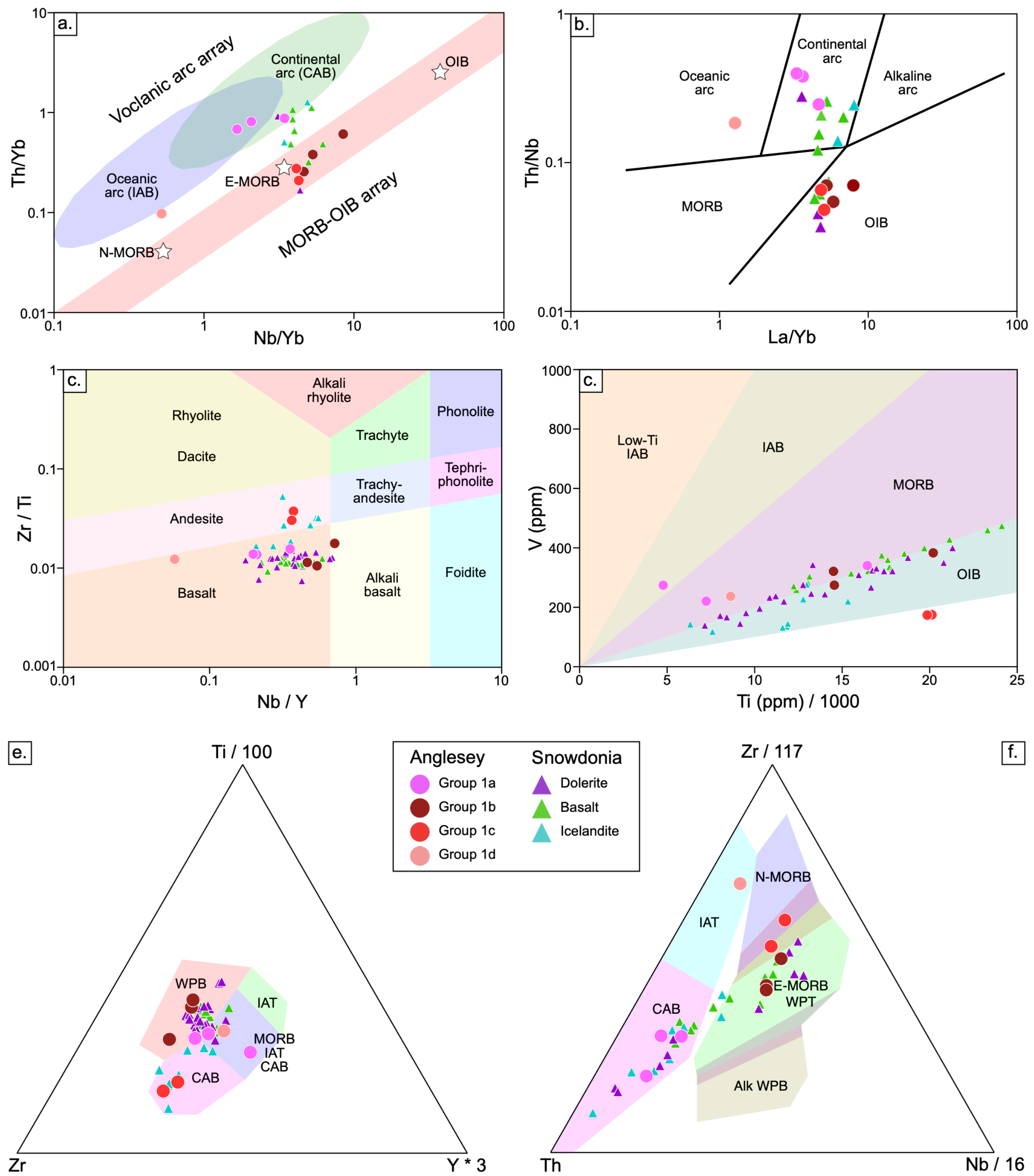

Figure 6.4: Elemental classification diagrams of Group 1 dolerite intrusives plotted against mafic-intermediate magmatic Ordovician rocks from Snowdonia showing (a) tectonic classification of MORB-OIB and VAB arrays (Pearce 2014); (b) tectonic classification using REE patterns (Hollocher et al. 2012); (c) volcanic rock type classification (Pearce 1996); (d) bivariate plot of Ti against V (Shervais 1982); ternary basalt tectonic classification diagram (Pearce and Cann 1973); and (f) ternary basalt tectonic classification diagram (Rollinson 1993). Snowdonia data from Howells et al. (1991); Thorpe et al. (1993b).

Ordovician dolerites in Snowdonia, along with basalts and icelandites, exhibit a compositional range from Group 1a (CAB) to Group 1b (E-MORB; see Figures 6.4a, b, e and f). Most sample follow a continuous Ti/V trend that straddles MORB and OIB fields (see Figure 6.4d). Ratios of Ti/V range from 17.6 – 63.2, with most data clustered within a range of 0.4 – 0.6. Although V contents may suffer from some mobility, the trend is well defined and low ratios are not indicative of an arc source. The rocks plot within – or along the boundary of – the basalt field, with the exception of Group 1c and a cluster of icelandites in the andesite field. This cluster can also be observed in Figure 6.4e, where they plot in the CAB field and exhibit relatively high Zr contents. Despite this clustering, Group 1c intrusives contain notably higher Zr (596 – 746 ppm) than the icelandites (380 – 411 ppm). The icelandites are mostly intrusive, although two samples belong to the Foel Grach Basalt Formation, part of the early stage Llewellyn Volcanic Group (Howells et al. 1991). Other icelandites, basalts and dolerites that hold affinity with Groups 1a and 1b are either intrusives, or related to the later, main magmatic stage – the Snowdon Volcanic Centre (SVC).

The multivariate plots in Figure 6.5 illustrate the close compositional similarities between SVC dolerites, basalts and icelandites with Groups 1a and 1b intrusives. REE patterns show consistent mean gradients (La/Lu_{PM} = 3.2 for icelandites; 2.9 for basalts; and 3.7 for dolerites). It seems likely that Groups 1a and 1b represent compositional endmembers of a shared source. Group 1c samples are enriched in HREE's relative to linked early magmatic icelandites (La/Lu_{PM} = 3.5 for Group 1c; 5.5 for icelandites), along with other HFSE's including Zr, Hf and Nb. The icelandites share a negative Ti anomaly but show enrichment in Th relative to Nb, also shown in Figure 6.5b.

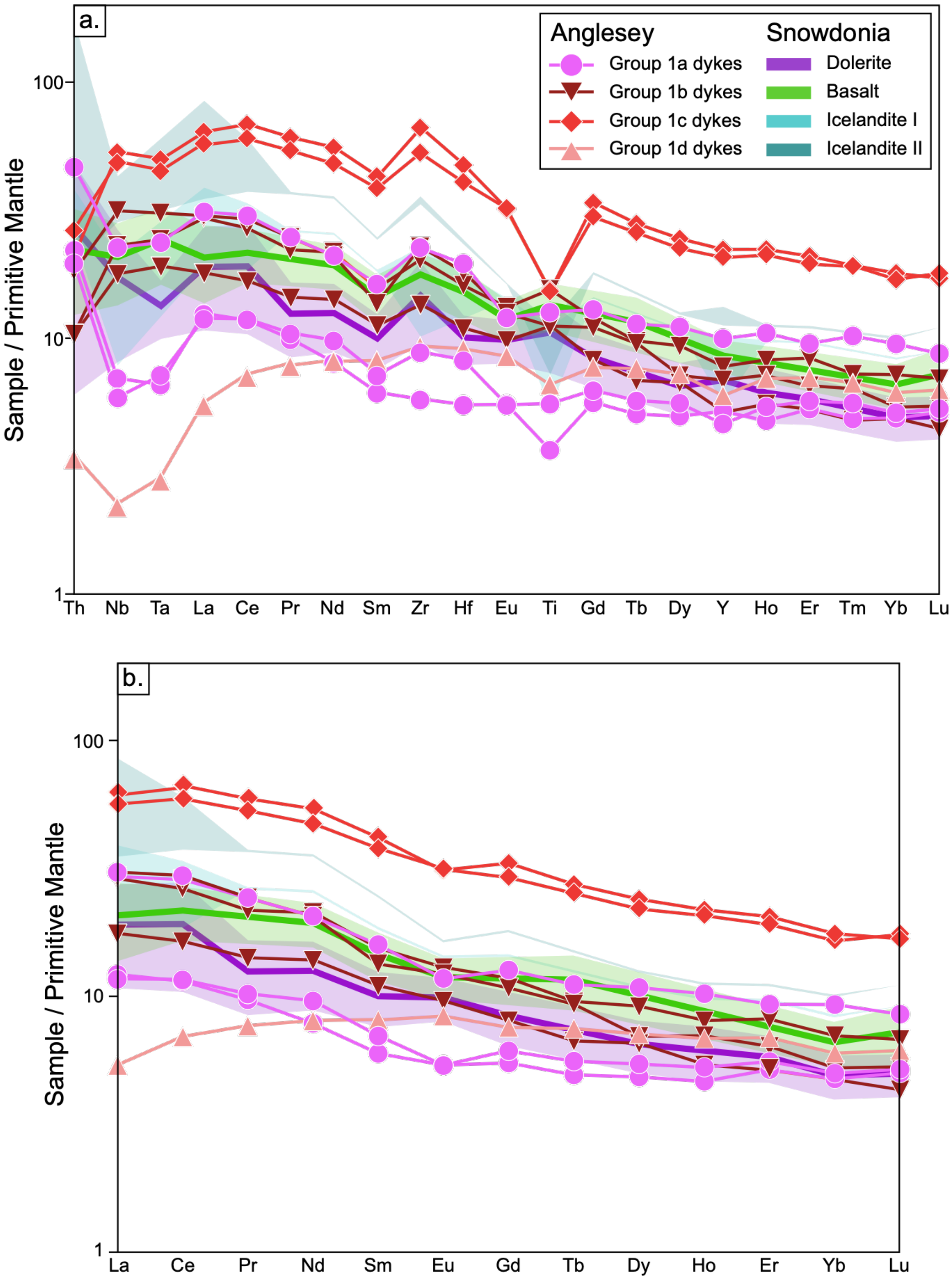

Figure 6.5: Multivariate diagrams of immobile elements plotting Group 1 intrusives from Anglesey against mafic-intermediate magmatic Ordovician rocks from Snowdonia, normalised to primitive mantle composition (Sun and McDonough 1989). Snowdonia data from Howells et al. (1991); Thorpe et al. (1993b).

Groups 1a and 1b plot on a continuous trend between E-MORB and CAB compositions, showing progressive enrichment of Th and depletion of Nb and Ta between the two endmembers respectively. The groups maintain relatively stable REE and Zr contents, suggesting that compositional variability is likely due to metasomatism proximal to subduction at the continental margin. Mafic rocks in the SVC are thought to originate from back-arc magmatism through extension around the Welsh Basin (Kokelaar 1988; Howells et al. 1991). This back-arc system is reflected geochemically and is the likely origin of intrusives from Groups 1a and 1b. Group 1c intrusives do not appear to be directly related to any included rocks from the Tremadoc-Caradoc series, and enrichment of Nb and Ta relative to Th suggests that it does not contain a metasomatized subduction component. While all mafic rocks in the Tremadoc-Caradoc series are enriched to E-MORB-like compositions, Group 1d intrusives contain an anomalous N-MORB signature and show no relation to this back-arc magmatism. It is possible, given the sampling locality, that they are related to gabbroic lenses scattered throughout the New Harbour Group on Holy Island.

Group 2

The single Group 2 intrusion (AN20038) represents a lamprophyre. Similar intrusions have been reported from the Midland Platform (Avalonia – Wrekin and Charnwood terranes), the Lake District (Ganderia) and throughout Laurentian and peri-Laurentian terranes in Scotland (Macdonald et al. 1985; Rock et al. 1988; Thorpe et al. 1993a; Shand et al. 1994). The intrusions are all thought to have been emplaced ca. 430 – 390 Ma (Rock et al. 1988). Lamprophyres have not previously been reported from the Welsh Caledonides (Thorpe et al. 1993a), so this occurrence could provide links to Avalonian or Ganderian terranes.

The ternary classification diagram in Figure 6.6a demonstrates that intrusives from all terranes are lamprophyres that comprise a single compositional cluster, although lamprophyres from Anglesey and the Charnwood Terrane are relatively depleted in K (K_2O = 0.57 – 0.82 wt. %) compared to other terranes (K_2O = 1.87 – 6.29 wt. %). The lamprophyres have high Al contents (Al_2O_3 = 10.01 – 17.24 wt. %) and plot between alkaline and calc-alkaline fields (see Figures 6.6b and c). Relatively low K and Si in Anglesey and Charnwood Terrane intrusives (SiO_2 = 45.81 – 48.75 wt. %) see them plot within the calc-alkaline and alkaline lamprophyre fields, whilst the majority of analyses plot between high-K calc-alkaline to shoshonite fields as calc-alkaline lamprophyres (see

Figure 6.6c). It is worth noting that K_2O contents may be influenced by alteration, particularly of biotite and feldspar components. Ranges in Mg# between terranes overlap closely with an overall range of 53.9 – 76.9, although most analyses plot between 55 – 70 (see Figure 6.6d).

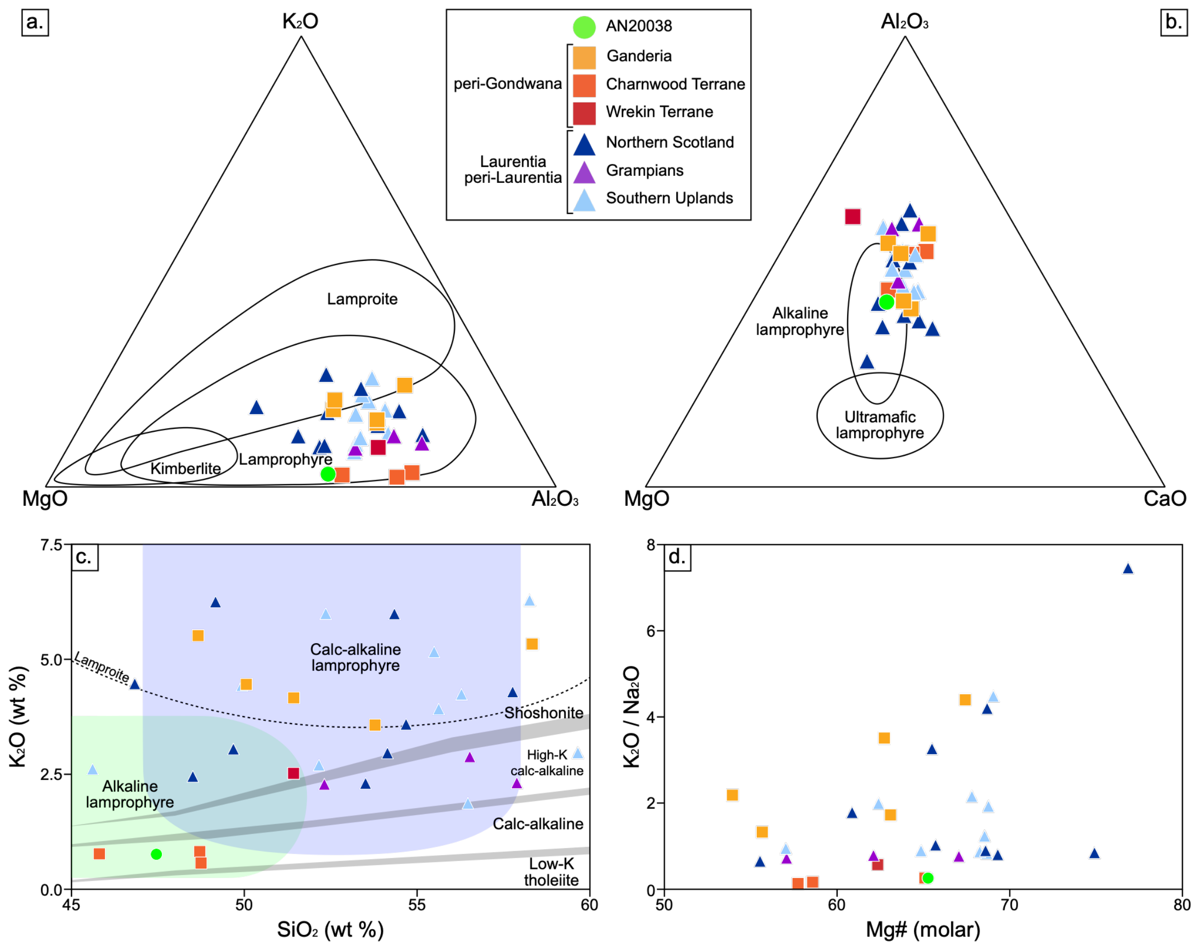

Figure 6.6: Major element diagrams for Group 2 intrusives plotted against Silurian-Devonian lamprophyres from associated peri-Gondwanan and Laurentian terranes in the British Isles (references in text) including (a) ternary kimberlite-lamproite-lamprophyre classification diagram (Bergman 1987); (b) ternary diagram distinguishing alkaline and ultramafic lamprophyres (Rock 1987); (c) alkaline affinity diagram with magma types and lamprophyre classification (Rollinson 1993; Raeisi et al. 2019); and (d) plot of potassic ratio against molar Mg#.

Lamprophyres plot between basalt and trachyte field based on HFSE ratios, with narrow Nb/Y ratio ranges (0.32 – 1.00). Avalonian intrusions have relatively low Zr/Ti ratios (0.008 – 0.015), with AN20038 slightly more evolved (Zr/Ti = 0.019), sitting between Avalonian and more evolved Laurentian (Zr/Ti = 0.021 – 0.116) and Ganderian (Zr/Ti = 0.027 – 0.043) lamprophyres (see Figure 6.7a). In Figure 6.7b, analyses plot largely below the Iceland array (Fitton et al. 1997), with less evolved Avalonian lamprophyres plotting along the array margin. Figures 6.7c and d plot incompatible Sr and Ba against compatible Cr and V in order to distinguish partial melting or fractional crystallisation as primary controls on compositions (Raeisi et al. 2019). While alteration may affect some of these results, degree of partial melting appears to predominantly influence compositions, with Avalonian lamprophyres originating from the greatest melt fraction, while lamprophyres from the Grampians are least evolved in Laurentia, and those from Northern Scotland the most evolved. In the ternary discrimination plot of Figure 6.7e, more evolved Laurentian analyses show high Zr contents, migrating from the within-plate alkali basalt field. In Figure 6.7f, analyses plot within the continental arc field, with the exceptions of the Wrekin Terrane intrusion in the MORB field and Charnwood Terrane samples in the island arc field due to their relatively high Ti contents.

Enrichment to alkaline OIB-like compositions is typically achieved by interaction between lithospheric mantle and upwelling volatile-rich melts from the asthenosphere (Gibson et al. 1995). Further enrichment towards continental arc compositions was likely driven by interactions with subducted material, given the high Ce/Nb (1.8 – 14.1) and Zr/Nb (9.3 – 53.6) ratios and predominantly shoshonite classification of the lamprophyres. Isotopic analyses of Laurentian lamprophyres suggests that metasomatism of mantle material led to enrichment and compositional variability from low degrees of partial melting (Shand et al. 1994). Metasomatism was likely caused by subduction-related melts and/or fluids (Macdonald et al. 1985; Rock et al. 1988; Shand et al. 1994). The lamprophyres were likely emplaced during thermal re-equilibration coinciding with the cessation of subduction and subsequent collision of Laurentia and Ganderia (Rock et al. 1988). Compositional distinctions between these lamprophyres and Avalonian lamprophyres may suggest a staggered collision of peri-Gondwanan terranes (Waldron et al. 2019b). Immobile element ratios demonstrate a close compositional relationship between AN20038 and Ganderian lamprophyres, as opposed to those from Avalonia.

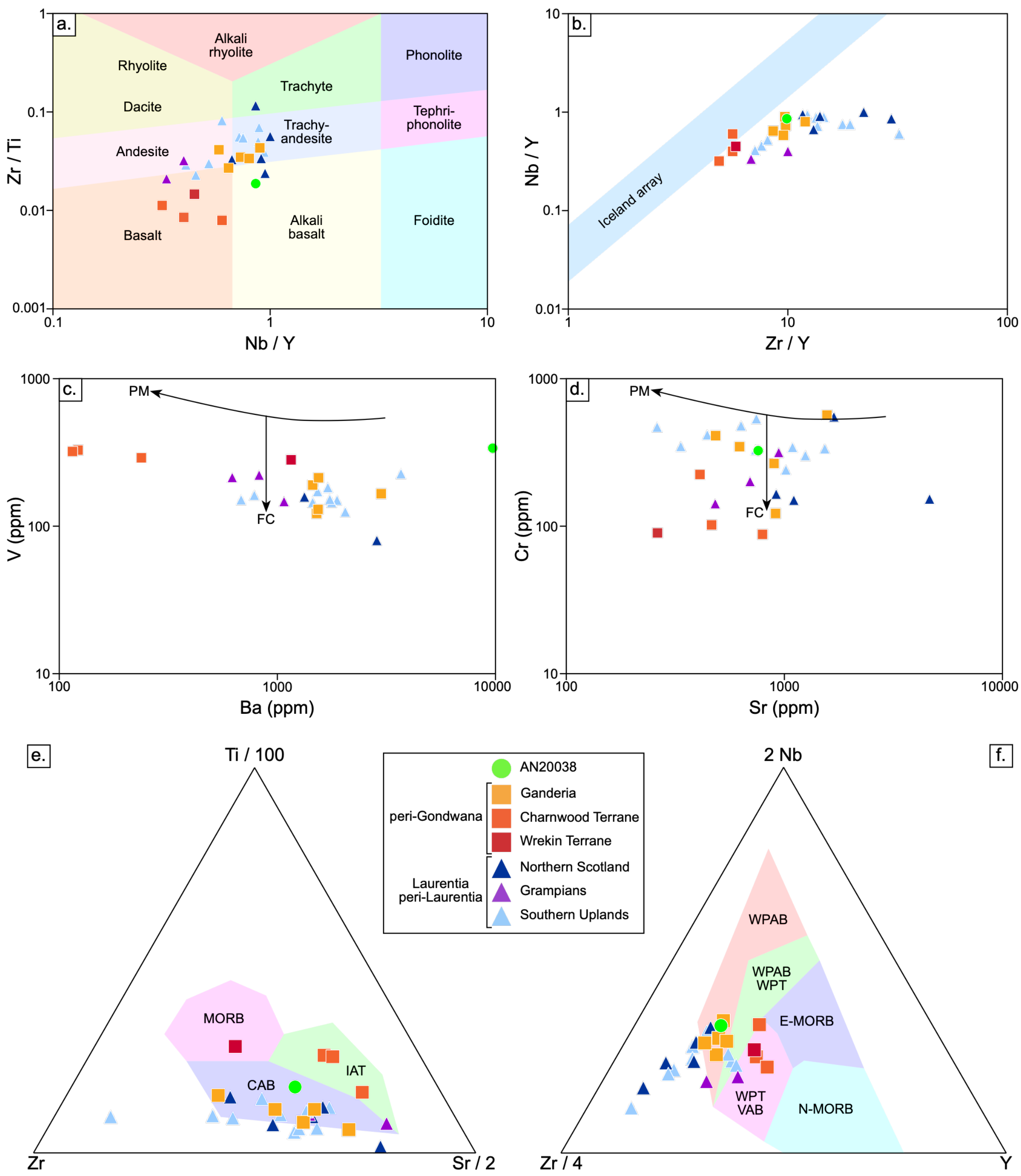

Figure 6.7: Trace element diagrams plotting Group 2 intrusives plotted against Silurian-Devonian lamprophyres from associated peri-Gondwanan and Laurentian terranes in the British Isles (references in text) including (a) volcanic rock type classification (Pearce 1996); magmatic evolution plot with reference to Iceland MORB-OIB array (Fitton et al. 1997); (c-d) bivariate plots of compatible against incompatible elements to distinguish compositional controls from partial melting (PM) and fractional crystallisation (FC); (e-f) ternary tectonic classification diagrams (Pearce and Cann 1973; Rollinson 1993).

6.2 MODEL OF FORMATION FOR THE MCT

The Monian subduction complex records a tectonic history of subduction at a continental margin, followed by a transition to a transcurrent regime, and finally, back-arc extension through renewed subduction. Zircon provenance studies across the MCT infer a consistent Gondwanan source for the Coedana, Aberffraw, Amlwch and Porth y Felin Terranes (Waldron et al. 2011; Pothier et al. 2015; Dartnall 2018; Waldron et al. 2019b). This implies that the terranes of the MCT all formed in the vicinity of Gondwana. More specifically, sediment sources were predominantly derived from the Amazonian craton, with the Gwna Complex likely formed between East Avalonia and Ganderia (Strachan 2012; Asanuma et al. 2017; Dartnall 2018; Schofield et al. 2020). Sediment provenance of the Cemaes Group has not been constrained but likely shares an affinity with Gondwana. Subsequent rifting separated peri-Gondwanan landmasses along the Avalonian arc front from the continent and led to their migration and eventual docking with the northern continent of Laurentia, driven by the back-arc opening of the Rheic Ocean (Murphy et al. 2004; Linnemann et al. 2008; Pollock et al. 2009; Nance et al. 2010; van Staal et al. 2012; Wen et al. 2020). The formation of units in the MCT predates this Ordovician-Devonian rifting process. However, the MCT still preserves evidence into the nature of this rifting.

By correlating data and interpretations collected in this study with evidence from across this tectonic province, Figure 6.8 illustrates a five-stage model for the development of the peri-Gondwanan rifting event, spanning from Late Neoproterozoic arc formation in Gondwana to Silurian collision with Laurentia. The model shows the MCT in relation to this system and highlights environments of formation for various units that have been covered in this study, including units of the MCT and later arc-related intrusives. The stages of tectonic evolution in the MCT – and the peri-Gondwanan terranes in general – are discussed in further detail below.

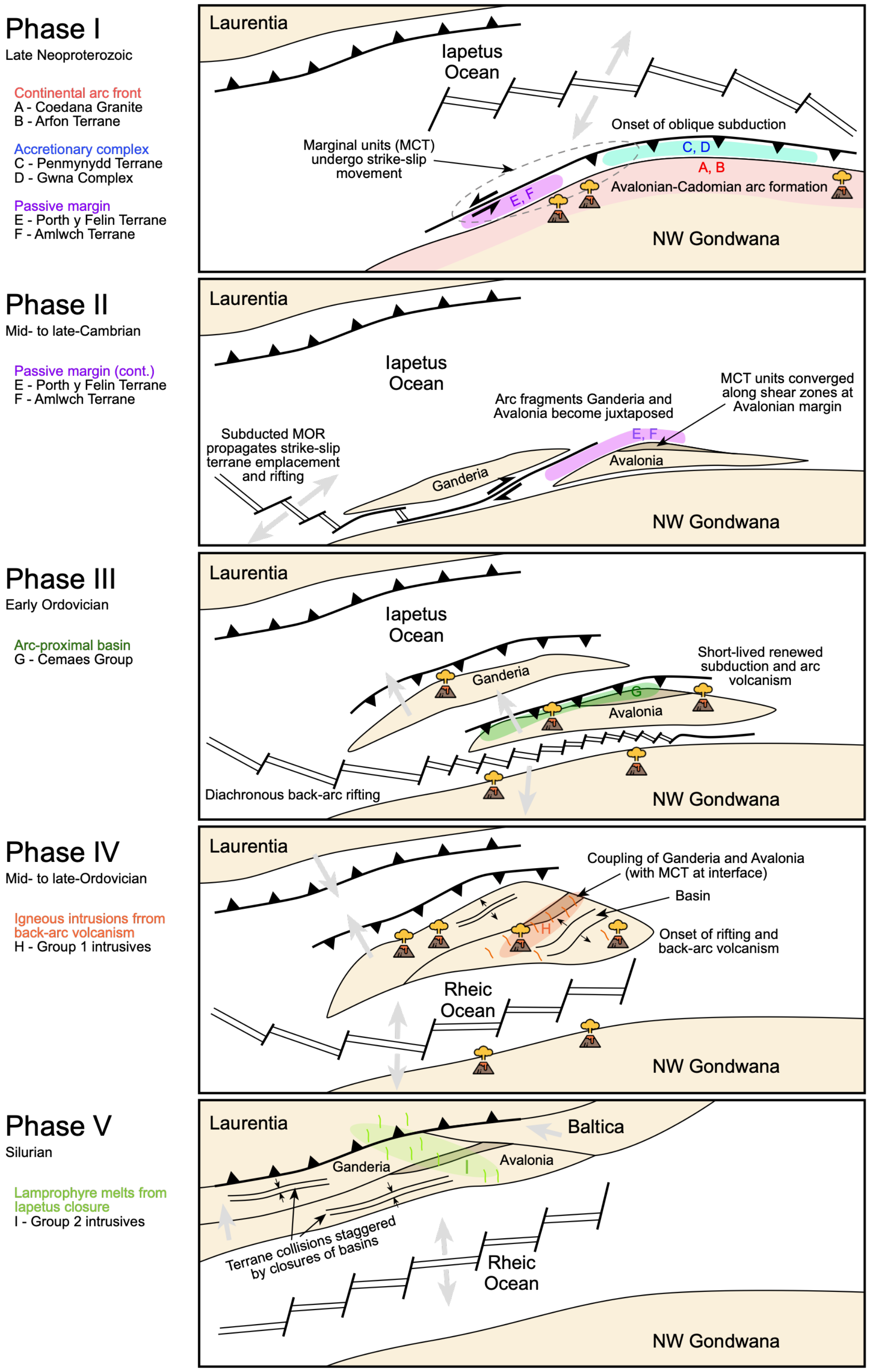

Figure 6.8: Schematic palinspastic model of the development of the peri-Gondwana rifting system showing five key phases of development between Late Neoproterozoic and Silurian. Units from the MCT, along with later arc-related intrusives, are marked by letters denoting the phase and environment of their formation. The model adopts a 'Baja-style' rifting mechanism, as discussed in Section 1.4.3 (Linnemann et al. 2008; Ackerman et al. 2019; Sánchez-García et al. 2019).

Phase I – Initial subduction

The initiation of subduction is recognised by the onset of continental arc magmatism in East Avalonia ca. 677 Ma (Tucker and Pharaoh 1991; Carney et al. 2000). Several breaks in magmatic activity through the late Neoproterozoic may represent episodes of soft arc-arc collision (van Staal et al. 2020). Late-stage Avalonian magmatism (ca. 570 – 550 Ma) coincides with the subduction of the Penmynydd Terrane (ca. 566 – 530 Ma) and formation of the Gwna Complex (from ca. 549 Ma), representing the earliest preserved indicators of subduction in the MCT (Dallmeyer and Gibbons 1987; Tucker and Pharaoh 1991; Compston et al. 2002; Asanuma et al. 2017; Dartnall 2018).

The Gwna Complex represents an accretionary system comprising OPS with varying components of oceanic and continent-derived material (see Figure 6.9). Recent studies have interpreted the Gwna Complex as an entirely sedimentary succession, with basaltic lenses entrained from the opening of an arc-proximal basin (Dartnall 2018; Schofield et al. 2020). However, repetitive imbrication of OPS units in Area I, along with rare but significant kinematic indicators indicate progressive tectonic underplating that is typical of accretionary complexes. Additionally, geochemical compositions of mafic rocks show no enrichment from subduction-related melts that would be expected in arc-related basins. Reconstructed OPS also records a complete ridge-trench transition, further indicating that the Gwna Complex comprises accreted sea floor material. Sequences do not contain assemblages of interbedded turbidites and volcanic rocks or bimodal magmatic products, as are common in rifting basins, or intrusive magmatic rocks apart from few localised examples, which have been discussed (see Section 5.1.4).

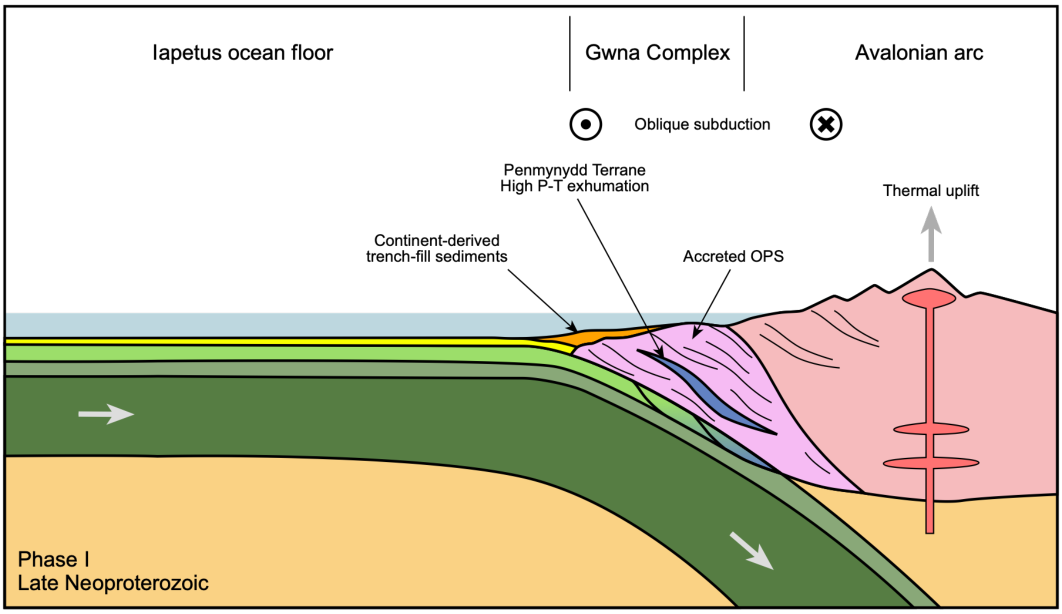

Figure 6.9: Schematic cross section of Phase I showing oblique subduction of the Iapetus ocean below the uplifting Avalonian arc on the continental margin of Gondwana, with accretion of Gwna Complex material and exhumation of High P-T Penmynydd Terrane material above the plate interface.

The Penmynydd Terrane is a key indicator of a subduction regime in the MCT and records peak deformation between greenschist and blueschist facies, comprising metabasites, dominant mica schists and subordinate chloritic schists and carbonates. Metabasites display rare pillow remnants and have very similar compositions to the Gwna Complex basalts, plotting within the MORB-OIB array. Metabasites and Gwna Complex basalts originate from the same oceanic source, exhibiting different subduction records from the same system (see Figure 6.9). Geochemical similarities also support the interpretation of the Gwna Complex being accretionary, if basalts from a shared source have undergone subduction and exhumation. Metasedimentary rocks surrounding the metabasic lenses are components of a similar OPS, with the dominant mica schists suggesting high input of continental material. Given the age of blueschist metamorphism on Anglesey, this would coincide with high rates of sediment input in early stages of Gwna Complex formation in Area II.

Reductions in continental sediment input between the formation of Area II and Area I coincide with the shutdown of East Avalonian and Ganderian arc magmatism (ca. 550 – 530 Ma) (Compston et al. 2002; Lin et al. 2007). Construction of the Welsh Basin around this time implies a tectonic shift that culminated in the cessation of subduction. In the aftermath, passive sedimentation led to the formation of the Porth y Felin and Amlwch Terranes (Phillips 1991b; Schofield et al. 2020).

Phase II – Transcurrent regime

The transition from a convergent to transcurrent regime during the Cambrian was gradual, and contemporaneous strike-slip terrane movement and late-stage Avalonian magmatism has been recognised (Gibbons and Horák 1990; O'Brien et al. 1994). In the MCT, the transcurrent regime is represented by NE-SW trending shear zones such as the MSFZ and BSZ, which were active mainly in the mid- to late-Cambrian. This led to the striking juxtaposition of Neoproterozoic and Cambrian terranes that characterises the MCT (see Figure 6.10). Inclusion of the Gwna Complex entirely within these strike-slip terranes indicates cessation of subduction in the early Cambrian.

Clasts of apparent felsic arc material and basement gneisses (Greenly 1919; Beckinsale and Thorpe 1979) entrained within the western margin of Penmynydd Terrane indicate interactions with fragments of continental arc along the BSZ during transcurrent shuffling of arc and arc-proximal slivers. This also led to the emplacement of the Coedana Terrane from the Avalonian arc into the centre of the MCT, surrounded by subduction-related rocks (Horák 1993; Gibbons and Horák 1996). Exhumation of the Penmynydd Terrane likely led to emplacement within the Gwna Complex as a paired metamorphic belt in an active subduction complex (Kawai et al. 2006; Kawai et al. 2007; Asanuma et al. 2015). Lack of clear high-angle faulting along the eastern margin with Gwna Complex Area IV may preserve this initial relationship, with the terrane being bound by high-angle shear zones elsewhere.

The Porth y Felin Terrane – and most likely the Amlwch Terrane – formed in response to unroofing and dissection of the East Avalonian arc during the transcurrent regime in a continental margin setting (Phillips 1991b). Subduction-centred tectonic models for the formation of the MCT (Kawai et al. 2006; Kawai et al. 2007; Asanuma et al. 2017) are limited by their omission of Cambrian transcurrent movement and arrangement of terranes. The model for the transcurrent organisation of older MCT units (Gibbons and Horák 1996) applies oblique subduction to account for simultaneous subduction and strike-slip activity. This would allow for the formation of the Gwna Complex and Penmynydd Terrane in subduction-dominated domains, while contemporaneous strike-slip sedimentation of the Porth y Felin Terrane is initiated in passive domains, with progressive strike-slip juxtaposition of the terranes along the continental margin.

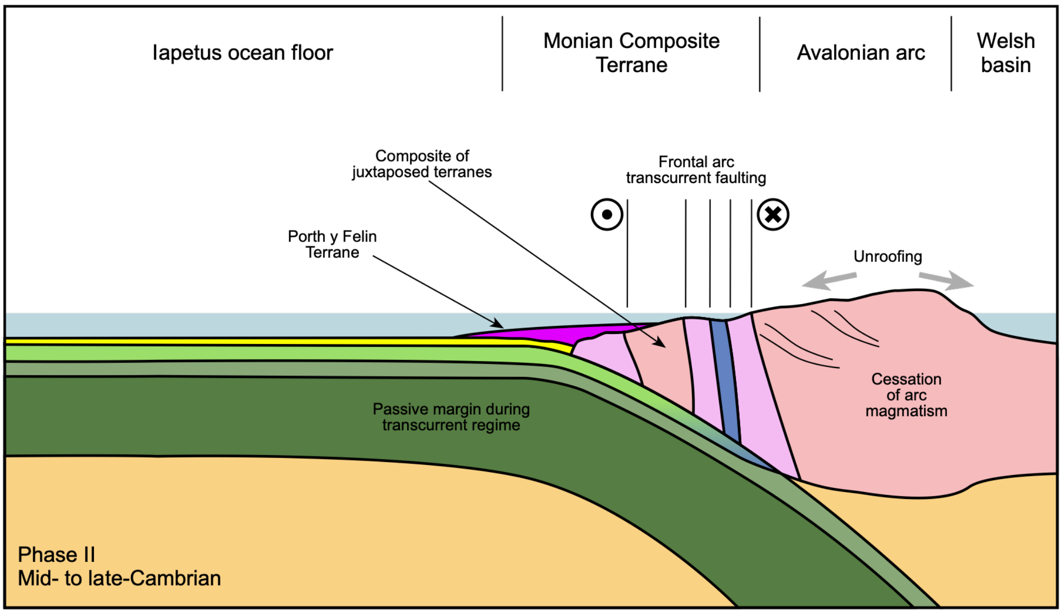

Figure 6.10: Schematic cross section of Phase II showing strike-slip juxtaposition of terranes along the Avalonian arc front including accreted and exhumed terranes along with arc fragments, while the Porth y Felin Terrane forms in a passive tectonic setting, leading to the assembly of the Monian Composite Terrane.

Phase III – Renewed subduction

Deposition of thick volcaniclastic sequences of the Porth Trefadog Formation seems to indicate the renewal of volcanic activity along the arc, and therefore the restarting of subduction (see Figure 6.11). The Cemaes Group post-dates Cambrian transcurrent deformation and is unconformably overlain by subaerial Floian sequences, suggesting an early Ordovician age. This would coincide with arc-related magmatic renewal in Snowdonia during the Tremadocian (Kokelaar 1988; Brenchley et al. 2006; Strachan 2012). The Porth Trefadog volcaniclastics are very compositionally similar to felsic-intermediate rhyolites proven to be produced in Snowdonia within the later Llewellyn Volcanic Centre (Howells et al. 1991). Volcaniclastic deposition grades into the olistostromal deposits of the Porth Swtan Formation during a period of uplift and tectonic instability. While the Cemaes Group formed within the vicinity of the arc, it is unclear whether it represents soft accretion at a continental margin or forearc basin deposition. It comprises entirely continentally derived clasts with no evidence of OPS accretion. Tonian carbonate clasts (Horák and Evans 2011) represent a change in sediment provenance, likely brought on by the relocation of cratonic sedimentary sequences from the arc interior to the continental margin during Phase II. The overlying angular unconformity favours a proximal basin setting, as opposed to a continental margin that would have remained active.

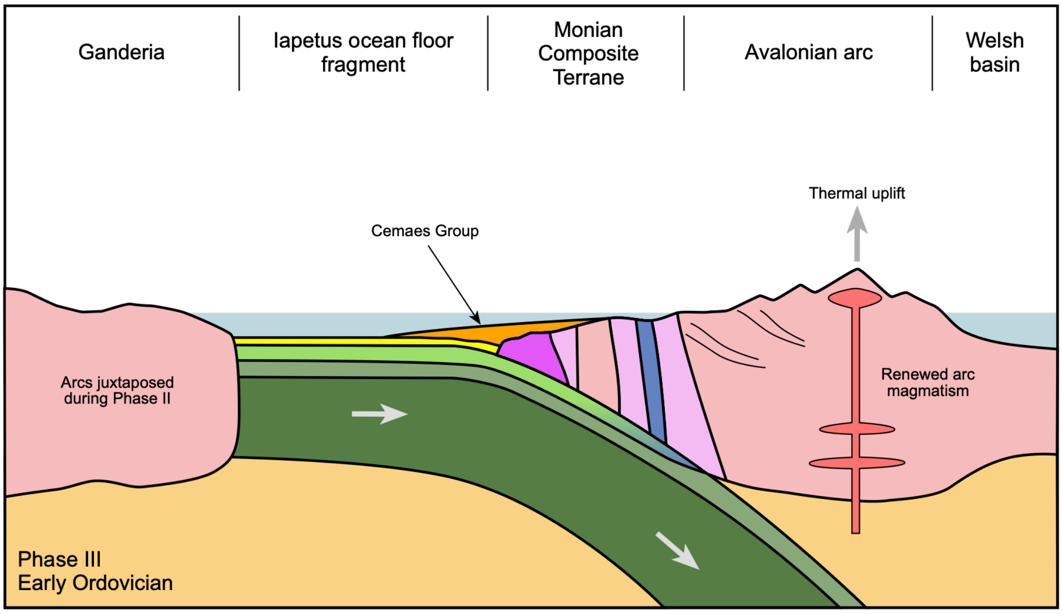

Figure 6.11: Schematic cross section of Phase III showing short-lived renewed subduction beneath the Avalonian margin, causing volcanism and uplift leading to the formation of the Cemaes Group.

Alternatively, the provenance of Porth y Felin Terrane material suggests a dominant sediment source to the north (Phillips 1991b). Formation of the Porth y Felin Terrane took place partly contemporaneously and partly after the formation of the Gwna Complex (Collins and Buchan 2004; Asanuma et al. 2017; Dartnall 2018; Schofield et al. 2020). Transcurrent movement of terranes was in part synmagmatic, facilitated by oblique subduction (Gibbons and Horák 1990). The presence of a northern source of still Gondwanan origin suggests that the MCT had been emplaced behind another frontal arc terrane during the transcurrent regime, likely Ganderia. This means that formation of the Cemaes Group may not represent renewed subduction in Avalonia, with the MCT spliced between coupled arc slivers (Strachan 2012). Short-lived Tremadocian arc magmatism, however, suggests that although these arc slivers were proximal, they were not connected by the lower Ordovician (Kokelaar 1988; Strachan 2012). The Cemaes Group is therefore likely indicative of short-term subduction renewal along the Avalonian margin as a result of arc magmatism and subsequent uplift.

Phase IV – Rifting of the peri-Gondwanan terranes

The transition from arc magmatism to back-arc basin magmatism in Snowdonia during the mid-Ordovician signifies the rifting of peri-Gondwanan landmasses from the margin of Avalonia (Kokelaar 1988; Howells et al. 1991; Thorpe et al. 1993b; Sánchez-García et al. 2003; Brenchley et al. 2006; Pollock et al. 2009; Strachan 2012; Sánchez-García et al. 2019). Dolerite dykes across Anglesey (Groups 1a and 1b) exhibit back-arc basin signatures that suggest an emplacement linked to this magmatic activity, more specifically related to the Snowdon Volcanic Centre (Howells et al. 1991). These dykes comfortably post-date rocks of the MCT. The Floian unconformity marks both the end of the MCT and the end of arc magmatism in Snowdonia, as Monian and Avalonian terranes are overstepped by correlating extension-related sedimentary sequences (Bates 1972; Beckly 1987; Pothier et al. 2015).

The apparent lack of accreted rocks within or around the vicinity of the MCT from this secondary subduction regime may indicate efficient net-passive rifting, or an erosive margin. Another possibility is that the progression of arc magmatism to back-arc basin magmatism in Snowdonia may signify the soft coupling of peri-Gondwanan landmasses, seeing East Avalonia – fronted by the MCT – dock with Ganderia to the north (see Figure 6.12). The Cemaes Group may therefore represent mélange developed at the continental margin that became accreted through this coupling. In the Sandbian stage, arc magmatism initiates across Ganderian Leinster-Lakesman Terrane, in Leinster, the Isle of Mann, the Lake District and eastern England (Branney and Soper 1988; Pharaoh et al. 1993; Barnes et al. 2006; Fritschle et al. 2018), suggesting the initiation of a main arc front along the northern margin of Ganderia (Brenchley et al. 2006; Strachan 2012).

Two models of peri-Gondwanan rifting were outlined in Section 1.4.3, including a 'Baja-style' rift system and a 'Caribbean-style' system. One major difference between the models is the rotation of landmasses. The Caribbean-style rifting requires rotation of landmasses, whereas the Baja-style model allows for simple translation. Area I of the Gwna Complex preserves consistent subduction polarity towards the SE, evinced by bedding-foliation asymmetry, progressive downstepping of OPS units and shear indicators, along with a consistent SE-dipping stratigraphy. Continuous unit orientations across multiple study localities can be used to infer a consistent SE subduction polarity for the Gwna Complex, despite local interferences in Areas II and IV, most likely through later deformation.

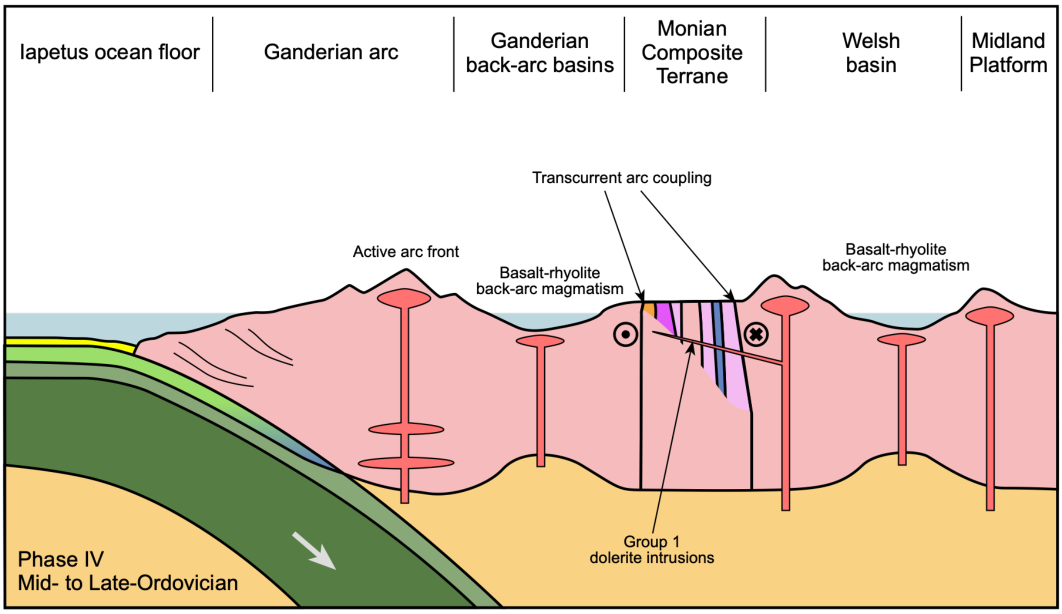

Figure 6.12: Schematic cross section of Phase IV showing rifted peri-Gondwanan landmasses (Avalonia and Ganderia) that have undergone arc coupling, resulting in cessation of arc magmatism in Snowdonia and accretion in the MCT.

Geographically, the MCT sits to the NW of Snowdonia and the Avalonian Composite Terrane, with perpendicularly striking subduction-related units. Additionally, to the SE of Avalonia sit Cadomian terranes, which remained along the Gondwanan margin after the departure of the Avalonian landmasses. Assuming that the Gwna Complex represents subduction along the margin of Gondwana – which provenance studies would suggest (Dartnall 2018; Waldron et al. 2019b) – and that it is backed by the East Avalonian arc (Gibbons and Horák 1996; Kawai et al. 2007), its subduction polarity has not changed relative to those landmasses. This would favour rifting in line with the Baja-style model, contrary to recent interpretations (Waldron et al. 2014b; Schofield et al. 2020).

To accommodate the Caribbean-style model, the MCT must either represent an East Avalonian back-arc environment, or the continental margin of Ganderia. The back-arc of East Avalonia is well defined by the Welsh Basin, which formed contemporaneously with the MCT from the Cambrian (Brenchley et al. 2006; Waldron et al. 2011; Pothier et al. 2015). It has been previously established that the Gwna Complex does not represent a back-arc basin. Additionally, the Gwna Complex does not show the correct subduction polarity to represent the rotated continental margin of Ganderia. A third possibility is that the Monian subduction complex formed at the front of an arc fragment involved in arc-arc collision with the Gondwanan margin, trapping the MCT between Ganderia and

Avalonia. The arc amalgamation could then have rotated through Caribbean-style rifting. However, combining the rotational arc-arc collision model of van Staal et al. (2020) with subsequent Caribbean-style rifting would require a total shift in rotational direction, effectively repeating rotational rifting in reverse. Additionally, relevant peri-Gondwanan arc-arc collisions would have occurred between 600 – 550 Ma, which predates ongoing Gwna Complex sedimentation.

A potential issue to resolve for Baja-style rifting is the placement of a mid-ocean ridge. The model uses the oblique subduction of a spreading centre as a mechanism of initiating rifting along the continental margin, following a transcurrent regime driven by strike-slip faulting between downgoing ridge segments (Sánchez-García et al. 2019). However, mid-ocean ridge subduction has also been presented as a possible explanation for rapid volcanic shutdown across Ganderia and East Avalonia in the Katian stage (Strachan 2012). Despite this, the Baja-style rift system is most appropriate to apply to the MCT and surrounding terranes, based on observations presented in this study.

Phase V – Collision with Laurentia

A lamprophyre intrusion marks the closure of the Iapetus Ocean as the peri-Gondwanan landmasses collide with Laurentia (Murphy et al. 2004; Nance et al. 2010; van Staal et al. 2012; Waldron et al. 2014a; Waldron et al. 2019a), as illustrated in Figure 6.13. Geochemical similarities with other lamprophyres of known age place the intrusion at ca. 430 – 390 Ma (Rock et al. 1988). The lamprophyres occur across Avalonian and Ganderian terranes, along with peri-Laurentian and Laurentian, representing the amalgamation of multiple landmasses along the Laurentian margin (Macdonald et al. 1985; Rock et al. 1988; Thorpe et al. 1993a; Shand et al. 1994). The Anglesey lamprophyre shows closer geochemical similarities to the Ganderian lamprophyres than those from other domains, perhaps indicating a close relationship upon reaching Laurentia, adding further evidence to the theory of a coupled arc during rifting (see Figure 6.12). Separation of the MCT and Arfon Terrane from East Avalonian terranes on the Midland Platform (southern Britain) likely led to staggered collisions with Laurentia (Waldron et al. 2019a). Lamprophyre compositional similarities between Anglesey and those in the Lake District, rather than in the southern Avalonian terranes, is likely a reflection of this staggered collision and resulting lamprophyric magmatism.

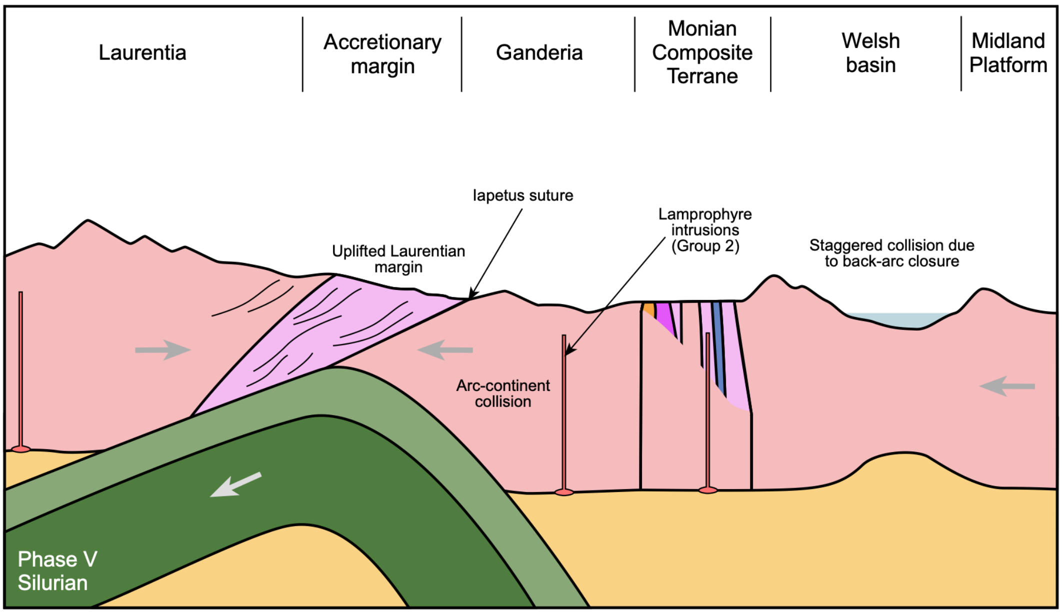

Figure 6.13: Schematic cross section of Phase V showing the staggered collision of peri-Gondwanan terranes along the margin of Laurentia, leading to closure of the Iapetus ocean and production of lamprophyric melts (Group 2).

CHAPTER VII
Geoheritage on Anglesey – GeoMôn collaboration

7.1 OVERVIEW OF GEOHERITAGE ON ANGLESEY

GeoMôn is a UNESCO Global Geopark that encapsulates the Isle of Anglesey, having held the status since 2010. The aim of GeoMôn is to promote tourism and education for the benefit of Anglesey's economy and heritage (Campbell et al. 2017). It promotes the incredibly diverse, condensed geology and geomorphology of the island and has erected information boards in thirteen sites, with some sites including geotrails. As with many geoparks in the UK, GeoMôn struggles somewhat with general awareness of geoheritage in relation to comparable ecological heritage sites and organisations (Wimbledon and Smith-Meyer 2012). Crucial identified methods of increasing the visibility and awareness of the geopark include boosting its presence at key geosites and improving online resources.

The Isle of Anglesey features some spectacular and popular geosites such as Parys Mountain and South Stack. Among these, one of the most important geosites is Newborough Nature Reserve. The site is a major tourist attraction for the island, with an estimated 450, 000 visitors in 2017 (data provided by Natural Resources Wales). The site is seen as a prime locality to raise the profile and awareness of GeoMôn, while better showcasing the incredible geology of the geosite to a larger audience. A major scientific focus of this project has been the Gwna Complex, which includes Newborough Nature Reserve. The collaboration with GeoMôn for this project at this site will use scientific findings from mapping and sampling across the site to influence decisions on increasing the geoheritage value of the site.

7.1.1 Newborough as a geoheritage site

Llanddwyn Island has long been recognised as an important geosite on Anglesey. It has long held GCR status and has been a key locality in numerous scientific studies (Carney et al. 2000; Kawai et al. 2008; Maruyama et al. 2010a). Two iterations of field guides of Anglesey have also included recommended trails around the island (Treagus 2008; Campbell et al. 2017). Llanddwyn Island is also a popular fieldtrip destination for schools, universities, and general interest groups. Despite its status, the adjacent Gwna Complex geology that continues inland into Newborough Forest is relatively obscure.

Extensive geological mapping and sampling of Newborough Nature Reserve (Gwna Complex Area I) in Chapter 2 highlighted the continuation of the geology of Llanddwyn Island northwards into Newborough Forest. While Llanddwyn Island was a key locality in observing disordered mélange, outcrops in Newborough Forest display key preserved stratigraphic relationships, which were crucial to reconstructing the OPS of the Gwna Complex in Chapter 6. Included in these key relationships are the transitional relationship between pillow basalts and overlying carbonates, the rip-out clasts of chert within sandstones and the continuation of hyaloclastites at the base of volcanic domains. In addition, rock types such as silty mudstone, siliciclastic sandstone and massive basalt on a mappable scale do not occur on Llanddwyn Island. These relationships, while somewhat implied on Llanddwyn island, provide much greater certainty to an overall geological story of the Gwna Complex. Many of the relationships and rock types are observed towards the top of Unit 4, which marks the continuation from Llanddwyn Island and the pillow basalts along the causeway. Uncovering these crucial relationships and geological continuation has enabled this section of Newborough Forest – roughly equating to the bounds of Unit 4 – to be included into the Newborough Warren GCR site and the Newborough & Llanddwyn RIGS.

7.1.2 Geopark presence in Newborough

One of thirteen GeoMôn 'geoboards' is stationed along the northern coast of Llanddwyn Island. The pilot's cottages – which are typically accessible seasonally – in the south of the island also contain several information boards about the site. Two iterations of geotrail recommendations for Llanddwyn Island have been published on with involvement from GeoMôn (Treagus 2008; Campbell et al. 2017) and some online information is also available, although there is no additional on-site infrastructure to accompany the trails. Resources to encourage engagement from passive visitors – which make up the vast majority of traffic – are otherwise limited.

In Newborough Forest, a short, linear geotrail runs along dirt path with very low traffic, skirting along the upper parts of Unit 4c. Although it is referred to briefly in field guides (Campbell et al. 2017), very little additional information is readily available and no signage exists to find the trail from higher traffic areas. With the geoboard and pilot's cottages both residing on Llanddwyn Island – which is inaccessible at high tide – those visitors who do not visit the island have very limited exposure to geological information throughout the site.

GeoMôn runs sporadic geological tours of the site for a wide range of audiences including geopark members, school fieldtrips, casual interest groups and research groups. These geological tours typically involve visiting localities in Newborough Forest and on Llanddwyn Island. As of writing, however, there is no geotrail in place that connects the areas, despite both being essential in providing a full geological story of the site. A new geotrail that links the most important localities of Newborough Forest and Llanddwyn Island is therefore proposed, with accompanying on-site and online material.

7.2 GEOTRAIL ASSESSMENT

The proposed geotrail will aim to utilise both the scientific significance and practical benefits of both areas. While Llanddwyn Island is overwhelmingly popular, particularly with passive visitors, it has the drawback of accessibility issues. Newborough Forest can therefore compensate for this, ensuring that the geotrail can always be engaged.

7.2.1 Geotrail placement justifications

Figure 7.1 shows the geological map of Newborough (presented in Chapter 2) with existing footpaths overlain. A series of 31 potential localities have been identified on the map. The localities were chosen based on having reasonable access from an existing footpath, and an outcropping area that could be comfortably and clearly observed by multiple visitors at a time. Potential trail routes have been applied to best link the potential localities. An overview of selected localities can be found in Table 7.1.

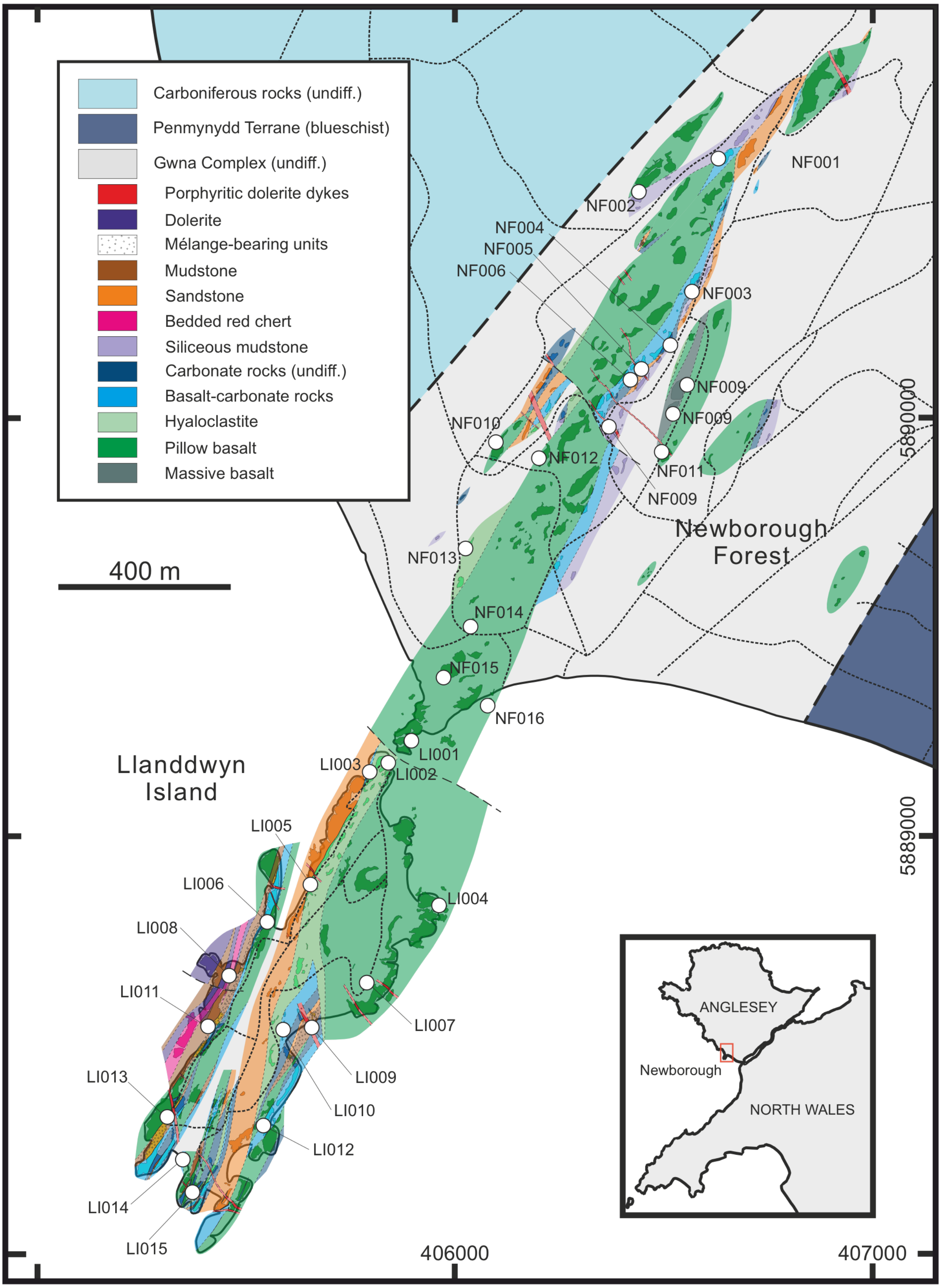

Figure 7.1: Geological map of Newborough Nature Reserve geosite with existing paths overlain and potentially suitable geotrail localities identified.

Table 7.1: Overview of selected potential localities for Newborough Nature Reserve geotrail proposal. Localities 'NF' located in Newborough Forest; localities 'LI' located on Llanddwyn Island.

Locality	Main features	Description
NF001	Multiple lithologies	Large outcrops of sandstones, basalt-carbonates, silty mudstones and pillow basalts in fenced area. Outcrops separated with no clear contacts. Large sizes and good exposure show variety of characteristics for multiple lithologies. Good, clear access from main pathway.
NF002	Volcs – pillow lavas	Towering pillow lava face showing deformed pillows in fenced area with lots of vegetation obscuring pathway. Situated close to main pathway.
NF003	Carbonates	Relatively small basalt-carbonate and carbonate outcrop showing good lithological transition but poorly maintained.
NF004	Carbonates	Large cliff exposure of carbonates with impressive jasper deposits throughout and occasional pillow lava. Evidence of Neolithic cave visible in cliff face.
NF005	Basalt-carbonates Dykes	Excellent pillow lava – carbonate transition visible in backwall, along with dolerite dyke. Outcrop is approx. 50 m from pathway up moderate slope.
NF006	Basalt-carbonates	Backwall and boulders with intricate basalt-carbonate interaction textures, along with outcrops along floor of sandstones and silty mudstones including key evidence for stratigraphic relationships. Access up moderate slope from pathway.
NF007	Volcs – lava flow	Potential occurrence of columnar jointing in massive basalt. Feature is speculative and not clearly presented. Easy access but outcrop overgrown.
NF008	Volcs – lava flow	Massive basalt that is locally autobrecciated. Jasper and Fe-rich deposits along joints create colourful outcrop. Easily accessed from dirt path.
NF009	Sedimentary rocks	Striking outcrop of silty mudstone showing intricate folding and soft-sediment deformation, situated at corner of dirt pathways. Photos of outcrop that predate the forest provide a point of historical/cultural value.
NF010	Volcs – pillow lavas	Pillow basalts in gently dipping cliff face along main pathway. Cliff face orientated along strike of pillows so clear shapes are difficult to observe.
NF011	Volcs – pillow lavas Dykes	Well exposed, contained pillow basalt outcrop with shapes visible in three dimensions and clear interpillow jasper. Also hosts dolerite dyke. Opposite small pond of ecological interest.
NF012	Volcs – pillow lavas	Good exposure of pillow basalts in face of headland accessed 50 m from dirt path across moderate vegetation cover. Has historical aspect of images from Greenly's fieldwork, showing area before forest was planted and covering significance of history of geological studies on Anglesey.
NF013	Volcs - hyaloclastite	Hyaloclastites exposed in contained outcrop next to main pathway with good access and exposure in three dimensions.
NF014	Volcs – pillow lavas	Mound of pillow lavas along main pathway that are smaller and less extensive than those on the causeway, but more easily accessible and sheltered.
NF015	Volcs – pillow lavas	Continuation of pillow lavas onto sand dunes and causeway, accessed along routes across soft sand with multiple excellent, large exposures that can be viewed in three dimensions. (Linked with LI001).
NF016	Volcs – pillow lavas	Small outcrop of pillow lavas on beach that are less impressive than the main causeway outcrops but have good exposures of interpillow jasper and epidote.

Table 7.1 continued.

Locality	Main features	Description
LI001	Volcs – pillow lavas	Excellent, extensive pillow lavas exposed along causeway in multiple easily accessible outcrops. (Linked with NF016).
LI002	Volcs - hyaloclastite	Headland around inlet shows sheared hyaloclastites with numerous hand specimen-sized fragments on ground that display intricate volcanic textures.
LI003	Volcs - hyaloclastite	Continuation of LI002 along beach, where headland shows clearer sea washed examples of hyaloclastite textures along with sheared lower contact. Only accessible at low tide.
LI004	Volcs – pillow lavas	Multiple headlands of pillow lavas along beaches to explore extensive volcanic features. Requires low tide and partly inaccessible seasonally.
LI005	Shearing & mélange	Sheared contact between sandstone and hyaloclastite visible between pathway and small dropdown to beach.
LI006	Shearing & mélange	Viewpoint overlooking sheared ridge showing the extent of deformation along strike with view, easily visible next to pathway if prompted.
LI007	Volcs – pillow lavas	Alternative pathway (with some steps) across island winds through region of pillow lavas, with exposures on island and over headland along coast. Excellent viewpoint to observe several fine examples of raised beaches.
LI008	Sedimentary rocks	Excellent red cherts exposure on headland overlooking coast, a short deviation from pathway. Headland can be explored further but on less accessible terrain, showing colourful mudstones and doleritic sills.
LI009	Dykes	Outcrop protruding between two bays structured around large planar dolerite dyke clearly crosscutting Gwna material. Bay has excellent views across Snowdonia and is good observation point for marine wildlife.
LI010	Basalt-carbonate	Basalt-carbonate transition exposed in cliff face and surrounding boulders along back of bay. Access limited seasonally and difficult to approach cliff.
LI011	Shearing & mélange Sedimentary rocks	Headland of bay showing multiple lithologies including colourful sheared mudstones, carbonates, hyaloclastites and basalts. Includes mélange-bearing mudstones that can be seen clearly on way back. Involves descent downhill from path and small amount of scrambling, only accessible with low tide.
LI012	Basalt-carbonate	Cliff face exposure of sheared basalt-carbonate rocks with scattered outcrops on beach show intricate relationships between rocks related to their deformation, but primary transition not clear. Low tide needed.
LI013	Shearing & mélange Volcs – pillow lavas Dykes	Low-lying rocky headland showing mélange-bearing mudstones and vesicular pillow lavas, along with carbonates and basalt-carbonates at the base of Llanddwyn lighthouse. Dolerite dyke also crosscuts the locality. Some exposures require low tide and area not easy to manoeuvre around.
LI014	Shearing & mélange	Striking, clearly defined outcrop of deformed pillow lavas at centre of bay, accessed across beach. Pillows show range of features such as large amounts of interpillow jasper or carbonates, along with intense carbonate veining.
LI015	Shearing & mélange Dykes	Spectacular mélange exposure across bay in headland and scattered outcrops along beach showing vivid colours of contrasting lithologies and extreme deformation features. Dolerite dyke with multiple generations of magmatism crosscuts area. Best seen at low tide.

While any trail route of Llanddwyn Island is largely dictated by its size and available pathways, Newborough Forest is much more expansive. The pathway of the current forest geotrail runs along a critical area of geological significance, also with relatively good exposure close that sits close to an existing pathway. This area is necessary to include in the new proposed geotrail. A major drawback of the current forest geotrail is its lack of connections to main walkways. There are several options to link the forest geotrail to the causeway for access to Llanddwyn Island. These options showcase different geological aspects and will be considered as potential trail routes. Two potential forest trails have therefore been proposed, and the relative value of each will be determined in order to recommend the best option. Outside of the outcrops covered in these two options, other outcrops such as around Units 1, 6 and 7 are not particularly viable for a trail route. Each would considerably increase the length of the trail, are not well exposed and do not add any new information that is not covered elsewhere to some extent.

The proposed geotrail will incorporate both Newborough Forest and Llanddwyn Island as a single trail but will ideally be split between the two regions (Llanddwyn Island – Ynys; Newborough Forest – Coed). These regions will act as their own shorter, contained geotrails for those who cannot – or do not wish to – engage in the full trail. Suitable trail route options based around potential localities are outlined in Figure 7.2. To design the proposed geotrail, potential localities will be evaluated to determine their relative value across a range of factors.

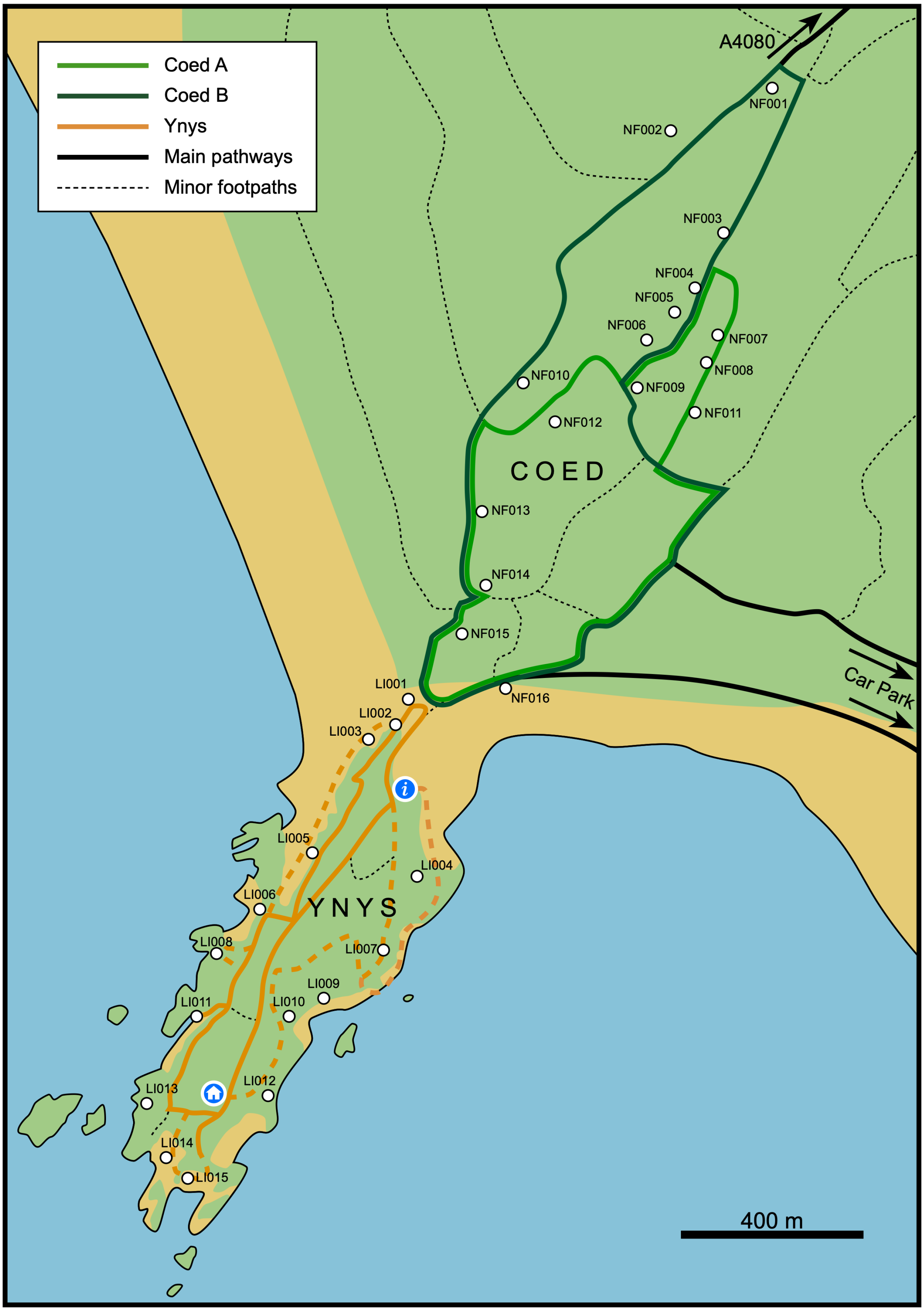

Figure 7.2: Potential localities and trail routes for Newborough Nature Reserve geotrail proposal.

7.2.2 Assessment criteria for evaluating localities

Since the 1980's, geoconservation, geoheritage and geotourism has developed into an increasingly expanding field globally, largely due to the creation of geoparks through organisations such as UNESCO, IUGS and ProGEO, amongst others. On a national scale in the UK, this was propagated by the introduction of SINCS and RIGS (Burek 2008), along with GCR sites (Wimbledon et al. 1995). As a result, methods of evaluating the potential value of geosites quantitatively have since been developed to assist in preserving, promoting, and managing sites of geological/geomorphological significance, known as geosites. Early methods focused on scientific significance to quantify the value of a site, generally based around the conservation of geosites (Wimbledon et al. 1999; Panizza 2001; Coratza and Giusti 2005). More recently, as geotourism has subsequently increased in popularity, studies have been conducted to determine the values sought from geosites (Hose 2008; Mao et al. 2009; Dowling 2011; Dowling 2013). The need to adapt evaluation methods to consider other factors such as aesthetic value and tourist potential has been realised and implemented (Pralong 2005; Różycka and Migoń 2014; Mikhailenko et al. 2017). Recent attempts to create a comprehensive assessment scheme for geosites aim to balance these values between the interests of the wide variety of potential visitors, from academic researchers to passive tourists (Pereira et al. 2007; Reynard et al. 2007; Kubalíková 2013; Tomić and Božić 2014; Miljković et al. 2018; Suzuki and Takagi 2018).

Geosite evaluation schemes are generally intended to be applied to overall sites, but have also been used to evaluate subsites within geosites (Reynard et al. 2007; Suzuki and Takagi 2018). Evaluation of potential geotrail localities in Newborough will use an adaptation of these published evaluation schemes to determine relative values of selected localities. The aim will be to determine which sites demonstrate enough value to include in the trail and to identify issues within the geotrail that will require management. While the numerous iterations of comprehensive geosite evaluation schemes are flexible in their application, they are often based around generalised criteria as a result. When assessing localities within a single geosite, the criteria can be modified to accentuate the overall values and conditions of the site. For example, if distance between sites is a consideration, values can be assigned based around appropriate distance ranges for that site, rather than using generalised ranges that produce a lower resolution in results. Additionally, factors such as economic value in terms of generated income or tourist numbers (Reynard et al. 2007; Fassoulas et al. 2012) are not applicable as they can only realistically be determined for the geosite as a whole.

Evaluation criteria have been developed using both qualitative and quantitative methods. In order to quantitatively determine values related to intangible values such as importance and beauty, measurable values must be implemented that pertain to the value (Bruschi and Cendrero 2005). The assessment criteria aim to use measurable values wherever applicable in order to manage ambiguity and biases.

Sites will be evaluated based on six key principles: educational value, scientific value, tourism value, aesthetic value, accessibility, and state of conservation. Educational and scientific values may appeal more towards experts and informed visitors, while tourist and aesthetic values may be favoured by unaware or casual visitors. Accessibility and conservation values are more related to practicalities and site management purposes. Each principle will be divided between three subcategories. A score from 1 – 4 will be attributed to each subcategory, where a higher score reflects greater value. Each principal value is therefore scored out of 12, giving localities an overall score out of a maximum 72. The assessment criteria for each principal value are discussed below. Table 7.2 details the evaluation and scoring criteria for each of the six principal values.

Table 7.2: Scoring and evaluation criteria for potential geotrail localities.

ID	Value	Scoring criteria			
		1	**2**	**3**	**4**
Ved	**Educational value**				
Ved1	Representativeness	None	Unusual/ less relevant feature	Important/ repeated feature	Key feature to overall story
Ved2	Number of features	No educational features	Single feature	Two features	More than two features
Ved3	Suitable number of visitors	0-5	5-20	20-50	>50
Vsc	**Scientific value**				
Vsc1	Rarity of features	Not unique to region	Not unique to area	Not unique but prime example	Only example in area
Vsc2	Clarity of understanding	None	Speculative	Multiple interpretations	Established understanding
Vsc3	Significance to understanding	No bearing	Mapped and sampled	Featured in observations	Featured in discussion
Vto	**Tourist value**				
Vto1	Ecological heritage	None	Single minor feature	Multiple/major features	Well-known feature
Vto2	Cultural/historic importance	None	Single minor feature	Multiple/major features	Well-known feature
Vto3	Nearby activities	None	Near minor pathway	Near major pathway	Near active visitor spots
Vae	**Aesthetic value**				
Vae1	Aesthetics of outcrop	Scattered or unclear outcrops	Outcrop area poorly defined	Visually clear outcrop area	Obvious outcrop with striking appearance
Vae2	Ease of recognising features	Difficult with guide	Noticeable with guide	Clear with prompt	Clear without explanation
Vae3	Aesthetics of locality	Views give negative perception	No significant features in plain landscape	Great view in plain landscape	Great view of distant landscape
Vsa	**Safety & accessibility**				
Vsa1	Condition of access	Some scrambling	Access off path (difficult)	Access off path (easy)	Direct access from path
Vsa2	Distance between localities	> 500 m	250 – 500 m	100 – 250 m	< 100 m
Vsa3	Limiting factors	Often inaccessible	Inaccessible seasonally/at mid tide	Periodic limited exposure/access	No limitations
Vss	**Sustainability**				
Vss1	Access maintenance	Route needs improvement	Overgrown or damaged route	Occasional route maintenance needed	No maintenance foreseen
Vss2	Outcrop maintenance	No/poor outcrop visibility	Features obstructed	Visible, needs maintaining	Clear exposure
Vss3	State of protection	None	SSSI	RIGS	GCR

Ved: educational value

Educational values focus on how useful a locality is regarding an overarching geological story for the site. Representativeness (Ved1) determines the importance of the features at a locality to the overall story, ranking from no importance to crucial (Pralong 2005; Serrano and González-Trueba 2005; Pereira et al. 2007; Vujičić et al. 2011). Number of features (Ved2) is an intrinsic value recording the number of distinct educational observations at a locality (Bruschi and Cendrero 2005; Pereira et al. 2007; Różycka and Migoń 2014). Localities with multiple lithologies or textural features, for example, will score higher in this category than localities with a single feature.

As mentioned, GeoMôn runs geological tours in Newborough, and this proposed geotrail will provide a basis for those trips. Additionally, schools and universities regularly visit Anglesey for geological fieldtrips. The suitable number of visitors (Ved3) as a value accounts for the area and form of a locality, along with considerations for any vulnerability in preserving a locality (Vujičić et al. 2011). This is an important consideration when organising tours or fieldwork.

Vsc: scientific value

Rarity (Vsc1), or uniqueness, refers to how many similar localities exist both across the geosite and across the regional area of Anglesey (Reynard et al. 2007; Tomić and Božić 2014; Miljković et al. 2018). Pillow lavas, for example are common across the geosite but are rarely found elsewhere, whereas dolerite dykes are common occurrences both in the geosite and across Anglesey. Localities with outstanding examples of common features will be valued above others. Scoring for this category will consider individual areas rather than the whole geosite in consideration of visitors undertaking the trail is a single area only.

Clarity of understanding (Vsc2) relates to the certainty of understanding of an outcrop, where poorly understood outcrops score lower. Those that are well understood, where features and interpretations can be confidently communicated without ambiguity will score highly. Clarity of understanding and rarity are commonly used criteria in scoring the scientific value of a geosite (Pralong 2005; Zouros 2007).

Scientific value (Vsc3) is commonly quantified in part on the basis of scientific publications, where more recognised or higher impact publications score higher (Bruschi and Cendrero 2005; Rybár 2010; Różycka and Migoń 2014; Suzuki and Takagi 2018). This factor cannot be properly considered on an outcrop-scale basis. As a substitute, scientific significance will score the importance of localities to this study, given that it provides the first comprehensive geological study across both areas, scored on whether an outcrop was mapped, sampled, or featured in observations or discussions. On a larger scale, the Ynys trail area would score highly through studies of Llanddwyn Island being published in journals such as Gondwana Research (Kawai et al. 2008) and Geological Society of London Special Publications (Maruyama et al. 2010a). In contrast, the relatively uncovered geology of the Coed trail would score low, despite being geologically continuous.

Vto: tourist value

Tourist value is crucial to public engagement, particularly with passive tourists and those with casual interest. The values of both ecological (Vto1) and historic/cultural (Vto2) significance consider factors that broaden the interests of a locality, raising its passive appeal. While these values may be considered together (Różycka and Migoń 2014; Suzuki and Takagi 2018), they are typically approached as separate values where historic/cultural value may be divided further (Bruschi and Cendrero 2005; Reynard et al. 2007; Miljković et al. 2018). While the entirety of the geosite is part of a nature reserve, some localities may incorporate additional ecological or geomorphic significance. Historical/cultural values consider factors that are both related and unrelated to the geological story of the geosite, as demonstrated in Figure 7.3a.

The value of nearby attractions (Vto3) relates to the positioning of localities relative to visitor traffic and is therefore also important in the potential to engage passive tourists. While this value typically applies to major attractions near large-scale geosites (Rybár 2010; Tomić and Božić 2014; Suzuki and Takagi 2018), the same principles can be applied to a smaller locality-sized scale here. Major attractions at the site, such as Goleudy Twr Mawr (lighthouse on Llanddwyn Island), draw visitors, so nearby sites have a higher potential to engage visitors. Localities on major paths will experience greater visibility than those on minor pathways, while localities off pathways are likely to be visited only by engaged visitors who actively seek them.

Vae: aesthetic value

The aesthetic values of a locality refer to the visual appeal of the locality along with the ease to approach and observe an outcrop and its features. Outcrop aesthetics (Vae1) are difficult to characterise objectively and apply to not only the beauty of an outcrop – based on the prominence of shapes, colours and textures, such as those in Figure

7.3b (Pralong 2005; Reynard et al. 2007) – but also the ease of identifying, viewing and moving around an outcrop based on its form and accounting for any obstructions (Vujičić et al. 2011; Tomić and Božić 2014). Ease of recognising features (Vae2) scores how clear and apparent geological features are to visitors and is linked broadly to outcrop aesthetics, accounting for more of an educational aspect as opposed to touristic.

Location aesthetics (Vae3) – separate from outcrop aesthetics – values beauty of the surrounding area, with more beautiful surroundings valued higher by visitors. This is often weighted by number of viewpoints within range of a geosite (Vujičić et al. 2011; Tomić and Božić 2014), but more arbitrary classifications describing the quality of landscapes have also been used (Reynard et al. 2007; Rybár 2010) and would be more appropriate here.

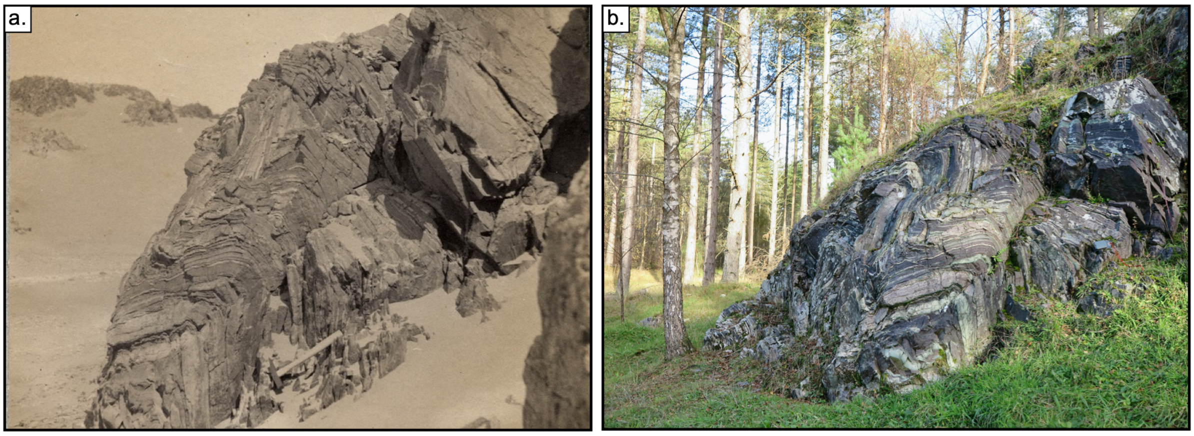

Figure 7.3: Locality NF009 demonstrating (a) historical heritage through old images from the field excursions of Edward Greenly predating the plantation of Newborough Forest and (b) high outcrop aesthetic value through vivid, contrasting colour of folded sedimentary layers. Image from 7.3a sourced from BGS archives.

Vsa: safety & accessibility value

Safety is of course a key aspect that must be accounted for in any proposal. At Newborough, potential localities and trails pose no significant safety issues beyond those expected from an outdoor trail and will not be a major factor in scoring criteria. The largest risk is the tidal nature of Llanddwyn Island, however ample warning measures are already in place. The tide does significantly limit accessibility however, and to ensure fair scoring of coastal localities, additional limitations (Vsa3) will consider the reduced accessibility or exposure of a locality at mid tide as opposed to high tide. Additional limitations also consider other factors such as inaccessibility due to seasonal nesting.

Condition of access (Vsa1) refers to how easy a locality is to reach, and therefore how many people will have the ability to access it (Bruschi and Cendrero 2005; Rybár 2010; Suzuki and Takagi 2018). While some criteria account for the presence of footpath markings or signposts (Różycka and Migoń 2014), this will not be considered here, and the issue of infrastructure will be covered in Section 7.3.

Distance between localities (Vsa2) scores the average distance between the nearest two localities, where shorter distances are preferable (Różycka and Migoń 2014; Suzuki and Takagi 2018). Appropriate distances were chosen based on the range between localities.

Vss: site sustainability value

Site sustainability relates to any potential upkeep and maintenance that may need to be considered at a given locality (Pereira et al. 2007; Reynard et al. 2007; Różycka and Migoń 2014). Access (Vss1) and outcrop maintenance (Vss2) score the likelihood of a locality or pathway deteriorating and consider initial improvements that would need to be made. Unkept pathways may reduce or restrict accessibility, hide direction signs or information boards, and may impact location aesthetics. Unkept outcrops will have a reduced aesthetic value, becoming less visually impressive and potentially masking important features. More importantly, they risk being damaged over time, diminishing the value of a locality. While site management is ultimately in control of these factors, outcrops with less need for maintenance are preferable, and localities which score low should be highlighted to site management.

The state of protection (Vss3) will be determined by the degree of conservation that protects a locality (Coratza and Giusti 2005; Zouros 2007; Rybár 2010). Newborough Nature Reserve is a well-protected site, and all its land is managed by Natural Resources Wales. Outcrops considered for the geotrail all fall under some forms of conservation protections. Localities of Newborough Nature Reserve are designated into up to four states of conservation. The Anglesey AONB (area of outstanding natural beauty), encompasses the majority of the island's coastline, including Newborough Nature Reserve. The site (Newborough Warren – Ynys Llanddwyn) is also a designated SSSI (site of special scientific interest). The boundaries of these sites are shown in Figure 7.4. Llanddwyn Island and western parts of Newborough Forest also have RIGS (regionally important geological/geomorphological site) and GCR (geological conservation review site) classification, although not all outcrops mapped fall within these site boundaries. RIGS are considered to be secondary to GCR sites in terms of preservation importance, and SSSI's have been largely replaced by the latter designations in terms of importance since their conception (Wimbledon and Smith-Meyer 2012).

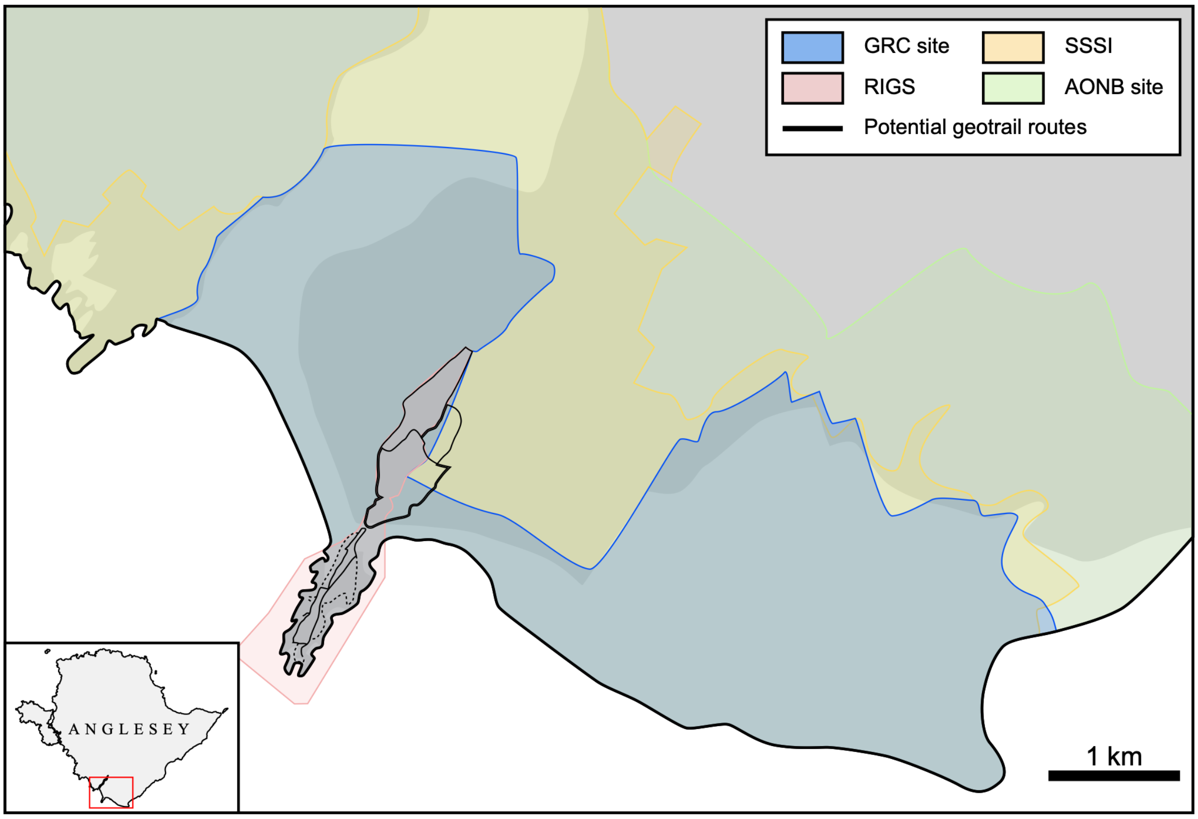

Figure 7.4: Delineation of current conservation sites across SE Anglesey. Data published by Natural Resources Wales.

7.2.3 Evaluation of potential localities

Table 7.3 outlines the scores for each value for the selected potential geosite localities, also assigning an overall score (Vsum). Suzuki and Takagi (2018) introduced a hexagonal visual representation of evaluation results that highlights the strengths and shortcomings of individual values of a site. This approach has been adapted in Figures 7.5 and 7.6, which shows the evaluation results of selected localities for the prospective Newborough Nature Reserve geotrail from Newborough Forest (Coed) and Llanddwyn Island (Ynys) respectively.

Table 7.3: Evaluation scores for potential geosite localities.

Locality	Ved	Vsc	Vto	Vae	Vsa	Vss	Vsum
NF001	10	7	6	7	6	9	45
NF002	7	9	6	7	4	8	41
NF003	7	8	5	7	10	10	47
NF004	8	10	7	9	11	8	53
NF005	10	12	5	10	10	10	57
NF006	9	11	5	8	10	9	52
NF007	5	5	5	6	11	6	38
NF008	8	11	5	8	11	9	52
NF009	8	10	6	10	11	11	56
NF010	7	8	6	7	9	10	47
NF011	8	9	6	9	12	7	51
NF012	7	9	7	9	9	9	50
NF013	9	11	6	9	10	11	56
NF014	9	8	6	10	10	11	54
NF015	10	10	7	12	11	12	62
NF016	8	9	6	11	11	12	57
LI001	10	10	7	12	11	12	62
LI002	8	9	6	8	11	12	54
LI003	10	10	6	9	8	12	55
LI004	9	8	6	11	4	12	50
LI005	8	11	5	7	8	11	50
LI006	8	9	6	10	10	11	54
LI007	7	8	6	10	10	11	52
LI008	10	11	5	8	9	10	53
LI009	8	7	6	10	6	12	49
LI010	7	8	7	9	6	10	47
LI011	10	11	8	8	6	9	52
LI012	6	8	5	9	7	12	47
LI013	9	10	8	8	8	11	54
LI014	7	9	10	11	10	12	59
LI015	11	10	9	11	8	12	61

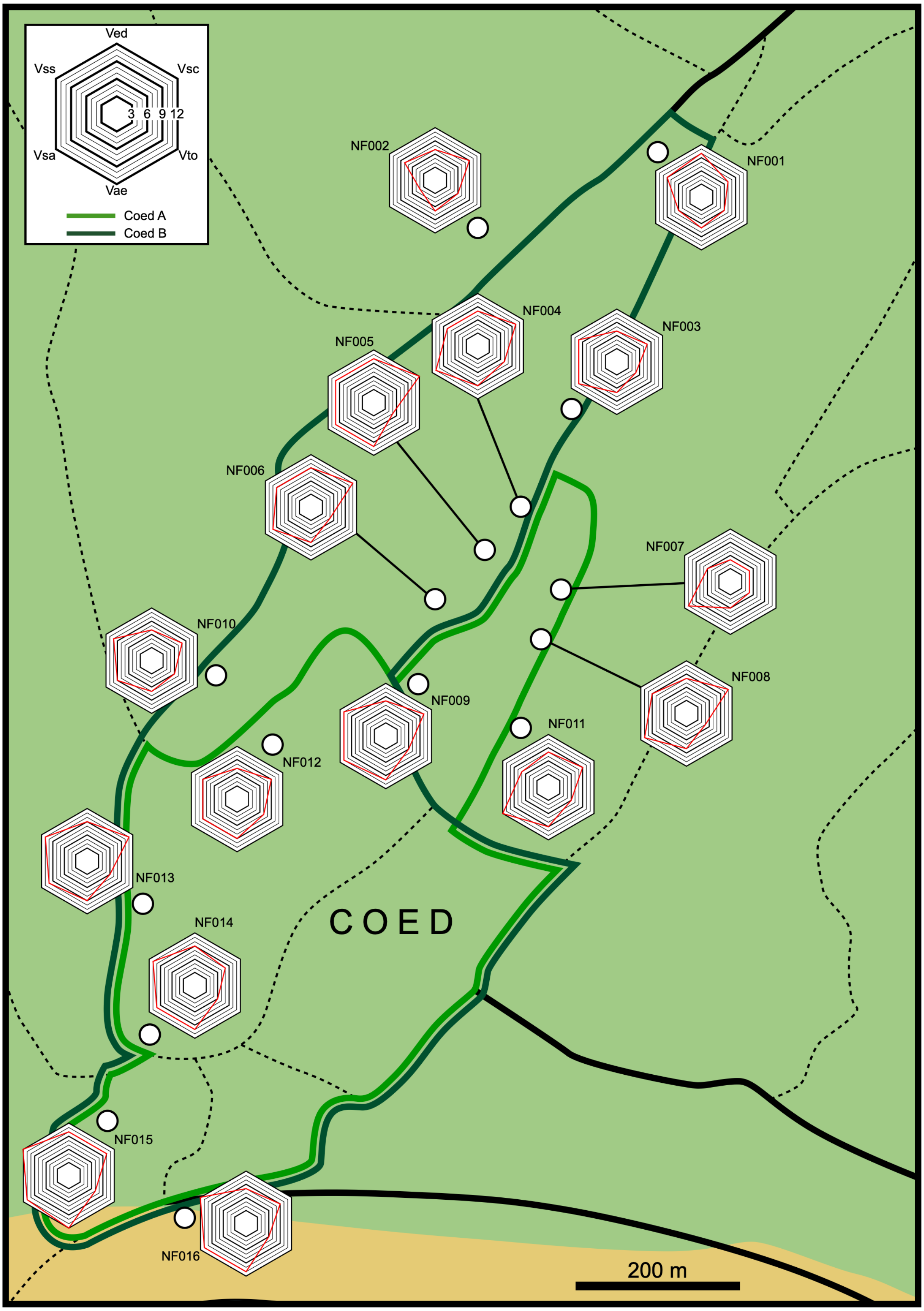

Figure 7.5: Visualisation of evaluation scores for potential localities of the Coed geotrail proposal.

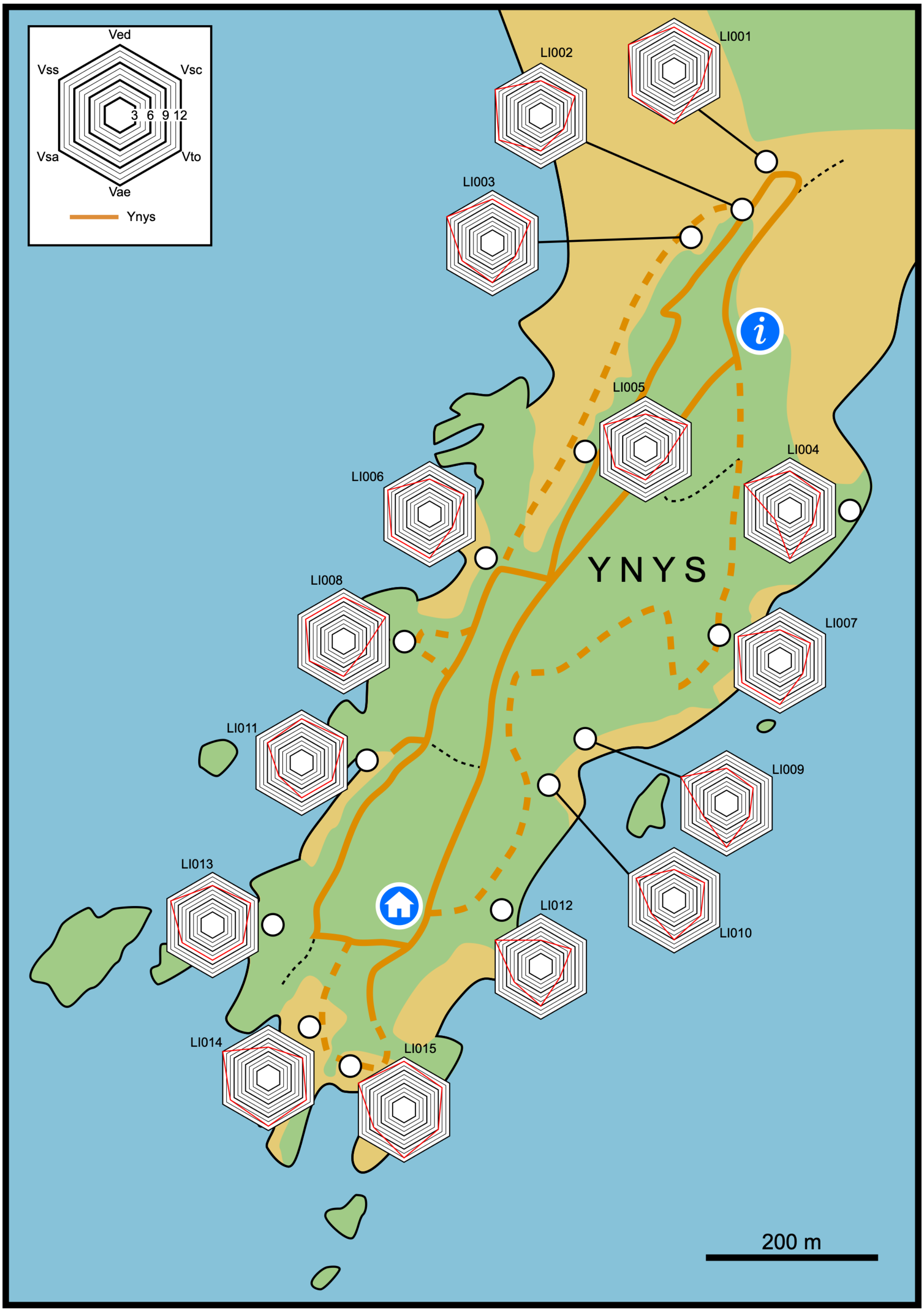

Figure 7.6: Visualisation of evaluation scores for potential localities of the Ynys geotrail proposal.

Localities score within an overall range of 38 – 62. The two localities that score above 60 are LI001/NF15 (causeway pillow lavas) and LI015 (Porth Twr Bach mélange), with both sites benefit from high aesthetic values. Scores across the areas are evenly weighted, with Coed localities averaging scores of 51.1 overall and those from Ynys averaging scores of 53.3. Ynys localities score notably higher in conservation value on average (Ynys – 11.3; Coed 9.5), ranking higher in all three factors. Ynys also has higher touristic value (Ynys – 6.7; Coed 5.9), benefitting from higher visitor traffic and tourist activities. Aesthetic value is closely balance between the two areas (Ynys – 9.4; Coed 8.9), with Ynys having a slightly higher average due to high location aesthetic scores, despite Coed localities averaging higher in other factors. Ynys also averages marginally higher in educational and scientific values. Conversely, Coed localities score much higher in safety and accessibility on average (Ynys – 8.1; Coed – 9.8) due to better path access and lack of limiting factors.

Coed routes A and B each include four unique localities. Localities on Coed A score 38, 52, 51 and 50, while Coed B localities all score below 50 (45, 41, 47 and 47). Coed A localities NF007, NF008 and NF011 have the drawbacks of lower conservation status, while Coed B localities NF001 and NF002 score low in accessibility value due to access limitations and greater distances between localities. Localities from both trails have accessibility drawbacks due to necessary pathway/access improvements. NF007 and NF008 provide the benefit of exhibiting massive lava flows, which are not found at any other proposed locality, scoring eleven in scientific value as a result.

Out of the 31 evaluated localities, eight scored below 50 overall and should not be considered for the geotrail. Some localities create pairs which exhibit the same or similar features in close proximity (NF014 and NF015, LI002 and LI003, LI004 and LI007, LI010 and LI012). To reduce the total number of localities, higher scoring duplicates should be recommended from these eight highlighted localities. While NF005 and NF006 both exhibit basalt-carbonate interactions nearby, both sites show different textures and have different additional features, so should be considered independently. LI003 scores marginally higher than LI002 (LI003 – 55; LI002 – 54) but scores lower in accessibility value due to tidal limitations. It may be advisable to use LI002 as a primary site with directions to LI003 as an option for those visiting at low tide.

7.2.4 Geotrail recommendations

Recommended geotrail routes and localities are outlined in Figure 7.7. The trail is divided into two separate trails (Coed and Ynys), which combine along the causeway (NF015/LI001). A total of 17 localities are included, including ten on the Coed trail and eight on the Ynys trail. Coed route A was favoured over Coed route B due to the greater overall value of its localities, better accessibility and shorter total distance (Coed A – 2.7 km; Coed B – 3.9 km). The overall trail uses the beach car park as a base for tours planned in advance, but trails can be started from the causeway, where the trail should be promoted on the information board.

Potential issues to address

Sites 1 and 2 (NF011 and NF008 respectively) fall marginally (< 200 m) outside of the current boundaries of the RIGS and GCR site. Their inclusion in the geotrail, and therefore the overall geological story of the geosite, should be reflected in their conservation classification. Additionally, NF008 exhibits unique properties not seen elsewhere in the geosite or elsewhere in the Gwna Complex, and therefore efforts should be made to improve its conservation status. Sites 1 and 2 also require additional work to properly link the trail to Site 3.

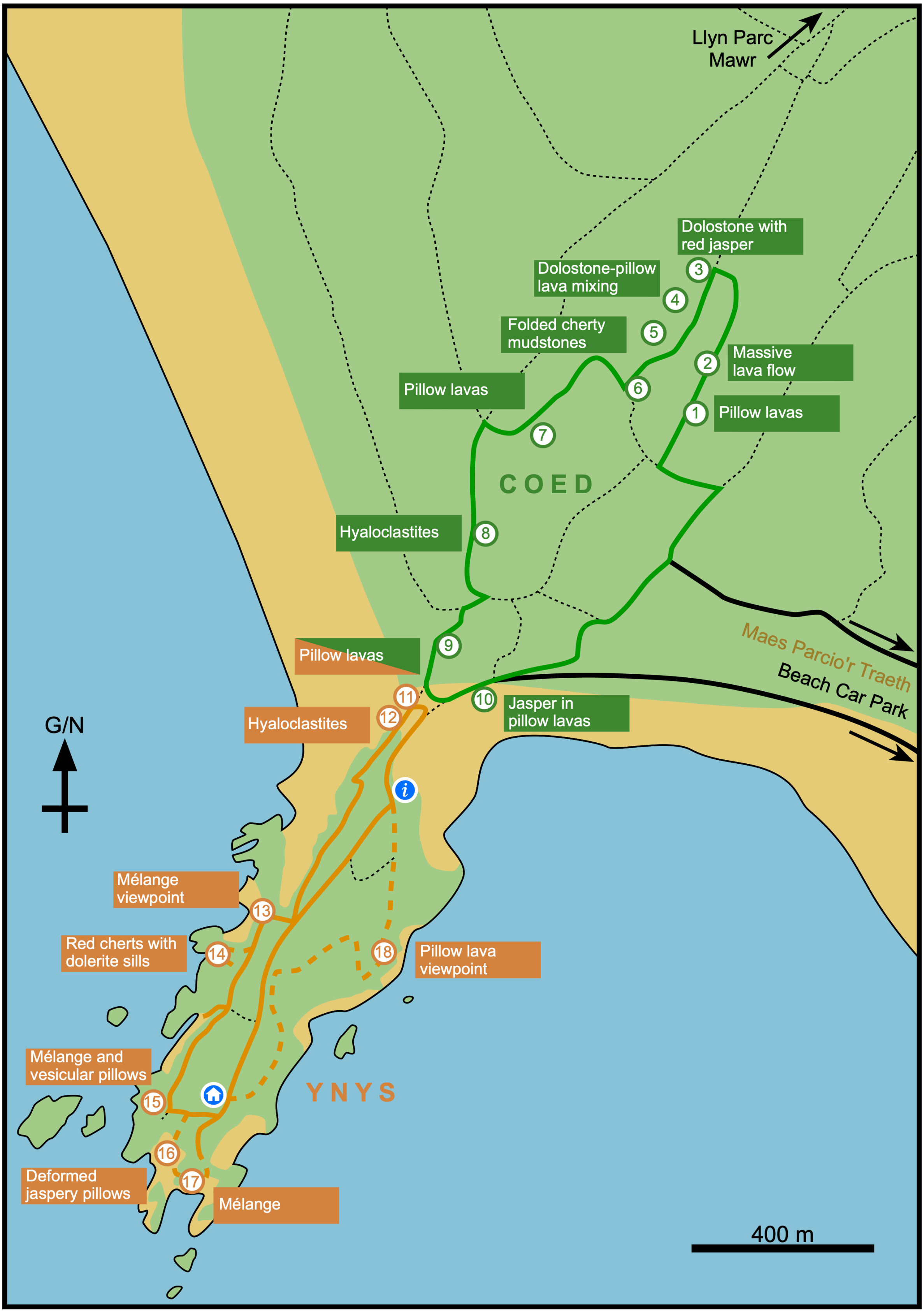

Figure 7.7: Newborough Nature Reserve geotrail recommendation.

7.3 SITE EVALUATION AND PROPOSED IMPROVEMENTS

The criteria used in Section 7.2 was developed to compare the value of individual localities within a geosite but not necessarily to evaluate the geosite itself. Factors that were constants across the geosite – or across the Ynys or Coed areas – were omitted as they served no comparative purpose, while scorings were weighted within the range of conditions of the selected localities. For example, Vss1 (safety and accessibility of access) does not include a score for requiring safety equipment, since no safety equipment is required at any of the suggested localities.

One major factor that was omitted from the evaluation scheme was the issue of tourist information and site infrastructure (Coratza and Giusti 2005; Rybár 2010; Vujičić et al. 2011; Tomić and Božić 2014; Miljković et al. 2018; Suzuki and Takagi 2018). This is because current information is fragmented and not based around the new proposed trail, so would negatively affect the value of new sites. Tourist information must be discussed for the proposed trail though and is perhaps best done regarding the whole geosite, as opposed to individual localities.

7.3.1 Overall site evaluation

Figure 7.8 shows the results for Ynys, Coed and the geosite as a whole (a combination of Ynys and Coed) when evaluated using the criteria of Suzuki and Takagi (2018). The full details of this evaluation scheme can be found in Appendix F. The criteria are designed as a comprehensive evaluation scheme that has been applied to over 30 geosites. It places heavy emphasis on to availability and quality of tourist information, which comprises one of six key values, while also influencing the educational value.

The overall site earns a sum value of 52. The highest scored value is conservation, scoring eleven. This falls just short of a maximum score because of the lower protection state of NF011 and NF008, but could be improved by expanding the current boundaries of the RIGS or GCR site. Tourism and accessibility values both score nine, which realistically cannot be improved upon. Ynys scores nine in touristic value compared to a score of six for Coed. This reflects the scoring in Section 7.2, where Ynys benefits from greater aesthetic value and the presence of higher traffic tourist attractions. Conversely, Coed scores marginally higher than Ynys for safety and accessibility value. This difference is based on safety aspects, while accessibility differences are not as well distinguished as in Section 7.2. Scientific value scores nine overall, which could be improved with further research and publications. Coed scores relatively low (seven) due to lack of inclusion in past publications, which does not adequately reflect its true scientific value.

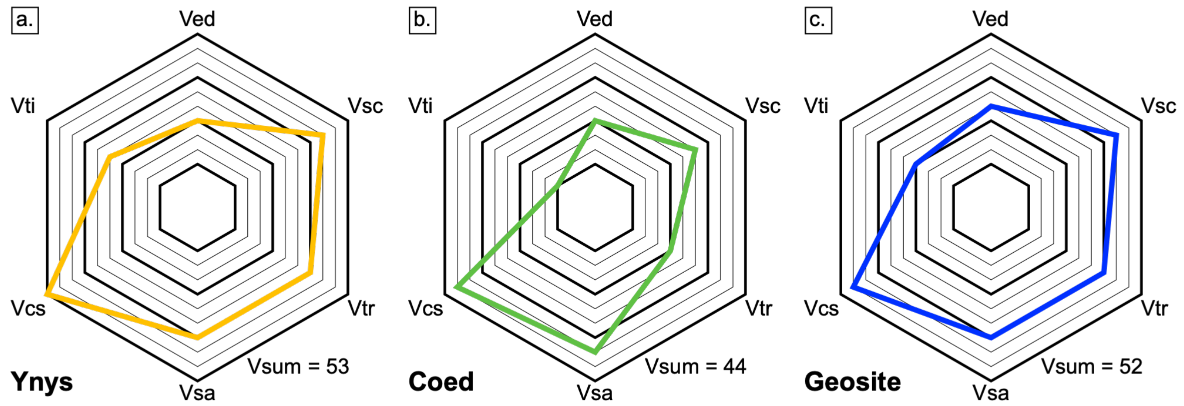

Figure 7.8: Results of applying geosite areas to the geosite evaluation scheme developed by Suzuki & Takagi (2018). Ved – educational value; Vsc – scientific value; Vtr – touristic value; Vsa – safety & accessibility value; Vcs – conservation value; Vti – tourist information value.

In all three areas, the tourist information and educational values are low, being the only values to score below nine. Tourist information scores seven from Ynys and overall due to the presence of an online island trail and the site geoboard, boosted by three points earned due to the availability of bilingual information (Welsh and English). Coed scores a minimum three points due to lack of information. The implementation of uniform information that covers the overall geosite for both on-site and online materials could increase the tourist information value of the geosite to eleven potentially.

Educational value is similarly hampered for each area by the minimal score for ease of understanding panels. This also negatively impacts the ease of understanding, limiting educational value to a maximum score of six. Otherwise, the overall geosite scores higher in representativeness than the individual sites, accounting for the slightly higher overall educational value score. The implementation of panels would increase the educational value of the overall site from seven to eleven potentially, depending on panel quality.

To increase the value of both sites by practical means, the implementation of information boards at localities and direction markers on paths are necessary. The value can be further boosted by promoting the geotrail either at the trail base (car park) or on the information board at the causeway of Llanddwyn Island. Further value can be added in the production of a leaflet to accompany the new trail, along with updating current online information to include both trail areas.

7.3.2 On-site tourist information material

To accompany the geotrail proposal, a leaflet was designed (available in Appendix G) for potential distribution at the geosite. The leaflet includes practical information and general information about GeoMôn in order to promote interest in the geopark and attract visitors to other geosites. Brief technical and geological backgrounds are included to add context to the geological story. The leaflet inset includes a geotrail map and general overview information about the rock types seen at different localities. Similarly, a new geoboard is proposed giving an overview of the geotrail and geological story, along with practical information.

More detailed information about individual sites should be included on discrete panels to be implemented at most localities (with some practical exceptions). The panels should detail the features found at the locality and how to recognise them, as well as pointing out any other heritage significance of the site.

7.3.3 Online tourist information material

Online material is targeted more towards potential visitors with an existing, active interest in geology, and therefore more details can be explored. Along with making online versions of the on-site material available in appropriate format, a virtual fieldtrip of the geosite is proposed as an educational tool. The relevance and usage of virtual fieldtrips has increased exponentially since 2020 and is now seen as a viable alternative to onsite fieldtrips. It is therefore beneficial to provide remote resources for an area of geological significance with a high educational value.

The fieldtrip is integrated through Google Earth, who provide relatively extensive coverage of the main pathways of the site with the Streetview feature. Information for sites will be accompanied by images showing overviews of the outcrops and details of any particular features, with explanatory diagrams where appropriate. To provide a more immersive tool, 3D models of some outcrops were produced using photogrammetry. This is particularly useful in understanding features such as pillow lavas. The models are more engaging than still images as they involve user interactions, and they also allow users to explore details with more independence.

Photogrammetry methodology

Images were captured using either handheld camera or UAV (drone). Permission was first obtained from Natural Resources Wales (site management) to operate a UAV within Newborough Forest and along the causeway (restricted on Llanddwyn Island). Images were acquired in a grid pattern, varying height, lateral position, distance, and camera angle. Approximately 80 – 200 images were captured for an outcrop depending on its size, shape complexity, and resolution of details. Overview images were captured from long distance (>10 m) to delineate the overall outcrop, then mid-distance (approximately 5 – 10 m) images captured most outcrop details. Points of particular interest or intricate details were captured in greater detail with close-up (< 5 m) images. All images must have clear overlap with other images to identify reference points.

Figure 7.9: Textured 3D model of pillow basalts from locality NF015.

Models were processed using Agisoft Metashape. Firstly, photos were aligned by identifying reference points to calculate the image orientation and position. A sparse point cloud was built from the aligned images. From this sparse point cloud, bounding dimensions for the outcrop were set, removing any distant features or background. Noise and any obstructive features such as trees were also removed. A dense point cloud was then built by calculating camera depth, creating detailed 3D parameters for the model. Any remaining noise was further removed before generating a polygonal mesh from the dense point cloud, building the model shape. A texture was then built onto the polygon mesh to complete the model, such as the example shown in Figure 7.9.

7.4 CONCLUSIONS

The new geotrail proposal for Newborough Nature Reserve combines localities from Llanddwyn Island and Newborough Forest to create a complete geological story of the geosite that previous iterations have not been able to show. In Newborough Forest, evidence of deformation and mélange formation is largely covered beneath the forest floor, with only larger undeformed OPS units exposed. On Llanddwyn Island, accretionary deformation is seen clearly, but the story of OPS is more difficult to recognise and communicate clearly. Both areas also exhibit lithologies not seen in the other area. The new trail proposal aims to create an accessible, flexible trail spanning across both areas to provide a comprehensive, uniform overview of the geology and other heritage available in the geosite. It aims to increase engagement of passive and casual visitors by increasing on-site awareness and information, and including localities with higher visitor traffic. The geotrail – with accompanying onsite and online information – should make the geology widely accessible and act as a template for future tours and fieldtrips.

The application and adaptation of geosite assessment models (GAM's) for use in evaluating localities within a single geosite shows how these assessment schemes may be expanded and developed in the future. Current GAM's account for many generalised factors that may not have the resolution to distinguish small-scale differences. This is seen by the close accessibility values of Ynys and Coed using the GAM of Suzuki and Takagi (2018) relative to the model presented here, based in the parameters of the geosite.

While there is clear merit in developing universal geosite evaluation schemes, as shown in Section 7.3, perhaps the most effective use for evaluation schemes is on a smaller scale where scoring can be tailored towards the specific parameters of the area to achieve a better resolution of values. Alternatively, universal evaluation schemes are an effective way to recognise values and shortcomings at a geosite, although contrasting results based on the scheme implemented (Štrba et al. 2014) should be taken into account.

7.4.1 Scope for implementation for other sites

The process of geosite evaluation has proven useful in determining the relative value of localities within a geosite, as well as evaluating geosites in general. This localised, focused approach can be used to propose or improve geotrails at other geosites across the island. On a larger scale, an evaluation model could be developed to assess potential geosites across Anglesey, similar to implementations at other geoparks (Serrano and González-Trueba 2005; Pereira et al. 2007; Zouros 2007; Vujičić et al. 2011; Tomić and Božić 2014). A specified geosite evaluation model within the parameters present on Anglesey could be used to identify particular values of geosites – or their potential value – to prioritise which geosites should be further promoted or focused on for further engagement projects. It can also be used – as has been done here – to identify shortcomings that can be resolved or improved.

Development of virtual fieldtrips for other geotrails and geosites throughout the geopark is also possible using the techniques outlined here. The implementation of 3D models may be particularly useful in some coastal locations, where features in cliff faces cannot be observed up close. However, restrictions on UAV operations are enforced across the areas of several geosites – particularly in Western Anglesey – due to their proximity to airfields and nature reserves.

CHAPTER VIII
Conclusions

The subduction complex of the Monian Composite Terrane records two separate periods of ocean plate subduction at the front of the Avalonian arc system, separated by a transient transcurrent regime. Initial subduction is recorded through the high P-T Penmynydd Terrane and the accretionary Gwna Complex. Secondary subduction is recorded by the Cemaes Group, beginning with magmatic renewal and volcaniclastic deposition, and grading into olistostrome formation through continental uplift.

The Gwna Complex represents subduction-related accretion of ocean floor material. Variable states of preservation – from imbricated tectonic slices partially preserving OPS, to chaotic block-in-matrix mélange – are controlled largely by terrigenous sediment input at the subduction trench. Stratigraphic reconstructions reveal two potential interpretations of OPS. Thick basal magmatic layers of basalts show variable compositions that range between tholeiitic N-MORB and alkaline OIB, along a single, continuous evolutionary trend. In addition to geochemical variability, its relatively common accretion as thick units, and basalt-carbonate interactions at the upper surface, raise the possibility of a seamount origin. The basalts show great geochemical similarities with off-axis seamounts from the East Pacific Rise.

Additionally, a secondary intraplate magmatic event was recognised in Area I, likely representing petit-spot magmatism in response to subducting plate flexure. Subtle geochemical variations differentiate petit-spots from plume-derived seamounts, although more work is needed to constrain and properly define the properties of petit-spots for accurate identification in accreted sequences. The recognition of two potential seamount systems that are not derived from mantle plumes highlights the need for further understanding and representation of less prominent ocean floor features.

Discrepancies in the preservation of lithologies within low-shear OPS units are explained by dual OPS models, accounting for seamount OPS and adjacent sea floor OPS, where pelagic sedimentation is dominated by carbonate rocks and siliceous sequences respectively. A composite OPS for the Gwna Complex describes a full ridge-trench transition, including a basaltic base topped by pelagic sediments that grade into hemi-pelagic, and finally overlain by clastic sediment deposited around a subduction trench from erosion of a proximal continental arc.

The volume of terrigenous sediment input has affected accretion styles throughout the Gwna Complex. In Area I, low sedimentation has led to the preservation of predominantly basalts and distal sea floor sediments, isolating weak pelitic layers and confining block-in-matrix mélange formation within sporadic, thin mudstone occurrences. In other study areas – particularly Area II – much higher sedimentation rates lead to accretion of predominantly thick turbidite sequences and olistostromes. Weak pelite-dominated material becomes intermixed and facilitates regional-scale block-in-matrix mélange formation, largely disintegrating stratigraphic order of accreted material.

Blueschist facies metabasites of the Penmynydd Terrane exhibit relict pillow lava textures and are geochemically similar to basalts from the Gwna Complex. They likely originate from the same oceanic substrate, and were subjected to different subduction processes. The general structure of the Penmynydd Terrane resembles the Gwna Complex at higher P-T conditions, comprising thick, orientated metabasite lenses suspended in a massive, highly foliated metapelitic matrix with subordinate carbonate and quartzite clasts, that resemble a similar, disintegrated ridge-trench OPS.

Recognition of subduction-related units, and information such as subduction polarity, can provide context to the wider geological evolution of the MCT and surrounding regional area. By the nature of a composite terrane, not all units of the MCT could be studied in this project. Several units, namely the Porth Trecastell Formation and the Amlwch Terrane, remain rather ambiguous and require more detailed studies. Additionally, U-Pb studies of detrital zircons from the Cemaes Group could determine depositional age and sediment provenance to scrutinise interpretations presented in this study. Attempts to further constrain age relationships in the Gwna Complex may also be helpful in determining more robust models for the development of the accretionary system. Additionally, ages of lower units of OPS could be used to give context to oceanic events, such as anoxic sedimentation and intraplate magmatism.

REFERENCES

Ackerman, L. et al. 2019. Architecture and composition of ocean floor subducted beneath northern Gondwana during Neoproterozoic to Cambrian: A palinspastic reconstruction based on Ocean Plate Stratigraphy (OPS). *Gondwana Research* 76, pp. 77–97. doi: 10.1016/j.gr.2019.07.001.

Agard, P., Yamato, P., Jolivet, L. and Burov, E. 2009. Exhumation of oceanic blueschists and eclogites in subduction zones: Timing and mechanisms. *Earth Science Reviews* 92(1–2), pp. 53–79. doi: 10.1016/j.earscirev.2008.11.002.

Allan, J.F., Batiza, R. and Lonsdale, P. 1987. Petrology and Chemistry of Lavas from Seamounts Flanking the East Pacific Rise Axis, 21°N°: Implications Concerning the Mantle Source Composition for Both Seamount and Adjacent EPR Lavas. In: Keating, B. H., Fryer, P., Batiza, R., and Boehlert, G. W. eds. *Geophysical Monograph Series*. Washington, D. C.: American Geophysical Union, pp. 255–282.

Allott & Lomax 1988. *Wylfa 'B' power station pre-application studies, report on civil engineering aspects*.

Alt, J.C. 2004. Alteration of the upper oceanic crust: mineralogy, chemistry and processes. In: Davis, E. E. and Elderfield, H. eds. *Hydrogeology of the Oceanic Lithosphere*. Cambridge: Cambridge University Press, pp. 495–533.

Alt, J.C. and Teagle, D.A.H. 2003. Hydrothermal alteration of upper oceanic crust formed at a fast-spreading ridge: mineral, chemical, and isotopic evidence from ODP Site 801. *Chemical Geology* 201(3–4), pp. 191–211. doi: 10.1016/S0009-2541(03)00201-8.

Anderson, M., Wanless, V.D., Perfit, M., Conrad, E., Gregg, P., Fornari, D. and Ridley, W.I. 2021. Extreme Heterogeneity in Mid-Ocean Ridge Mantle Revealed in Lavas From the 8°20′N Near-Axis Seamount Chain. *Geochemistry, Geophysics, Geosystems* 22(1).

Annen, C., Blundy, J.D. and Sparks, R.S.J. 2006. The Genesis of Intermediate and Silicic Magmas in Deep Crustal Hot Zones. *Journal of Petrology* 47(3), pp. 505–539. doi: 10.1093/petrology/egi084.

Asanuma, H. et al. 2015. Reconstruction of ocean plate stratigraphy in the Gwna Group, NW Wales: Implications for the subduction–accretion process of a latest Proterozoic trench-forearc. *Tectonophysics* 662, pp. 195–207. doi: 10.1016/j.tecto.2015.04.016.

Asanuma, H. et al. 2017. New isotopic age data constrain the depositional age and accretionary history of the Neoproterozoic-Ordovician Mona Complex (Anglesey-Lleyn, Wales). *Tectonophysics* 706–707, pp. 164–195. doi: 10.1016/j.tecto.2017.03.017.

Bach, W., Hegner, E., Erzinger, J. and Satir, M. 1994. Chemical and isotopic variations along the superfast spreading East Pacific Rise from 6 to 30□S. *Contributions to Mineralogy and Petrology* 116(4), pp. 365–380. doi: 10.1007/BF00310905.

Bach, W., Jöns, N. and Klein, F. 2013. Metasomatism Within the Ocean Crust. In: *Metasomatism and the Chemical Transformation of Rock*. Lecture Notes in Earth System Sciences. Berlin, Heidelberg: Springer Berlin Heidelberg, pp. 253–288.

Bamousa, A.O. 2008. *Structural analysis and tectonic significance of the Carmel Head thrust belt, Anglesey, North Wales*. PhD Thesis, University of Leicester.

Banno, S. and Sakai, C. 1989. Geology and metamorphic evolution of the Sanbagawa metamorphic belt, Japan. *Geological Society, London, Special Publications* 43(1), pp. 519–532. doi: 10.1144/GSL.SP.1989.043.01.50.

Barber, A.J. and Max, M.D. 1979. A new look at the Mona Complex (Anglesey, North Wales). *Journal of the Geological Society* 136(4), pp. 407–432. doi: 10.1144/gsjgs.136.4.0407.

Barnes, R.P., Branney, M.J., Stone, P. and Woodcock, N.H. 2006. The Lakesman Terrane: the Lower Palaeozoic record of the deep marine Lakesman Basin, a volcanic arc and foreland basin. In: Brenchley, P. J. and Rawson, P. F. eds. *The Geology of England and Wales*. First. The Geological Society of London, pp. 103–129.

Barr, S.M., Davis, D.W., Kamo, S. and White, C.E. 2003. Significance of U–Pb detrital zircon ages in quartzite from peri-Gondwanan terranes, New Brunswick and Nova Scotia, Canada. *Precambrian Research* 126(1–2), pp. 123–145. doi: 10.1016/S0301-9268(03)00192-X.

Barr, S.M., White, C.E., Davis, D.W., McClelland, W.C. and van Staal, C.R. 2014. Infrastructure and provenance of Ganderia: Evidence from detrital zircon ages in the Brookville terrane, southern New Brunswick, Canada. *Precambrian Research* 246, pp. 358–370. doi: 10.1016/j.precamres.2014.03.022.

Barrat, J.A. and Nesbitt, R.W. 1996. Geochemistry of the Tertiary volcanism of Northern Ireland. *Chemical Geology* 129, pp. 15–38.

Bates, D.E.B. 1972. The Stratigraphy of the Ordovician rocks of Anglesey. *Geological Journal* 8(1), pp. 29–58. doi: 10.1002/gj.3350080104.

Bates, D.E.B. 1974. The structure of the Lower Palaeozoic rocks of Anglesey, with special reference to faulting. *Geological Journal* 9(1), pp. 39–60. doi: 10.1002/gj.3350090104.

Batiza, R., Storms, M.A. and Allan, J.F. eds. 1995. *Proceedings of the Ocean Drilling Program, 142 Scientific Results*. Ocean Drilling Program. Available at: http://www-odp.tamu.edu/publications/142_SR/142TOC.HTM [Accessed: 24 May 2022].

Bebout, G.E. 1995. The impact of subduction-zone metamorphism on mantle-ocean chemical cycling. *Chemical Geology* 126(2), pp. 191–218. doi: 10.1016/0009-2541(95)00118-5.

Becker, K. and Davis, E.E. 2004. In situ determinations of the permeability of the igneous oceanic crust. In: Davis, E. E. and Elderfield, H. eds. *Hydrogeology of the Oceanic Lithosphere*. Cambridge: Cambridge University Press, pp. 189–224.

Beckinsale, R.D. and Thorpe, R.S. 1979. Rubidium-strontium whole-rock isochron evidence for the age of metamorphism and magmatism in the Mona Complex of Anglesey. *Journal of the Geological Society* 136(4), pp. 433–439. doi: 10.1144/gsjgs.136.4.0433.

Beckly, A.J. 1987. Basin development in North Wales during the Arenig. *Geological Journal* 22(S1), pp. 19–30. doi: 10.1002/gj.3350220504.

Beier, C., Haase, K.M. and Turner, S.P. 2012. Conditions of melting beneath the Azores. *Lithos* 144–145, pp. 1–11. doi: 10.1016/j.lithos.2012.02.019.

Bergman, S.C. 1987. Lamproites and other potassium-rich igneous rocks: a review of their occurrence, mineralogy and geochemistry. *Geological Society, London, Special Publications* 30(1), pp. 103–190. doi: 10.1144/GSL.SP.1987.030.01.08.

Bevins, R.E., Horák, J.M., Evans, A.D. and Morgan, R. 1996. Palaeogene dyke swarm, NW Wales: evidence for Cenozoic sinistral fault movement. *Journal of the Geological Society* 153(2), pp. 177–180. doi: 10.1144/gsjgs.153.2.0177.

Bhatia, M.R. and Crook, K.A.W. 1986. Trace element characteristics of graywackes and tectonic setting discrimination of sedimentary basins. *Contributions to Mineralogy and Petrology* 92(2), pp. 181–193. doi: 10.1007/BF00375292.

Biscaye, P.E. 1965. Mineralogy and Sedimentation of Recent Deep-Sea Clay in the Atlantic Ocean and Adjacent Seas and Oceans. *Geological Society of America Bulletin* 76(7), p. 803. doi: 10.1130/0016-7606(1965)76[803:MASORD]2.0.CO;2.

Blake, J.F. 1888. On the Monian System of Rocks. *Quarterly Journal of the Geological Society* 44(1–4), pp. 463–547. doi: 10.1144/GSL.JGS.1888.044.01-04.36.

Bonnand, P., Doucelance, R., Boyet, M., Bachèlery, P., Bosq, C., Auclair, D. and Schiano, P. 2020. The influence of igneous processes on the chromium isotopic compositions of Ocean Island basalts. *Earth and Planetary Science Letters* 532, p. 116028. doi: 10.1016/j.epsl.2019.116028.

Boudreau, B.P., Middelburg, J.J., Hofmann, A.F. and Meysman, F.J.R. 2010. Ongoing transients in carbonate compensation: COMPENSATION TRANSIENTS. *Global Biogeochemical Cycles* 24(4), p. n/a-n/a. doi: 10.1029/2009GB003654.

Branney, M.J. and Soper, N.J. 1988. Ordovician volcano-tectonics in the English Lake District. *Journal of the Geological Society* 145(3), pp. 367–376. doi: 10.1144/gsjgs.145.3.0367.

Brenchley, P.J., Rushton, A.W.A., Howells, M. and Cave, R. 2006. Cambrian and Ordovician: the early Palaeozoic tectonostratigraphic evolution of the Welsh Basin, Midland and Monian Terranes of Eastern Avalonia. In: Brenchley, P. J. and Rawson, P. F. eds. *The Geology of England and Wales*. First. The Geological Society of London, pp. 25–74.

British Geological Survey 1980. Geological Map, England and Wales. Special Sheet, Solid with Drift edition, 1: 50 000 series.

Brown, E.H. 1977. The Crossite Content of Ca-Amphibole as a Guide to Pressure of Metamorphism. *Journal of Petrology* 18(1), pp. 53–72. doi: 10.1093/petrology/18.1.53.

Brown, M. 1998. Unpairing metamorphic belts: P–T paths and a tectonic model for the Ryoke Belt, southwest Japan. *Journal of Metamorphic Geology* 16, pp. 3–22. doi: 10.1111/j.1525-1314.1998.00061.x.

Brown, M. 2002. Plate margin processes and 'paired' metamorphic belts in Japan: Comment on 'Thermal e¡ects of ridge subduction and its implications for the origin of granitic batholith and paired metamorphic belts' by H. Iwamori. *Earth and Planetary Science Letters* 199, pp. 483–492.

Brown, M. 2007. Metamorphic Conditions in Orogenic Belts: A Record of Secular Change. *International Geology Review* 49(3), pp. 193–234. doi: 10.2747/0020-6814.49.3.193.

Bruschi, V.M. and Cendrero, A. 2005. Geosite evaluation; can we measure intangible values? *Italian Journal of Quaternary Sciences* 18(1), pp. 293–306.

Buchs, D.M., Baumgartner, P.O., Baumgartner-Mora, C., Bandini, A.N., Jackett, S.-J., Diserens, M.-O. and Stucki, J. 2009. Late Cretaceous to Miocene seamount accretion and mélange formation in the Osa and Burica Peninsulas (Southern Costa Rica): episodic growth of a convergent margin. *Geological Society, London, Special Publications* 328(1), pp. 411–456. doi: 10.1144/SP328.17.

Buchs, D.M., Hoernle, K. and Grevemeyer, I. 2015. Seamounts. In: Harff, J., Meschede, M., Petersen, S., and Thiede, J. eds. *Encyclopedia of Marine Geosciences*. Dordrecht: Springer Netherlands, pp. 1–11.

Buchs, D.M., Pilet, S., Cosca, M., Flores, K.E., Bandini, A.N. and Baumgartner, P.O. 2013. Low-volume intraplate volcanism in the Early/Middle Jurassic Pacific basin documented by accreted sequences in Costa Rica: ACCRETED SEAMOUNT IN COSTA RICA. *Geochemistry, Geophysics, Geosystems* 14, pp. 1552–1568. doi: 10.1002/ggge.20084.

Burek, C.V. 2008. History of RIGS in Wales: an example of successful cooperation for geoconservation. *Geological Society, London, Special Publications* 300(1), pp. 147–171. doi: 10.1144/SP300.12.

Cabanis and Lecolle, M. 1989. The La/10-Y/15-Nb/8 diagram: A tool for distinguishing volcanic series and discovering crustal mixing and/or contamination. *Comptes Rendus de l'Academie des Sciences, Serie 2, Sciences de la Terre* 309, p. 20.

Campbell, S., Wood, M. and Windley, B.F. 2017. *Footsteps Through Time. The Rocks and Landscape of Anglesey Explained*. 2nd ed. Wales, UK: Geomôn, Isle of Anglesey County Council.

Cann, J.R. 1970. Rb, Sr, Y, Zr and Nb in some ocean floor basaltic rocks. *Earth and Planetary Science Letters* 10(1), pp. 7–11. doi: 10.1016/0012-821X(70)90058-0.

Carney, J.N., Joint Nature Conservation Committee and British Geological Survey eds. 2000. *Precambrian rocks of England and Wales*. Peterborough: Joint Nature Conservation Committee.

Cawood, P.A., Hawkesworth, C.J., Pisarevsky, S.A., Dhuime, B., Capitanio, F.A. and Nebel, O. 2018. Geological archive of the onset of plate tectonics. *Philosophical Transactions of the Royal Society A: Mathematical, Physical and Engineering Sciences* 376.

Chen, S. et al. 2019. Iron isotope fractionation during mid-ocean ridge basalt (MORB) evolution: Evidence from lavas on the East Pacific Rise at 10°30′N and its implications. *Geochimica et Cosmochimica Acta* 267, pp. 227–239. doi: 10.1016/j.gca.2019.09.031.

Choi, H., Kim, S. and Park, S. 2021. Magnetic Constraints on Off-Axis Seamount Volcanism in the Easternmost Segment of the Australian-Antarctic Ridge. *Geochemistry, Geophysics, Geosystems* 22(9).

Clift, P. and Vannucchi, P. 2004. Controls on tectonic accretion versus erosion in subduction zones: Implications for the origin and recycling of the continental crust. *Reviews of Geophysics* 42, p. RG2001. doi: 10.1029/2003RG000127.

Cocks, L.R.M. and Torsvik, T.H. 2002. Earth geography from 500 to 400 million years ago: a faunal and palaeomagnetic review. *Journal of the Geological Society* 159(6), pp. 631–644. doi: 10.1144/0016-764901-118.

Cocks, L.R.M. and Torsvik, T.H. 2006. European geography in a global context from the Vendian to the end of the Palaeozoic. *Geological Society, London, Memoirs* 32(1), pp. 83–95. doi: 10.1144/GSL.MEM.2006.032.01.05.

Collins, Alans. and Buchan, C. 2004. Provenance and age constraints of the South Stack Group, Anglesey, UK: U–Pb SIMS detrital zircon data. *Journal of the Geological Society* 161(5), pp. 743–746. doi: 10.1144/0016-764904-036.

Comodi, P. and Zanazzi, P.F. 1996. Effects of temperature and pressure on the structure of lawsonite. *American Mineralogist* 81, pp. 833–841. doi: 10.2138/am-1996-7-805.

Compston, W., Wright, A.E. and Toghill, P. 2002. Dating the Late Precambrian volcanicity of England and Wales. *Journal of the Geological Society* 159(3), pp. 323–339. doi: 10.1144/0016-764901-010.

Condie, K.C. 1997. *Plate tectonics and crustal evolution*. 4th ed. Oxford ; Boston: Butterworth Heinemann.

Condie, K.C. 2018. A planet in transition: The onset of plate tectonics on Earth between 3 and 2 Ga? *Geoscience Frontiers* 9(1), pp. 51–60. doi: 10.1016/j.gsf.2016.09.001.

Condon, D.J. and Prave, A.R. 2000. Two from Donegal: Neoproterozoic glacial episodes on the northeast margin of Laurentia. *Geology* 28(10), pp. 951–954.

Coombs, M.L., Clague, D.A., Moore, G.F. and Cousens, B.L. 2004. Growth and collapse of Waianae Volcano, Hawaii, as revealed by exploration of its submarine flanks: WAIʻANAE VOLCANO, HAWAII. *Geochemistry, Geophysics, Geosystems* 5(8).

Coratza, P. and Giusti, C. 2005. Methodological Proposal for the Assessment of the Scientific Quality of Geomorphosites. *Italian Journal of Quaternary Sciences* 18(1), pp. 307–313.

Courtillot, V., Davaille, A., Besse, J. and Stock, J. 2003. Three distinct types of hotspots in the Earth's mantle. *Earth and Planetary Science Letters* 205(3–4), pp. 295–308. doi: 10.1016/S0012-821X(02)01048-8.

Cousens, B.L. and Clague, D.A. 2015. Shield to Rejuvenated Stage Volcanism on Kauai and Niihau, Hawaiian Islands. *Journal of Petrology* 56(8), pp. 1547–1584. doi: 10.1093/petrology/egv045.

Cowan, D.S. 1985. Structural styles in Mesozoic and Cenozoic mélanges in the western Cordillera of North America. *Geological Society of America Bulletin* 96, pp. 451–462.

Cullers, R.L. and Podkodyrov, V.N. 2000. Geochemistry of the Mesoproterozoic Lakhanda shales in southeastern Yakutia, Russia: implications for mineralogical and provenance control, and recycling. *Precambrian Research* 104(1–2), pp. 77–93. doi: 10.1016/S0301-9268(00)00090-5.

Dallmeyer, R.D. and Gibbons, W. 1987. The age of blueschist metamorphism in Anglesey, North Wales: evidence from ^{40}Ar/^{39}Ar mineral dates of the Penmynydd schists. *Journal of the Geological Society* 144(6), pp. 843–850. doi: 10.1144/gsjgs.144.6.0843.

Dartnall, R. 2018. *Depositional framework of the Gwna Group mélanges of Anglesey and north-west Wales, UK*. PhD Thesis, University of Birmingham.

Davies, G.R., Gledhill, A. and Hawkesworth, C. 1985. Upper crystal recycling in southern Britain: Evidence from Nd and Sr isotopes. *Earth and Planetary Science Letters* 75, pp. 1–12.

Davis, A.S. and Clague, D.A. 2000. President Jackson Seamounts, northern Gorda Ridge: Tectonomagmatic relationship between on- and off-axis volcanism. *Journal of Geophysical Research: Solid Earth* 105(B12), pp. 27939–27956. doi: 10.1029/2000JB900291.

Davis, A.S., Gray, L.B., Clague, D.A. and Hein, J.R. 2002. The Line Islands revisited: New 40 Ar/ 39 Ar geochronologic evidence for episodes of volcanism due to lithospheric extension: LINE ISLANDS REVISITED. *Geochemistry, Geophysics, Geosystems* 3(3), pp. 1–28. doi: 10.1029/2001GC000190.

De la Roche, H., Leterrier, J., Grandclaude, P. and Marchal, M. 1980. A classification of volcanic and plutonic rocks using R 1 R 2 -diagram and major-element analyses — Its relationships with current nomenclature. *Chemical Geology* 29(1–4), pp. 183–210. doi: 10.1016/0009-2541(80)90020-0.

Debaille, V., Blichert-Toft, J., Agranier, A., Doucelance, R., Schiano, P. and Albarede, F. 2006. Geochemical component relationships in MORB from the Mid-Atlantic Ridge, 22–35°N. *Earth and Planetary Science Letters* 241(3–4), pp. 844–862. doi: 10.1016/j.epsl.2005.11.004.

Delavault, H., Chauvel, C., Sobolev, A. and Batanova, V. 2015. Combined petrological, geochemical and isotopic modeling of a plume source: Example of Gambier Island, Pitcairn chain. *Earth and Planetary Science Letters* 426, pp. 23–35. doi: 10.1016/j.epsl.2015.06.013.

Dickinson, W.R. 2006. Geotectonic evolution of the Great Basin. *Geosphere* 2(7), pp. 353–368. doi: 10.1130/GES00054.1.

Dixon, J., Clague, D.A., Cousens, B., Monsalve, M.L. and Uhl, J. 2008. Carbonatite and silicate melt metasomatism of the mantle surrounding the Hawaiian plume: Evidence from volatiles, trace elements, and radiogenic isotopes in rejuvenated-stage lavas from Niihau, Hawaii: VOLATILES AND TRACE ELEMENTS IN LAVAS. *Geochemistry, Geophysics, Geosystems* 9(9), p. n/a-n/a. doi: 10.1029/2008GC002076.

Dong, Y. et al. 2020. Important role of magma mixing in generating the late Carboniferous Tayuan Complex during subduction of the Paleo-Asian oceaic plate beneath the Xing'an–Erguna Massif, NE China: Evidence from petrology, geochemistry, and zircon U–Pb–Hf isotopes. *Lithos*.

Dostal, J., Dupuy, C. and Dudoignon, P. 1996. Distribution of boron, lithium and beryllium in ocean island basalts from French Polynesia: implications for the B/Be and Li/Be ratios as tracers of subducted components. *Mineralogical Magazine* 60(401), pp. 563–580. doi: 10.1180/minmag.1996.060.401.03.

Dowling, R.K. 2011. Geotourism's Global Growth. *Geoheritage* 3(1), pp. 1–13. doi: 10.1007/s12371-010-0024-7.

Dowling, R.K. 2013. Global Geotourism – An Emerging Form of Sustainable Tourism. *Czech Journal of Tourism* 2(2).

Droop, G.T.R. 1987. A general equation for estimating Fe 3+ concentrations in ferromagnesian silicates and oxides from microprobe analyses, using stoichiometric criteria. *Mineralogical Magazine* 51(361), pp. 431–435. doi: 10.1180/minmag.1987.051.361.10.

Dupuy, C., Barsczus, H.G., Dostal, J., Vidal, P. and Liotard, J.-M. 1989. Subducted and recycled lithosphere as the mantle source of ocean island basalts from southern Polynesia, central Pacific. *Chemical Geology* 77(1), pp. 1–18. doi: 10.1016/0009-2541(89)90010-7.

Edina LIDAR Digimap Service 2016. Lidar Composite Digital Terrain Model Wales 50 cm Resolution [ASC Geospatial Data]. Available at: http://digimap.edina.ac.uk.

Edmond, J.M. et al. 1979. Ridge crest hydrothermal activity and the balances of the major and minor elements in the ocean: The Galapagos data. *Earth and Planetary Science Letters* 46(1), pp. 1–18. doi: 10.1016/0012-821X(79)90061-X.

Eijsink, A. 2017. *Deformation mechanisms in the Gwna mélange on Anglesey (UK) and the implications for aseismic subduction zones*. MSc Thesis, Utrecht University.

Ellis, E. 2009. *The geochemistry and petrology of the Palaeogene dykes of Anglesey: are they related to the Antrim basalts?* MESci Thesis, Cardiff University.

Ernst, W.G. 1973. Blueschist metamorphism and P-T regimes in active subduction zones. *Tectonophysics* 17, pp. 255–272.

Eskola, P. 1921. The mineral facies of rocks. *Norsk Geologisk Tidsskrift* 6, pp. 142–194.

Eskola, P. 1939. Die metamorphen Gesteine. In: Barth, T. F. W., Correns, C. W., and Eskola, P. eds. *Die Entstehung der Gesteine*. Berlin: Springer, p. 422.

Evans, B.W. 1990. Phase relations of epidote-blueschists. *Lithos* 25(1–3), pp. 3–23. doi: 10.1016/0024-4937(90)90003-J.

Fagereng, Å. and Sibson, R.H. 2010. Mélange rheology and seismic style. *Geology* 38(8), pp. 751–754. doi: 10.1130/G30868.1.

Fassoulas, C., Mouriki, D., Dimitriou-Nikolakis, P. and Iliopoulos, G. 2012. Quantitative Assessment of Geotopes as an Effective Tool for Geoheritage Management. *Geoheritage* 4(3), pp. 177–193. doi: 10.1007/s12371-011-0046-9.

Festa, A., Dilek, Y., Pini, G.A., Codegone, G. and Ogata, K. 2012. Mechanisms and processes of stratal disruption and mixing in the development of mélanges and broken formations: Redefining and classifying mélanges. *Tectonophysics* 568–569, pp. 7–24. doi: 10.1016/j.tecto.2012.05.021.

Festa, A., Pini, G.A., Dilek, Y. and Codegone, G. 2010. Mélanges and mélange-forming processes: a historical overview and new concepts. *International Geology Review* 52(10–12), pp. 1040–1105. doi: 10.1080/00206810903557704.

Festa, A., Pini, G.A., Ogata, K. and Dilek, Y. 2019. Diagnostic features and field-criteria in recognition of tectonic, sedimentary and diapiric mélanges in orogenic belts and exhumed subduction-accretion complexes. *Gondwana Research* 74, pp. 7–30. doi: 10.1016/j.gr.2019.01.003.

Fettes, D.J., Desmons, J., Árkai, P. and International Union of Geological Sciences eds. 2007. *Metamorphic rocks: a classification and glossary of terms: recommendations of the International Union of Geological Sciences Subcommission on the Systematics of Metamorphic Rocks*. Cambridge ; New York: Cambridge University Press.

Fike, D.A., Grotzinger, J.P., Pratt, L.M. and Summons, R.E. 2006. Oxidation of the Ediacaran Ocean. *Nature* 444(7120), pp. 744–747. doi: 10.1038/nature05345.

Fitton, J.G., Saunders, A.D., Norry, M.J., Hardarson, B.S. and Taylor, R.N. 1997. Thermal and chemical structure of the Iceland plume. *Earth and Planetary Science Letters* 153, pp. 197–208. doi: 10.1016/S0012-821X(97)00170-2.

Floyd, P.A. and Winchester, J.A. 1978. Identification and discrimination of altered and metamorphosed volcanic rocks using immobile elements. *Chemical Geology* 21(3–4), pp. 291–306. doi: 10.1016/0009-2541(78)90050-5.

Foulger, G.R. and Jurdy, D.M. eds. 2007. *Plates, plumes, and planetary processes*. Boulder, Colo: Geological Society of America.

Fowler, A.P.G. and Zierenberg, R.A. 2016. Elemental changes and alteration recorded by basaltic drill core samples recovered from in situ temperatures up to 345°C in the active, seawater-recharged Reykjanes geothermal system, Iceland: REYKJANES CORE ELEMENT GAINS AND LOSSES. *Geochemistry, Geophysics, Geosystems* 17(11), pp. 4772–4801. doi: 10.1002/2016GC006595.

Franzson, H., Zierenberg, R. and Schiffman, P. 2008. Chemical transport in geothermal systems in Iceland. *Journal of Volcanology and Geothermal Research* 173(3–4), pp. 217–229. doi: 10.1016/j.jvolgeores.2008.01.027.

Fritschle, T. et al. 2018. Peri-Gondwanan Ordovician arc magmatism in southeastern Ireland and the Isle of Man: Constraints on the timing of Caledonian deformation in Ganderia. *GSA Bulletin*.

Gale, A., Dalton, C.A., Langmuir, C.H., Su, Y. and Schilling, J.-G. 2013. The mean composition of ocean ridge basalts: MEAN MORB. *Geochemistry, Geophysics, Geosystems* 14, pp. 489–518. doi: 10.1029/2012GC004334.

Garapić, G., Jackson, M.G., Hauri, E.H., Hart, S.R., Farley, K.A., Blusztajn, J.S. and Woodhead, J.D. 2015. A radiogenic isotopic (He-Sr-Nd-Pb-Os) study of lavas from the Pitcairn hotspot: Implications for the origin of EM-1 (enriched mantle 1). *Lithos* 228–229, pp. 1–11. doi: 10.1016/j.lithos.2015.04.010.

García-Casco, A., Proenza, J.A. and Iturralde-Vinent, M.A. 2011. Subduction Zones of the Caribbean: the sedimentary, magmatic, metamorphic and ore-deposit records. *Geologica Acta* 9(3–4), pp. 217–224. doi: 10.1344/105.00001745.

Gibbons, W. 1981. Glaucophanic amphibole in a Monian shear zone on the mainland of N Wales. *Journal of the Geological Society* 138(2), pp. 139–143. doi: 10.1144/gsjgs.138.2.0139.

Gibbons, W. 1983a. Stratigraphy, subduction and strike-slip faulting in the Mona Complex of North Wales—a review. *Proceedings of the Geologists' Association* 94(2), pp. 147–163. doi: 10.1016/S0016-7878(83)80006-6.

Gibbons, W. 1983b. The Monian 'Penmynydd Zone of Metamorphism' in Llŷn, North Wales. *Geological Journal* 18(1), pp. 21–41. doi: 10.1002/gj.3350180103.

Gibbons, W. 1987. Menai Strait fault system: An early Caledonian terrane boundary in north Wales. *Geology* 15, pp. 744–747.

Gibbons, W. and Ball, M.J. 1991. A discussion of Monian Supergroup stratigraphy in northwest Wales. *Journal of the Geological Society* 148(1), pp. 5–8. doi: 10.1144/gsjgs.148.1.0005.

Gibbons, W. and Gyopari, M. 1986. A greenschist protolith for blueschist in Anglesey, U.K. In: *Geological Society of America Memoirs*. Geological Society of America, pp. 217–228.

Gibbons, W. and Horák, J. 1990. Contrasting metamorphic terranes in northwest Wales. *Geological Society, London, Special Publications* 51, pp. 315–327. doi: 10.1144/GSL.SP.1990.051.01.20.

Gibbons, W. and Horák, J.M. 1996. The evolution of the Neoproterozoic Avalonian subduction system: Evidence from the British Isles. In: *Special Paper 304: Avalonian and related peri-Gondwanan terranes of the Circum-North Atlantic*. New York: Geological Society of America, pp. 269–280.

Gibbons, W. and Mann, A. 1983. Pre-Mesozoic lawsonite in Anglesey, northern Wales: Preservation of ancient blueschists. *Geology* 11, pp. 3–6.

Gibbons, W. and McCarroll, D. 1993. *Geology of the country around Aberdaron, including Bardsey Island*. London, UK: Memoir of the British Geological Survey.

Gibbons, W., Tietzsch-Tyler, D., Horák, J.M. and Murphy, F.C. 1994. Precambrian rocks in Anglesey, southwest Llyn and southeast Ireland. In: Gibbons, W. and Harris, A. L. eds. *A revised correlation of Precambrian rocks in the British Isles*. London, UK: Geological Society, London, Special Report No. 22, pp. 75–84.

Gibbons, W. and Young, T.P. 1999. Mid-Caradoc magmatism in central Llyn, rhyolite petrogenesis, and the evolution of the Snowdonia volcanic corridor in NW Wales. *Journal of the Geological Society, London* 156, pp. 301–316.

Gibson, S.A., Thompson, R.N., Dickin, A.P. and Leonardos, O.H. 1995. High-Ti and low-Ti mafic potassic magmas: Key to plume-lithosphere interactions and continental flood-basalt genesis. *Earth and Planetary Science Letters* 136(3–4), pp. 149–165. doi: 10.1016/0012-821X(95)00179-G.

Goss, A.R. et al. 2010. Geochemistry of lavas from the 2005-2006 eruption at the East Pacific Rise, 9°46′N-9°56′N: Implications for ridge crest plumbing and decadal changes in magma chamber compositions: GEOCHEMISTRY OF LAVAS FROM 2005-2006 EPR ERUPTION. *Geochemistry, Geophysics, Geosystems* 11(5), p. n/a-n/a. doi: 10.1029/2009GC002977.

Greenly, E. 1900. III.—On the Age of the Later Dykes of Anglesey. *Geological Magazine* 7, pp. 160–164. doi: 10.1017/S0016756800177039.

Greenly, E. 1919. *The Geology of Anglesey*. Memoir of the Geological Survey of Great Britain.

Greenly, E. 1920. One inch geological map of Anglesey.

Gregg, P., Hebert, L., Montési, L. and Katz, R. 2012. Geodynamic Models of Melt Generation and Extraction at Mid-Ocean Ridges. *Oceanography* 25(1), pp. 78–88. doi: 10.5670/oceanog.2012.05.

Grevemeyer, I., Kaul, N., Villinger, H. and Weigel, W. 1999. Hydrothermal activity and the evolution of the seismic properties of upper oceanic crust. *Journal of Geophysical Research: Solid Earth* 104(B3), pp. 5069–5079. doi: 10.1029/1998JB900096.

Guice, G.L. 2019. *Origin and geodynamic significance of ultramafic- mafic complexes in the North Atlantic and Kaapvaal Cratons*. PhD Thesis, Cardiff, UK: Cardiff University.

Haase, K.M., Fretzdorff, S., Mühe, R., Garbe-Schönberg, D. and Stoffers, P. 2009. A geochemical study of off-axis seamount lavas at the Valu Fa Ridge: Constraints on magma genesis and slab contributions in the southern Tonga subduction zone. *Lithos* 112(1–2), pp. 137–148. doi: 10.1016/j.lithos.2009.05.041.

Hailwood, E.A., Maddock, R.H., Fung, T. and Rutter, E.H. 1992. Palaeomagnetic analysis of fault gouge and dating fault movement, Anglesey, North Wales. *Journal of the Geological Society* 149(2), pp. 273–284. doi: 10.1144/gsjgs.149.2.0273.

Hajná, J., Žák, J., Dörr, W., Kachlík, V. and Sláma, J. 2018. New constraints from detrital zircon ages on prolonged, multiphase transition from the Cadomian accretionary orogen to a passive margin of Gondwana. *Precambrian Research* 317, pp. 159–178. doi: 10.1016/j.precamres.2018.08.013.

Hajná, J., Žák, J. and Kachlík, V. 2014. Growth of accretionary wedges and pulsed ophiolitic mélange formation by successive subduction of trench-parallel volcanic elevations. *Terra Nova* 26(4), pp. 322–329. doi: 10.1111/ter.12103.

Hajná, J., Žák, J., Kachlík, V., Dörr, W. and Gerdes, A. 2013. Neoproterozoic to early Cambrian Franciscan-type mélanges in the Teplá–Barrandian unit, Bohemian Massif: Evidence of modern-style accretionary processes along the Cadomian active margin of Gondwana? *Precambrian Research* 224, pp. 653–670. doi: 10.1016/j.precamres.2012.11.007.

Hanano, D., Weis, D., Scoates, J.S., Aciego, S. and DePaolo, D.J. 2010. Horizontal and vertical zoning of heterogeneities in the Hawaiian mantle plume from the geochemistry of consecutive postshield volcano pairs: Kohala-Mahukona and Mauna Kea-Hualalai: GEOCHEMISTRY OF POSTSHIELD VOLCANO PAIRS. *Geochemistry, Geophysics, Geosystems* 11(1), p. n/a-n/a. doi: 10.1029/2009GC002782.

Hansen, J., Jerram, D.A., McCAFFREY, K. and Passey, S.R. 2009. The onset of the North Atlantic Igneous Province in a rifting perspective. *Geological Magazine* 146, pp. 309–325. doi: 10.1017/S0016756809006347.

Hanyu, T. et al. 2013. Geochemical diversity in submarine HIMU basalts from Austral Islands, French Polynesia. *Contributions to Mineralogy and Petrology* 166(5), pp. 1285–1304. doi: 10.1007/s00410-013-0926-x.

Hanyu, T., Kimura, J.-I., Katakuse, M., Calvert, A.T., Sisson, T.W. and Nakai, S. 2010. Source materials for inception stage Hawaiian magmas: Pb-He isotope variations for early Kilauea: INCEPTION STAGE HAWAIIAN MAGMAS. *Geochemistry, Geophysics, Geosystems* 11(3), p. n/a-n/a. doi: 10.1029/2009GC002760.

Harker, A. 1887. IV.—Woodwardian Museum Notes: on some Anglesey Dykes. II. *Geological Magazine* 4, pp. 546–552. doi: 10.1017/S0016756800190612.

Hart, S.R., Blijsztajn, J. and Craddock, C. 1995. Cenozoic volcanism in Antarctica: Jones Mountains and Peter I Island. *Geochimica et Cosmochimica Acta* 59(16), pp. 3379–3388. doi: 10.1016/0016-7037(95)00212-I.

Hart, S.R. and Jackson, M.G. 2014. Ta'u and Ofu/Olosega volcanoes: The "Twin Sisters" of Samoa, their P, T, X melting regime, and global implications. *Geochemistry, Geophysics, Geosystems* 15(6), pp. 2301–2318. doi: 10.1002/2013GC005221.

Hastie, A.R., Kerr, A.C., Pearce, J.A. and Mitchell, S.F. 2007. Classification of Altered Volcanic Island Arc Rocks using Immobile Trace Elements: Development of the Th–Co Discrimination Diagram. *Journal of Petrology* 48(12), pp. 2341–2357. doi: 10.1093/petrology/egm062.

Hauri, E.H. and Hart, S.R. 1997. Rhenium abundances and systematics in oceanic basalts. *Chemical Geology* 139(1–4), pp. 185–205. doi: 10.1016/S0009-2541(97)00035-1.

Hawthorne, F.C., Oberti, R., Harlow, G.E., Maresch, W.V., Martin, R.F., Schumacher, J.C. and Welch, M.D. 2012. Nomenclature of the amphibole supergroup. *American Mineralogist* 97, pp. 2031–2048. doi: 10.2138/am.2012.4276.

Hayashi, K.-I., Fujisawa, H., Holland, H.D. and Ohmoto, H. 1997. Geochemistry of ~1.9 Ga sedimentary rocks from northeastern Labrador, Canada. *Geochimica et Cosmochimica Acta* 61(19), pp. 4115–4137. doi: 10.1016/S0016-7037(97)00214-7.

Hékinian, R. 1982. *Petrology of the Ocean Floor*. Amsterdam: Elsevier.

Henslow, J. 1822. Geological description of Anglesea, volume 1. *Transactions of the Cambridge Philosophical Society* 1, pp. 359–452.

Hernández-Uribe, D., Palin, R.M., Cone, K.A. and Cao, W. 2021. Petrological Implications of Seafloor Hydrothermal Alteration of Subducted Mid-Ocean Ridge Basalt. *Journal of Petrology* 61(9), pp. 1–18. doi: 10.1093/petrology/egaa086.

Hibbard, J.P., Van Staal, C.R. and Rankin, D.W. 2007. A comparative analysis of pre-Silurian crustal building blocks of the northern and the southern Appalachian orogen. *American Journal of Science* 307(1), pp. 23–45. doi: 10.2475/01.2007.02.

Hildenbrand, A., Weis, D., Madureira, P. and Marques, F.O. 2014. Recent plate re-organization at the Azores Triple Junction: Evidence from combined geochemical and geochronological data on Faial, S. Jorge and Terceira volcanic islands. *Lithos* 210–211, pp. 27–39. doi: 10.1016/j.lithos.2014.09.009.

Hillier, J.K. 2007. Pacific seamount volcanism in space and time. *Geophysical Journal International* 168(2), pp. 877–889. doi: 10.1111/j.1365-246X.2006.03250.x.

Hirano, N. et al. 2006. Volcanism in Response to Plate Flexure. *Science* 313, pp. 1426–1428. doi: 10.1126/science.1128235.

Hirano, N. 2011. Petit-spot volcanism: A new type of volcanic zone discovered near a trench. *Geochemical Journal* 45(2), pp. 157–167. doi: 10.2343/geochemj.1.0111.

Hirano, N. et al. 2019. Petit-spot volcanoes on the oldest portion of the Pacific plate. *Deep Sea Research Part I: Oceanographic Research Papers* 154, p. 103142. doi: 10.1016/j.dsr.2019.103142.

Hirano, N., Kawamura, K., Hattori, M., Saito, K. and Ogawa, Y. 2001. A new type of intra-plate volcanism; Young alkali-basalts discovered from the subducting Pacific Plate, Northern Japan Trench. *Geophysical Research Letters* 28, pp. 2719–2722. doi: 10.1029/2000GL012426.

Hirano, N., Machida, S., Abe, N., Morishita, T., Tamura, A. and Arai, S. 2013. Petit-spot lava fields off the central Chile trench induced by plate flexure. *Geochemical Journal* 47(2), pp. 249–257. doi: 10.2343/geochemj.2.0227.

Holland, T.J.B. and Richardson, S.W. 1979. Amphibole zonation in metabasites as a guide to the evolution of metamorphic conditions. *Contributions to Mineralogy and Petrology* 70(2), pp. 143–148. doi: 10.1007/BF00374442.

Hollocher, K., Robinson, P., Walsh, E. and Roberts, D. 2012. Geochemistry of amphibolite-facies volcanics and gabbros of the Storen Nappe in extensions west and southwest of Trondheim, western gneiss region, Norway: A key to correlations and paleotectonic settings. *American Journal of Science* 312(4), pp. 357–416. doi: 10.2475/04.2012.01.

Horák, J.M. 1993. *The late Precambrian Coedana and Sarn Complexes, north-west Wales - A geochemical and petrological study*. PhD Thesis, Cardiff, UK: University of Wales.

Horák, J.M., Doig, R., Evans, J.A. and Gibbons, W. 1996. Avalonian magmatism and terrane linkage: new isotopic data from the Precambrian of North Wales. *Journal of the Geological Society* 153, pp. 91–99. doi: 10.1144/gsjgs.153.1.0091.

Horák, J.M. and Evans, J.A. 2011. Early Neoproterozoic limestones from the Gwna Group, Anglesey. *Geological Magazine* 148(1), pp. 78–88. doi: 10.1017/S0016756810000464.

Horák, J.M. and Gibbons, W. 1986. Reclassification of blueschist amphiboles from Anglesey, North Wales. *Mineralogical Magazine* 50(357), pp. 533–535. doi: 10.1180/minmag.1986.050.357.18.

Hori, T. and Sakaguchi, H. 2011. Mechanism of décollement formation in subduction zones: Décollement formation in subduction zones. *Geophysical Journal International* 187(3), pp. 1089–1100. doi: 10.1111/j.1365-246X.2011.05204.x.

Hose, T.A. 2008. Towards a history of geotourism: definitions, antecedents and the future. *Geological Society, London, Special Publications* 300(1), pp. 37–60. doi: 10.1144/SP300.5.

Howells, M.F., Reedman, A.J. and Campbell, S.D.G. 1991. *Ordovician (Caradoc) marginal basin volcanism in Snowdonia (north-west Wales)*. London: HM Stationery Office.

Hsü, K.J. 1968. Principles of mélanges and their bearing on the Franciscan-Knoxville paradox. *Geological Society of America Bulletin* 79, pp. 1063–1074.

Hsü, K.J. 1974. Mélanges and their distinction from olistostromes. In: Dott, R. H. and Shaver, R. H. eds. *Modern and Ancient Geosynclinal Sedimentation*. SEPM (Society for Sedimentary Geology), pp. 321–333.

von Huene, R., Ranero, C.R. and Watts, P. 2004. Tsunamigenic slope failure along the Middle America Trench in two tectonic settings. *Marine Geology* 203(3–4), pp. 303–317. doi: 10.1016/S0025-3227(03)00312-8.

Humphreys, E.R. and Niu, Y. 2009. On the composition of ocean island basalts (OIB): The effects of lithospheric thickness variation and mantle metasomatism. *Lithos* 112, pp. 118–136. doi: 10.1016/j.lithos.2009.04.038.

Humphris, S.E., Melson, W.G. and Thompson, R.N. 1980. 34. Basalt weathering on the East Pacific Rise and the Galapagos spreading center, Deep Sea Drilling Project Leg 54. In: *Initial Reports of the Deep Sea Drilling Project, 54.* Initial Reports of the Deep Sea Drilling Project. U.S. Government Printing Office.

Irvine, T.N. and Baragar, W.R.A. 1971. A Guide to the Chemical Classification of the Common Volcanic Rocks. *Canadian Journal of Earth Sciences* 8(5), pp. 523–548. doi: 10.1139/e71-055.

Isozaki, Y., Maruyama, S. and Furuoka, F. 1990. Accreted oceanic materials in Japan. *Tectonophysics* 181, pp. 179–205. doi: 10.1016/0040-1951(90)90016-2.

Jackson, M.G. et al. 2007. The return of subducted continental crust in Samoan lavas. *Nature* 448(7154), pp. 684–687. doi: 10.1038/nature06048.

Jaroslow, G.E., Smith, D.K. and Tucholke, B.E. 2000. Record of seamount production and off-axis evolution in the western North Atlantic Ocean, 25°25′-27°10′N. *Journal of Geophysical Research: Solid Earth* 105(B2), pp. 2721–2736. doi: 10.1029/1999JB900253.

Jenner, F.E. and O'Neill, H.St.C. 2012. Analysis of 60 elements in 616 ocean floor basaltic glasses: TECHNICAL BRIEF. *Geochemistry, Geophysics, Geosystems* 13(2), p. n/a-n/a. doi: 10.1029/2011GC004009.

Jicha, B.R., Singer, B.S. and Valentine, M.J. 2013. 40Ar/39Ar Geochronology of Subaerial Ascension Island and a Re-evaluation of the Temporal Progression of Basaltic to Rhyolitic Volcanism. *Journal of Petrology* 54(12), pp. 2581–2596. doi: 10.1093/petrology/egt058.

Johns, W.D., Grim, R.E. and Brad, W.F. 1954. Quantitative Estimations of Clay Minerals by Diffraction Methods. *SEPM Journal of Sedimentary Research* Vol. 24.

Johnson, T.E., Kirkland, C.L., Gardiner, N.J., Brown, M., Smithies, R.H. and Santosh, M. 2019. Secular change in TTG compositions: Implications for the evolution of Archaean geodynamics. *Earth and Planetary Science Letters* 505, pp. 65–75. doi: 10.1016/j.epsl.2018.10.022.

Jordan, B.R., Fowler, A.-R., Mahmoud, B.E.D., El-Saiy, A.K. and Abdelghanny, O. 2008. Peperites and associated pillow lavas subjacent to the Oman Ophiolite. *Journal of Volcanology and Geothermal Research* 173(3–4), pp. 303–312. doi: 10.1016/j.jvolgeores.2008.01.019.

Kameda, J., Okamoto, A., Sato, K., Fujimoto, K., Yamaguchi, A. and Kimura, G. 2017. Opal-CT in chert beneath the toe of the Tohoku margin and its influence on the seismic aseismic transition in subduction zones. *Geophysical Research Letters* 44(2), pp. 687–693. doi: 10.1002/2016GL071784.

van de Kamp, P.C. 2008. Smectite-Illite-Muscovite Transformations, Quartz Dissolution, and Silica Release in Shales. *Clays and Clay Minerals* 56(1), pp. 66–81. doi: 10.1346/CCMN.2008.0560106.

Kawai, T. et al. 2007. Geotectonic framework of the Blueschist Unit on Anglesey–Lleyn, UK, and its role in the development of a Neoproterozoic accretionary orogen. *Precambrian Research* 153, pp. 11–28. doi: 10.1016/j.precamres.2006.11.002.

Kawai, T., Windley, B.F., Terabayashi, M., Yamamoto, H., Isozaki, Y. and Maruyama, S. 2008. Neoproterozoic glaciation in the mid-oceanic realm: An example from hemi-pelagic mudstones on Llanddwyn Island, Anglesey, UK. *Gondwana Research* 14, pp. 105–114. doi: 10.1016/j.gr.2007.12.008.

Kawai, T., Windley, B.F., Terabayashi, M., Yamamoto, H., Maruyama, S. and Isozaki, Y. 2006. Mineral isograds and metamorphic zones of the Anglesey blueschist belt, UK: implications for the metamorphic development of a Neoproterozoic subduction-accretion complex. *Journal of Metamorphic Geology* 24, pp. 591–602. doi: 10.1111/j.1525-1314.2006.00656.x.

Keller, T., Katz, R.F. and Hirschmann, M.M. 2017. Volatiles beneath mid-ocean ridges: Deep melting, channelised transport, focusing, and metasomatism. *Earth and Planetary Science Letters* 464, pp. 55–68. doi: 10.1016/j.epsl.2017.02.006.

Kelley, D.S., Baross, J.A. and Delaney, J.R. 2002. Volcanoes, Fluids, and Life at Mid-Ocean Ridge Spreading Centers. *Annual Review of Earth and Planetary Sciences* 30, pp. 385–491. doi: 10.1146/annurev.earth.30.091201.141331.

Kelley, K.A., Kingsley, R. and Schilling, J.-G. 2013. Composition of plume-influenced mid-ocean ridge lavas and glasses from the Mid-Atlantic Ridge, East Pacific Rise, Galápagos Spreading Center, and Gulf of Aden: PLUME-INFLUENCED MORB. *Geochemistry, Geophysics, Geosystems* 14(1), pp. 223–242. doi: 10.1002/ggge.20049.

Kent, R.W. and Fitton, J.G. 2000. Mantle Sources and Melting Dynamics in the British Palaeogene Igneous Province. *Journal of Petrology* 41, pp. 1023–1040. doi: 10.1093/petrology/41.7.1023.

Keppie, J.D., Nance, R.D., Murphy, J.B. and Dostal, J. 2003. Tethyan, Mediterranean, and Pacific analogues for the Neoproterozoic–Paleozoic birth and development of peri-Gondwanan terranes and their transfer to Laurentia and Laurussia. *Tectonophysics* 365(1–4), pp. 195–219. doi: 10.1016/S0040-1951(03)00037-4.

Kerr, A.C. 2014. Oceanic Plateaus. In: Holland, H. D. and Turekian, K. K. eds. *Treatise on Geochemistry*. 2nd edition. Oxford, UK: Elsevier, pp. 631–667.

Kerr, A.C. and Tarney, J. 2005. Tectonic evolution of the Caribbean and northwestern South America: The case for accretion of two Late Cretaceous oceanic plateaus. *Geology* 33(4), p. 269. doi: 10.1130/G21109.1.

Kimura, G. et al. 2012. Tectonic mélange as fault rock of subduction plate boundary. *Tectonophysics* 568–569, pp. 25–38. doi: 10.1016/j.tecto.2011.08.025.

Kipf, A. et al. 2014. Seamounts off the West Antarctic margin: A case for non-hotspot driven intraplate volcanism. *Gondwana Research* 25(4), pp. 1660–1679. doi: 10.1016/j.gr.2013.06.013.

Kiss, G., Molnár, F. and Palinkaš, L.A. 2008. Volcanic facies and hydrothermal processes in Triassic pillow basalts from the Darnó Unit, NE Hungary. *Geologia Croatica* 61(2–3), pp. 385–394.

Kitamura, Y. and Kimura, G. 2012. Dynamic role of tectonic mélange during interseismic process of plate boundary mega earthquakes. *Tectonophysics* 568–569, pp. 39–52. doi: 10.1016/j.tecto.2011.07.008.

Kogiso, T., Tatsumi, Y., Shimoda, G. and Barsczus, H.G. 1997. High μ (HIMU) ocean island basalts in southern Polynesia: New evidence for whole mantle scale recycling of subducted oceanic crust. *Journal of Geophysical Research: Solid Earth* 102(B4), pp. 8085–8103. doi: 10.1029/96JB03892.

Kohnstamm, M.A. and Mann, A. 1981. Transcurrent faulting and the anomalous position of pre-Carboniferous Anglesey - Matters Arising. *Nature* 293, p. 762.

Kokelaar, P. 1988. Tectonic controls of Ordovician arc and marginal basin volcanism in Wales. *Journal of the Geological Society* 145(5), pp. 759–775. doi: 10.1144/gsjgs.145.5.0759.

Kopf, A.J. 2002. Significance of mud volcanism. *Reviews of Geophysics* 40(2), p. 1005. doi: 10.1029/2000RG000093.

Kubalíková, L. 2013. Geomorphosite assessment for geotourism purposes. *Czech Journal of Tourism* 2(2), pp. 80–104. doi: 10.2478/cjot-2013-0005.

Kuno, H. 1968. Differentiation of basalt magmas. In: Hess, H. H. and Poldervaart, A. eds. *Basalts: The Poldervaart treatise on rocks of basaltic composition*. New York: Interscience, pp. 623–688.

Kusky, T. et al. 2020. Mélanges through time: Life cycle of the world's largest Archean mélange compared with Mesozoic and Paleozoic subduction-accretion-collision mélanges. *Earth-Science Reviews* , p. 103303. doi: 10.1016/j.earscirev.2020.103303.

Kusky, T.M., Bradley, D.C. and Haeussler, P. 1997. Progressive deformation of the Chugach accretionary complex, Alaska, during a paleogene ridge-trench encounter. *Journal of Structural Geology* 19(2), pp. 139–157. doi: 10.1016/S0191-8141(96)00084-3.

Kusky, T.M., Windley, B.F., Safonova, I., Wakita, K., Wakabayashi, J., Polat, A. and Santosh, M. 2013. Recognition of ocean plate stratigraphy in accretionary orogens through Earth history: A record of 3.8billion years of sea floor spreading, subduction, and accretion. *Gondwana Research* 24(2), pp. 501–547. doi: 10.1016/j.gr.2013.01.004.

Larrea, P., França, Z., Lago, M., Widom, E., Galé, C. and Ubide, T. 2013. Magmatic Processes and the Role of Antecrysts in the Genesis of Corvo Island (Azores Archipelago, Portugal). *Journal of Petrology* 54(4), pp. 769–793. doi: 10.1093/petrology/egs084.

Lassiter, J.C., Blichert-Toft, J., Hauri, E.H. and Barsczus, H.G. 2003. Isotope and trace element variations in lavas from Raivavae and Rapa, Cook–Austral islands: constraints on the nature of HIMU- and EM-mantle and the origin of mid-plate volcanism in French Polynesia. *Chemical Geology* 202(1–2), pp. 115–138. doi: 10.1016/j.chemgeo.2003.08.002.

Le Maitre, R.W. 2002. *Igneous Rocks: a classification and glossary of terms recommendations of the international union of geological sciences, subcommission on the systematics of igneous rocks*. 2nd ed. Cambridge: Cambridge university press.

Leah, H., Fagereng, Å., Groome, N. and Buchs, D.M. 2022. Heterogeneous subgreenschist deformation in an exhumed sediment-poor mélange. *In Press* , p. 42.

Leake, B.E. 1971. On aluminous and edenitic hornblendes. *Mineralogical Magazine* 38(296), pp. 389–407. doi: 10.1180/minmag.1971.038.296.01.

Leake, B.E. et al. 1997. Nomenclature of amphiboles: Report of the subcommittee on amphiboles of the International Mineralogical Association, Commission on new minerals and mineral names. *The Canadian Mineralogist* 35, pp. 219–246.

Lefeuvre, B., Agard, P., Verlaguet, A., Dubacq, B. and Plunder, A. 2020. Massive formation of lawsonite in subducted sediments from the Schistes Lustrés (W. Alps): Implications for mass transfer and decarbonation in cold subduction zones. *Lithos* .

Leterrier, J., Maury, R.C., Thonon, P., Girard, D. and Marchal, M. 1982. Clinopyroxene composition as a method of identification of the magmatic affinities of paleo-volcanic series. *Earth and Planetary Science Letters* 59(1), pp. 139–154. doi: 10.1016/0012-821X(82)90122-4.

Li, Z.-X., Evans, D.A.D. and Halverson, G.P. 2013. Neoproterozoic glaciations in a revised global palaeogeography from the breakup of Rodinia to the assembly of Gondwanaland. *Sedimentary Geology* 294, pp. 219–232. doi: 10.1016/j.sedgeo.2013.05.016.

Lin, S., Davis, D.W., Barr, S.M., Van Staal, C.R., Chen, Y. and Constantin, M. 2007. U-Pb Geochronological Constraints On The Evolution Of The ASPY Terrane, Cape Breton Island: Implications For Relationships Between ASPY And BRAS D'OR Terranes And Ganderia In The Canadian Appalachians. *American Journal of Science* 307(2), pp. 371–398. doi: 10.2475/02.2007.03.

Linnemann, U., Pereira, F., Jeffries, T.E., Drost, K. and Gerdes, A. 2008. The Cadomian Orogeny and the opening of the Rheic Ocean: The diacrony of geotectonic processes constrained by LA-ICP-MS U–Pb zircon dating (Ossa-Morena and Saxo-Thuringian Zones, Iberian and Bohemian Massifs). *Tectonophysics* 461(1–4), pp. 21–43. doi: 10.1016/j.tecto.2008.05.002.

Liou, J.G., Graham, S.A., Maruyama, S. and Zhang, R.Y. 1996. Characteristics and Tectonic Significance of the Late Proterozoic Aksu Blueschists and Diabasic Dikes, Northwest Xinjiang, China. *International Geology Review* 38(3), pp. 228–244. doi: 10.1080/00206819709465332.

Liou, J.G., Maruyama, S., Wang, X. and Graham, S. 1990. Precambrian blueschist terranes of the world. *Tectonophysics* 181, pp. 97–111. doi: 10.1016/0040-1951(90)90010-6.

Liu, C., Wang, Z., Raub, T.D., Macdonald, F.A. and Evans, D.A.D. 2014. Neoproterozoic cap-dolostone deposition in stratified glacial meltwater plume. *Earth and Planetary Science Letters* 404, pp. 22–32. doi: 10.1016/j.epsl.2014.06.039.

Lloyd, G.E. 2018. Syntectonic quartz vein evolution during progressive deformation. *Geological Society, London, Special Publications* 487, pp. 127–151. doi: 10.1144/SP487.3.

Locock, A.J. 2014. An Excel spreadsheet to classify chemical analyses of amphiboles following the IMA 2012 recommendations. *Computers & Geosciences* 62, pp. 1–11. doi: 10.1016/j.cageo.2013.09.011.

Macdonald, R., Thorpe, R.S., Gaskarth, J.W. and Grindrod, A.R. 1985. Multi-component origin of Caledonian lamprophyres of northern England. *Mineralogical Magazine* 49(353), pp. 485–494. doi: 10.1180/minmag.1985.049.353.01.

Machida, S., Hirano, N., Sumino, H., Hirata, T., Yoneda, S. and Kato, Y. 2015. Petit-spot geology reveals melts in upper-most asthenosphere dragged by lithosphere. *Earth and Planetary Science Letters* 426, pp. 267–279. doi: 10.1016/j.epsl.2015.06.018.

Mallick, S., Salters, V.J.M. and Langmuir, C.H. 2019. Geochemical Variability Along the Northern East Pacific Rise: Coincident Source Composition and Ridge Segmentation. *Geochemistry, Geophysics, Geosystems* 20(4), pp. 1889–1911. doi: 10.1029/2019GC008287.

Maltman, A.J. 1975. Ultramafic rocks in Angleseytheir non-tectonic emplacement. *Journal of the Geological Society* 131(6), pp. 593–603. doi: 10.1144/gsjgs.131.6.0593.

Maltman, A.J. 1977. Serpentinites and related rocks of Anglesey. *Geological Journal* 12(2), pp. 113–128. doi: 10.1002/gj.3350120202.

Maltman, A.J. 1979. Tectonic emplacement of ophiolitic rocks in the Precambrian Mona Complex of Anglesey. *Nature* 277, p. 327.

Mann, A. 1986. *Geological studies within the Mona Complex of central Anglesey, North Wales*. PhD Thesis, Cardiff University.

Mao, I., Robinson, A.M. and Dowling, R.K. 2009. Potential Geotourists: An Australian Case Study. *Journal of Tourism* 10(1), pp. 71–80.

Markl, G. and Baumgartner, L. 2002. pH changes in peralkaline late-magmatic fluids. *Contributions to Mineralogy and Petrology* 144(3), pp. 331–346. doi: 10.1007/s00410-002-0401-6.

Maruyama, S. 1997. Pacific-type orogeny revisited: Miyashiro-type orogeny proposed. *The Island Arc* 6, pp. 91–120. doi: 10.1111/j.1440-1738.1997.tb00042.x.

Maruyama, S., Kawai, T. and Windley, B.F. 2010a. Ocean plate stratigraphy and its imbrication in an accretionary orogen: the Mona Complex, Anglesey–Lleyn, Wales, UK. *Geological Society, London, Special Publications* 338(1), pp. 55–75. doi: 10.1144/SP338.4.

Maruyama, S. and Liou, J.G. 1988. Petrology of Franciscan Metabasites Along the Jadeite-Glaucophane Type Facies Series, Cazadero, California. *Journal of Petrology* 29, pp. 1–37. doi: 10.1093/petrology/29.1.1.

Maruyama, S., Liou, J.G. and Terabayashi, M. 1996. Blueschists and Eclogites of the World and Their Exhumation. *International Geology Review* 38, pp. 485–594. doi: 10.1080/00206819709465347.

Maruyama, S., Masago, H., Katayama, I., Iwase, Y., Toriumi, M., Omori, S. and Aoki, K. 2010b. A new perspective on metamorphism and metamorphic belts. *Gondwana Research* 18(1), pp. 106–137. doi: 10.1016/j.gr.2010.03.007.

Matley, C.A. 1899. On the Geology of Northern Anglesey. *Quarterly Journal of the Geological Society* 55(1–4), pp. 635–675. doi: 10.1144/GSL.JGS.1899.055.01-04.38.

Matley, C.A. 1928. The Pre-Cambrian Complex and Associated Rocks of South-Western Lleyn, Carnarvonshire. *Quarterly Journal of the Geological Society* 84(1–4), pp. 440–447. doi: 10.1144/GSL.JGS.1928.084.01-04.17.

Matsuda, T. and Isozaki, Y. 1991. Well-documented travel history of Mesozoic pelagic chert in Japan: From remote ocean to subduction zone. *Tectonics* 10(2), pp. 475–499. doi: 10.1029/90TC02134.

Matsumoto, M., Wallis, S., Aoya, M., Enami, M., Kawano, J., Seto, Y. and Shimobayashi, N. 2003. Petrological constraints on the formation conditions and retrograde P-T path of the Kotsu eclogite unit, central Shikoku. *Journal of Metamorphic Geology* 21, pp. 363–376. doi: 10.1046/j.1525-1314.2003.00449.x.

Max, M.D. and Roddick, J.C. 1989. Age of metamorphism in the Rosslare Complex, S.E. Ireland. *Proceedings of the Geologists' Association* 100, pp. 113–121. doi: 10.1016/S0016-7878(89)80070-7.

McConnell, B.J., Morris, J.H. and Kennan, P.S. 1999. A comparison of the Ribband Group (southeastern Ireland) to the Manx Group (Isle of Man) and Skiddaw Group (northwestern England). *Geological Society, London, Special Publications* 160(1), pp. 337–343. doi: 10.1144/GSL.SP.1999.160.01.22.

McIlroy, D. and Horák, J.M. 2006. Neoproterozoic: the late Precambrian terranes that formed Eastern Avalonia. In: Brenchley, P. J. and Rawson, P. F. eds. *The Geology of England and Wales*. The Geological Society of London, pp. 9–23.

Mertz, D.F., Weinrich, A.J., Sharp, W.D. and Renne, P.R. 2001. Alkaline intrusions in a near-trench setting, Franciscan Complex, California: Constraints from geochemistry, petrology, and 40Ar/39Ar chronology. *American Journal of Science* 301, pp. 877–911. doi: 10.2475/ajs.301.10.877.

Métrich, N., Zanon, V., Créon, L., Hildenbrand, A., Moreira, M. and Marques, F.O. 2014. Is the 'Azores Hotspot' a Wetspot? Insights from the Geochemistry of Fluid and Melt Inclusions in Olivine of Pico Basalts. *Journal of Petrology* 55(2), pp. 377–393. doi: 10.1093/petrology/egt071.

Mikhailenko, A.V., Nazarenko, O.V., Ruban, D.A. and Zayats, P.P. 2017. Aesthetics-based classification of geological structures in outcrops for geotourism purposes: a tentative proposal. *Geologos* 23(1), pp. 45–52. doi: 10.1515/logos-2017-0004.

Miljković, Đ. et al. 2018. Geosite Assessment Using Three Different Methods; a Comparative Study of the Krupaja and the Žagubica Springs – Hydrological Heritage of Serbia. *Open Geosciences* 10(1), pp. 192–208. doi: 10.1515/geo-2018-0015.

Millet, M.-A., Doucelance, R., Baker, J.A. and Schiano, P. 2009. Reconsidering the origins of isotopic variations in Ocean Island Basalts: Insights from fine-scale study of São Jorge Island, Azores archipelago. *Chemical Geology* 265(3–4), pp. 289–302. doi: 10.1016/j.chemgeo.2009.04.005.

Miyashiro, A. 1961. Evolution of metamorphic belts. *Journal of Petrology* 2, pp. 277–311.

Miyashiro, A. 1994. *Metamorphic petrology*. London: UCL Press.

Monié, P. and Agard, P. 2009. Coeval blueschist exhumation along thousands of kilometers: Implications for subduction channel processes: INSIGHTS INTO SUBDUCTION CHANNEL PROCESSES. *Geochemistry, Geophysics, Geosystems* 10(7), pp. 1–12. doi: 10.1029/2009GC002428.

Montgomery, H. and Kerr, A.C. 2009. Rethinking the origins of the red chert at La Désirade, French West Indies. *Geological Society, London, Special Publications* 328(1), pp. 457–467. doi: 10.1144/SP328.18.

Moore, D.E. 1984. Metamorphic History of a High-Grade Blueschist Exotic Block from the Franciscan Complex, California. *Journal of Petrology* 25(1), pp. 126–150. doi: 10.1093/petrology/25.1.126.

Morgan, J.K., Clague, D.A., Borchers, D.C., Davis, A.S. and Milliken, K.L. 2007. Mauna Loa's submarine western flank: Landsliding, deep volcanic spreading, and hydrothermal alteration: MAUNA LOA'S WESTERN FLANK. *Geochemistry, Geophysics, Geosystems* 8(5), p. n/a-n/a. doi: 10.1029/2006GC001420.

Morimoto, N. et al. 1988. Nomenclature of Pyroxenes. *Mineralogical Magazine* 52(367), pp. 535–550. doi: 10.1180/minmag.1988.052.367.15.

Mottl, M.J. 1983. Metabasalts, axial hot springs, and the structure of hydrothermal systems at mid-ocean ridges. *GSA Bulletin* 94(2), pp. 161–180.

Mougel, B., Agranier, A., Hemond, C. and Gente, P. 2014. A highly unradiogenic lead isotopic signature revealed by volcanic rocks from the East Pacific Rise. *Nature Communications* 5(1), p. 4474. doi: 10.1038/ncomms5474.

Muir, M.D., Bliss, G.M., Grant, P.R. and Fisher, M.J. 1979. Palaeontological evidence for the age of some supposedly Precambrian rocks in Anglesey, North Wales. *Journal of the Geological Society* 136, pp. 61–64. doi: 10.1144/gsjgs.136.1.0061.

Murphy, F.C. 1990. Basement-cover relationships of a reactivated Cadomian mylonite zone: Rosslare Complex, SE Ireland. *Geological Society, London, Special Publications* 51, pp. 329–339. doi: 10.1144/GSL.SP.1990.051.01.21.

Murphy, J.B., Pisarevsky, S.A., Nance, R.D. and Keppie, J.D. 2004. Neoproterozoic—Early Paleozoic evolution of peri-Gondwanan terranes: implications for Laurentia-Gondwana connections. *International Journal of Earth Sciences* 93, pp. 659–682.

Nance, R.D. et al. 2008. Neoproterozoic-early Palaeozoic tectonostratigraphy and palaeogeography of the peri-Gondwanan terranes: Amazonian v. West African connections. *Geological Society, London, Special Publications* 297(1), pp. 345–383. doi: 10.1144/SP297.17.

Nance, R.D. et al. 2010. Evolution of the Rheic Ocean. *Gondwana Research* 17(2–3), pp. 194–222. doi: 10.1016/j.gr.2009.08.001.

Nance, R.D. and Thompson, M.D. 1996. Avalonian and related peri-Gondwanan terranes of the circum-North Atlantic: An introduction. In: *Special Paper 304: Avalonian and related peri-Gondwanan terranes of the Circum-North Atlantic*. Geological Society of America, pp. 1–7.

Nedimović, M.R., Carbotte, S.M., Diebold, J.B., Harding, A.J., Canales, J.P. and Kent, G.M. 2008. Upper crustal evolution across the Juan de Fuca ridge flanks. *Geochemistry, Geophysics, Geosystems* 9(9), pp. 1–23. doi: 10.1029/2008GC002085.

Nemčok, M., Schamel, S. and Gayer, R.A. 2005. *Thrustbelts: structural architecture, thermal regimes and petroleum systems*. Cambridge ; New York: Cambridge University Press.

Nisbet, E.G. and Pearce, J.A. 1977. Clinopyroxene composition in mafic lavas from different tectonic settings. *Contributions to Mineralogy and Petrology* 63(2), pp. 149–160. doi: 10.1007/BF00398776.

Niu, Y. 2021. Lithosphere thickness controls the extent of mantle melting, depth of melt extraction and basalt compositions in all tectonic settings on Earth – A review and new perspectives. *Earth-Science Reviews*.

Niu, Y. and Batiza, R. 1997. Trace element evidence from seamounts for recycled oceanic crust in the Eastern Pacific mantle. *Earth and Planetary Science Letters* 148(3–4), pp. 471–483. doi: 10.1016/S0012-821X(97)00048-4.

Niu, Y., Regelous, M., Wendt, I.J., Batiza, R. and O'Hara, M.J. 2002. Geochemistry of near-EPR seamounts: importance of source vs. process and the origin of enriched mantle component. *Earth and Planetary Science Letters* 199(3–4), pp. 327–345. doi: 10.1016/S0012-821X(02)00591-5.

Niu, Y., Wilson, M., Humphreys, E.R. and O'Hara, M.J. 2012. A trace element perspective on the source of ocean island basalts (OIB) and fate of subducted ocean crust (SOC) and mantle lithosphere (SML). *Episodes* 35(2), pp. 310–327.

Nutt, M.J.C. and Smith, E.G. 1981. Transcurrent faulting and the anomalous position of pre-Carboniferous Anglesey. *Nature* 290(5806), pp. 492–495. doi: 10.1038/290492a0.

O'Brien, S.J., Tucker, R.D. and O'Driscoll, C.F. 1994. Neoproterozoic basement-cover relationships and the tectono-magmatic record of the Avalon Zone on the Hermitage Peninsula and environs, Newfoundland. In: *New Perspectives in the Appalachian-Caledonian orogen*., p. 21.

Ogata, K., Mutti, E., Pini, G.A. and Tinterri, R. 2012. Mass transport-related stratal disruption within sedimentary mélanges: Examples from the northern Apennines (Italy) and south-central Pyrenees (Spain). *Tectonophysics* 568–569, pp. 185–199. doi: 10.1016/j.tecto.2011.08.021.

Onishi, C.T., Kimura, G., Hashimoto, Y., Ikehara-Ohmori, K. and Watanabe, T. 2001. Deformation history of tectonic melange and its relationship to the underplating process and relative plate motion: An example from the deeply buried Shimanto Belt, SW Japan. *Tectonics* 20(3), pp. 376–393. doi: 10.1029/1999TC001154.

Otsuki, M. and Banno, S. 1990. Prograde and retrograde metamorphism of hematite-bearing basic schists in the Sanbagawa belt in central Shikoku. *Journal of Metamorphic Geology* 8, pp. 425–439. doi: 10.1111/j.1525-1314.1990.tb00629.x.

Palin, R.M., Santosh, M., Cao, W., Li, S.-S., Hernández-Uribe, D. and Parsons, A. 2020. Secular change and the onset of plate tectonics on Earth. *Earth-Science Reviews* .

Palin, R.M. and White, R.W. 2016. Emergence of blueschists on Earth linked to secular changes in oceanic crust composition. *Nature Geoscience* 9(1), pp. 60–64. doi: 10.1038/ngeo2605.

Panizza, M. 2001. Geomorphosites: Concepts, methods and examples of geomorphological survey. *Chinese Science Bulletin* 46(S1), pp. 4–5. doi: 10.1007/BF03187227.

Parsons, B. and Sclater, J.G. 1977. An analysis of the variation of ocean floor bathymetry and heat flow with age. *Journal of Geophysical Research* 82(5), pp. 803–827. doi: 10.1029/JB082i005p00803.

Pearce, J.A. 1976. Statistical Analysis of Major Element Patterns in Basalts. *Journal of Petrology* 17(1), pp. 15–43. doi: 10.1093/petrology/17.1.15.

Pearce, J.A. 1996. A User's Guide to Basalt Discrimination Diagrams. In: Wyman, D. A. ed. *Trace Element Geochemistry of Volcanic Rocks: Applications for Massive Sulphide Exploration: Geological Association of Canada, Short Course Notes*., pp. 79–113.

Pearce, J.A. 2008. Geochemical fingerprinting of oceanic basalts with applications to ophiolite classification and the search for Archean oceanic crust. *Lithos* 100, pp. 14–48. doi: 10.1016/j.lithos.2007.06.016.

Pearce, J.A. 2014. Geochemical Fingerprinting of the Earth's Oldest Rocks. *Geology* 42(2), pp. 175–176. doi: 10.1130/focus022014.1.

Pearce, J.A. and Cann, J.R. 1973. Tectonic setting of basic volcanic rocks determined using trace element analyses. *Earth and Planetary Science Letters* 19(2), pp. 290–300. doi: 10.1016/0012-821X(73)90129-5.

Pearce, J.A. and Peate, D.W. 1995. Tectonic implications of the composition of volcanic arc magmas. *Annual Review of Earth and Planetary Sciences* 23, pp. 251–285.

Pereira, M., Chichorro, M., Linnemann, U., Eguiluz, L. and Silva, J. 2006. Inherited arc signature in Ediacaran and Early Cambrian basins of the Ossa-Morena Zone (Iberian Massif, Portugal): Paleogeographic link with European and North African Cadomian correlatives. *Precambrian Research* 144(3–4), pp. 297–315. doi: 10.1016/j.precamres.2005.11.011.

Pereira, P., Pereira, D. and Caetano Alves, M.I. 2007. Geomorphosite assessment in Montesinho Natural Park (Portugal). *Geographica Helvetica* 62(3), pp. 159–168. doi: 10.5194/gh-62-159-2007.

Perfit, M.R. 2001. Mid-ocean Ridge Geochemistry And Petrology. In: *Encyclopedia of Ocean Sciences*. Elsevier, pp. 1778–1788.

Perfit, M.R. and Chadwick, W.W. 1998. Magmatism at Mid-Ocean Ridges: Constraints from Volcanological and Geochemical Investigations. In: Roger Buck, W., Delaney, P. T., Karson, J. A., and Lagabrielle, Y. eds. *Geophysical Monograph Series*. Washington, D. C.: American Geophysical Union, pp. 59–115.

Pharaoh, T., Haslam, R., Hough, E., Kirk, K., Leslie, G., Schofield, D. and Heafford, A. 2020. The Môn–Deemster–Ribblesdale fold–thrust belt, central UK: a concealed Variscan inversion belt located on weak Caledonian crust. *Geological Society, London, Special Publications* 490, pp. 153–176. doi: 10.1144/SP490-2018-109.

Pharaoh, T.C., Brewer, T.S. and Webb, P.C. 1993. Subduction-related magmatism of late Ordovician age in eastern England. *Geological Magazine* 130(5), pp. 647–656. doi: 10.1017/S0016756800020951.

Phillips, E. 1991a. Progressive deformation of the South Stack and New Harbour Groups, Holy Island, western Anglesey, North Wales. *Journal of the Geological Society* 148, pp. 1091–1100. doi: 10.1144/gsjgs.148.6.1091.

Phillips, E. 1991b. The lithostratigraphy, sedimentology and tectonic setting of the Monian Supergroup, western Anglesey, North Wales. *Journal of the Geological Society* 148(6), pp. 1079–1090. doi: 10.1144/gsjgs.148.6.1079.

Pickering, K.T. and Hiscott, R.N. 2016. *Deep-marine systems: processes, deposits, environments, tectonics and sedimentation*. Chichester, West Sussex ; Hoboken, NJ: John Wiley & Sons Inc.

Piercey, S.J. 2011. The setting, style, and role of magmatism in the formation of volcanogenic massive sulfide deposits. *Mineralium Deposita* 46(5–6), pp. 449–471. doi: 10.1007/s00126-011-0341-z.

Piper, J.D.A. 1976. Magnetic properties of Precambrian pillow lavas of the Mona Complex and a related dyke swarm, Anglesey, Wales. *Geological Journal* 11(2), pp. 189–201. doi: 10.1002/gj.3350110206.

Pollack, H.N. 2007. Thermal characteristics of the Archean. In: De Wit, M. J. and Ashwal, L. D. eds. *Oxford monographs on geology and geophysics*. Oxford, UK: Claredon Press, pp. 223–232.

Pollock, J.C., Hibbard, J.P. and Sylvester, P.J. 2009. Early Ordovician rifting of Avalonia and birth of the Rheic Ocean: U–Pb detrital zircon constraints from Newfoundland. *Journal of the Geological Society* 166(3), pp. 501–515. doi: 10.1144/0016-76492008-088.

Pothier, H.D., Waldron, J.W.F., Schofield, D.I. and DuFrane, S.A. 2015. Peri-Gondwanan terrane interactions recorded in the Cambrian–Ordovician detrital zircon geochronology of North Wales. *Gondwana Research* 28(3), pp. 987–1001. doi: 10.1016/j.gr.2014.08.009.

Potter, P.E., Maynard, J.B. and Depetris, P.J. 2010. *Mud and mudstones: introduction and overview*. Berlin: Springer.

Pourteau, A., Scherer, E.E., Schorn, S., Bast, R., Schmidt, A. and Ebert, L. 2019. Thermal evolution of an ancient subduction interface revealed by Lu–Hf garnet geochronology, Halilbağı Complex (Anatolia). *Geoscience Frontiers* 10(1), pp. 127–148. doi: 10.1016/j.gsf.2018.03.004.

Pralong, J.-P. 2005. A method for assessing tourist potential and use of geomorphological sites. *Géomorphologie : relief, processus, environnement* 11(3), pp. 189–196. doi: 10.4000/geomorphologie.350.

Prestvik, T., Barnes, C.G., Sundvoll, B. and Duncan, R.A. 1990. Petrology of Peter I Øy (Peter I Island), West Antarctica. *Journal of Volcanology and Geothermal Research* 44(3–4), pp. 315–338. doi: 10.1016/0377-0273(90)90025-B.

Prigmore, J.K., Butler, A.J. and Woodcock, N.H. 1997. Rifting during separation of Eastern Avalonia from Gondwana: Evidence from subsidence analysis. *Geology* 25(3), p. 203. doi: 10.1130/0091-7613(1997)025<0203:RDSOEA>2.3.CO;2.

Pu, J.P. et al. 2016. Dodging snowballs: Geochronology of the Gaskiers glaciation and the first appearance of the Ediacaran biota. *Geology* 44(11), pp. 955–958. doi: 10.1130/G38284.1.

Quesada, C. 2006. The Ossa-Morena Zone of the Iberian Massif: a tectonostratigraphic approach to its evolution. *Zeitschrift der Deutschen Gesellschaft für Geowissenschaften* 157(4), pp. 585–595. doi: 10.1127/1860-1804/2006/0157-0585.

Raase, P. 1974. Al and Ti contents of hornblende, indicators of pressure and temperature of regional metamorphism. *Contributions to Mineralogy and Petrology* 45(3), pp. 231–236. doi: 10.1007/BF00383440.

Raeisi, D., Gholoizade, K., Nayebi, N., Babazadeh, S. and Nejadhadad, M. 2019. Geochemistry and mineral composition of lamprophyre dikes, central Iran: implications for petrogenesis and mantle evolution. *Journal of Earth System Science* 128(3), p. 74. doi: 10.1007/s12040-019-1110-0.

Raymond, L.A. 1984. Classification of Melanges. *Geological Society of America, Special Paper* 198, pp. 7–20.

Reedman, A.J., Leveridge, B.E. and Evans, R.B. 1984. The Arfon Group ('Arvonian') of north Wales. *Proceedings of the Geologists' Association* 95, pp. 313–322.

Regalla, C.A., Rowe, C.D., Harrichhausen, N., Tarling, M.S. and Singh, J. 2018. Styles of underplating in the Marin Headlands terrane, Franciscan complex, California. In: *Geology and Tectonics of Subduction Zones: A Tribute to Gaku Kimura*. Geological Society of America.

Reinhard, A.A., Jackson, M.G., Blusztajn, J., Koppers, A.A.P., Simms, A.R. and Konter, J.G. 2019. "Petit Spot" Rejuvenated Volcanism Superimposed on Plume-Derived Samoan Shield Volcanoes: Evidence From a 645-m Drill Core From Tutuila Island, American Samoa. *Geochemistry, Geophysics, Geosystems* 20, pp. 1485–1507. doi: 10.1029/2018GC007985.

Remitti, F., Vannucchi, P., Bettelli, G., Fantoni, L., Panini, F. and Vescovi, P. 2011. Tectonic and sedimentary evolution of the frontal part of an ancient subduction complex at the transition from accretion to erosion: The case of the Ligurian wedge of the northern Apennines, Italy. *Geological Society of America Bulletin* 123(1–2), pp. 51–70. doi: 10.1130/B30065.1.

Reynard, E., Fontana, G., Kozlik, L. and Scapozza, C. 2007. A method for assessing 'scientific' and 'additional values' of geomorphosites. *Geographica Helvetica* 62(3), pp. 148–158. doi: 10.5194/gh-62-148-2007.

Rhodes, J.M., Huang, S., Frey, F.A., Pringle, M. and Xu, G. 2012. Compositional diversity of Mauna Kea shield lavas recovered by the Hawaii Scientific Drilling Project: Inferences on source lithology, magma supply, and the role of multiple volcanoes: COMPOSITIONAL DIVERSITY OF HSDP LAVAS. *Geochemistry, Geophysics, Geosystems* 13(3), p. n/a-n/a. doi: 10.1029/2011GC003812.

Richardson, S.W. 1970. The relation between a petrogenetic grid, facies series and the geothermal gradient in metamorphism. *Fortschrifte Mineralogische* 47, pp. 65–76.

Robertson, A.H.F. 2019. Patuki and Croisilles melanges in South Island, New Zealand: genesis related to Permian subduction–accretion processes. In: *Paleozoic-Mesozoic geology of South Island, New Zealand: Subduction-related processes adjacent to SE Gondwana.* Geological Society, London, Memoirs. London, UK: Geological Scoiety of London, pp. 119–156.

Rock, N.M.S. 1987. The nature and origin of lamprophyres: an overview. *Geological Society, London, Special Publications* 30(1), pp. 191–226. doi: 10.1144/GSL.SP.1987.030.01.09.

Rock, N.M.S., Gaskarth, J.W., Henney, P.J. and Shand, P. 1988. Late Caledonian dyke-swarms of Northern Britain: some preliminary petrogenic and tectonic implications of their province-wide distribution and chemical variation. *Canadian Mineralogist* 26, pp. 3–22.

Rojay, B., Yaliniz, K.M. and Altiner, D. 2001. Tectonic Implications of Some Cretaceous Pillow Basalts from the North Anatolian Ophiolitic Mélange(Central Anatolia-Turkey) to the Evolution of Neotethys. *Turkish Journal of Earth Sciences* 10(3), p. 11.

Rollinson, H.R. 1993. *Using geochemical data: evaluation, presentation, interpretation*. Harlow, Essex, England : New York: Longman Scientific & Technical ; Copublished in the U.S. with J. Wiley & Sons.

Rosenbauer, R.J., Bischoff, J.L. and Zierenberg, R.A. 1988. The Laboratory Albitization of Mid-Ocean Ridge Basalt. *The Journal of Geology* 96(2), pp. 237–244. doi: 10.1086/629213.

Roser, B.P. and Korsch, R.J. 1986. Determination of Tectonic Setting of Sandstone-Mudstone Suites Using SiO2 Content and K2O/Na2O Ratio. *The Journal of Geology* 94(5), pp. 635–650. doi: 10.1086/629071.

Roser, B.P. and Korsch, R.J. 1988. Provenance signatures of sandstone-mudstone suites determined using discriminant function analysis of major-element data. *Chemical Geology* 67(1–2), pp. 119–139. doi: 10.1016/0009-2541(88)90010-1.

Ross, P.-S. and Bédard, J.H. 2009. Magmatic affinity of modern and ancient subalkaline volcanic rocks determined from trace-element discriminant diagrams. Polat, A. ed. *Canadian Journal of Earth Sciences* 46(11), pp. 823–839. doi: 10.1139/E09-054.

Różycka, M. and Migoń, P. 2014. Visitors' background as a factor in geosite evaluation. The case of Cenozoic volcanic sites in the Pogórze Kaczawskie region, SW Poland. *Geotourism / Geoturystyka* 38–39(1), p. 3. doi: 10.7494/geotour.2014.38-39.3.

Ruiz Cruz, M.D. 2010. Zoned Ca-amphibole as a new marker of the Alpine metamorphic evolution of phyllites from the Jubrique unit, Alpujárride Complex, Betic Cordillera, Spain. *Mineralogical Magazine* 74(4), pp. 773–796. doi: 10.1180/minmag.2010.074.4.773.

Rushton, A.W.A., Brück, P.M., Molyneux, S.G., Williams, M. and Woodcock, N.H. eds. 2011. *A Revised Correlation of the Cambrian Rocks on the British Isles*. First. The Geological Society of London.

Ryan, M.C., Helland-Hansen, W., Johannessen, E.P. and Steel, R.J. 2009. Erosional vs. accretionary shelf margins: the influence of margin type on deepwater sedimentation: an example from the Porcupine Basin, offshore western Ireland. *Basin Research* 21(5), pp. 676–703. doi: 10.1111/j.1365-2117.2009.00424.x.

Rybár, P. 2010. Assessment of attractiveness (value) of geotouristic objects. *Acta Geoturistica* 1(2), pp. 13–21.

Saccani, E. 2015. A new method of discriminating different types of post-Archean ophiolitic basalts and their tectonic significance using Th-Nb and Ce-Dy-Yb systematics. *Geoscience Frontiers* 6(4), pp. 481–501. doi: 10.1016/j.gsf.2014.03.006.

Safonova, I., Biske, G., Romer, R.L., Seltmann, R., Simonov, V. and Maruyama, S. 2016a. Middle Paleozoic mafic magmatism and ocean plate stratigraphy of the South Tianshan, Kyrgyzstan. *Gondwana Research* 30, pp. 236–256. doi: 10.1016/j.gr.2015.03.006.

Safonova, I., Kojima, S., Nakae, S., Romer, R.L., Seltmann, R., Sano, H. and Onoue, T. 2015. Oceanic island basalts in accretionary complexes of SW Japan: Tectonic and petrogenetic implications. *Journal of Asian Earth Sciences* 113, pp. 508–523. doi: 10.1016/j.jseaes.2014.09.015.

Safonova, I., Maruyama, S., Kojima, S., Komiya, T., Krivonogov, S. and Koshida, K. 2016b. Recognizing OIB and MORB in accretionary complexes: A new approach based on ocean plate stratigraphy, petrology and geochemistry. *Gondwana Research* 33, pp. 92–114. doi: 10.1016/j.gr.2015.06.013.

Safonova, I.Yu. 2008. Geochemical evolution of intraplate magmatism in the Paleo-Asian Ocean from the Late Neoproterozoic to the Early Cambrian. *Journal of Petrology* 16, pp. 492–511. doi: 10.1134/S0869591108050056.

Safonova, I.Yu. 2009. Intraplate magmatism and oceanic plate stratigraphy of the Paleo-Asian and Paleo-Pacific Oceans from 600 to 140 Ma. *Ore Geology Reviews* 35(2), pp. 137–154. doi: 10.1016/j.oregeorev.2008.09.002.

Safonova, I.Yu. and Santosh, M. 2014. Accretionary complexes in the Asia-Pacific region: Tracing archives of ocean plate stratigraphy and tracking mantle plumes. *Gondwana Research* 25, pp. 126–158. doi: 10.1016/j.gr.2012.10.008.

Saito, T. et al. 2015. Geochemistry of accreted metavolcanic rocks from the Neoproterozoic Gwna Group of Anglesey–Lleyn, NW Wales, U.K.: MORB and OIB in the Iapetus Ocean. *Tectonophysics* 662, pp. 243–255. doi: 10.1016/j.tecto.2015.08.015.

Sánchez-García, T., Bellido, F., Pereira, M.F., Chichorro, M., Quesada, C., Pin, Ch. and Silva, J.B. 2010. Rift-related volcanism predating the birth of the Rheic Ocean (Ossa-Morena zone, SW Iberia). *Gondwana Research* 17(2–3), pp. 392–407. doi: 10.1016/j.gr.2009.10.005.

Sánchez-García, T., Chichorro, M., Solá, A.R., Álvaro, J.J. and Díez-Montes, A. 2019. The Cambrian-Early Ordovician Rift Stage in the Gondwanan Units of the Iberian Massif. In: Quesada, C. and Oliveira, J. T. eds. *The Geology of Iberia: A Geodynamic Approach*. Switzerland: Springer Nature.

Sánchez-García, T., Quesada, C., Bellido, F., Dunning, G.R. and González del Tánago, J. 2008. Two-step magma flooding of the upper crust during rifting: The Early Paleozoic of the Ossa Morena Zone (SW Iberia). *Tectonophysics* 461(1–4), pp. 72–90. doi: 10.1016/j.tecto.2008.03.006.

Sánchez-García, T., Bellido, F. and Quesada, C. 2003. Geodynamic setting and geochemical signatures of Cambrian–Ordovician rift-related igneous rocks (Ossa-Morena Zone, SW Iberia). *Tectonophysics* 365(1–4), pp. 233–255. doi: 10.1016/S0040-1951(03)00024-6.

Sano, H. and Kanmera, K. 1991. Collapse of ancient oceanic reef complex—what happened during collision of Akiyoshi reef complex? Sequence of collisional collapse and generation of collapse products. *Journal of the Geological Society of Japan* 97, pp. 631–644.

Sano, T. and Yamashita, S. 2019. Evolution, hydrothermal assimilation, and ascent of magma inferred from volatile contents in MORB glasses: An example from thick lava pile at IODP Site 1256. *Lithos* 346–347, p. 105143. doi: 10.1016/j.lithos.2019.07.010.

Sarrionandia, F., Carracedo Sánchez, M., Eguiluz, L., Ábalos, B., Rodríguez, J., Pin, C. and Gil Ibarguchi, J.I. 2012. Cambrian rift-related magmatism in the Ossa-Morena Zone (Iberian Massif): Geochemical and geophysical evidence of Gondwana break-up. *Tectonophysics* 570–571, pp. 135–150. doi: 10.1016/j.tecto.2012.07.023.

Sato, T. et al. 2015. Redox condition of the late Neoproterozoic pelagic deep ocean: 57Fe Mössbauer analyses of pelagic mudstones in the Ediacaran accretionary complex, Wales, UK. *Tectonophysics* 662, pp. 472–480. doi: 10.1016/j.tecto.2015.08.002.

Sato, Y. et al. 2018. Direct ascent to the surface of asthenospheric magma in a region of convex lithospheric flexure. *International Geology Review* 60, pp. 1231–1243. doi: 10.1080/00206814.2017.1379912.

Schilling, J.G., Zajac, M., Evans, R., Johnston, T., White, W., Devine, J.D. and Kingsley, R. 1983. Petrologic and geochemical variations along the Mid-Atlantic Ridge from 29 degrees N to 73 degrees N. *American Journal of Science* 283(6), pp. 510–586. doi: 10.2475/ajs.283.6.510.

Schlanger, S.O., Jackson, E.D., and et al. 1976. *Initial Reports of the Deep Sea Drilling Project, 33*. U.S. Government Printing Office.

Schmidt, M.W. and Poli, S. 2003. Generation of Mobile Components during Subduction of Oceanic Crust. In: Holland, H. D. and Turekian, K. K. eds. *Treatise on Geochemistry*. Elsevier-Pergamon, pp. 567–591.

Schofield, D.I., Evans, J.A., Millar, I.L., Wilby, P.R. and Aspden, J.A. 2008. New U–Pb and Rb–Sr constraints on pre-Acadian tectonism in North Wales. *Journal of the Geological Society* 165(5), pp. 891–894. doi: 10.1144/0016-76492008-044.

Schofield, D.I., Leslie, A.G., Wilby, P.R., Dartnall, R., Waldron, J.W.F. and Kendall, R.S. 2020. Tectonic evolution of Anglesey and adjacent mainland North Wales. *Geological Society, London, Special Publications* 503, pp. 371–390. doi: 10.1144/SP503-2020-9.

Schofield, D.I., Potter, J., Barr, S.M., Horák, J.M., Millar, I.L. and Longstaffe, F.J. 2016. Reappraising the Neoproterozoic 'East Avalonian' terranes of southern Great Britain. *Gondwana Research* 35, pp. 257–271. doi: 10.1016/j.gr.2015.06.001.

Sengör, A.M.C. 2003. The repeated rediscovery of mélanges and its implications for the possibility and the role of objective evidence in the scientific enterprise. *Special paper-Geological Society of America* 373, pp. 385–445. doi: 10.1130/0-8137-2373-6.385.

Serrano, E. and González-Trueba, J.J. 2005. Assessment of geomorphosites in natural protected areas: the Picos de Europa National Park (Spain). *Géomorphologie : relief, processus, environnement* 11(3), pp. 197–208. doi: 10.4000/geomorphologie.364.

Shackleton, R.M. 1954. The structure and succession of Anglesey and the Lleyn Peninsula. *Advancement of Science* 11, pp. 106–108.

Shackleton, R.M. 1969. The Precambrian of North Wales. In: Wood, D., S. ed. *The Precambrian and Lower Palaeozoic rocks of Wales*. Cardiff, UK: University of Wales Press, pp. 1–18.

Shackleton, R.M. 1975. Precambrian rocks of Wales. In: Harris, A. L., Shackleton, R. M., Watson, J., Downie, C., Harland, W. B., and Moorbath, S. eds. *A correlation of the Precambrian rocks in the British Isles*. Edinburgh, UK: Geological Society, London, Special Report No. 6, pp. 76–82.

Shand, P., Gaskarth, J.W., Thirlwall, M.F. and Rock, N.M.S. 1994. Late caledonian lamprophyre dyke swarms of South-Eastern Scotland. *Mineralogy and Petrology* 51(2–4), pp. 277–298. doi: 10.1007/BF01159733.

Shellnutt, J.G., Owen, J.V., Yeh, M.-W., Dostal, J. and Nguyen, D.T. 2019. Long-lived association between Avalonia and the Meguma terrane deduced from zircon geochronology of metasedimentary granulites. *Scientific Reports* 9(1), pp. 1–11. doi: 10.1038/s41598-019-40673-9.

Shervais, J.W. 1982. Ti-V plots and the petrogenesis of modern and ophiolitic lavas. *Earth and Planetary Science Letters* 59(1), pp. 101–118. doi: 10.1016/0012-821X(82)90120-0.

Shibuya, T., Aoki, K., Komiya, T. and Maruyama, S. 2010. Stratigraphy-related, low-pressure metamorphism in the Hardey Syncline, Hamersley Province, Western Australia. *Gondwana Research* 18(1), pp. 213–221. doi: 10.1016/j.gr.2010.01.002.

Shields, G.A. 2005. Neoproterozoic cap carbonates: a critical appraisal of existing models and the plumeworld hypothesis. *Terra Nova* 17(4), pp. 299–310. doi: 10.1111/j.1365-3121.2005.00638.x.

Silver, E.A. and Beutner, E.C. 1980. Melanges. *Geology* (8), pp. 32–34.

Sinton, J.M. and Detrick, R.S. 1992. Mid-ocean ridge magma chambers. *Journal of Geophysical Research* 97, pp. 197–216. doi: 10.1029/91JB02508.

Sinton, J.M. and Fryer, P. 1987. Mariana Trough lavas from 18°N: Implications for the origin of back arc basin basalts. *Journal of Geophysical Research* 92(B12), p. 12782. doi: 10.1029/JB092iB12p12782.

Sisson, T.W., Kimura, J.-I. and Coombs, M.L. 2009. Basanite–nephelinite suite from early Kilauea: carbonated melts of phlogopite–garnet peridotite at Hawaii's leading magmatic edge. *Contributions to Mineralogy and Petrology* 158(6), pp. 803–829. doi: 10.1007/s00410-009-0411-8.

Soper, N.J. and Dunning, F.W. 2005. Structure and sequence of the Ingleton Group, basement to the central Pennines of northern England. *Proceedings of the Yorkshire Geological Society* 55(4), pp. 241–261. doi: 10.1144/pygs.55.4.241.

Spear, F.S. 1995. *Metamorphic phase equilibria and pressure-temperature-time paths*. 2nd edition. Washington, D.C: Mineralogical Society of America.

van Staal, C.R. and Barr, S.M. 2012. Lithospheric architecture and tectonic evolution of the Canadian Appalachians and associated Atlantic Margin. *Geological Association of Canada Special Papers* , pp. 41–95.

van Staal, C.R., Barr, S.M., McCausland, P.J.A., Thompson, M.D. and White, C.E. 2020. Tonian–Ediacaran tectonomagmatic evolution of West Avalonia and its Ediacaran–early Cambrian interactions with Ganderia: an example of complex terrane transfer due to arc–arc collision? *Geological Society, London, Special Publications* 503, pp. 143–167. doi: 10.1144/SP503-2020-23.

van Staal, C.R., Barr, S.M. and Murphy, J.B. 2012. Provenance and tectonic evolution of Ganderia: Constraints on the evolution of the Iapetus and Rheic oceans. *Geology* 40(11), pp. 987–990.

van Staal, C.R., Sullivan, R.W. and Whalen, J.B. 1996. Provenance and tectonic history of the Gander Zone in the Caledonian/Appalachian orogen: Implications for the origin and assembly of Avalon. In: Nance, R. D. and Thompson, M. D. eds. *Avalonian and Related Peri-Gondwanan Terranes of the Circum-North Atlantic*. Special paper. Boulder, Colorado: Geological Society of America, pp. 347–368.

Staudigel, H. and Hart, S.R. 1983. Alteration of basaltic glass: Mechanisms and significance for the oceanic crust-seawater budget. *Geochimica et Cosmochimica Acta* 47(3), pp. 337–350. doi: 10.1016/0016-7037(83)90257-0.

Staudigel, H., Hart, S.R. and Richardson, S.H. 1981. Alteration of the oceanic crust: Processes and timing. *Earth and Planetary Science Letters* 52(2), pp. 311–327. doi: 10.1016/0012-821X(81)90186-2.

Stone, P. and Evans, J.A. 1995. Nd-isotope study of provenance patterns across the British sector of the Iapetus Suture. *Geological Magazine* 132(5), pp. 571–580. doi: 10.1017/S0016756800021233.

Strachan, R.A. 2012. Late Neoproterozoic to Cambrian Accretionary History of Eastern Avalonia and Armorica on the Active Margin of Gondwana. In: Woodcock, N. and Strachan, R. eds. *Geological History of Britain and Ireland*. Chichester, UK: John Wiley & Sons, Ltd, pp. 133–149.

Strachan, R.A., Collins, A.S., Buchan, C., Nance, R.D., Murphy, J.B. and D'Lemos, R.S. 2007. Terrane analysis along a Neoproterozoic active margin of Gondwana: insights from U–Pb zircon geochronology. *Journal of the Geological Society* 164(1), pp. 57–60. doi: 10.1144/0016-76492006-014.

Štrba, L. et al. 2014. Geosite assessments: comparison of methods and results. *Current Issues in Tourism* 18(5), pp. 496–510. doi: 10.1080/13683500.2014.882885.

Stroncik, N.A. and Schmincke, H.-U. 2001. Evolution of palagonite: Crystallization, chemical changes, and element budget. *Geochemistry, Geophysics, Geosystems* 2(7), pp. 1–43. doi: 10.1029/2000GC000102.

Stroncik, N.A. and Schmincke, H.-U. 2002. Palagonite – a review. *International Journal of Earth Sciences* 91(4), pp. 680–697. doi: 10.1007/s00531-001-0238-7.

Suetsugu, D., Steinberger, B. and Kogiso, T. 2013. Mantle Plumes and Hotspots. In: *Reference Module in Earth Systems and Environmental Sciences*. Elsevier, pp. 1–8.

Sun, S. -s. and McDonough, W.F. 1989. Chemical and isotopic systematics of oceanic basalts: implications for mantle compositionand processes. *Geological Society, London, Special Publications* 42, pp. 313–345. doi: 10.1144/GSL.SP.1989.042.01.19.

Suzuki, D.A. and Takagi, H. 2018. Evaluation of Geosite for Sustainable Planning and Management in Geotourism. *Geoheritage* 10, pp. 123–135. doi: 10.1007/s12371-017-0225-4.

Takamasa, A., Nakai, S., Sahoo, Y., Hanyu, T. and Tatsumi, Y. 2009. W isotope compositions of oceanic islands basalts from French Polynesia and their meaning for core–mantle interaction. *Chemical Geology* 260(1–2), pp. 37–46. doi: 10.1016/j.chemgeo.2008.11.018.

Tardy, Y. and Duplay, J. 1994. Chapter 5 Stability Fields of Smectites and Illites Including Glauconites as a Function of Temperature and Chemical Composition. In: *Developments in Sedimentology*. Elsevier, pp. 95–132.

Tatsumi, Y. and Eggins, S. 1995. *Subduction zone magmatism*. Cambridge, Mass., USA: Blackwell Science.

Taylor, B. and Martinez, F. 2003. Back-arc basin basalt systematics. *Earth and Planetary Science Letters* 210(3–4), pp. 481–497. doi: 10.1016/S0012-821X(03)00167-5.

Teagle, D.A.H., Alt, J.C., Umino, S., Miyashita, S., Banerjee, N.R., Wilson, D.S., and Expedition 309/312 Scientists eds. 2006. *Proceedings of the IODP, 309/312*. Integrated Ocean Drilling Program.

Teagle, D.A.H., Wilson, D.S., Acton, G.D. and Vanko, D.A. eds. 2007. *Proceedings of the Ocean Drilling Program, 206 Scientific Results*. Ocean Drilling Program. Available at: http://www-odp.tamu.edu/publications/206_SR/206TOC.HTM [Accessed: 24 May 2022].

Terabayashi, M. 1988. Actinolite-forming reaction at low pressure and the role of Fe2+-Mg substitution. *Contributions to Mineralogy and Petrology* 100(3), pp. 268–280. doi: 10.1007/BF00379738.

Thompson, G., Bryan, W.B. and Humphris, S.E. 1989. Axial volcanism on the East Pacific Rise, 10–12°N. *Geological Society, London, Special Publications* 42(1), pp. 181–200. doi: 10.1144/GSL.SP.1989.042.01.12.

Thomson, B.J., Hurowitz, J.A., Baker, L.L., Bridges, N.T., Lennon, A.M., Paulsen, G. and Zacny, K. 2014. The effects of weathering on the strength and chemistry of Columbia River Basalts and their implications for Mars Exploration Rover Rock Abrasion Tool (RAT) results. *Earth and Planetary Science Letters* 400, pp. 130–144. doi: 10.1016/j.epsl.2014.05.012.

Thorpe, R.S. 1972. Ocean floor basalt affinity of Precambrian glaucophane schist from Anglesey. *Nature Physical Science* 240, pp. 164–166.

Thorpe, R.S. 1978. Tectonic emplacement of ophiolite rocks in the Precambrian Mona Complex of Anglesey. 276, pp. 57–58.

Thorpe, R.S. 1993. Geochemistry and eruptive environment of metavolcanic rocks from the Mona Complex of Anglesey, North Wales, U.K. *Geological Magazine* 130(1), pp. 85–91. doi: 10.1017/S0016756800023748.

Thorpe, R.S., Beckinsale, R.D., Patchett, P.J., Piper, J.D.A., Davies, G.R. and Evans, J.A. 1984. Crustal growth and late Precambrian-early Palaeozoic plate tectonic evolution of England and Wales. *Journal of the Geological Society* 141, pp. 521–536. doi: 10.1144/gsjgs.141.3.0521.

Thorpe, R.S., Gaskarth, J.W. and Henney, P.J. 1993a. Composite Ordovician lamprophyre (spessartite) intrusions around the Midlands Microcraton in central Britain. *Geological Magazine* 130(5), pp. 657–663. doi: 10.1017/S0016756800020963.

Thorpe, R.S., Leat, P.T., Mann, A.C., Howells, M.F., Reedman, A.J. and Campbell, S.D.G. 1993b. Magmatic Evolution of the Ordovician Snowdon Volcanic Centre, North Wales (UK). *Journal of Petrology* 34(4), pp. 711–741. doi: 10.1093/petrology/34.4.711.

Tietzsch-Tyler, D. and Phillips, E. 1989. Extended Abstract: Correlation of the Monian Supergroup in NW Anglesey with the Cahore Group in SE Ireland. *Journal of the Geological Society* 146, pp. 417–418. doi: 10.1144/gsjgs.146.3.0417.

Tomić, N. and Božić, S. 2014. A modified Geosite Assessment Model (M-GAM) and its Application on the Lazar Canyon area (Serbia). *Int. J. Environ. Res.* 8(4), pp. 1041–1052.

Totten, M. and Blatt, H. 1993. Alterations in the Non-Clay-Mineral Fraction of Pelitic Rocks Across the Diagenetic to Low-Grade Metamorphic Transition, Ouachita Mountains, Oklahoma and Arkansas. *Journal of Sedimentary Research* 63(5), pp. 899–908. doi: 10.1306/D4267C3F-2B26-11D7-8648000102C1865D.

Treagus, J. 2007. Metamorphic zones in the Anglesey blueschist belt and implications for the development of a Neoproterozoic subduction-accretion complex: discussion. *Journal of Metamorphic Geology* 25, pp. 507–508. doi: 10.1111/j.1525-1314.2007.00709.x.

Treagus, J. 2008. *Anglesey geology: a field guide = Daeareg Ynys Môn: arweinlyfr maes*. Ludlow: Seabury Salmon & Associates.

Treagus, J.E., Treagus, S.H. and Woodcock, N.H. 2013. The significance of the boundary between the Rhoscolyn and New Harbour formations on Holy Island, North Wales, to the deformation history of Anglesey. *Geological Magazine* 150(3), pp. 519–535. doi: 10.1017/S0016756812000775.

Trindade, R.I.F. and Macouin, M. 2007. Palaeolatitude of glacial deposits and palaeogeography of Neoproterozoic ice ages. *Comptes Rendus Geoscience* 339(3–4), pp. 200–211. doi: 10.1016/j.crte.2007.02.006.

Troll, V.R. and Carracedo, J.C. 2016. The Geology of La Palma. In: *The Geology of the Canary Islands*. Elsevier, pp. 101–180.

Tsujimori, T. and Ernst, W.G. 2014. Lawsonite blueschists and lawsonite eclogites as proxies for palaeo-subduction zone processes: a review. *Journal of Metamorphic Geology* 32, pp. 437–454. doi: 10.1111/jmg.12057.

Tucker, R.D. and Pharaoh, T.C. 1991. U-Pb zircon ages for Late Precambrian igneous rocks in southern Britain. *Journal of the Geological Society* 148(3), pp. 435–443. doi: 10.1144/gsjgs.148.3.0435.

Turner, F.J. 1981. *Metamorphic petrology: mineralogical, field, and tectonic aspects*. 2nd edition. Washington: McGraw-Hill.

Uenzelmann-Neben, G., Schmidt, D.N., Niessen, F. and Stein, R. 2012. Intraplate volcanism off South Greenland: caused by glacial rebound?: Intraplate volcanism off South Greenland. *Geophysical Journal International* 190, pp. 1–7. doi: 10.1111/j.1365-246X.2012.05468.x.

Ujiie, K. 2002. Evolution and kinematics of an ancient décollement zone, mélange in the Shimanto accretionary complex of Okinawa Island, Ryukyu Arc. *Journal of Structural Geology* 24(5), pp. 937–952. doi: 10.1016/S0191-8141(01)00103-1.

Valentine, G.A. and Hirano, N. 2010. Mechanisms of low-flux intraplate volcanic fields—Basin and Range (North America) and northwest Pacific Ocean. *Geology* 38, pp. 55–58. doi: 10.1130/G30427.1.

Valley, J.W. et al. 2005. 4.4 billion years of crustal maturation: oxygen isotope ratios of magmatic zircon. *Contributions to Mineralogy and Petrology* 150(6), pp. 561–580. doi: 10.1007/s00410-005-0025-8.

Vannucchi, P., Sak, P.B., Morgan, J.P., Ohkushi, K., Ujiie, K., and the IODP Expedition 334 Shipboard Scientists 2013. Rapid pulses of uplift, subsidence, and subduction erosion offshore Central America: Implications for building the rock record of convergent margins. *Geology* 41(9), pp. 995–998. doi: 10.1130/G34355.1.

Vujičić, M.D., Vasiljević, D.A., Marković, S.B., Hose, T.A., Lukić, T., Hadžić, O. and Janićević, S. 2011. Preliminary geosite assessment model (gam) and its application on Fruška gora mountain, potential geotourism destination of Serbia. *Acta geographica Slovenica* 51(2), pp. 361–376. doi: 10.3986/AGS51303.

Wakabayashi, J. 2017. Structural context and variation of ocean plate stratigraphy, Franciscan Complex, California: insight into mélange origins and subduction-accretion processes. *Progress in Earth and Planetary Science* 4(1), p. 18. doi: 10.1186/s40645-017-0132-y.

Wakita, K. 2012a. Mappable features of mélanges derived from Ocean Plate Stratigraphy in the Jurassic accretionary complexes of Mino and Chichibu terranes in Southwest Japan. *Tectonophysics* 568–569, pp. 74–85. doi: 10.1016/j.tecto.2011.10.019.

Wakita, K. 2012b. Mappable features of mélanges derived from Ocean Plate Stratigraphy in the Jurassic accretionary complexes of Mino and Chichibu terranes in Southwest Japan. *Tectonophysics* 568–569, pp. 74–85. doi: 10.1016/j.tecto.2011.10.019.

Wakita, K. 2015. OPS mélange: a new term for mélanges of convergent margins of the world. *International Geology Review* 57(5–8), pp. 529–539. doi: 10.1080/00206814.2014.949312.

Wakita, K. 2019. Tectonic setting required for the preservation of sedimentary mélanges in Palaeozoic and Mesozoic accretionary complexes of southwest Japan. *Gondwana Research* 74, pp. 90–100. doi: 10.1016/j.gr.2019.03.006.

Wakita, K. and Metcalfe, I. 2005. Ocean Plate Stratigraphy in East and Southeast Asia. *Journal of Asian Earth Sciences* 24(6), pp. 679–702. doi: 10.1016/j.jseaes.2004.04.004.

Waldron, J.W.F. et al. 2014a. Ganderia–Laurentia collision in the Caledonides of Great Britain and Ireland. *Journal of the Geological Society* 171, pp. 555–569. doi: 10.1144/jgs2013-131.

Waldron, J.W.F., Schofield, D.I. and Murphy, J.B. 2019a. Diachronous Paleozoic accretion of peri-Gondwanan terranes at the Laurentian margin. *Geological Society, London, Special Publications* 470, pp. 289–310. doi: 10.1144/SP470.11.

Waldron, J.W.F., Schofield, D.I., Murphy, J.B. and Thomas, C.W. 2014b. How was the Iapetus Ocean infected with subduction? *Geology* 42, pp. 1095–1098. doi: 10.1130/G36194.1.

Waldron, J.W.F., Schofield, D.I., Pearson, G., Sarkar, C., Luo, Y. and Dokken, R. 2019b. Detrital zircon characterization of early Cambrian sandstones from East Avalonia and SE Ireland: implications for terrane affinities in the peri-Gondwanan Caledonides. *Geological Magazine* 156, pp. 1217–1232. doi: 10.1017/S0016756818000407.

Waldron, J.W.F., Schofield, D.I., White, C.E. and Barr, S.M. 2011. Cambrian successions of the Meguma Terrane, Nova Scotia, and Harlech Dome, North Wales: dispersed fragments of a peri-Gondwanan basin? *Journal of the Geological Society* 168(1), pp. 83–98. doi: 10.1144/0016-76492010-068.

Wang, K., Hu, Y., von Huene, R. and Kukowski, N. 2010. Interplate earthquakes as a driver of shallow subduction erosion. *Geology* 38(5), pp. 431–434. doi: 10.1130/G30597.1.

Wang, X.-J. et al. 2018. Recycled ancient ghost carbonate in the Pitcairn mantle plume. *Proceedings of the National Academy of Sciences* 115(35), pp. 8682–8687. doi: 10.1073/pnas.1719570115.

Warren, C.J. 2013. Exhumation of (ultra-)high-pressure terranes: concepts and mechanisms. *Solid Earth* 4(1), pp. 75–92. doi: 10.5194/se-4-75-2013.

Waters, C.L. et al. 2020. Sulfide mantle source heterogeneity recorded in basaltic lavas from the Azores. *Geochimica et Cosmochimica Acta* 268, pp. 422–445. doi: 10.1016/j.gca.2019.10.012.

Watson, E.B., Wark, D.A. and Thomas, J.B. 2006. Crystallization thermometers for zircon and rutile. *Contributions to Mineralogy and Petrology* 151(4), pp. 413–433. doi: 10.1007/s00410-006-0068-5.

Watts, A.B. 2001. *Isostasy and flexure of the lithosphere*. Cambridge ; New York: Cambridge University Press.

Weaver, C.E. 1961. Clay minerals of the Ouachita structural belt and adjacent foreland. In: Flawn, P. T. ed. *The Ouachita system*. Austin, Tx, USA: University of Texas Press, pp. 147–162.

Wen, B., Evans, D.A.D., Anderson, R.P. and McCausland, P.J.A. 2020. Late Ediacaran paleogeography of Avalonia and the Cambrian assembly of West Gondwana. *Earth and Planetary Science Letters* 552, p. 116591. doi: 10.1016/j.epsl.2020.116591.

van der Werff, W. 1995. Structure and morphotectonics of the accretionary prism along the Eastern Sunda-Western Banda Arc. *Journal of Southeast Asian Earth Sciences* 11(4), pp. 309–322. doi: 10.1016/0743-9547(94)00038-G.

Wessel, P., Sandwell, D. and Kim, S.-S. 2010. The Global Seamount Census. *Oceanography* 23, pp. 24–33. doi: 10.5670/oceanog.2010.60.

Wimbledon, W.A.P. et al. 1995. The development of a methodology for the selection of British geological sites for conservation: Part 1. *Modern Geology* 20, pp. 159–202.

Wimbledon, W.A.P., Andersen, S., Cleal, C.J., Cowie, J., Erikstad, L., Karis, L. and Suominen, V. 1999. Geological world heritage; GEOSITES; a global comparative site inventory to enable prioritisation for conservation. *Memorie Descritive della Carta Geologica d'Italia* 54, pp. 45–60.

Wimbledon, W.A.P. and Smith-Meyer, S. eds. 2012. *Geoheritage in Europe and its conservation*. Oslo: ProGEO.

Winter, J.D. 2010. *Principles of igneous and metamorphic petrology*. 2nd edition. New York: Prentice Hall.

Wood, D., S. 1974. Ophiolites, Melanges, Blueschists, and Ignimbrites: Early Caledonian Subduction in Wales? In: Dott, R. H. and Shaver, R. H. eds. *Modern and Ancient Geosynclinal Sedimentation*. SEPM (Society for Sedimentary Geology).

Wood, D.A. 1980. The application of a ThHfTa diagram to problems of tectonomagmatic classification and to establishing the nature of crustal contamination of basaltic lavas of the British Tertiary Volcanic Province. *Earth and Planetary Science Letters* 50(1), pp. 11–30. doi: 10.1016/0012-821X(80)90116-8.

Wood, M. 2012. The Historical Development of the Term 'Mélange' and Its Relevance to the Precambrian Geology of Anglesey and the Lleyn Peninsula in Wales, UK. *Journal of Geography (Chigaku Zasshi)* 121(1), pp. 168–180. doi: 10.5026/jgeography.121.168.

Wood, M. and Nicholls, G.D. 1973. Precambrian stromatolitic limestones from Northern Anglesey. *Nature Physical Science* 241, p. 65.

Woodcock, N.H. and Morris, J.H. 1999. Debris flows on the Ordovician margin of Avalonia: Lady Port Formation, Manx Group, Isle of Man. *Geological Society, London, Special Publications* 160(1), pp. 121–138. doi: 10.1144/GSL.SP.1999.160.01.09.

Woodcock, N.H., Soper, N.J. and Strachan, R.A. 2007. A Rheic cause for the Acadian deformation in Europe. *Journal of the Geological Society* 164(5), pp. 1023–1036. doi: 10.1144/0016-76492006-129.

Woodhead, J.D. and McCulloch, M.T. 1989. Ancient seafloor signals in Pitcairn Island lavas and evidence for large amplitude, small length-scale mantle heterogeneities. *Earth and Planetary Science Letters* 94(3–4), pp. 257–273. doi: 10.1016/0012-821X(89)90145-3.

Workman, R.K. et al. 2004. Recycled metasomatized lithosphere as the origin of the Enriched Mantle II (EM2) end-member: Evidence from the Samoan Volcanic Chain: RECYCLED METASOMATIZED LITHOSPHERE. *Geochemistry, Geophysics, Geosystems* 5(4), p. n/a-n/a. doi: 10.1029/2003GC000623.

Xu, C. et al. 2018. Cold deep subduction recorded by remnants of a Paleoproterozoic carbonated slab. *Nature Communications* 9(1), p. 2790. doi: 10.1038/s41467-018-05140-5.

Yamamoto, J., Korenaga, J., Hirano, N. and Kagi, H. 2014. Melt-rich lithosphere-asthenosphere boundary inferred from petit-spot volcanoes. *Geology* 42, pp. 967–970. doi: 10.1130/G35944.1.

Yan, Z., Xiao, W., Aitchison, J.C., Yuan, C., Liu, C. and Fu, C. 2021. Age and origin of accreted ocean plate stratigraphy in the North Qilian belt, NE Tibet Plateau: evidence from microfossils and geochemistry of cherts and siltstones. *Journal of the Geological Society* 178(6), pp. jgs2020-231. doi: 10.1144/jgs2020-231.

Yang, A.Y., Langmuir, C.H., Cai, Y., Michael, P., Goldstein, S.L. and Chen, Z. 2021. A subduction influence on ocean ridge basalts outside the Pacific subduction shield. *Nature Communications* 12(1), p. 4757. doi: 10.1038/s41467-021-25027-2.

Yang, S., Humayun, M. and Salters, V.J.M. 2018. Elemental Systematics in MORB Glasses From the Mid-Atlantic Ridge. *Geochemistry, Geophysics, Geosystems* 19(11), pp. 4236–4259. doi: 10.1029/2018GC007593.

Yardley, B.W.D. 1989. *An introduction to metamorphic petrology*. Harlow, Essex, England : New York: Longman Scientific & Technical ; Wiley.

Zagorevski, A., van Staal, C.R., McNicoll, V., Rogers, N. and Valverde-Vaquero, P. 2008. Tectonic architecture of an arc-arc collision zone, Newfoundland Appalachians. In: *Special Paper 436: Formation and Applications of the Sedimentary Record in Arc Collision Zones*. Geological Society of America, pp. 309–333.

Zagorevski, A., van Staal, C.R., McNicoll, V.J., Hartree, L. and Rogers, N. 2012. Tectonic evolution of the Dunnage Mélange tract and its significance to the closure of Iapetus. *Tectonophysics* 568–569, pp. 371–387. doi: 10.1016/j.tecto.2011.12.011.

Zanon, V. and Pimentel, A. 2015. Spatio-temporal constraints on magma storage and ascent conditions in a transtensional tectonic setting: The case of the Terceira Island (Azores). *American Mineralogist* 100(4), pp. 795–805. doi: 10.2138/am-2015-4936.

Zanon, V. and Viveiros, F. 2019. A multi-methodological re-evaluation of the volcanic events during the 1580 CE and 1808 eruptions at São Jorge Island (Azores Archipelago, Portugal). *Journal of Volcanology and Geothermal Research* 373, pp. 51–67. doi: 10.1016/j.jvolgeores.2019.01.028.

Zhang, G.-L. and Smith-Duque, C. 2014. Seafloor basalt alteration and chemical change in the ultra thinly sedimented South Pacific. *Geochemistry, Geophysics, Geosystems* 15(7), pp. 3066–3080. doi: 10.1002/2013GC005141.

Zhu, W. et al. 2011. Neoproterozoic tectonic evolution of the Precambrian Aksu blueschist terrane, northwestern Tarim, China: Insights from LA-ICP-MS zircon U–Pb ages and geochemical data. *Precambrian Research* 185, pp. 215–230. doi: 10.1016/j.precamres.2011.01.012.

Zouros, N.C. 2007. Geomorphosite assessment and management in protected areas of Greece Case study of the Lesvos island – coastal geomorphosites. *Geographica Helvetica* 62(3), pp. 169–180. doi: 10.5194/gh-62-169-2007.